Materials Horizons: From Nature to Nanomaterials

Komal Rizwan
Muhammad Bilal
Tahir Rasheed
Tuan Anh Nguyen *Editors*

Hybrid Nanomaterials

Biomedical, Environmental and Energy Applications

Springer

Materials Horizons: From Nature to Nanomaterials

Series Editor

Vijay Kumar Thakur, School of Aerospace, Transport and Manufacturing, Cranfield University, Cranfield, UK

Materials are an indispensable part of human civilization since the inception of life on earth. With the passage of time, innumerable new materials have been explored as well as developed and the search for new innovative materials continues briskly. Keeping in mind the immense perspectives of various classes of materials, this series aims at providing a comprehensive collection of works across the breadth of materials research at cutting-edge interface of materials science with physics, chemistry, biology and engineering.

This series covers a galaxy of materials ranging from natural materials to nanomaterials. Some of the topics include but not limited to: biological materials, biomimetic materials, ceramics, composites, coatings, functional materials, glasses, inorganic materials, inorganic-organic hybrids, metals, membranes, magnetic materials, manufacturing of materials, nanomaterials, organic materials and pigments to name a few. The series provides most timely and comprehensive information on advanced synthesis, processing, characterization, manufacturing and applications in a broad range of interdisciplinary fields in science, engineering and technology.

This series accepts both authored and edited works, including textbooks, monographs, reference works, and professional books. The books in this series will provide a deep insight into the state-of-art of Materials Horizons and serve students, academic, government and industrial scientists involved in all aspects of materials research.

Review Process

The proposal for each volume is reviewed by the following:

1. Responsible (in-house) editor
2. One external subject expert
3. One of the editorial board members.

The chapters in each volume are individually reviewed single blind by expert reviewers and the volume editor.

Komal Rizwan · Muhammad Bilal · Tahir Rasheed ·
Tuan Anh Nguyen
Editors

Hybrid Nanomaterials

Biomedical, Environmental and Energy Applications

Springer

Editors
Komal Rizwan
Department of Chemistry
University of Sahiwal
Sahiwal, Pakistan

Tahir Rasheed
Department of Chemistry and Chemical Engineering
Shanghai Jiao Tong University
Shanghai, China

Muhammad Bilal
School of Life Science and Food Engineering
Huaiyin Institute of Technology
Huaian, China

Tuan Anh Nguyen
Institute of Tropical Technology
Vietnam Academy of Science and Technology
Hanoi, Vietnam

ISSN 2524-5384 ISSN 2524-5392 (electronic)
Materials Horizons: From Nature to Nanomaterials
ISBN 978-981-19-4537-3 ISBN 978-981-19-4538-0 (eBook)
https://doi.org/10.1007/978-981-19-4538-0

This Springer imprint is published by the registered company Springer Nature Singapore Pte Ltd.
The registered company address is: 152 Beach Road, #21-01/04 Gateway East, Singapore 189721, Singapore

Preface

Hybrid nanomaterials represent the interface between two worlds of chemistry. These are novel conjugates of organic (ligands, biomolecules, pharmaceutical substances, polymers, etc.) and inorganic (metal ions, salts, metal) clusters or particles, oxides, non-metallic, etc.) materials. The combination of various structural layouts and components with different interactions, including covalent, dispersion, electrostatic, hydrogen bonding and π-complexation, etc., provides an endless variety of novel task-specific materials. Hybrid materials possess enhanced physical and chemical properties and novel functionalities compared to single components owing to their size on the nanoscale. The porosity of hybrid materials is controllable, and their exposure to surface functional groups promotes them as potential candidates for diversified applications as environment, optics, bio-imaging, electronics, medicine, catalysis, sensors, energy, and energy storage, diagnosis, etc. Advanced architectures based on organic–inorganic hybrids promote continuous innovations and provide a driving force for progress in different technological fields, particularly drug delivery, energy applications, and material science.

During the last decades, hybrid nanomaterials have been developed largely. Characteristics of hybrid nanomaterials may be modified post-synthetically. Coupling molecular engineering and processing helps fabricate hybrids of different shapes, morphologies, compositions, and versatile functionalities. These novel hybrid materials possess enhanced electrical and optical features, improved conductivity, luminescence, selectivity, rigidity, porosity, and chemical potential. Thereof, organic–inorganic hybrid nanomaterials are at cutting edge in many fields, especially biomedical, environmental remediation, and energy-based devices. In this way, the use of organic, inorganic hybrid nanomaterials should be advantageous in designing modern technologies.

The use of organic–inorganic nanohybrids in biomedical, energy, and bioremediation research has yielded a slew of new data in recent years, allowing researchers to gain a better understanding of key pathways and gain new insights into the fabrication and application of nanohybrids in various life domains. The emergence, fabrication, structural analysis, current status, problems, and future prospects of organic–

inorganic nanohybrids in their new avatars for environmental remediation have all been covered in Chaps. 1–4.

A great deal of interest has been drawn to organic and inorganic nanohybrids because of their advantageous properties and potential uses in the healthcare industry. Chapters 5–7 describe the applications of organic–inorganic nanohybrids in biomedical fields such as medicines, cancer treatment, drug delivery, and tissue engineering.

Environmental pollution is a severe issue around the globe, and there is a need to design environment-friendly materials for their facile application to remediation of the environment. The demand for nanohybrid materials with potential environmental remediation increases day by day due to their overwhelming environmental impacts. The advanced techniques used in environmental remediation and detection devices, such as electrochemical sensors, are sustainable alternatives to keep the environment clean and safe. Nanohybrid composites are significant materials for sensing, detecting, and removing environmental pollutants from soil, wastewater, and air. Chapters 8–11 portray the role of organic–inorganic nanohybrids in sensing volatile organic compounds, heavy metals, humidity, UV, gases, and others. Chapters 12–14 describe the potential role of organic–inorganic nanohybrids in removing different pollutants from wastewater, soil, and air.

Energy storage is becoming increasingly important for diverse areas such as renewable energy, electric vehicles, grid reliability, and consumer electronics. Flexible electronic devices have been widely used in energy storage and sensor systems due to their flexibility and biocompatibility. These applications require long-lasting and economic systems that can store and deliver energy on demand. Moreover, their easy fabrication and lightweight properties have raised the demand for medical devices and portable electronics. Currently, different flexible electronic devices are made up of organic–inorganic compounds, e.g., carbon materials, metal oxides and polymers, which significantly improve the efficacy of these devices. However, the growing use of these flexible devices in our daily lives gives scientists a significant challenge to make advancements in these devices regarding materials and fabrication. Chapters 15–21 have given an insight into the significant role of organic–inorganic nanohybrids in energy applications. Chapter 22, entitled "Toxicology, Stability, and Recycling of Organic–Inorganic Nanohybrids" provides details about the toxic effects of organic–inorganic nanohybrids and their stability in various environments. Chapter 23 provides a synoptic view of the challenges and future prospective of organic–inorganic nanohybrids.

As editors, we have sincerely attempted to provide a comprehensive account and role of state-of-the-art organic–inorganic nanohybrids as biomedical tools, energy applications, sensing and remediation of pollutants from various matrices. The book offers more insights into the fabrication of organic–inorganic hybrid nanomaterials, their advantages, self-assembly, and their applications in diversified fields, specifically in the biomedical field, energy devices, sensors, and environmental remediation. This book shall also provide insight into tools, tricks, and challenges associated with

fabrication techniques and future challenges and risks. All chapters include fundamentals of the processes involved, which will provide a broad-spectrum and cross-disciplinary audience of academic institutions and research institutes with up-to-date and comprehensive ideas on organic–inorganic nanohybrids, as well as know-how of appropriate bioremediation technology for environmental remediation to students, researchers, and scientists in the fields of chemistry, biology, biotechnology, pharmacology, and biochemistry. We also hope that the book will also be handy for the engineering consultants, industrial waste managers, and regulators representing government and non-government/private organizations.

We gratefully acknowledge all the authors for their contributions to the book.

Sahiwal, Pakistan

Dr. Komal Rizwan
Corresponding Editor

Acknowledgments

The book, *Hybrid Nanomaterials: Biomedical, Environmental and Energy Applications*, is the result of dedicated efforts of numerous individuals; the editors, were not alone but assisted by many people, many of whom deserve special mention. We would like to acknowledge and appreciate the efforts of all the contributors who responded to our request and shared their knowledge enthusiastically with us in the form of manuscript containing the recent and updated information on the topic and made this primer a reality.

Dr. Komal Rizwan would love to dedicate this book to her beloved father, **Khan Mahboob Rizwani (late)**. His unconditional support, love and blessings throughout life have given her strength and determination to accomplish her goals, and all his efforts in her life made her eligible to this level to pay role as a scientist.

Dr. Komal Rizwan would like to thank **Prof. Dr. Shahid Munir**, Chairman, Punjab Higher Education Commission, Pakistan (Former-Vice Chancellor, University of Jhang) for his kind support to complete this book. His constructive comments helped out in editing some of the manuscripts for value addition and his efforts are highly appreciated.

Dr. Komal Rizwan expresses her sincere gratitude to our Co-editor **Dr. Muhammad Bilal** for his kind moral support and guidance, which proved highly useful to complete this book. In addition, he took his valuable time to critically review the individual manuscript of this book.

We wish to acknowledge our students, past and present, who provided the stimulation for the continuation of this work that made it possible. We want to thank our teachers/mentors–who, in their way, have a true passion for science and an insistence that the right experiments are done. She is always grateful to her Ph.D. supervisor, **Dr. Muhammad Zubair**, Chairman, Department of Chemistry, Government College University Faisalabad, Pakistan, for the tremendous academic support that they provided to her during her doctoral studies.

We would also like to thank Springer Nature for giving us the opportunity to accomplish the project and share the knowledge with the scientific and academic fraternity. We are particularly indebted to Ms. Priya Vyas, Editor, Springer, for the

execution of the publishing agreement, motivation, encouragement, support, and her valuable suggestions.

We are grateful to Ms. Silky Abhay Sinha, in her role as Project Coordinator at Springer, for constant critical advice and invaluable support and coordinating the entire project and ensuring the smooth production of this book. She systematically managed the book's production schedule and progress; without her prodding, this book would never have been completed. We wish to warmly and gratefully acknowledge the many publishing professionals at Springer Nature whose consistent encouragement, hard work, and careful attention to detail contributed much to the clarity of both the text and the artwork which helped to make *Hybrid Nanomaterials: Biomedical, Environmental and Energy Applications.*

The team of Springer Nature has played a great role throughout, always helpful and supportive. Finally, we would like to apologize in advance for any errors that may occur in the text and express our heartfelt embarrassment. We should be pleased to receive any suggestions on the content and style of *Hybrid Nanomaterials: Biomedical, Environmental and Energy Applications*, from students, professionals, environmentalists, environmental engineers, scientists, and policymakers, all of which will be given serious consideration for inclusion in any further editions.

Dr. Komal Rizwan
Corresponding Editor

Contents

1 Introduction to Organic–Inorganic Nanohybrids 1
Hassan Zeb and Asim Riaz

2 Structural Design of Organic–Inorganic Nanohybrids 29
Muhammad Tanveer, Muhammad Imran, Shoomaila Latif, Nazim Hussain, and Muhammad Bilal

3 Fabrication of Organic–Inorganic Nanohybrids 37
Muhammad Rashid, Shoomaila Latif, Muhammad Imran, Ayesha Mumtaz, Nazim Hussain, and Muhammad Bilal

4 Synthesis of Organic–Inorganic Nanohybrids-Based Polymeric Nanocomposites 53
Ahmad Shakeel, Komal Rizwan, Ujala Farooq, and Saima Yasin

5 Organic–Inorganic Nanohybrids in Medicine 77
Sameera Shafi, Saba Zafar, Zohaib Sarwar, Muhammad Hassan Rasool, and Tahir Rasheed

6 Organic–Inorganic Nanohybrids in Cancer Treatment 107
Hira Amjad, Komal Rizwan, Muhammad Baber, and Shahid Iqbal

7 Organic–Inorganic NanoHybrids in Tissue Engineering and Drug Delivery Applications 133
Shahzad Maqsood Khan, Saba Zia, and Nafisa Gull

8 Organic–Inorganic Nanohybrid-Based Electrochemical Biosensors 151
Aneeqa Batool, Tauqir A. Sherazi, and Syed Ali Raza Naqvi

9 Organic–Inorganic Nanohybrids Based Sensors for Volatile Organic Compounds 175
Syed Salman Shafqat, Asma Mukhtar, Syed Rizwan Shafqat, Muhammad Adnan Asghar, Muhammad Rizwan, Dure Najaf Iqbal, and Tahir Rasheed

10 Organic-Inorganic Nanohybrid-Based Sensors for Metal Ions Sensing 201
Madeeha Batool and Hafiz Muhammad Junaid

11 Organic-Inorganic Nanohybrids-Based Sensors for Gases, Humidity, UV and Others 227
Sohail Shahzad, Komal Rizwan, and Muhammad Zubair

12 Application of Organic-Inorganic Nanohybrids in Wastewater Treatment 247
Azka Abdur Rehman, Zaeem Bin Babar, Shahid Munir, Mashhood Urfi, Sumaira Kanwal, Muhammad Naeem Ashraf, and Komal Rizwan

13 Organic–Inorganic Nanohybrids for the Removal of Environmental Pollutants 277
Zaeem Bin Babar, Ariha Shahi, Abdul Rauf, Hamed Sattar, and Komal Rizwan

14 Tungstate-Based Nanohybrid Materials for Wastewater Treatment 311
Junaid Munawar, Ehsan Ullah Rashid, Shahid Nawaz, Sayed Ali Abbas Sherazi, Muhammad Ali, Abbas Rahdar, Komal Rizwan, and Muhammad Bilal

15 Organic–Inorganic nanohybrids in Dye-Sensitized Solar Cells 329
Osama Majeed Butt, Muhammad Zaffar, Muhammad Shakeel Ahmad, Komal Rizwan, Adnan Daud Khan, and Muhammad Saad Rehan

16 Organic–Inorganic Nanohybrids in Supercapacitors 359
Muhammad Abbas, Syed Fahad Bin Haque, Yafen Tian, John P. Ferraris, and Kenneth J. Balkus Jr.

17 Organic–Inorganic Nanohybrids in Flexible Electronic Devices 385
Rabia Akhtar, Ameer Fawad Zahoor, Asim Mansha, Sajjad Ahmad, Muhammad Irfan, Kulsoom Ghulam Ali, and Bushra Parveen

18 Organic–Inorganic Nanohybrids for Light Harvesting Application 405
Syed Muhammad Ali Trimzi, Muhammad Wajahat Ali, Ataf Ali Altaf, and Samia Kausar

19 Organic–Inorganic Nanohybrids as Thermoelectric Materials 419
Muhammad Ayyaz, Noor-ul-Huda Altaf, Mohsin Khan, Ambreen Ashar, Sehrish Maqsood, Muhammad Yasin Naz, and Shazia Shukrullah

20 Organic–Inorganic Nanohybrids in Fuel Cell Applications 445
Abdul Rauf, Mashhood Urfi, Zaeem Bin Babar, Shahid Iqbal, and Komal Rizwan

21 Organic–Inorganic Nanohybrids in Advanced Batteries 461
Aqsa Iqbal, Ataf Ali Altaf, Javeria Shoukat, Anila, Shaheed Ullah, and Samia Kausar

22 Toxicology, Stability, and Recycling of Organic–Inorganic Nanohybrids 485
Shahzad Maqsood Khan, Sidra Saleemi, and Hafiz Abdul Mannan

23 Application Scope, Challenges and Future Perspectives of Organic–Inorganic Nanohybrids 499
Hina Liaquat, Shoomaila Latif, Muhammad Imran, Nazim Hussain, and Muhammad Bilal

About the Editors

Dr. Komal Rizwan is currently working as an Assistant Professor in the Chemistry Department, Faculty of Science, University of Sahiwal, Pakistan. She earned her Ph.D. in chemistry from Government College University, Pakistan in 2017 and also carried out research work at University of Pennsylvania, USA. She has won 3 prestigious scholarships from higher education commission, Pakistan. She has published more than 100 scientific contributions in the form of research, reviews and book chapters in various areas of sciences. She has an H-index of 24 along with 2000 citations. She is serving as lead editor of two books and serves as scientific reviewer in numerous peer reviewed journals. Dr. Rizwan's research group is working in multiple research directions mainly focused on material chemistry, environmental chemistry, organic synthesis, visible light photoredox couplings, transition metal catalyzed cross couplings and click chemistry. Her group is also focusing on synthesis of nonlinear optical compounds and computational part of her lab contributes to a fundamental understanding of the electronic structure and properties of nonlinear optical materials that are being considered in the design of electro-optics.

Dr. Muhammad Bilal is working as an Associate Professor in the School of Life Science and Food Engineering, Huaiyin Institute of Technology, China. He received his Ph.D. from Shanghai Jiao Tong University with a specialization in Bioengineering and Applied Biotechnology. He has published more than 800 scientific contributions in the form of research, reviews, book chapters and scientific articles in various areas of science & engineering. He has an H-index = 64 with more than 16000 citations. He is an editorial board member of journals of national and international repute and has edited several special issues and books. His research interests include bioengineering, environmental biotechnology, nanotechnology, bio-catalysis, enzyme engineering, immobilization, chemical modifications and industrial applications of microbial enzymes, bioremediation of hazardous and emerging pollutants, liquid, and solid waste management – valorization of agro-industrial wastes and biomaterials for bioenergy.

Dr. Tahir Rasheed is currently working as a researcher at the School of Chemistry and Chemical Engineering, Shanghai Jiao Tong University, China. He received his Ph.D. and degree in Polymer Chemistry and postdoctoral research from the same university. Dr. Rasheed has published over 100 scientific contributions in various areas of science and engineering. His research interests focus on multiple disciplines including controllable synthesis, characterization and self-assembly of alternating copolymers, hyper-branched polymers, with special emphasis on their potential applications in the field of sensing and biosensing, enzyme mimic, catalysis, solid polymer electrolytes and energy storage devices (i.e. supercapacitor and Li-ion batteries).

Dr. Tuan Anh Nguyen is presently working in the Institute for Tropical Technology, Vietnam Academy of Science and Technology. He completed his B.Sc. in Physics from Hanoi University in 1992, and his Ph.D. in Chemistry from Paris Diderot University (France) in 2003. He was a Visiting Scientist at Seoul National University (South Korea, 2004) and the University of Wollongong (Australia, 2005). He worked as a Postdoctoral Research Associate and Research Scientist at Montana State University (USA), 2006–2009. In 2012, he was appointed as Head of Microanalysis Department at the Institute for Tropical Technology (Vietnam Academy of Science and Technology). He has managed 4 Ph.D. theses as thesis director and 3 are in progress. Dr. Nguyen has edited 38 books and 5 books published.

Chapter 1
Introduction to Organic–Inorganic Nanohybrids

Hassan Zeb and Asim Riaz

1 Introduction

Advanced material development for variety of applications keeping the norms of sustainable strategy has gained significant importance in current century [1]. Starting with the consumption of naturally occurring raw materials, recent advancements focused on modifications of these natural moieties motivated by specific application as well as higher efficacies. Materials can either be classified as "organic (based on living or once-living matter)" or "inorganic (coming from non-living matter or minerals)." Both have separate applications; however, they can produce miracles when used in combination.

"Hybrid" stems from "hybrid," a Latin term which means mixed strain [2]. As per The International Union of Pure and Applied Chemistry (IUPAC), definition of hybrid material, is that "material composed of an intimate mixture of inorganic components, organic components, or both types of components where the components diffuse into each other at nanometer level" [3]. This includes composite materials of all types including metal–metal, polymer–polymer, metal–ceramic, metal–polymer, and polymer–ceramic composites. In a classical way, the term "composite" was attributed to macroscale mixing or for the blends with noncovalent interactions and the term "hybrid" where components are bonded by covalent interactions [4]. In modern days, however, this distinction has got dim and both the terms are used interchangeably.

Basically, a hybrid material is the one which comprises of at least two materials. Philosophy behind merging two materials together is to obtain a new material

H. Zeb (✉)
Institute of Energy & Environmental Engineering, University of the Punjab, Q&A Campus, Lahore, Pakistan
e-mail: hassanzeb.ieee@pu.edu.pk

A. Riaz
Department of Chemical Engineering, Khwaja Fareed University of Engineering & Information Technology, Rahim Yar Khan, Pakistan

K. Rizwan et al. (eds.), *Hybrid Nanomaterials*, Materials Horizons: From Nature to Nanomaterials, https://doi.org/10.1007/978-981-19-4538-0_1

depicting the properties of both parent materials as well as additional properties resulting from the synergetic effect [2, 5]. As a matter of fact, characteristics of hybrids are actually more than just sum of the individual characteristics of parent materials, and this synergy is usually associated with the interface between the two materials [6]. Merger of organic–inorganic materials to form a hybrid first started with an aim of amplifying the properties of polymeric materials such as clay particles added to polymeric matrices to increase its mechanical strength [7]. However, recent advancements in field of hybridization of organics and inorganics go far beyond mere mechanical boost and cover an outstanding range of applications including energy storage, efficiencies of electronic devices, catalysis, biomedical sciences, etc. [5, 8]. This certainly has a positive impact on quality of life in terms of resource management as well as environmental remediation. In order to have a long-term positive impact, synthesis of these hybrid to be greener as well.

The field of hybrid materials, not new however, is rapidly growing and continuously expanding owing to not only ambitious requirements on properties of materials but also requirement on adherence to environmentally benign practices while synthesizing those materials. In fact, nature provided humans the concept of crossbreeding of organic and mineral components. Highly efficient composite structures which include biological parts such as bones, ivory, shells, teeth, and ferritin were all the result of biomineralization and have been existing for thousands of centuries. These biological components incorporate biopolymers (cellulose, proteins, sugars etc.) with inorganics moieties (calcium, iron, silica, carbonates, phosphates, etc.) [9]. However, for the last 3 decades, the recent surge in the area of organic–inorganic hybrids is the result of bringing together research communities with their own infrastructures, distinct fields and hence customized approaches.

This chapter discusses a few examples of nanohybrid materials in the fields of energy and environment and biomedical sciences as shown in Fig. 1. However, to give readers a better understanding about the evolution of these modern hybrid materials, let us first go through a brief history of different classes of these hybrids.

2 History of Modern Hybrids

2.1 Silicon Chemistry and Silicates

Beginning of the silicon period, known as the basis in the creation of advanced hybrids, was the seventeenth century. Although “glass technology” has been there since 3000 BC, the rise of new silicon technology is mild in term of reaction conditions, allowing it to work nicely with organic components. New synthetic pathways leading to organosilicon precursors and molecular silicon were pivotal in the development of contemporary chemistry of silicon. This development can be accredited to Swedish scientist, J. J. Berzelius, also known for his vital contributions to the discovery of new elements, chemical notation, and atomic weight, who was a modern

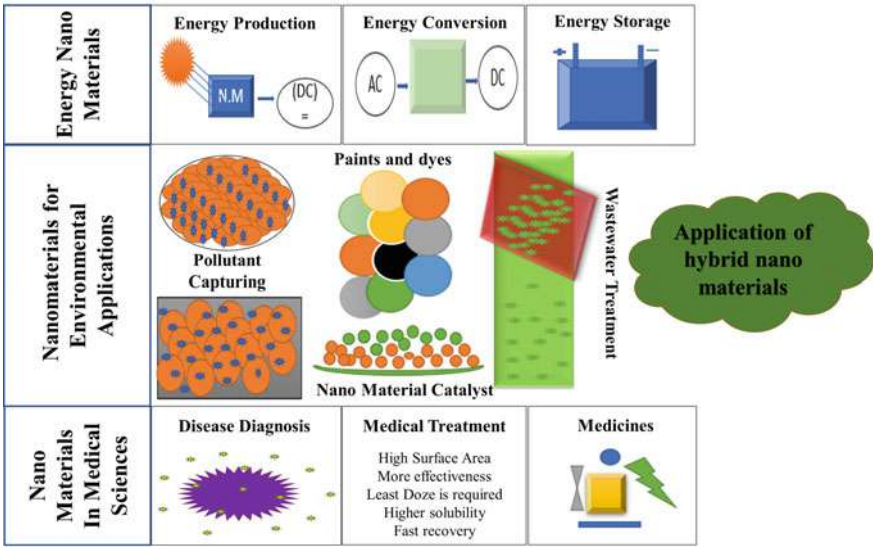

Fig. 1 Schematic, depicting few examples of applications of nanohybrids in the fields of energy, environment, and biomedical sciences

chemistry pioneer. Berzelius created two groundbreaking reactions in 1824, which he revealed in 1843 that he discovered, by coincidence though, the separation of elemental silicon by heating potassium fluorosilicate and potassium metal together [10]. The other discovery was the production of silicon halides, particularly $SiCl_4$, starting with isolated silicon. $SiCl_4$ is a key precursor for the forthcoming inorganic polymerization.

2.2 Hybrids Based on Clay

The earliest contemporary composites consisting of organic–inorganic components were presumably made utilizing layered clay particles like smectites (phyllosilicates and montmorillonite) and organic cations to replace the inorganic cations which is present in between layers, as Hendricks [11] and Gieseking [12] described at the start of 1940s. This similar sort of clay mineral was later developed by Bradley [13] and MacEwan [14] to create organic–inorganic hybrids. Notably, the intercalation technique used to create organic–clay hybrids may be used to create numerous 2D solids, paving the path for future important breakthroughs in organic–inorganic hybrid materials [15]. Clay–organic hybrids gained early prominence due to vast their industrial utilization as filler and additives in polymer like clay–polymer nanohybrids, as specialized sorbents, as rheological agents, and recently in specific applications for future materials [16]. As stated earlier, important research by Hendricks,

Gieseking, MacEwan, and Bradley performed in the 1940s, laid the foundation for modern production of organoclays which have been surfaced over last two decades [17]. This sort of hybrid is one of the most widely used around the globe currently. Each year, thousands of tons of organoclays are manufactured for important market sectors in vast applications, such as oil spill cleanup, pollution adsorption, greases, rheological agents for paints, pesticides, enzymes, and other biologically active materials support, and polymer fillers.

The production of polymer–clay nanocomposites (PCNs) represent a significant step forward in the application of organoclays. In 1961, initial reports by Blumstein showed that the polymer intercalates in the layered clays by homopolymerization of monomers contributing to well-structured polymer–clay hybrid composites [18]. Theng modified the very first monograph dedicated exclusively to the disclosure of the modern polymer–clay interactions in 1979 [19]. However, after groundbreaking research leading to PCN invention by Fukushima et al. [20] in 1985, this issue once again came into the light after many decades. For the first time, Toyota researchers discovered clay delamination producing very highly dispersed polymers. This discovery symbolizes a breakthrough in science and technology, not only for using clays as to reinforce polymer's charges but also to incorporate functionality into hybrid materials [21]. PCN was initially studied for its rheological and mechanical properties, but later on, the additional features of PCN including electrical conductivity were explored as functional nanocomposites. Deuel created the first organic silicate derivatives in 1952. He reacted silanol groups of montmorillonite clay with the diazomethane to form covalent linkages between silicate network and the organic groups. However, the lack of Si–OH groups in this silicate raised numerous questions among scientists [22]. The reaction of organosilanes with clays and some other silicates in acidic conditions produced very stable organic–inorganic hybrids. The organic derivatives of vermiculite, sepiolite, and chrysotile were then prepared using this one-pot co-hydrolysis method [23].

Carbon-clay-based conducting hybrid nanocomposite materials were synthesized either by in situ production of graphene-like substances or by direct assembling of carbonaceous materials like sepiolite with graphite nanoplatelets and certain other clay minerals or multiwalled carbon nanotubes (MWCNTs) [24]. These hybrid materials have intriguing physicochemical properties that each element of interest offers, making them suitable for many applications such as their incorporation in polymers. So, the cheap graphite nanoplatelet–clay hybrids with small doping of MWCNTs have recently been described for their use as a nanofiller in polymer hybrids, resulting in considerable electrical conductivity while also improving mechanical properties of interest for a variety of applications [25]. In fact, the idea of combining clay and graphite originates from the pencil discovery by N. J. Conté in 1795, who demonstrated that combining graphite powder and clay minerals produces carbon–clay composite materials that can be treated as sticks and serve as the basis for the fabrication of traditional pencil cores [25].

2.2.1 Biohybrids Based on Clay

Biohybrids are created by combining biologically derived molecules with inorganic substrates such as carbonates, silicates, and phosphates. These materials are made up of clay minerals, microfibrous clays like sepiolite, and layered clays like montmorillonite which are manufactured using building block methods [26]. The most intriguing attribute of these biohybrids is most likely their incredible bioactivity. In addition to the invention of novel vaccines based on organically altered sepiolite that demonstrate a considerably greater efficiency than current influenza vaccines [27], they may be employed as viral particle carriers for the production of thermally stable vaccines (e.g., Influenza A) [28].

2.3 Zeolite-Based Hybrids

In the 1950s and 1960s, the zeolite community, like clays, began hybridizing and integrating organic groups, but from a very different perspective. Zeolites are alkali and alkaline earth metal hydrated aluminosilicates consisted of interconnected tetrahedra of silica and alumina that create 3D crystalline formations with well-defined microporosity by controlled condensation. Because of the uniform sizes and openings of microcavities, zeolites help to sort molecules; as a result, they have been called "molecular sieves" and used for catalysis, purification, separation, ion exchange, and detergents.

The earliest example of zeolite hybridization, according to Barrer and Denny, was the crystalline aluminosilicates that are metal cation-free synthesized by adding alkylammonium [29]. The structure-directing effect was caused using bigger organic cations, which increased the pore size and structural range of zeolites. In 1966, Kerr reported the novel synthesis of ZK-5, a very stable molecular sieve, in the presence of quaternary ammonium ions, which had outstanding hydrocarbon separation performance [30]. In addition to its charge-balancing and template functions, organic guest cations impose a charge density constraint on the zeolite framework, producing materials with a higher Si/Al ratio, which allows zeolites to be acidity controlled.

Barrer's hypothesis was confirmed by Mobil Oil in the 1970s when they synthesized ZSM-5 zeolite with high Si/Al ratio (with Si/Al > 10), showing shape selective catalytic features as well as high thermal stability. The crystallization of aluminosilicate frameworks consisting of three rings with Si/Al ratios between 10 and 30 was caused by trispyrrolidinium cation which served as a templating agent during the synthesis of ZSM-18 [31]. Interestingly, a pure SiO_2-based molecular sieve known as "silicalite" was developed by using identical methods [32]. This organic–inorganic synthesis method was eventually extended to additional molecular sieve families (e.g., the AlPO4-n series) [33] and constituted a revolution in the production of zeolites for catalytic purposes, propelling academic investigations in the decades that followed [34].

2.4 Ceramics and Glasses Derived from Sol–Gel Technique

Initially, the "sol–gel" science was quite progressive which was motivated by practical, if not technical, demands; in fact, the sol–gel science emerged after the sol–gel technology [35]. In the 1930s, Geffcken and Berger reported some pioneering work on sol–gel coatings (Schott Glaswerke Company) [36]. Between the mid-1950s and the 1970s, the "sol–gel" domain began to cluster. It all began in the ceramic sector in 1952–1956 with the work of Rustum Roy [37].

A milestone in the glass community was the sol–gel pathway to produce optical coatings of crystalline, glassy crystalline, and glassy systems consisting of multicomponents without melting and it was manifested by H. Dislich in the beginning of 1970s [38]. In the early 1980s, scientists like D. Ulrich, C. J. Brinker, and J. D. Mackenzie, and D. Ulman, hosted the first scientific seminar bringing together experts working on glasses and ceramics as well as other subjects including silicones [39], optics, and mechanical engineering [40]. In the 1980s, metallorganic and silicone chemists like H. Schmidt and K. Andrianov presented the first organically altered molecular precursor (organoalkoxysilanes) synthesis [41].

Although the sol–gel method had been studied broadly and understood for silica. In the late 1980s, other transition–metal oxides were synthesized by scientists like Livage et al. who defined standard principles for condensation of transition metal oxides, aligning system reactivity to electronegativities [42]. The release of G. Scherer, and C. J. Brinker's book "Sol–Gel Science" in 1990 [43] laid the foundation of a distinct discipline of physics and chemistry devoted to the sol–gel process. In the 1990s, understanding of sol–gel silica materials had progressed to the point that material properties could be modified by selecting proper processing conditions. Adapted shaping techniques produce SiO_2 materials with regulated morphology and porosity like monoliths [44], powders with defined shape [45], or films [46].

2.4.1 Polymer Nanocomposites from Sol–Gel Technique

Due to their extraordinary processability, and versatility at moderate conditions, in the late 1970s, sol–gel compounds were easily coupled with organic polymers to form inorganic–organic hybrid materials of class I or II [47]. Back in 1980s, the main motive to couple sol–gel technique with the organic polymerization was the mechanical reinforcing of plastics. In 1985, G. Wilkes and J. Mark invented "ceramers", a novel type of composite material, using a sol–gel technique that combined polymers with metal oxo polymers.

In the 1980s, the fundamental motivation to combine sol–gel technique with the organic polymerization was the mechanical reinforcing of plastics [48]. In the early, 1990s Novak tried (and succeeded) in synthesizing interpenetrated inorganic–organic networks via simultaneous inorganic and organic polymerization [49]. A method

presented by K. Matyjaszewski based on transfer of an atom aided radical polymerization to form block copolymers and homopolymers from surfaces based on silicon [50]. It was a signification development in hybridization process.

2.4.2 Biohybrids Based on Sol–Gel Technique

During the same time period, numerous researchers working on "sol–gel" began bridging the gap between biology and the sol–gel method by enclosing biomolecules in silica matrices to create bioactive hybrids. In 1990, D. Avnir presented groundbreaking research in which an enzyme, such as alkaline phosphatase (ALP), was trapped in a silica gel [51]. In the 1993, Sanchez and Audebert produced a novel electrochemical biosensor by trapping glucose oxydase in silica gels [52].

Similarly, Livage and colleagues immobilized parasite protozoa (Leishmania do novani infantum) in silica matrices and employed an enzyme-linked immunosorbent test to perform specific antigen/antibody reactions for the diagnosis of visceral leishmaniasis [53]. The same research group, after ten years, showed that the viability of Serratia marcescens bacteria trapped in silica gel may be greatly enhanced by "quorum sensing," i.e., intercellular signals molecules [54]. Silica–based sol–gel materials are now key players in the development of diverse biomaterials for a variety of biological applications, including drug delivery and bioscaffolds [55].

2.5 Mesoporous Nanomaterials

The mesoporous materials emerged from converging sol–gel chemistry and organic templating techniques that had previously been used for clay-zeolite hybrids [56]. Kuroda (Waseda University, Japan) and colleagues were the first to report the synthesis of SiO_2 mesoporous materials in 1990 [57]. Researchers from Mobil Oil presented the "liquid–crystal templating" technology in 1992. Kresge et al. described the production of mesoporous materials with ordered porous structure resulted from the condensation of silicate substance between self-assembled ionic surfactant micelles in a 1992 paper. Kresge's contribution on liquid–crystal templating ushered in a new era of sophisticated mesoporous materials, particularly those with changeable composition [58] and bigger pore sizes. In 1994, Stucky and colleagues described a method for synthesizing periodic mesostructured composites including cationic or anionic surfactants and a variety of metal oxides (other than silica) [59]. Electrostatic templates, on the other hand, resulted in a porous but unstable network. Tanev et al., in 1995, reported a neutral templating technique based on hydrogen bonding interactions and self-assembly among neutral primary amine micelles and neutral inorganic precursors [60].

Several researchers reported the production of large pore silica compounds between 1997 and 1998. As templating agents, Goltner and Antonietti used amphiphilic block copolymers [61]. Using polyakylene oxide, a triblock copolymer,

as a micellar structuring agent, Stucky and colleagues synthesized a mesoporous silica material with larger pore size (5–30 nm). This mesoporous silica material was labeled as SBA-15 (or Santa Barbara amorphous type material) [62]. Mesoporous metal oxides materials with large pores (including ZrO_2, TiO_2, Nb_2O_5, Ta_2O_5, Al_2O_3, WO_3, SnO_2, and HfO_2 and mixed oxides $SiTiO_4$, $SiAlO_{3.5}$, Al_2TiO_5, ZrW_2O_8, and $ZrTiO_4$) having semicrystalline frameworks may later be manufactured by utilizing the same type of block copolymers [63].

Ryoo et al. introduced the "nanocasting" approach, which uses inorganic mesoporous materials as a "hard template" for the formation of mesoporous carbons (denoted CMK-1) [64]. The polymer precursors may be impregnated into the silica mesoporous template, which could then be polymerized to form a continuous network surrounding the silica network, as Knox et al. reported more than 10 years ago [65].

Inorganic compounds generated from sol–gel were not the only ones caused by the organic template technique. Using a direct polymer templating technique, Cölfen, Nassif, and colleagues successfully developed mesoporosity in ionic crystals [66]. Zwitterionic PEO–$(RGD)_5$ block copolymers containing aqueous solution was precipitated to form mesoporous crystalline calcite. The double-hydrophilic block copolymer was the "binding block" having zwitterionic peptide sequence, facilitating stability, nucleation inhibition and templating of amorphous precursor particles [66].

2.6 Hierarchically Structured and Multiscale Materials

The advent of templating techniques paved the path for the development of multiscale, hierarchically organized materials, which were made possible by integrative tactics including the smart combination of sophisticated processing, sol–gel chemistry, and multiple templating [67]. Flexible processing techniques [68] for shaping mesoporous materials as films [69], particles [70], fibers [71], and patterns [72] were developed, owing to the advent of so-called evaporation induced self-assembly strategies described by Brinker and coworkers and Baskaran et al. at the end of the 1990s. By mixing polymer latex particles with micelles, Antonietti and coworkers in 1998 suggested a multiple templating technique for the manufacture of hierarchical porous silica having bimodal pore size distribution which ranged 20–400 nm [73].

Multiscale shaping of hybrid and inorganic materials was first attempted at the end of 1990s by using a combination of soft-chemistry procedures such as organic templating. Soft-lithography techniques were also proposed by Xia and Whitesides in same era [74]. In the years afterward, several more processing/shaping processes had been developed, and this approach has now attained a high level of technological maturity [75]. As a result, the key characteristics of mesoporous and hierarchical materials (high surface area and broad composition range) enable them to be used in catalysis, optics, biology, medicine, electronics, energy, and nanofluidics [76].

2.7 Coordination Polymers

Hybrid coordination polymers made up of metal ions or clusters joined by organic linkers have a long history (dating back to Prussian Blue); however, the discovery of "metal–organic frameworks" in the mid-1990s drew a lot of attention [77]. The United States government originally backed the development of metal-containing coordination polymers in the 1940s–1960s, with the goal of generating materials with better thermal stabilities than ordinary polymers for the space program. Saito and colleagues crystallized bis(adiponitrilo)copper(I) structures made of tetrahedral Cu(–CN)4 units combined by organic species of varying lengths in 1959, including the first three dimensional, four connected networks [78]. C. E. Carraher Jr published many papers in the 1970s that focused on the development of metal–organic oligomers and polymers [78]. R. Robson, a coordination chemist with a strong background in crystallography and XRD characterization, made a significant contribution in the late 1980s. Robson and Hoskins published an infinite, non-interpenetrated, cationic framework with the formula [Cu(TCTPM)]+ in 1989 [79]. Kitagawa and Kondo, in 1998, proposed a chronological as well as a functional categorization of porous coordination polymers [80].

Originally defined in 1995, the term MOFs (metal–organic frameworks) was first used to describe a material with the formula Cu(4,4′-bpy)1.5NO_3(H_2O)1.25, which had an open diamond-like structure [81]. It was shown in 2002 that by varying the functionality and length of the linkers, different isoreticular "MOF-5" frameworks may be produced [82].

One of the earliest and most notable instances of third generation porous coordination polymers explored since the early 2000s is their reversible responsiveness and flexibility [83]. The MOF community has grown significantly in recent years, and several different porous coordination polymers have been awarded their "lettre de noblesse" [84]. In recent years, a new era of porous hybrid materials has begun [85] with the development of processing and shaping techniques to support their use in fields such as catalysis, sensing, energy storage, electronics, nanomedicine, and photonics [86].

Following sections of this chapter provide a few examples of applications of hybrid materials in the fields of energy and environment and biomedical sciences with a particular focus on the hybrids based on biological systems.

3 Organic–Inorganic Materials in Energy and Environment Applications

3.1 Polysaccharide-Based Hybrids

While poly-ionic liquids (PILs) as a category of functional materials have distinct advantages like durability, mechanical properties, and processibility, for the production of nanohybrids, eyebrows are raised about their environmental friendliness. Polysaccharides, however, are an excellent option to their environmentally benign nature, low cost, natural abundance, and a number of other benefits such as toughness, and formability, low density, and flexibility [87]. Despite the fact that there are several polysaccharides accessible and are being used as nanohybrids in the field of energy and environment, this section picks up a few examples of polysaccharides-based hybrid materials with several inorganic components.

3.1.1 Carbon Nanotube/Reduced Graphene Oxide/Cellulose Nanofiber Hybrids

Highly efficient energy storage systems with high power and energy densities, lightweight, high flexibility, great durability, cheap cost, and environmental friendliness are in high demand [88]. Because of their high capacitances, supercapacitors are an excellent choice for these devices [89]. Despite these promising features, various obstacles, such as high raw material costs and/or difficult production techniques, continue to pose a bottleneck for their practical deployment. All of this demands a growing interest in developing thin, flexible, lightweight supercapacitors made of novel, cost-effective, and sustainable/renewable materials [90].

To solve this issue, a new form of all-solid-state supercapacitor based on carbon nanotube (CNT)/reduced graphene oxide (RGO)/cellulose nanofiber (CNF) hybrid aerogels was devised and manufactured without the use of electroactive additives, current collectors, or binders [91]. This leads to the development of multifunctional cellulose hybrid materials. Excellent aspect ratios, exceptional mechanical strength and flexibility, and outstanding hydrophilicity are all characteristics of CNFs generated from cellulose [92]. Aerogels made from them are also very porous, have a large surface area, and have good electrolyte/absorption characteristics. CNFs have similar features to graphene-based porous carbon materials, such as environmental compatibility, high specific surface area, efficient electrical conductivity, and ultralow density [93].

CNTs, on the other hand too, have gained plenty of attention for application as supercapacitor electrodes. This is owing to their characteristics of mechanical strength, electrical conductivity, and surface area [94]. In order to produce electrodes with good power density, high specific capacitance, energy density, and remarkable cyclic stability, CNT/RGO/CNF hybrid aerogels were fabricated (Fig. 2) in a

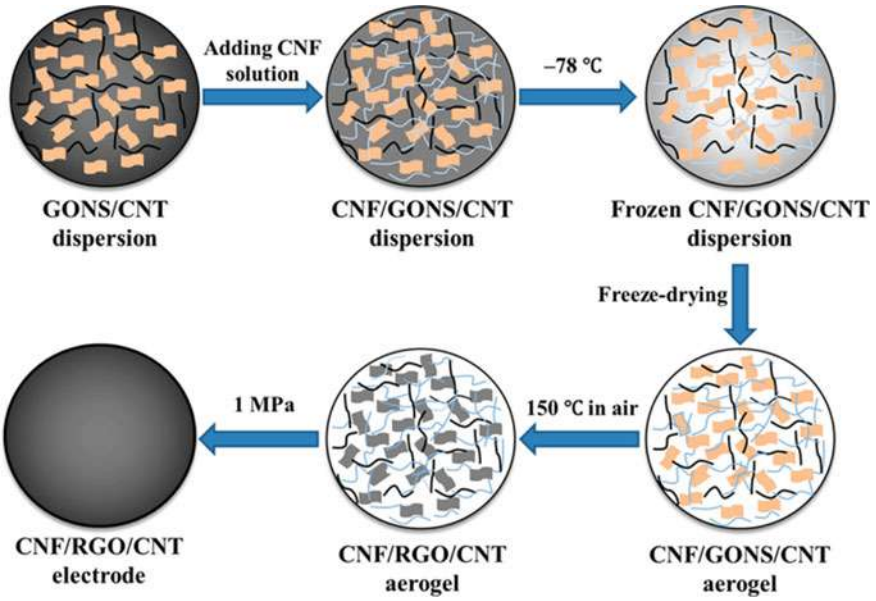

Fig. 2 Schematic representation of CNF/RGO/CNT electrode fabrication process [91] (Image permission from ACS)

simple and environmentally friendly manner with an aim of combining the superior characteristics of discrete components.

For the following reasons, the CNT/RGO/CNF hybrid combination demonstrated higher electrochemical performance: (i) highly hydrophilic CNFs allowing intimate contact between polymer-gel electrolyte and the electrodes, coupled with the generation of highly porous 3D network obtained via freeze-drying, enhance diffusion pathways for the electrolyte; (ii) production of additional conduction pathways between the layers of graphene nanosheets by the introduction of CNTs; and (iii) presence of CNFs and CNTs prevent the aggregation of graphene. These types of less expensive and environmentally benign materials could be used in the construction of rechargeable energy storage systems with low cost, greater flexibility, and lesser weight.

3.1.2 Carbon Nanotube/Lithium Titanate/Cellulose Nanofiber Hybrids

Commercially available electronic materials are typically made of nonrenewable, nonbiodegradable, and occasionally possibly hazardous materials (e.g., gallium arsenide). When discarded, these material build up a trash which is not environmentally beneficial [95]. Demand for ecologically friendly, lightweight, thin, flexible, up-scalable, and portable energy storage devices is increasing at a rapid rate. Lithium-ion batteries (LIBs), being the most auspicious future-generation source of

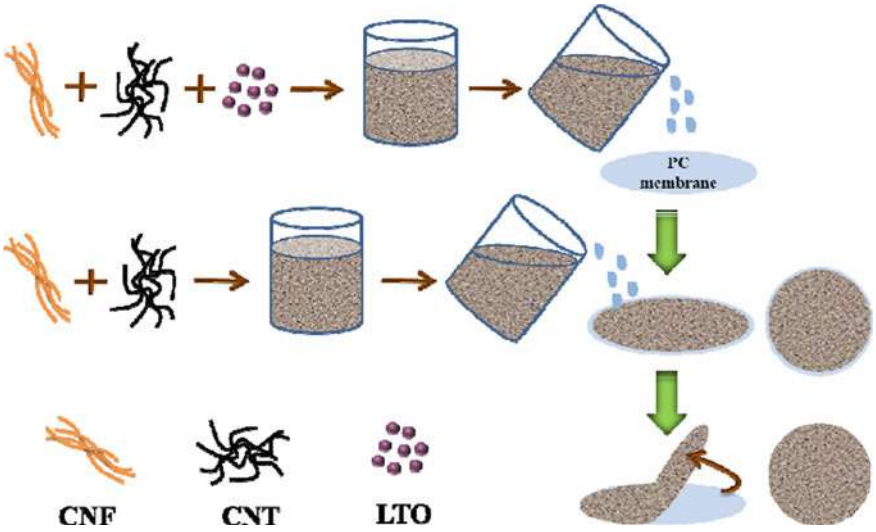

Fig. 3 Schematic representation of rapid assembling, free-standing but flexible hybrid film consisting of CNT/LTO/CNF [97] (Image permission from ACS)

energy and power storage technology, are employed in several types of electronic devices [96]. However, for the fabrication of flexible LIBs, the use of toxic organic solvents, metal current collectors (e.g., Ni, Al, and Cu), and synthetic polymer binders based on fluorine (e.g., fluorinated glycidyl azide) must be taken into account.

A free-standing flexible hybrid network film consisting of lithium titanate/carbon nanotube/ cellulose nanofiber (CNT/LTO/CNF) was created through extrusion process in aqueous media with controlled pressure (Fig. 3) [97]. It replaced synthetic polymers and traditional harmful solvents with CNF generated from biomass, which is renewable, compatible, and biodegradable, and it presents itself as an ideal contender to be used as dispersant [98], separator [99], and binder [100] for flexible electronics assembling.

These flexible type of electrode materials (single-/dual-layer) are very promising for flexible electronics that are high-performance, low-cost, and ecologically benign.

3.1.3 Phosphorylated Graphene Oxide/Chitosan Hybrids

Polymer exchange membrane fuel cells (PEMFCs) are among the most propitious renewable energy technologies. One of the key components of a PEMFC is ionomers-based proton exchange membrane (PEM) which determines system performance such as electricity cost, durability, and power density [101]. Nafion has excellent characteristics as an ionomer because of its microstructure which provides an efficient proton conductivity, and exceptional electrochemical and chemical stabilities, and hence is among the most investigated ionomers [102].

Apart from these benefits, Nafion has a number of disadvantages, including reduced dissociation ability at temperatures below 100 °C, high cost, poor mechanical strength, and low conductivities. This makes those PEMs more relevant which exhibit better thermal stability and higher proton conductivity at high temperature in non-aqueous medium [103].

Phosphoric acid groups which serve as proton carriers exhibit higher binding energy with water (47.3 $kJmol^{-1}$) and lower proton transfer energy (37.2 $kJmol^{-1}$) which make them promising non-aqueous polyelectrolytes conducting proton. This is due to re-establishment of hydrogen bond formation and breakage as well as structure diffusion of protonic defects between phosphoric species. Phosphoric acid groups are added to polymeric membrane structure in three different ways: (i) associating them to inorganic nanofillers, (ii) doping them into the membrane in liquid state, and (ii) binding them to polymer backbone [104].

Efficient conductivity of proton requires high phosphonation degree; however, excessive swelling might result in a rapid deterioration in structural stability. Phosphoric acid is immobilized over inorganic nanofillers to obtain high conductivity is an effective technique to prevent unwanted swelling and leaching, resulting in mechanically stable membranes of nanohybrids [105].

Chitosan, which is obtained by deacetylation of chitin, has both hydroxyl groups and reactive amino groups may serve as chemically resistant and exceptional film forming material which is also considered as eco-friendly. With a good proton transport ability, chitosan may act as a low-fuel crossover and a low-cost candidate for Nafion. Chitosan itself has discrete ion nanochannel and hence shows poor proton conductivity; however, when coupled with nanofillers functionalized with acid and formed into a matrix of membrane, it acts like a bridge and improves proton transfer ability significantly [106]. Resulting membranes also show good mechanical stability. 2D sheets of GO, having a thickness of a single atom, high conductivity of proton, and electronic insulation; may be used a nanofillers in PEMs with further introduction of other functional groups [107]. Nanosheets of phosphorylated graphene oxide are coupled with chitosan matrix to construct membranes of nanohybrid to satisfy the above mentioned requirements [108]. Phosphoric acid-functionalized GO membrane was synthesized through distillation–precipitation polymerization and then implanted onto the chitosan matrix (Fig. 4) [109].

Under anhydrous conditions, these membranes of nanohybrid material with efficient proton conductivity can produce greater H_2/O_2 fuel cell efficiencies than those of chitosan controlled and GO-filled ones [108].

3.1.4 Polyaniline/Tin Oxide/Chitosan Ternary Hybrid

Electrochemical capacitors' markets and uses are expanding, owing to their ability to bridge the gap between traditional capacitors having small charge–discharge time periods and the ones with higher discharge duration. Such capacitors use conducting polymers as spacers and metal oxides as pseudo-capacitive materials. However,

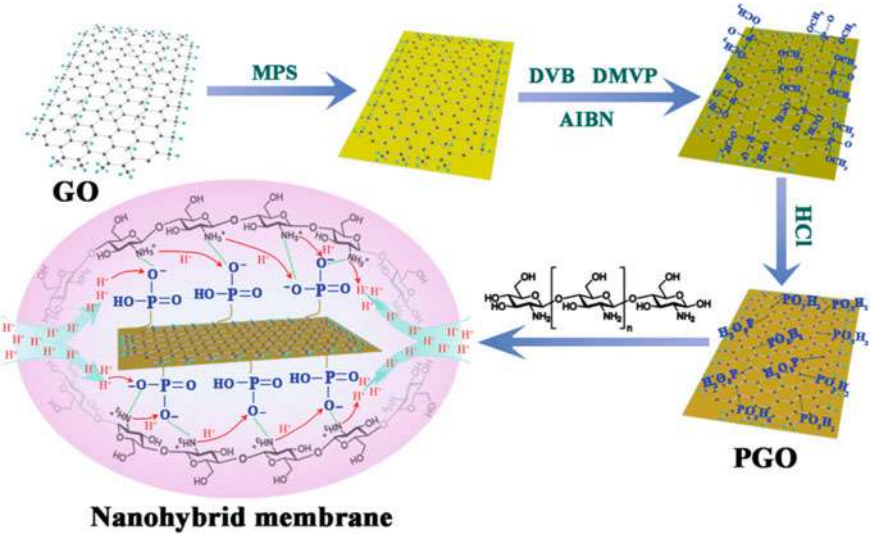

Fig. 4 Scheme representation of PGO and CS-PGO interface domain for proton transfer [108] (Image permission from Elsevier)

their poor cycle stability and high electrical resistance limit their use in supercapacitors [109]. A number of conducting polymers including polyaniline, polythiophene and polypyrole have recently got a lot of attention; particularly polyaniline because of its better controlled optical and electrical properties, longer environmental stability, lower cost than comparative conducting polymers, ease of preparation, redox behavior, and lower operating temperature [110]. Their areas of application include anticorrosion coatings, microelectronic devices, pseudo-capacitors, and organic lightweight batteries [111]. Producing hybrid composites of conducting polymers and polysaccharides is really intriguing. Because of the good qualities of individual components and amazing synergistic effect concurrently, chitosan, as the second most abundant biopolymer on earth, can be used to build hybrid composites with inorganic materials [112]. Tin oxide (SnO_2), an n-type semiconductor having high capacitance and high bandgap ($E_g = 3.6$ eV), is a low-cost promising material for antireflective coatings in solar cells, gas sensing, and energy storage [113]. As a result, a chitosan/SnO_2/polyaniline hybrid was synthesized via chemical precipitation and in situ polymerization [114]. This ternary hybrid serves as a promising option for supercapacitor applications as an electrode material.

3.2 Protein-Based Hybrids

Along with a better knowledge of physical phenomena, there has been a significant push to use (fibrillar) biopolymers extracted from renewable sources instead

of polymers derived from fossil sources in such devices [115]. The scientific world has turned to orthodox and familiar materials that have been exploited for hundreds of years in the quest for fossil-free polymers. Four biopolymers particularly are highlighted in this regard: (i) the most abundant biopolymer present in green plants and algae; cellulose, (ii) the second most abundant fibrillar biopolymer found in diatoms, insects, fungi, and crustaceans; chitin, (iii) the most abundant protein in the animal kingdom found in most vertebrates, cartilage, bones, tendons, corneas, and skin; collagen, and (iv) a traditional commodity protein used in medical sutures and textiles; silk [115].

The knowledge of chemical synthesis when combined with understanding of self-organization mechanisms and molecular recognition from biologically derived systems to build and maneuver novel hybrids consisting of supramolecular functional systems can prove handy to replace their current counterpart materials and technologies [116]. Applications of organic–inorganic nanohybrids in the fields of energy conversion, energy storage, and environmental remediation have been discussed with few examples in this section.

3.2.1 Silk/Nanoparticle Hybrid

Silk has long been utilized as a textile, a biomaterial [117] and an engineering material [118] due to its compatibilities with biological systems as well as easier degradation. In the recent years, increased knowledge of relationship between composition and properties of different varieties of silk has helped to give this polymer a new lease on life, both as a stand-alone material [119] and as a part of excellent-performing hybrid materials and composites [120]. Silk has been utilized to make lithium-ion batteries by acting as a template for the production of Fe_3O_4 hollow spheres, which are then pyrolyzed to produce a continuous coating of carbon on the particles. Over 180 cycles, particles derived from silk and coated with carbon demonstrated a very high capacity of 900 mA h g^{-1} [121]. The solvothermal synthesis of Fe_2O_3 from a solution comprising silk fibroin and iron (III) chloride was used to make the anode. The Fe_3O_4–carbon hollow spheres were created by calcining the Fe_2O_3–silk hollow spheres in Ar at 600 °C. Electronic conductivity values >1 S cm^{-1} and ionic conductivities >10^{-2} S cm^{-1} are required in a number of electrochemical applications [122]. Gold NWs ≈1 kS cm^{-1} [123], iridium films ≈10 kS cm^{-1} [124], multiwall CNTs ≈10–4 S cm^{-1} [125], ascorbic acid-reduced graphene oxide (Asc-RGO) ≈0.6 S cm^{-1} [126] and hydrazine-reduced graphene oxide (N-RGO) ≈36 S cm^{-1} [127] are the conductivities produced from the combination of different hybrid nanomaterials. The capacity to construct well-distributed systems is a critical stage in the preparation of effective heaters. Silk is a great protein polymer for this activity because of its high concentration of cysteine groups. Wan et al. produced a silk-gold nanoparticle hybrid with various gold NP concentrations and placed it on an Al/Si Schottky diode, measuring the photo-thermoelectric effect (Fig. 5) [128].

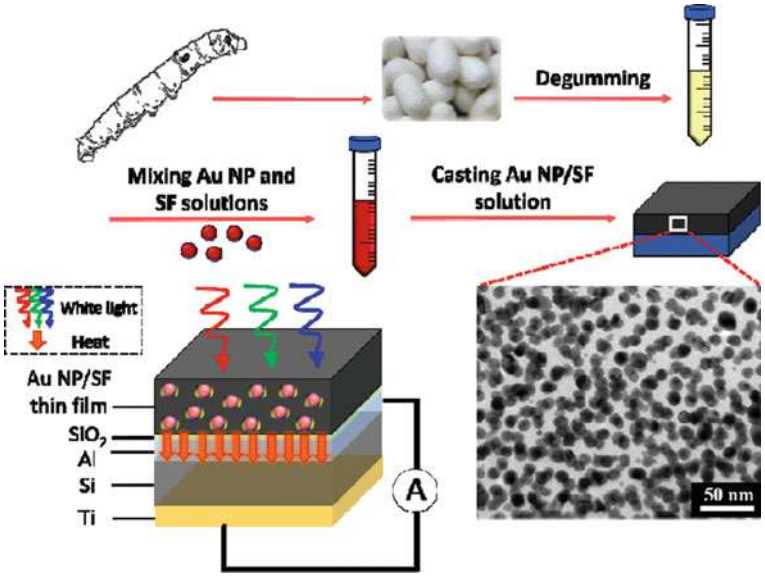

Fig. 5 Schematic of silk-gold nanoparticle fabrication and irradiation of white light of hybrid on a Al/Si Schottky diode [128] (Image permission from ACS)

3.2.2 Collagen/Nanoparticle Hybrids

In the animal kingdom, the protein which is present in the most abundant form is collagen, which consists of three polypeptide chains, and it can be extracted from cartilage, bones, tendons, corneas, and skin of mammals [129]. It can also be obtained as a by-product of tanning industry. The mechanical qualities of collagen (tendon collagen have a toughness of 7.5 MJm^{-3} stiffness of 1.5 GPa, extensibility of 12%, and strength of 0.15 GPa [130] combined with the abundant supply of raw material lead to a highly valuable component that can be used in a variety of applications. A few examples of collagen-based inorganic material (hybrids) in the field of energy and environment are discussed below.

Collagen's mechanical qualities, as previously stated, make it an appealing component for the manufacture of elastic devices. Park et al. showed the manufacture of a flexible cable battery with zinc–air electrodes that meets the mechanical criteria imposed by the desired bendability [131].

The battery system consisted of a collagen-based gel like polymer electrolyte, an anode of zinc and an air electrode with iron carbide as metal catalysts (Fig. 6).

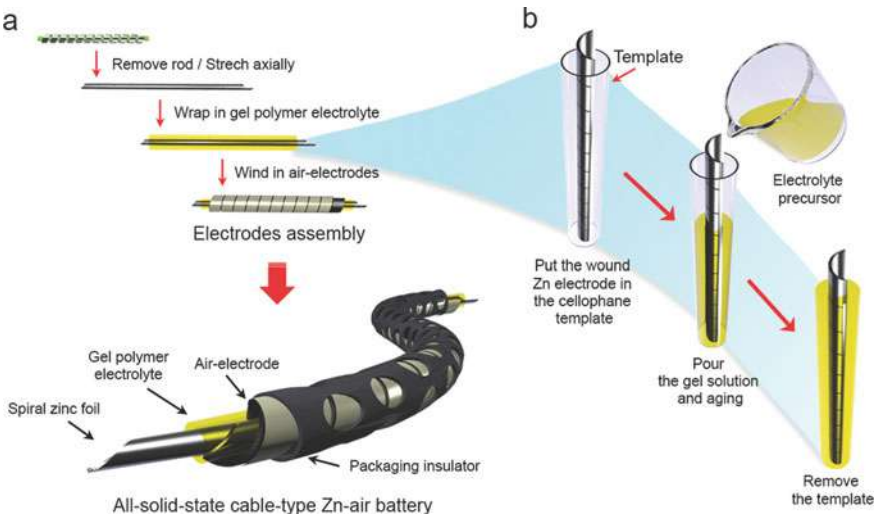

Fig. 6 Schematic representation of assembly of the zinc/gel/air battery (**a**), and preparation of the gel electrolyte (**b**) [131] (Image with permission from John Wiley & Sons)

4 Coordination Polymers for Medical Applications

4.1 Crystalline Versus Amorphous

Due to the potential multifunctional characteristics, hybrid nanoparticles have emerged in wide range of applications including, i.e., catalysis [132], electronic devices [133], electrical memory devices [134], gas separation and cleaning [135], sensors, [136] etc. The field of medicine, however, is relatively new avenue where hybrid nanomaterials are anticipated to have a wide influence. Potential applications in the field of medicines extend from a finely administered discharge of therapeutic agents to imaging applications [137]. Because of the difference in size of these particles from proteins, tissues and cells [138] and the requirement of increased retention effect (EPR) and permeability as a way of quietly approaching the affected tissues [139], the design of these particles is crucial. In addition, biocompatibility and stability are the other required for nanohybrids to be used in biological systems. Hybrid therapeutic agents can also offer incentives like higher active ingredient bearing, reduced toxicity, increased accumulation of drug, fine tuning of drug release, real-time monitoring of treatment response, etc. [140].

Inorganic (metal)–organic (polymer) are the most predominant candidate being used as nanohybrid materials in medicines which can further be classified as nanoscale coordination polymers (NCPs, amorphous form) and nanoscale metal–organic frameworks (NMOFs, crystalline form). NCPs exist both as porous and nonporous materials, whereas NMOFs usually refer to porous matter. Like other hybrid materials, NCPs/NMOFs also result in synergetic effect of combining pure

organic and inorganic moieties which assists researchers for its diverse therapeutic applications as compared to classical nanomaterials in medicinal applications. Their potentials advantages include;

(a) Fine tuning of surface functionalization for specific application
(b) Effective modification of chemical properties based on the metal–ligand combination
(c) Control of biodegradability
(d) Higher tunability of structure, composition, and porosity for better encapsulation of the target.

NMOFs represent the most researched hybrid materials for biomedical application. They are distinct type of organic–inorganic composites made up from the self-assembling of inorganic building blocks and precisely tuned organic linkers resulting in everlasting porous structures, high surface area and hence higher drug loading ability. These kinds of structures also present an effective control over drug dispensing which is one of their unique characteristics. Moreover, their crystallinity allows better investigation of drug capture-drug dispensing response [141]. NCPs, on the other hand, have come to light recently with their first study published in 2005 [142] following a rapid increase in investigations indicating prompt interest of research fraternity engaged in the field of biomedicines.

Currently, both NMOFs and NCPs, owing to their exceptional characteristics, are being used in biomedical field including therapeutics, diagnosis, drug capturing, delivery and dispensing, biomedical imaging, optical imaging, etc. Few applications of both types of hybrids have been discussed in the following pages.

4.1.1 Drug Delivery

The understanding and utilization of NCPs/NMOFs have produced new opportunities for the chemotherapeutic cure of cancer. Encapsulation of anticancer medicine by nanoparticle permits customized architectures which ensure controlled release of the medicine. Platinum-based chemotherapeutics examples are mostly reported because of its predominance in the cure of cancer. A recent rise in research aiming to modify platinum-based agents to produce systems through mechanisms different from conventional platinum-based systems to addresses the issue of their slow entrance. Various strategies and the use of nanodelivery instruments have been introduced for the incorporation of platinum active molecules into nanomedicines [143].

A group of researchers at University of North Caroline, headed by Wenbin Lin, produced a series of work in 2009 [144], 2013 [145], and in 2014 [146] incorporating Pt(IV) in MOFs structures and in NCPs. Pt(IV) is anticipated to attack cancer cells selectively and be reduced to Pt(II) because of the ability of cancer cells to create a reducing environment. The ensuing systems are generally coated with silica shell or bilayer of lipid and thereafter functionalized with active targeting molecules and/or PEG. Nano-system produced in this way exhibits exceptional circulation of blood,

slow drug release, excessive drug loadings and greater efficacy and effectiveness at a very low dose of drug as compared to free drugs. These systems can also bear various drugs to be used for multiple therapies [147], enabling the simultaneous delivery of more than one active specie having distinct mechanisms of action.

4.1.2 Doxorubicin

Coordination of Zn(II) with 1, 4-bis (imidazole-1-ylmethyl) benzene NCPs with the encapsulation of doxorubicin and other cancer inhibiting agents was first reported by Ruiz-Molina et al. [148]. Doxorubicin is a chemical entity used for broad spectrum cancer treatment. As compared to free drugs, these hybrid nanoparticles present a remarkable in vitro anticancer activity and greater cytotoxicity against the cancer cells.

Other examples of such systems where an anticancer drug was encapsulated in NCPs/NMOFs/MOFs are methotrexate in NMOFs [149], methotrexate in NCPs [150], camptothecin in MOFs [151], camptothecin in NCPs [152], 5-fluorouracil in MOFs [153], and 5-fluorouracil in NMOFs [154].

4.2 Photodynamic Therapy (PDT) and Photothermal (PTT) Therapy

Photodynamic and photothermal therapies (commonly known as PDT and PTT) are productive anticancer treatments which include the administration of cancer cells localizing photosensitizer (PS) subsequently activated by light for heat generation in case of PDT or exceedingly cytotoxic reactive oxygen species (ROS) for the case of PTT, which rapidly starts killing cancer cells selectively. These therapies are preferred alternatives to radiotherapy as well as to surgery which are considered relatively more dangerous and toxic.

Lin et al. surfaced the first application of metal–porphyrin NMOFs as highly effective nanohybrid material for cancer control by PDT [155]. In vitro and in vivo anticancer nanostructure is obtained by simultaneous implementation of PDT and chemotherapy. Similarly, PTT uses heat produced from near infrared irradiated photothermal agents to fight cancer cells, and Liu et al. first reported the development of metal–organic polymer at nanoscale for PTT of tumor [156]. Both PDT and PTT have great potential as cancer treatment therapy in future; however, they are still at very early stage as therapeutic procedure.

4.3 Biomedical Imaging

Superparamagnetic oxide of iron nanoparticles, quantum dots, and noble metals have been used as nanoparticles as contrast agents for medical imaging [157]. Tunability and versatility in many biomedical imaging procedures, particularly in optical imaging (OI) and magnetic resonance imaging (MRI), are the key advantages that can be obtained for metal–organic polymeric nanostructures.

OI has been used very effectively in recent times to distinguish the infected and healthy cells without damaging the cells themselves. This is due to their ability of different dye accumulations. In the diagnosis of cancer, different studies prove to be efficient for OI where NCPs/NMOFs carrying luminescent lanthanides [158], fluorescent dyes [157], and phosphorescent species [160] have been used. NMOFs also exhibit a shift in emissive properties, and this property has been utilized as aqueous phase detection of different species using NMOFs as biosensor [161].

In vivo OI use in humans is limited; however when combined with other techniques like MRI or positron emission tomography (PET), it can be used in fluorescent-guided surgery procedures [162]. Similarly, hybrid nanoparticles having more than one contrast agents allow combining multiple imaging modalities and improve resolution of each of these techniques. A number of studies have utilized metal–organic polymeric nanomaterials for OI and MRI; however, the pioneering work was performed by Lin et al. with NMOFs containing Zr/Hf [160] or iodinated aromatic molecules [163]. The structural and compositional diversity of NCPs/NMOFs permit contrast agents and therapeutic drugs the provision of real-time monitoring of drug delivery and treatment response of cancer cells. More work is required to establish the in vivo behavior of NCPs/NMOFs for preclinical guidelines on their safety and efficacy.

Concluding this section, NCPs/NMOFs are being used for biomedical applications, and they further have great potential as they present a number of advantages over existing systems as have been discussed above.

5 Concluding Remarks

Parallel to inorganic material research, the production and isolation of organic species with accurately monitored surface qualities and dimensions has triggered the expansion of fascinating new materials with wide range of applications. Because some of these components have a biological basis, numerous composite materials and hybrids are being designed along the lines of natural composites, i.e., bioinspiration and biomimicry. The utilization of biologically derived components at nanoscale poses a number of problems, as the characteristics of the components might vary significantly between individual species. It is still necessary to develop techniques enabling others to control the size and qualities, to isolate, and to extract the biological component. T. Saito and A. Isogai of Tokyo University proposed the TEMPO-mediated oxidation approach as one such mechanism. An approach that has allowed precise control

of cellulosic component for surface characteristics and, in some circumstances, for dimension stability. To exploit sustainable materials with definitive characteristics in the fabrication of composites and hybrid materials will undoubtedly have a significant impact on scientific progress, but it may also leave a significant social impact in countries which are still at developing stage, as the processes that enable access to these plentiful components are expected to be available at lesser price and their availability may become wider to become cheaper and more widely available. After all, the materials and their ancestors covered in this chapter are ancient elements just waiting to be retrieved.

References

1. Unterlass MM (2016) Green synthesis of inorganic-organic hybrid materials: state of the art and future perspectives. Eur J Inorg Chem 2016(8):1135–1156
2. Nikolaev A (2004) Die Etymologie von altgriechischem hybris. Glotta: zeitschrift für griechische und lateinische sprache 80(1):211–230
3. Alemán J et al (2007) Definitions of terms relating to the structure and processing of sols, gels, networks, and inorganic-organic hybrid materials (IUPAC Recommendations 2007). Pure Appl Chem 79(10):1801–1829
4. de Clippel F et al (2013) Tailoring nanohybrids and nanocomposites for catalytic applications. Green Chem 15(6):1398–1430
5. Shakeel A et al (2022) Advanced polymeric/inorganic nanohybrids: an integrated platform for gas sensing applications. Chemosphere, 133772
6. Judeinstein P, Sanchez C (1996) Hybrid organic–inorganic materials: a land of multidisciplinarity. J Mater Chem 6(4):511–525
7. Gao F (2004) Clay/polymer composites: the story. Mater Today 7(11):50–55
8. Letcher TM, Scott JL (2012) Materials for a sustainable future. Royal Society of Chemistry
9. Faivre D, Godec TU (2015) From bacteria to mollusks: the principles underlying the biomineralization of iron oxide materials. Angew Chem Int Ed 54(16):4728–4747
10. Rocke AJ (2010) Bibliography. Image and reality: Kekulé, Kopp, and the scientific imagination. University of Chicago Press, pp 341–368
11. Hendricks SB (1941) Base exchange of the clay mineral montmorillonite for organic cations and its dependence upon adsorption due to van der Waals forces. J Phys Chem 45(1):65–81
12. Gieseking J (1939) The mechanism of cation exchange in the montmorillonite-beidellite-nontronite type of clay minerals. Soil Sci 47(1):1–14
13. Bradley WF (1945) Molecular associations between montmorillonite and some polyfunctional organic liquids. J Am Chem Soc 67(6):975–981
14. MacEwan D (1948) Complexes of clays with organic compounds. I. Complex formation between montmorillonite and halloysite and certain organic liquids. Trans Faraday Soc 44:349–367
15. Lagaly G, Beneke K (1991) Intercalation and exchange reactions of clay minerals and non-clay layer compounds. Colloid Polym Sci 269(12):1198–1211
16. Ruiz-Hitzky E, Aranda P, Serratosa JM (2004) Clay-organic interactions: organoclay complexes and polymer-clay. Handbook of layered materials, p 91
17. He H et al (2014) Synthesis of organoclays: a critical review and some unresolved issues. Appl Clay Sci 100:22–28
18. Blumstein A (1961) Polymerization in adsorbed layers. Bull Soc Chim Fr 5:899–914
19. Theng BKG (2012) Formation and properties of clay-polymer complexes. Elsevier
20. Fukushima Y et al (1988) Swelling behaviour of montmorillonite by poly-6-amide. Clay Miner 23(1):27–34

21. Kharisov BI, Kharissova OV, Ortiz-Mendez U (2016) CRC concise encyclopedia of nanotechnology. CRC Press
22. Brown G, Greene-Kelly R, Norrish K (1952) Organic derivatives of montmorillonite. Clay Miner Bull 1(7):214–220
23. Fripiat JJ, Mendelov E, Organic derivatives of silicates. I. Chrysotile methyl derivative. Bulletin De La Societe Chimique De France 1968(2):483–492
24. Zapata L et al (1972) Organosilicon derivatives. 2. Vinyl and allyl derivatives of chrysotile and vermiculite. Bulletin de la Société Chimique de Paris, 54
25. Ruiz-Hitzky E et al (2016) Clay-graphene nanoplatelets functional conducting composites. Adv Funct Mater 26(41):7394–7405
26. Ruiz-Hitzky E et al (2011) Hybrid and biohybrid silicate based materials: molecular vs. block-assembling bottom–up processes. Chem Soc Rev 40(2):801–828
27. Doner H, Mortland M (1969) Benzene complexes with copper (II) montmorillonite. Science 166(3911):1406–1407
28. Wicklein B et al (2012) Lipid-based bio-nanohybrids for functional stabilisation of influenza vaccines. Eur J Inorg Chem 2012(32):5186–5191
29. Barrer RM, Denny PJ (2001) Hydrothermal chemistry of the silicates. Part IX. Nitrogenous aluminosilicates. J Chem Soc (Resumed) 1961:971–982
30. Kerr GT (1963) Zeolite ZK-5: a new molecular sieve. Science 140(3574):1412
31. Lawton SL, Rohrbaugh WJ (1990) The framework topology of ZSM-18, a novel zeolite containing rings of three (Si, Al)-O species. Science 247(4948):1319–1322
32. Flanigen EM et al (1978) Silicalite, a new hydrophobic crystalline silica molecular sieve. Nature 271(5645):512–516
33. Flanigen EM, Patton RL, Wilson ST (1988) Structural, synthetic and physicochemical concepts in aluminophosphate-based molecular sieves. In: Grobet PJ, et al (eds) Studies in surface science and catalysis. Elsevier, pp 13–27
34. Corma A et al (1994) Acidity and stability of MCM-41 crystalline aluminosilicates. J Catal 148(2):569–574
35. Dimitriev Y, Ivanova Y, Iordanova R (2008) History of sol-gel science and technology. J Univ Chem Technol Metall 43(2):181–192
36. Aqueous and nonaqueous sol-gel chemistry, in metal oxide nanoparticles in organic solvents: synthesis, formation, assembly and application. Springer London, London, pp 7–18 (2009)
37. Roy R (1987) Ceramics by the solution-sol-gel route. Science 238(4834):1664–1669
38. Dislich H (1971) New routes to multicomponent oxide glasses. Angew Chem, Int Ed Engl 10(6):363–370
39. Kaiser A, Schmidt H, Bottner H (1985) Preparation of membranes based on heteropolysiloxanes. J Membr Sci 22(2–3):257–268
40. Mackenzie J, Ulrich D (1990) Sol-gel optics, present status and future trends. In: 34th annual international technical symposium on optical and optoelectronic applied science and engineering, vol 1328. SPIE
41. Andrianov K, Zhdanov A, Levin VY (1978) Some physical properties of organosilicon ladder polymers. Annu Rev Mater Sci 8(1):313–326
42. Livage J, Henry M, Sanchez C (1988) Sol-gel chemistry of transition metal oxides. Prog Solid State Chem 18(4):259–341
43. Brinker CJ, Scherer GW (2013) Sol-gel science: the physics and chemistry of sol-gel processing. Elsevier Inc., Academic Press, Boston, US
44. Hench LL, Ulrich DR (1986) Science of ceramic chemical processing. Wiley-Interscience, Weinheim
45. Sakka S, Kamiya K (1982) The sol-gel transition in the hydrolysis of metal alkoxides in relation to the formation of glass fibers and films. J Non-Cryst Solids 48(1):31–46
46. Yang C-C, Josefowicz JY, Alexandru L (1980) Deposition of ultrathin films by a withdrawal method. Thin Solid Films 74(1):117–127
47. Sanchez C, Ribot F, Lebeau B (1999) Molecular design of hybrid organic-inorganic nanocomposites synthesized via sol-gel chemistry. J Mater Chem 9(1):35–44

48. Tan JC, Cheetham AK (2011) Mechanical properties of hybrid inorganic–organic framework materials: establishing fundamental structure–property relationships. Chem Soc Rev 40(2):1059–1080
49. Novak BM, Davies C (1991) " Inverse" organic-inorganic composite materials. 2. Free-radical routes into nonshrinking sol-gel composites. Macromolecules 24(19):5481–5483
50. Matyjaszewski K et al (1999) Polymers at interfaces: using atom transfer radical polymerization in the controlled growth of homopolymers and block copolymers from silicon surfaces in the absence of untethered sacrificial initiator. Macromolecules 32(26):8716–8724
51. Braun S et al (1990) Biochemically active sol-gel glasses: the trapping of enzymes. Mater Lett 10(1–2):1–5
52. Audebert P, Demaille C, Sanchez C (1993) Electrochemical probing of the activity of glucose oxidase embedded sol-gel matrixes. Chem Mater 5(7):911–913
53. Barreau J-Y et al (1994) Fixation and immunological reactivity of parasitic protozoa in sol-gel matrices. Comptes Rendus de L'academie des sciences. Serie III, Sciences de la vie 317(7):653–657
54. Nassif N et al (2004) Bacteria quorum sensing in silica matrices. J Mater Chem 14(14):2264–2268
55. Vallet-Regí M, Colilla M, González B (2011) Medical applications of organic–inorganic hybrid materials within the field of silica-based bioceramics. Chem Soc Rev 40(2):596–607
56. Galarneau A, Barodawalla A, Pinnavaia TJ (1995) Porous clay heterostructures formed by gallery-templated synthesis. Nature 374(6522):529–531
57. Yanagisawa T et al (1990) Trimethylsilyl derivatives of alkyltrimethylammonium–kanemite complexes and their conversion to microporous SiO_2 materials. Bull Chem Soc Jpn 63(5):1535–1537
58. Tanev PT, Chibwe M, Pinnavaia TJ (1994) Titanium-containing mesoporous molecular sieves for catalytic oxidation of aromatic compounds. Nature 368(6469):321–323
59. Huo Q et al (1994) Generalized synthesis of periodic surfactant/inorganic composite materials. Nature 368(6469):317–321
60. Tanev PT, Pinnavaia TJ (1995) A neutral templating route to mesoporous molecular sieves. Science 267(5199):865–867
61. Goltner CG, Antonietti M (1997) Mesoporous materials by templating of liquid crystalline phases. Wiley Online Library
62. Zhao D et al (1998) Triblock copolymer syntheses of mesoporous silica with periodic 50 to 300 angstrom pores. Science 279(5350):548–552
63. Yang P et al (1998) Generalized syntheses of large-pore mesoporous metal oxides with semicrystalline frameworks. Nature 396(6707):152–155
64. Ryoo R, Joo SH, Jun S (1999) Synthesis of highly ordered carbon molecular sieves via template-mediated structural transformation. J Phys Chem B 103(37):7743–7746
65. Knox JH, Kaur B, Millward GR (1986) Structure and performance of porous graphitic carbon in liquid chromatography. J Chromatogr A 352:3–25
66. Page MG et al (2008) Mesoporous calcite by polymer templating. Cryst Growth Des 8(6):1792–1794
67. Mann S et al (1997) Sol−gel synthesis of organized matter. Chem Mater 9(11):2300–2310
68. Faustini M et al (2014) From chemical solutions to inorganic nanostructured materials: a journey into evaporation-driven processes. Chem Mater 26(1):709–723
69. Lu Y et al (1997) Continuous formation of supported cubic and hexagonal mesoporous films by sol–gel dip-coating. Nature 389(6649):364–368
70. Bruinsma PJ et al (1997) Mesoporous silica synthesized by solvent evaporation: spun fibers and spray-dried hollow spheres. Chem Mater 9(11):2507–2512
71. Huo Q et al (1997) Room temperature growth of mesoporous silica fibers: a new high-surface-area optical waveguide. Adv Mater 9(12):974–978
72. Fan H et al (2000) Rapid prototyping of patterned functional nanostructures. Nature 405(6782):56–60

73. Antonietti M et al (1998) Synthesis of mesoporous silica with large pores and bimodal pore size distribution by templating of polymer latices. Adv Mater 10(2):154–159
74. Xia Y, Whitesides GM (1998) Soft lithography. Annu Rev Mater Sci 28(1):153–184
75. Su B-L, Sanchez C, Yang X-Y (2012) Hierarchically structured porous materials: from nanoscience to catalysis, separation, optics, energy, and life science. Wiley
76. Faustini M et al (2010) Bottom-up approach toward titanosilicate mesoporous pillared planar nanochannels for nanofluidic applications. Chem Mater 22(20):5687–5694
77. Schoedel A, Yaghi OM (2016) Porosity in metal–organic compounds. Wiley, Chichester, UK
78. Abd-El-Aziz AS, Manners I (2007) Frontiers in transition metal-containing polymers. Wiley
79. Hoskins BF, Robson R (1989) Infinite polymeric frameworks consisting of three dimensionally linked rod-like segments. J Am Chem Soc 111(15):5962–5964
80. Kitagawa S, Kondo M (1998) Functional micropore chemistry of crystalline metal complex-assembled compounds. Bull Chem Soc Jpn 71(8):1739–1753
81. Yaghi O, Li H (1995) Hydrothermal synthesis of a metal-organic framework containing large rectangular channels. J Am Chem Soc 117(41):10401–10402
82. Eddaoudi M et al (2002) Systematic design of pore size and functionality in isoreticular MOFs and their application in methane storage. Science 295(5554):469–472
83. Min KS, Suh MP (2000) Silver (I)−polynitrile network solids for anion exchange: anion-induced transformation of supramolecular structure in the crystalline state. J Am Chem Soc 122(29):6834–6840
84. Chui SS-Y et al (1999) A chemically functionalizable nanoporous material [Cu3(TMA)2(H2O)3]n. Science 283(5405):1148–1150
85. Maurin G et al (2017) The new age of MOFs and of their porous-related solids. Chem Soc Rev 46(11):3104–3107
86. Clemente-León M et al (2011) Multifunctionality in hybrid magnetic materials based on bimetallic oxalate complexes. Chem Soc Rev 40(2):473–497
87. Baughman RH, Zakhidov AA, Heer Wad (2002) Carbon nanotubes—the route toward applications. Science 297(5582):787–792
88. Liu C, Li F, Ma L, Cheng H-M (2010) Advanced materials for energy storage. Adv Mater 22(8):E28–E62
89. Wang G, Zhang L, Zhang J (2012) A review of electrode materials for electrochemical supercapacitors. Chem Soc Rev 41(2):797–828
90. Liu L et al (2014) Nanostructured graphene composite papers for highly flexible and foldable supercapacitors. Adv Mater 26(28):4855–4862
91. Zheng Q et al (2015) Cellulose nanofibril/reduced graphene oxide/carbon nanotube hybrid aerogels for highly flexible and all-solid-state supercapacitors. ACS Appl Mater Interfaces 7(5):3263–3271
92. Moon RJ et al (2011) Cellulose nanomaterials review: structure, properties and nanocomposites. Chem Soc Rev 40(7):3941–3994
93. You B, Jiang J, Fan S (2014) Three-dimensional hierarchically porous all-carbon foams for supercapacitor. ACS Appl Mater Interfaces 6(17):15302–15308
94. Futaba DN et al (2006) Shape-engineerable and highly densely packed single-walled carbon nanotubes and their application as super-capacitor electrodes. Nat Mater 5(12):987–994
95. Jung YH et al (2015) High-performance green flexible electronics based on biodegradable cellulose nanofibril paper. Nat Commun 6(1):1–11
96. Du L et al (2014) Flexible supercapacitors based on carbon nanotube/MnO_2 nanotube hybrid porous films for wearable electronic devices. J Mater Chem A 2(41):17561–17567
97. Cao S et al (2015) Integrated fast assembly of free-standing lithium titanate/carbon nanotube/cellulose nanofiber hybrid network film as flexible paper-electrode for lithium-ion batteries. ACS Appl Mater Interfaces 7(20):10695–10701
98. Li Y et al (2015) Nanocellulose as green dispersant for two-dimensional energy materials. Nano Energy 13:346–354
99. Leijonmarck S et al (2013) Single-paper flexible Li-ion battery cells through a paper-making process based on nano-fibrillated cellulose. J Mater Chem A 1(15):4671–4677

100. Kim G et al (2011) Use of natural binders and ionic liquid electrolytes for greener and safer lithium-ion batteries. J Power Sources 196(4):2187–2194
101. Zhang H, Shen PK (2012) Advances in the high performance polymer electrolyte membranes for fuel cells. Chem Soc Rev 41(6):2382–2394
102. Mauritz KA, Moore RB (2004) State of understanding of Nafion. Chem Rev 104(10):4535–4586
103. Kreuer K-D (2014) Ion conducting membranes for fuel cells and other electrochemical devices. Chem Mater 26(1):361–380
104. Jung G-B et al (2012) Membrane electrode assemblies doped with H_3PO_4 for high temperature proton exchange membrane fuel cells. Int J Hydrogen Energy 37(18):13645–13651
105. Zhao Y et al (2014) Enhanced proton conductivity of the hybrid membranes by regulating the proton conducting groups anchored on the mesoporous silica. J Power Sources 270:292–303
106. Li Y et al (2013) Recent advances in the fabrication of advanced composite membranes. J Mater Chem A 1(35):10058–10077
107. Karim MR et al (2013) Graphene oxide nanosheet with high proton conductivity. J Am Chem Soc 135(22):8097–8100
108. Bai H et al (2015) Anhydrous proton exchange membranes comprising of chitosan and phosphorylated graphene oxide for elevated temperature fuel cells. J Membr Sci 495:48–60
109. Chen F, Liu P, Zhao Q (2012) Well-defined graphene/polyaniline flake composites for high performance supercapacitors. Electrochim Acta 76:62–68
110. Wang J et al (2009) Removal of aqueous Hg(II) by polyaniline: sorption characteristics and mechanisms. Environ Sci Technol 43(14):5223–5228
111. Rakhi R, Chen W, Alshareef HN (2012) Conducting polymer/carbon nanocoil composite electrodes for efficient supercapacitors. J Mater Chem 22(11):5177–5183
112. Anandhavelu S, Thambidurai S (2013) Effect of annealing temperature on optical and electrochemical properties of chitosan–ZnO nanostructure. Ionics 19(6):903–909
113. Sun Z et al (2013) Electrical property and characterization of nano-SnO_2/wollastonite composite materials. Mater Res Bull 48(3):1013–1019
114. Karpuraranjith M, Thambidurai S (2016) Twist fibrous structure of CS–SnO_2–PANI ternary hybrid composite for electrochemical capacitance performance. RSC Adv 6(46):40567–40576
115. Gandini A (2011) The irruption of polymers from renewable resources on the scene of macromolecular science and technology. Green Chem 13(5):1061–1083
116. Yuan J, Antonietti M (2011) Poly(ionic liquid)s: polymers expanding classical property profiles. Polymer 52(7):1469–1482
117. Altman GH et al (2003) Silk-based biomaterials. Biomaterials 24(3):401–416
118. Pérez-Rigueiro J et al (1998) Silkworm silk as an engineering material. J Appl Polym Sci 70(12):2439–2447
119. Porter D, Guan J, Vollrath F (2013) Spider silk: super material or thin fibre? Adv Mater 25(9):1275–1279
120. Studart AR (2012) Towards high-performance bioinspired composites. Adv Mater 24(37):5024–5044
121. Sheng W et al (2015) Silk-regulated hierarchical hollow magnetite/carbon nanocomposite spheroids for lithium-ion battery anodes. Nanotechnology 26(11):115603
122. Tarascon JM, Armand M (2001) Issues and challenges facing rechargeable lithium batteries. Nature 414(6861):359–367
123. Dong B-J, Lu Q (2014) Conductive Au nanowires regulated by silk fibroin nanofibers. Front Mater Sci 8(1):102–105
124. Lin H et al (2014) Electron transport and bulk-like behavior of Wiedemann-Franz law for sub-7 nm-thin iridium films on silkworm silk. ACS Appl Mater Interfaces 6(14):11341–11347
125. Yoon SH et al (2007) Electrically conducting silk fibroin microspheres by incorporation of multiwalled carbon nanotubes on their surfaces. Materials science forum. Trans Tech Publ
126. Liang B et al (2014) Fabrication and application of flexible graphene silk composite film electrodes decorated with spiky Pt nanospheres. Nanoscale 6(8):4264–4274

127. Lu Z, Mao C, Zhang H (2015) Highly conductive graphene-coated silk fabricated via a repeated coating-reduction approach. J Mater Chem C 3(17):4265–4268
128. Tsao SH et al (2015) White-light-induced collective heating of gold nanocomposite/Bombyx mori silk thin films with ultrahigh broadband absorbance. ACS Nano 9(12):12045–12059
129. Fratzl P (2008) Collagen: structure and mechanics, an introduction. In: Fratzl P (ed) Collagen: structure and mechanics. Springer US, Boston, MA, pp 1–13
130. Omenetto FG, Kaplan DL (2010) New opportunities for an ancient material. Science 329(5991):528–531
131. Park J et al (2015) All-solid-state cable-type flexible Zinc-air battery. Adv Mater 27(8):1396–1401
132. Chughtai AH et al (2015) Metal–organic frameworks: versatile heterogeneous catalysts for efficient catalytic organic transformations. Chem Soc Rev 44(19):6804–6849
133. Zhang S et al (2005) Enhanced infrared photovoltaic efficiency in PbS nanocrystal/semiconducting polymer composites: 600-fold increase in maximum power output via control of the ligand barrier. Appl Phys Lett 87(23):233101
134. Portney NG, Martinez-Morales AA, Ozkan M (2008) Nanoscale memory characterization of virus-templated semiconducting quantum dots. ACS Nano 2(2):191–196
135. Chaemchuen S et al (2013) Metal–organic frameworks for upgrading biogas via CO_2 adsorption to biogas green energy. Chem Soc Rev 42(24):9304–9332
136. Liu X et al (2012) Facile synthesis of thermally stable poly(N-vinylpyrrolidone)-modified gold surfaces by surface-initiated atom transfer radical polymerization. Langmuir 28(25):9451–9459
137. Ma Z, Moulton B (2011) Recent advances of discrete coordination complexes and coordination polymers in drug delivery. Coord Chem Rev 255(15–16):1623–1641
138. Albanese A, Tang PS, Chan WC (2012) The effect of nanoparticle size, shape, and surface chemistry on biological systems. Annu Rev Biomed Eng 14:1–16
139. Ruiz-Hernandez E, Baeza A, Vallet-Regi M (2011) Smart drug delivery through DNA/magnetic nanoparticle gates. ACS Nano 5(2):1259–1266
140. Kim CS et al (2013) Triggered nanoparticles as therapeutics. Nano Today 8(4):439–447
141. Furukawa H et al (2013) The chemistry and applications of metal-organic frameworks. Science 341(6149):1230444
142. Oh M, Mirkin CA (2005) Chemically tailorable colloidal particles from infinite coordination polymers. Nature 438(7068):651–654
143. Johnstone TC, Suntharalingam K, Lippard SJ (2016) The next generation of platinum drugs: targeted Pt(II) agents, nanoparticle delivery, and Pt(IV) prodrugs. Chem Rev 116(5):3436–3486
144. Taylor-Pashow KM et al (2009) Postsynthetic modifications of iron-carboxylate nanoscale metal−organic frameworks for imaging and drug delivery. J Am Chem Soc 131(40):14261–14263
145. Huxford-Phillips RC et al (2013) Lipid-coated nanoscale coordination polymers for targeted cisplatin delivery. RSC Adv 3(34):14438–14443
146. Liu D et al (2014) Self-assembled nanoscale coordination polymers with trigger release properties for effective anticancer therapy. Nat Commun 5(1):1–11
147. Poon C et al (2015) Self-assembled nanoscale coordination polymers carrying oxaliplatin and gemcitabine for synergistic combination therapy of pancreatic cancer. J Control Release 201:90–99
148. Imaz I et al (2010) Coordination polymer particles as potential drug delivery systems. Chem Commun 46(26):4737–4739
149. Huxford RC et al (2012) Lipid-coated nanoscale coordination polymers for targeted delivery of antifolates to cancer cells. Chem Sci 3(1):198–204
150. Xing L, Cao Y, Che S (2012) Synthesis of core–shell coordination polymer nanoparticles (CPNs) for pH-responsive controlled drug release. Chem Commun 48(48):5995–5997
151. Zhuang J et al (2014) Optimized metal–organic-framework nanospheres for drug delivery: evaluation of small-molecule encapsulation. ACS Nano 8(3):2812–2819

152. Imaz I et al (2011) Metal–biomolecule frameworks (MBioFs). Chem Commun 47(26):7287–7302
153. Sun CY et al (2011) Chiral nanoporous metal-organic frameworks with high porosity as materials for drug delivery. Adv Mater 23(47):5629–5632
154. Lucena FRS et al (2013) Induction of cancer cell death by apoptosis and slow release of 5-fluoracil from metal-organic frameworks Cu-BTC. Biomed Pharmacother 67(8):707–713
155. Lu K, He C, Lin W (2014) Nanoscale metal–organic framework for highly effective photodynamic therapy of resistant head and neck cancer. J Am Chem Soc 136(48):16712–16715
156. Yang Y et al (2016) Nanoscale metal–organic particles with rapid clearance for magnetic resonance imaging-guided photothermal therapy. ACS Nano 10(2):2774–2781
157. Selvan ST et al (2010) Functional and multifunctional nanoparticles for bioimaging and biosensing. Langmuir 26(14):11631–11641
158. Deng K et al (2015) Aptamer-mediated up-conversion core/MOF shell nanocomposites for targeted drug delivery and cell imaging. Sci Rep 5(1):1–7
159. Novio F et al (2014) Carboxyl group ($-CO_2H$) functionalized coordination polymer nanoparticles as efficient platforms for drug delivery. Chem Eur J 20(47):15443–15450
160. Liu D, Huxford RC, Lin W (2011) Phosphorescent nanoscale coordination polymers as contrast agents for optical imaging. Angew Chem Int Ed 50(16):3696–3700
161. Kumar P, Deep A, Kim K-H (2015) Metal organic frameworks for sensing applications. TrAC, Trends Anal Chem 73:39–53
162. Van Dam G et al (2011) Intraoperative tumor-specific fluorescence imaging in ovarian cancer by folate receptor. Nat Med 17(10):1315–1319
163. DeKrafft KE et al (2009) Iodinated nanoscale coordination polymers as potential contrast agents for computed tomography. Angew Chem 121(52):10085–10088

Chapter 2
Structural Design of Organic–Inorganic Nanohybrids

Muhammad Tanveer, Muhammad Imran, Shoomaila Latif, Nazim Hussain, and Muhammad Bilal

1 Introduction

A brief description on understanding the structural layout of mixing herbal–inorganic additives as the nanohybrids drugs services is accompanied by the excellent properties and uses of organic–inorganic nanohybrids (OINHs). In advance, recently showing the applications and programmed uses of these hybrids. Then, excellent fabrication and structural design techniques are given as functionalization, one-pot synthesis, wrapping, and electrospinning strategies [1]. Brief conditions which can be addressed to adopt their structural design and multipurpose uses of nanohybrid drugs provide their wider applications. They may be discussed as the approach regarding their therapeutic use, and in emerging technology such as dendrimers, micelles, polymers, carbon nanotubes (CNTs), liposomes hybridizing with inorganic nanomaterials which encompass mesoporous silica, layered of double hydroxides, halloysites, iron oxide and hydroxyapatite to produce OINHs as flexible drug transport shops with improved traits and structurally changed and better drug, magnetic or receptor-targeted delivery of medicine [2].

A new magnetic nanohybrid containing the non-steroid anti-inflammatory medication diclofenac (DIC) intercalated Mg–Al layered double hydroxide (LDH) on magnesium ferrite particles was created using one-step precipitation self-assembly.

M. Tanveer · M. Imran
Centre for Inorganic Chemistry, School of Chemistry, University of the Punjab, Lahore, Pakistan
e-mail: imran.hons@pu.edu.pk

S. Latif
School of Physical Sciences, University of the Punjab, Lahore, Pakistan

N. Hussain
Centre for Applied Molecular Biology, University of the Punjab, Lahore, Pakistan

M. Bilal (✉)
School of Life Science and Food Engineering , Huaiyin Institute of Technology, Huaian, China
e-mail: bilaluaf@hotmail.com

K. Rizwan et al. (eds.), *Hybrid Nanomaterials*, Materials Horizons: From Nature to Nanomaterials, https://doi.org/10.1007/978-981-19-4538-0_2

The measurements of ICP, FTIR, and XRD praepostor that magnetic nanohybrid comprise of every disseminated intravascular coagulation-lactate dehydrogenase (DIC-LDH) nanocrystallite and magnesium ferrite stages. The magnetic nanohybrid gives a nicely explicit center-shell structure as indicated by the TEM picture and the diameter of the shell ranges between 90 and 150 nm. Because of a heterogeneous nucleation and crystal boom approach with the introduction of the magnetic core, the sheltered DIC-LDH nanocrystallites in magnetic hybrid have lesser measurements and a significantly less crisp hexagonal shape than natural DIC-LDH nanocrystalline [3]. Due to many smaller periods of the encased DIC-LDH nanoparticles on the magnetic center's surface, the magnetic nanohybrid's in vitro drug launch charge changed, becoming higher and more suitable. The kinetic statistics show that the discharge of DIC out from magnetic nanohybrid is controlled by particle diffusion, with the discharge rate decreasing with particle length and the level of aggregation of the hybrid magnetic debris. Furthermore, the obtained nanohybrid clearly demonstrates a substantial magnetism response, hinting that it might be utilized in magnetic drugs [4].

The structural design and study of fluorescent nanohybrids based on p-extended hydroxyoxophosphole ligands mounted onto ZnO nanoparticles. Due to a powerful aggregation-induced emission effect, the limitation of the organic fluorophore' intramolecular movements during each aggregate's generation in solution or processing into thin films, office work shockingly excitonic materials. The interactions between the herbal and inorganic opposite numbers have been studied using theoretical calculations and X-ray photoemission spectroscopy (XPS) investigation. Preliminary studies show that such nanohybrids can be used as actual solution excitonic strata in organic light emitting diodes (OLEDs) for photo and spectroscopic applications [5].

2 History of Structural Design of OINHS

The latest history 2021 in the journal of "Materials today" defined the structural layout and synthesis of many OINHs and may be discussed with specific elements in their structures. Here is the artwork included the use of sodium citrate to reduce Ag ion into Ag steel in its nanoscale form and the chemical manufacture of Ag metal nanoparticles. FTIR, XRD, and AFM are used to detect the nanoparticles. For Ag NPs and MnO_2 NPs, the mostly peak become 5 nm and 2.5 nm, respectively. Furthermore, the novelty comes from the usage of a natural substance 5-methoxy-2-mercaptobenzimidazole (MBBI) for the manufacturing of herbal–inorganic nanohybrids that permeate the ply of FTIR and XRD [6].

Organic/inorganic nanohybrids (OINHs) captivated incredible attention because of its unique design, commendatory possessions, and auspicious strategy in the biomedical realm. Substantial endeavor was assembled to pattern adaptable nanohybrids. Numerous polymers provide distinct disciplines for multifunctional systems with collective qualities among one-of-a-kind natural additions. It focuses on

herbal/inorganic nanohybrids constructed of inorganic nanoparticles and polymers, as well as their format and biological applications. We begin with a quick overview of a growing number of structural layout options for sensitive herbal/inorganic nanohybrids. Nanohybrid applications and capacities, morphology-based homes, and nanohybrid self-assembly will be demonstrated [7].

Whereas large stages of nanocomposites are thought to conjugate into hybrid form, the hybrid structure, composition, and interactions depend on the nanohybrid's final potential. The reduced hydrophilic surface of inorganic nanoparticles, as is widely known, prevents their direct application in pharmaceuticals. Surface functionalization was used to solve this problem. Natural species and the inorganic nanoparticle surface should both have the appropriate inclinations for this. For contrast, the existence of Iron-O bonds and hyroxyl bonds on the surface, as well as −OH groups and −COOH groups on the organic moiety, is significant in the preparation of IONP.

In recent years, scientists and chemists have been interested in organic/inorganic nanohybrid materials since the inorganic and organic components in those hybrids appear to be structurally ambiguous so it is not easy to regulate them at the molecular level in comparison to difficulties and structural challenges. Furthermore, the majority of these materials are ultimately made up of inorganic additions on their personal constituents and the natural components are without a doubt, hired as templates. In recent years, an entirely new design of layered natural/inorganic nanocomposites, made up of molecules that are amphiphilic in nature with a covalent link between a few of the silicate and the surfactant, has been proposed. Because nanohybrid precursors can create 3D networks at some point in the self-assembling procedure, in which organic part are covalently connected with strong C-Silicon bonds via inorganic layers, these substances may have a capacity.

Recently, a special type of natural/inorganic nanohybrids "cerasome" in aqueous medium using self-assembling of lipidic organotrialkoxysilanes to shape bilayer vesicles with a silicate floor have been prepared by sol–gel reaction method. We initially organoalkoxysilane(1) is compiled with triethoxysilyl head which is a hydrophobic. When organoalkoxysilne was treated with the sol–gel method, the amphiphiles with the silanol head clumped produced morphologically persistent multilayer vesicles. The cerasome is made up of lipids (hemispheric bilayer membrane) having a hydrated segment, similar to a liposome, and is further protected on its surface by a silicate scaffolding (Fig. 1).

In addition to the triethoxysilyl element, we created a cerasome formed lipid with a quaternary ammonium structure on the top of the molecule. While liposomes are widely employed for bio membrane designs as well as helpful nanocapsules, its morphological fragility is often a source of concern for delicate concerns. In the presence of a silicate layer on to the side of the cerasome was thought to solve this problem. Furthermore, the cerasome is a one-of-a-kind herbal–inorganic nanohybrid with a carefully constructed nanostructure. With the help of cerasome-forming lipid, we can determine the thickness of each herbal layer, inorganic layer, and vesicular distance. Cerasome is essentially controlled using classic monodispersed liposome preparation methods. We looked at the role of lipid molecule pinnacle organization during hydrolysis inside the cerasome, the connections between pH and the sol–gel

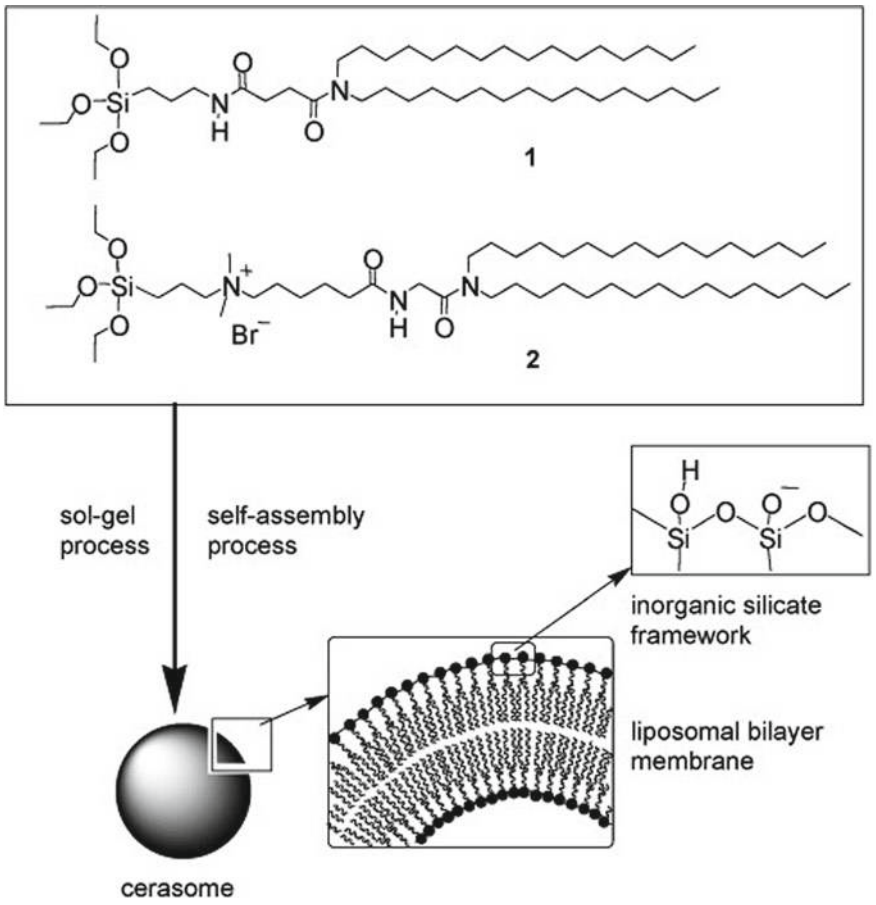

Fig. 1 Cerasome-lipid forming nanohybrid structure. Reproduced from [7] with permission from John Wiley and Sons. Copyright © 2007 WILEY-VCH Verlag GmbH & Co. KGaA, Weinheim

method settings must be in consideration. Furthermore, cerasome characterization is accomplished by a series of physical assays that reveal the structure of cerasome-forming lipids molecules, their shape, and physiochemical characteristics.

There are some important points that should be remembered regarding OIHNS.

- Organic–inorganic nanohybrids (OINHs) are considered to be the effective applications of many studies and industrial fields due to their specific and flexible structural design.
- The applications of OIH in biosensors, chemical analysis, and environmental tracking are highlighted in this chapter. A technique for metrological traceability dimension and standardization of OINHs as well as an illustration of the usefulness of mathematical modeling in biosensors is also presented morphologically. [8].

3 OINHS Classification Based on Interactions

Steel-to-carbon linkages that are stable during hydrolysis processes are present in OINHs, as are alkoxy groups (R-OM bonds) which might play a role relying on the composition of the natural–inorganic junction. Nanohybrid compounds can be categorized in two primary classes based on interactions (Fig. 2) [9]:

1. Hybrid structures with sensitive additive interactions (Van der Waals forces, H-bonding) [11].
2. Chemical bonds, either covalent or ionic-covalent, connect organic and inorganic components. The magnificence of OIH (Type/Class I) describes the physical relationship (pi-pi contact, H-bond, etc.) between natural and inorganic constituents. Class I OIH compounds are the simplest, despite the fact that both natural and inorganic components have unique intentional activities on their bases [12]. Aside from that, OIH compounds are in a hybrid phase, separation between organic–inorganic additives occur. Mostly proven employing different center-shell structures, inorganic detritus, or other nanostructures embedded in an organic (e.g., polymer) matrix, that dictates functionality in the photocatalysis, biosensors, and other applications.

These two main classes can be summarized as:

1. One which shows **physical interaction**:
   (a) Sol–gel matrices will be embedded by an organic dye
   (b) An organic monomer in sol–gel matrices
   (c) An inorganic polymer embedded in a polymer
   (d) Ordered organic–inorganic structures.
2. 2nd which shows **chemical interaction**:

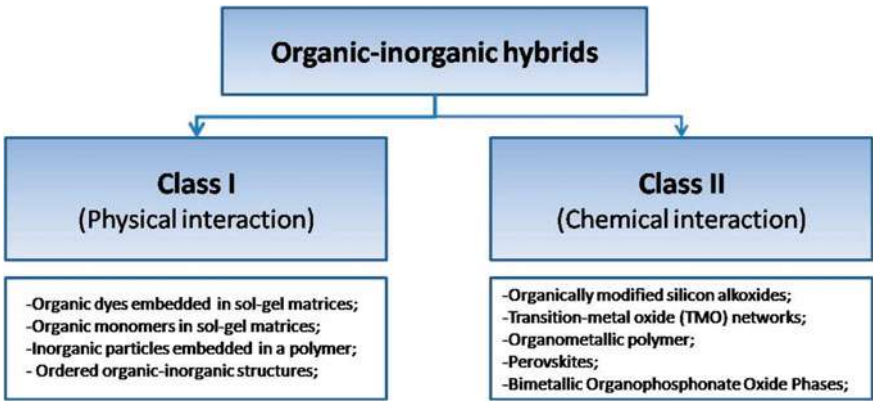

Fig. 2 Classification of organic–inorganic hybrids based on the interactions [10]. This article is an open access article distributed under the terms and conditions of the Creative Commons Attribution (CC BY) license (http://creativecommons.org/licenses/by/4.0/)

(a) Organically modified silicon alkoxide.
(b) Transition–metal oxide (TMO) networks
(c) Organometallic polymer
(d) Perovskites
(e) Bimetallic organophosphonate oxide phases.

In terms of unique hybrid nanomaterials, advanced nanotechnology in terms of morphology has emerged unexpectedly, determining various programs in everyday living existence in order to improve the general populace. Silica, iron, gold, hydroxyapatite, and double hydroxide-based nanohybrids (DHN) have shown promising results in biological uses such as bioimaging, therapeutic transport, and photothermal or dynamic therapy [13]. Furthermore, recent development in the transformation of nanohybrid compounds is critical; the reason is that they offer remarkable NIR imaging capabilities as well as benefits that might be effective in treating underground malignant cells. Our present overview emphasizes current trends in natural–inorganic nanohybrid structural arrangement, as well as their applications in bioimaging, medication delivery, and phototherapy [14].

4 Classification of Nanohybrids on the Basis of Material Used

Now, OINHs can be classified into the following:

- Organic–inorganic
- Inorganic–inorganic
- Bioinorganic.

Because of their unique structural and material qualities, they have shown their value. With the resources of standard solid-state processes, obtaining such new properties is tough. As a result, in the rapidly developing field of nanomedicine, which is entirely based on nanotechnology, it is critical to develop superior hybrid nanomaterials with precise properties using artificial methods such as chemical vapor deposition, Langmuir–Blodgett method, self-meeting, and reaction strategies. Certain molecules are reversibly interpolated into 2D host lattices to generate an extension of nanohybrids with advanced characteristics, which includes inorganic–inorganic, natural–inorganic, and bioinorganic hybrids [15]. It's also worth noting that recent advances in nanochemistry have aided in the development of novel nanohybrids, including creative multifunctional rising nanohybrids, without a doubt by editing the molecular re-association of heterogeneously oriented organic–inorganic substances. Advanced research has allowed us to develop a large number of nanohybrid materials with already known or unknown properties that could be useful for drug development, bifurcation, and other applications.

Due to the synergetic functions of such nanohybrid substances, this unique discovery becomes particularly fascinating for producing analogous hybrid materials. A simple exfoliation/restacking process, for example, can produce very photocatalytic inorganic–inorganic nanohybrids. Several procedures have been set out to develop useful nanohybrids based entirely on inorganic–chemical techniques: for example, nanoporous hybrids that can be used for both releasing and loading computing agents; this form of hybrid organic–inorganic substances has offered ascend to special nanohybrids with versatile properties. Moreover, the combination of multiple nanomaterials, the resulting hybrids must be greater in therapeutic potential [16].

Hybrid systems have grown in popularity as a result of their more versatile uses and applications, as well as their structural shape [17]. Each herbal and inorganic ingredient in textiles has multiple, greater molecular, thermal, and mechanical features in organic–inorganic hybrid materials. When contrasted to solitary inorganic components, hybrid fabric offers a variety of innovation merits. Because of their clinical usage, these innovation assets and programs of natural–inorganic hybrid compounds have saved numerous lives [16].

References

1. Faustini M, Nicole L, Ruiz-Hitzky E, Sanchez C (2018) History of organic–inorganic hybrid materials: prehistory, art, science, and advanced applications. Adv Func Mater 28(27):1704158
2. Manatunga DC, Godakanda VU, de Silva RM, de Silva KN (2020) Recent developments in the use of organic–inorganic nanohybrids for drug delivery. Wiley Interdisc Rev Nanomed Nanobiotechnol 12(3):e1605
3. Zhang H, Pan D, Zou K, He J, Duan X (2009) A novel core-shell structured magnetic organic-inorganic nanohybrid involving drug-intercalated layered double hydroxides coated on a magnesium ferrite core for magnetically controlled drug release. J Mater Chem 19(19):3069–3077
4. Phelipot J, Ledos N, Dombray T, Duffy MP, Denis M, Wang T, Didane Y, Gaceur M, Bao Q, Liu X, Fahlman M, Delugas P, Mattoni A, Tondelier D, Geffroy B, Bouit P-A, Margeat O, Ackermann J, Hissler M (2022) Highly emissive layers based on organic/inorganic nanohybrids using aggregation induced emission effect. Adv Mater Technol 7(1):2100876
5. Adnan LA, Alheety NF, Majeed AH, Alheety MA, Akbaş H (2021) Novel organic-inorganic nanohybrids (MnO_2 and Ag nanoparticles functionalized 5-methoxy-2-mercaptobenzimidazole): one step synthesis and characterization. Mater Today: Proc 42:2700–2705
6. Zhao N, Yan L, Zhao X, Chen X, Li A, Zheng D, Zhou X, Dai X, Xu FJ (2018) Versatile types of organic/inorganic nanohybrids: from strategic design to biomedical applications. Chem Rev 119(3):1666–1762
7. Katagiri K, Hashizume M, Ariga K, Terashima T, Kikuchi JI (2007) Preparation and characterization of a novel organic–inorganic nanohybrid "cerasome" formed with a liposomal membrane and silicate surface. Chem Eur J 13(18):5272–5281
8. Ha CS, Nagappan S (2018) Hydrophobic and superhydrophobic organic-inorganic nanohybrids. Jenny Stanford Publishing
9. Choi G, Rejinold NS, Piao H, Choy JH (2021) Inorganic–inorganic nanohybrids for drug delivery, imaging and photo-therapy: recent developments and future scope. Chem Sci 12(14):5044–5063

10. Silina YE, Gernaey KV, Semenova D, Iatsunskyi I (2020) Application of organic-inorganic hybrids in chemical analysis, bio-and environmental monitoring. Appl Sci 10(4):1458
11. Sanchez C, Soler-Illia GDA, Ribot F, Lalot T, Mayer CR, Cabuil V (2001) Designed hybrid organic−inorganic nanocomposites from functional nanobuilding blocks. Chem Mater 13(10):3061–3083
12. Laine RM, Sanchez C, Brinker CJ, Giannelis E (1998) Organic/inorganic hybrid materials (No. CONF-980405). Materials Research Society, Warrendale, PA (United States)
13. Schmidt H, Jonschker G, Goedicke S, Mennig M (2000) The sol-gel process as a basic technology for nanoparticle-dispersed inorganic-organic composites. J Sol-Gel Sci Technol 19(1):39–51
14. Kresge AC, Leonowicz ME, Roth WJ, Vartuli JC, Beck JS (1992) Ordered mesoporous molecular sieves synthesized by a liquid-crystal template mechanism. Nature 359(6397):710–712
15. Sanchez C, Shea KJ, Kitagawa S (2011) Recent progress in hybrid materials science. Chem Soc Rev 40(2):471–472
16. Vallet-Regí M, Colilla M, González B (2011) Medical applications of organic–inorganic hybrid materials within the field of silica-based bioceramics. Chem Soc Rev 40(2):596–607
17. Shakeel A, Rizwan K, Farooq U, Iqbal S, Altaf AA (2022) Advanced polymeric/inorganic nanohybrids: an integrated platform for gas sensing applications. Chemosphere, 133772

Chapter 3
Fabrication of Organic–Inorganic Nanohybrids

Muhammad Rashid, Shoomaila Latif, Muhammad Imran, Ayesha Mumtaz, Nazim Hussain, and Muhammad Bilal

1 Organic–Inorganic Nanohybrids

Organic and inorganic substance heteronanoparticles are what nanohybrids are referred to as. Organic and inorganic components are arranged into distinct domains in their makeup. In addition to combining the original functionalities of both organic and inorganic components, nanohybrids also integrate both organic and inorganic functions. They undoubtedly provide entirely new and advanced properties and functions due to the interaction between their parts, like expected and desirable electrical, optical, and magnetic properties [1].

2 Strategies of Fabrication for Organic–Inorganic Nanohybrids

There are many ways to make organic–inorganic nanohybrids, and they all work that has been developed. The following are the five major strategies used in the manufacturing of organic–inorganic nanohybrids.

M. Rashid · M. Imran
Centre for Inorganic Chemistry, School of Chemistry, University of the Punjab, Lahore 54000, Pakistan
e-mail: imran.hons@pu.edu.pk

S. Latif
School of Physical Sciences, University of the Punjab, Lahore, Pakistan

A. Mumtaz · N. Hussain
Centre for Applied Molecular Biology, University of the Punjab, Lahore, Pakistan

M. Bilal (✉)
School of Life Science and Food Engineering, Huaiyin Institute of Technology, Huaian, China
e-mail: bilaluaf@hotmail.com

K. Rizwan et al. (eds.), *Hybrid Nanomaterials*, Materials Horizons: From Nature to Nanomaterials, https://doi.org/10.1007/978-981-19-4538-0_3

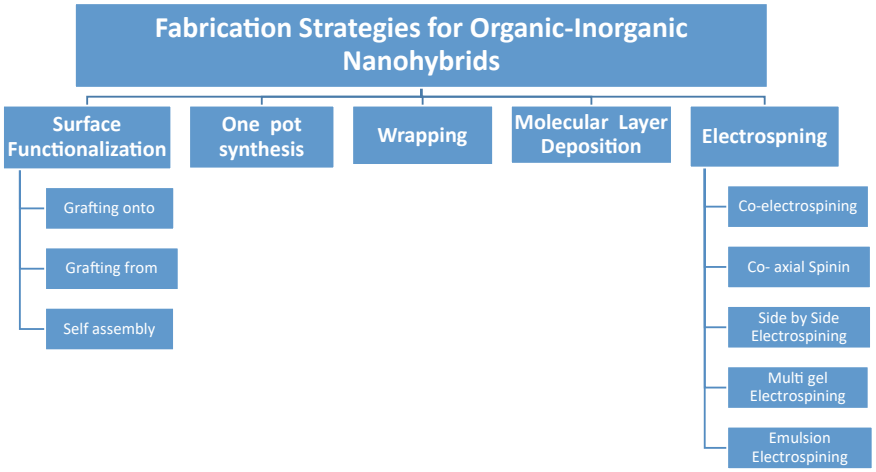

Fig. 1 Fabrication of organic–inorganic nanohybrids

- Functionalization of the surface.
- One-pot synthesis.
- Wrapping.
- Electrospinning.
- Molecular layer deposition.

Figure 1 depicts an overview of multiple fabrication strategies. For the design and synthesis of nanohybrids with our specialized and most necessary qualities, we searched for and developed method(s) that may give important facts and details for the organic–inorganic hybrid fabrication techniques described in this Chaps. 2 and 3.

2.1 Surface Functionalization

Organic–inorganic nanohybrid materials have been of significant scientific interest, and the inorganic and organic qualities make them very technical. Due to their nanoscale size, inorganic nanoparticles exhibit intriguing magnetic, optical, electrical, and catalytic capabilities. As a result, their high surface-to-volume ratio might lead to losing critical qualities. It is possible to manage this issue by applying chemically or physically end-tethered polymer chains to the surfaces of inorganic nanomaterials [4].

The most widely used and operating method for the fabrication of nanohybrids is the surface functionalization of inorganic nanoparticles. Because surface engineering is the method, it has proven possible to create a mix of organic and inorganic components. It is a vital tool for using distinct characteristics of nanohybrids in

various applications. In most cases, providing polymers to surface functionalization properties can give biocompatible hydrophilic surfaces to nanohybrids. It can also give functional groups that can be utilized for targeting or delivery goals using biomolecular targets such as peptides of proteins or genes [5].

2.1.1 "Grafting onto" Method

The easiest way to integrate NPS and polymers is to directly and quickly graft polymers or any other biomolecules (as may be necessary) onto the surface of produced nanoparticles. In this scenario, the molecular weight of the grafted polymer is critical, and it must be determined, fixed, and maintained at a constant level. Adequate and proper conjugation procedures may be used to carry out this process, which is also known as chemical replacement. Steric hindrance plays a critical role in limiting the grafting density in these circumstances. As a result, it has been shown that a compromise will be reached between synthetic convenience and commensurate efficacy [6].

Designing multifunctional nanocarriers is relevant for medication delivery with well-suited features, the detection of cancer, and the delivery of different treatments, among other applications. To improve the efficiency of photothermal treatment and photoswitchable targeted theranostics, hollow-structured CuS@Cu_2S@Au nanoshell/satellite nanoparticles may be used in conjunction with these applications. The surface production of various forms of nanohybrids may be used to determine the presence of a photoswitchable targeting effect [7].

We have completed the design and development of low-toxic, multifunctional heteronanostructures comprising cellulose nanocrystal (CNC)-gold nanoparticle hybrids wrapped in low-toxic, hydroxyl-rich polycations, as well as the synthesis of these heteronanostructures. To achieve effective cancer treatment, heteronanostructures may be employed to combine a variety of functionalities that are most appropriate for the situation. Cellulose nanocrystals (CNCs) with the best rod-like shape for high cellular uptake have been employed and sustained as substrates to carry spherical gold nanorods (Au NRs) or gold nanoparticles (Au NPs) via gold-thiolate bonds more effectively and efficiently as well as to provide heterolayered nanohybrids of CNC-Au NRs or CNC-Au NPs. CNC-Au NRs. It is then implanted into the surface of the nanohybrids through host–guest contact and gold–thiolate bonding, with PEG functioning as an intermediate and spacer at this stage in the process. They are great examples of gene carriers, such as the CNC-Au-PGEA heteronanostructures that have been constructed.

2.1.2 Method of "Grafting from"

Consequently, it is fundamentally a technique that starts from the bottom up: Polymers emerge from the surface of NPs by surface-initiated polymerization, resulting in greater grafting densities. The introduction of alternative initiators for controlled

surface started polymerization has made it feasible to attach the densely tethered polymer brushes using this approach, which has allowed for the development of new materials. After that, as a consequence, control over the polymer brush's versatility and chemical resilience is accessible and under control, while the synthetic flexibility allows for the simple insertion of functional groups [9]. Many distinct instances of nanohybrids that have been constructed using the "grafting from" technique have been described in detail in this section.

Differential photoluminescence properties of lanthanide-doped up conversion nanoparticles (UCNPs) are very useful and beneficial in various biomedical applications. A polymer coating applied on UCNPs may give additional essential qualities such as in vivo biocompatibility and stability and the potential to be used in drug delivery applications. This is a crucial characteristic since it allows for exact monitoring of the modification process. It is also significant because it will not have an unfavorable effect on the luminescence properties of UCNPs. To construct an organic polymer shell, visible light was used to graft it onto the surface of UCNPs. Photon energy/electron transfer–reversible addition–fragmentation chain transfer polymerization may be regulated by using this shell, which is effective (PET-RAFT). Several variables may be manipulated, including the grafting density, kinetics of polymerization, and chain thickness, and exploited by monitoring the monomer to RAFT agent ratio or the length of time the polymer chains are exposed to light. Additionally, the process of polymerization was given functional temporal control as a result of it. Furthermore, the polymerization process may be launched, paused, or terminated with the simple switch of the light source on and off. This increased the luminescence of silica-coated UCNPs because the polymer shell suffocated surface defects and prevented solvents from deactivating the UCNPs, among other things. With the results of this research, we may begin to construct UCNPs with regulated qualities, which will be helpful in many other applications [10].

By linking two or three Fe_3O_4 nanoparticles in line with the silica covering, we were able to swiftly create peapod-like one-dimensional nanoparticles. When PGMA from the silane-linked initiator was grafted onto the surfaces of $Fe_3O_4@SiO_2$ nanoparticles, it was feasible to generate an opening reaction for gene transfer with enough ethanolamine. $Fe_3O_4@SiO_2$PGEA nanohybrids [11] facilitate gene transfer due to their one-dimensional shape and magnetic responsiveness. It is possible to create nanohybrids with a wide variety of functionalities using the RAFT polymerization technique as an easy "grafting from" method. CTAs for nanohybrids are most often based on silane- or amine-functionalized nanoparticle immobilization. After a silane-containing CTA has been connected, the Fe_3O_4 nanospheres may be surface-initiated RAFT to graft S-benzyl S′-trimethoxysilyl propyl tricarbonate [12].

Surface-initiated ROP has been used to create nanohybrids. To achieve the highest biocompatibility and solubility, hyperbranched polyglycerol (HPG), which has many hydroxyl groups, was grafted onto MoS_2 nanosheets [13]. The hydroxyl groups on MoS_2's surface were duplicated and fused with the 1-thioglycerol (TG) ligand and subsequently acted as an activator for anionic ROP. The MoS_2-g-HPG nanohybrids that have been created might be further united with specific functional chemistries. Rhodamine B, for example, is a fluorescent dye. Aziridine cationic ROP was used

to graft this PEI onto the surface of single-walled carbon nanotubes that had been functionalized with amines (SWCNTs). This is how genetic material is passed down across the generations [14].

2.1.3 Method of Self-assembly

It is a spontaneous and fast bottom-up process that occurs worldwide. It is the main fundamental procedure to develop excellent biological systems. Using this self-assembly method to create intelligent nanohybrids is seen as a promising and realistic technique [15]. Nanohybrids based on organic and inorganic components self-assembly are shown in this area because of unique interactions. These interactions often make use of host–guest molecular recognition with switchability and selectivity. Most often, host–guest molecular recognition with inherent switchability and selectivity is used in the classic cyclodextrin–adamantane (CDAd) assembly method. Because of its small molecular size and good biocompatibility, CD is often employed to construct gatekeepers for MSNs [16].

A simple block copolymer-facilitated liquid deposition, followed by a direct heat treatment, is possible technique used to pattern silicon surfaces with effectively ordered nanoperforated $TiO_{(2)}$ layers. The surfactant patterning agent's molecular mass determines the crater diameter, always between 10 and 50 nm. Nanostructured heterogeneous surfaces (nanoholes with $SiO_{(2)}$ bottom surfaces and $TiO_{(2)}$ walls) occur when two separate perfluorinated organic groups are utilized selectively. These nanoholes were demonstrated to acquire the substrate surface and then selectively distribute both functions on the surface using water-contact-angle measurements to confirm the Cassie link [17]. Manufacturing of KALA/heparin–biotin/heparin/chitosan/$CaCO_3$ nanohybrids (KALA/HPB/HP/CTS/$CaCO_3$) with active targeting, pH sensitivity, and cell-penetrating properties was carried out to develop a simple process for designing multifunctional drug carriers and formulating a new intelligent drug delivery platform for the development of a new innovative drug delivery platform. Through self-assembly, all of the functionally active components were integrated into the nanoparticles. The applicability of the nanohybrid as a medication delivery carrier for anticancer agents was investigated. To compare, HP/CTS, HP/CTS/$CaCO_3$, and HPB/HP/CTS/$CaCO_3$ nanohybrids were also produced and compared with one another. Through dynamic light scattering, it was possible to determine the sizes and size distributions of the nanohybrids (DLS). Various techniques, including FTIR, XPS, TEM, and thermogravimetric analysis, were used to examine the nanohybrids' surface characteristics and structure (TGA). The $CaCO_3$-containing nanohybrids showed pH-sensitive drug release behavior and could be employed to effectively enhance drug release after loading doxorubicin hydrochloride (DOX) into the nanohybrid and measuring in vitro drug release [18].

MNPs functionalized with organic ligands (organic MNPs) have garnered much interest in recent years for their usage in biomedical applications. Nanohybrids that combine the capabilities of organic ligands with the superparamagnetic properties of MNPs for diagnostic imaging and treatment may enhance blood circulation time,

tumor targeting, and cellular absorption. For a range of biomedical applications, the ability to modify the composition, chemical–physical, and biological characteristics of distinct inorganic ligands and MNPs enables sophisticated manipulating of their interactions [19].

New nanomaterials like CNC–organic MMT have been developed and built via electrostatic self-assembly, which expands the application of nanomaterials like cellulose nanocrystals and montmorillonite that are already in use in other ways. By adhering the needle-like CNTs to the surface of the two-dimensional OMMT, they were discovered to form the three-dimensional nanohybrid according to the morphological features of the two materials. The experiment's findings show that both CNC and OMMT were preserved in the nanohybrid. The Zeta potentials of cellulose nanocrystals and OMMT were measured to demonstrate electrostatic adsorption. This work showed that the lamellar structure of OMMT may cover sulfur groups on the CNC surface and have a shielding effect on heat transmission, resulting in an enhancement in the temperature stability of the nanohybrid. Using a nanohybrid with the principal function of a functional nanostructure, we predict synergistic effects in polymer nanocomposites, which might be a helpful technique for developing high-performance polymer nanocomposites.

Method of One-Pot Synthesis

Recently, the one-pot synthesis has become an essential atom-economical approach for different chemical transformations in a single pot without involving the purification of intermediate compounds. This simple approach does not involve the separation process at each step, thereby reducing the reaction duration, minimizing chemical resources, and being responsible for a high atom economy. This environmentally benign strategy has attracted much attention to synthesizing and fabricating all kinds of nanomaterials. Further, this approach has acquired a new aspect of sustainability with the participation of biomolecules such as proteins, DNA, and phytochemicals as safe capping and reducing agents [21].

Nanohybrid composites (MnFMC, CoFMC) with outstanding Pb(II) removal capacity have been synthesized using a one-pot solvothermal synthesis. Experiments on the adsorption capacity of the nanohybrids have been conducted using both equilibrium and kinetic methods. MFe_2O_4 nanoparticles and CDs and MoS_2 with a high surface area may be combined to generate nanohybrids that display excellent adsorption performance by taking advantage of cation substitution on the surface of MFe_2O_4 nanoparticles and CDs, as demonstrated in this work. The reusability of these nanohybrids and their ability to reduce the effluent lead content to ppb levels, which satisfy the WHO drinking water standard, make them promising candidates for the purification of drinking water [16].

It was possible to create a well-linked molybdenum disulfide nanohybrid (NC-MoS_2) using a one-pot hydrothermal synthesis technique doped with nitrogen and inserted into carbon. The material was then used as a novel adsorbent for the uptake of tetracycline (TC) from water and was effective. Intercalating nitrogen-doped carbon into MoS_2 nanosheets enhances interlayer spacing, surface area, and functional groups. Different interactions, such as hydrogen bonding, hydrophobicity, and

molecule stacking, affect adsorption [22]. An effective room temperature ammonia (NH_3) gas sensor has been created using a zinc oxide (ZnO)—polyaniline (PANI) nanohybrid that was created in a single pot of synthesis. Materials were examined to determine their morphological, structural, thermal, compositional, and optical characteristics. The structural and morphological analyses demonstrated that ZnO particles were well-integrated into the PANI matrix. The ability of ZnO-PANI nanohybrids to detect gas has been examined in detail. The findings suggested that ZnO-PANI nanohybrids are highly selective for NH_3, have a short reaction time, and have excellent stability [23].

The one-pot synthesis of sodium dodecyl sulfate (SDS) organomodified LDH Zn_2Al (GLIB) increased colloidal stability and usefulness. The GLIB data showed zero-order zinc release kinetics from the LDH matrix (2.96% 0.002 ppm), which matched findings from an acid medium [24]. GLIB data showed zero-order kinetics of zinc release from the LDH matrix, consistent with release in a simulated intestinal media. Using manganese ferrite nanoparticles functionalized with Schiff base and enclosed in a layer of silica, a heterogeneous catalyst was synthesized, and then copper was added. FTIR spectroscopy, FESEM, energy-dispersive X-ray spectroscopy, DTG analysis, and X-ray powder diffraction were utilized to evaluate the synthesized hybrid material.

Synthesis of N-arylquinolines and 1,4-dihydropyridines under mild reaction conditions was made possible with the help of the organic–inorganic nanohybrid catalyst that was created during the fabrication process. Catalytic activity was high under optimal circumstances, and the desired products were produced with high yields. 1-methyl-3-(3-trimethoxysilylpropyl) chloride of 1H imidazole-3 ion. It has been possible to manufacture and analyze Ni@zeolite-Y-based nanostructured materials (Ni@zeolite-Im-IL) using several analytical methods such as EDX, BET, FT-IR, FE SEM, TGA-DTG, and XRD. To create this nanohybrid, first Ni_{2+} and 3-chloropropyltriethoxysilane (CPTES) were swapped, and then N-methylimidazole was used to functionalize the imidazolium chloride ionic liquid. Ni@zeolite-Im-IL nanohybrid showed intense activity in the one-pot reaction of thiourea methylcarbonyls and iodine at 80 °C in dimethyl sulfoxide with good yields (85–98%). Condensation of aromatic aldehydes with o-arylendiaminein in ethyl alcohol at room temperature catalyzed the production of 2-aryl benzimidazoles with good yields (90–98%). This efficient synthetic technique has the advantages of shorter reaction durations, greater purity, easier product separation, outstanding yields, superior activity, stability, and reusability. Because of these advantages, this is one of the most intriguing prospects in green chemistry.

Copper iodide-polypyrrole nanohybrids Cui-PPy has been synthesized in a single step. The manufacturing method is time-controlled and concentration-dependent to create nanoscale metal salt/polymer hybrid structures. Different experimental variables, such as synthesis duration, component addition sequence, and reagent concentration, have been studied concerning dimensionality structure and end-product yield. Synthetic settings allow for a marshite CuI content in the nanohybrid of 60–90 weight percent. Conditions for fabricating nanosized CuI dispersed throughout the polypyrrole matrix. The manufactured nanosized metal-polymer hybrid materials

have been discovered to exhibit high repeatability and morphological stability. Cyclic voltammetry tests have validated the electrochemical activity of the nanohybrids. One-pot synthesis for hybrid nanodimensional copper iodide-polypyrrole manufacturing meets green chemistry requirements and is very efficient for future biosensor development [27].

2.2 Method of Wrapping

This is a technique for combining inorganic and organic elements in nanohybrids via noncovalent interactions. Aside from precipitation or chemical reaction techniques, organic components play an essential role in forming NPs, including all of these or some of the inorganic NPs. To create nanohybrids, organic and inorganic components may be combined to form nanostructures. Fe_2O_3, Fe_3O_4, SnO_2, and Ag nanospheres were synthesized and constructed from isopropyl alcohol and a few key phenols [28], which included Fe_2O_3, Fe_3O_4, and SnO_2. Nonsolvent-assisted counterion complexation is used to fabricate and create multifunctional nanocarriers based on chitosan/gold nanorod (CS-AuNR) hybrid nanospheres. This procedure is straightforward and does not need the use of any solvent. The anticancer agent cisplatin is subsequently inserted or not into the freshly generated hybrid nanospheres, which benefit and employ the loading area provided by the spherical chitosan matrix in the process. Following in vitro cell investigations, when used as contrast agents for real-time cell imaging, the CS-AuNR hybrid nanospheres may also be used to kill cancer cells by emitting a near-infrared thermotherapy nanodevice. Due to the unique optical qualities supplied by the gold nanorods that have been encapsulated and trapped, this has occurred [29]. There are many prominent examples, including multifunctional nanocarriers for applications such as cell imaging, drug delivery, and other near-IR photothermal therapy, to name a few.

Using this method, inorganic nanoparticles may be enclosed in an organic matrix by either direct encapsulation or self-assembly inside the matrix. As part of the manufacturing process, chemical reactions and precipitation are used to create core–shell structures that are concentric or eccentric in shape, with the polymer or organic molecules wrapping around the inorganic core. PEG-Au-PAA/mSiO_2-LA of the octopus-type Janus nanoparticles (NPs) are fabricated with dual-stimuli responsive properties to pH and NIR light and targeting specificity for use in use in synergistic chemo-photothermal cancer therapy in vitro and in vivo. To synthesize homogenous Au@poly(acrylic acid) (PAA) Janus nanoparticles, a straightforward approach has been established (JNPs). A mesoporous silica (mSiO_2) shell and gold branches are grown on the JNPs, which are then treated with methoxy-poly(ethylene glycol)-thiol (PEG) to increase their stability and lactobionic acid (LA), which is utilized to target tumors specifically, using the JNPs as templates. The Janus NPs (PEG-OJNP-LA) were used to evaluate the octopus-type PEG-Au-PAA/mSiO_2-LA composite, demonstrating dual-responsive release properties in both the pH and pH NIR regions when tested [30].

Photothermal properties of chitosan nanospheres encapsulated with gold nanorods and indocyanine green (ICG) and photodynamic treatment have been synthesized and manufactured. It has an adsorption range of 650–900 nm for the hybrid nanospheres, 180 nm in diameter, and spherical [31]. Successful loading of ICG and protection against rapid hydrolysis are two advantages of using the spherical chitosan matrix.

Preparation of CdSe/ZnS quantum dot encapsulated chitosan nanospheres (CS-QD) in an aqueous solution with the assistance of ethanol is possible by utilizing counterion complexation assisted by ethanol, which is a simple and straightforward approach. Chitosan spherical matrix provided loading room for multiple QDs, but the encapsulated QDs also provided distinctive fluorescence features to the synthesized CS-QD hybrid nanospheres. As a result, these hybrid nanospheres are highly biocompatible and optically stable in the physiological environment [32]. Iron oxide nanoparticles encased in hydrophilic chitosan nanospheres were synthesized using an aqueous solution and nonsolvent-assisted counterion complexation of iron oxide nanoparticles. Hybrid nanospheres were compared to free iron oxide nanoparticles in terms of molar transverse relaxivity rate in this experiment, r2, and the manufactured hybrid nanospheres achieved a maximum of 533 Fe mM1 s1. The chitosan nanospheres are most likely to blame for the high r2 value [33]. This study produced high-quality heterodimers combining lanthanide-doped UCNPs and porphyrinic nanoscale metal–organic frameworks (nMOF). UCNPs absorb low-energy photons, which are subsequently transferred to the nMOFs, which activate porphyrins to produce singlet oxygen due to their interactions with the nanoparticles. In addition, the method makes it easier to make heterodimers with variable upconversion nanoparticle size and dual NIR light-harvesting functionalities [34].

In this study, emulsion polymerization processes were used to produce a variety of spherical and nonspherical magnetite–polyester (Fe_3O_4PS) composite colloids with superparamagnetic cores that were either concentrically or eccentrically aligned within polystyrene shells, with the concentrically aligned cores being the most common. The emulsion polymerization processes were used to create a variety of spherical and nonspherical magnetite–polyester. In addition to the effects of swelling and phase separation, it was observed that the interfacial tension formed between the monomer-swollen polymer shell and the inorganic core was responsible for the swelling and phase separation, which may be employed to build as well as to determine the structure and morphology of composite colloids Colloidal particles with an anisotropic structure, homogeneous size, and magnetic control are particularly well suited as building blocks for the fabrication of innovative functional materials and devices [35].

2.3 Electrospinning Method

Electrospinning is a simple, cost-effective, adaptable, and commonly used process for producing nanofibers from a range of polymers. It is gaining popularity as more people learn about it. In this procedure, the polymer is first dissolved in a suitable

solvent to produce a polymer solution, which is then concentrated and subjected to an electrical potential gradient of a significant magnitude. A buildup of charge on the surface of the liquid droplet tip occurs as a result of this. At some point, when the accumulated electrical charge overcomes the surface tension of the polymer solution, a charged jet is produced, which flows toward a grounded metal plate [35]. During this procedure, the solvent is evaporated, and the fibers may be produced at the surface of the ground metal plate. Electrospinning has recently piqued researchers' interest as a potential drug delivery method because of its high surface-area-to-volume ratio, variable porosity, and surface functionalization capacity. Electrospinning has recently piqued researchers' interest as a potential drug delivery method [37]. This is due to its high surface-area-to-volume ratio, variable porosity, and surface functionalization capacity. Various components, including as collagen, CTS, and gelatin, have been employed for this purpose by targeting their usage for skin and wound applications [38]. Also, synthetic polymers like poly(lactic acid) have been employed in combination with them (PLA), polyethylene oxide (PEO), and copolymers, such as poly(lactic-co-glycolic acid) (PLGA). Collagen, CTS, and gelatin are examples of natural polymers that have been used for this purpose.

For the first time, co-electrospinning was used to customize the resulting fibers' properties further. Combinations of polymers in the same solvent and combinations of various polymer solutions are electrospun using a conventional electrodelaminating apparatus (classical electrospinning device) [36]. This study used co-electrospinning to create electrospun inorganic–organic nanofiber-supported anion exchange materials, then tested their performance. SWCNTs were employed to link imidazolium-functionalized polysulfone nanofibers to imidazolium-functionalized polysulfone nanotubes in the construction of these materials. FMWCNT inorganic nanofibers can adapt along the axis of the electrospun nanofibers, which is a unique property when subjected to a high-voltage electrostatic field was demonstrated, and this solved the problem of simple agglomeration of FMWCNTs in cast-composite anion exchange membranes, which worked in conjunction with the polymer nanofibers to support the membrane. In an electrospun composite film, small X-rays revealed that ion clusters are bound to the total, indicating paths of endless and lower-energy barriers for hydroxide transport [39].

Using the co-electrospinning method, biocompatible and biomimetic nanofibrous scaffolds of polyamide-6,6 (PA-6,6) mixed with biopolymer chitosan were synthesized in a single step shown to be biocompatible and biomimetic. The osteophilic environment provided by the nanocomposite electrospun scaffold mats aids in cell growth and biomineralization by promoting proliferation and differentiation. Furthermore, compared to pristine PA-6,6, the biomineralization of the nanohybrid electrospun mats revealed more significant potential for the nucleation of bioactive calcium phosphate (Ca/P) nanoparticles (bioactive Ca/P) during the biomineralization process. The biomimetic character of scaffolds, in addition, has been shown to increase the viability and regeneration of preosteoblast (MC3T3-E1) cells [40].

Coaxial electrospinning is one of the most significant technological developments, in which a concentric spinneret with two distinct diameters is used. Inside and outer spinnerets are emptied of polymer solutions. Using electric forces applied

to both polymer solutions like single-nozzle electrospinning resulted in considerable stretching of polymer jets due to the direct tugging and development of electrically generated bending disturbances. By adjusting the flow of liquid and the voltage applied, researchers could produce fibers with a core–shell structure. To make fibers from materials that cannot be created by electrospinning on their own [36], coaxial electrospinning is utilized [41]. It was decided to employ PAN as the filament-forming polymer matrix to develop an electrospinnable polyacrylonitrile (PAN) solution as the core fluid in the experiment. To execute the modified coaxial electrospinning process, silver nitrate ($AgNO_3$) solution was used as the sheath fluid at various flow rate ratios between the sheath and the core of the electrospinning apparatus. It was shown that using $AgNO_3$ solution as the sheath fluid in coaxial electrospinning made it easier to get the smaller diameter, functionally coated nanofibers, which made a difference in the material's antibacterial activity [41].

2.4 Molecular Layer Deposition

Atomic layer deposition is a technique that has been used for a long time. The ALD process has been used to produce relatively essential inorganic compounds, such as nitrides and binary oxides, often found in nature. Experimental molecular layer deposition (MLD) research conducted in the 1990s, which provided organic polymers, significantly increased the available materials spectrum. Molecular layer deposition (MLD) is a technique for depositing an organic thin film that allows for consistent and exact control of the film's thickness throughout the deposition.

Nanohybrid superlattices may be created using the (MLD) approach in a gas phase. Layer-by-layer development may be regulated under vacuum conditions in this procedure, making it compatible with atomic layer deposition (ALD). SAOL is formed at 170 °C using MLD with step-by-step adsorptions of C-terminated alkylsilane and zirconium hydroxyl with O_2 activation, which results in self-assembled organic layers (SAOL). Using ALD and $H_2O/Zr(OC(CH_3)_3)_4$ surface-saturating processes, a ZrO_2 inorganic monolayer is synthesized at the same temperature using an ALD procedure. An organic–inorganic nanohybrid film made of SAOL-ZrO_2 has excellent insulating characteristics, solid mechanical stability, and a very high dielectric constant k (about 16).

Thin-film transistors based on pentacene use a dielectric thickness of 23 nm [43]. To create an "aluminum alkoxide" (aluminum alkoxide) thin film, MLD used trimethylaluminum (TMA and hydroquinone). The thickness and roughness of HQ-TMA alone films drop and rise slower than those of the diethylene glycol-TMA counterpart when exposed to a humidity state of 50% at 25 °C. The thickness of the annealed silicon layer decreased, and graphitic carbon areas appeared after thermal annealing at temperatures between 300 and 800 °C under vacuum, as shown by Auger, Raman, and XPS investigations. To create a p-type semiconductor, the nanohybrids had to be annealed, which increased electrical conductivity [44].

Molecular layer deposition [MLD] is the preferred technique for fabricating organic–inorganic hybrid superlattice films. The adsorption of 2,4-hexagon-1,6-diol and $TiCl_4$ at 100 °C substrate temperature and subsequent UV polymerization were used to generate thin layers of polydiacetylene [PDA] using the molecular layer deposition technique. Surface-saturation reactions with $TiCl_4$ and water (H_2O) were used to deposit titanium oxide [TiO_2] inorganic layers. The development of the nanohybrid films was shown to be self-limiting using ellipsometry measurement. The transmission electron microscopy (TEM) analysis of titanium oxide thin films crosslinked with polydiacetylene (PDA) was used to evaluate the MLD growth rate of the films, which revealed that the films are amorphous superlattices. It was discovered that the mechanical and thermal stability of the TiOPDA-TiO_2 nanohybrid superlattice films were outstanding [45].

Thin-film transistors with active semiconducting channel layers have been made via molecular layer deposition of N-type organic–inorganic nanohybrid superlattices produced at a relatively low temperature of 150 °C for the formation of active semiconducting channel layers. These nanohybrid superlattices are made up of inorganic layers such as ZnO, which provide mechanical and thermal stability and the possibility for semiconducting properties. However, self-assembled organic layers (SAOLs) allow for more structural flexibility. They have exceptional mechanical and thermal stability and high field-effect mobility. Using the nanohybrid semiconductor in p–n junction diodes, pentacene compatibility is excellent [46].

3 Conclusion

There has been a great deal of interest in nanohybrids comprising organic and inorganic components in recent years. Nanohybrids have achieved remarkable success thanks to the fast development of synthesis techniques for inorganic nanoparticles and organic components. Because synthetic techniques for inorganic nanoparticles are well-established, surface-functionalized nanohybrids continue to rule the roost. Other fundamental techniques such as molecular layer deposition, one-pot synthesis, wrapping and electrospinning, and others are promoted.

References

1. Zhao N, Yan L, Zhao X, Chen X, Li A, Zheng D, Zhou X, Dai X, Xu FJ (2018) Versatile types of organic/inorganic nanohybrids: from strategic design to biomedical applications. Chem Rev 119(3):1666–1762
2. Krasia-Christoforou T (2015) Organic-inorganic polymer hybrids: synthetic strategies and applications. Hybrid and hierarchical composite materials. Springer, Cham, pp 11–63
3. Manatunga DC, Godakanda VU, de Silva RM, de Silva KN (2020) Recent developments in the use of organic-inorganic nanohybrids for drug delivery. Wiley Interdisc Rev Nanomed Nanobiotechnol 12(3):e1605
4. Achilleos DS, Vamvakaki M (2010) End-grafted polymer chains onto inorganic nano-objects. Materials 3(3):1981–2026
5. Kalia S, Haldorai Y (eds) (2015) Organic-inorganic hybrid nanomaterials, vol 267. Springer, New York, NY, USA
6. Gao H, Matyjaszewski K (2007) Synthesis of molecular brushes by "grafting onto" method: a combination of ATRP and click reactions. J Am Chem Soc 129(20):6633–6639
7. Deng X, Li K, Cai X, Liu B, Wei Y, Deng K, Xie Z, Wu Z, Ma P, Hou Z, Cheng Z, Lin J (2017) A hollow-structured CuS@ Cu_2S@ Au nanohybrid: synergistically enhanced photothermal efficiency and photoswitchable targeting effect for cancer theranostics. Adv Mater 29(36):1701266
8. Hu Y, Wen C, Song L, Zhao N, Xu FJ (2017) Multifunctional hetero-nanostructures of hydroxyl-rich polycation wrapped cellulose-gold hybrids for combined cancer therapy. J Control Release 255:154–163
9. Bensabeh N, Ronda JC, Galià M, Cádiz V, Lligadas G, Percec V (2018) SET-LRP of the hydrophobic biobased menthyl acrylate. Biomacromol 19(4):1256–1268
10. Bagheri A, Arandiyan H, Adnan NNM, Boyer C, Lim M (2017) Controlled direct growth of polymer shell on upconversion nanoparticle surface via visible light-regulated polymerization. Macromolecules 50(18):7137–7147
11. Wang R, Hu Y, Zhao N, Xu FJ (2016) Well-defined peapod-like magnetic nanoparticles and their controlled modification for effective imaging-guided gene therapy. ACS Appl Mater Interfaces 8(18):11298–11308
12. Qin S, Wang L, Zhang X, Su G (2010) Grafting poly (ethylene glycol) monomethacrylate onto Fe_3O_4 nanoparticles to resist nonspecific protein adsorption. Appl Surf Sci 257(3):731–735
13. Xuan H, Dai W, Zhu Y, Ren J, Zhang J, Ge L (2018) Self-Healing, antibacterial, and sensing nanoparticle coating and its excellent optical applications. Sens Actuators, B Chem 257:1110–1117
14. Zheng SG, Xu HX, Chen HR (2013) Nano/microparticles and ultrasound contrast agents. World J Radiol 5(12):468
15. Yu J, Ju Y, Zhao L, Chu X, Yang W, Tian Y, Sheng F, Lin J, Liu F, Dong Y, Hou Y (2016) Multistimuli-regulated photochemothermal cancer therapy remotely controlled via Fe5C2 nanoparticles. ACS Nano 10(1):159–169
16. Aznar E, Oroval M, Pascual Ll, Murguía JR, Martínez-Máñez R, Sancenón F (2016) Chem Rev 116:561–718
17. Fisher A, Kuemmel M, Järn M, Linden M, Boissière C, Nicole L, Sanchez C, Grosso D (2006) Surface nanopatterning by organic/inorganic self-assembly and selective local functionalization. Small 2(4):569–574
18. Liang P, Liu CJ, Zhuo RX, Cheng SX (2013) Self-assembled inorganic/organic hybrid nanoparticles with multi-functionalized surfaces for active targeting drug delivery. J Mater Chem B 1(34):4243–4250
19. Yang HY, Li Y, Lee DS (2021) Functionalization of magnetic nanoparticles with organic ligands toward biomedical applications. Adv NanoBiomed Res 1(5):2000043
20. Liu H, He H, Huang B (2020) Cellulose nanocrystals-organic montmorillonite nanohybrid material by electrostatic self-assembly. J Appl Polym Sci 137(41):49263

21. Krishnan S, Bhardwaj SK, Liu S, Xing R, Chavali M (2021) Handbook of greener synthesis of nanomaterials and compounds
22. Li S, Huang W, Yang P, Li Z, Xia B, Li M, Xue C, Liu D (2021) One-pot synthesis of N-doped carbon intercalated molybdenum disulfide nanohybrid for enhanced adsorption of tetracycline from aqueous solutions. Sci Total Environ 754:141925
23. Das M, Sarkar D (2017) One-pot synthesis of zinc oxide-polyaniline nanocomposite for fabrication of efficient room temperature ammonia gas sensor. Ceram Int 43(14):11123–11131
24. Leão AD, Alvarez-Lorenzo C, Soares-Sobrinho JL (2020) One-pot synthesis of the organomodified layered double hydroxides-glibenclamide biocompatible nanoparticles. Colloids Surf, B 193:111055
25. Ahadi N, Mobinikhaledi A, Bodaghifard MA (2020) One-pot synthesis of 1, 4-dihydropyridines and N-arylquinolines in the presence of copper complex stabilized on $MnFe_2O_4$ (MFO) as a novel organic–inorganic hybrid material and magnetically retrievable catalyst. Appl Organomet Chem 34(10):e5822
26. Kalhor M, Zarnegar Z (2022) 1-Methylimidazolium ionic liquid supported on Ni@ zeolite-Y: fabrication and performance as a novel multi-functional nanocatalyst for one-pot synthesis of 2-aminothiazoles and 2-aryl benzimidazoles. Res Chem Intermed 48(2):519–540
27. Konakov AO, Dremova NN, Khodos II, Koch M, Zolotukhina EV, Silina YE (2021) One-pot synthesis of copper iodide-polypyrrole nanocomposites. Chemosensors 9(3):56
28. Ali N, Bilal M, Khan A, Ali F, Khan H, Khan HA, Iqbal HM (2021) Fabrication strategies for functionalized nanomaterials. Nanomaterials: synthesis, characterization, hazards and safety. Elsevier, pp 55–95
29. Guo R, Zhang L, Qian H, Li R, Jiang X, Liu B (2010) Multifunctional nanocarriers for cell imaging, drug delivery, and near-IR photothermal therapy. Langmuir 26(8):5428–5434
30. Zhang L, Chen Y, Li Z, Li L, Saint-Cricq P, Li C, Lin J, Wang C, Su Z, Zink JI (2016) Tailored synthesis of octopus-type Janus nanoparticles for synergistic actively-targeted and chemo-photothermal therapy. Angew Chem Int Ed 55(6):2118–2121
31. Chen R, Wang X, Yao X, Zheng X, Wang J, Jiang X (2013) Near-IR-triggered photothermal/photodynamic dual-modality therapy system via chitosan hybrid nanospheres. Biomaterials 34(33):8314–8322
32. Lin Y, Zhang L, Yao W, Qian H, Ding D, Wu W, Jiang X (2011) Water-soluble chitosan-quantum dot hybrid nanospheres toward bioimaging and biolabeling. ACS Appl Mater Interfaces 3(4):995–1002
33. Lin Y, Wang S, Zhang Y, Gao J, Hong L, Wang X, Wu W, Jiang X (2015) Ultra-high relaxivity iron oxide nanoparticles confined in polymer nanospheres for tumor MR imaging. J Mater Chem B 3(28):5702–5710
34. Li Y, Di Z, Gao J, Cheng P, Di C, Zhang G, Liu B, Shi X, Sun L-D, Li L, Yan CH (2017) Heterodimers made of upconversion nanoparticles and metal–organic frameworks. J Am Chem Soc 139(39):13804–13810
35. Ge J, Hu Y, Zhang T, Yin Y (2007) Superparamagnetic composite colloids with anisotropic structures. J Am Chem Soc 129(29):8974–8975
36. Hu X, Liu S, Zhou G, Huang Y, Xie Z, Jing X (2014) Electrospinning of polymeric nanofibers for drug delivery applications. J Control Release 185:12–21
37. Haider A, Haider S, Kang IK (2018) A comprehensive review summarizing the effect of electrospinning parameters and potential applications of nanofibers in biomedical and biotechnology. Arab J Chem 11(8):1165–1188
38. Contreras-Cáceres R, Cabeza L, Perazzoli G, Díaz A, López-Romero JM, Melguizo C, Prados J (2019) Electrospun nanofibers: recent applications in drug delivery and cancer therapy. Nanomaterials 9(4):656
39. Gong X, Dai Y, Yan X, Wu X, Wang Q, Zhen D, Li T, Chen W, He G (2018) Electrospun imidazolium functionalized multiwalled carbon nanotube/polysulfone inorganic-organic nanofibers for reinforced anion exchange membranes. Int J Hydrogen Energy 43(46):21547–21559
40. Shrestha BK, Mousa HM, Tiwari AP, Ko SW, Park CH, Kim CS (2016) Development of polyamide-6, 6/chitosan electrospun hybrid nanofibrous scaffolds for tissue engineering application. Carbohyd Polym 148:107–114

41. Yu DG, Zhou J, Chatterton NP, Li Y, Huang J, Wang X (2012) Polyacrylonitrile nanofibers coated with silver nanoparticles using a modified coaxial electrospinning process. Int J Nanomed 7:5725
42. Sundberg P, Karppinen M (2014) Organic and inorganic–organic thin film structures by molecular layer deposition: a review. Beilstein J Nanotechnol 5(1):1104–1136
43. Lee BH, Im KK, Lee KH, Im S, Sung MM (2009) Molecular layer deposition of ZrO_2-based organic–inorganic nanohybrid thin films for organic thin film transistors. Thin Solid Films 517(14):4056–4060
44. Lee S, Baek G, Lee JH, Choi DW, Shong B, Park JS (2018) Facile fabrication of p-type Al_2O_3/carbon nanocomposite films using molecular layer deposition. Appl Surf Sci 458:864–871
45. Yoon KH, Han KS, Sung MM (2012) Fabrication of a new type of organic-inorganic hybrid superlattice films combined with titanium oxide and polydiacetylene. Nanoscale Res Lett 7(1):1–6
46. Park Y, Han KS, Lee BH, Cho S, Lee KH, Im S, Sung MM (2011) High performance n-type organic–inorganic nanohybrid semiconductors for flexible electronic devices. Org Electron 12(2):348–352

Chapter 4
Synthesis of Organic–Inorganic Nanohybrids-Based Polymeric Nanocomposites

Ahmad Shakeel, Komal Rizwan, Ujala Farooq, and Saima Yasin

1 Introduction

Polymeric nanocomposites are of great importance in different fields [74]. Synthesis of hybrid nanocomposites based on organic (polymer) and inorganic components has gained serious attention of researchers due to their extensive range of applications in biomedical, environment, and energy-related areas. Progress in polymer science has created an opportunity to produce an extensive range of materials having superior mechanical, electroactive, and thermal properties [55]. In addition to this direction of developing new nanocomposites, researchers are continuously exploring novel techniques to prepare hybrid nano-materials by combining desirable features of polymers and nanoparticles. In literature, various challenges have been mentioned in preparing polymeric nanocomposites with desired features [68, 87]. The major limitation for producing nanocomposites at a commercial scale is the absence of

A. Shakeel (✉)
Laboratory of Process Engineering, NeptunLab, Department of Microsystems Engineering (IMTEK), Albert Ludwig University of Freiburg, 79110 Freiburg, Germany
e-mail: ahmad.shakeel@neptunlab.org

Freiburg Materials Research Center (FMF), Albert Ludwig University of Freiburg, 79104 Freiburg, Germany

Department of Chemical, Polymer and Composite Materials Engineering, University of Engineering and Technology, New Campus (KSK), Lahore 54890, Pakistan

K. Rizwan
Department of Chemistry, University of Sahiwal, Sahiwal 57000, Pakistan

U. Farooq
Department of Aerospace Structures and Materials, Faculty of Aerospace Engineering, Delft University of Technology, Kluyverweg 1, 2629 HS Delft, The Netherlands

S. Yasin
Department of Chemical Engineering, University of Engineering and Technology, Lahore 39161, Pakistan

K. Rizwan et al. (eds.), *Hybrid Nanomaterials*, Materials Horizons: From Nature to Nanomaterials, https://doi.org/10.1007/978-981-19-4538-0_4

economical methods for nanoparticle dispersion into the polymer matrix. The aggregation of nanomaterials hinders its benefits associated to the dimension (nanoscale), and hence, well-dispersed and isolated nanoparticles within the polymer matrix are needed. Hence, there is a need to develop synthesis methods that are effective on nanoscale yet appropriate for macroscopic processing. Researchers have developed a range of synthesis methods for preparing polymer nanocomposites which include direct processing, in situ polymerization, sol–gel, etc. [44]. Table 1 provides an overview of benefits and limitations of different synthetic routes for polymer based nanocomposites.

Table 1 Benefits and limitations of different conventional techniques for preparing polymeric nanocomposites

Synthesis method	Benefits	Limitations
Melt blending	• Well-adapted for mass-scale industrial applications • Economical • Wide spectrum of materials can be employed • Environmental-friendly	• Poor dispersion of nanomaterials, particularly at higher concentrations • High temperature and/or shearing is required
Solution blending	• Appropriate for membrane/film formation • Better dispersion of nanofiller • Recommended for thermally sensitive polymer	• Higher capital cost • Compatibility between polymer and solvent is critical • Aggregation of polymer chains after solvent evaporation • Environmental restrictions
In situ polymerization	• Enhanced dispersion of nanofiller • Both thermoplastics and thermosets can be used • Permits the grafting or exfoliation of polymers on filler surface	• Complex processing steps • Expensive reactants • Not appropriate for all types of polymers and elastomers
Sol–gel	• Higher-quality product • High potential for developing hybrid materials	• Unsatisfactory bonding • High permeability • Expensive raw material
Electrochemical	• Short reaction time • Simple and easy operation • Eco-friendly • High-purity product	• Limited surface area of electrode which hinders large-scale production

2 Synthesis Routes

Synthesis of polymer nanocomposites via suitable processing technique is vital in order to get high-performance nanocomposites. Several approaches have been developed to prepare polymeric nanocomposites including in situ preparation and direct processing [87]. The direct mixing process involves the dispersion of desired nanomaterial into polymer matrix either by melt, mechanical, or solution blending. However, uniform dispersion of nanomaterial is a major challenge of this approach [79]. In contrast, in situ polymerization technique solves the above-mentioned problem by creating a polymer microenvironment to synthesize the desired nanomaterial from its precursors through series of reactions [54]. This method is gaining interest because of the ease of controlling the morphology and particle size within the composite. The most important processing methods (Fig. 1) for polymer nanocomposites have been explained below.

2.1 Direct Processing

This technique is based on the dispersion of nanofiller into the polymer matrix using heating, solvent, or mechanical action, which makes it a top-down approach. This method is extensively used for preparing polymeric composites due to the sustainable bulk production and lower cost. This approach results in nanocomposites with one- or two-dimensional structures having particles within the range of submicron to nanoscale. In order to attain homogenous dispersion of filler into the polymer matrix,

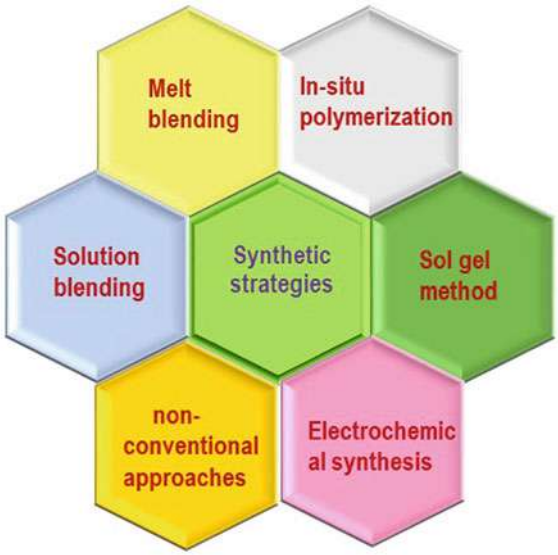

Fig. 1 Various routes for synthesis of organic–inorganic nanohybrids-based polymer nanocomposites

several approaches have been developed such as adding stabilizers or dispersants, adjusting process parameters (mixing speed, temperature, time, etc.), and chemical modification of polymers [87]. There are two main approaches for direct mixing of fillers and polymer.

2.1.1 Melt Blending

Melt blending is a typical procedure to disperse nanofiller into the continuous matrix for producing thermoplastic or elastomer-based nanocomposites. It involves the usage of a suitable processing machine (i.e., extruder or ultrasonicator) for applying required shear forces at high temperatures (usually above the glass transition temperature of polymer) in order to melt the polymer, followed by the addition and mixing of the filler for achieving uniform filler distribution [79]. Typically, melt mixing is performed in the presence of an inert gas like nitrogen, argon, etc. [33]. Melt mixing possesses several inherent advantages such as environmental-friendly due to the absence of any solvent, economical, and convenient because of the compatibility with large-scale industrial processes (i.e., extrusion and injection molding) and applicability for both polar and aploar polymers [54].

Saleh and Jawad prepared the graphene nanoplatelet (Gr NP) and polystyrene-based nanocomposites by dispersing Gr NP into the polystyrene matrix using a small batch mixer at 190 °C and a mixing speed of 100 rpm for 10 min. The prepared nanocomposite was then pressed in a compression molding machine at 25 MPa and 220 °C for 10 min, in order to prepare the samples for characterization [3]. Alig and colleagues explained the correlation between the morphologies obtained for carbon nanotube-based nanocomposite and the processing conditions [6]. Furthermore, they described the dispersion process of filler into the polymer matrix in four steps: (i) wetting of filler aggregates with polymer, (ii) infiltration of polymeric chains into the filler aggregates, (iii) dispersion of filler aggregates by erosion and rupture, and (iv) distribution of individual carbon nanotubes into the polymer. Similarly, different polymeric nanocomposites such as graphene-polypropylene, exfoliated graphite-poly(methyl methacrylate), graphene-polycarbonate, graphene oxide-poly(ethylene-2,6-naphthalate) have been prepared via melt blending for different applications [76].

However, the distribution of filler into the polymer matrix is less efficient in case of melt blending as compared to the solution blending due to the higher viscosity of melt, which can be further enhanced by modifying the surface of fillers, tuning the interactions between the filler and polymer matrix, using solvent together with melt processing, etc. For instance, the distribution of graphene nanoplatelet into the polypropylene matrix was enhanced by using solvent (mixture of *p*-xylene and *N*,*N*-dimethylform-amide)-assisted melt blending process, which eventually resulted in better mechanical properties of nanocomposites [47].

In another study, the dispersion of filler (carbon black, carbon nanotube, and graphene nanoplatelet) into the polymer matrix was enhanced by installing an ultrasonic device at the extruder [96]. The vibration caused by the ultrasonic device helped

in breaking the filler aggregates (or removing the air trapped inside the polymer) during mixing and hence, enhancing the filler distribution. Likewise, the dispersion of graphene sheets in polypropylene (PP) was improved by modifying PP by using triethylaluminum and rar-Ethylenebis(1-indenyl) zirconium dichloride ($EBIZrCI_2$), which resulted in terminally hydroxylated PP [21]. The modified PP and graphene sheets were first heated in tetradecane at 200 °C followed by melt mixing with PP, in order to prepare the nanocomposite.

Moreover, the application of high temperature for melt blending is known to damage the surface modification of fillers, leading to inhomogeneous distribution of filler. For instance, alkyl ammonium modified organoclays was observed to degrade at temperatures greater than 140 °C, whereas the melt blending temperature was within the range of 190–220 °C [2]. This issue can be solved by using the thermally stable modification of filler or by performing the blending process at lower temperatures [58]. Hence, in order to attain good dispersion of filler and better mechanical properties of nanocomposites, several parameters are important to consider including surface modification of fillers, processing conditions, and compatibility between filler and matrix.

2.1.2 Solution Blending

Solution blending is another common processing method for producing polymeric nanocomposites. The overall procedure can be divided into three steps: (i) dispersion of nanofiller in appropriate solvent using agitation, (ii) mixing of polymer and nanofiller solutions, and (iii) removal of solvent by evaporation or solvent coagulation [29]. Polymers are typically dissolvable in a variety of solvents including water, cyclohexane, chloroform, acetone, dimethylformamide (DMF), toluene, tetrahydrofuran, etc. [54]. The selection of suitable solvent is mainly governed by the dispersibility of nanofiller and/or solubility of polymer [7]. The same solvent can be used for both nanofiller and polymer matrix. This method facilitates the dispersion of nanofiller into the polymer matrix with the help of solvent. However, this synthetic approach is not suitable for the insoluble polymers. Moreover, the removal of solvent imposes environmental restrictions, which limits its applicability from small scale to industrial scale [79].

For example, Marroquin and colleagues prepared chitosan-based nanocomposite by dispersing Fe_3O_4 and multi-walled carbon nanotubes (MWCNTs) using solvent blending [52]. Firstly, the nanofillers (Fe_3O_4 and MWCNTs) were distributed in distilled water by ultrasonication for 1 h, followed by the addition of chitosan and acetic acid. Magnetic stirring of the mixture was performed for 2 h and then ultrasonicated for 30 min. The prepared mixture was then degassed and vacuum dried to produce the nanocomposite. Likewise, Taha and Alzara reported the development of polyvinyl alcohol (PVA) and $SrTiO_3$-based nanocomposites [78]. PVA powder was firstly dissolved in distilled water at 80 °C and stirred for 60 min. $SrTiO_3$ powder was then incorporated into the PVA solution and agitated for 1 h. The resulting mixture

was poured into a glass dish and dried at 80 °C. In another study, the poly(ether-ether-ketone) (PEEK) and MWCNTs-based nanocomposites have been synthesized via solution blending [39]. First of all, *N*-methyl-2-pyrrolidone (NMP) solvent was used to disperse MWCNTs by ultrasonication for 15 min. PEEK powder was dissolved in dichloroacetic acid (DCA) at 185 °C and cooled down to room temperature. The PEEK solution was then added into the MWCNTs solution and manually shaken to mix the solution. The resulting mixture was filtered and washed with methanol and deionized water to remove the residual solvents. The obtained precipitates were dried at 80 °C to obtain nanocomposite powder, which were finally injection molded to prepare the required samples.

In addition to the single polymer matrix, binary/ternary polymer mixture has also been reported in literature to prepare nanocomposites. For example, Lu and colleagues produced nanocomposites, based on boron nitride (BN) as a filler and mixture of polystyrene (PS) and polypropylene (PP) as a polymer matrix, through solution blending method [48]. Polystyrene particles were firstly dissolved in DMF at 80 °C via magnetic stirring followed by the addition of BN platelets into the PS solution and vigorously stirred. The PP microspheres were then added into the PS/BN mixture and coagulated in deionized water. The resultant granules were filtered, washed by DI water, and dried at 80 °C. The characterization samples were prepared by pressing the granules at 170 °C under 10 MPa for 15 min. In order to further enhance the filler distribution and to avoid the filler aggregation and stack up problems, grafting to/from and chemical functionalization approaches are typically used to prepare polymeric nanocomposite. For instance, phase transfer techniques [22], lyophilization methods [20], and surfactants [46] were utilized to facilitate the solution blending of graphene into the polymer matrix.

2.2 In Situ Polymerization

In situ polymerization method is a bottom-up approach in which polymers and nanomaterials are formed within the final composite system with the help of series of chemical reactions catalyzed by suitable agents (radiation, heat, initiator, catalyst, etc.) [7]. Typically, there are three approaches for preparing polymeric nanocomposites using in situ method: (i) Nanomaterial precursor is preloaded onto the polymer matrix, which forms required nanomaterial after chemical reaction, (ii) monomers (instead of polymer matrix) along with the nanomaterials forms the starting mixture, and (iii) both monomers and nanomaterial precursors are mixed through an appropriate solvent, followed by the in situ polymerization and chemical reactions to form nanomaterials [87]. The second option (combination of monomer and nanomaterial) avoids the aggregation of nanofiller within the polymer matrix, which eventually results in excellent dispersion of nanofiller and better interfacial interaction with polymers. Moreover, this second approach also alters the physical characteristics of the resultant polymer nanocomposite due to the intercalation or grafting of polymer structures within/on the layers of nanomaterials. This intercalation and homogeneous

distribution of nanomaterials within the polymer matrix allows the development of partially exfoliated structures [29]. However, this method also has several limitations such as requirement of expensive reactants, complex processing steps, and not suitable for all types of polymers and elastomers [79].

The production of polypyrrole and reduced graphene oxide (r-GO)-based nanocomposites using chemical oxidative in situ polymerization method has been reported [75]. The nanomaterial was dispersed in CTAB/APS mixture using ultrasonic bath for 10 h. Pyrrole monomer was then added to this stable suspension, and the required nanocomposite was obtained after the polymerization. The prepared nanocomposite was washed, followed by overnight drying in a vacuum oven at 60 °C. Likewise, polymeric nanocomposites based on polyaniline and montmorillonite using in situ polymerization approach have been fabricated [41]. In short, clay particles were distributed in distilled water using ultrasonicator for 10 min. Then, the solution of aniline in HCl was slowly added to the clay suspension, followed by the slow addition of APS (oxidizing agent) under magnetic stirring. For complete polymerization at 0 °C, the suspension was stirred for 4 h and a dark green polymer nanocomposite was obtained by vacuum filtration. The obtained composite was washed with water and acetone followed by overnight drying in vacuum oven at 50 °C.

Hou and colleagues reported the preparation of nanocomposites based on waterborne polyurethane (WPU) as a polymer matrix and combination of graphene oxide (GO) and carbon black (CB) as nanomaterials [36]. First of all, the mixture of monomer (isophorone diisocyanate) and polypropylene glycol was stirred in a container at 85 °C for 3 h. Then, mixture of NMP/DMPA along with the few drops of dibutyltin dilaurate was incorporated into the system under stirring for 2 h, to obtain NCO-terminated prepolymer. Nanomaterials (CB and GO) were then dispersed in the prepared mixture and stirred at high speed for 2 h. Neutralizer (TEA) and viscosity reducer (acetone) were added, and the mixture was stirred for 45 min and cooled down to 45 °C. Mixture of EDA and water was then added dropwise under extensive stirring, and the nanocomposite dispersion was finally obtained. Similarly, the highly conductive polymeric nanocomposites based on polypyrrole and Zeolite nanoparticles using in situ polymerization method have been synthesized [35]. Firstly, nanoparticles were dispersed into the mixture of distilled water and CH_3Cl by stirring for 1 h. Then, monomer was incorporated into the suspension with continuous stirring for 4 h. After 3 h, the obtained composite material was filtered, washed, and dried in an oven. The oxidizing agent ($FeCl_3$) was then added dropwise to initiate the polymerization process at 0 °C or 25 °C. In another study, Nicosia and colleagues compared the photocatalytic activity of TiO_2-poly(methyl methacrylate) nanocomposites synthesized by solution blending and in situ polymerization for water pollution remediation [60]. The results revealed that the chemical-physical interactions between the nanomaterials and polymer matrix was significantly influenced by in situ polymerization approach, which eventually boosted the photocatalytic degradation of dyes.

2.3 Sol–Gel Method

Synthesis of polymeric nanocomposites via sol–gel method is an old technique; however, recently, it is getting famous for preparing structurally advanced and functionalized hybrid materials. This method is quite similar to the in situ polymerization method, which involves the nanomaterial precursor and polymer matrix along with the suitable reagent (solvent, heating, radiation, etc.). In short, the nanomaterial precursor is dissolved in a suitable solvent and mixed with polymer matrix in precise molar ratios [87]. This mixture then undergoes a series of hydrolytic (or non-hydrolytic in case of organic solvents) and condensation reactions followed by nucleophilic substitution reaction facilitated by polymer matrix, which results in sol formation. Sol can be understood as a colloidal suspension having almost non-interacting particles. This sol then converts into a (wet) gel system due to the crosslinking reactions and the formation of interconnected network of particles facilitated by agitation and/or temperature changes. This wet gel eventually leads to the formation of polymeric nanocomposite after the drying procedure [67]. Typical nanomaterials used for preparing polymer nanocomposites through sol–gel technique include alumina, silica, titania, and vanadia. However, silica-based materials are commonly used because of their lower cost and highly stable Si–O bond [65]. In this method, polymer nanocomposites are synthesized by having either physical or chemical interactions between the inorganic nanomaterials and organic polymers. This method does not involve separate steps or additional energy to distribute the nanomaterials within the polymer matrix. Other benefits of this technique include high purity and uniformity of product, low sintering temperature, easily controllable reaction, better forming ability, etc. On the other hand, this method also inherits some drawbacks such as requirement of expensive and toxic precursors, difficulty in making crystalline nanocomposites, brittle fracture of product due to the volatility of solvents, and longer preparation times (i.e., few days to weeks) [79].

For instance, Factori and colleagues reported the development of polymer nanocomposite based on ZnO and poly(vinyl alcohol) (PVA) via sol–gel technique under microwave heating [26]. PVA was firstly dissolved in hot DI water followed by the incorporation of ethyl alcohol, acetic acid, and $Zn(NO_3)_2.6H_2O$ into the solution. The prepared solution was then poured into the round bottom flask and placed on a microwave reactor. The mixture was maintained at 100 °C via microwave irradiation of varying power as a heating source, which eventually resulted in polymer nanocomposite. Phase inversion phenomenon was further used to prepare polymer nanocomposite films. Likewise, Besancon et al. used non-hydrolytic sol–gel technique along with reactive extrusion to produce polypropylene (PP) and titanium dioxide-based polymer nanocomposites [16]. PP was firstly added into the co-rotating twin screw extruder at 200 °C followed by the addition of nanomaterial precursor and other reactants. After adding reactants, the temperature was increased up to 240 °C in a certain region of extruder. A vacuum pump was installed to extract the by-products. The prepared nanocomposite was obtained at the exit of die and cooled under air flow. In order to further remove the residual by-products, Soxhlet extraction technique was

used with ethyl acetate as a solvent at 110 °C for 72 h. In another study, Behnam and colleagues fabricated the polyurethane and carbon nanotubes (CNTs)-based polymer nanocomposites with enhanced thermal stability using sol–gel method [14]. In short, CNTs were distributed in tetrahydrofuran (THF) and sonicated for 30 min followed by the addition of polyurethane, tetraethyl orthosilicate (TEOS), and DI water into the mixture. Then, formic acid was incorporated into the mixture under continuous stirring until complete solvent evaporation.

2.4 Electrochemical Synthesis

Electrochemical synthesis is a simple chemical procedure for preparing polymeric nanocomposites, which is typically performed on electrochemical workstation. Commonly used monomers for this processing technique include aniline, thiophene, and pyrrole [65]. Generally, there are three electrodes present during the electrochemical synthesis: (i) working electrode, (ii) counter electrode, and (iii) reference electrode. This methodology is an excellent way to directly prepare the polymeric nanocomposite film on the surface of electrode. The main controlling parameters of electrochemical synthesis process include current density or applied potential and the amount of charges integrated in the system. This approach offers many advantages including operational simplicity, short reaction time, eco-friendly, and easier to control. Moreover, this technique avoids the use of oxidant; hence, greater purity of the final product can be achieved. However, the mass production using this technique is not feasible because of the limited surface area of the working electrode [79].

For example, Fani and colleagues reported the fabrication of polymeric nanocomposite biosensor based on polypyrrole, reduced graphene oxide, and gold nanoparticles via electrochemical method [28]. In short, the working electrode (screen printed carbon electrode) was first cleaned with H_2SO_4 and DI water followed by drying at room temperature. Then, the mixture of reduced graphene oxide, pyrrole, $HAuCl_4$, and l-Cys in PBS was sonicated for 20 min and electrodeposited onto the electrode surface using voltammetric sweep. Similarly, Saeb and Zenali synthesized the polymeric nanocomposite (polyaniline-TiO_2-gold nanoparticles) sensor for hydrazine detection using electrochemical technique [71]. Firstly, the electrode (glassy carbon electrode) surface was polished using 0.3 mm alumina-based abrasive paper followed by rinsing with deionized (DI) water. The electrode was then sonicated for 10 min in a mixture of water and ethanol, in order to eliminate the remaining alumina particles. TiO_2 nanoparticles were dispersed in DI water by using ultrasonicator for 30 min and then dropped onto the electrode surface and allowed to dry at ambient temperature. After drying, the electrode was rinsed with DI water to remove the residual nanoparticles. The prepared electrode was then submerged in a mixture of aniline and H_2SO_4, and the electro-polymerization of aniline was performed with a potential window of −0.2 to 0.8 V for 5 cycles. Then, the solution of Au in chloroauric acid was electrodeposited on the electrode surface using cyclic voltammetry.

In another study, Yan and colleagues fabricated the multi-layer polymer nanocomposite (chitosan silver nanoparticles) coating for pH-dependent controlled release of active compounds using a two-step electrochemical synthesis approach [86]. The electrodeposition of chitosan was performed by using a two-electrode workstation: (i) working electrode made of stainless steel wire of 0.4 mm diameter and (ii) counter electrode made of platinum wire. All the electrodes were sonicated in ethanol, acetone, and water for 5 min for removing the impurities. Then, the two electrodes were partially immersed in chitosan solution (chitosan and nitric acid), and a constant current density (2.5 A m^{-2}) was applied for particular time. In the next step, the chitosan-coated electrode was soaked in the solution of $AgNO_3$ and $NaNO_3$ for 12 h to allow complete loading of silver ions. The electrode was removed from the solution, then gently washed with DI water followed by the application of a cathodic voltage (5 V) for particular time to allow the electrochemical reduction of silver ions to the nanoparticles. In the end, the prepared polymeric nanocomposite was washed with DI water, removed from the electrode surface using tweezers, and freeze-dried for further analysis.

2.5 Nonconventional Methods

In addition to the above-mentioned techniques, researchers have investigated some other approaches as well such as template-based synthesis, electrospinning to produce polymer nanocomposites with improved properties due to the better dispersion of nanofiller into the polymer matrix.

2.5.1 Template-Based Synthesis

In this approach, an inert material acts as a framework or skeleton for the in situ polymerization of monomer. The template-based synthesis is typically used to prepare polymer nanocomposites with porous structures. For example, Wang et al. reported the sacrificial template synthesis of N-doped carbon, molybdenum disulfide (MoS_2) nanosheets, and polypyrrole (PPy)-based hollow nanocomposites for sodium storage performance [84]. The result showed that the MoS_2 nanosheets were protected by PPy and N-doped carbon via Mo–N bonds, which inhibits the volume change and prevents the aggregation and fracture of electrode. Moreover, the external PPy and inner N-doped carbon effectively accelerated the Na-ion transport. Likewise, Zhang et al. [94] produced PPy nanostructure with platinum and gold nanoparticles using a reactive template based on manganese oxide (MnO_2) nanowires. The reactive template (MnO_2 nanowires) induced one-dimensional polymerization of monomers, and the simultaneous dissolution of template provided the hollow tube-like structure. The nanoparticles content in the prepared nanocomposites can simply be varied by manipulating the amount of precursors. However, this technique is not suitable when complex composite system is required.

2.5.2 Electrospinning Method

This method is typically used to prepare polymer nanocomposites in the form of nanofibers by applying high voltage. This approach is a modification of solvent blending; i.e., polymer and nanomaterial are dispersed/dissolved into a solvent to obtain homogeneous solution. Then, a hydraulic syringe is filled with this solution, and the nanofibers are extruded under high voltage to overcome the surface tension. For example, [19] utilized electrospinning technique to prepare poly(ethylene oxide) or poly(vinyl pyrrolidone) and iron oxide nanoparticles-based nanofibrous network. Metal organic framework based on poly(methyl methacrylate) and zirconium via electrospinning technique has been synthesized [53]. This approach is highly suitable to produce uniform morphology and size of nanofibers. Table 2 provides an overview of different polymer nanocomposites along with their synthesis route.

3 Conclusion

Synthesis of hybrid nanocomposites based on organic (polymer) and inorganic components has gained serious attention of researchers due to their extensive range of applications. Integration of inorganic nanomaterials to polymeric components is excellent tool to confer their unique characteristics to polymeric materials. Polymeric nanocomposites showed great conductivity, large surface area, high porosity, significant catalytic, electric and optical potential. These composites may possess weak interactions like hydrogen bonding and Van der Waals forces, and some nanocomposites possess strong interactions at the interface as well. Different synthetic routes have been developed for the preparation of polymeric nanocomposites as in situ polymerization, melt blending, solution blending, sol–gel, and electrochemical synthesis. The polymeric nanocomposites synthesized through these approaches showed intriguing features which have been explored in applications of electronic devices, different sensors, and in biomedicines. Different synthetic approaches have different limitations such as direct mixing process involves the dispersion of desired nanomaterial into polymer matrix either by melt, mechanical, or solution blending. However, uniform distribution of nanomaterial is a major challenge of this approach. In contrast, in situ polymerization method solves the above-mentioned problem by creating a polymer microenvironment to synthesize the desired nanomaterial from its precursors through series of reactions. This method is gaining interest because of the ease of controlling the morphology and particle size within the composite. Still problem exists to enhance the conductivity control, the morphology, shape size, and composition of polymeric nanocomposites, so future developments must focus on improving the synthetic protocols, and novel assembly approaches should be introduced.

Table 2 Overview of different polymer nanocomposites prepared via different techniques

Polymer material	Inorganic material	Composite preparation method	Application	Refs.
Polyamide	Organoclay	In situ polymerization	–	[10]
Polyaniline	Montmorillonite	In situ polymerization	Removal of dye	[41]
Polypyrrole	Molybdenum diselenide	In situ polymerization	Photocatalytic degradation of dye	[57]
Poly(methyl methacrylate)	Titanium dioxide	In situ polymerization	Photocatalytic degradation of xenobiotic	[60]
Polyaniline	Graphene oxide-camphorsulfonic acid	In situ polymerization	Electromagnetic wave absorption and anti-corrosion	[85]
Polyaniline	Graphene oxide	In situ polymerization	Removal of dye	[4]
Polyaniline	Manganese dioxide	In situ polymerization	Energy storage	[38]
Polypyrrole	Zeolite	In situ polymerization	Electrode for super-capacitors	[35]
Polyimide	Paraffin-barium titanate	In situ polymerization	Energy storage	[64]
Polyaniline-chitosan	Montmorillonite	Intercalation and in situ polymerization	Removal of dye	[56]
Poly(*o*-anisidine)	Carbon nanotubes-graphene	In situ polymerization	Electrode for super-capacitors	[17]
Poly(methyl methacrylate)	Graphene nanoplatelets	In situ polymerization	Gamma-ray absorption	[15]
Polyaniline	Phosphotungstic acid-titania	In situ polymerization	Anode for methanol fuel cells	[45]
Polyaniline	Reduced graphene oxide-zinc oxide	In situ polymerization	Electrode for super-capacitors	[62]

(continued)

Table 2 (continued)

Polymer material	Inorganic material	Composite preparation method	Application	Refs.
Polyaniline	Graphene oxide-titanium dioxide	In situ polymerization	Photocatalytic degradation of dye	[12]
Polyaniline	Cadmium sulfide quantum dots	In situ polymerization	Solar cell and photovoltaic	[66]
Polyaniline	Graphene oxide-manganese sulfide	In situ polymerization	Electrode for super-capacitors	[88]
Polypyrrole	Zinc spinel ferrite-silicon dioxide	Sol–gel and in situ polymerization	Electromagnetic wave absorption	[32]
Polypyrrole	Nickel zinc ferrite	In situ polymerization	Degradation of organic pollutants	[59]
Polypyrrole	Zinc ferrite-graphitic carbon nitride	In situ polymerization	Degradation of organic pollutants	[23]
Poly(methyl methacrylate)	Reduced graphene oxide-hematite	In situ polymerization	Energy storage	[82]
Waterborne polyurethane	Graphene oxide	In situ polymerization	Anti-corrosion	[36]
Polypyrrole	Aluminum fumarate metal–organic framework	In situ polymerization	Removal of heavy metal	[90]
Polyaniline	Nickel zinc ferrite	In situ polymerization	Electromagnetic wave absorption	[43]
Poly(butylene succinate)	Nanoboehmite	In situ polymerization	–	[40]
Poly(methyl methacrylate)	MXene-zinc oxide	In situ polymerization	Dielectric materials	[83]
Polyindole	Copper–alumina	In situ polymerization	Sensing of ammonia gas	[72]
Polypyrrole	Titanium dioxide	Polymerization followed by sonication	Degradation of organic pollutants	[89]

(continued)

Table 2 (continued)

Polymer material	Inorganic material	Composite preparation method	Application	Refs.
Polythiophene	Zinc oxide	Sol–gel and in situ polymerization	Degradation of organic pollutants	[27]
Poly(vinyl alcohol)	Zinc oxide	Microwave-assisted sol–gel	UV shielding and anti-microbial	[26]
Polypropylene	Titanium dioxide	Sol–gel and reactive extrusion	–	[16]
Poly(vinyl alcohol)	Zinc oxide	Sol–gel and self-propagation	Electrode material and electrochemical sensor	[1]
Poly(vinyl chloride)	Cadmium sulfide	Sol–gel and spin coating	Photocatalytic degradation of dye	[70]
Polyamide	Hydroxylated boron nitride	Melt blending	Thermal management	[34]
Poly(methyl methacrylate)	Alumina	Melt blending	–	[9]
Poly(vinyl alcohol)-poly(vinyl pyrrolidone)	Montmorillonite	Melt blending	Dielectric material	[73]
Polylactide-polycaprolactone	Silicon dioxide-multi-walled carbon nanotubes	Melt blending	EMI shielding	[49]
Polypropylene	Multi-walled carbon nanotubes	Melt blending	Wear resistance	[63]
High-density polyethylene	Calcium carbonate	Melt blending	Dielectric material	[5]
Polypropylene-polylactide	Nanoclay	Melt blending	Biodegradable material	[51]
High-density polyethylene	Electrochemically exfoliated graphene	Melt blending	–	[11]
Linear low-density polyethylene-poly(ethylene-co-methyl acrylate)	Graphene-carbon nanotubes	Melt blending	–	[61]

(continued)

Table 2 (continued)

Polymer material	Inorganic material	Composite preparation method	Application	Refs.
Poly(butylene adipate-co-terephthalate)	Multi-walled carbon nanotube-zinc oxide	Melt blending	Packaging material	[30]
Poly(vinyl alcohol)	Strontium titanate	Solution blending	Dielectric materials	[78]
Chitosan	Graphene oxide	Solution blending	Electrical and opto-electronic devices at high frequency	[25]
Poly(ether-ether-ketone)	Multi-walled carbon nanotubes	Solution blending	High-temperature applications	[39]
Poly(ethylene-co-vinyl acetate)	α-zirconium phosphate	Solution blending	–	[95]
Poly(vinyl pyrrolidone)-poly(ethylene oxide)	Alumina-silica	Solution blending	Optical and opto-electronic devices	[24]
Polyaniline-sulfonated polyetherimide	Sodium alanate-multi-walled carbon nanotubes-titanium dioxide	Solution blending	Hydrogen storage	[13]
Polystyrene-polypropylene	Boron nitride	Solution blending and hot pressing	Thermal management material	[48]
Polyurethane	Functionalized graphene-functionalized carbon nanotubes	Solution blending	–	[69]
Poly(vinyl alcohol)	Graphene oxide-sodium montmorillonite	Solution blending and evaporation	Removal of dye	[8]
Poly(vinyl alcohol)-poly(vinyl pyrrolidone)	Nanographene	Solution blending	–	[37]
Polypyrrole	Reduced graphene oxide-gold nanoparticles	Electrochemical synthesis	Virus DNA detection	[28]

(continued)

Table 2 (continued)

Polymer material	Inorganic material	Composite preparation method	Application	Refs.
Poly(*N*-phenyl-o-phenylenediamine)	Titanium carbide-titanium dioxide	Electrochemical synthesis	Uric acid detection	[91]
Chitosan	Silver nanoparticles	Electrochemical synthesis	Biomedical and tissue engineering	[86]
Polypyrrole	Reduced graphene oxide-multi-walled carbon nanotubes	Electrochemical synthesis	Dopamine detection	[42]
Polyaniline	Titanium oxide-gold nanoparticles	Electrochemical synthesis	Hydrazine detection	[71]
Polyaniline	Reduced graphene oxide-gold nanoparticles-manganese dioxide	Electrochemical synthesis	Electrode for super-capacitors	[80]
Polyaniline	Reduced graphene oxide-silver nanoflower	Electrochemical synthesis	DNA detection	[81]
Poly(3,4-ethylenedioxythiophene)-poly(thiomethyl 3,4-ethylenedioxythiophene)	Gold nanoparticles	Electrochemical synthesis	Nitrite detection	[31]
Polyaniline	Graphitic carbon nitride-cadmium oxide	Electrochemical synthesis	Detection of antibiotics	[18]
Chitosan	Manganese oxide-aluminum oxyhydroxide	Electrochemical synthesis	Removal of organic pollutants	[77]
Polyaniline	Graphitic carbon nitride-titanium dioxide	Electrochemical polycondensation and soaking adsorption	Removal of organic pollutants	[97]

(continued)

Table 2 (continued)

Polymer material	Inorganic material	Composite preparation method	Application	Refs.
Poly(vinyl pyrrolidone)	Bismuth oxybromide	Precipitation	Removal of organic pollutants	[92]
Polythiophene	Bismuth oxyiodide	In situ precipitation	Removal of organic pollutants	[50]
Polythiophene	Manganese oxide	Mechanical mixing and sonication	Removal of organic pollutants	[98]
Polyaniline	Indium oxide	Impregnation method	Removal of organic pollutants	[93]

References

1. Abebe B, Murthy HCA, Zereffa EA, Adimasu Y (2021) Synthesis and characterization of ZnO/PVA nanocomposites for antibacterial and electrochemical applications. Inorg Nano-Metal Chem 51(8):1127–1138. https://doi.org/10.1080/24701556.2020.1814338
2. Abedi S, Abdouss M (2014) A review of clay-supported Ziegler-Natta catalysts for production of polyolefin/clay nanocomposites through in situ polymerization. Appl Catal A 475:386–409
3. Al-Saleh MH, Abdul Jawad S (2016) Graphene nanoplatelet-polystyrene nanocomposite: dielectric and charge storage behaviors. J Electron Mater 45(7):3532–3539. https://doi.org/10.1007/s11664-016-4505-6
4. Ali Khan M, Govindasamy R, Ahmad A, Siddiqui MR, Alshareef SA, Hakami AAH, Rafatullah M (2021) Carbon based polymeric nanocomposites for dye adsorption: synthesis, characterization, and application. Polymers 13(3):419
5. Ali SFA, Elsad RA, Mansour SA (2021) Enhancing the dielectric properties of compatibilized high-density polyethylene/calcium carbonate nanocomposites using high-density polyethylene-g-maleic anhydride. Polym Bull 78(3):1393–1405. https://doi.org/10.1007/s00289-020-03164-w
6. Alig I, Pötschke P, Lellinger D, Skipa T, Pegel S, Kasaliwal GR, Villmow T (2012) Establishment, morphology and properties of carbon nanotube networks in polymer melts. Polymer 53(1):4–28
7. Amor G, Vázquez A, Kharisov BI (2021) Chapter 17—greener synthesis of nanocomposites and nanohybrids. In: Kharisov B, Kharissova O (eds) Handbook of greener synthesis of nanomaterials and compounds. Elsevier, Amsterdam, pp 389–404
8. Arabkhani P, Asfaram A, Ateia M (2020) Easy-to-prepare graphene oxide/sodium montmorillonite polymer nanocomposite with enhanced adsorption performance. J Water Process Eng 38:101651. https://doi.org/10.1016/j.jwpe.2020.101651
9. Arimatéia RR, Hanken RB, Oliveira AD, Agrawal P, Freitas NL, Silva ES et al (2021) Effect of alumina on the properties of poly(methyl methacrylate)/alumina composites obtained by melt blending. J Thermoplast Compos Mater 34(4):451–471. http://doi.org/10.1177/0892705719843167
10. Baniasadi H, Trifol J, Ranta A, Seppälä J (2021) Exfoliated clay nanocomposites of renewable long-chain aliphatic polyamide through in-situ polymerization. Compos B Eng 211:108655. https://doi.org/10.1016/j.compositesb.2021.108655
11. Bansala T, Verma P, Vashisth A, Hope JT, Yakovlev S, Uppili S et al (2021) High-density polyethylene reinforced by low loadings of electrochemically exfoliated graphene via melt recirculation approach. J Appl Polym Sci 138(20):50448. http://doi.org/10.1002/app.50448
12. Baruah S, Kumar S, Nayak B, Puzari A (2021) Optoelectronically suitable graphene oxide-decorated titanium oxide/polyaniline hybrid nanocomposites and their enhanced photocatalytic activity with methylene blue and rhodamine B dye. Polym Bull 78(3):1703–1720. https://doi.org/10.1007/s00289-020-03182-8
13. Beatrice CAG, Moreira BR, de Oliveira AD, Passador FR, de Almeida Neto GR, Leiva DR, Pessan LA (2020) Development of polymer nanocomposites with sodium alanate for hydrogen storage. Int J Hydrogen Energy 45(8):5337–5346. https://doi.org/10.1016/j.ijhydene.2019.06.169
14. Behnam R, Roghani-Mamaqani H, Salami-Kalajahi M (2019) Preparation of carbon nanotube and polyurethane-imide hybrid composites by sol–gel reaction. Polym Compos 40(S2):E1903–E1909. https://doi.org/10.1002/pc.25193
15. Bel T, Muhammettursun M, Kocacinar E, Erman E, Gul FB, Dogan E et al (2021) Improvement of thermal stability and gamma-ray absorption in microwave absorbable poly(methyl methacrylate)/graphene nanoplatelets nanocomposite. J Appl Polym Sci 138(36):50897. http://doi.org/10.1002/app.50897
16. Besançon M, Wang Y, Ylla N, Cinquin V, Mutin H, Alauzun J et al (2021) Non-hydrolytic sol–gel synthesis of polypropylene/TiO_2 composites by reactive extrusion. J Sol-Gel Sci Technol 99(1):39–54. http://doi.org/10.1007/s10971-021-05548-4

17. Bonakdar M, Hosseini SR, Ghasemi S (2021) Poly(o-anisidine)/carbon nanotubes/graphene nanocomposite as a novel and cost-effective supercapacitor material. Mater Sci Eng B 267:115099. https://doi.org/10.1016/j.mseb.2021.115099
18. Bonyadi S, Ghanbari K, Ghiasi M (2020) All-electrochemical synthesis of a three-dimensional mesoporous polymeric g-C3N4/PANI/CdO nanocomposite and its application as a novel sensor for the simultaneous determination of epinephrine, paracetamol, mefenamic acid, and ciprofloxacin. New J Chem 44(8):3412–3424. https://doi.org/10.1039/C9NJ05954G
19. Burke L, Mortimer CJ, Curtis DJ, Lewis AR, Williams R, Hawkins K et al (2017) In-situ synthesis of magnetic iron-oxide nanoparticle-nanofibre composites using electrospinning. Mater Sci Eng C 70:512–519. http://doi.org/10.1016/j.msec.2016.09.014
20. Cao Y, Feng J, Wu P (2010) Preparation of organically dispersible graphene nanosheet powders through a lyophilization method and their poly(lactic acid) composites. Carbon 48(13):3834–3839. https://doi.org/10.1016/j.carbon.2010.06.048
21. Chammingkwan P, Matsushita K, Taniike T, Terano M (2016) Enhancement in mechanical and electrical properties of polypropylene using graphene oxide grafted with end-functionalized polypropylene. Materials 9(4):240
22. Choi E-Y, Han TH, Hong J, Kim JE, Lee SH, Kim HW, Kim SO (2010) Noncovalent functionalization of graphene with end-functional polymers. J Mater Chem 20(10):1907–1912. https://doi.org/10.1039/B919074K
23. Das KK, Patnaik S, Mansingh S, Behera A, Mohanty A, Acharya C, Parida KM (2020) Enhanced photocatalytic activities of polypyrrole sensitized zinc ferrite/graphitic carbon nitride n-n heterojunction towards ciprofloxacin degradation, hydrogen evolution and antibacterial studies. J Colloid Interface Sci 561:551–567. https://doi.org/10.1016/j.jcis.2019.11.030
24. Dhatarwal P, Sengwa RJ (2021) Nanofiller controllable optical parameters and improved thermal properties of (PVP/PEO)/Al_2O_3 and (PVP/PEO)/SiO_2 nanocomposites. Optik 233:166594. https://doi.org/10.1016/j.ijleo.2021.166594
25. Dhayal V, Hashmi SZ, Kumar U, Choudhary BL, Dalela S, Dolia SN, Alvi PA (2021) Optical and electrical properties of biocompatible and novel (CS–GO) polymer nanocomposites. Opt Quant Electron 53(1):53. https://doi.org/10.1007/s11082-020-02723-9
26. Factori IM, Amaral JM, Camani PH, Rosa DS, Lima BA, Brocchi M et al (2021) ZnO nanoparticle/poly(vinyl alcohol) nanocomposites via microwave-assisted sol–gel synthesis for structural materials, UV shielding, and antimicrobial activity. ACS Appl Nano Mater 4(7):7371–7383. http://doi.org/10.1021/acsanm.1c01334
27. Faisal M, Harraz FA, Jalalah M, Alsaiari M, Al-Sayari SA, Al-Assiri MS (2020) Polythiophene doped ZnO nanostructures synthesized by modified sol-gel and oxidative polymerization for efficient photodegradation of methylene blue and gemifloxacin antibiotic. Mater Today Commun 24:101048. https://doi.org/10.1016/j.mtcomm.2020.101048
28. Fani M, Rezayi M, Pourianfar HR, Meshkat Z, Makvandi M, Gholami M, Rezaee SA (2021) Rapid and label-free electrochemical DNA biosensor based on a facile one-step electrochemical synthesis of rGO–PPy–(L-Cys)–AuNPs nanocomposite for the HTLV-1 oligonucleotide detection. Biotechnol Appl Biochem 68(3):626–635. https://doi.org/10.1002/bab.1973
29. Fawaz J, Mittal V (2014) Synthesis of polymer nanocomposites: review of various techniques. In: Synthesis techniques for polymer nanocomposites, pp 1–30
30. Ge F-F, Tsou C-H, Yuan S, De Guzman MR, Zeng C-Y, Li J et al (2021) Barrier performance and biodegradability of antibacterial poly(butylene adipate-co-terephthalate) nanocomposites reinforced with a new MWCNT-ZnO nanomaterial. Nanotechnology 32(48):485706. http://doi.org/10.1088/1361-6528/ac1b52
31. Ge Y, Jamal R, Zhang R, Zhang W, Yu Z, Yan Y et al (2020) Electrochemical synthesis of multilayered PEDOT/PEDOT-SH/Au nanocomposites for electrochemical sensing of nitrite. Microchim Acta 187(4):248. http://doi.org/10.1007/s00604-020-4211-1
32. Ge Y, Li C, Waterhouse GIN, Zhang Z, Yu L (2021) $ZnFe_2O_4$@SiO_2@polypyrrole nanocomposites with efficient electromagnetic wave absorption properties in the K and Ka band regions. Ceram Int 47(2):1728–1739. https://doi.org/10.1016/j.ceramint.2020.08.290

33. Guo F, Aryana S, Han Y, Jiao Y (2018) A review of the synthesis and applications of polymer-nanoclay composites. Appl Sci 8(9):1696
34. Guo H, Xu T, Zhou S, Jiang F, Jin L, Song N, Ding P (2021) A technique engineered for improving thermal conductive properties of polyamide-6 composites via hydroxylated boron nitride masterbatch-based melt blending. Compos B Eng 212:108716. https://doi.org/10.1016/j.compositesb.2021.108716
35. Hamidouche F, Ghebache Z, Boudieb N, Sanad MMS, Djelali N-E (2021) Enhancing the supercapacitive and conductivity properties of polypyrrole via in-situ polymerization with HY zeolite nanoparticles. J Inorg Organomet Polym Mater 31(2):704–715. https://doi.org/10.1007/s10904-020-01707-2
36. Hou L, Zhou M, Gu Y, Chen Y (2020) WPU/CB/GO nanocomposites: in situ polymerization preparation, thermal, and anticorrosion performance evaluation. J Appl Polym Sci 137(21):48716. https://doi.org/10.1002/app.48716
37. Hussein S, Abd-Elnaiem A, Ali N, Mebed A (2020) Enhanced thermo-mechanical properties of poly(vinyl alcohol)/poly(vinyl pyrrolidone) polymer blended with nanographene. Curr Nanosci 16(6):994–1001. https://doi.org/10.2174/1573413716666200310121947
38. Izwan Misnon I, Jose R (2021) Charge storage in the PANI–α-MnO_2 polymer–nanocomposite system. Mater Today Proc 41:513–519. https://doi.org/10.1016/j.matpr.2020.05.235
39. Jiang Z, Chen Q, Zhu Z, Tsai C-Y, Zhao M, Sue H-J et al (2021) Well-dispersed poly(ether-ether-ketone)/multi-walled carbon nanotube nanocomposites prepared via a simple solution mixing approach. Polym Int 70(8):1090–1098. http://doi.org/10.1002/pi.6227
40. Kahkesh S, Rafizadeh M (2020) Flame retardancy and thermal properties of poly(butylene succinate)/nano-boehmite composites prepared via in situ polymerization. Polym Eng Sci 60(9):2262–2271. https://doi.org/10.1002/pen.25468
41. Kalotra S, Mehta R (2021) Synthesis of polyaniline/clay nanocomposites by in situ polymerization and its application for the removal of acid green 25 dye from wastewater. Polym Bull 78(5):2439–2463. https://doi.org/10.1007/s00289-020-03222-3
42. Kathiresan V, Thirumalai D, Rajarathinam T, Yeom M, Lee J, Kim S et al (2021) A simple one-step electrochemical deposition of bioinspired nanocomposite for the non-enzymatic detection of dopamine. J Anal Sci Technol 12(1):5. http://doi.org/10.1186/s40543-021-00260-y
43. Kaur B, Tanwar R, Mandal UK (2020) Effect of nanoparticles concentration on thermal, magnetic and electrical properties of $Ni_{0.5}Zn_{0.5}Fe_2O_4$ based polyaniline nanocomposites by in-situ polymerisation. Colloids Surf A Physicochem Eng Aspects 599:124798. http://doi.org/10.1016/j.colsurfa.2020.124798
44. Khan FSA, Mubarak NM, Khalid M, Walvekar R, Abdullah EC, Mazari SA et al (2020) Magnetic nanoadsorbents' potential route for heavy metals removal—a review. Environ Sci Pollut Res 27(19):24342–24356. http://doi.org/10.1007/s11356-020-08711-6
45. Lakshmi MS, Wabaidur SM, Alothman ZA, Johan MR, Ponnusamy VK, Dhanusuraman R (2021) Phosphotungstic acid-titania loaded polyaniline nanocomposite as efficient methanol electro-oxidation catalyst in fuel cells. Int J Energy Res 45(6):8243–8254. https://doi.org/10.1002/er.5950
46. Lee HB, Raghu AV, Yoon KS, Jeong HM (2010) Preparation and characterization of poly(ethylene oxide)/graphene nanocomposites from an aqueous medium. J Macromol Sci Part B 49(4):802–809. https://doi.org/10.1080/00222341003603701
47. Lee MG, Lee S, Cho J, Jho JY (2020) Improving dispersion and mechanical properties of polypropylene/graphene nanoplatelet composites by mixed solvent-assisted melt blending. Macromol Res 28(12):1166–1173. https://doi.org/10.1007/s13233-020-8144-7
48. Liu B, Li Y, Fei T, Han S, Xia C, Shan Z, Jiang J (2020) Highly thermally conductive polystyrene/polypropylene/boron nitride composites with 3D segregated structure prepared by solution-mixing and hot-pressing method. Chem Eng J 385:123829. https://doi.org/10.1016/j.cej.2019.123829
49. Liu Y, He H, Tian G, Wang Y, Gao J, Wang C et al (2021) Morphology evolution to form double percolation polylactide/polycaprolactone/MWCNTs nanocomposites with ultralow percolation threshold and excellent EMI shielding. Compos Sci Technol 214:108956. http://doi.org/10.1016/j.compscitech.2021.108956

50. Ma Y, Xu Y, Ji X, Xie M, Jiang D, Yan J et al (2020) Construction of polythiophene/$Bi_4O_5I_2$ nanocomposites to promote photocatalytic degradation of bisphenol a. J Alloys Compd 823:153773. http://doi.org/10.1016/j.jallcom.2020.153773
51. Mandal DK, Bhunia H, Bajpai PK, Chaudhari CV, Dubey KA, Varshney L, Kumar A (2021) Preparation and characterization of polypropylene/polylactide blends and nanocomposites and their biodegradation study. J Thermoplast Compos Mater 34(6):725–744. https://doi.org/10.1177/0892705719850601
52. Marroquin JB, Rhee KY, Park SJ (2013) Chitosan nanocomposite films: enhanced electrical conductivity, thermal stability, and mechanical properties. Carbohyd Polym 92(2):1783–1791. https://doi.org/10.1016/j.carbpol.2012.11.042
53. McCarthy DL, Liu J, Dwyer DB, Troiano JL, Boyer SM, DeCoste JB et al (2017) Electrospun metal–organic framework polymer composites for the catalytic degradation of methyl paraoxon. New J Chem 41(17):8748–8753. http://doi.org/10.1039/C7NJ00525C
54. Md Said NH, Liu W-W, Khe C-S, Lai C-W, Zulkepli NN, Aziz A (2021) Review of the past and recent developments in functionalization of graphene derivatives for reinforcement of polypropylene nanocomposites. Polym Compos 42(3):1075–1108. https://doi.org/10.1002/pc.25922
55. Mehmood A, Khan FSA, Mubarak NM, Tan YH, Karri RR, Khalid M et al (2021) Magnetic nanocomposites for sustainable water purification—a comprehensive review. Environ Sci Pollut Res 28(16):19563–19588. http://doi.org/10.1007/s11356-021-12589-3
56. Minisy IM, Salahuddin NA, Ayad MM (2021) Adsorption of methylene blue onto chitosan–montmorillonite/polyaniline nanocomposite. Appl Clay Sci 203:105993. https://doi.org/10.1016/j.clay.2021.105993
57. Mittal H, Khanuja M (2021) Hydrothermal in-situ synthesis of MoSe2-polypyrrole nanocomposite for efficient photocatalytic degradation of dyes under dark and visible light irradiation. Sep Purif Technol 254:117508. https://doi.org/10.1016/j.seppur.2020.117508
58. Mittal V (2009) Optimization of polymer nanocomposite properties. Wiley, Hoboken
59. Nag S, Ghosh A, Das D, Mondal A, Mukherjee S (2020) $Ni_{0.5}Zn_{0.5}Fe_2O_4$/polypyrrole nanocomposite: a novel magnetic photocatalyst for degradation of organic dyes. Synth Met 267:116459. http://doi.org/10.1016/j.synthmet.2020.116459
60. Nicosia A, Vento F, Di Mari GM, D'Urso L, Mineo PG (2021) TiO_2-based nanocomposites thin film having boosted photocatalytic activity for xenobiotics water pollution remediation. Nanomaterials 11(2):400
61. Nunes MABS, de Matos BR, Silva GG, Ito EN, de Melo TJA, Fechine GJM (2021) Hybrids nanocomposites based on a polymer blend (linear low-density polyethylene/poly(ethylene-co-methyl acrylate) and carbonaceous fillers (graphene and carbon nanotube). Polym Compos 42(2):661–677. https://doi.org/10.1002/pc.25856
62. Palsaniya S, Nemade HB, Dasmahapatra AK (2021) Hierarchical PANI-RGO-ZnO ternary nanocomposites for symmetric tandem supercapacitor. J Phys Chem Solids 154:110081. https://doi.org/10.1016/j.jpcs.2021.110081
63. Poornima C, Mallik US, Shivasiddaramaiah AG, Pushpalakshmi N, Puneeth BS (2021) Evaluation of wear characteristics of PP/MWCNT nanocomposites. Mater Today Proc 46:2477–2482. https://doi.org/10.1016/j.matpr.2021.01.404
64. Pu L, Tang J, Gu X, Jin T, Zeng B, Liu J, Huang X (2021) Dielectric and energy storage properties of nanocomposites with core–shell paraffin-engineered $BaTiO_3$ in polyimides. J Mater Sci Mater Electron 32(5):5886–5897. https://doi.org/10.1007/s10854-021-05309-7
65. Rahman MA, Habib ML, Chisty AH, Mallik AK, Khan MN, Haque P, Rahman MM (2022) Organic–inorganic polymer hybrids for water and wastewater treatment. In: Lichtfouse E, Muthu SS, Khadir A (eds) Inorganic-organic composites for water and wastewater treatment, vol 1, pp 29–54. Springer, Singapore
66. Rasool A, Rizvi TZ, Nayab S, Iqbal Z (2021) Electrical properties of cadmium sulfide quantum dots and polyaniline based nanocomposites. J Alloy Compd 854:156661. https://doi.org/10.1016/j.jallcom.2020.156661

67. Rathi G, Choudhry A, Khan S, Sharma A, Tara N, Abdulla NK et al (2021) Chapter 36—multifunctional organic-inorganic materials for water treatment. In: Ahamad A, Siddiqui SI, Singh P (eds) Contamination of water. Academic Press, Cambridge, pp 529–540
68. Rizwan K, Rahdar A, Bilal M, Iqbal HMN (2021) MXene-based electrochemical and biosensing platforms to detect toxic elements and pesticides pollutants from environmental matrices. Chemosphere 132820. https://doi.org/10.1016/j.chemosphere.2021.132820
69. Rostami A, Moosavi MI (2020) High-performance thermoplastic polyurethane nanocomposites induced by hybrid application of functionalized graphene and carbon nanotubes. J Appl Polym Sci 137(14):48520. https://doi.org/10.1002/app.48520
70. Rouabah N, Boudine B, Nazir R, Zaabat M, Sebais M, Halimi O et al (2021) Structural, optical and photocatalytic properties of PVC/CdS nanocomposites prepared by soft chemistry method. J Inorg Organomet Polym Mater 31(3):1102–1110. http://doi.org/10.1007/s10904-020-01752-x
71. Saeb E, Asadpour-Zeynali K (2021) Facile synthesis of TiO_2@PANI@Au nanocomposite as an electrochemical sensor for determination of hydrazine. Microchem J 160:105603. https://doi.org/10.1016/j.microc.2020.105603
72. Sankar S, Naik AA, Anilkumar T, Ramesan MT (2020) Characterization, conductivity studies, dielectric properties, and gas sensing performance of in situ polymerized polyindole/copper alumina nanocomposites. J Appl Polym Sci 137(38):49145. https://doi.org/10.1002/app.49145
73. Sengwa RJ, Dhatarwal P (2021) PVA/MMT and (PVA/PVP)/MMT hybrid nanocomposites for broad-range radio frequency tunable nanodielectric applications. Mater Lett 299:130081. https://doi.org/10.1016/j.matlet.2021.130081
74. Shakeel A, Rizwan K, Farooq U, Iqbal S, Altaf AA (2022) Advanced polymeric/inorganic nanohybrids: an integrated platform for gas sensing applications. Chemosphere 133772
75. Shumaila, Khan S, Khan ZMSH, Husain M, Zulfequar M (2020) Facile synthesis of highly conducting polypyrrole and reduced graphene oxide nanocomposites for low-turn-on electron field emitters. J Phys Chem Solids 143:109522. https://doi.org/10.1016/j.jpcs.2020.109522
76. Singh V, Joung D, Zhai L, Das S, Khondaker SI, Seal S (2011) Graphene based materials: past, present and future. Prog Mater Sci 56(8):1178–1271
77. Sultana S, Ahmad N, Ahmad E, Sabir S, Khan MZ (2020) Electrochemical synthesis of novel aluminium oxyhydroxide-decorated MnO_2/chitosan nanocomposite with efficient photocatalytic and antibacterial activity. Nanotechnol Environ Eng 5(2):20. https://doi.org/10.1007/s41204-020-00083-z
78. Taha TA, Alzara MAA (2021) Synthesis, thermal and dielectric performance of PVA-$SrTiO_3$ polymer nanocomposites. J Mol Struct 1238:130401. https://doi.org/10.1016/j.molstruc.2021.130401
79. Tajik S, Beitollahi H, Nejad FG, Dourandish Z, Khalilzadeh MA, Jang HW et al (2021) Recent developments in polymer nanocomposite-based electrochemical sensors for detecting environmental pollutants. Ind Eng Chem Res 60(3):1112–1136. http://doi.org/10.1021/acs.iecr.0c04952
80. Taravati Ahmad P, Jaleh B, Khazalpour S, Gharehbaghi R, Varma RS (2021) Electrochemical fabrication of rGO/PANI-Au-γMnO_2 nanocomposites as supercapacitor electrode materials. J Mater Sci Mater Electron 32(3):3038–3053. https://doi.org/10.1007/s10854-020-05054-3
81. Tran LT, Tran HV, Dang HTM, Nguyen AV, Tran TH, Huynh CD (2021) Electrosynthesis of electrochemically reduced graphene oxide/polyaniline nanowire/silver nanoflower nanocomposite for development of a highly sensitive electrochemical DNA sensor. RSC Adv 11(32):19470–19481. https://doi.org/10.1039/D1RA01301G
82. Ul-Haq Y, Murtaza I, Mazhar S, Ullah R, Iqbal M, Zeeshan ul H et al (2020) Dielectric, thermal and mechanical properties of hybrid PMMA/RGO/Fe_2O_3 nanocomposites fabricated by in-situ polymerization. Ceram Int 46(5):5828–5840. http://doi.org/10.1016/j.ceramint.2019.11.033
83. Ul Haq Y, Murtaza I, Mazhar S, Ahmad N, Qarni AA, Ul Haq Z et al (2020) Investigation of improved dielectric and thermal properties of ternary nanocomposite PMMA/MXene/ZnO fabricated by in-situ bulk polymerization. J Appl Polym Sci 137(40):49197. http://doi.org/10.1002/app.49197

84. Wang G, Bi X, Yue H, Jin R, Wang Q, Gao S, Lu J (2019) Sacrificial template synthesis of hollow C@MoS_2@PPy nanocomposites as anodes for enhanced sodium storage performance. Nano Energy 60:362–370. https://doi.org/10.1016/j.nanoen.2019.03.065
85. Wang H, Ren H, Jing C, Li J, Zhou Q, Meng F (2021) Two birds with one stone: graphene oxide@sulfonated polyaniline nanocomposites towards high-performance electromagnetic wave absorption and corrosion protection. Compos Sci Technol 204:108630. https://doi.org/10.1016/j.compscitech.2020.108630
86. Yan K, Xu F, Wei W, Yang C, Wang D, Shi X (2021) Electrochemical synthesis of chitosan/silver nanoparticles multilayer hydrogel coating with pH-dependent controlled release capability and antibacterial property. Colloids Surf B 202:111711. https://doi.org/10.1016/j.colsurfb.2021.111711
87. Yashas SR, Shahmoradi B, Wantala K, Shivaraju HP (2021) Potentiality of polymer nanocomposites for sustainable environmental applications: a review of recent advances. Polymer 233:124184. https://doi.org/10.1016/j.polymer.2021.124184
88. Yasoda KY, Kumar S, Kumar MS, Ghosh K, Batabyal SK (2021) Fabrication of MnS/GO/PANI nanocomposites on a highly conducting graphite electrode for supercapacitor application. Mater Today Chem 19:100394. https://doi.org/10.1016/j.mtchem.2020.100394
89. Yuan X, Kobylanski MP, Cui Z, Li J, Beaunier P, Dragoe D et al (2020) Highly active composite TiO_2-polypyrrole nanostructures for water and air depollution under visible light irradiation. J Environ Chem Eng 8(5):104178. https://doi.org/10.1016/j.jece.2020.104178
90. Zayan S, Elshazly A, Elkady M (2020) In situ polymerization of polypyrrole @ aluminum fumarate metal-organic framework hybrid nanocomposites for the application of wastewater treatment. Polymers 12(8):1764
91. Zenasni M, Quintero-Jaime A, Salinas-Torres D, Benyoucef A, Morallón E (2021) Electrochemical synthesis of composite materials based on titanium carbide and titanium dioxide with poly(N-phenyl-o-phenylenediamine) for selective detection of uric acid. J Electroanal Chem 895:115481. https://doi.org/10.1016/j.jelechem.2021.115481
92. Zhang B, Zhang M, Zhang L, Bingham PA, Li W, Kubuki S (2020) PVP surfactant-modified flower-like BiOBr with tunable bandgap structure for efficient photocatalytic decontamination of pollutants. Appl Surf Sci 530:147233. https://doi.org/10.1016/j.apsusc.2020.147233
93. Zhang F, Li X, Zhao Q, Chen G, Zhang Q (2020) High-performance In_2O_3@PANI core@shell architectures with ultralong charge carriers lifetime for photocatalytic degradation of gaseous 1,2-dichlorobenzene. Appl Catal B 263:118278. https://doi.org/10.1016/j.apcatb.2019.118278
94. Zhang J, Liu X, Zhang L, Cao B, Wu S (2013) Reactive template synthesis of polypyrrole nanotubes for fabricating metal/conducting polymer nanocomposites. Macromol Rapid Commun 34(6):528–532. https://doi.org/10.1002/marc.201200757
95. Zhao M, Baker J, Jiang Z, Zhu Z, Wu H-M, Wu J-L et al (2021) Preparation of well-exfoliated poly(ethylene-co-vinyl acetate)/α-zirconium phosphate nanocomposites. Langmuir 37(15):4550–4561. http://doi.org/10.1021/acs.langmuir.1c00146
96. Zhong J, Isayev AI, Zhang X (2016) Ultrasonic twin screw compounding of polypropylene with carbon nanotubes, graphene nanoplates and carbon black. Eur Polym J 80:16–39. https://doi.org/10.1016/j.eurpolymj.2016.04.028
97. Zhou Q, Zhao D, Sun Y, Sheng X, Zhao J, Guo J, Zhou B (2020) g–C3N4–and polyaniline-co-modified TiO_2 nanotube arrays for significantly enhanced photocatalytic degradation of tetrabromobisphenol A under visible light. Chemosphere 252:126468. https://doi.org/10.1016/j.chemosphere.2020.126468
98. Zia J, Aazam ES, Riaz U (2020) Highly efficient visible light driven photocatalytic activity of MnO_2 and polythiophene/MnO_2 nanohybrids against mixed organic pollutants. J Mol Struct 1207:127790. https://doi.org/10.1016/j.molstruc.2020.127790

Chapter 5
Organic–Inorganic Nanohybrids in Medicine

Sameera Shafi, Saba Zafar, Zohaib Sarwar, Muhammad Hassan Rasool, and Tahir Rasheed

1 Introduction

Because of their beneficial physicochemical features, nanohybrids comprising the organic and inorganic parts have received considerable recognition in the bio-related systems field [79]. Organic/inorganic nanohybrids, such as snail-shells and teeth, can be found in nature and are made up of biological macromolecules and inorganic salts due to nanoscale hybridization [141]. Organic/inorganic nanohybrids are hetero-nanoparticles with separate domains made up of organic and inorganic components [128, 147]. Hybridization at the nanoscale has a unique property that distinguishes it from similar bulk materials [142], making it useful in clinical application [16, 118]. When nanoparticles (NPs) aggregate in tumor regions, the enhanced permeation and persistence (EPR) impact may help to facilitate their preferred aggregation [119]. To achieve acceptable therapeutic effects, a variety of these nanohybrid niosomes were used to carry medicines and biomolecules [79, 193]. The gold nanoparticles and iron oxide can be used in up conversion for the synthesis of NPs [31, 202] to introduce PET, CT, MR, and FL imaging [7]. Furthermore, organic components are essential for nanohybrid biocompatibility and stability. Site-specific dosage and regulated drug distribution are essential for delivering chemotherapy to the sick site while avoiding damage to healthy tissue. This is especially important for reducing chemotherapy side effects [167]. In general, the organic components of natural nanohybrids could provide stimulations, selectivity, foreign compound loading, biodegradability, and controlled drug release. To make organic/inorganic nanohybrids, techniques such as

S. Shafi · S. Zafar · Z. Sarwar · M. H. Rasool
Institute of Chemistry, The Islamia University of Bahawalpur, Bahawalnagar, Pakistan
e-mail: Sameera.shafi@iub.edu.pk

T. Rasheed (✉)
Interdisciplinary Research Center for Advanced Materials, King Fahd University of Petroleum and Minerals, Dhahran 31261, Saudi Arabia
e-mail: tahir.rasheed@kfupm.edu.sa

K. Rizwan et al. (eds.), *Hybrid Nanomaterials*, Materials Horizons: From Nature to Nanomaterials, https://doi.org/10.1007/978-981-19-4538-0_5

"grafting from," "grafting onto," and self-assembly could be used [208]. To achieve this goal, this presentation will examine recent developments in a number of natural nanohybrids for medicinal applications such as medication administration, gene delivery, photodynamic treatment (such as laser scanning), scanning, and multimodal systems. It then focuses on fundamental ideas and mechanisms in medicinal application. Nanohybrids that can be used for tomography, medication, and optics therapy will be categorized and talked about. To demonstrate the ideas of novel nanohybrid systems, several design justifications will be discussed. Organic and inorganic constituents' roles, and also their interaction, will be investigated further [208].

2 Innovations in Biomedical Nanohybrid Manufacturing

2.1 Organic Species

Biomimetic nanohybrids can be made from a variety of organic species. Inorganic nanoparticles (NPs) typically require functionalization of their surfaces to control interactions with living organisms [1, 81]. Aside from being hydrophobic or poisonous, inorganic nanoparticles' sealing ligands may not be suited for biomedical purposes after synthesis. Alternatives to encapsulating the interface with inorganic or organic materials might reduce or improve the cytotoxic effects and other properties [12]. Organic species have higher versatility in terms of usefulness, dispersibility, stability, and biocompatibility. To achieve maximum NPs' absorption and selectivity, the correct organic species can be applied to the surface [199]. Silane-functionalized silica NPs and thiol-functionalized Au NPs are two examples of functionalization that can be applied to nanoparticles [199].

2.1.1 Small Molecules

Alkoxysilane groups can be bound to the surface of silica NPs using tiny organic chemicals as APTMS, APTES, and APCP. These compounds are utilized to form nanohybrid structures. Additional activities can be introduced or biological gene transport capabilities can be directly imparted by using APTES amides as an attractive electrostatic connection [67]. It was developed by connecting DAA to the HA backbone by amide linkages and then using the amphiphilic block copolymers that resulted from this process to create micelles. For medicinal purposes, gold nano crystals were created by reducing $HAuCl_4$ with a DAA component [225]. Furthermore, 2-propionic-3-methylmaleic anhydride (CDM) is a common bridge among copolymers used to create pH-sensitive polymers due to its specific cleavage at the tumor site (pH 6.8) [22].

2.1.2 Synthetic Polymers

For nanohybrid applications, polymeric ligands offer a wider range of options because both the components and the structures can be tailored to meet specific needs [114]. Nanohybrids may benefit from PEG's medicinal applications and hydrophilicity, which inhibit permeation rates and enhance biocompatibility, as the most prevalent polymer. Plus, PEG is a bioinert, nonimmunogenic ingredient that has been officially approved as an additive (FDA). As a result of the need for high colloidal stability in medical applications, hydrophilic PEG was frequently utilized to pre-treat nanoparticles (NPs) [169]. It has been discovered that PEG-functionalized silica NPs had a longer blood circulation and a low rate of organ entrapment, as opposed to silica NPs with carboxyl-terminated small molecules and silica NPs with hydroxyl groups [53]. When PEG-terminated NPs are used as delivery carriers, they exhibit superior bioavailability of drugs, efficient localization to cancerous locations, and enhanced renal clearance [165, 186, 189]. Nonviral gene carriers like PEI, PAMAM, and PDMAEMA can condense nucleic acids for gene delivery by forming electrostatic bonds with them [124].

2.1.3 Biological Molecules

Biological components are frequently employed in nanohybrids in order to improve cytocompatibility, dispersion, and, in particular, active target selectivity, among other things [112]. In addition to antibodies [40] and aptamers [83], biomolecules such as peptides [168] and peptide ligands are also commonly used to attain biological identification of certain receptor molecules or antigens on marked cells [126]. An aptamer can easily be attached to the surface of an amine-functionalized NP by means of carbodiimide coupling chemistry [65] to boost their ability to identify malignant cells [54]. Tumor cells with strong transferrin receptor expression can also be targeted with transferrin [23].

2.2 Inorganic Nanoparticles

Top-down and bottom-up techniques can be used to make inorganic nano powders that have a nanometer scale in the 1–100 nm range. Biocompatibility and nontoxicity are requirements for medicinal application. However, improved surface crosslinking is required for proper solution and dispersion in physiological fluids [56, 126]. The nucleation and growth processes will determine the ultimate NP morphology. Many ligands are required to cap crystal formation at the nanoscale, like surfactants or polymeric compounds. These interactions will change how quickly each crystal face grows and how big it gets. This will have a big impact on how NPs move through the body and how well they penetrate [13, 42, 56].

2.2.1 Gold Nanoparticles

Due to their bioactivity, gold nanoparticles (Au NPs) are extensively used metallic nanoparticles in biomedicine currently. There are many ways to modify the morphology of gold nanoparticles, such as altering the ratio of gold ions, reductants, and caps [11, 36]. Due to the same significant optical absorption in the preferred near-infrared (NIR) region, it is possible to use gold nano-shells as well as nanorods for photothermal therapy and photoacoustic imaging [103]. A bathochromic photoactivity in the NIR band was observed in gold nanocaps or semi-shells with distinct cavities [103].

2.2.2 Silica Nanoparticles

Silica NPs are good prospects for medical applications, particularly in medicines and gene administration, due to their controlled form, great porosity, accessibility of simple surface chemistry, and cytocompatibility [188, 205]. The well-known Stöber technique can be used to produce a narrow size distribution of silica nanoparticles with a dimension range of 50 nm to 2 m [160]. Silica hollow NPs can be made using flexible templates such as nano-emulsions, vacuoles, and microcapsules [75, 213]. The flexible templating technique is also used in their production [136]. It is widely accepted that silicate NPs are degradable, but the process may take a long time because of the dense silicate network [80]. Various ways have been devised to produce biodegradable silica nanoparticles in order to speed up their decomposition and removal [170, 221].

2.2.3 Fe_3O_4 Nanoparticulates

Nanoparticulates of Fe_3O_4 have shown considerable promise in medicinal applications, for example, drugs delivery, remedial platforms, and MRI [38, 88, 97, 100]. Salts of Fe^{+2} and Fe^{+3} (equimolar ratio of 1:2) interacted chemically with the base within water to synthesize stable Fe_3O_4 nanoparticles [41, 138]. Hydrothermal synthesis, the polyol process [71], and the thermal decomposition [72] processes are also used for iron NPS synthesis. As a surface modification, iron acetyl acetonate thermally decomposes in benzyl ether in the presence of oleic acid, yielding nano-cubes with dimensions 20–160 nm [84]. With the assistance of transferrin and ferritin, the surplus ions created by Fe_3O_4 nanoparticles will be eliminated by storage and transit well with the assistance of transferrin and ferritin, respectively. An individual's iron storage proteins, dose, and surface-coating ligands all influence how quickly Fe_3O_4 NPs degrade in the body [84].

2.2.4 Quantum Dots (QDs)

There has been a huge pact of concern in the potential bioapplications of semiconductor quantum dots, particularly multimodal bioimaging systems, due to their natural ocular properties [97, 111, 196]. Because of their enduring photostability, strong photoluminescence (PL) quantum efficiency, size tunability, and narrow-band emissions, quantum dots are suitable fluorescent probes for monitoring critical biological processes [10]. A submissive film, like ZnS, CdS, or CdSe, is commonly placed over top of the QD core in order to maintain or increase the PL quantum yield [151]. Water-soluble QDs are required for the biomedical field, and ligand switch over is required for these quantum dots containing organic ligands. Aqueous QD manufacturing, conversely, is more convenient for a wide variety of uses [78]. Graphene, MoS_2, WS_2, and MXene are just a few of the new 2D QDs that have recently been developed. Their 2-dimensional layered materials have been scaled down to make these miniatures. Sadly, this is an all-too-common misconception [198].

2.2.5 Some More Nanoparticles of Inorganic Origin

In addition to the usual inorganic NPs, a range of NPs used in biological fields are being researched. Unusual prospects for up conversion luminescence imaging (UCL) include up conversion nanoparticles (UCNPs), which have the potential to convert lower energy near-infrared (NIR) light to higher energy ultraviolet/visible (UV/vis). Rare-earth elements have unique 4f orbitals, which give them special features [102, 110]. It is possible that medicinal applications could potentially make use of inorganic NPs like carbon nanomaterials and hetero-nanoparticles, as well as transition metal dichalcogenides, calcium phosphate, and calcium carbonate [45, 58].

2.3 Nanohybrid Nanofabrication Methodologies

Shell functionalization, pot-economic synthesis, and wrapping are the three types of techniques available. Figure 1 is typically successful in creating nanohybrids with compatible biosorbent surface and functional groups that can interact with molecules such as proteins or genomes in order to facilitate the targeting and administration of medicinal drugs [234]. An appropriate grafting density or coating thickness is required for the use of polymer brushes, which are polymer strings with one of their ends covalently bonded to something like a surface or interface [29]. Using "grafting from" or "grafting onto" procedures, polymer brushes can be grafted on top planer area of inorganic NPs. Polymer or biomolecule grafting onto the NP surface is the most efficient form of NP integration. Using metal–sulfur bonding, polymers having thiol groups can be grafted onto metallic surfaces. There are numerous examples

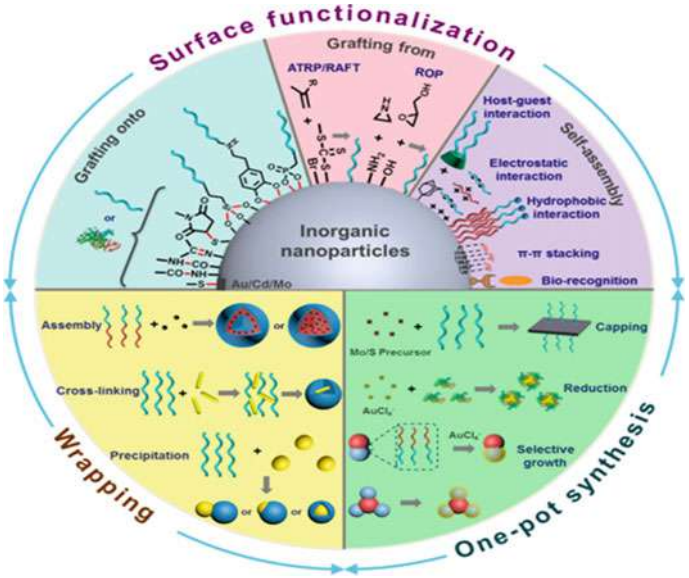

Fig. 1 Manufacturing of organic/inorganic nanohybrids through surface functionalization, wrapping, and one-pot synthesis [225]

of how Au NPs interact with thiolated polymers, the most common of which is the formation of Au-thiol bonds [24, 39, 180].

PEG-LA was created by conjugating lipoic acid (LA) with a dithiolane and forming PEG-LA, that have numerous dithiolane rings and can easily bond to gold surfaces [63]. As a side note, cellulose nanocrystals (CNC) can also be tailored with LA (CNCLA) to make them stick to Au NPs and nanorods (Fig. 2).

This is because CNC has hydroxyl groups on its surface [63]. Peptides containing thiol groups, such as RGD peptides (RGDSH), can form stable AuS bonds with Au NPs [210]. Additionally, thiol-ended and LA-conjugated polymers may be transferred to metallic surfaces via CdS [190], CuS [192], WS [19, 209], or BiS [20] bonding to create a variety of nanohybrids of polymers, MoS_2, Bi_2S_3, and hetero-nanoparticles. Another option is to graft carboxylic group-terminated NPs with amino group-terminated PEG (PEG-NH_2) onto carbon dots [64, 163], graphene oxide (GO), MoS_2 nanoflakes [37], UCNP [47], and Janus hetero-nanoparticles [61, 148]. Polymers and biomolecules have been grafted onto NP surfaces via Schiff base linkage and click reaction [105, 214]. Nanohybrids containing PEG and silica or silica-coated inorganic NPs could be created using the "grafting onto" procedure [145, 155, 162].

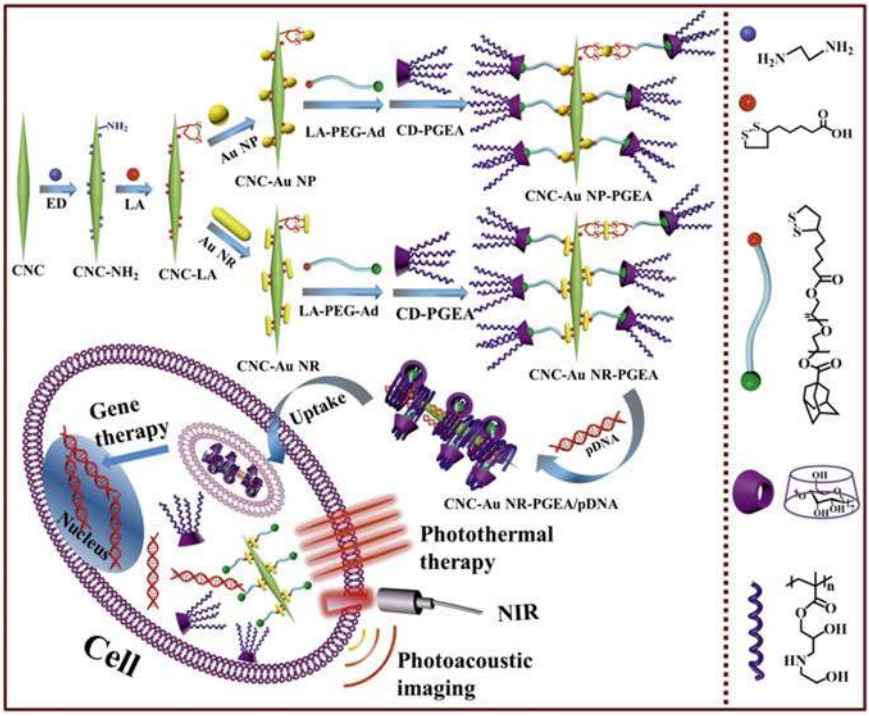

Fig. 2 Au NPs chemically modified with PDM-SS-PDM and CNC and Au coupled [63]

2.3.1 "Grafting From" Strategy

Bottom-up procedures that use surface-initiated polymerization to build polymers from the surfaces of NPs generate larger transplanting densities than "grafting onto" methods [8]. Immobilizing ATRP initiators on the surface of NPs is a simple and broadly practical approach. When it comes to attaching polymers, it is also important to have the right reaction system in place. The surface qualities and the complex formation of NPs will be considered in the immobilization of ATRP initiators. Gold's affinity for thiol or disulfide groups has had a significant impact on initiator conjugation, and the OH group on silica and metal oxide surfaces is commonly implicated in this process. At the same time, gene carriers containing ATRP inorganic nanoparticles have been proposed. To increase subcellular uptake and targeted delivery, using bovine serum albumin (BSA), Zhao et al. created BSA-Br by reacting BIBA with EDC and NHS in the presence of BSA. Polycationic PDMAEMA nanohybrids could be generated by ATRP grafting on Au [201].

Intriguingly, up to three of Fe_3O_4 NPs were used in a streak with a silica coating to create 1D peapod-like NPs [177]. Gene delivery was accomplished by performing a ring-opening reaction with excess ethanolamine after PGMA was grafted onto peapod-like Fe_3O_4@SiO_2 NPs by a silane-coupled initiator. The Fe_3O_4–SiO_2 PGEA

nanohybrids have increased gene transfection because of their one-dimensional structure and magnetic responsiveness. To track gene delivery in round or 1D custom graphics silica NPs, ATRP could be utilized to functionalize QD@SiO_2PGEA nanohybrids with various shapes. This can be utilized to monitor the central and midpoint QD alignment [207].

2.3.2 Self-assemblage Technique

Self-assembly, which is the underlying approach for constructing remarkable biological systems, happens everywhere in nature as a natural bottom-up association process [30, 173]. It is usual to use host guest bioreceptors with inbuilt specificity and switchability [173]. Organic/inorganic nanohybrid assemblage examples include noncovalent hydrophobic interactions, connections, and biorecognition. This hydrophobic PEGylated polymer, PEG-C18PMH, was created via the hydrophobic derivatization of the CNTs in the Dai group and has a hydrophobic C_{18} chain [135]. SWCNT nanohybrids, carbon nanohorns, and void Si/C nanospheres were constructed using this polymer as theranostic agents [14, 96, 215]. A pre-modified octadecyltrimethoxysilane-modified porous structure or organosilica could benefit from the doped surface as well (C_{18}TMS). Hydrophobic hydrophobic contact was used to readily make nanohybrids of PEG-C18PMH and silica-coated SWCNTs or Janus Au@SiO nanoparticles in order to treat cancer [60, 107]. To attain the necessary outcomes, piling is particularly important in the exterior modification of carbon nanomaterials, where it tackle in conjunction with carbon that is sp^2 hybridized and aromatic compounds to achieve the desired outcome [43, 226]. Carbon nanomaterials could also be used to assemble biomolecules having aromatic structures, such as DNA, on their surfaces. Scientists have developed nanohybrid ssDNA-carbon nanosphere nanoparticle hybrids that can be used to detect numerous cancer types, such as breast, prostate, and melanoma [91].

2.3.3 Pot-Economic Synthesis

Pot-economic: It is simple and fast to synthesize inorganic parts in the existence of organic components that function as capping agents on surface or act as precursors. In nearly all situations, the organic components are just caps and do not contribute to the process. A PEGylated MoS2 nanosheets of various sizes may be produced in a single solvothermal synthesis step [179]. P (OEGMA-co-MAA) was used to stabilize PEGylated ultrasmall Fe_3O_4 NPs generated by one-step coprecipitation. The oligo (ethylene glycol) component offered water solubility and cytocompatibility while the methacrylic acid segment anchored the copolymers to the iron oxide surface [116]. Different anchoring groups for three P (OEG-A) block copolymers were investigated using coprecipitation (phosphonic acid, carboxylic acid, and glycerol) [5].

2.3.4 Wrapping

Organic/inorganic nanohybrids can be formed through electrostatic interaction between organic and inorganic components, which is another extensively used method of producing them. Wrapping is another method of producing organic/inorganic nanohybrids. With the addition of isopropyl alcohol, it was possible to easily synthesize nanohybrids containing PAA and diversity of inorganic NPs, together with Fe_2O_3, Fe_3O_4, SnO_2, and Ag nanospheres, among others [93]. Concentric UCNP@PAA core–shell nanohybrids and Janus Au–PAA nanohybrids could be constructed using this simple and general method by growing the spherical Au NPs into Au branches further [101, 216]. When PEG and lactobionic acid are conjugated to the PAA and Au domains, they can improve their biocompatibility and tumor targeting. The resulting octopus-type nanohybrids have been shown to be a promising stage intended for active focused collective chemo-photothermal cancer therapy [153]. Metalorganic frameworks (nMOF) can be wrapped or grown around inorganic NPs to create nanohybrids. Incidentally, the amino-functionalized octahedral iron carboxylate nMOF shell coating on the UCNP cores produced the eccentric and octahedral coreshell hybrids [95].

3 Nanohybrids with Organic and Inorganic Components and Their Functions

Complementary contact of two segments at the nanoscale may result in the formation of new characteristics, which has the potential to be useful in the development and manufacturing of highly lucrative nanohybrids. Nanohybrids could help scientists figure out how materials are made, how they look, how they work, and how they can be used.

3.1 Organic Parts

The endurance and cytocompatibility of nanohybrids are influenced by organic components such as biomolecules, synthetic polymers, and biomaterials. Additionally, the organic segments of the nanohybrids typically contain more than one type of organic component, such as functionalization and attacking selectivity of particular small molecules and biomolecules.

3.1.1 Stimuli Responsiveness

Nanohybrids that are adaptive in nature that reflect changes in physiological circumstances are critical in limiting the harmful influence of the normal region [146, 164]. To take advantage of tumors' slightly acidic extrinsic pH (6.07.0) and endosomal intrinsic pH (4.56.5), pH responsiveness has been frequently utilized. Drug release gatekeepers are often utilized because of their hydrophilic properties in acidic condition, which compares with their hydrophobic properties in neutral or alkaline solution [65, 230]. Using void silica NPs functionalized by means of PEG shielding and CD-Ad host–guest interaction, Cai et al. developed a pH-responsive chain release method for tumors [106]. The outer PEG layer's rational design ensured that the delivery system's blood circulation was prolonged by reducing nonspecific protein adsorption and cellular absorption. To enhance cell absorption, benzoic-imine bonds dissociated PEG at the tumor location when the carriers arrived. Apoptosis would next be induced in the cells by hydrolysis of the boronic acid-catechol ester linkers, which would remove the gatekeeper-CD and release medicines from the cell. The proven efficacy of drug delivery system that is pH-responsive, i.e., (HMSN-CD/Ad PEG), was demonstrated by delivering medications to tumor cells via the tumor microenvironment and preserving the advantages of PEG shielding [89]. Carbon dots that can be charged or uncharged were made by Zhao et al. by putting amino acid-functionalized carbon dots on them that were coated with an anionic polymer, PEG-(PAH/DMMA) [34]. To accomplish both dual- and triple-responsiveness, organic elements were used in the formulation. Iron oxide and thermo-responsive polymer (P) nanohybrids (DEGMA-co-PEGMA-b-[TMSPMA-co-VBA]) required a combination of pH and thermo-responsiveness; therefore, the drug DOX was conjugated at 40 °C by reacting amine groups with polymer aldehyde groups [55]. Zhao et al. used organic segments to create pH, redox, and light triple-responsive nanohybrids [223]. Disulfide bonds and *o*-nitrobenzyl esters were used as links to make the pH-responsive polymer PDEAEMA more useful on the surface of HMSNs by making it more acidic (Fig. 3).

3.1.2 Targeting

Medicinal uses, for example, drug delivery and functional imaging, benefit greatly from nanohybrids that are well suited for accumulation and absorption at the medication's intended site of action [217]. Both EPR-mediated tumor targeting and biological receptor-mediated tumor targeting are of tremendous interest [73]. This review study by Low et al. explains the organic design reasoning for the targeted delivery system's organic components, along with the identification of disease-specific receptors, targeting ligands, spacers, and cleavage linkers [159].

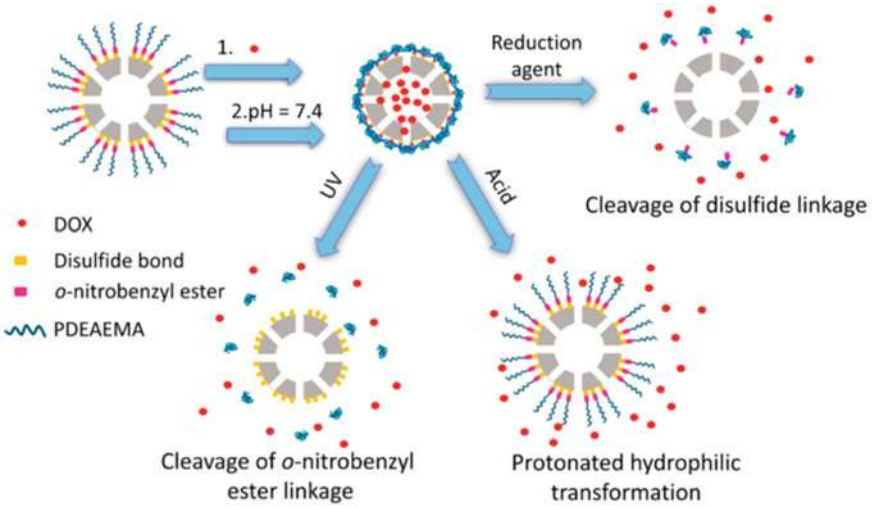

Fig. 3 Schematic representation for the structure of and different mechanisms of triggered drug release. Reproduced with permission from Ref. [223]. Copyright 2015 American Chemical Society

3.1.3 Guest Molecule Loading

Nanohybrids carry payloads such as drugs, genes, photosensitizers, proteins, or a mixture of these molecules in order to achieve diverse imaging or therapy [90]. Organic portions play an important role in guest molecule loading, in addition to the spongy structure of inorganic parts that capture payloads via corporeal interactions [137]. Physical and chemical forces such as inter-molecular, hydrophobic interaction, entrapment, and electrostatic attraction could be used to transport medicines via organic segments [4]. Furthermore, Schiff base bonds, amide bonds, or hydrazone bonds were used in nanohybrid ligands to connect the anticancer medication DOX to the polymers [74, 171]. PHEMA and PCB segments' organic ligands were linked via ester and diselenide linkages, respectively, to retinoic acid and simvastatin, both of which are used to treat Alzheimer's disease [94, 220]. For the anti-TB medication isoniazid (INH), Horwitz et al. created pH-responsive delivery systems based on MSNs in a recent study [70]. There are a number of hydrophobic medications that are transported in the hydrophobic cavities of organic parts, like kartogenin, Dox, and AB3 (a histone deacetylase inhibitor). Inner cores in these medications are made of hydrophobic PPhe as well as poly (4,5-dimethylbenzyl methacrylate) (PNBMA) [15, 123]. For the dispersal of biofilms and the death of cancer cells, nitric oxide (NO) was given using Au nanoparticles grafted with P (OEGMA)-bPVBC (P (OEGMA)-bPVBC) polymers [28]. Also, because of their electrostatic binding properties, nanohybrid ligands can bind negatively charged genes. Most commonly, polycations are the most common carriers of genetic information, and a range of PEI-modified inorganic NPs was created to assess their effectiveness as gene

carriers [150, 161, 197]. Boyer et al. used the "grafting onto" technique to functionalize Fe_2O_3 NPs with P (OEG-A) and P (DMAEA) functionalized NPs to address protein adsorption issues caused by polycation positive charge [9]. The nanohybrids' biocompatibility and lengthy circulation are enhanced by the anti-fouling shell of P (OEG-A) around the positively charged P (DMAEA) inner layer. The polycations and cation amphiphiles have also been developed by researchers, plus polysaccharide-based carriers from grafts of polymer. In light of these advances, nanohybrids for gene delivery could be developed in a new way [77, 158, 194].

3.1.4 Features with Multiple Purposes

To achieve many functions, the organic portions of nanohybrids could be integrated with other components. Disulfide linkages and tumor-specific compounds, for example, could enable redox-responsive medicine delivery [115, 133, 218]. As depicted in Fig. 4, to prevent nanohybrids from becoming trapped in RES, PEGylation is widely employed in multifunctional goods. This allows nanohybrids to be excreted mostly through the kidneys rather than the liver or spleen [69]. Organic disulfide linkages and polycations were used to achieve redox-responsiveness and gene loading [85, 187]. Tumor cell targeting is made easier using polysaccharides like HA, which not only aid in loading drugs into capsules and serving as gatekeepers [25, 33]. One of the advantages of using transferrin and the lipophilic triphenylphosphonium cation as a PTT agent was the ability to simultaneously target cancer cells and mitochondria [48].

3.2 Inorganic Parts

The nanohybrids' inorganic components serve as a bridge between regulated production and possible biomedical applications. Inorganic NPs have been extensively studied, and a few relevant reviews have been published [12, 97, 143]. We discuss the optic, electromagnetic, and other properties of inorganic nanoparticles (NPs) in this paper, as well as the usual qualities and associated components that inorganic parts contribute to the corresponding nanohybrids [183].

3.2.1 Optical Properties and Other Uses

Quantum confinement effects on the intrinsic optical properties of fluorescent NPs like QDs make them ideal for use in biological imaging. It is extremely difficult to use QDs for cell and in vivo imaging because of the toxicity of heavy metal ions associated with them [166]. Lee et al. used ultrasound (US) irradiation to create a collection of nontoxic ZnxS-AgyIn1-yS2 QDs by means of enhanced optical (PL) features that were also nontoxic, according to their findings [161]. Regardless of

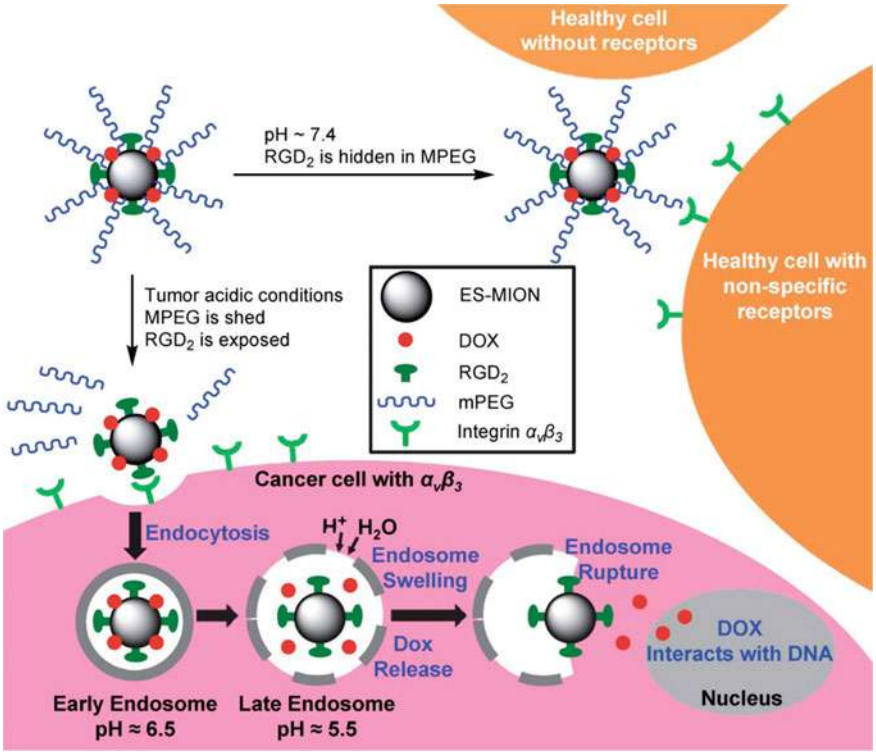

Fig. 4 Fabrication of Fe_3O_4-RGD-mPEG nanohybrids to minimize nonspecific absorption by healthy cells. The acid-labile linker is disrupted in the tumor microenvironment, allowing RGD to connect to cancer cells. Reused with consent from Ref. [149]. Copyright 2017 American Chemical Society

the size of the QDs, they emit a bright light at room temperature. Cellular imaging and siRNA treatment can be tracked using the increased FL of QDs within cells. To minimize cytotoxicity, QDs can be coated with polymer, BSA, or silica before hybridization [99, 190, 207]. After being coupled with a peptide that target at tumor, the nanohybrids might produce effective cancer imaging. Wan et al. demonstrated the internal creation of NIR-fluorescent Ag_2S QDs in tumor cells cultured on GSH-rich surfaces [154]. Detectable Ag_2S QD NIR FL emission with elevated effectiveness and remarkable optical stability was discovered when the precursors were injected into cells, providing new clues for the biosynthetic route and imaging applications [108].

3.2.2 Magnetism and Their Related Uses

For therapeutic applications, NPs with magnetic characteristics are particularly intriguing since they can be employed for magnetic tracking, MRI, and magnetic hyperthermia all at once [38, 140]. As the T_2 relaxation period of the protons adjacent water molecules increases, this magnetic activity aids MRI by increasing contrast. Additionally, NPs' superparamagnetism, which allows them to soak up and turn the radiation of an oscillating magnetic field (AMF) into heat, could aid hyperthermia remedy as well. In terms of magnetic NPs, SPIONs are now the most often and extensively studied, accounting for over half of all research. They are used in T_2 MRI contrast agents to monitor and provide feedback on the therapy process. Fe_3O_4 NPs were used as the inorganic cores of versatile nanohybrids by Kang and colleagues for targeted tumor treatment [200]. As a result, Pseudomonas aeruginosa biofilms were detachable by the local heating of polymer Fe_3O_4 NPs for enhanced antimicrobial therapy [50, 129]. The magnetic properties of Fe_3O_4 NPs may also benefit Fe_3O_4 NPs. According to some, MPI has the benefits of active targeting, fewer emissions, and virtually no background from tissues, among other things [44, 46].

3.2.3 Functions Associated with Electrical Properties

For example, reflex of inorganic NPs with superior electrical properties like gold, molybdenum disulfide, and nanotubes can be used to promote tissue regeneration. Proliferation and differentiation of stem cells into specialized cell types, including such brain cells, could be improved using "electro-stimulated" techniques [51, 181]. Human embryonic stem cells (hESC) were shown to be influenced by electrical stimulation by fibronectin-coated Au NPs [185]. The improved anticancer impact of electrochemotherapy was attributed to magnified electro-stimulation mediated by SWCNTs. For Parkinson's disease patients, electromagnetized PEGylated Au NPs were found to assist in straightforward lineage remodeling and the regeneration of dopaminergic neuron activity when subjected to specific electromagnetic fields by researchers [210]. The transformation of stem cells into cardiomyocytes was aided by the application of electric carbon nanotubes [125].

3.2.4 Other Properties

The fact that organic NPs can act as medications is even more intriguing. In an acidic intracellular environment, a Pt nanocluster assembly proposed by Hyeon et al. would breakdown to release Pt nanoclusters. Toxic Pt ions were released by the Pt nanocrystals with specific surface area to kill HCC cells via DNA damage and overcome cisplatin resistance [191]. Nanoparticles of Titanium oxide with discrete energy-band structures, employed in photodynamic cancer therapy, can be used to separate electrons and holes [52].

3.3 Interdependent Characteristics of Organic and Inorganic Parts

When the organic and inorganic components of a nanohybrid work together, it has the potential to provide a synergistic effect and novel activities. Phototrigger-controlled drug-release carriers could likewise be constructed via the emission of UCNPs. As compared to conventional light-based drug delivery systems, NIR-initiated UCNPs-based medications have exhibited considerable potential in the geographic and temporal determination of medicinal release [2]. UCNPs with a yolk-shell structure were loaded with amino-coumarin, a trigger, and chlorambucil, an anticancer drug [224]. The hypoxic aspect of the tumor microenvironment frequently limits PDT. An improved therapeutic impact of PDT might be achieved by combining the organic and inorganic components together. PCCN nanohybrids like PpIX-PEG-RGD and CCN could, for example, have carbon dots doped into the carbon nitride. This could help water split, lower the band gap, and increase red light absorption, for example [227]. As the natural and non-living (mineral part) components of the nanohybrids maintained their individual characteristics, they displayed cooperative capabilities that were complementary to one other. Carbon dots on PEG-CS hybrid nanogels proceeds well in this method since they were nontoxic. The hybrid nanogels are made up of carbon dots that glow in the dark, thermoplastic PEG, and pH-sensitive chitosan [172]. To control the release of DOX from nanogels, CS must have been employed to monitor pH variations between 5.0 and 7.4. By using NIR irradiation, carbon dots embedded in the thermo-responsive PEG framework released drugs. It is possible that photothermal inorganic NPs and organic components could work together to target or release medicines through hyperthermia [26]. In another example of this, chemically conjugated cancer medications could be delivered in a manner that responds to both the acidic milieu in which malignant cells thrive and the magnetic hyperthermia produced by acicular $Fe_3O_4@SiO_2$ NPs [27].

3.4 Functional Nanohybrids with Varying Morphological Features

According to some researchers, the shape of nanoparticles (NPs) may influence the way they interact with biomolecules. Nanohybrids' skeletal anatomy features and functionalities, as well as their concomitant biological reactions, such as cell uptake and targeted administration, cytotoxicity, and clearance, are of great interest to scientists. Both silica and gold NPs' cellular absorption efficiencies are expected to be size-dependent [21, 113, 232]. Nanohybrids of MSN and folic acid (48, 72, and 100 nm) were created and tested for cancer-targeted medication delivery in vivo [219]. When tested on tumors, the 48-nm nanohybrids performed best and were found to be more readily absorbed by the cancer cells [82, 86]. Nanohybrids' form effects may be much more intricate than their size influences. Numerous studies have

demonstrated that the internalization of nanoparticles depends on their shape (NPs). For the most part, one-dimensional nanostructures with a greater aspect ratio (such as nanotubes, rods, and worms) are projected to boost cell absorption in excess of normal spheres of nanomaterial (like gold nanoparticles) (nanoNPs) [42, 68, 121, 130]. The bigger aspect ratio APTES-SiO_2 nanohybrids were shown to have a larger effect on cell activity, including growth, bond strength, migration, and death [68]. Additionally, the structure of the nanohybrids may influence their in vivo properties, such as biodistribution, clearance, and tumor tissue penetration [13, 67]. Tang et al. discovered that shorter APTES-SiO_2 nanohybrids were easily confined to the liver, but longer ones were primarily dispersed in the spleen. However, PEGylated silica nanohybrids of both dimensions were reported to be increased in the lungs of experimental individuals. Silica nanoparticles with rough surfaces have been effectively manufactured in the form of virus-, rambutan-, raspberry-, or flower-like structures, and it has been discovered that these structures improve cellular absorption effectiveness by increasing adherence to bacterial or cell surfaces [131, 156, 157]. There is a growing interest in using nanohybrids with PEGA-functionalized silica nanocapsules and Au nanorod cores in tandem with PA/CT to guide gene, chemotherapy, and photothermal therapies [18].

4 Multipurpose Medicinal Applications

Nanohybrids comprising organic and inorganic materials, as described in Sect. 3, have significant potential in a wide range of biomedical applications. Three categories are used to categorize these applications: diagnostic imaging and therapeutic imaging.

4.1 Flexible Imaging

To name just a few of the imaging methods in which they are employed, NPs are found in everything from CT scans to positron emission tomographies (PET) to ultrasonic imaging [97]. Anatomical, physiological, and metabolic phenomena are predicted to be accurately captured by these imaging modalities. When analyzing clinical data, it is critical to be able to see physical structures clearly so that doctors can make the right treatment decisions [152, 231]. MR pictures with a high signal contrast on T_1-weighted images are known as T_1-weighted because it measures longitudinal relaxation with a positive contrast. There is a negative contrast and a dark signal contrast in photos that are T_2-weighted because T_2 denotes transverse relaxation. Contrast agents are usually used to make MRI more sensitive by shortening the time it takes for T_1 or T_2 to relax, which is called the r1 or r2 relaxivity [62]. Metal chelating complexes, such as Gd^{3+}- and Mn^{2+}-based T_1 contrast agents, are commonly used to make T1 contrast agents. MRI T_1-weighted with Gd^{3+}, which has

seven unpaired electrons, is widely used in the medical field. The T_2 contrast agents are predominantly Fe_3O_4 NPs [62, 88]. Fe_3O_4 NPs are commonly operationalized by PEG to increase their cytocompatibility and circulation time of blood, both of which are important for improving contrast efficiency in MRI scans and other diagnostic procedures [59, 144]. Compounds like peptides are added to the organic components of these nanohybrids to improve the resolution of sick tissues when they are scanned with targeted MRI, as seen in this illustration [127, 182].

4.1.1 Luminescence Imaging

Because optical FL imaging uses no ionizing radiation and is hence noninvasive, it gives the most eye-catching data. The newly developed NIR FL imaging, which also includes larger imaging in the second NIR band (NIR-II, 1000–1700 nm), has deep penetration and outstanding spatial resolution [57, 76]. The inorganic components of nanohybrids are typically responsible for their luminous characteristics. Luminescent carbon dots or spherical nanoparticles are often made with PEG or PVP to make them more biocompatible for imaging in the body [92, 206].

4.1.2 Imaging with Other Modalities

PA imaging is capable because it is premised on sound waves that move with heat and can go deeper than optical imaging can. According to experts, CT imaging is thought to have multidimensional and density resolution compared to other imaging modalities. Shi et al. generated acetylated generation 5 (G5) PAMAM dendrimer-encased Au NPs using a one-pot process, and these NPs showed great promise for use in CT imaging of cancer cells [174]. Real-time monitoring of gastrointestinal bleeding is also possible using MPI. This would be a safe and sensitive situation [211].

4.1.3 Multimodal Imaging

Because of the recompense of immediate response, good selection, spatial/chronological/contrast resolution, and high penetration, multimodal imaging is much sought after [37, 87, 88]. Multimodal contrast agents based on organic/inorganic nanohybrids may be productive for a range of imaging purposes. In terms of spatial and density resolution, CT imaging is believed to be superior to many other modalities. Shi et al. generated acetylated generation 5 (G5) PAMAM dendrimer-encased Au NPs using a one-pot process, and these NPs showed great promise for use in CT imaging of cancer cells [174]. The intranasal administration of glucose-coated Au NPs, as demonstrated by Ropovtzer et al., allowed for in vivo CT imaging of exosomes within the brain, a technique that has the potential to serve as a very sensitive diagnostic platform for a wide range of

brain disorders [6]. NPs made of silica or calcium carbonate are commonly utilized in US imaging. The nanohybrids of MWCNTs, PEI, and a monoclonal antibody were found to be useful for targeted US imaging of malignant tumors [186, 189].

4.2 Diverse Therapies

However, effective therapy demands additional efforts due to the fact that flexible imaging allows for the reliable and sensitive detection of infectious regions for early diagnosis [32]. Phototherapy (PTT and PDT), chemotherapy, genetic testing, radiation therapy, and multimodal therapy are all being studied a lot right now, and they are all being looked at very closely [32].

4.2.1 Phototherapy

It is a harmless light-induced remedy that is mostly local in nature and has the potential to minimize damage to healthy tissues. It is common for PTT monotherapy nanohybrids to be constructed from nanostructured inorganic materials with high NIR absorption, such as Au [175, 178] and Zn [178, 181, 184], GO [204], MoS2 [17, 179], Cu2 XSe [17, 35] and Ti_3C_2 [98] PDT, in contrast to PTT, is an oxygen-dependent phototherapy that uses photosensitizers. Improvements in tumor oxygenation may, in this case, lead to improved overall performance. The activation of the light sensitizer promotes the death of cancer cells by releasing deadly ROS. Designing nanohybrids with hydrophobic photoenergetic agents (PHAs) in mind is necessary for better efficacy in photodynamic therapy. Silica [117], calcium carbonate [132], and calcium phosphosilicate are examples of inorganic NPs [3].

4.2.2 Chemotherapy

In the future, nanohybrids could be used to carry chemotherapeutic medications. Mesopores or hollow gaps can be exploited to deliver medications to MSNs with large specific regions [105, 148, 219, 228]. As described in Sect. 3.1, organic portions of nanohybrids can provide responsiveness, targeting, or multifunctions for controlled drug delivery. PEGylated Janus $Fe_3O_4SiO_2$ NPs were created to target liver cancer therapy [148]. Another promising class of drug delivery systems was found in dextran-functionalized iron oxide nanocages. It is interesting that the cage shape affects drug release and cell absorption in a way that makes medicines more effective [139].

4.2.3 Gene Transfer Treatment

GT shows potential treatment strategy for inherited diseases that involves therapeutic nucleic acid insertion into cells. Nanohybrids of organic and inorganic materials have the potential to be excellent choices. As gene carriers, polycations with charge groups such as amino (NH_2) and imino (NH) might be used [124, 195]. Nonviral gene carriers such as PEI are used to condense DNA through electrostatic interactions between the organic cationic sections of nanohybrids [157, 197]. For "Nanoscript" platforms, nanohybrids could be used to integrate tiny compounds with gold or magnetic NPs to control gene expression. Using a platform like this, stem cells could be encouraged to differentiate into neurons or muscle cells [134]. Cooperative PTT/GT boosted PTT efficacy, which resulted in an increased anticancer impact. In particular, the nanohybrids containing HA and porous hollow structures are of interest. A combination of tumor starvation therapy and low-temperature photothermal therapy was prepared using Prussian blue nanoparticles (NPs) in this work (PTT) [229]. Tumor starvation therapy relies on glucose oxidase as a glucose consumer and a source of gluconic acid for glucose consumption. Nanohybrids with MnO_2 NPs increased PDT efficiency by producing oxygen to overcome tumor hypoxia hypoxic conditions [222].

4.3 Therapy Directed by Imaging

It would be excellent if therapy processes could be monitored in order to gather vital information that could be used to adjust treatment. Researchers are working Therapy Directed by Imaging, which relies on logical methods for making nanohybrids that combine good features and functions into a single structure so that they can be used to treat people.

4.3.1 Monomodal Imaging-Guided Therapy

MRI has received the greatest research into imaging-guided therapy of any imaging modality. MRI imaging-guided therapy in the T1 mode frequently employs magnetic components like Mn^{2+}, Gd^{3+}, or amorphous Fe NPs [122, 212]. CoP NPs or amorphous Fe_3O_4 for T1/T2 dual-mode and FeS2, Fe_3O_4@Gd_2O_3 for T2 mode [104, 203]. PDT, SDT, or chemotherapy using MnO_2 or Mn-doped silica NPs, which react with malignant cells H_2O_2 to create O_2 and overcome malignant hypoxia, is common [109, 233]. Fe_3O_4 nanoparticles covered with red blood cell membranes were generated using a microfluidic electroporation technique. In order to accomplish noninvasive anticancerous theragnosis, Fedorova et al. proposed allowing NIR FL image tracking and PDT to function independently [120]. Inorganic NPs' cavities could release medication when illuminated with NIR light. Intriguingly, NIR pretreatment improved PA imaging with the NIR-triggered targeting nanohybrids.

4.3.2 Imaging-Guided Remedy with Multimodality

For example, organic/inorganic nanohybrids may either have inorganic theranostic NPs or an amalgamation of both of these components that can perform multimodal imaging and therapy. As a gatekeeper and gene carrier, CD-PGEA was used to load medications into mesoporous silica. PTT and CD-PGEA deconstruction were both facilitated by the photothermal action mediated by Au NRs during NIR irradiation, allowing for NIR-triggered medicine discharge. A multimodal imaging-guided PTT/GT/chemotherapy was created because of this [49, 66, 176]. When creating polypyrrole/MSN yolk-shell nanohybrids, the poly pyrrole core was used as a photothermal polymer for PA imaging and PTT, while the MSN shell and intermediate space were used to load perfluorohexane as a contrast for better US imaging [49].

5 Conclusions and Perspectives

When it comes to designing nanohybrids, the complimentary characteristics and functionalities of natural and synthetic component is one of the most exciting aspects. Because it offers a novel technique that looks to be beneficial for diagnosing and monitoring therapeutic processes, the use of nanohybrids for imaging-guided therapy needs greater study. Among other things, the scope of immunization research will be broadened as a result of these findings. Because of their amazing versatility, it is feasible that organic/inorganic nanohybrids will serve as a cutting-edge benchmark for prospective medical applications and customized therapy.

References

1. Albanese A et al (2012) The effect of nanoparticle size, shape, and surface chemistry on biological systems. Annu Rev Biomed Eng 14:1–16
2. Bagheri A et al (2016) Lanthanide-doped upconversion nanoparticles: emerging intelligent light-activated drug delivery systems. Adv Sci 3(7):1500437
3. Barth BM et al (2011) Targeted indocyanine-green-loaded calcium phosphosilicate nanoparticles for in vivo photodynamic therapy of leukemia. ACS Nano 5(7):5325–5337
4. Basuki JS et al (2013) Grafting of P (OEGA) onto magnetic nanoparticles using Cu (0) mediated polymerization: comparing grafting "from" and "to" approaches in the search for the optimal material design of nanoparticle MRI contrast agents. Macromolecules 46(15):6038–6047
5. Basuki JS et al (2014) A block copolymer-stabilized co-precipitation approach to magnetic iron oxide nanoparticles for potential use as MRI contrast agents. Polym Chem 5(7):2611–2620
6. Betzer O et al (2017) In vivo neuroimaging of exosomes using gold nanoparticles. ACS Nano 11(11):10883–10893
7. Biju V (2014) Chemical modifications and bioconjugate reactions of nanomaterials for sensing, imaging, drug delivery and therapy. Chem Soc Rev 43(3):744–764

8. Boyer C et al (2016) Copper-mediated living radical polymerization (atom transfer radical polymerization and copper (0) mediated polymerization): from fundamentals to bioapplications. Chem Rev 116(4):1803–1949
9. Boyer C et al (2010) Anti-fouling magnetic nanoparticles for siRNA delivery. J Mater Chem 20(2):255–265
10. Bruchez Jr M et al (1998) Semiconductor nanocrystals as fluorescent biological labels. Science 281(5385):2013–2016
11. Brust M et al (1994) Synthesis of thiol-derivatised gold nanoparticles in a two-phase liquid–liquid system. J Chem Soc Chem Commun (7):801–802
12. Burda C et al (2005) Chemistry and properties of nanocrystals of different shapes. Chem Rev 105(4):1025–1102
13. Chauhan VP et al (2011) Fluorescent nanorods and nanospheres for real-time in vivo probing of nanoparticle shape-dependent tumor penetration. Angew Chem 123(48):11619–11622
14. Chen D et al (2014) Photoacoustic imaging guided near-infrared photothermal therapy using highly water-dispersible single-walled carbon nanohorns as theranostic agents. Adv Func Mater 24(42):6621–6628
15. Chen G et al (2017) Neuroendocrine tumor-targeted upconversion nanoparticle-based micelles for simultaneous nir-controlled combination chemotherapy and photodynamic therapy, and fluorescence imaging. Adv Func Mater 27(8):1604671
16. Chen G et al (2016) Nanochemistry and nanomedicine for nanoparticle-based diagnostics and therapy. Chem Rev 116(5):2826–2885
17. Chen L et al (2017) One-pot synthesis of MoS2 nanoflakes with desirable degradability for photothermal cancer therapy. ACS Appl Mater Interfaces 9(20):17347–17358
18. Chen X et al (2018) Rattle-structured rough nanocapsules with in-situ-formed gold nanorod cores for complementary gene/chemo/photothermal therapy. ACS Nano 12(6):5646–5656
19. Cheng L et al (2014) PEGylated WS2 nanosheets as a multifunctional theranostic agent for in vivo dual-modal CT/photoacoustic imaging guided photothermal therapy. Adv Mater 26(12):1886–1893
20. Cheng Y et al (2018) Deep-level defect enhanced photothermal performance of bismuth sulfide–gold heterojunction nanorods for photothermal therapy of cancer guided by computed tomography imaging. Angew Chem Int Ed 57(1):246–251
21. Chithrani BD et al (2006) Determining the size and shape dependence of gold nanoparticle uptake into mammalian cells. Nano Lett 6(4):662–668
22. Dai Y et al (2017) Nanoparticle design strategies for enhanced anticancer therapy by exploiting the tumour microenvironment. Chem Soc Rev 46(12):3830–3852
23. Daniels TR et al (2006) The transferrin receptor part I: biology and targeting with cytotoxic antibodies for the treatment of cancer. Clin Immunol 121(2):144–158
24. del Mar Encabo-Berzosa M et al (2017) The effect of PEGylated hollow gold nanoparticles on stem cell migration: potential application in tissue regeneration. Nanoscale 9(28):9848–9858
25. Deng L et al (2016) Hybrid iron oxide–graphene oxide–polysaccharides microcapsule: a micro-matryoshka for on-demand drug release and antitumor therapy in vivo. ACS Appl Mater Interfaces 8(11):6859–6868
26. Deng X et al (2017) A hollow-structured CuS@ Cu2S@ Au nanohybrid: synergistically enhanced photothermal efficiency and photoswitchable targeting effect for cancer theranostics. Adv Mater 29(36):1701266
27. Dunn AE et al (2014) Spatial and temporal control of drug release through pH and alternating magnetic field induced breakage of Schiff base bonds. Polym Chem 5(10):3311–3315
28. Duong HT et al (2014) Functional gold nanoparticles for the storage and controlled release of nitric oxide: applications in biofilm dispersal and intracellular delivery. J Mater Chem B 2(31):5003–5011
29. Edmondson S et al (2004) Polymer brushes via surface-initiated polymerizations. Chem Soc Rev 33(1):14–22
30. Elacqua E et al (2017) Molecular recognition in the colloidal world. Acc Chem Res 50(11):2756–2766

31. Fan W et al (2016) On the latest three-stage development of nanomedicines based on upconversion nanoparticles. Adv Mater 28(21):3987–4011
32. Fan W et al (2017) Nanotechnology for multimodal synergistic cancer therapy. Chem Rev 117(22):13566–13638
33. Feng Q et al (2016) Tumor-targeted and multi-stimuli responsive drug delivery system for near-infrared light induced chemo-phototherapy and photoacoustic tomography. Acta Biomater 38:129–142
34. Feng T et al (2016) Charge-convertible carbon dots for imaging-guided drug delivery with enhanced in vivo cancer therapeutic efficiency. ACS Nano 10(4):4410–4420
35. Feng W et al (2015) Flower-like PEGylated MoS2 nanoflakes for near-infrared photothermal cancer therapy. Sci Rep 5(1):1–13
36. Frens G (1973) Controlled nucleation for the regulation of the particle size in monodisperse gold suspensions. Nat Phys Sci 241(105):20–22
37. Gai S et al (2014) Recent progress in rare earth micro/nanocrystals: soft chemical synthesis, luminescent properties, and biomedical applications. Chem Rev 114(4):2343–2389
38. Gallo J et al (2013) Magnetic nanoparticles as contrast agents in the diagnosis and treatment of cancer. Chem Soc Rev 42(19):7816–7833
39. Gao F et al (2017) Biocompatible cup-shaped nanocrystal with ultrahigh photothermal efficiency as tumor therapeutic agent. Adv Func Mater 27(24):1700605
40. Gao X et al (2004) In vivo cancer targeting and imaging with semiconductor quantum dots. Nat Biotechnol 22(8):969–976
41. Ge S et al (2009) Facile hydrothermal synthesis of iron oxide nanoparticles with tunable magnetic properties. J Phys Chem C 113(31):13593–13599
42. Geng Y et al (2007) Shape effects of filaments versus spherical particles in flow and drug delivery. Nat Nanotechnol 2(4):249–255
43. Georgakilas V et al (2016) Noncovalent functionalization of graphene and graphene oxide for energy materials, biosensing, catalytic, and biomedical applications. Chem Rev 116(9):5464–5519
44. Gleich B, Weizenecker J (2005) Tomographic imaging using the nonlinear response of magnetic particles. Nature 435(7046):1214–1217
45. Gong L et al (2017) Two-dimensional transition metal dichalcogenide nanomaterials for combination cancer therapy. J Mater Chem B 5(10):1873–1895
46. Goodwill PW et al (2012) X-space MPI: magnetic nanoparticles for safe medical imaging. Adv Mater 24(28):3870–3877
47. Guan M et al (2015) Multifunctional upconversion–nanoparticles–trismethylpyridylporphyrin–fullerene nanocomposite: a near-infrared light-triggered theranostic platform for imaging-guided photodynamic therapy. NPG Asia Mater 7(7):e205–e205
48. Guo R et al (2016) Mitochondria-targeting magnetic composite nanoparticles for enhanced phototherapy of cancer. Small 12(33):4541–4552
49. Guo R et al (2018) A yolk–shell nanoplatform for gene-silencing-enhanced photolytic ablation of cancer. Adv Func Mater 28(14):1706398
50. Guo R et al (2010) Multifunctional nanocarriers for cell imaging, drug delivery, and near-IR photothermal therapy. Langmuir 26(8):5428–5434
51. Guo W et al (2016) Self-powered electrical stimulation for enhancing neural differentiation of mesenchymal stem cells on graphene–poly (3, 4-ethylenedioxythiophene) hybrid microfibers. ACS Nano 10(5):5086–5095
52. Han X et al (2018) Oxygen-deficient black titania for synergistic/enhanced sonodynamic and photoinduced cancer therapy at near infrared-II biowindow. ACS Nano 12(5):4545–4555
53. He X et al (2008) In vivo study of biodistribution and urinary excretion of surface-modified silica nanoparticles. Anal Chem 80(24):9597–9603
54. Herr JK et al (2006) Aptamer-conjugated nanoparticles for selective collection and detection of cancer cells. Anal Chem 78(9):2918–2924
55. Hervault A et al (2016) Doxorubicin loaded dual pH-and thermo-responsive magnetic nanocarrier for combined magnetic hyperthermia and targeted controlled drug delivery applications. Nanoscale 8(24):12152–12161

56. Hinde E et al (2017) Pair correlation microscopy reveals the role of nanoparticle shape in intracellular transport and site of drug release. Nat Nanotechnol 12(1):81–89
57. Hong G et al (2017) Near-infrared fluorophores for biomedical imaging. Nat Biomed Eng 1(1):1–22
58. Hou C-H et al (2009) The fabrication and characterization of dicalcium phosphate dihydrate-modified magnetic nanoparticles and their performance in hyperthermia processes in vitro. Biomaterials 30(27):4700–4707
59. Hu F et al (2006) Preparation of biocompatible magnetite nanocrystals for in vivo magnetic resonance detection of cancer. Adv Mater 18(19):2553–2556
60. Hu H et al (2017) Synthesis of Janus Au@ periodic mesoporous organosilica (PMO) nanostructures with precisely controllable morphology: a seed-shape defined growth mechanism. Nanoscale 9(14):4826–4834
61. Hu Y et al (2017) A comparative study of clinical intervention and interventional photothermal therapy for pancreatic cancer. Adv Mater 29(33):1700448
62. Hu Y et al (2018) Construction of iron oxide nanoparticle-based hybrid platforms for tumor imaging and therapy. Chem Soc Rev 47(5):1874–1900
63. Hu Y et al (2017) Multifunctional hetero-nanostructures of hydroxyl-rich polycation wrapped cellulose-gold hybrids for combined cancer therapy. J Control Release 255:154–163
64. Huang P et al (2012) Light-triggered theranostics based on photosensitizer-conjugated carbon dots for simultaneous enhanced-fluorescence imaging and photodynamic therapy. Adv Mater 24(37):5104–5110
65. Huang X et al (2012) Synthesis of hetero-polymer functionalized nanocarriers by combining surface-initiated ATRP and RAFT polymerization. Small 8(23):3579–3583
66. Huang X et al (2016) NaYF4: Yb/Er@ PPy core–shell nanoplates: an imaging-guided multimodal platform for photothermal therapy of cancers. Nanoscale 8(2):1040–1048
67. Huang X et al (2011) The shape effect of mesoporous silica nanoparticles on biodistribution, clearance, and biocompatibility in vivo. ACS Nano 5(7):5390–5399
68. Huang X et al (2010) The effect of the shape of mesoporous silica nanoparticles on cellular uptake and cell function. Biomaterials 31(3):438–448
69. Huang X et al (2013) Mesenchymal stem cell-based cell engineering with multifunctional mesoporous silica nanoparticles for tumor delivery. Biomaterials 34(7):1772–1780
70. Hwang AA et al (2015) pH-responsive isoniazid-loaded nanoparticles markedly improve tuberculosis treatment in mice. Small 11(38):5066–5078
71. Hyeon T (2003) Chemical synthesis of magnetic nanoparticles. Chem Commun (8):927–934
72. Hyeon T et al (2001) Synthesis of highly crystalline and monodisperse maghemite nanocrystallites without a size-selection process. J Am Chem Soc 123(51):12798–12801
73. Jain RK (2012) Delivery of molecular and cellular medicine to solid tumors. Adv Drug Deliv Rev 64:353–365
74. Jang H et al (2014) Facile synthesis and intraparticle self-catalytic oxidation of dextran-coated hollow Au–Ag nanoshell and its application for chemo-thermotherapy. ACS Nano 8(1):467–475
75. Jatupaiboon N et al (2015) A facile microemulsion template route for producing hollow silica nanospheres as imaging agents and drug nanocarriers. J Mater Chem B 3(16):3130–3133
76. Jeong S et al (2017) Cancer-microenvironment-sensitive activatable quantum dot probe in the second near-infrared window. Nano Lett 17(3):1378–1386
77. Jiang S, Cao Z (2010) Ultralow-fouling, functionalizable, and hydrolyzable zwitterionic materials and their derivatives for biological applications. Adv Mater 22(9):920–932
78. Jing L et al (2016) Aqueous based semiconductor nanocrystals. Chem Rev 116(18):10623–10730
79. Jokerst JV, Gambhir SS (2011) Molecular imaging with theranostic nanoparticles. Acc Chem Res 44(10):1050–1060
80. Kempen PJ et al (2015) Theranostic mesoporous silica nanoparticles biodegrade after pro-survival drug delivery and ultrasound/magnetic resonance imaging of stem cells. Theranostics 5(6):631

81. Kim B et al (2010) Tuning payload delivery in tumour cylindroids using gold nanoparticles. Nat Nanotechnol 5(6):465–472
82. Kim BH et al (2011) Large-scale synthesis of uniform and extremely small-sized iron oxide nanoparticles for high-resolution T1 magnetic resonance imaging contrast agents. J Am Chem Soc 133(32):12624–12631
83. Kim D et al (2010) A drug-loaded aptamer–gold nanoparticle bioconjugate for combined CT imaging and therapy of prostate cancer. ACS Nano 4(7):3689–3696
84. Kim D et al (2009) Synthesis of uniform ferrimagnetic magnetite nanocubes. J Am Chem Soc 131(2):454–455
85. Kim J et al (2016) Single-layered MoS2–PEI–PEG nanocomposite-mediated gene delivery controlled by photo and redox stimuli. Small 12(9):1184–1192
86. Kucheryavy P et al (2013) Superparamagnetic iron oxide nanoparticles with variable size and an iron oxidation state as prospective imaging agents. Langmuir 29(2):710–716
87. Lee D-E et al (2012) Multifunctional nanoparticles for multimodal imaging and theragnosis. Chem Soc Rev 41(7):2656–2672
88. Lee N et al (2015) Iron oxide based nanoparticles for multimodal imaging and magnetoresponsive therapy. Chem Rev 115(19):10637–10689
89. Lei M et al (2017) Activated surface charge-reversal manganese oxide nanocubes with high surface-to-volume ratio for accurate magnetic resonance tumor imaging. Adv Func Mater 27(30):1700978
90. Li C et al (2014) Gold-coated Fe_3O_4 nanoroses with five unique functions for cancer cell targeting, imaging, and therapy. Adv Func Mater 24(12):1772–1780
91. Li C et al (2015) Mesoporous carbon nanospheres featured fluorescent aptasensor for multiple diagnosis of cancer in vitro and in vivo. ACS Nano 9(12):12096–12103
92. Li D et al (2018) Near-infrared excitation/emission and multiphoton-induced fluorescence of carbon dots. Adv Mater 30(13):1705913
93. Li L et al (2013) Generalized approach to the synthesis of reversible concentric and eccentric polymer-coated nanostructures. Small 9(6):825–830
94. Li Y et al (2018) Positively charged polyprodrug amphiphiles with enhanced drug loading and reactive oxygen species-responsive release ability for traceable synergistic therapy. J Am Chem Soc 140(11):4164–4171
95. Li Y et al (2015) Core–shell upconversion nanoparticle@ metal–organic framework nanoprobes for luminescent/magnetic dual-mode targeted imaging. Adv Mater 27(27):4075–4080
96. Liang C et al (2014) Tumor metastasis inhibition by imaging-guided photothermal therapy with single-walled carbon nanotubes. Adv Mater 26(32):5646–5652
97. Lim E-K et al (2015) Nanomaterials for theranostics: recent advances and future challenges. Chem Rev 115(1):327–394
98. Lin H et al (2017) Two-dimensional ultrathin MXene ceramic nanosheets for photothermal conversion. Nano Lett 17(1):384–391
99. Lin Y et al (2011) Water-soluble chitosan-quantum dot hybrid nanospheres toward bioimaging and biolabeling. ACS Appl Mater Interfaces 3(4):995–1002
100. Ling D et al (2015) Chemical synthesis and assembly of uniformly sized iron oxide nanoparticles for medical applications. Acc Chem Res 48(5):1276–1285
101. Liu B et al (2015) Poly (acrylic acid) modification of Nd3+-sensitized upconversion nanophosphors for highly efficient UCL imaging and pH-responsive drug delivery. Adv Func Mater 25(29):4717–4729
102. Liu C et al (2014) Are rare-earth nanoparticles suitable for in vivo applications? Adv Mater 26(40):6922–6932
103. Liu H et al (2012) Targeting gold nanoshells on silica nanorattles: a drug cocktail to fight breast tumors via a single irradiation with near-infrared laser light. Adv Mater 24(6):755–761
104. Liu J et al (2018) A new co-P nanocomposite with ultrahigh relaxivity for in vivo magnetic resonance imaging-guided tumor eradication by chemo/photothermal synergistic therapy. Small 14(7):1702431

105. Liu J et al (2017) Safe and effective reversal of cancer multidrug resistance using sericin-coated mesoporous silica nanoparticles for lysosome-targeting delivery in mice. Small 13(9):1602567
106. Liu J et al (2016) Hollow mesoporous silica nanoparticles facilitated drug delivery via cascade pH stimuli in tumor microenvironment for tumor therapy. Biomaterials 83:51–65
107. Liu J et al (2015) Mesoporous silica coated single-walled carbon nanotubes as a multi-functional light-responsive platform for cancer combination therapy. Adv Func Mater 25(3):384–392
108. Liu X et al (2016) Tumor-targeted multimodal optical imaging with versatile cadmium-free quantum dots. Adv Func Mater 26(2):267–276
109. Liu Y et al (2018) Engineering multifunctional RNAi nanomedicine to concurrently target cancer hallmarks for combinatorial therapy. Angew Chem Int Ed 57(6):1510–1513
110. Liu Z et al (2013) Long-circulating Gd_2O_3: Yb3+, Er3+ up-conversion nanoprobes as high-performance contrast agents for multi-modality imaging. Biomaterials 34(6):1712–1721
111. Louie A (2010) Multimodality imaging probes: design and challenges. Chem Rev 110(5):3146–3195
112. Low PS et al (2008) Discovery and development of folic-acid-based receptor targeting for imaging and therapy of cancer and inflammatory diseases. Acc Chem Res 41(1):120–129
113. Lu F et al (2009) Size effect on cell uptake in well-suspended, uniform mesoporous silica nanoparticles. Small 5(12):1408–1413
114. Lundqvist M et al (2008) Nanoparticle size and surface properties determine the protein corona with possible implications for biological impacts. Proc Natl Acad Sci 105(38):14265–14270
115. Luo Z et al (2014) Intracellular redox-activated anticancer drug delivery by functionalized hollow mesoporous silica nanoreservoirs with tumor specificity. Biomaterials 35(27):7951–7962
116. Lutz J-F et al (2006) One-pot synthesis of PEGylated ultrasmall iron-oxide nanoparticles and their in vivo evaluation as magnetic resonance imaging contrast agents. Biomacromolecules 7(11):3132–3138
117. Ma X et al (2015) Targeted delivery of 5-aminolevulinic acid by multifunctional hollow mesoporous silica nanoparticles for photodynamic skin cancer therapy. ACS Appl Mater Interfaces 7(20):10671–10676
118. Ma X et al (2011) Theranostic nanoparticles engineered for clinic and pharmaceutics. Acc Chem Res 44(10):1114–1122
119. Maeda H et al (2013) The EPR effect for macromolecular drug delivery to solid tumors: improvement of tumor uptake, lowering of systemic toxicity, and distinct tumor imaging in vivo. Adv Drug Deliv Rev 65(1):71–79
120. Mangadlao JD et al (2018) Prostate-specific membrane antigen targeted gold nanoparticles for theranostics of prostate cancer. ACS Nano 12(4):3714–3725
121. Meng H et al (2011) Aspect ratio determines the quantity of mesoporous silica nanoparticle uptake by a small GTPase-dependent macropinocytosis mechanism. ACS Nano 5(6):4434–4447
122. Mi P et al (2015) Hybrid calcium phosphate-polymeric micelles incorporating gadolinium chelates for imaging-guided gadolinium neutron capture tumor therapy. ACS Nano 9(6):5913–5921
123. Min KH et al (2012) The tumor accumulation and therapeutic efficacy of doxorubicin carried in calcium phosphate-reinforced polymer nanoparticles. Biomaterials 33(23):5788–5797
124. Mintzer MA, Simanek EE (2009) Nonviral vectors for gene delivery. Chem Rev 109(2):259–302
125. Mooney E et al (2012) The electrical stimulation of carbon nanotubes to provide a cardiomimetic cue to MSCs. Biomaterials 33(26):6132–6139
126. Nam J et al (2013) Surface engineering of inorganic nanoparticles for imaging and therapy. Adv Drug Deliv Rev 65(5):622–648
127. Nasr SH et al (2018) Detection of β-amyloid by sialic acid coated bovine serum albumin magnetic nanoparticles in a mouse model of Alzheimer's disease. Small 14(3):1701828

128. Nguyen KT, Zhao Y (2015) Engineered hybrid nanoparticles for on-demand diagnostics and therapeutics. Acc Chem Res 48(12):3016–3025
129. Nguyen T-K et al (2015) Iron oxide nanoparticle-mediated hyperthermia stimulates dispersal in bacterial biofilms and enhances antibiotic efficacy. Sci Rep 5(1):1–15
130. Niikura K et al (2013) Gold nanoparticles as a vaccine platform: influence of size and shape on immunological responses in vitro and in vivo. ACS Nano 7(5):3926–3938
131. Niu Y et al (2013) Nanoparticles mimicking viral surface topography for enhanced cellular delivery. Adv Mater 25(43):6233–6237
132. Nomoto T et al (2016) Calcium phosphate-based organic–inorganic hybrid nanocarriers with pH-responsive on/off switch for photodynamic therapy. Biomater Sci 4(5):826–838
133. Palanikumar L et al (2015) Noncovalent polymer-gatekeeper in mesoporous silica nanoparticles as a targeted drug delivery platform. Adv Func Mater 25(6):957–965
134. Patel S et al (2015) Inducing stem cell myogenesis using nanoscript. ACS Nano 9(7):6909–6917
135. Prencipe G et al (2009) PEG branched polymer for functionalization of nanomaterials with ultralong blood circulation. J Am Chem Soc 131(13):4783–4787
136. Qi G et al (2010) Facile and scalable synthesis of monodispersed spherical capsules with a mesoporous shell. Chem Mater 22(9):2693–2695
137. Qiao H et al (2017) Targeting osteocytes to attenuate early breast cancer bone metastasis by theranostic upconversion nanoparticles with responsive plumbagin release. ACS Nano 11(7):7259–7273
138. Qiu J et al (2005) Preparation and characterization of porous ultrafine Fe_2O_3 particles. Mater Res Bull 40(11):1968–1975
139. Rampersaud S et al (2016) The effect of cage shape on nanoparticle-based drug carriers: anticancer drug release and efficacy via receptor blockade using dextran-coated iron oxide nanocages. Nano Lett 16(12):7357–7363
140. Reddy LH et al (2012) Magnetic nanoparticles: design and characterization, toxicity and biocompatibility, pharmaceutical and biomedical applications. Chem Rev 112(11):5818–5878
141. Ruiz-Hitzky E et al (2010) Advances in biomimetic and nanostructured biohybrid materials. Adv Mater 22(3):323–336
142. Sanchez C et al (2005) Applications of hybrid organic–inorganic nanocomposites. J Mater Chem 15(35–36):3559–3592
143. Sapsford KE et al (2013) Functionalizing nanoparticles with biological molecules: developing chemistries that facilitate nanotechnology. Chem Rev 113(3):1904–2074
144. Sarigiannis Y et al (2016) Synthesis and evaluation of condensed magnetic nanocrystal clusters with in vivo multispectral optoacoustic tomography for tumour targeting. Biomaterials 91:128–139
145. Schick I et al (2014) Multifunctional two-photon active silica-coated Au@ MnO Janus particles for selective dual functionalization and imaging. J Am Chem Soc 136(6):2473–2483
146. Seidi F et al (2018) Designing smart polymer conjugates for controlled release of payloads. Chem Rev 118(7):3965–4036
147. Shakeel A et al (2022) Advanced polymeric/inorganic nanohybrids: an integrated platform for gas sensing applications. Chemosphere 133772
148. Shao D et al (2016) Janus "nano-bullets" for magnetic targeting liver cancer chemotherapy. Biomaterials 100:118–133
149. Shen Z et al (2017) Multifunctional theranostic nanoparticles based on exceedingly small magnetic iron oxide nanoparticles for T1-weighted magnetic resonance imaging and chemotherapy. ACS Nano 11(11):10992–11004
150. Shim MS, Kwon YJ (2012) Stimuli-responsive polymers and nanomaterials for gene delivery and imaging applications. Adv Drug Deliv Rev 64(11):1046–1059
151. Smith AM et al (2008) Bioconjugated quantum dots for in vivo molecular and cellular imaging. Adv Drug Deliv Rev 60(11):1226–1240
152. Smith BR, Gambhir SS (2017) Nanomaterials for in vivo imaging. Chem Rev 117(3):901–986

153. Song G et al (2018) Janus iron oxides@ semiconducting polymer nanoparticle tracer for cell tracking by magnetic particle imaging. Nano Lett 18(1):182–189
154. Song G et al (2014) Hydrophilic molybdenum oxide nanomaterials with controlled morphology and strong plasmonic absorption for photothermal ablation of cancer cells. ACS Appl Mater Interfaces 6(6):3915–3922
155. Song G et al (2013) A low-toxic multifunctional nanoplatform based on Cu9S5@ $mSiO_2$ core-shell nanocomposites: combining photothermal-and chemotherapies with infrared thermal imaging for cancer treatment. Adv Func Mater 23(35):4281–4292
156. Song H et al (2016) Silica nanopollens enhance adhesion for long-term bacterial inhibition. J Am Chem Soc 138(20):6455–6462
157. Song H et al (2017) Plasmid DNA delivery: nanotopography matters. J Am Chem Soc 139(50):18247–18254
158. Srinivas R et al (2009) Cationic amphiphiles: promising carriers of genetic materials in gene therapy. Chem Soc Rev 38(12):3326–3338
159. Srinivasarao M, Low PS (2017) Ligand-targeted drug delivery. Chem Rev 117(19):12133–12164
160. Stöber W et al (1968) Controlled growth of monodisperse silica spheres in the micron size range. J Colloid Interface Sci 26(1):62–69
161. Subramaniam P et al (2012) Generation of a library of non-toxic quantum dots for cellular imaging and siRNA delivery. Adv Mater 24(29):4014–4019
162. Sun Q et al (2017) A photoresponsive and rod-shape nanocarrier: single wavelength of light triggered photothermal and photodynamic therapy based on AuNRs-capped & Ce6-doped mesoporous silica nanorods. Biomaterials 122:188–200
163. Tang J et al (2013) Carbon nanodots featuring efficient FRET for real-time monitoring of drug delivery and two-photon imaging. Adv Mater 25(45):6569–6574
164. Tong R et al (2014) Smart chemistry in polymeric nanomedicine. Chem Soc Rev 43(20):6982–7012
165. Torchilin V (2011) Tumor delivery of macromolecular drugs based on the EPR effect. Adv Drug Deliv Rev 63(3):131–135
166. Tsoi KM et al (2013) Are quantum dots toxic? Exploring the discrepancy between cell culture and animal studies. Acc Chem Res 46(3):662–671
167. Ulbrich K, Hola K, Subr V, Bakandritsos A, Tucek J, Zboril R (2016) Chem Rev 116:5338–5431
168. Von Maltzahn G et al (2011) Nanoparticles that communicate in vivo to amplify tumour targeting. Nat Mater 10(7):545–552
169. Walkey CD et al (2012) Nanoparticle size and surface chemistry determine serum protein adsorption and macrophage uptake. J Am Chem Soc 134(4):2139–2147
170. Wang D et al (2014) Fabrication of single-hole glutathione-responsive degradable hollow silica nanoparticles for drug delivery. ACS Appl Mater Interfaces 6(15):12600–12608
171. Wang F et al (2011) Doxorubicin-tethered responsive gold nanoparticles facilitate intracellular drug delivery for overcoming multidrug resistance in cancer cells. ACS Nano 5(5):3679–3692
172. Wang H et al (2015) Biocompatible PEG-chitosan@ carbon dots hybrid nanogels for two-photon fluorescence imaging, near-infrared light/pH dual-responsive drug carrier, and synergistic therapy. Adv Func Mater 25(34):5537–5547
173. Wang H et al (2016) Design and synthesis of core–shell–shell upconversion nanoparticles for NIR-induced drug release, photodynamic therapy, and cell imaging. ACS Appl Mater Interfaces 8(7):4416–4423
174. Wang H et al (2011) Computed tomography imaging of cancer cells using acetylated dendrimer-entrapped gold nanoparticles. Biomaterials 32(11):2979–2988
175. Wang H et al (2013) Folic acid-modified dendrimer-entrapped gold nanoparticles as nanoprobes for targeted CT imaging of human lung adenocarcinoma. Biomaterials 34(2):470–480
176. Wang J et al (2016) MoS2 quantum dot@ polyaniline inorganic–organic nanohybrids for in vivo dual-modal imaging guided synergistic photothermal/radiation therapy. ACS Appl Mater Interfaces 8(37):24331–24338

177. Wang R et al (2016) Well-defined peapod-like magnetic nanoparticles and their controlled modification for effective imaging guided gene therapy. ACS Appl Mater Interfaces 8(18):11298–11308
178. Wang S et al (2010) Photothermal effects of supramolecularly assembled gold nanoparticles for the targeted treatment of cancer cells. Angew Chem 122(22):3865–3869
179. Wang S et al (2015) Biocompatible PEGylated MoS2 nanosheets: controllable bottom-up synthesis and highly efficient photothermal regression of tumor. Biomaterials 39:206–217
180. Wang S et al (2018) Adjuvant photothermal therapy inhibits local recurrences after breast-conserving surgery with little skin damage. ACS Nano 12(1):662–670
181. Wang S et al (2017) A nanostructured molybdenum disulfide film for promoting neural stem cell neuronal differentiation: toward a nerve tissue-engineered 3D scaffold. Adv Biosyst 1(5):1600042
182. Wang T et al (2018) Timely visualization of the collaterals formed during acute ischemic stroke with Fe_3O_4 nanoparticle-based MR imaging probe. Small 14(23):1800573
183. Wang X et al (2016) Synthesis, properties, and applications of hollow micro-/nanostructures. Chem Rev 116(18):10983–11060
184. Wang Y et al (2013) Comparison study of gold nanohexapods, nanorods, and nanocages for photothermal cancer treatment. ACS Nano 7(3):2068–2077
185. Woo DG et al (2009) The effect of electrical stimulation on the differentiation of hESCs adhered onto fibronectin-coated gold nanoparticles. Biomaterials 30(29):5631–5638
186. Wu H et al (2014) Prostate stem cell antigen antibody-conjugated multiwalled carbon nanotubes for targeted ultrasound imaging and drug delivery. Biomaterials 35(20):5369–5380
187. Wu M et al (2016) Large pore-sized hollow mesoporous organosilica for redox-responsive gene delivery and synergistic cancer chemotherapy. Adv Mater 28(10):1963–1969
188. Wu S-H et al (2013) Synthesis of mesoporous silica nanoparticles. Chem Soc Rev 42(9):3862–3875
189. Wu X et al (2014) Recent development of silica nanoparticles as delivery vectors for cancer imaging and therapy. Nanomed Nanotechnol Biol Med 10(2):297–312
190. Wu Y et al (2012) A quantum dot photoswitch for DNA detection, gene transfection, and live-cell imaging. Small 8(22):3465–3475
191. Xia H et al (2016) pH-sensitive Pt nanocluster assembly overcomes cisplatin resistance and heterogeneous stemness of hepatocellular carcinoma. ACS Cent Sci 2(11):802–811
192. Xiao Q et al (2013) A core/satellite multifunctional nanotheranostic for in vivo imaging and tumor eradication by radiation/photothermal synergistic therapy. J Am Chem Soc 135(35):13041–13048
193. Xie J et al (2010) Nanoparticle-based theranostic agents. Adv Drug Deliv Rev 62(11):1064–1079
194. Xu F-J (2018) Versatile types of hydroxyl-rich polycationic systems via O-heterocyclic ring-opening reactions: from strategic design to nucleic acid delivery applications. Prog Polym Sci 78:56–91
195. Xu F, Yang W (2011) Polymer vectors via controlled/living radical polymerization for gene delivery. Prog Polym Sci 36(9):1099–1131
196. Xu G et al (2016) New generation cadmium-free quantum dots for biophotonics and nanomedicine. Chem Rev 116(19):12234–12327
197. Xu X et al (2018) Precision-guided nanospears for targeted and high-throughput intracellular gene delivery. ACS Nano 12(5):4503–4511
198. Xu Y et al (2018) Recent progress in two-dimensional inorganic quantum dots. Chem Soc Rev 47(2):586–625
199. Xu ZP et al (2006) Inorganic nanoparticles as carriers for efficient cellular delivery. Chem Eng Sci 61(3):1027–1040
200. Yan H et al (2018) "All-in-one" nanoparticles for trimodality imaging-guided intracellular photo-magnetic hyperthermia therapy under intravenous administration. Adv Func Mater 28(9):1705710

201. Yan P et al (2014) A facile strategy to functionalize gold nanorods with polycation brushes for biomedical applications. Acta Biomater 10(8):3786–3794
202. Yang D et al (2015) Current advances in lanthanide ion (Ln 3+)-based upconversion nanomaterials for drug delivery. Chem Soc Rev 44(6):1416–1448
203. Yang K et al (2018) Cooperative assembly of magneto-nanovesicles with tunable wall thickness and permeability for MRI-guided drug delivery. J Am Chem Soc 140(13):4666–4677
204. Yang K et al (2012) The influence of surface chemistry and size of nanoscale graphene oxide on photothermal therapy of cancer using ultra-low laser power. Biomaterials 33(7):2206–2214
205. Yang P et al (2012) Functionalized mesoporous silica materials for controlled drug delivery. Chem Soc Rev 41(9):3679–3698
206. Yang S-T et al (2009) Carbon dots for optical imaging in vivo. J Am Chem Soc 131(32):11308–11309
207. Yang Y et al (2016) Facile synthesis of wormlike quantum dots-encapsulated nanoparticles and their controlled surface functionalization for effective bioapplications. Nano Res 9(9):2531–2543
208. Yi C et al (2017) Anisotropic self-assembly of hairy inorganic nanoparticles. Acc Chem Res 50(1):12–21
209. Yong Y et al (2015) Tungsten sulfide quantum dots as multifunctional nanotheranostics for in vivo dual-modal image-guided photothermal/radiotherapy synergistic therapy. ACS Nano 9(12):12451–12463
210. Yoo J et al (2017) Electromagnetized gold nanoparticles mediate direct lineage reprogramming into induced dopamine neurons in vivo for Parkinson's disease therapy. Nat Nanotechnol 12(10):1006–1014
211. Yu EY et al (2017) Magnetic particle imaging for highly sensitive, quantitative, and safe in vivo gut bleed detection in a murine model. ACS Nano 11(12):12067–12076
212. Yu L et al (2016) "Manganese extraction" strategy enables tumor-sensitive biodegradability and theranostics of nanoparticles. J Am Chem Soc 138(31):9881–9894
213. Yuan J-J et al (2007) Cross-linking of cationic block copolymer micelles by silica deposition. J Am Chem Soc 129(6):1717–1723
214. Zeng X et al (2017) A drug-self-gated mesoporous antitumor nanoplatform based on pH-sensitive dynamic covalent bond. Adv Func Mater 27(11):1605985
215. Zhang J et al (2017) Degradable hollow mesoporous silicon/carbon nanoparticles for photoacoustic imaging-guided highly effective chemo-thermal tumor therapy in vitro and in vivo. Theranostics 7(12):3007
216. Zhang L et al (2016) Tailored synthesis of octopus-type Janus nanoparticles for synergistic actively-targeted and chemo-photothermal therapy. Angew Chem Int Ed 55(6):2118–2121
217. Zhang L et al (2014) Chemical modification of inorganic nanostructures for targeted and controlled drug delivery in cancer treatment. J Mater Chem B 2(5):452–470
218. Zhang L et al (2011) Multifunctional and degradable zwitterionic nanogels for targeted delivery, enhanced MR imaging, reduction-sensitive drug release, and renal clearance. Biomaterials 32(20):4604–4608
219. Zhang Q et al (2014) Biocompatible, uniform, and redispersible mesoporous silica nanoparticles for cancer-targeted drug delivery in vivo. Adv Func Mater 24(17):2450–2461
220. Zhang R et al (2016) Traceable nanoparticle delivery of small interfering RNA and retinoic acid with temporally release ability to control neural stem cell differentiation for Alzheimer's disease therapy. Adv Mater 28(30):6345–6352
221. Zhang S et al (2013) Controllable drug release and simultaneously carrier decomposition of SiO_2-drug composite nanoparticles. J Am Chem Soc 135(15):5709–5716
222. Zhang W et al (2018) Oxygen-generating MnO_2 nanodots-anchored versatile nanoplatform for combined chemo-photodynamic therapy in hypoxic cancer. Adv Func Mater 28(13):1706375
223. Zhang Y et al (2015) Polymer-coated hollow mesoporous silica nanoparticles for triple-responsive drug delivery. ACS Appl Mater Interfaces 7(32):18179–18187
224. Zhao L et al (2014) Near-infrared photoregulated drug release in living tumor tissue via yolk-shell upconversion nanocages. Adv Func Mater 24(3):363–371

225. Zhao N et al (2018) Versatile types of organic/inorganic nanohybrids: from strategic design to biomedical applications. Chem Rev 119(3):1666–1762
226. Zhao Y-L, Stoddart JF (2009) Noncovalent functionalization of single-walled carbon nanotubes. Acc Chem Res 42(8):1161–1171
227. Zheng D-W et al (2016) Carbon-dot-decorated carbon nitride nanoparticles for enhanced photodynamic therapy against hypoxic tumor via water splitting. ACS Nano 10(9):8715–8722
228. Zheng X-Y et al (2017) Gd-dots with strong ligand–water interaction for ultrasensitive magnetic resonance renography. ACS Nano 11(4):3642–3650
229. Zhou J et al (2018) Engineering of a nanosized biocatalyst for combined tumor starvation and low-temperature photothermal therapy. ACS Nano 12(3):2858–2872
230. Zhou J et al (2015) Silica nanotubes decorated by pH-responsive diblock copolymers for controlled drug release. ACS Appl Mater Interfaces 7(6):3618–3625
231. Zhou Z et al (2017) T1–T2 dual-modal magnetic resonance imaging: from molecular basis to contrast agents. ACS Nano 11(6):5227–5232
232. Zhu J et al (2013) Size-dependent cellular uptake efficiency, mechanism, and cytotoxicity of silica nanoparticles toward HeLa cells. Talanta 107:408–415
233. Zhu P et al (2018) Nanoenzyme-augmented cancer sonodynamic therapy by catalytic tumor oxygenation. ACS Nano 12(4):3780–3795
234. Zoppe JO et al (2017) Surface-initiated controlled radical polymerization: state-of-the-art, opportunities, and challenges in surface and interface engineering with polymer brushes. Chem Rev 117(3):1105–1318

Chapter 6
Organic–Inorganic Nanohybrids in Cancer Treatment

Hira Amjad, Komal Rizwan, Muhammad Baber, and Shahid Iqbal

1 Cancer

Cancer is considered to be the second most deadly disease by World Health Organization and GLOBOCAN in 2020 which is killing people exponentially assuming the disease rate to 28.4 million by 2040 [1]. The causes of this disease in developing and developing countries range from smoking to petty injuries [2]. The abnormal growth or uncontrolled growth of body cells is termed as tumor cells, cancer cells, or malignant cells. Cancer cells can penetrate the normal cells and body tissues and can destroy the immune system of body, making the body more prone to any disease whether the bacterial or the viral and eventually encumbering the body functioning [3]. The range of deterioration of tissues may lead to skin cancer, lung cancer, breast cancer, liver cancer, bone marrow cancer, colorectal cancer, prostate cancer, cervical cancer, and leukemia [4]. The cancer in different types also imparts unique lineaments not only uncontrolled growth but also abnormal division, hindrance from programmed cell death, lack of proper signaling, tissue incursion, uncontrolled blood vessel construction, and lastly metastases. There are a number of reasons that may lead to this abnormality including genetic factor, ionizing radiation, exposure to carcinogenic chemical compounds, and pathogens [5]. Moreover, the symptoms of cancers are

H. Amjad
Department of Chemistry, Government College University Lahore, Lahore 54000, Pakistan

K. Rizwan (✉)
Department of Chemistry, University of Sahiwal, Sahiwal 57000, Pakistan
e-mail: komal.rizwan45@yahoo.com

M. Baber
Institute of Molecular Biology and Biotechnology, Bahauddin Zakariya University, Multan, Pakistan

S. Iqbal
Department of Chemistry, School of Natural Sciences (SNS), National University of Sciences and Technology (NUST), H-12, Islamabad 46000, Pakistan

K. Rizwan et al. (eds.), *Hybrid Nanomaterials*, Materials Horizons: From Nature to Nanomaterials, https://doi.org/10.1007/978-981-19-4538-0_6

also different for different types of malignances with weight loss, intense pain, dizziness, digestive system problems, fatigue, changes in lumps, skin changes, or even acne [6].

2 Therapeutic Approach

The therapeutic method ranges from medication to chemotherapy to surgery. However, most of the time, it is combination of two therapies to avoid resistance of disease as well as its eradication. The most important thing in treatment is response of drug and drug resistance by the apoptotic proteins and cancer cells [7]. Despite of number of methods for the treatment of cancer, the death rate is high which may be due to uninformed exact cause of cancer. A major cause for the non-survival is late diagnosis of this disease, so there is need to adopt such methods that cause least side effects with maximum percentage of effectiveness [8].

2.1 Immunotherapy

The prime treatment in practice and research is immunotherapy which is defined as the treatment of cancer by using the substances that increase the immune system against tumor cells and regenerate the autoimmune system for combating the cancer cells. Lately, it has been reported that the immunotherapy against the tumor cells not only induces immune system but also inhibits metastasis and stimulating antitumor response system against recurrence [9, 10].

2.2 Surgery

The surgery comprises of removal of tumor cells using instruments that involves abrading, cutting, and suturing. The surgery further consisted of a number of methods including the targeted removing of cancer cells using laser, cryosurgery, electrosurgery, and microscopic controlled surgery [11–15]. However, it cannot be denied that every procedure brings some risk and side effects with it. The different side effects and risks included severe blood loss, adverse reactions, even damage to the vital organs, severe pain after surgery, discomfort, circulatory clot formation, and infections. The surgery also mostly shaded with the stage of cancer and area of prevailing cancer cells which may be from delocalized to localized area to mere hand to vital organs.

2.3 Radiation Therapy

Another major way includes radiation therapy, which is based upon the eradication of cancer cells upon the bombardment of ionizing radiation, while the ionizing substances are mostly osmium, platinum, and cobalt. The different type of radiation therapy treats different cancers including lung cancer, neck and head cancer, rectal cancer, prostate cancer, cervical cancer, and osteosarcoma [16]. The most common method used for the treatment of cancer is chemotherapy which can be in use for the third stage of cancer. The cancer treatment using chemotherapy is based upon killing of cancer cells using different chemicals without infecting the surrounding cells and other vital organs [17].

3 Nanomedicine

Nanomedicine has paved its way for the best results due to targeted technique of action. They have vast application for the drug discovery and drug delivery system. Variety of different physical and chemical properties of nanoparticles due variety in their surface properties, shape, size, and charge that in turn causes impact on stability in blood, their cellular intake, volume distribution, in vivo distribution, half-life and functioning with the abnormal cells in body [18]. Thus, they could increase the therapeutic ability as well as diagnostic ability due to their elevated properties to be used in the field of medical sciences.

3.1 Size

The size of nanoparticle is very crucial for not only its formation but also as its administration as drug. The optimal size for a nanoparticle as drug delivery agent is 100–200 nm [19]. The particle with more size can undergo accumulation in spleen leading to its removal through reticulo-endothelial system, while the less size undergoes rapid clearance from the circulation system through the extravasation or the renal clearance, so the optimal size results in uptake of nanoparticles to the liver and avoids filtration through spleen [20].

3.2 Shape

The shape of nanoparticle is also very important for their cellular uptake. The reason is the spleen exhibits filtration of asymmetric units, so the spherical nanoparticles result

in the functioning after avoiding spleen filtration as compared to the hemispherical particles [21–23].

3.3 Surface Properties

Surface properties are an important factor affecting the blood circulation period. The main factor includes opsonization which is association of nanoparticles with the blood proteins or opsonins including complement proteins and immunoglobulins. These proteins are destined to recognize the foreign entity and macrophages activation. Thus, the surface property modifies the circulation time of nanoparticles through the tissues and blood [24].

3.4 Specified Releasing Property

The specified releasing property of nanoparticles makes them the best alternative to other therapeutics. They are mostly encapsulated to reach the target site, release and act in best possible way. Thus, the specified concentration of medicine can be used for disease instead of conventional drug which is mostly given in high concentration, so the target site for the medicine can have the required results, while it also causes huge side effects on other body parts. The drug level in plasma for the nanoparticles remains constant and releases at specific site with maximum results and no side effects to other vital organs [25].

4 Targeted Cancer Therapy

The anticancer drug must possess two properties that help in increase chances of patient survival, which are as follows:

- They must target the specific tumor site instead of any other organ.
- They must kill the tumor cell or malignant cell selectively with imparting any effect on healthy cells.

The targeted therapy for nanoparticle in this regard has two different approaches containing passive targeting and active targeting [26].

4.1 Passive Targeting

The most important factor in passive targeting includes size, circulation time of nanoparticle, and microenvironment of tumor. This tactic enhances the efficacy and drug bioavailability as nanodrug reaches the targeted site using tumor vasculature [27]. This specificity is due to huge gaps between adjacent endothelial cells of tumor cells, making a specification in angiogenic blood vessels. The defective and leaky tumor vasculature also has more secretion due to certain mediators like nitric oxide, fibroblast growth factor, vascular endothelial growth factor, and prostaglandins [28]. Thus, the additive factors for tumor vasculature are termed as enhanced permeability and retention effect which enable nanodrugs to accumulate in tumors and destroy them. The microenvironment for the tumor is also very specific from the normal one as they have high metabolic rate, high-level oxygen, and more nutrients. Thus creating such environment tumor cells, they end up acidic environment for survival by releasing enzymes like matrix metalloproteinase while taking over glycolysis pathway for energy supply and nutrient [29].

4.2 Active Targeting

Sometimes, the passive targeting is not that much effective because the permeability of tumor vessels does not have the same pathway throughout due to lack of enhanced permeability and retention effect [30]. This problem can be overcome by targeted drug delivery which depends upon the following factor.

- The tumor cells must have more receptor sites for the targeted drugs than the normal cells.
- They must be expressed on tumor cells.

The receptor-mediated endocytosis undergoes drug internalization. The drug releases in cytoplasm occur after reaching the target organelle due to endosomes [31].

5 Nanodrugs in Different Forms

As ideal drug delivery system and theranostics, nanoparticles have high potential of handling major problems including high dosages, intolerance, instability, and low bioavailability. The therapeutic drugs using nanoparticles proved to be the great source of help in combating this disease [32]. The different types of nanoparticles include magnetic nanoparticles, polymeric nanoparticles, dendrimers, ceramic nanoparticles, carbon nanoparticle, and metallic-based nanoparticles. In attempt to form better nanodrugs for the purpose of theranostics, nanohybrid is a new approach

that indicates the mixing of different materials at nanoscale level for the formation of effective materials [33].

5.1 Nanohybrid

The nano word relates to particles with 0.1–100 nm size. They have been widely used in different fields including agriculture, food industry, material science, and medicines and diagnostics [34]. These particles have been specifically used for medical purposes including biological barriers passage, recognizing diseased cells for treatment and eradication. Thus, nanotechnology is specifically being used in medical sciences for the diagnosis purposes as well as treatment. The nanosized organic molecules and inorganic metal oxides combine to form nanohybrid which has mostly better biological activities as well as physicochemical properties due to high surface area-to-volume ratio with high stability at high room temperature and pressure. These nanosized particles are further divided into nanorods, nanotubes, nanobelts, and nanoflower. The nanohybrids consist of number of oxides including zinc, aluminum, cadmium, titanium, etc. along with organic material including graphene, graphene oxide, chitosan, etc. It may also include enzymes or biological species as organic source [35].

5.2 Organic–Inorganic Nanohybrids

The organic–inorganic nanohybrids have organic and inorganic portion on nanoscale. The inorganic nanoparticle is meant to provide multi-functionality due to smaller size with targeting aptitude, prominent optical, electrical, and mechanical properties [36]. The organic nanocarrier is meant to enhance versatility in hydrophilic and hydrophobic drugs along with better efficacy and bioavailability. However, the organic carriers are readily identified by the immune system and suffer chemical and thermal stability. The inorganic carriers have problem with dispersity and stability due to surface functionalization, so the organic carrier mixing enhances stability, biocompatibility, and biodegradability while minimizing the side effects and targeted approach. Thus, the organic–inorganic nanohybrids gained a huge attention for years due to their favorable physicochemical properties. The nanohybrids not only express the individual behavior of the constituents but also properties owing to the synergistic effect [37].

5.3 *Preparation of Nanohybrids*

There are certain strategies reported for the preparation of nanohybrids mainly divided into covalent and non-covalent conjugation which are further described below (Fig. 1).

5.3.1 Synthesis Through Covalent Conjugation

Various ligands for instance polyethylene glycol (PEG), oligonucleotides, peptides, and some other polymers are made up of covalent conjugations and are tested extensively for the nanoparticles surface modification [38]. The most abundant groups of these ligands include amino, carboxyl, thiol, and imidazole among some others. Between these abundant groups, thiol has been used largely for fabrication of nanohybrids using covalent conjugation. Kim and co-workers were successful in amalgamation of PEG-b-poly (L-lysine) (PEG-PLL) along with thiol moieties at ω-end of PLL. Using Au-sulfur covalent bond, thiol groups were further used for the conjugation of these polymers on gold NPs which was done after complexation of polymers with siRNA. While administrating via saphenous, these nanoparticles demonstrated prolonged circulation time within blood and remarkably ameliorate the siRNA accumulation onto sites presenting tumors as compared to the controls. In the meantime, higher level of (GSH) intracellular glutathione may effect the stability of the NPs by triggering the siRNA release, presenting the reverse nanoparticles stability in relevance to negative charges gold nanoparticles surface and thiol exchange [39].

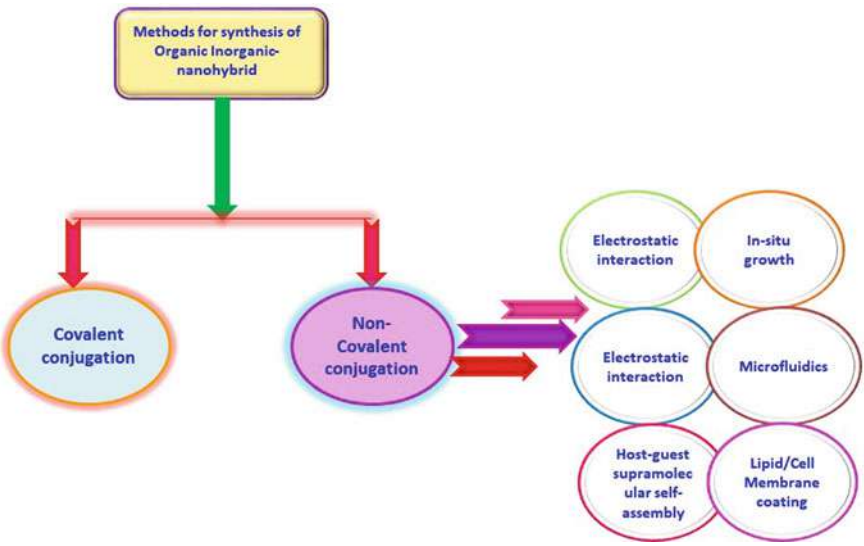

Fig. 1 Methods for fabrication of organic–inorganic nanohybrids

For mesoporous silica nanoparticles applications, these modified surfaces impede premature release, or triggering of selective cargos should also be taken into account. Successful thermo-responsive ultrasound-responsive polymers to silica nanoparticles were grafted by Paris and co-workers. Silylated polymers were formed by functionalizing aminopropyl triethoxysilane with poly(2-(2-methoxyethoxy) ethylmethacrylate-co-2-tetrahydropyranyl methacrylate (p(MEO2MA-co-THPMA)) which was then grafted to silica nanoparticles surface using silanol chemistry. Consequently, these nanoparticles which are hybrid in nature can then be combined with cargos at relatively low temperature of around (40 °C), owing to the conformation of open polymer. After which without premature release of these loaded cargos at physiological temperature, these polymers are collapsed at 37 °C causing the pores closure enabling these nanoparticles to carry the loaded cargos. Upon exposure to ultrasonic irradiation, the polymer changes its form from hydrophobicity to a coil-like structure releasing the carrier cargo at a designated site by opening its gates [40].

5.3.2 Synthesis Through Non-covalent Conjugation

5.3.2.1 Electrostatic Interaction

This is a simple assembling approach involving the interaction between negatively and positively charged materials. It is a very versatile method, since it involves many charged molecules which can be used, mainly involving synthetic polyelectrolytes and natural electrolytes [41]. Lee and colleagues by using protease nanoparticles composite in nature, layer-by-layer deposition of negatively charged siRNA and positively charged biodegradable poly-L-lysine forged on gold nanoparticles. Three layers of siRNA and four layers of poly-L-lysine were successfully coated. Since poly-L-lysine degradation is slow, it allowed the gradually slow release of siRNA complexed in nature presenting an extended silencing effect on genes. Moreover, the layers of siRNA number were related to this silencing effect. Nanohybrids inorganic–inorganic in nature were also formulated through interaction involving electrostatics. For instance, copper sulfide citrate-capped nanosatellites and zirconium-labeled hollow mesoporous silica were self-congregated to form core-satellite nanoconstructs by the use of electrostatic interaction. These nanoconstructs were multifaceted and could easily be utilized as imaging receptors by using positron emission tomography, Cerenkov luminescence, fluorescence, and Cerenkov-resonance energy transfer and can further help by being local photodynamic therapy and photothermal therapy agents [42].

5.3.2.2 Nano-precipitation

Another robust and scalable process of forming drug nanoparticles has been determined as nanoprecipitation. As this process is quite simple and quick, easier to reproduce within practice, thereof it is recommended and preferred. Zhu and colleagues by using this nanoprecipitation method produced nanoceria-doped semiconducting nanoparticles polymer. The process mainly depends on interactions hydrophobic in nature in between different components. By using thermal decomposition of cerium precursors in organic solution and through coating hydrophobic oleyl amine, nanoceria is prepared [43].

Triblock copolymer (PEG-b-PEG-b-PEG) has been utilized with good water solubility to co-precipitate poly(cyclopentadithiophene-altbenzothiadiazole) bestowing the SPNs. The redoxorubicin activity of the nanoceria was undisturbed and had no negative impact by using this procedure since mixed valence, i.e., Ce^{4+} and Ce^{3+} after nanoprecipitation retained their states. In the near-infrared region, PCPDTBT showed strong absorption rate, and the nanoceria was able to change its oxidation states due to pH conditions since the high surface oxygen density was present, making it a ROS scavenger which is also smart regulator. The same combination bestowed nanoceria-doped semiconducting nanoparticles polymer with photodynamic properties which were only pH dependent, hence increasing the use of phototherapy microenvironment of tumors acidic in nature while showing quite reduction in healthy tissues potential side effects [44].

Shen and co-workers by using two-step co-precipitation method produced Fe_3O_4/Gd_2O_3 nanoparticles with poly(acrylic acid). These nanohybrids hastened the reaction of Fenton in cancerous cells because of increased concentration of local Fe^{3+}, Fe^{2+}, and H_2O_2. Moreover, the capability of these nanoparticles to respond to intrinsic magnetic resonance imaging was used to evaluate and check response by tumor [45].

5.3.2.3 Host–Guest Supramolecular Self-assembling Approach

Molecular recognition between several molecules using non-covalent interactions as hydrogen bonding, hydrophobic interaction, electrostatic, and π-π stacking is known as supramolecular self-assembly [46]. The guest–host nanosystem supramoleculars are distributed on the basis of utilized host units, like cyclodextrins, metal–organic hosts, cucurbiturils, and calixarenes. For instance, by applying discrete metallacage loading to encapsulate a photosensitizer with therapeutic organoplatinum (II), Yu and co-workers formed an inclusion complex between host–guest, hence helping the photosensitizer and chemotherapeutic agent co-delivery within a single nanosystem. Taking edge of this increased retention (EPR) and permeability effect by targeting actively, these nanosystems showed a quite significant effect in antitumor activity against tumor resisting the drug [47].

5.3.2.4 In Situ Growth

In situ growth can be used to develop hybrid nanoparticles in pre-existing nanostructures. By the use of in situ growth method, Min and co-workers prepared calcium carbonate-loaded doxorubicin nanoparticles by a copolymer block template for ultrasound imaging and antitumor activity. This copolymer block template calcium carbonate proved to be beneficial due to mineralization, since it was simple method which produces nanocarriers capable of loading various cancer therapeutics within core of calcium carbonate [48]. Other researchers also utilized in situ growth method to insert gold nanoparticles in nanostructures to increase their vitality. For example, by using in situ generation process, gold nanoparticles containing polymersomes were prepared separately and by injecting this pre-designed gold nanoparticles into hydrophilic core [49].

Further studies showed that in situ growth presented better result in various in vitro and in vivo studies due to high-density packaging and gold nanoparticles homogenous distribution in polymersomes lamella. Drug seepage was effectively refined at pH 7.4 resulting in increased systematic circulation time. These outcomes suggested that gold nanoparticles produced by in situ process have great potential for improved stability of vesicles and suppression of tumor. Another group presented that growth of gold nanoparticles on surface of metal organic framework by use of in situ process can easily stabilize the nanocomposite allowing it to be used as radio sensitizers increasing the radiation energy in the tumor effectively [50].

5.3.2.5 Microfluidics

Technologies involving microfluidics are beneficial for producing nanosized and microsized delivery system for drugs which not only can produce high throughput, reproducible, and well-preserved manner particles but also can easily form three-dimensional environments with flowing continuously mimicking the pathological and physiological processes in micro-environments [51]. For instance, inorganic–organic hybrid nanocomposites were generated by Cheheltani and co-workers by loading gold nanoparticles in polydicarboxylatophenoxy phosphazene (PCPP) nanomatrix biodegradable in nature. Using microfluidic device, homogenous Au-PCPP was produced which had the ability of size controlling of gold-PCPP by changing PEG-poly-L-lysine copolymer block within formulation. In another instance, the mixture of the unsaturated phospholipids in liquid state and saturated phospholipid in powdered form was used to fabricate monodisperse H_2O in oil and in the double emulsion templates having shell core framework utilizing microfluidics glass capillary. The low transition temperature of the unsaturated phospholipids in powdered form was overcame by this technique and also it solved the limitation of solubility of saturated phospholipid, and it also improved the stable monodisperse phospholipid vesicles fabrication [52].

5.3.2.6 Lipid/Cell Membrane Coating

Nanoparticles (NPs) usually face short circulation, high toxicity, cellular-resistance and poor stability, limiting their applications in biomedical sciences. For the purpose of delivering nanocarriers, lipids are considered to be highly bio-compatible and which is the reason of its over extensive usage. To yield highly stable nanohybrids and biocompatibility, lipid shell coating is an effective method. For example, by the rehydration of thin films of lipids containing phosphatidylcholine, cholesterol and distearoylphosphoethanolamine-polyethyleneglycol-biotin along with ND-complexes nanodiamonds (ND)-lipids particles hybrid in nature are produced. The smaller ND clusters and charge-based inhibited accumulation were stabilized by thin lipid films [53].

Additional to these synthetic lipids, various cell membrane types like erythrocytes, platelets, stem cells, and cancer cells have gotten a lot of attention during cancer therapy. The successful combination of membrane vesicles with dual target binding and immune escaping functions was achieved. Upconversion nanoparticles (UCNPs) with cancer membrane cell were shielded by Rao and co-workers by integrating the core ability of UCNP to near-infrared radiation conversion to visible light, hence using it for in vivo imaging of tumor, showing this construct ability in therapy and diagnosis. Likewise, cell membranes containing cancer were coated on silica nanoparticles increasing in vivo and in vitro anticancer efficiency and by reduction in systematic toxicity [54].

Immune-related functions are carried out by leukocytes since they are made up of subsets such as T cells, neutrophils, macrophages, dendritic cells, and some others. One of the research groups reported that silicon particles coated with the leukocyte membrane cell which are nanoporous may easily and successfully escape from immune phagocytosis and could transport the carrier through reconstructed inflamed endothelium. Moreover, these leuko-like reserved their main functionality after being injected in vivo, representing better tumor targeting and increased circulation time [55]. The most fascinating thing observed is that erythrocyte-coated nanoparticles in membrane were capable of achieving longer circulating cargo delivery by bypassing systemic clearance and macrophage uptake [56].

Platelet membrane is also an important membrane which has been explored in this regard which is enrolled naturally to vascular injury site to jumpstart a phase of events resulting in production+ of clot triggering the healing process. Providing a novel biomimetic platform delivery, the stem cells have the ability to target tumor in the form of cancer therapy. Many cell types have been observed owing to their distinctive properties, while single nanoparticle containing multiple cell types was desired during incorporation. At present, this unfolding biomimetic nanotechnology is starting to enter a mature phase and work is being done for its positive impact clinically [57].

6 Functionalization by Hybrid Strategies

The mixture of two or more inorganic and organic components having specific chemical and unique physical properties is known as hybrid nanomaterials. By utilizing these hybrid materials with different strategies, we can make the most of their unique features to outweigh their previously existing shortcomings while achieving the required aims.

6.1 Enhancement of Encapsulation Efficacy and Biocompatibility

Anticancer medication like cisplatin, doxorubicin, and paclitaxel which are used conventionally usually and almost always causes systematic toxicity due to its gathering in normal tissues limiting their usage in the chemotherapy. Potential of such drugs can be improved by using encapsulation of hybrid drug delivery system which is a direct approach based on polyacrylic acid (PAA)-coated ultrasmall superparamagnetic iron oxide NPs (PAA-USPIOs). Yang and colleagues made a cisplatin-loaded, GE11 peptide-conjugated theranostic system (GE11-PDA-Pt-USPIOs) and polydopamine-coated for tumor hypoxia modulation, and image-guided MRI/photoacoustic (PA) chemoradiotherapy of cancer cells. Activated cisplatin with complexing of the carboxylic groups PAA was loaded due to this thick PAA coating on USPIOs [58].

Improving the package efficiency is also an important strategy starting with the material itself. Great compatibility and biodegradability of calcium carbonate are thought to be the best carrier for various hydrophilic and hydrophobic-based drugs. Ultrahigh-content nanomaterials, microgel were prepared by Wang and co-workers (up to 92% wt%); gelatin was prepared by casting process, utilizing templates of porous calcium carbonate. By the use of this technique, diffusion constraints can be overcome with the decrease in nanoparticles during production of microgels, hence gaining a high-content loading platform for either hydrophobic or hydrophilic NPs [59].

6.2 Enhancement in Solubility and Stability

Due to poor bioavailability, many trial drugs failed to progress because of aqueous insolubility. The low stability and poor solubility of various molecules found in this aqueous medium under different conditions and unfathomable biodistributions limit intravenous administration, hence limiting concentration of the drug at target tissues. Hybrid nanotechnology gave a new meaning to the concept of metal complex delivery. For improvement of nanoparticles stability, protective shells like hydrophilic

polymers like PEG are used. The particular usage of Ru (II)-polypyridyl complexes for imaging and PDT has peeked a lot of interest. However, due to high display of lipophilicity in these Ru (II)-polypyridyl complexes, it results in poor aqueous solubility. Zhang and colleagues functionalized the Ru (II)-polypyridyl complexes with polyethylene glycol (Ru-PEG) to enhance the aqueous medium solubility and the bioavailability [60].

6.3 Improvement of Targeted Delivery

Accumulation of different macromolecules in the tumors is preferential because of retention (EPR) effect and enhanced permeability which plays important role in nanomaterials and macromaterials delivery to tumors. Active targeting is receiving much attention as compared to passive EPR targeting effect. Ligand-mediated targeting also called as the active targeting refers to drugs conferring or the active binding of carriers to targeted sites using ligands in nanoparticles surface for specific retention by targeted cell. The key style includes probe molecules coupling like antibodies, sugar chains, nucleic acid aptamers, and polypeptides via physical or chemical means which can bind precisely to receptors surface over exposed in tissues, diseased organs, cells, and subcellular domains. For active targeting of nanoparticles, high-affinity protein named Affibodies (Afbs) has been used which are smaller than normal antibodies [61].

Using supramolecular interaction, they decorated the silica nanoparticles surface loaded with human epidermal growth factor receptor 2 (HER2) and camptothecin (CPT) by binding Afbs. This case proclaimed deep insights into supermolecularly built protein corona shield usage as a ligand targeting and regulating bridge between biological systems and nanoparticles. Solid tumors and macrophages have overexposed folate receptors, making them easy and most desired target for nanoparticles by using receptor-mediated endocytosis. Iridium sulfide (IrSx) nanoparticles prepared by PEG conjugated and modifying IrSx were reported by Zhang and co-workers which can be used for targeting ligands folate for multimodal imaging-guided chemophotothermal combination therapy [62].

6.4 Drug Release Behavior Control

For controlled drug delivery, various silica nanoparticles have been employed for having excellent properties like high pore volume, broad diversity in surface functionalizing, and high surface area as multifunctional carriers for numerous hybrid material construction. To elude premature cargo release of the drug and to regulate drug release by hybrid modification, researchers have used these properties of silica nanoparticles. A novel thermo-responsive hybrid magnetic mesoporous silica nanocarriers have been reported by Baeza and co-workers which release the proteins,

different cargo drugs, and small compounds loaded within branches of polymers and also inside the mesoporous matrix in reaction to an external altering magnetic field [63]. The grafting of light-responsive polymers to silica nanoparticles by Lai and co-workers allowed the drug release in response to light. Endogenous stimuli (e.g., changes in pH, concentration of enzymes or specific analytes, or doxorubicin potential) and exogenous stimuli (i.e., magnetic fields, electric fields, ultrasounds, temperature, and light) are used for stimuli-responsive drug delivery systems' development. A new gradient two-stage rocket mimetic nanocarriers and doxorubicin-responsive nanocarriers for improved tumor accumulation and chemotherapy has been developed by Jia and co-workers which triggers doxorubicin reaction of different types according to the difference between intracellular GSH concentration and extracellular microenvironment, resulting in degradation of nanocarriers and drug release. These drug delivery systems based on stimuli response were developed through hybrids of inorganic–organics [64].

7 Different Types of the Organic–Inorganic Nanohybrids

While there is a huge range of conjugation between nanomaterials leading to nanohybrids, their type, interaction as well as composition matters a lot in defining their functionality. Commonly, less hydrophilic inorganic nanoparticle surface hinders their application as drugs which is usually overwhelmed by the surface functionality. Hence for the desired results, the choice of organic as well as inorganic nanoparticle surface must be wise. It has been noted that the formation of organic–inorganic hybrid must have an –OH bond or –COOH bond on the surface for the organic group [65].

7.1 Clay-Based Nanohybrids

The clay-based nanohybrids are further classified into clay-polymer nanohybrids and LDH-based nanohybrids which are discussed below:

7.1.1 Clay-Polymer-Based Nanohybrids

Clay minerals including smectites ($AlSi_2O_5(OH)_xH_2O$) (montmorillonite-MMT), fibrous clay mineral, hectorites (laponite), kaolinite ($Si_2Al_2O_5(OH)_4$), and derived LDHs are explored to use in drug delivery system [66]. The interaction of clay with organic molecules like polymers imparts special features as drug molecules which certainly depends upon the physicochemical properties as well as functional groups of the organic groups, while the swelling ability, adsorptivity, ion exchange capacity, porosity, and surface area of mineral clay make the drug more potent [67, 68].

Moreover, biocompatibility, biodegradability, hydrophobicity, and hydrophilicity also increase the efficiency of hybrid clay-polymer as drug. The combination of polymer and clay is to be performed in three different ways comprising of intercalated nanocomposite, phase-separated microcomposite, and exfoliated nanocomposite [69].

The clay-based nanohybrids are reported to act as drug delivery by encapsulation process. The laponite has been stated as clay-polymer nanohybrids to encapsulate ciprofloxacin and methotrexate for the tumor therapy with enhanced effect than the free drugs [70].

7.1.2 LDH-Based Nanohybrids

A set of brucite-like clay comprises of anionic layers which are indicated as LDH. They are composed of layers of divalent or trivalent metal cations, making a layer of net positive charge in hydroxide layers. The extra positive charges due to cations are neutralized with exchangeable gallery anions present within the layers. The interlayer hydrogen bonds, gallery anions, and the electrostatic interaction embrace the layers at a place to form the fine 3D structure [71, 72]. In the presence of exchangeable ions in huge capacity, the negatively charged drug molecules or biomolecules intercalate in the LDH layers spacing for the positively charged layers, making the drugs highly penetrating through the cellular membranes. Hence, the LDH has the high potential for the drugs with anions or negative charges like DNA, amino acids, vitamins, and synthetic compounds to pass the cellular membrane as therapeutic drugs [73].

The effect of Raloxifene hydrochloride, a hydrophobic anticancer drug, has been studied as pure drug and LDH-ZnFe intercalated clay-polymer-based nanohybrids. The significant results for the drug delivery system were shown by the intercalated nanohybrid as compared to the drug alone, while in vitro antitumor efficacy was also enhanced. The in vivo studies with same also showed the better results with the hybrid composition rather the pure drug [74].

7.2 Organic-Based Nanohybrids

The nanohybrids can be organic-based which are mixture of different transition metal oxide along with the organic-based components that can be solely the compounds or the biomolecules. They can be further classified as carbon nanotubes-based nanohybrids, liposomes-based nanohybrids, and dendrimers-based nanohybrids [65].

7.2.1 Carbon Nanotube-Based Nanohybrids

Carbon nanotubes have been considered as drug carriers for the last few years due to their suitable size, surface area, better aspect ratio, cell penetration, and easy functionalization. Conventionally, carbon nanotubes for better functioning have been in use after coupling with TiO_2, iron, and hydroxyapatite [75].

The anticancer drug, doxorubicin when combined with TiO_2–Au nanoparticle carbon nanotubes, enhances the biocompatibility and efficiency of drug at low pH as confirmed in zebra fish by hemolysis. The mean transit test and fluorescence imaging also confirmed their antiproliferative effect on breast cancer cells [76].

Currently, the ferromagnetic carbon nanotubes have been observed for the loading of drugs like 5-fluorouracil, 1,8-naphthalimide, and purpurin for the treatment of colon cancer, melanoma, and colon adenocarcinoma cells, while iron hydroxyapatite carbon nanotubes have also shown better response for the administration and effect of doxorubicin for the treatment of cancer [67].

7.2.2 Liposomes-Based Nanohybrids

The liposomes are also very helpful in the eradication of cancer cells by the drug delivery system. Though naturally occurring, they can be combined with anticancer drug or may be loaded upon. The main issue with the liposomes is the stability one, and they mostly burst rapidly making the drug to leave the system ghastly and minimizing the therapeutic dosage and leaving behind the side effects only. Thus, the problem can be solved using silica or any ceramic layer to combine it with, so it leads the liposomal stability making the resultant termed as cerasome [77]. Due to super stable entity, they can be loaded upon the hydrophobic, hydrophilic as well as amphiphilic compounds. Another fact for the recommendation is the presence of liposomal bilayer for holding the silica and ceramic layer making the cerasome so stable and less denser leading to better more biodegradable, biocompatible, and functionalization for bioconjugation than the simple silica nanoparticles. The lipid layers along with liposomes make the siloxane network, but due to high durability, the drug permeability is mostly very low along with insufficient drug release. Thus, primary or slight degradation of lipid can make the process easy by the introduction of pore in the siloxane network [78, 79]. Hence, doxorubicin-loaded cerasome with better lipid composition leads to the best cytotoxic effect along with better efficacy and accumulating efficiencies against the breast cancer cells. Another anticancer drug named paclitaxel loaded with cerasome has also been reported to be effective for the treatment of solid tumor. This dual-labeled cerasome also enables us to identify the tumor cells as well as cancer cells both through the MRI and NIR florescence [80].

7.2.3 Dendrimer-Based Nanohybrids

The 3D (3-dimensional) polymer assemblies with branched structure constituted of internal cavities and reasonable surfaces are dendrimers [81]. The host–guest complex forming nature of dendrimers making electrostatic interaction or hydrogen bonding while being non-degradable and non-toxic makes them most favorable to be used in drug delivery system for the treatment of diseases including cancer. Thus for this purpose, different inorganic particles like silica, iron, and gold nanoparticles are conjugated with the dendrimers, resulting in different assemblies for the treatment of cancer [82]. The conjugation of silica polyamidoamine with dendrimer in nanosystem was introduced for the delivery of anthocyanin, where antiproliferative effect on neuroblastoma cells was prominent [83]. Similarly, magnetic dendrimer conjugate loaded upon silica polyamidoamine for methyl prednisolone succinate delivery for the cancer treatment proved to be very efficient, while polyamidoamine conjugated with 3-aminopropylsilane can be assigned for the delivery of ibuprofen, salicylic acid, and chlorogenic acid [84]. Similarly, PEGylated Au-polyamidoamine nanodendrimer was composed to load curcumin for the theranostic approach for colorectal adenocarcinoma [85].

7.3 Inorganic and Metal-Based Nanohybrids

As indicated by the name, the mixing of inorganic nanoparticles in different organic compounds is said to be inorganic–organic nanohybrids. As far as chemotherapy is considered, mostly gold, silver, and titanium have been under practice. The most specific properties for their consideration are their bioaccumulation, less toxicity, inertness, and ability to conduct heat [65]. The application of nanohybrids is given in table, while few nanohybrids will be discussed in concise detail.

7.3.1 Gold Nanoparticles

The gold has a unique property of better catalytic activity that enables it to be used for the effective drug delivery system. The gold nanoparticles not only reported as drug delivery entity but also in tumor detection, multidrug resistant, photodynamics, photothermal therapy, and imaging [86]. In a study, the epimer of doxorubicin, i.e., epirubicin is coupled with gold nanoparticle in lipid bilayer of liposomes for the passive drug delivery in cancer treatment. The release of drug in this case was slow and smooth with dependency on pH which showed its advantage for endocytosis. The cytotoxicity of this coupling was described by the epirubicin encapsulation in liposomes that permits the slow diffusion of drug to the site of action making least side effect to other normal cells and increasing the therapeutic effect against cancer. Another notable factor for this coupling is formation of reactive oxygen species that varies the mitochondrial membrane permeability and prompts apoptosis [87, 88].

In another study, dextran-grafted polyacrylamide was embedded with gold nanoparticles to form nanohybrids that for the delivery of doxorubicin or cisplatin. The hybrid along with the drugs was tested against breast cancer cells, human T-cell leukemia, human histiocytic lymphoma cells, and myelogenous leukemia cells, and mostly, the results were remarkable [89, 90].

The gold nanoparticles along with polyvinylpyrrolidone have also been used for the delivery of doxorubicin for the treatment of lung cancer due to specific delivery and less cytotoxicity, while in another study, organic compounds like Herceptin and oxaliplatin were laden on gold nanoparticles of oleic acid, iron oxide, oleylamine, and then coated by polyethylene glycol to find out their toxicity and effect on cancer cells [91]. The results showed that oxaliplatin along with gold nanoparticles of iron oxide embedded in Herceptin was more promising for human estrogen receptor 2 targeted chemotherapy for gastric cancer [92].

7.3.2 Silica-Based Nanohybrids

Silica nanoparticles comprising of both mesoporous and non-porous particles, are supposed to be the best for the drug delivery and cancer treatment due to their large surface area, pore structure, better surface functionalization, better drug loading ability, and stability. The stimuli-responsive silica organic nanohybrids respond on low pH specifically in extracellular environment and with high glutathione level in intracellular environment [93].

In another study, it was observed that morpholin group assists the release of doxorubicin with the change of pH environment due to activity of tumor. The acidic environment due to tumor permits the morpholin to protonate and breaking the acid-sensitive hydrazine linkage for functioning of doxorubicin [94]. The similar process was studied rending the mesoporous silica nanoparticles to reverse charge for the releasing of doxorubicin in bovine serum albumin and adenocarcinomic human alveolar basal epithelial cells [95].

Silica organic nanohybrids combining with silica nanohybrids on cancer cells and cancer ligands using active targeting approach have been achieved on different receptors like epidermal growth factor receptor, folic acid, transferrin, human epidermal growth factor receptor 2, and different ligands [96]. The folate-conjugated lipid layer along with silica organic nanohybrids has been applied to mesoporous silica nanoparticles after coating on doxorubicin for the treatment of multidrug-resistant cancer cells. The study also showed that this made the doxorubicin to show higher drug ability more than 97% for over 7 days at low pH which is significant indeed [97].

In another attempt, the silica organic nanohybrids functionalized by mesoporous amine and combined with folate receptor have been made to observe the programmed and image delivery of doxorubicin drug in folate receptor which was expressed in HeLa cells. Similarly, the hyaluronic acid has also designed with silica organic nanohybrids for the delivery of doxorubicin along with quercetin for the chemotherapy of gastric carcinoma cells [98].

7.3.3 Iron Oxide-Based Nanohybrids

Iron oxide nanoparticles have been under great attention due to their superparamagnetic nature that leads to unique mechanical, physical, chemical, and thermal properties. Due to their momentarily external attractive forces and magnetic responsiveness to travel to specific site of action, they have been specifically used in the field of biomedical sciences [99]. The unique character of binding with specific antibodies and ligands like epidermal growth factor receptor, human epidermal receptor 2, folic acid, and transferrin leads to targeted drug delivery to cancer cells and avoiding side effects by the anticancer agent at different sites [100].

It has also been observed that there are certain drawbacks of iron oxide nanohybrids in therapeutic application including quick removal from the system, rapid oxidation, and aggregation. This can be avoided by using certain organic moieties and polymeric coating to provide colloidal stability, decrease toxicity, increase toxicity, and steric stability, thus improving the stimuli responsiveness and binding to release drugs [101].

The different polymers have been studied to combine with iron oxide nanoparticles to bind with different receptors. The combining entities include liposomes, dendrimers, carboxymethyl cellulose, poloxamer heparin polymer, and graphene oxide [102].

In recent studies, the anticancer drug delivery was assisted by the iron oxide nanohybrids combined with heparin poloxamer shell structure that binds with the hydrophobic and hydrophilic drugs due to poloxamer and targets tumor due to heparin [103]. Similarly in another study, the iron oxide nanohybrids combined with carboxymethyl cellulose had been loaded with doxorubicin for the therapeutic and hyperthermic effect on brain cancer cells. The hyperthermic effect by the external magnetic effect increases the therapeutic effect of nanohybrids against the brain cancer cells [104].

In another study, graphene oxide combined with iron oxide organic nanohybrids for the anticancer drug delivery of doxorubicin while recently the guided delivery of doxorubicin to neuroblastoma cells having iron oxide loaded with graphene oxide with better results like high loading, pH sensitive, anticancer effect, and controlled releasing has also been observed [105].

7.3.4 Zinc Oxide-Based Nanohybrids

The presence of cancer cells or benign tumor creates the acidic environment, and the zinc ion having the capacity to dissociate in such surroundings which producing reactive oxygen species makes it promising to consider as anticancer agent. The zinc oxide nanohybrids due to pH-dependent behavior may be considered for targeted drug delivery for cancer treatment, as the drug may combine to them through electrostatic, covalent, or Vander Waals interaction. The further improvement can be made possible by using tumor-specified ligands on the specific sites [106]. In a study, the phenol boronic acid has been used as the targeted ligand combined with zinc oxide

nanohybrids to distribute curcumin to the breast cancer cells, where the targeted ligand responds to the sialic acid present up there. However, it was also observed that the nanohybrids along with the targeted drug released 56% as compared to 8.2% with curcumin [107].

The zinc oxide nanohybrids in coupling with other inorganic nanoparticles lead to the formation of unique drug carriers and anticancer drugs. In order to examine such case, TiO_2 coupled with zinc oxide and graphene oxide shell structure has been used for curcumin delivery with pH impact to the colon as targeted drug delivery system [108]. In this coupling, the mesoporous titanium oxide was first blended with zinc oxide coating and then augmented to graphene oxide suspension. The amalgamation is due to unique property of zinc oxide to release in pH gradient making it more potent to use in colon cancer. In another study, zinc oxide is blended with silicon oxide for the delivery of doxorubicin making a high impact on cancer cells [109].

8 Conclusion

Cancer has been acknowledged as the most deadly disease to kill millions of people every year. The therapeutic approach for this disease leads to a number of different processes including immunotherapy, surgery, radiation therapy, and nanomedicine which lead to another dimension for its treatment. The formation of these nanomedicines is also very specific in their parameters as per their shape, size, and surface property, making the mechanism of their action in different ways including passive and active targeting. The preparation of these nanomedicine or here specifically organic–inorganic nanohybrids is formed using two different strategies, i.e., covalent conjugation and non-covalent conjugation. The recent development in organic–inorganic nanohybrids generated the way for the treatment of cancer in its different types. They are in constant development to overcome the drawbacks in the system of treatment. The formation of different organic–inorganic nanohybrids also faces different problems including their stability and dispersity. The organic moiety in this nanohybrids mixture enhances the targeting ability, biocompatibility, and biodegradability, while the inorganic moiety adds the quality of optical activity and magnetic targeting resulting a phenomenal quality for the treatment of many disease including different types of cancer. Though the nanohybrids formation is very critical process, but their formation is still very challenging due to their lack of yield, safety issues, absence of reproducibility, reduced efficiency, delicacy, and cytotoxicity. They may be prepared in laboratory, but on larger scale or bulk formation, the unfortunate problems and hurdles make them impossible to appoint as a drug. The glitches can be removed by the cautious study of each and every aspect of formation of these nanohybrids. Further number of new combination of different organic and inorganic nanohybrids must be introduced which can avoid any problem in the way of proving nanohybrids as nanomedicine for the treatment of cancer on global level.

References

1. Siegel RL, Miller KD, Jemal A (2019) Cancer statistics. CA Cancer J Clin 69(1):734
2. Sung H, Ferlay J, Siegel RL, Laversanne M, Soerjomataram I, Jemal A, Bray F (2021) Global cancer statistics 2020: GLOBOCAN estimates of incidence and mortality worldwide for 36 cancers in 185 countries. CA Cancer J Clin 71(3):209–249
3. Jain A, Gautam L, Vishwakarma N, Sharma R, Mody N, Dubey S, Vyas SP (2018) Emergence of polymer-lipid hybrid systems in healthcare scenario. In: Multifunctional nanocarriers for contemporary healthcare applications. IGI Global, USA, p 448470
4. Riley RS, June CH, Langer R, Mitchell MJ (2019) Delivery technologies for cancer immunotherapy. Nat Rev Drug Discov 18(3):175–196
5. Jain A, Mahira S, Majoral J-P, Bryszewska M, Khan W, Ionov M (2019) Dendrimer mediated targeting of siRNA against polo-like kinase for the treatment of triple negative breast cancer. J Biomed Mater Res Part A 107(9):19331944
6. Nam J, Son S, Park KS, Zou W, Shea LD, Moon JJ (2019) Cancer nanomedicine for combination cancer immunotherapy. Nat Rev Mater 4(6):398–414
7. Kalia VC, Patel SK, Cho BK, Wood TK, Lee JK (2021) Emerging applications of bacteria as antitumor agents. In: Seminars in cancer biology. Academic Press, Cambridge
8. Massari F, Rizzo A, Mollica V, Rosellini M, Marchetti A, Ardizzoni A, Santoni M (2021) Immune-based combinations for the treatment of metastatic renal cell carcinoma: a meta-analysis of randomised clinical trials. Eur J Cancer 154:120–127
9. Christofi T, Baritaki S, Falzone L, Libra M, Zaravinos A (2019) Current perspectives in cancer immunotherapy. Cancers 11(10):1472
10. Dong Y, Siegwart DJ, Anderson DG (2019) Strategies, design, and chemistry in siRNA delivery systems. Adv Drug Deliv Rev 144:133–147
11. Chen G, Qian Y, Zhang H, Ullah A, He X, Zhou Z, Shen J (2021) Advances in cancer theranostics using organic-inorganic hybrid nanotechnology. Appl Mater Today 23:101003
12. Gautam L, Jain A, Shrivastava P, Vyas S, Vyas SP (2021) Emergence of novel targeting systems and conventional therapies for effective cancer treatment. In: Nano drug delivery strategies for the treatment of cancers. Academic Press, Cambridge, pp 1–35
13. Hameed S, Mo S, Mustafa G, Bajwa SZ, Khan WS, Dai Z (2020) Immunological consequences of nanoparticle-mediated antitumor photoimmunotherapy. Adv Ther 3(5):1900101
14. Liu J-Y, Deng J-Y, Zhang N-N, Liu H-F, Sun W-L, He W-T et al (2019) Clinical significance of skip lymph-node metastasis in pN1 gastric-cancer patients after curative surgery. Gastroenterol Rep 7(3):193198
15. Liu Y, Chen X-G, Yang PP, Qiao Z-Y, Wang H (2019) Tumor microenvironmental pH and enzyme dual responsive polymer-liposomes for synergistic treatment of cancer immunochemotherapy. Biomacromolecules 20(2):882892
16. Majumdar APN (2019) Preclinical animal tumor models to study prevention of colon cancer recurrence by curcumin. In: Animal models in cancer drug discovery. Elsevier, Amsterdam, p 293307
17. Marra G, Valerio M, Emberton M, Heidenreich A, Crook JM, Bossi A, Pisters LL (2019) Salvage local treatments after focal therapy for prostate cancer. Eur Urol Oncol 2(5):526538
18. McDonnell NA, Funk RK, Foote RL, Kalra S, Neben-Wittich MA (2019) Treatment of tracheobronchial amyloidosis with external beam radiation therapy. Int J Radiat Oncol Biol Phys 104(1):238
19. Arbain NH, Basri M, Salim N, Wui WT, Rahman MBA (2018) Development and characterization of aerosol nanoemulsion system encapsulating low water soluble quercetin for lung cancer treatment. Mater Today Proc 5:S137S142
20. Rout SR, Gowtham K, Sheikh A, Parvez S, Dandela R, Kesharwani P (2022) Recent advances and future prospective of hybrid drug delivery systems. In: Hybrid nanomaterials for drug delivery. Woodhead Publishing, UK, pp 357–374
21. Zhang X, Wang S, Cheng G, Yu P, Chang J, Chen X (2021) Cascade drug-release strategy for enhanced anticancer therapy. Matter 4(1):26–53

22. Ajdary M, Moosavi M, Rahmati M, Falahati M, Mahboubi M, Mandegary A, Jangjoo S, Mohammadinejad R, Varma R (2018) Health concerns of various nanoparticles: a review of their in vitro and in vivo toxicity. Nanomaterials 8:634
23. Yang G, Phua SZF, Bindra AK, Zhao Y (2019) Degradability and clearance of inorganic nanoparticles for biomedical applications. Adv Mater 31(10):1805730
24. Seaberg J, Montazerian H, Hossen MN, Bhattacharya R, Khademhosseini A, Mukherjee P (2021) Hybrid nanosystems for biomedical applications. ACS Nano 15(2):2099–2142
25. Ding Y, Li Z, Jaklenec A, Hu Q (2021) Vaccine delivery systems toward lymph nodes. Adv Drug Deliv Rev 179:113914
26. Zeng Y, Xiang Y, Sheng R, Tomás H, Rodrigues J, Gu Z et al (2021) Polysaccharide-based nanomedicines for cancer immunotherapy: a review. Bioact Mater 6(10):3358–3382
27. Zhang YN, Lazarovits J, Poon W, Ouyang B, Nguyen LN, Kingston BR, Chan WC (2019) Nanoparticle size influences antigen retention and presentation in lymph node follicles for humoral immunity. Nano Lett 19(10):7226–7235
28. Shimizu K, Iyoda T, Okada M, Yamasaki S, Fujii SI (2018) Immune suppression and reversal of the suppressive tumor microenvironment. Int Immunol 30(10):445–455
29. Hao M, Chen B, Zhao X, Zhao N, Xu FJ (2020) Organic/inorganic nanocomposites for cancer immunotherapy. Mater Chem Front 4(9):2571–2609
30. Cassetta L, Pollard JW (2018) Targeting macrophages: therapeutic approaches in cancer. Nat Rev Drug Discov 17(12):887–904
31. Gu Z, Liu T, Tang J, Yang Y, Song H, Tuong ZK et al (2019) Mechanism of iron oxide-induced macrophage activation: the impact of composition and the underlying signaling pathway. J Am Chem Soc 141(15):6122–6126
32. Liu X, Yan B, Li Y, Ma X, Jiao W, Shi K et al (2020) Graphene oxide-grafted magnetic nanorings mediated magnetothermodynamic therapy favoring reactive oxygen species-related immune response for enhanced antitumor efficacy. ACS Nano 14(2):1936–1950
33. He L, Nie T, Xia X, Liu T, Huang Y, Wang X, Chen T (2019) Designing bioinspired 2D MoSe2 nanosheet for efficient photothermal-triggered cancer immunotherapy with reprogramming tumor-associated macrophages. Adv Func Mater 29(30):1901240
34. Pathria P, Louis TL, Varner JA (2019) Targeting tumor-associated macrophages in cancer. Trends Immunol 40(4):310–327
35. Frtús A, Smolková B, Uzhytchak M, Lunova M, Jirsa M, Kubinová Š et al (2020) Analyzing the mechanisms of iron oxide nanoparticles interactions with cells: a road from failure to success in clinical applications. J Controlled Release 328:59–77
36. Wang X, Zhong X, Li J, Liu Z, Cheng L (2021) Inorganic nanomaterials with rapid clearance for biomedical applications. Chem Soc Rev 50(15):8669–8742
37. Kargozar S, Mozafari M (2018) Nanotechnology and nanomedicine: start small, think big. Mater Today Proc 5(7):15492–15500
38. Choi G, Rejinold NS, Piao H, Choy JH (2021) Inorganic–inorganic nanohybrids for drug delivery, imaging and photo-therapy: recent developments and future scope. Chem Sci 12(14):5044–5063
39. Martinelli C, Pucci C, Ciofani G (2019) Nanostructured carriers as innovative tools for cancer diagnosis and therapy. APL Bioeng 3(1):011502
40. Dong Y, Chen Y, Zhu D, Shi K, Ma C, Zhang W et al (2020) Self-assembly of amphiphilic phospholipid peptide dendrimer-based nanovectors for effective delivery of siRNA therapeutics in prostate cancer therapy. J Controlled Release 322:416–425
41. Cucchiarini M, Madry H (2019) Biomaterial-guided delivery of gene vectors for targeted articular cartilage repair. Nat Rev Rheumatol 15(1):18–29
42. Nikolaeva OY, Liubota RV, Zotov OS, Vereshchako RI (2021) Cancer immunotherapy: current opportunities and perspectives. Pract Oncol 4(2):25–38
43. Mi Y, Hagan CT IV, Vincent BG, Wang AZ (2019) Emerging nano-/microapproaches for cancer immunotherapy. Adv Sci 6(6):1801847
44. Yu G, Zhu B, Shao L, Zhou J, Saha ML, Shi B et al (2019) Host–guest complexation-mediated codelivery of anticancer drug and photosensitizer for cancer photochemotherapy. Proc Nat Acad Sci 116(14):6618–6623

45. Zhou J, Rao L, Yu G, Cook TR, Chen X, Huang F (2021) Supramolecular cancer nanotheranostics. Chem Soc Rev 50(4):2839–2891
46. Conejos-Sánchez I, Đorđević S, Medel M, Vicent MJ (2021) Polypeptides as building blocks for image-guided nanotherapies. Curr Opin Biomedi Eng 20:100323
47. Yang C, Mi X, Su H, Yang J, Gu Y, Zhang L et al (2019) GE11-PDA-Pt@ USPIOs nanoformulation for relief of tumor hypoxia and MRI/PAI-guided tumor radio-chemotherapy. Biomater Sci 7(5):2076–2090
48. Wang A, Li J, Dong Q, Wang S, Jian H, Wang M et al (2019) Preparation of microgels with ultrahigh payload of various hydrophilic and hydrophobic inorganic nanoparticle composites up to 92 wt%. ACS Appl Mater Interfaces 11(4):4408–4415
49. Chen J, Zhu Y, Wu C, Shi J (2020) Nanoplatform-based cascade engineering for cancer therapy. Chem Soc Rev 49(24):9057–9094
50. Saveleva MS, Eftekhari K, Abalymov A, Douglas TE, Volodkin D, Parakhonskiy BV, Skirtach AG (2019) Hierarchy of hybrid materials—the place of inorganics-in-organics in it, their composition and applications. Front Chem 7:179
51. Juthani R, Madajewski B, Yoo B, Zhang L, Chen PM, Chen F et al (2020) Ultrasmall core-shell silica nanoparticles for precision drug delivery in a high-grade malignant brain tumor model. Clin Cancer Res 26(1):147–158
52. Zakery M, Ensafi AA, Kazemifard N, Rezaei B (2020) Novel histamine fluorosensor based on modified environmental friendly carbon nanoparticles from gum tragacanth. IEEE Sens J 20(22):13229–13235
53. Gardinier TC, Kohle FF, Peerless JS, Ma K, Turker MZ, Hinckley JA et al (2019) High-performance chromatographic characterization of surface chemical heterogeneities of fluorescent organic–inorganic hybrid core–shell silica nanoparticles. ACS Nano 13(2):1795–1804
54. Li Z, Hu J, Yang L, Zhang X, Liu X, Wang Z, Li Y (2020) Integrated POSS-dendrimer nanohybrid materials: current status and future perspective. Nanoscale 12(21):11395–11415
55. Halicka K, Cabaj J (2021) Electrospun nanofibers for sensing and biosensing applications—a review. Int J Mol Sci 22(12):6357
56. Yu H, Zhu T, Xie J, Du J, Sun C, Wang J et al (2019) Preparation of inorganic-organic-framework nanoscale carries as a potential platform for drug delivery. Adv Eng Mater 21(2):1800626
57. Wu J, Xi J, Chen H, Li S, Zhang L, Li P, Wu W (2022) Flexible 2D nanocellulose-based SERS substrate for pesticide residue detection. Carbohyd Polym 277:118890
58. Liang X, Liu Y, Wen K, Jiang W, Li Q (2021) Immobilized enzymes in inorganic hybrid nanoflowers for biocatalytic and biosensing applications. J Mater Chem B 9(37):7597–7607
59. Tang Q, Zhang L, Tan X, Jiao L, Wei Q, Li H (2019) Bioinspired synthesis of organic–inorganic hybrid nanoflowers for robust enzyme-free electrochemical immunoassay. Biosens Bioelectron 133:94–99
60. Wang Y, Yan J, Wen N, Xiong H, Cai S, He Q et al (2020) Metal-organic frameworks for stimuli-responsive drug delivery. Biomaterials 230:119619
61. Liu J, Huang J, Zhang L, Lei J (2021) Multifunctional metal–organic framework heterostructures for enhanced cancer therapy. Chem Soc Rev 50(2):1188–1218
62. Huang X, Hu J, Li Y, Xin F, Qiao R, Davis TP (2019) Engineering organic/inorganic nanohybrids through RAFT polymerization for biomedical applications. Biomacromolecules 20(12):4243–4257
63. Ma C, Malessa A, Boersma AJ, Liu K, Herrmann A (2020) Supercharged proteins and polypeptides. Adv Mater 32(20):1905309
64. Cheng X, Xu HD, Ran HH, Liang G, Wu FG (2021) Glutathione-depleting nanomedicines for synergistic cancer therapy. ACS Nano 15(5):8039–8068
65. Zhao N, Yan L, Zhao X, Chen X, Li A, Zheng D et al (2018) Versatile types of organic/inorganic nanohybrids: from strategic design to biomedical applications. Chem Rev 3:1666–1762
66. Panahi Y, Gharekhani A, Hamishehkar H, Zakeri-milani P, Gharekhani H (2019) Stomach-specific drug delivery of clarithromycin using a semi interpenetrating polymeric network hydrogel made of montmorillonite and chitosan: synthesis, characterization and in vitro drug release study. Adv Pharmeceutical Bull 9(1):159–173

67. Li H, Zhang Z, Godakanda VU, Chiu Y, Angkawinitwong U, Patel K et al (2019) The effect of collection substrate on electrospun ciprofloxacin-loaded poly (vinylpyrrolidone) and ethyl cellulose nanofibers as potential wound dressing materials. Mater Sci Eng C 104:109917
68. Godakanda VU, Li H, Alquezar L, Zhao L, Zhu L, de Silva R et al (2019) Tunable drug release from blend poly(vinyl pyrrolidone)-ethyl cellulose nanofibers. Int J Pharm 562:172–179
69. García-Guzmán P, Medina-Torres L, Calderas F, Bernad-Bernad MJ, Gracia-Mora J, Mena B, Manero O (2018) Characterization of hybrid microparticles/montmorillonite composite with raspberry-like morphology for atorvastatin controlled release. Colloids Surf B 167:397–406
70. Silva JM, Barud HS, Meneguin AB, Constantino VRL, Ribeiro SJL (2019) Inorganic-organic bio-nanocomposite films based on laponite and cellulose nanofibers (CNF). Appl Clay Sci 168:428–435
71. Wang H, Wu J, Zheng L, Cheng X (2018) Preparation and properties of ZnAl layered double hydroxide/polycaprolactone nanocomposites for use in drug delivery. Polym Plast Technol Eng 1–9
72. Senapati S, Shukla R, Tripathi YB, Mahanta AK, Rana D, Maiti P (2018) Engineered cellular uptake and controlled drug delivery using two dimensional nanoparticle and polymer for cancer treatment. Mol Pharm 15(2):679–694
73. Mahanta AK, Senapati S, Paliwal P, Krishnamurthy S, Hemalatha S, Maiti P (2019) Nanoparticle-induced controlled drug delivery using chitosan-based hydrogel and scaffold: application to bone regeneration. Mol Pharm 16(1):327–338
74. Yazdani P, Mansouri E, Eyvazi S, Yousefi V, Kahroba H, Hejazi MS et al (2019) Layered double hydroxide nanoparticles as an appealing nanoparticle in gene/plasmid and drug delivery system in C2C12 myoblast cells. Artifi Cells Nanomed Biotechnol 47(1):436–442
75. Simon J, Flahaut E, Golzio M (2019) Overview of carbon nanotubes for biomedical applications. Materials 12(4):1–21
76. Karthika V, Kaleeswarran P, Gopinath K, Arumugam A, Govindarajan M, Alharbi NS et al (2018) Biocompatible properties of nano-drug carriers using TiO_2-Au embedded on multiwall carbon nanotubes for targeted drug delivery. Mater Sci Eng C 90:589–601
77. Zhang N, Yan F, Liang X, Wu M, Shen Y, Chen M et al (2018) Localized delivery of curcumin into brain with polysorbate 80-modified cerasomes by ultrasound-targeted microbubble destruction for improved Parkinsons disease therapy. Theranostics 8(8):2264–2277
78. Hameed S, Bhattarai P, Dai Z (2018) Cerasomes and bicelles: hybrid bilayered nanostructures with silica-like surface in cancer theranostics. Front Chem 6:1–17
79. Gileva A, Sarychev G, Kondrya U, Mironova M, Sapach A, Selina O et al (2019) Lipoamino acid-based cerasomes for doxorubicin delivery: preparation and in vitro evaluation. Mater Sci Eng C 100:724–734
80. Bagheri AR, Li C, Zhang X, Zhou X, Aramesh N, Zhou H, Jia J (2021) Recent advances in covalent organic frameworks for cancer diagnosis and therapy. Biomater Sci 9:5745–5761
81. Huang D, Wu D (2018) Biodegradable dendrimers for drug delivery. Mater Sci Eng C 90:713–727
82. Kesharwani P, Choudhury H, Meher JG, Pandey M, Gorain B (2019) Dendrimer-entrapped gold nanoparticles as promising nanocarriers for anticancer therapeutics and imaging. Prog Mater Sci 103:484–508
83. Maryo LS, Haghnazari N, Keshavarzi F, Zhaleh H, Seidi F (2018) Synthesis of poly (amidoamine) (PAMAM) dendrimer-based chitosan for targeted drug delivery and cell therapy. J Basic Res Med Sci 5(4):6–13
84. Kurczewska J, Cegłowski M, Messyasz B, Schroeder G (2018) Dendrimer-functionalized halloysite nanotubes for effective drug delivery. Appl Clay Sci 153:134–143
85. Alibolandi M, Hoseini F, Mohammadi M, Ramezani P, Einafshar E, Taghdisi SM et al (2018) Curcumin-entrapped MUC-1 aptamer targeted dendrimer-gold hybrid nanostructure as a theranostic system for colon adenocarcinoma. Int J Pharm 549(1–2):67–75
86. Singh P, Pandit S, Mokkapati VRSS, Garg A, Ravikumar V, Mijakovic I (2018) Gold nanoparticles in diagnostics and therapeutics for human cancer. Int J Mol Sci 19(7):1979

87. Wang L, Pei J, Cong Z, Zou Y, Sun T, Davitt F et al (2019) Development of anisamide-targeted PEGylated gold nanorods to deliver epirubicin for chemo-photothermal therapy in tumor-bearing mice. Int J Nanomed 14:1817
88. Mehmandoust M, Erk N, Karaman C, Karimi F, Salmanpour S (2021) Sensitive and selective electrochemical detection of epirubicin as anticancer drug based on nickel ferrite decorated with gold nanoparticles. Micromachines 12(11):1334
89. Kutsevol N, Harahuts Yu, Shton I, Borikun T, Storchai D, Lukianova N, Chekhun V (2018) In vitro study of toxicity of hybrid gold-polymer composites. Mol Cryst Liq Cryst 671(1):1–8
90. Kutsevol N, Kuziv Y, Bezugla T, Chumachenko V, Chekhun V (2020) Multicomponent nanocomposites for complex anti-cancer therapy: effect of aggregation processes on their efficacy. Int J Polym Sci 2020(Article ID 9627954):7
91. Mahalunkar S, Yadav AS, Gorain M, Pawar V, Braathen R, Weiss S et al (2019) Functional design of pH-responsive folate-targeted polymer-coated gold nanoparticles for drug delivery and in vivo therapy in breast cancer. Int J Nanomed 14:8285
92. Khongkow M, Yata T, Boonrungsiman S, Ruktanonchai UR, Graham D, Namdee K (2019) Surface modification of gold nanoparticles with neuron-targeted exosome for enhanced bloodbrain barrier penetration. Sci Rep 9(1):8278
93. Manatunga DC, Godakanda VU, de Silva RM, de Silva KN (2020) Recent developments in the use of organic–inorganic nanohybrids for drug delivery. Wiley Interdisc Rev Nanomed Nanobiotechnol 12(3):e1605
94. Ilhan-Ayisigi E, Yesil-Celiktas O (2018) Silica-based organic-inorganic hybrid nanoparticles and nanoconjugates for improved anticancer drug delivery. Eng Life Sci 18(12):882–892
95. Yuan X, Peng S, Lin W, Wang J, Zhang L (2019) Multistage pH-responsive mesoporous silica nanohybrids with charge reversal and intracellular release for efficient anticancer drug delivery. J Colloid Interface Sci 555:82–93
96. Samanta S, Pradhan L, Bahadur D (2018) Mesoporous lipid-silica nanohybrids for folate-targeted drug-resistant ovarian cancer. New J Chem 42(4):2804–2814
97. Zhao S, Sun S, Jiang K, Wang Y, Liu Y, Wu S, Li Z (2019) In situ synthesis of fluorescent mesoporous silica—carbon dot nanohybrids featuring folate receptor—overexpressing cancer cell targeting and drug delivery. Nano-Micro Lett 0123456789:1–32
98. Fang J, Zhang S, Xue X, Zhu X, Zhu S, Song S et al (2018) Quercetin and doxorubicin co-delivery using mesoporous silica nanoparticles enhance the efficacy of gastric carcinoma chemotherapy. Int J Nanomed 13:5113–5126
99. Liu JF, Jang B, Issadore D, Tsourkas A (2019) Use of magnetic fields and nanoparticles to trigger drug release and improve tumor targeting. Wiley Interdisc Rev Nanomed Nanobiotechnol 11:e1571
100. Satpathy M, Wang L, Zielinski RJ, Qian W, Wang YA, Mohs AM et al (2019) Targeted drug delivery and image-guided therapy of heterogeneous ovarian cancer using HER2-targeted theranostic nanoparticles. Theranostics 9(3):778–795
101. Vallabani NVS, Singh S (2018) Recent advances and future prospects of iron oxide nanoparticles in biomedicine and diagnostics. 3 Biotech 8(6):1–23
102. Shukla RK, Kumar A, Kansara K, Dhawan A, Patel P, Pandya A, Shanker R (2018) Corrigendum: synthesis of biocompatible iron oxide nanoparticles as a drug delivery vehicle. Int J Nanomed 13:4207–4208
103. Vangijzegem T, Stanicki D, Laurent S (2019) Magnetic iron oxide nanoparticles for drug delivery: applications and characteristics. Expert Opin Drug Deliv 16(1):69–78
104. Carvalho SM, Leonel AG, Mansur AAP, Carvalho IC, Krambrock K, Mansur HS (2019) Bifunctional magnetopolymersomes of iron oxide nanoparticles and carboxymethylcellulose conjugated with doxorubicin for hyperthermo-chemotherapy of brain cancer cells. Biomater Sci 7(5):2102–2122
105. Lerra L, Farfalla A, Sanz B, Cirillo G, Vittorio O, Voli F et al (2019) Graphene oxide functional nanohybrids with magnetic nanoparticles for improved vectorization of doxorubicin to neuroblastoma cells. Pharmaceutics 11(1):1–17

106. Sadhukhan P, Kundu M, Rana S, Kumar R, Das J (2019) Microwave induced synthesis of ZnO nanorods and their efficacy as a drug carrier with profound anticancer and antibacterial properties. Toxicol Rep 6:176–185
107. Kundu M, Sadhukhan P, Ghosh N, Chatterjee S, Manna P, Das J, Sil PC (2019) pH-responsive and targeted delivery of curcumin via phenylboronic acid-functionalized ZnO nanoparticles for breast cancer therapy. J Adv Res 18:161–172
108. Zamani M, Rostami M, Aghajanzadeh M, Kheiri Manjili H, Rostamizadeh K, Danafar H (2018) Mesoporous titanium dioxide@ zinc oxide–graphene oxide nanocarriers for colon-specific drug delivery. J Mater Sci 53(3):1634–1645
109. Zhang X, Liang X, Ma X, Hou R, Li X, Wang F (2019) Highly stable near-infrared dye conjugated cerasomes for fluorescence imagingguided synergistic chemo-photothermal therapy of colorectal cancer. Biomater Sci 7(7):2873–2888

Chapter 7
Organic–Inorganic NanoHybrids in Tissue Engineering and Drug Delivery Applications

Shahzad Maqsood Khan, Saba Zia, and Nafisa Gull

1 Introduction

Organic–inorganic nanohybrids (OINHs) which comprise of distinct inorganic and organic constituents are fascinating because they merge both components and achieve the synergistic properties of both [1–4]. OINHs are extensively found in nature like mollusk teeth and shells, which comprised of bio macromolecules as organic moiety and inorganic ingredients via nanoscale hybridization [5]. Inorganic nanoparticles like iron, gold, silver oxide, and quantum dots have captivating magnetic, electrical and optical properties making them suitable candidate for the development of multi-functional nanohybrids [3]. The unique nanoscale hybridization possesses considerably prominent properties than respective bulk materials [6], which is demanding for pharmaceutical applications [7, 8]. Enhanced permeation and retention effect causes appropriate nanoparticles accumulation in tumour area [9]. In modern era, with increasing demand of personalized therapy [10], efforts have been done to assess the response of treatment and notion of theranostics [11]. In this perspective, OINHs assimilating metals, polymers and semiconductors can be potential candidates for newly developed biomaterials.

In OINHs, inorganic nanoparticles provide porous structure and organic moieties tender different functional groups make them favourable for controlled release pattern and drug loading capacity [4, 12]. Due to these aspects, OINHs have directed to the modern drug delivery field with enthralling characteristics. However, functionality of OINHs can be modulated using control composition of each phase, morphology and the surface identity during their synthesis according to the demand of drug release pattern [13–17].

Surface functionalization of organic moieties including biomolecules, small molecules and polymers is needed to make better dispersibility of nanoparticles for

S. M. Khan (✉) · S. Zia · N. Gull
Institute of Polymer and Textile Engineering, University of the Punjab, Lahore, Pakistan
e-mail: shahzad.ipte@pu.edu.pk

K. Rizwan et al. (eds.), *Hybrid Nanomaterials*, Materials Horizons: From Nature to Nanomaterials, https://doi.org/10.1007/978-981-19-4538-0_7

biomedical applications [18]. Furthermore, organic constituents are also demanded to ensure the stability and biocompatibility of nanohybrids [19]. To reduce the side effects of chemotherapy, controlled and site-specific targeting drug release pattern are important to target the pathological region without damaging the healthy tissues [20]. Distinct tumour microenvironment-based approaches are proposed for the synthesis and design of theranostic agents [21, 22]. Mostly, organic constituent of OINHs induce the functions like controlled release manner, biodegradability, guest molecule loading, targeting and stimuli responsiveness [23]. The design of morphology, composition and surface property of nanohybrids proffers them with modulated characteristics and paves the path for diverse biomedical applications [24].

2 Constituents of Organic–Inorganic Nanohybrids

2.1 Organic Constituents

2.1.1 Cellulose

Cellulose is one of the utmost and plentiful biomaterials currently available. It is mostly produced from plants and some bacteria. It is water insoluble fibrous and tough material. All these characteristics play a vital role for the adherence of plant structure and stable cell walls. Cellulose chains are organized in the form of bundles or microfibrils which results in the building of cell walls of the plants. This helps in the support of the firmness of the plant structure and makes cellulose a biomaterial that has high strength and additional higher mechanical characteristics. Microcrystalline cellulose is a material that is widely used in different applications including tissue engineering and drug delivery [25].

2.1.2 Starch

Starch is another dominant biomass available on earth, generated as energy storing fragment for plants. Pure starch is formed by the combination of two kinds of molecules, and that combination has branched amylopectin and linear/helical amylose. Starch is unscented, tasteless white powder that is insoluble in cold water and alcohol. The functional and physio-chemical characteristics of starch isolate them from diverse botanical resources like wheat, rice, corn and potato which makes them beneficial for range of pharmaceutical and biomedical applications. Its properties like excellent swell ability, solubility in favourable solvents, gelatinization, mechanical behaviour, rheological characteristics and enzymatic digestibility are of ultimate prominence which make it suitable for distinct applications like bone fixation and replacement. It is also utilized as transporter for the controlled drug delivery systems

and other bioactive agents. Starch is chemically reformed with added reactive sites, can carry biologically active complexes and valuable biocompatible carriers that can be certainly metabolized in human body [26].

2.1.3 Chitosan

Chitosan is a distinctive biopolymer, a chitin derivative, earned a noteworthy importance in the field of tissue engineering and drug release system. It is extracted from the exoskeleton of crustaceans like crabs and in the plants cell envelope like fungal hyphae (mushrooms) [27–30]. Due to its extraordinary properties in engineering, technology and biological fields, it is used to produce nanohybrid materials. Combination of chitosan with silica or nanosilica by sol–gel method can be used for development of nanohybrid materials having both properties of organic and inorganic components. As silica in micro or nano form have decisive role for bio mineralization, so it is used for stimulation of biomaterials as biological response [31–33].

2.1.4 Alginate

Alginate is an anionic brown seaweed extracted natural polymer, (1,4)-linked β-D-mannuronate (M) and α-L-guluronate (G) residues are the building blocks of alginate. It is biocompatible, cost-effective when added with divalent cations and results in mild gelation. It is widely studied for several biomedical applications. Alginate gels have been extensively used in several biomedical areas, including wound healing, tissue/bone regeneration and used as systems for studying mammalian cell cultures [34].

2.1.5 Poly(Ethylene Glycol)

Poly(ethylene glycol) (PEG) is water-soluble polymer and used for biomedical applications as it has nonimmunogenicity and low toxicity. These promising properties of PEG have made it a right selection for surface modified biomaterials [35]. The end-group derivatization and chemical conjugation with a range of biological molecules such as polypeptides, polysaccharides, polynucleotides, and small organic molecules under mild physiological conditions is possible because it is easily soluble in water [36].

2.2 Inorganic Constituents

2.2.1 Silica

It is the key component of rock-forming minerals in magmatic and metamorphic rocks. It is a significant element of sediments and soils. An approach for synthesizing a dual-modality and theranostic silica nanohybrids is studied that have outstanding characteristics for optical imaging, magnetic resonance imaging and in drug delivery system. Silica nanohybrids are composed of two key components: $CuInS_2$/ZnS quantum dots and magnetite nanocrystals, having an outer silica shell that is grafted with PEG and amine groups to improve biocompatibility and successive bio conjugation, respectively [37].

2.2.2 Halloysite Nanoclay

Aiming clays for their key features, halloysite nanoclay has myriad impact. Its molecular formula is $Al_2Si_2O_5(OH)_4nH_2O$, alumina silicate abundantly available in nature, whereas Al is inclined in gibbsite-like octahedral formations of Al–OH groups and groups of Si–O are formed like tetrahedral sheet [38]. Nanohybrids made up of electro-spun poly(L-lactic) acid nanofibers with halloysite clay have high tensile strength, young's modulus, and fracture analysis [39]. Nano-micro scaffold with 3-week drug delivery tenure was fabricated using nanohybrid of halloysite nanoclay with metronidazole drug and doped with poly(caprolactone)/gelatin microfibres have controlled drug delivery applications. This nanoclay can also be used for the manufacturing of membranes with increased anisotropic mechanical properties [40]. Grafting of nanohalloysite nanoclay with PEG amine enhances cellular uptake and improves water-soluble antioxidant activity and can be used in tissue engineering applications [41].

2.2.3 Quantum Dots

Nanotechnology has high score in the current healthcare industry. Although, initial focus was only on taming the features of pre-existent therapeutic and investigative modalities. However, last few years have perceived quite a lot of innovative moieties regarding therapeutic and diagnostic prospective, this also helped in the development of the supramolecular assemblies having simple mechanisms through nanoengineering. Quantum dots are such case, has been useful to the diagnostic and therapeutic field. They were firstly employed in determination of surface kinetics, but now these are efficaciously used in drug delivery systems as agents and diagnostic markers [42].

3 Fabrication Techniques of Organic–Inorganic Nanohybrids

The prerequisite to produce stable hybrid nanoparticles is the production of such nanohybrids which can join inorganic and organic components. These strong interactions are obtained by different bonding patterns like non-covalent physical interactions (Class I) or by covalent chemical bonds (Class II). Non-covalent physical interactions have a number of interactions including van der Waal forces and hydrogen bonding [43]. For the production of 1st generation biohybrid materials, Class I type bonding is normally favoured [44]. Class II nanohybrids fabrication depends on binding of nanoparticles surface with polymers thus enhancing stronger metal to ligand coordination. Class II route often produce nanohybrid materials with excellent colloidal stability and narrow size in biological media. Such materials also offer tunable surface activity which is favourable condition for formation of biological nanohybrids for biomedical applications. Amphiphilic polymers or polyelectrolytes are normally used for fabrication of Class I nanohybrids by hydrophobic or electrostatic interactions. During synthesis, removal of solvents or organic phase produces materials with variable architectures. In polymers, accurate control of these hybrid aggregates enhances the performance of nanohybrids due to combination of properties of parent inorganic components which therefore produces a nanohybrid material with entirely new and advanced properties. Moreover, these self-assembled amphiphilic polymer structures serve as a base material as nanotemplates to produce nanohybrids. Such produced nanohybrids have controlled size and morphology [45]. Certain stimuli-responsive moieties can also be incorporated into polymers or inorganic systems. These moieties can persuade a changeable assembly to produce nanohybrid materials in a specific biological environment [46].

Till now, various approaches have been subjected for the fabrication of organic–inorganic hybrid materials. Later, efforts were also in progress to analyse their characteristic properties with required morphologies and enhanced mechanical properties so that nanohybrid materials with high performance can be fabricated. These approaches include layer-by-layer (LbL) self-assembly, in situ fabrication and electrospinning. Based on structure of cationic polymers, multiple techniques have been employed for the synthesis of organic or inorganic nanohybrid gene carriers. It includes electrospinning, self-assembly and wrapping strategies [47, 48]. Few fabrication techniques of OINHs are given below in detail.

3.1 Blended Electrospinning

Electrospinning is an economical, newly developed, and widely used technique to produce nanofibres from polymers. It is considered as one of the most simple and adaptable method for the fabrication of nanohybrid materials. This can be achieved by mixing of nanoparticles with polymers and subject them for electrospinning.

Such simple mixing of materials and then formation of nanohybrid fibres results in the development of biocompatible nanohybrid materials with enhanced mechanical properties which can be used for various biological applications. Before subjecting to electrospinning, the polymer solution is mixed with nanoparticles and stirred to produce a uniform stable colloidal solution. Often this process is of long duration and resulted evenly distributed nanoparticles in polymer solution [49].

3.2 Layer-by-Layer (LbL) Method

LbL self-assembly is one of the important methods, especially for the surface modification of the nanohybrid materials or their composites. This technique can also be used for the deposition of different multilayers on the nanomaterials surface to develope modified nanohybrids [50]. Already synthesized nanofibres by electrospinning are used as substrate. This substrate is then used to deposit inorganic–organic materials by electrostatic self-assembly for the development of nanohybrid materials [51].

3.3 In Situ Fabrication

This method can be used to obtain hybrid nanofibres. In this mode, in situ polymerization is used to prepare nanoparticles in polymer solution which afterward subjected to electrospinning for production of hybrid nanofibres. Moreover, polymer nanofibres doped with inorganic nanoparticles precursors like metal ions can be firstly generated and then inorganic nanoparticles are produced by in situ growth. This is helpful to produce such nanofibres which have uniform particle spreading in fibres and due to in situ method particle aggregation is avoided. However, this method is used for the fabrication of hybrid nanofibres which are doped with metal or metal oxide nanoparticles due to in situ generation of the inorganic nanoparticles [52].

3.4 Co-axial Electrospinning

In this method, a co-axial spinneret with outer and inner needle is used. Various nanohybrid materials in the form of fibres with different morphologies can be obtained by adjustment of the flow rate of both inner and outer polymer solution with variable compositions [53] which helps to produce nanohybrid composite fibres with different mechanical properties. FePt nanoparticles in poly-ε-caprolactone nanofibres can be obtained by this process [54]. Co-axial electrospinning mode need more stringent control on parameters of electrospinning process like voltage, flow rate and

concentration of electrospinning solution, than blended electrospinning, as core and shell fluids are electrospun collectively in co-axial electrospinning [55].

3.5 Melt Intercalation

This technique can be considered as a "grafting on" approach. Layered silicates are used for mixing with polymers in molten form which helps polymer to creep in interlayer spaces forming intercalated or exfoliated nanoparticles. This crawling depends on the compatibility of polymers and layered surface [56]. On the other side, for grafting from approach, an organic layer is added by surface initiated free radical polymerization reactions. Monomer, solvent and catalysts are required for grafting. This mode produces nanohybrids with multifunctional and tunable properties [57].

3.6 One-Pot Synthesis

It is simple, easy, and efficient mode to produce nanohybrids, in which inorganic part is directly formed by one step reaction in the presence of organic parts which exert as surface capping agents. Normally, organic parts do not take part during the reaction, and they only play the capping role. Multiple functional groups are added on inorganic nanoparticles surface which is helpful for enhancing ligating ability of nanoparticles [58].

3.7 Wrapping Technique

Wrapping of organic molecules is another method for the fabrication of nanohybrids by non-covalent interactions. Inorganic nanoparticles are added with organic molecule which act as matrix by self-assembly process or by direct encapsulation. In synthesis process, the core shell structure is wrapped by polymer molecules [24]. Moreover, the other functional groups which are organic, have metallic ions that produce core shell like structure by coordinate bonds [59].

4 Organic–Inorganic Nanohybrids in Tissue Engineering

Nanohybrid materials, especially in ultrathin form, are novel for tissue engineering and regenerative medicines (TERM) preparation. These structures are quasi structures which are two-dimensional, having thickness up to sub-micrometric level like average near about hundreds of nanometres with several square centimetres surface

area which enable them to be used for broad range of applications. They are used in biological or chemical sensors and in nanoelectronic devices for ultra-conformable circuits and electrodes. They are also used for formation of encapsulation schemes for storage of hydrogen-based materials. Moreover, nanohybrids have major applications now in biomedical field like tissue engineering [60].

Nanohybrid materials in hydrogel form are rapidly using as artificial biomaterial scaffolds. These nanohybrids produce microenvironment in three-dimensional form for TERM. It involves several biomedical applications including not only repair but also replacement and regeneration of tissues which are very problematic to heal and are damaged. Normally the procedure adopted for tissue repair is by taking healthy tissues from a donor, i.e. allograft or from patients own body, i.e. autograft, but there are many drawbacks in both procedures like scarcity of donor, mismatching problem which cause tissue rejection and failure of graft. Therefore, new tissues are developed from very low number of recipients which is archetypical of modern TERM. These newly fabricated tissues are made of host cells, tissue scaffolds and growth factors of animals. As plastic surfaces are not alleged to organisms' cellular environment due to their hard and flat nature which is due to interactions of extracellular matrix (ECM) with cellular tissue homeostasis. This is formed due to three-dimensional communication network establishment [61].

For patients suffering from osteoporosis-related facture, trauma, and skeletal diseases, use of nanohybrids in bone tissue engineering provides an important and powerful pathway for health care of individuals. In order to develop the function of native bone ECM, during the past decades, a promising work is done for designing of nanohybrid materials-based scaffolds which are produced by using biopolymers. These scaffolds made up of nanohybrid materials are used for tissue regeneration and for the reconstruction and remodelling of bone defect sites. These modes are successfully employed to treat and restoration of complex bones [62].

Aerogels are one of the important materials which is used in environmental and biomedical applications due to tuneable and exclusive possessions and ease in functionalization. The characteristic three-dimensional open network structure of aerogels helps to access the external fluids of biological body, thus helping in controlled communication with inner vigorous exteriors. As aerogels with their nanohybrids have a lot of versatility, therefore, they are used in different applications including catalysis, CO_2 seizure, oil and water separation, drug and medicine delivery [63]. Several biopolymers are in use for bio-aerogels manufacturing which might involve collagen, gelatin, whey proteins, polysaccharides (alginate, cellulose and chitosan), etc. [64]. Those nanohybrid aerogel structures which are silica-based, produce materials which have ability of forming adjustable mechanical and chemical properties. This will also help in the improvement of biomaterials characteristics like noncytotoxicity, biocompatibility, bioactivity, biodegradability, etc. [65].

Different natural and synthetic polymers are used for tissue regeneration in bones. Amongst natural polymers, polysaccharides and proteins are prominent because their cytocompatibility is similarity to ECM of instinctive tissues [66]. In biomedical engineering and biotechnology fields, to increase starch matrix performance use of natural polymers like bamboo, plant, and bacterial cellulose and fibre-based starch matrix has

been increased. For the development of bone structures and scaffolds, nanohybrids made up of fibre-based composites increased a lot in recent years [67]. Nanofibres of polymers have close resemblance with bone tissues, so they help in rapid growth, calcination process, proliferation, and growth. Amongst such polymers, silk fibroin is one of the important fibrous biopolymers having good biological properties along with slow degradation rate and enhanced mechanical properties. High oxygen permeability of silk fibroin makes it favourable material for slow regeneration of tissues as bone [68]. Due to these prominent features, these nanofibres are widely used for bone tissue scaffolding manufacturing [69].

Nanohybrid materials are required to be biocompatible and biodegradable so that osteoblast adhesion and proliferation should be enhanced. This enhancement should be induced without any harmful effect. Another important polymer which is used for the development of nanohybrid materials is carboxymethyl cellulose which is used in many biomedical applications. The crosslinked 3D carboxymethyl cellulose is used for tissue engineering because of metal ions harmful effects to osteoblasts. Zirconia is an important tetravalent metal, cationic in nature and has very interesting chemistry. It exists in pure, nano and in ionic forms. It has exceptional mechanical properties, good corrosion resistivity, biologically inert and used as alloy for bone implantation. Due to the nontoxic behaviour of the zirconia in nano form, it has no adverse effect on osteoblast. It can also be added to cell culture in controlled concentrations and in scaffold forming nanohybrids for biomedical purposes like proliferation, stem cell and orthopaedics [70].

Halloysite clay in nano form is also one of the important materials used for the nanohybrid development to be used in tissue engineering applications like tissue fabrication, drug delivery and cell labelling. Still there is challenge for the preparation of biocompatible natural nanotubes with wider lumen. Such halloysite nanotubes can load bio macromolecules or fluorescent beacons. These nanotubes have raised the potential for drug delivery agent in cytoplasm as it has ability to internalize by diffusion and accumulation in the specified area [71]. The foremost application of halloysite based nanohybrids in imaging cellular circulation labelling in tissues. This imaging can also be facilitated by incorporation of dyes to support laser scanning confocal imaging, or by enhanced dark-field imaging [72]. Halloysite hybrid-based drug-loaded nanocontainers are internalized by the cells. The drug is released by different modes like triggering a reaction, enzyme stimulation or activation by thermal means. Halloysite clay can be chemically treated by many ways to change the organics side of its structure. A favourable approach to alter halloysite nanohybrids is that no prominent change is required in whole structure except only the tube which are endings by functionalized inorganic [73] or organic stoppers giving stimuli responsiveness to release the attached drug. Halloysite nanohybrids can also be doped with proteins and acids. Such doped materials also used modifiers [74] for intra-cellular tissue engineering scaffolds for gene delivery. These nanohybrids can also be used for the modification of surfaces of artificial tissue scaffolds with increased mechanical properties due to nanohalloysite [75]. Chitosan and halloysite based nanohybrids also have excellent mechanical and thermal properties which are synthesized by freeze-drying method [76].

5 Organic–Inorganic Nanohybrids in Drug Delivery

The use of OINHs in drug release application provide better pharmacokinetic, pharmacodynamic profiles and therapeutic index of the drugs [77, 78]. Additionally, shape and suitable size of the nanoparticles easily infuse through leaky vasculature in cancer cells or through cell membranes [79, 80]. A surplus of nanocarriers with inorganic and organic origins are using over the years to adsorb or encapsulate drugs. Iron oxide nanoparticles [81, 82] mesoporous silica nanoparticles [83, 84] and double layered hydroxides [85] are highlighted as inorganic nanocarriers. Amongst organic nanocarriers, liposomes [86], carbon nanotubes [87], dendrimers [88] solid lipid nanoparticles, micelles, nanogels and polymeric nanoparticles have been significantly used. Out of inorganic and organic nanocarriers, inorganic ones are preferably used to get targeting ability with smaller particle size as well as provide multifunctionality owing to electrical, mechanical and optical properties. While organic nanocarriers are used to provide biodegradability and diversity in loading of hydrophobic and hydrophilic drugs [89].

Different OINHs based on clays like sapiolite, montmorillonite, palygorskite, kaolin, etc., are greatly explored in drug release applications [90–92]. Interaction between inorganic constituent clay and organic part polymer or drug molecule is due to the different mechanisms depends upon the physico-chemical properties of the organic compounds, available functional groups and type of clay. Among all mechanisms, ion exchange is mostly used [93]. This mechanism along with swelling capacity [94] and adsorptivity [95] of clay cause the potential use of clay based hybrid materials in extended delivery system [96], site-specific delivery systems [97] and drug solubility improvement systems [98]. Improved characteristics like enhanced ion exchange capacity, porosity and surface area can boost clay drug interaction which is accounted for the extended release of drugs [99]. Required characteristics of natural clays can further be improved by using polymeric additives and chemical and thermal treatments [100].

Among all clays, sodium montmorillonite is preferably used due to its high ion exchange capacity and intercalation ability. A hybrid composite of gelatin microparticles and montmorillonite is reported for controlled drug release system at pH below the isoelectric point with drug entrapment efficiency up to 67%. This hybrid composite also shown better rheological properties with strong affinity with mucin at pH 1.6 showing its viability at stomach pH [101]. In another study, variable amount of montmorillonite was added in siloxane-poly(ethylene oxide) and regulated the nanostructural properties of hybrids which consequently controlled the delivery of sodium diclofenac. This varied addition of exfoliated silicate controlled the water uptake and eventually release of sodium diclofenac via mass transport barrier which can be used in prolonged treatment of painful conditions [102].

Silica particles are encapsulated in organic components and silanol groups are functionalized which are present at outer and inner surfaces to be used for drug delivery system [103]. Luo et al. reported that silica nanoparticles loaded

with doxorubicin and coated on gelatin shell which were crosslinked with N,N′-bis(acryloyl)cystamine to develop redox responsive nanogated mechanism. This nanohybrid shown better potent anticancer effect and cellular internalization for A549 cells compared to the pure doxorubicin [104].

Thi et al. prepared super paramagnetic iron oxide nanoparticles by coprecipitation method on which poloxamer-heparin copolymer was coated. This core shell structure can interact with hydrophobic and hydrophilic drugs due to the inclusion of poloxamer having tumour targeting capacity due to heparin for anticancer drug delivery. This nanohybrid showed the safe usability due to biocompatibility of the polymer, improved anticancer effect against HeLa cell lines and controlled release of doxorubicin over five days [105]. In another study, core shells of carboxymethyl cellulose and ironoxide nanohybrids were prepared which were loaded with doxorubicin which showed chemotherapeutic and hyperthermic effect against glioblastoma brain cancer cells [58]. Some more studies with iron oxide nanoparticles were also conducted to achieve both magnetic targeting capability and hyperthermic effect [106].

Sawant and Bamane prepared zinc oxide based core shell nanohybrids by using PEG linked with beta-cyclodextrin loaded with curcumin in which beta-cyclodextrin provided controlled drug release and PEG improved the biocompatibility and water dispersibility. It showed the 88% release of curcumin at pH 4.8 and 45–50% at physiological pH to make it suitable for tumour microenvironment. It showed the bifunctional therapeutic effect by improved apoptotic activity against breast cancer cells and moderate antibacterial activity against *Staphylococcus aureus*. Luminescent properties of zinc oxide make it capable for cellular imaging during drug administration [107].

Hydroxyapatite based nanohybrids were prepared by functionalization of alginate with hydroxyapatite having iron oxide core which showed the controlled release of curcumin and 6-gingerol at pH 5.3 for 6–7 days against liver and breast cancer cells [108]. Another core shell system of hydroxyapatite and gum acacia was prepared which showed controlled release of naringin over 28 days with strong effective antiproliferative effect against osteosarcoma cells. This system also showed antibacterial activity against *Escherichia coli* and *S. aureus* proliferation [109].

Dendrimers are synthetic 3D polymer assemblies with highly branched structures comprise of functional surfaces and internal cavities. They develop host–guest complex with drugs via hydrogen bonding and electrostatic interactions which make them capable for drug delivery systems [110]. Due to their nondegradable nature, inorganic nanoparticles like silica, iron, gold, etc., are conjugated with dendrimers to develop nontoxic dendritic structures [111, 112].

Silica polyamidoamine dendrimer nanoconjugate was developed for anthocyanin release for which antiproliferative effect of the drug-loaded carrier investigated on the neuroblastoma cells showed improved toxic effect for seven days and highlighted its anticancer potential [113]. Magnetic nanodendrimers were fabricated using silica polyamidoamine and iron oxide nanoparticles for the release of methyl prednisolone succinate for cancer treatment [111].

Micelles are amphiphilic molecules with hydrophilic head group and hydrophobic tails developing circular structure in aqueous medium. They can overcome the issues like cellular penetration, toxicity, solubility and show stimuli responsiveness in targeted drug release [114]. Pluronic-b-poly(L-lysine) micelles coated with gold nanoparticles were prepared for NIR induced paclitaxel release showed improved cellular uptake by MDA MB231 breast cancer cells [115]. A triblock copolymer has hydroxamic acid functionalized centre ligate with iron oxide and loaded with doxorubicin and paclitaxel to develop theranostic micelle based nanohybrids which have ability to use in magnetic resonance imaging [116]. Lipase sensitive polyurethane micelles decorated with silver nanoparticles which have antibacterial activity show profound antibacterial effect against *S. aureus* and *E. coli* [117].

6 Conclusion

Recent development of OINHs has gained much attention due to their applications in tissue engineering and drug delivery fields. Hybrid structures are preferred to overcome the issues like poor dispersibility and solubility of individual systems. In OINHs, inorganic moieties provide magnetic, electrical, and optical properties while organic constituents enhance the biodegradability, biocompatibility and targeting ability of drugs. Different types of inorganic nanoparticles like silica oxide, iron oxide, gold oxide, zinc oxide and hydroxyapatite, etc., and organic moieties like biomolecules, synthetic polymers and small molecules are used to prepare OINHs. They are fabricated by different facile techniques like LbL assembly, wrapping, in situ fabrication, one pot synthesis and blended and co-axial electrospinning etc. However, fabrication of OINHs is critical because its use in different applications is challenging due to the cytotoxicity, lack of reproducibility, delicacy, and poor efficiency. By deep understanding of in vitro and in vivo conditions and interaction of OINHs with biological constituents inside the body, they can be used in biomedical application like tissue engineering and drug release systems.

References

1. Molina M, Asadian-Birjand M, Balach J, Bergueiro J, Miceli E, Calderón M (2015) Stimuli-responsive nanogel composites and their application in nanomedicine. Chem Soc Rev 44:6161–6186
2. Nguyen KT, Zhao Y (2015) Engineered hybrid nanoparticles for on-demand diagnostics and therapeutics. Acc Chem Res 48:3016–3025
3. Guo K, Zhao X, Dai X, Zhao N, Xu FJ (2019) Organic/inorganic nanohybrids as multifunctional gene delivery systems. J Gene Med 21
4. Shakeel A et al (2022) Advanced polymeric/inorganic nanohybrids: an integrated platform for gas sensing applications. Chemosphere 133772
5. Ruiz-Hitzky E, Darder M, Aranda P, Ariga K (2010) Advances in biomimetic and nanostructured biohybrid materials. Adv Mater 22:323–336

6. Sanchez C, Julián B, Belleville P, Popall M (2005) Applications of hybrid organic−inorganic nanocomposites. J Mater Chem 15:3559–3592
7. Chen G, Roy I, Yang C, Prasad PN (2016) Nanochemistry and nanomedicine for nanoparticle-based diagnostics and therapy. Chem Rev 116:2826–2885
8. Ma X, Zhao Y, Liang XJ (2011) Theranostic nanoparticles engineered for clinic and pharmaceutics. Acc Chem Res 44:1114–1122
9. Maeda H, Nakamura H, Fang J (2013) The EPR effect for macromolecular drug delivery to solid tumors: improvement of tumor uptake, lowering of systemic toxicity, and distinct tumor imaging in vivo. Adv Drug Deliv Rev 65:71–79
10. Ryu JH, Lee S, Son S, Kim SH, Leary JF, Choi K, Kwon IC (2014) Theranostic nanoparticles for future personalized medicine. J Control Release 190:477–484
11. Lim EK, Kim T, Paik S, Haam S, Huh YM, Lee K (2015) Nanomaterials for theranostics: recent advances and future challenges. Chem Rev 115:327–394
12. Samanta S, Pradhan L, Bahadur D (2018) Mesoporous lipid-silica nanohybrids for folate-targeted drug-resistant ovarian cancer. New J Chem 42:2804–2814
13. Manatunga DC, Godakanda VU, de Silva RM, de Silva KN (2019) Recent developments in the use of organic–inorganic nanohybrids for drug delivery. WIREs Nanomed Nanobiotechnol 12
14. Pippa N, Chronopoulos DD, Stellas D, Fernández-Pacheco R, Arenal R, Costas Demetzos NT (2017) Design and development of multi-walled carbon nanotube-liposome drug delivery platforms. Int J Pharm 528:429–439
15. Zhang X, Zhao Y, Cao L, Sun L (2018) Fabrication of degradable lemon-like porous silica nanospheres for pH/redox-responsive drug release. Sens Actuators B Chem 257:105–115
16. Gonzalez-Rodriguez R, Campbell E, Naumov A (2019) Multifunctional graphene oxide/iron oxide nanoparticles for magnetic targeted drug delivery dual magnetic resonance/ fluorescence imaging and cancer sensing. PLoS ONE 14:1–18
17. Liu S et al (2021) Engineered nanocellulose-based hydrogels for smart drug delivery applications. Int J Biol Macromol 181:275–290
18. Biju V (2014) Chemical modifications and bioconjugate reactions of nanomaterials for sensing, imaging, drug delivery and therapy. Chem Soc Rev 43:744–764
19. Qamar SA et al (2022) Carrageenan-based hybrids with biopolymers and nano-structured materials for biomimetic applications. Starch—Stärke 2200018
20. Ulbrich K, Hola K, Subr V, Bakandritsos A, Tucek J, Zboril R (2016) Targeted drug delivery with polymers and magnetic nanoparticles: covalent and noncovalent approaches, release control, and clinical studies. Chem Rev 116:5338–5431
21. Liu JN, Bu W, Shi J (2017) Chemical design and synthesis of functionalized probes for imaging and treating tumor hypoxia. Chem Rev 117:6160–6224
22. Dai Y, Xu C, Sun X, Chen X (2017) Nanoparticle design strategies for enhanced anticancer therapy by exploiting the tumor microenvironment. Chem Soc Rev 46:3830–3852
23. Kamaly N, Yameen B, Wu J, Farokhzad OC (2016) Degradable controlled-release polymers and polymeric nanoparticles: mechanisms of controlling drug release. Chem Rev 116:2602–2663
24. Zhao N, Yan L, Zhao X, Chen X, Li A, Zheng D, Zhou X, Dai X, Xu FJ (2018) Versatile types of organic/inorganic nanohybrids: from strategic design to biomedical applications. Chem Rev 3:1666–1762
25. Liu H, Li X, Wang S, Huang S, Wei C, Lv J (2014) Fabrication and thermal property of polyhedral oligomeric silsesquioxane (POSS)/microcrystalline cellulose (MCC) hybrids. J Carbohyd Chem 33:86–103
26. Kaur L, Singh J, Liu Q (2007) Starch—a potential biomaterial for biomedical applications. Nanomaterials and nanosystems for biomedical applications, pp 83–98
27. Reyes-Peces MV, Pérez-Moreno A, María de-los-Santos D, del Mar Mesa-Díaz M, Pinaglia-Tobaruela G, Vilches-Pérez JI, Fernández-Montesinos R, Salido M, de la Rosa-Fox N, Piñero M (2020) Chitosan-GPTMS-silica hybrid mesoporous aerogels for bone tissue engineering. Polymers 12:2723

28. Gull N, Khan SM, Khalid S, Zia S, Islam A, Sabir A, Sultan M, Hussain F, Khan RU, Butt MT (2020) Designing of biocompatible and biodegradable chitosan based crosslinked hydrogel for in vitro release of encapsulated povidone-iodine: a clinical translation. Int J Biol Macromol 164:4370–4380
29. Abo Elsoud MM, El Kady EM (2019) Current trends in fungal biosynthesis of chitin and chitosan. Bull Natl Res Centre 43:59
30. Gull N, Khan SM, Butt MT, Zia S, Khalid S, Islam A, Sajid I, Khan RU, King MW (2019) Hybrid cross-linked hydrogels as a technology platform for in vitro release of cephradine. Polym Adv Technol 30:2414–2424
31. Götz W, Tobiasch E, Witzleben S, Schulze M (2019) Effects of silicon compounds on biomineralization, osteogenesis, and hard tissue formation. Pharmaceutics 11:117
32. Gull N, Khan SM, Butt OM, Islam A, Shah A, Jabeen S, Khan SU, Khan A, Khan RU, Butt MT (2020) Inflammation targeted chitosan-based hydrogel for controlled release of diclofenac sodium. Int J Biol Macromol 162:175–187
33. Gull N, Khan SM, Butt MT, Khalid S, Shafiq M, Islam A, Asim S, Hafeez S, Khan RU (2019) In vitro study of chitosan-based multi-responsive hydrogels as drug release vehicles: a preclinical study. RSC Adv 9:31078–31091
34. Datta LP, Manchineella S, Govindaraju T (2019) Biomolecules-derived Biomaterials. Biomaterials 230:119633
35. Gull N, Khan SM, Islam A, Butt MTZ (2019) Hydrogels used for biomedical applications. In: Visakh PM, Bayraktar O, Menon G (eds) Bio monomers for green polymeric composites materials, pp 175–199
36. Pison U, Welte T, Giersig M, Groneberg DA (2006) Nanomedicine for respiratory diseases. Eur J Pharmacol 533:341–350
37. Hsu JC, Huang CC, Ou KL, Lu N, Mai FD, Chen JK, Chang JY (2011) Silica nanohybrids integrated with CuInS2/ZnS quantum dots and magnetite nanocrystals: multifunctional agents for dual-modality imaging and drug delivery. J Mater Chem 21:19257–19266
38. Wu Y, Zhang Y, Ju J, Yan H, Huang X, Tan Y (2019) Advances in halloysite nanotubes–polysaccharide nanocomposite preparation and applications. Polymers 11:987
39. Cai N, Dai Q, Wang Z, Luo X, Xue Y, Yu F (2015) Toughening of electrospun poly(l-lactic acid) nanofiber scaffolds with unidirectionally aligned halloysite nanotubes. J Mater Sci 50:1435–1445
40. Fakhrullin RF, Lvov YM (2016) Halloysite clay nanotubes for tissue engineering. Nanomedicine 11:2243–2246
41. Vikulina A, Voronin D, Fakhrullin R, Vinokurov V, Volodkin D (2020) Naturally derived nano- and micro-drug delivery vehicles halloysite, vaterite and nanocellulose. Royal Soc Chem 44
42. Ozkan M (2004) Quantum dots and other nanoparticles: what can they offer to drug discovery? Res Focus 9:1065–1071
43. Judeinstein P, Sanchez C (1996) Hybrid organic−inorganic materials: a land of multidisciplinarity. J Mater Chem 6:511–525
44. Luchini A, Vitiello G (2019) Understanding the nano-bio interfaces: lipid-coatings for inorganic nanoparticles as promising strategy for biomedical applications. Front Chem 7:343
45. Li X, Iocozzia J, Chen Y, Zhao S, Cui X, Wang W, Yu H, Lin S, Lin Z (2018) From precision synthesis of block copolymers to properties and applications of nanoparticles. Angew Chem Int Ed 57:2046–2070
46. Huang X, Hu J, Li Y, Xin F, Qiao R, Davis TP (2019) Engineering organic/inorganic nanohybrids through RAFT polymerization for biomedical applications. Biomacromolecules 20:4243–4257
47. Xu FJ (2018) Versatile types of hydroxyl-rich polycationic systems via O-heterocyclic ring-opening reactions: from strategic design to nucleic acid delivery applications. Prog Polym Sci 78:56–91
48. Zhao N, Yan L, Zhao X, Chen X, Li A, Zheng D, Zhou X, Dai X, Xu FJVersatile types of organic/inorganic nanohybrids: from strategic design to biomedical applications. Chem Rev 119:1666–1762

49. Barakat N, Abadir M, Sheikh F, Kanjwal M, Park S, Kim H (2010) Polymeric nanofibres containing solid nanoparticles prepared by electrospinning and their applications. Chem Eng J 156:487–495
50. Cao M, Zhao W, Wang L, Li R, Gong H, Zhang Y, Xu H, Lu J (2018) Graphene oxide-assisted accumulation and layer-by-layer assembly of antibacterial peptide for sustained release applications. ACS Appl Mater Interfaces 10:24937–24946
51. Luo Y, Wang S, Shen M, Qi R, Fang Y, Guo R, Cai H, Cao X, Tomas H, Zhu M, Shi X (2013) Carbon nanotube-incorporated multilayered cellulose acetate nanofibres for tissue engineering applications. Carbohyd Polym 91:419–427
52. Wang S, Wang C, Zhang B, Sun Z, Li Z, Jiang X, Bai X (2010) Preparation of Fe_3O_4/PVA nanofibres via combining in situ composite with electrospinning. Mater Lett 64:9–11
53. Avsar G, Agirbasli D, Agirbasli MA, Gunduz O, Oner ET (2018) Levan based fibrous scaffolds electrospun via co-axial and single-needle techniques for tissue engineering applications. Carbohyd Polym 193:316–325
54. Song T, Zhang YZ, Zhou TJ (2006) Fabrication of magnetic composite nanofibres of poly(epsilon-caprolactone) with FePt nanoparticles by coaxial electrospinning. J Magn Magn Mater 303:E286–E289
55. Huang W, Xiao Y, Shi X (2019) Construction of electrospun organic/inorganic hybrid nanofibres for drug delivery and tissue engineering applications. Adv Fiber Mater 1:32-45
56. Campbell K, Craig DQM, McNally T (2008) Poly(ethylene glycol) layered silicate nanocomposites for retarded drug release prepared by hot-melt extrusion. Int J Pharm 363:126–131
57. Zhang Y, Tang A, Yang H, Ouyang J (2015) Applications and interfaces of halloysite nanocomposites. Appl Clay Sci 119:8–17
58. Carvalho SM, Leonel AG, Mansur AAP, Carvalho IC, Krambrock K, Mansur HS (2019) Bifunctional magnetopolymersomes of iron oxide nanoparticles and carboxymethylcellulose conjugated with doxorubicin for hyperthermo-chemotherapy of brain cancer cells. Biomater Sci 7:2102–2122
59. Chowdhuri AR, Singh T, Ghosh SK, Sahu SK (2016) Carbon dots embedded magnetic nanoparticles @ chitosan @ metal organic framework as a nanoprobes for pH sensitive targeted anticancer drug delivery. ACS Appl Mater Interfaces 8:16573–16583
60. Vannozzi L, Gouveia P, Pingue P, Canale C, Ricotti L (2020) Novel ultrathin films based on a blend of PEG-b-PCL and PLLA and doped with ZnO nanoparticles. ACS Appl Mater Interfaces 12:21398–21410
61. Ng JY, Obuobi S, Chua ML, Zhang C, Hong S, Kumar Y, Gokhale R, Ee PL (2020) Biomimicry of microbial polysaccharide hydrogels for tissue engineering and regenerative medicine—a review. Carbohyd Polym 241
62. Shrestha BK, Shrestha S, Tiwari AP, Kim JI, Ko SW, Kim HJ, Park CH, Kim CS (2017) Bio-inspired hybrid scaffold of zinc oxide-functionalized multi-wall carbon nanotubes reinforced polyurethane nanofibres for bone tissue engineering. Mater Des 133:69–81
63. Ulker Z, Erkey C (2014) An emerging platform for drug delivery: aerogel based systems. J Control Release 177:51–63
64. Govindarajan D, Duraipandy N, Srivatsan KV, Lakra R, Korapatti PS, Jayavel R, Kiran MS (2017) Fabrication of hybrid collagen aerogels reinforced with wheat grass bioactives as instructive scaffolds for collagen turnover and angiogenesis for wound healing applications. ACS Appl Mater Interfaces 9:16939–16950
65. Reyes-Peces MV, Pérez-Moreno A, de-Los-Santos DM, Mesa-Díaz MD, Pinaglia-Tobaruela G, Vilches-Pérez JI, Fernández-Montesinos R, Salido M, de la Rosa-Fox N, Piñero M (2020) Chitosan-GPTMS-silica hybrid mesoporous aerogels for bone tissue engineering. Polymers 12
66. Peppas NA, Hilt JZ, Khademhosseini A, Langer R (2006) Hydrogels in biology and medicine: from molecular principles to bionanotechnology. Adv Mater 18:1345–1360
67. Mobini S, Solati-Hashjin M, Peirovi H, Osman NA, Gholipourmalekabadi M, Barati M, Samadikuchaksaraei A (2013) Bioactivity and biocompatibility studies on silk-based scaffold for bone tissue engineering. J Med Biol Eng 33:207–213

68. Vepari C, Kaplan DL (2009) Silk as a biomaterial. Prog Polym Sci 32:991–1007
69. Hadisi Z, Nourmohammadi J, Mohammadi J (2015) Composite of porous starch-silk fibroin nanofiber-calcium phosphate for bone regeneration. Ceram Int 41:10745–10754
70. Gaihre B, Jayasuriya AC (2016) Fabrication and characterization of carboxymethyl cellulose novel microparticles for bone tissue engineering. Mater Sci Eng C Mater Biol Appl 69:733–743
71. Vergaro V, Abdullayev E, Lvov YM, Zeitoun A, Cingolani R, Rinaldi R, Leporatti S (2010) Cytocompatibility and uptake of halloysite clay nanotubes. Biomacromolecules 11:820–826
72. Dzamukova MR, Naumenko EA, Rozhina EV, Trifonov AA, Fakhrullin RF (2015) Cell surface engineering with polyelectrolyte-stabilised magnetic nanoparticles: a facile approach for fabrication of artificial multicellular tissue-mimicking clusters. Nano Res 8:2515–2532
73. Wei W, Minullina R, Abdullayev E, Fakhrullin R, Mills D, Lvov Y (2014) Enhanced efficiency of antiseptics with sustained release from clay nanotubes. RSC Adv 4:488–494
74. Shamsi MH, Geckeler KE (2008) The first biopolymer-wrapped noncarbon nanotubes. Nanotechnology 19:075604
75. Olugebefola SC, Hamilton AR, Fairfield DJ, Sottos NR, White SR (2013) Structural reinforcement of microvascular networks using electrostatic layer-by-layer assembly with halloysite nanotubes. Soft Matter 10:544–548
76. Liu M, Wu C, Jiao Y, Xiong S, Zhou C (2013) Chitosan–halloysite nanotubes nanocomposite scaffolds for tissue engineering. J Mater Chem B 1:2078–2089
77. He H, Yuan D, Wu Y, Cao Y (2019) Pharmacokinetics and pharmacodynamics modeling and simulation systems to support the development and regulation of liposomal drugs. Pharmaceutics 11:1–22
78. Rizvi SAA, Saleh AM (2018) Applications of nanoparticle systems in drug delivery technology. Saudi Pharm J 26:64–70
79. Rothermich NO, Thomas MH, Phillips VK, Bergen W (1981) Clinical trial of penicillamine in rheumatoid arthritis. Arthritis Rheum 24:1473–1478
80. Mao Y et al (2021) Insight of nanomedicine strategies for a targeted delivery of nanotherapeutic cues to cope with the resistant types of cancer stem cells. J Drug Deliv Sci Technol 64:102681
81. Chandra Mohanta S, Saha A, Sujatha Devi P (2018) PEGylated Iron oxide nanoparticles for pH responsive drug delivery application. Mater Today: Proc 5:9715–9725
82. Vangijzegem T, Stanicki D, Laurent S (2019) Magnetic iron oxide nanoparticles for drug delivery: applications and characteristics. Expert Opin Drug Deliv 16:69–78
83. Vallet-Regí M, Colilla M, Izquierdo-Barba I, Manzano M (2018) Mesoporous silica nanoparticles for drug delivery: current insights. Molecules 23:1–19
84. Zhou Y, Quan G, Wu Q, Zhang X, Niu B (2018) Mesoporous silica nanoparticles for drug and gene delivery. Acta Pharmaceutica Sinica B 8:165–177
85. Kaassis AYA, Wei M, Williams GR (2016) New biocompatible hydroxy double salts and their drug delivery properties. J Mater Chem B 4:5789–5793
86. Alavi M, Karimi N, Safaei M (2017) Application of various types of liposomes in drug delivery systems. Adv Pharm Bull 7:3–9
87. Meng L, Zhang X, Lu Q, Fei Z, Dyson PJ (2012) Single walled carbon nanotubes as drug delivery vehicles: targeting doxorubicin to tumors. Biomaterials 33:1689–1698
88. Huang D, Wu D (2018) Biodegradable dendrimers for drug delivery. Mater Sci Eng C 90:713–727
89. Corma A, Díaz U, Arrica M, Fernández E, Ortega Í (2009) Organic-inorganic nanospheres with responsive molecular gates for drug storage and release. Ang Chem-Int Ed 48:6247–6250
90. Wilpiszewska K, Antosik AK, Spychaj T (2015) Novel hydrophilic carboxymethyl starch/montmorillonite nanocomposite films. Carbohyd Polym 128:82–89
91. Kong Y, Ge H, Xiong J, Zuo S, Wei Y, Yao C, Deng L (2014) Applied clay science palygorskite polypyrrole nanocomposite: a new platform for electrically tunable drug delivery. Appl Clay Sci 99:119–124

92. Zhang Y, Long M, Huang P, Yang H, Chang S, Hu Y (2016) Intercalated 2D nanoclay for emerging drug delivery in cancer therapy. Nano Res 3:1–11
93. Rajkumar S, Kevadiya BD, Bajaj HC (2015) Spheres as reservoirs of antidepressant drugs. Asian J Pharm Sci 10:452–458
94. Panahi Y, Gharekhani A, Hamishehkar H, Zakeri-milani P, Gharekhani H (2019) Stomach-specific drug delivery of clarithromycin using a semi interpenetrating polymeric network hydrogel made of montmorillonite and chitosan: synthesis, characterization and in vitro drug release study. Adv Pharm Bull 9:159–173
95. Joshi GV, Kevadiya BD, Mody HM, Bajaj HC (2012) Confinement and controlled release of quinine on chitosan-montmorillonite bionanocomposites. J Polym Sci Part A: Polym Chem 50:423–430
96. Jain S, Datta M (2015) Oral extended release of dexamethasone: montmorillonite-PLGA nanocomposites as a delivery vehicle. Appl Clay Sci 104:182–188
97. Mahkam M, Rafi AA, Gheshlaghi LM (2014) Preparation of novel pH-sensitive nanocomposites based on ionic-liquid modified montmorillonite for colon specific drug delivery system. Polym Compos 37:182–187
98. Zheng JP, Luan L, Wang HY, Xi LF, Yao KD (2007) Study on ibuprofen/montmorillonite intercalation composites as drug release system. Appl Clay Sci 36:297–301
99. Bello ML, Junior AM, Vieira BA, Dias LRS, De VP (2015) Sodium Montmorillonite/Amine-containing drugs complexes: new insights on intercalated drugs arrangement into layered carrier material. PLoS ONE 10:1–20
100. Wang Q, Zhang J, Zheng Y, Wang A (2014) Adsorption and release of ofloxacin from acid- and heat-treated halloysite. Colloids Surf B: Biointerfaces 113:51–58
101. García-guzmán P, Medina-torres L, Calderas F, Bernad-bernad MJ, Gracia-mora J (2019) Rheological mucoadhesion and cytotoxicity of montmorillonite clay mineral / hybrid microparticles biocomposite. Appl Clay Sci 180:105–202
102. Jesus CRN, Molina EF, Pulcinelli SH, Santilli CV (2018) Highly controlled diffusion drug release from ureasil-poly(ethylene oxide)-Na^+-montmorillonite hybrid hydrogel nanocomposites. ACS Appl Mater Interfaces 10:19059–19068
103. Ilhan-AyisigE, Yesil-Celiktas O (2018) Silica-based organic-inorganic hybrid nanoparticles and nanoconjugates for improved anticancer drug delivery. Eng Life Sci 18:882–892
104. Luo W, Xu X, Zhou B, He P, Li Y, Liu C (2019) Formation of enzymatic/redox-switching nanogates on mesoporous silica nanoparticles for anticancer drug delivery. Mater Sci Eng C 100:855–861
105. Thi TTH, Tran DHN, Bach LG, Quang HV, Nguyen DC, Park KD, Nguyen DH (2019) Functional magnetic core-shell system-based iron oxide nanoparticle coated with biocompatible copolymer for anticancer drug delivery. Pharmaceutics 11:1–13
106. Le TTH, Bui TQ, Ha TMT, Le MH, Pham HN, Ha PT (2018) Optimizing the alginate coating layer of doxorubicin-loaded iron oxide nanoparticles for cancer hyperthermia and chemotherapy. J Mater Sci 53:13826–13842
107. Sawant VJ, Bamane SR (2017) PEG-beta-cyclodextrin functionalized zinc oxide nanoparticles show cell imaging with high drug payload and sustained pH responsive delivery of curcumin in to MCF-7 cells journal of drug delivery science and technology PEG-beta-cyclodextrin functionalized. J Drug Deliv Sci Technol 43:397–408
108. Manatunga DC, de Silva RM, de Silva KMN, Wijeratne DT, Malavige GN, Williams G (2018) Fabrication of 6-gingerol, doxorubicin and alginate hydroxyapatite into a bio-compatible formulation: enhanced anti-proliferative effect on breast and liver cancer cells. Chem Cent J 12:1–13
109. Padmanabhan VP, Kulandaivelu R, Nellaiappan SNTS (2018) New core-shell hydroxyapatite/Gum-Acacia nanocomposites for drug delivery and tissue engineering applications. Mater Sci Eng C 92:685–693
110. Kurczewska J, Cegłowski M, Messyasz B, Schroeder G (2018) Dendrimer-functionalized halloysite nanotubes for effective drug delivery. Appl Clay Sci 153:134–143

111. Maryo LS, Haghnazari N, Keshavarzi F, Zhaleh H, Seidi F (2018) Synthesis of poly (amidoamine) (PAMAM) dendrimer-based chitosan for targeted drug delivery and cell therapy. J Basic Res Med Sci 5:6–13
112. Kesharwani P, Choudhury H, Meher JG, Pandey M, Gorain B (2019) Dendrimer-entrapped gold nanoparticles as promising nanocarriers for anticancer therapeutics and imaging. Prog Mater Sci 103:484–508
113. Yesil-Celiktas O, Pala C, Cetin-Uyanikgil EO, Sevimli-Gur C (2017) Synthesis of silica-PAMAM dendrimer nanoparticles as promising carriers in neuro blastoma cells. Anal Biochem 519:1–7
114. Hanafy NAN, El-Kemary M, Leporatti S (2018) Micelles structure development as a strategy to improve smart cancer therapy. Cancer 10:1–14
115. Sun Y, Wang Q, Chen J, Liu L, Ding L, Shen M, Li J, Han B, Duan Y (2017) Temperature-sensitive gold nanoparticle-coated pluronic-PLL nanoparticles for drug delivery and chemo-photothermal therapy. Theranostics 7:4424–4444
116. Bakewell SJ, Carie A, Costich TL, Sethuraman J, Semple JE, Sullivan B, Martinez GV, Dominguez-Viqueira W, Sill KN (2017) Imaging the delivery of drug-loaded, iron-stabilized micelles. Nanomedicine: Nanotechnol Biol Med 13:1353–1362
117. Su Y, Zhao L, Meng F, Wang Q, Yao Y, Luo J (2017) Silver nanoparticles decorated lipase-sensitive polyurethane micelles for on-demand release of silver nanoparticles. Colloids Surf B: Biointerfaces 152:238–244

Chapter 8
Organic–Inorganic Nanohybrid-Based Electrochemical Biosensors

Aneeqa Batool, Tauqir A. Sherazi, and Syed Ali Raza Naqvi

1 Sensors and Biosensors

Sensor is a device or a system that is used to detect the environmental changes in the form of signals transferred to the electronic devices such as computer processor [1]. Sensors generally consist of a sensing element and signal transducer, which produces signals usually electrical, thermal, optical, or magnetic in nature depending on the type of sensor. The sensing procedure involves the detection of analyte by sensing element, and the transducer changes this chemical event into suitable signal that with or without amplification used to determine the quality and quantity of analyte in the provided sample.

The sensors classified into number of ways depend on the mode of detection, display and conversion process. The sensors are also classified into active sensors and passive sensors. Active sensors require an external excitation signal, and output signal is displayed in continuous manner. Passive sensors are those which do not need an external excitation signals, and output signal is displayed in the form of discrete or digital data [2]. The other classification based on mode of detection of sensors, which involves chemical, electric, biological and radioactive. The conversion process of input to output is another way to classify sensors, i.e., photoelectric, thermoelectric, electrochemical, thermo-optic and electromagnetic. [3]. One of the simplest examples of sensor is light-dependent resistor (LDR) that performs on the bases of change in intensity of light with change in resistance by using their inverse relation. This LDR when connected to a voltage divider to check voltage drop across the LDR is used as light sensor [4].

A. Batool · T. A. Sherazi (✉)
Department of Chemistry, COMSATS University Islamabad, Abbottabad Campus 22060, Pakistan
e-mail: sherazi@cuiatd.edu.pk

S. A. R. Naqvi
Department of Chemistry, Government College University, Faisalabad 38000, Pakistan

K. Rizwan et al. (eds.), *Hybrid Nanomaterials*, Materials Horizons: From Nature to Nanomaterials, https://doi.org/10.1007/978-981-19-4538-0_8

The different types of sensors involve temperature sensors, color sensors, pressure sensors, light sensors, humidity sensors, IR sensor touch sensors, gas sensors, ultrasonic sensors, position sensors, weight and strain sensors. Different types of receptors such as physical, chemical and biochemical nature of receptors are available. Information is produced and generated at receptors, and transducer translates this information into useful analytical signals. Sensors have great importance due to their broad range of applications in automobiles, agriculture, medicine, water treatment and many other fields. The importance of sensors could be evaluated through their applications in different industrial process, which includes but not limited to monitoring, process control and in safety measures. The sensors also used in medical studies which involve diagnosis of diseases, monitoring of process and critical care.

The biosensors are analytical devices which comprise biological sensing element connected or integrated with transducer that convert biological response to analytical signals. The term biosensors were first introduced by Cabman, while Leyland C. Clark gives the basic concept of biosensors known as father of biosensors in 1960s. According to definition of biosensors given by IUPAC, "Biosensor are analytical device that ascribe results in form of electrical signals, which are independent of physical parameters like temperature and pH". The biological sensing element can be an enzyme, nucleic acid, plant or animal tissue, antibodies, organic or a whole organism. Biosensors are combination of physical and chemical sensing techniques that categorize these devices as advanced sensing appliances.

The biosensors are basically centered on receptor–transducer tool, which comprises three main sections as shown in the block diagram (Fig. 1). The first section is sensitive biological part, the second section is transducer that converts the coming signals from analyte, and third section is amplifier followed by processer and a display unit.

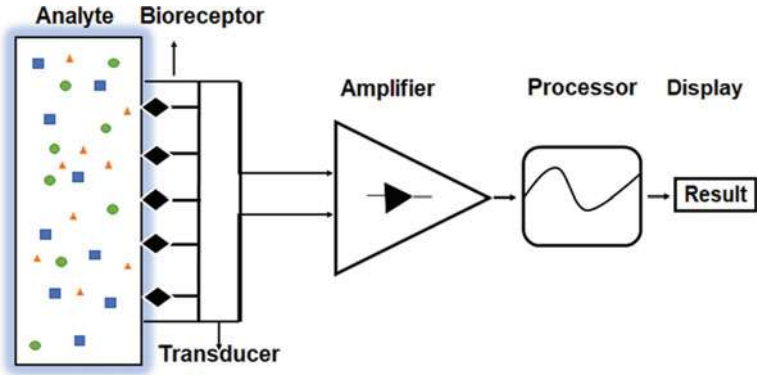

Fig. 1 Working principal of a biosensor

2 Classification of Biosensors

Biosensors are classified based on various factors such as sensing element, bioreceptor and mode of transducers. In general, biosensing elements are naturally evolved receptors that are immobilized on the surface of transducer through specific fabrication method. In the biosensors that involve transducer, the detection mode is physicochemical change that originates from the interaction of analyte with the sensing plateform. The biosensors including cell biosensors, immuno-biosensors, DNA biosensor, enzymes biosensors and biological tissues are classified on the basis of specific bioreceptor. Electrochemical biosensors, piezoelectric biosensors and optical biosensors are categorized on the basis of transducers mode. The classification of biosensors on the bases of biomolecule and transducer mode is summarized in Fig. 2.

2.1 Classification Based on Bioreceptor

2.1.1 Immuno-biosensors

Immunosensors are based on affinity of a specific antibody toward antigens. Antibodies are secreted by the immune system of an organism in response to the

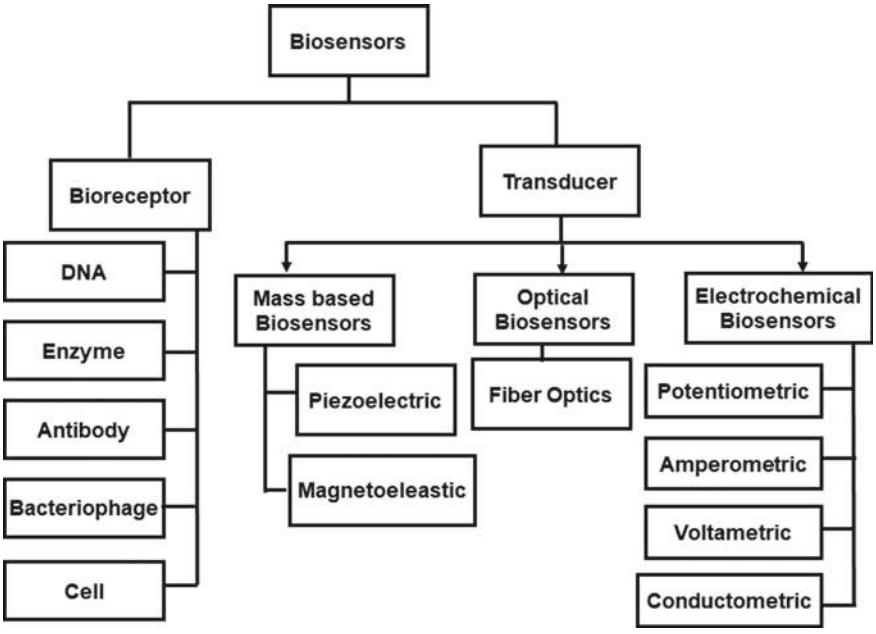

Fig. 2 Classification of biosensors on the bases on biosensing molecule and transducer mode

approach of alien biological compounds (antigens). The antigen present in the test sample binds with specific antibody through interimmunochemical interaction on the surface of transducer. Immunosensors are mainly used to detect participants of immunochemical reactions and monitoring a biological process [5].

2.1.2 Enzyme-Based Biosensors

Enzyme-based biosensors comprising enzyme as biorecognition element, which catalyzed a specific biological reaction and remains unchanged by the end of reaction. The specific enzyme catalyzes a particular biochemical reaction, and the progress is detected in the form of signals by the transducer. The most commonly used enzymes for sensing applications involve are hydrolase and oxidoreductase. The polymer microfluidic chip-based enzyme biosensor is an example of biosensor used for food safety measures [6].

2.1.3 DNA Biosensors

DNA biosensors consist of single-stranded DNA probe as sensing element that identify the complementary target DNA strands present in the sample and transducer generates results when the hybridization of DNA strand occurs with the help of hydrogen bonds. The important applications of DNA biosensors include the detection of DNA sequence in therapeutic monitoring and clinical samples.

2.1.4 Cell Biosensors

The cell biosensors embrace complete living cell itself as the biorecognition element. The sensing depends on the conditions of living cell to detect the intracellular and extracellular microenvironment, different physiological parameter, and produces reaction according to these conditions [7]. The whole cell biosensors are used to detect the presence or absence of certain chemicals under investigation, their concentration and toxicity.

2.1.5 Bacteriophage Biosensors

Bacteriophages also known as phages are viruses found in different environments such as soil, food and water. The propagation of bacteriophages takes place by following two different life cycles named as lytic and lysogenic. Lytic life cycle is based on binding of phages with host bacteria where these phages insert their DNA to the host. The host cell provides essential enzymes to multiply the phage DNA and produce progeny phage. These phages usually destroy the host bacteria in external environment and replicate themselves. After replication, proteins are form

using processes carried out by bacteria. Lysogenic cycle involves only DNA replication of virus when they inserted their DNA to host bacterial cell and not use their essential enzymes to produce proteins. As a result, the host bacterial cell is only used for replication of DNA and not to translate it into proteins [8]. In this sense, the bacteriophage is used as bioprobe in biosensors as they are specific and selective for host bacterial cell [9].

2.2 Classification Based on Transducer

2.2.1 Piezoelectric Biosensors

Piezoelectric biosensors consist of piezoelectric material as signal transducer, and the biosensing element is integrated with the piezoelectric material. The principle involved in this type of biosensors is characteristic reverberation recurrence. The piezoelectric material has positive and negative charge vibrations with characteristic frequencies. Interactions of biomolecules with the analytes present in the sample alters the resonance frequency that is detected. The recurrence vibrations can be controlled by an outer electrical system provided with specific current or potential. At the moment, any molecule present in the sample interacts with detecting element which causes recurrence move, which generates change in current provided by outer electric system, and this change is measured as source of detection. The efficiency of piezoelectric biosensors depends on the characteristic properties of piezoelectric materials. Mostly, quartz lithium niobate and lithium tentalate are used due to their good mechanical strength.

2.2.2 Magnetoelastic Biosensors

Magnetoelastic effect works as sensing principal in magnetoelastic biosensors, i.e., change in magnetic properties of material with the applied mechanical stress. The change in different environmental parameters involve temperature, humidity, pressure and viscosity could be determined by using magnetoelastic effect in sensors applications [10]. These biosensors are made up of magnetoelastic resonator, which is coated with filament of biomolecule. The magnetoelastic resonator is composed of a material that exhibits property of contraction and elongation along the direction of applied magnetic field, e.g., ferromagnetic wires or ribbons mostly iron-rich alloys immobilized with biosensing element. Any external stress that could variate the magnetic field can be assessed by magnetoelastic resonator through demonstrating corresponding changes in oscillating shape [11].

2.2.3 Thermal Biosensors

Thermal biosensors are analytical devises used to determine the change in temperature. These biosensors sense heat changes in the reaction medium, i.e., adsorption or evaluation of heat from biological reaction. Thermal biosensors were first developed in 1960s, and since then these are replacing calorimeter due to their sensitivity and overall performance. Thermal biosensors are used to determine the enzyme activity, various analytes in the test samples, metal ions and process monitoring.

2.2.4 Optical Biosensors

An optical biosensor is an analytical device comprising a biorecognition sensing element integrated with an optical transducer system. The optical biosensor is based on the principle of optical diffraction or electrochemiluminescence in which a protein is immobilized onto silicon wafer through covalent bonds, which is then exposed to UV light via a photograph veil that helps to selectively wind up antibodies just over the UV-exposed area [12]. The interaction between analyte and sensing element changes the light characteristic that is measured by transducer in the form of change in intensity, polarization, etc. These biosensors are mainly used to detect many chemical and biological species, industrial control processes, veterinary, and recognition of real-time processes.

2.2.5 Electrochemical Biosensors

Electrochemical transducer works as a sensing element in the electrochemical biosensors that convert biochemical information into useful signal like current or voltage [13]. Electrochemical biosensors are notable due to their fast analysis, low production cost, portability with greatly reduced size, high selectivity and low limit of detection. Any change in the test sample that causes change or generate current or potential could be measured by electrochemical biosensor. If the electrode system is used as transducer, then specifically electrochemical biosensors obtain. In general, electrochemical biosensors consist of three electrode systems, i.e., working electrode, auxiliary electrode and reference electrode. The electrode where concerned reaction take place is designated as working. The carbon, platinum, carbon-based composites, etc. can be used as working electrode. The auxiliary electrode, also known as current carrying electrode, is utilized for voltammetric and impedimetric measurements. Pt or graphite is commonly used to act as auxiliary electrode [14]. Electrochemical sensors hence classified in to three types, namely potentiometric sensors, amperometric sensors and impedance or admittance-based device.

In potentiometric biosensors, potential difference between sample and reference solution can be measured with the help of reference electrode. In amperometric sensors, potential is applied by potentiometer, and it is kept constant while current is being measured as a result of charge transfer reaction between analyte and working

electrode. Conductometric sensors depend on changing electrical conductivity of sensing material by providing sensory information when it comes in contact with the analyte [14].

3 Inorganic Materials Used for Biosensors

The immobilization of biomolecule on the surface of an inorganic material offers enhanced properties to resulted biosensors that include high chemical and thermal stability making them capable to operate under variant operating environment. Inorganic substrate often shows high biocompatibility after certain modification. Moreover, high catalytic activities and powerful load capacity make them suitable for wide use in biosensing applications. Au-electrode has also been used to immobilized biomolecule via different interactions like self-assembled monolayer with different functionalities. The process uses functional interface molecules to prepare self-assembled monolayer having two terminal functional groups. The functional group on one side is used for bonding with inorganic substrate, while the same molecule on the other end is active to immobilize the biomolecule. As an example, thiolation of Au electrode is performed prior to immobilization of biomolecule. Thiol helps to link the Au at one end forming –S–Au covalent bond, while it attaches biomolecule on the other end. In this way, the biomolecules are linked with Au nanoparticles without loss of electrochemical activity of the developed organic–inorganic hybrid system [15]. Although different notable substrates such as C, Pt, Si show biocompatibility and high thermal strength, sometime these experiences limitations due to presence of weak bonding with the modifying agent such as weak Au–S bond. Most metallic elements are biologically toxic and can generate problems if dissolved or leached out of an electrode.

Carbon is the most biocompatible material for biomolecules thus considered as suitable substrate for immobilization of biomolecule for sensing applications. In biosensor applications, the electrically conductive form of carbon utilized, i.e., graphite, carbon films, boron-doped diamond, glassy carbon and carbon paste. There are various methods that could be adopted to immobilize the biomolecules on the surface of carbon-based substrate. Among these methods, the most common is insertion reactions. The biomolecules have different alkene and alkyne groups, which can perform insertion reactions with the help of thermal or ultraviolet activation [16]. However, the immobilization of biomolecule on carbon-based substrate is time-consuming process. The immobilization via glutaraldehyde crosslinking increases both biological activity and kinetics of insertion process. The limitation is complexity of this immobilization process [17].

Silicon, just like carbon, is suitable substrate for biofunctional electrochemical sensors due to its characteristics similar to carbon, such as biocompatibility and electrical conductivity. The common immobilization method for silicon is also insertion reaction, but the major limitation while using Si as substrate for biosensors is spontaneous oxidation of Si to SiO_2 and the conductivity decreases abruptly as SiO_2 is

insulator. The formation of SiO_2 can be prevented by use of HF to form H- terminated Si^{3+} form self-assembled monolayer (SAMs).

Metal oxides can also be effective substrate for biofunctionalized application if their electric conductivity enhanced. The electrical conductivity of metal oxide can be improved by silanization, which involves activation of surface by -OH groups that result in formation of alkoxysilane polymer via Si–O–Si bonds. The polymer layer which forms at the surface bonded with biomolecule through specific functional group. The biofunctionalized surfaces form by this process are stable as compared to Au–S bonding, but the silanization process is not a standard process, and the results often vary with operating conditions like temperature, time, silane reagent, etc. Indium tin oxide is a tin-doped metal oxide having high electrical conductivity as well as optical transparency which is widely used in biosensors and provides better results.

TiO_2 is also considered as the most suitable substrate for biosensing application due to its characteristic properties. TiO_2 nanoparticles are semiconductive, biocompatible, physically and chemically stabile and exhibit photocatalytic activity [18]. The different methods such as silanization or phosphonate chemistry are available for the fabrication of biosensing element using TiO_2 surface. The inorganic substrate although provides the certain properties as a substrate for biomolecules, but there are some limitations while using inorganic material as a substrate for biorecognition element as summarized in Table 1.

Table 1 Inorganic substrates immobilized with biomolecules used in biosensor applications

Material	Interactions	Advantages	Disadvantages	References
Au	Au–S	Simple, biocompatibility	Poor storage stability, use for short duration	[19]
Si	Alkene insertion	Biocompatible	Efficiency loss due to SiO_2 formation	[20, 21]
Pt	Pt–S bond	Biocompatible, good strength		
TiO_2	Phosphonate	High chemical stability, high conductivity and biocompatibility	Low sensitivity due to low conductivity	[22]
MoS_2	Thiol adsorption		Low biocompatibility	[22]
Indium tin oxide	Phosphonate or silanization	High sensitivity, good conductivity	Brittle nature, not useful for flexible substrate	[23]

4 Organic Materials Used for Biosensors

The organic substrate experiences high sensitivity, low ionization potential and ease in fabrication process thus considered as a useful candidates for preparation of biosensors. The organic substrate used for sensor applications is mostly electronically conducting polymers, i.e., polyaniline used in biosensors for estimation of glucose, while urea and triglycerides also showed excellent sensing properties. Polypyrrole is also used as a host matrix for glucose oxidase and used for estimation of glucose in test sample [24]. Other major advantages of conducting polymers are their excellent compatibility with biomolecules in neutral solution as well as conductivity due to conjugated p-electrons. Moreover, it is easy to handle and fabricate the electrode surface using polymer matrix immobilized with biomolecule. The polymer matrixes themselves are very sensitive to the environment, which makes them suitable material for sensing applications [25, 26].

Another conducting polymer (Poly-5,2′: 5′,2″-terthiophene-3-carboxylic acid) immobilized with xanthine oxidase used for determination of xanthine in blood and urine samples [27]. In another study, the same polymer immobilized with cytochrome c_3 used in electrochemical sensors, i.e., determination of superoxide radicals in test samples [28]. The use of polymer offers ease in the immobilization of biomolecule on the surface of polymer.

The different kinds of organic substrate immobilized with biomolecules used for sensing applications are summarized in Table 2.

Graphene is also considered as an ideal organic substrate for biosensors due to its excellent properties, i.e., 2D structure, high electron mobility, flexibility and biocompatibility. The layered structure of graphene is due to delocalized p-bonds that are present above and below the basal plane due to sp^2 hybridization. This electronic delocalization provides electron mobility and high electronic conductivity to graphene. Another property of graphene is ambipolar electric effect, which provides resistivity at zero gate voltage. The 2D nanostructure of graphene enables the maximum area of graphene monolayer for sensing applications. The graphene is recognized as an ideal material for biosensors due to its superior electron mobility, biocompatibility and flexibility. The combination of unique properties exhibited by carbon nanotubes (CNTs) stimulated their use in biosensing applications. CNTs are effective electrode material due to their remarkable mechanical stability, large surface area and electrical conductivity due to presence of sp^2-hybridized adjacent carbon atoms. The single-walled carbon nanotubes act as support to immobilize biomolecules, utilizing different functional groups as source of interaction. The electrochemical biosensor prepared from carbon nanotubes immobilized with organophosphorus hydrolase is used for determination of organophosphate pesticides [34].

Despite several advantages, there are specific limitations associated with organic matrix for biosensing application that include low sensitivity , poisoning of elec-

Table 2 Organic substrate immobilized with biosensing element used in electrochemical biosensors

Organic substrate	Biorecognition element	Analyte	Immobilization of biomolecule	Advantages	References
Graphene modified by chitosan	Glucose oxidase	Glucose	Electron and proton transfer reactions	High conductivity of graphene, good biocompatibility of chitosan	[29]
Carbon nanotube (CNT)-doped polypyrrole	Glucose oxidase	Glucose	Electropolymerization	High selectivity and sensitivity	[30]
Carbon nanotube thin films	Single-strand DNA	Complementary DNA strand	Covalent interaction	Low detection limit	[31]
Nitrilotriacetic acid functionalized with polypyrrole	Glucose oxidase, DNA	Glucose, DNA	Bioactive linked entrapment	High sensitivity, simple immobilization	[32]
Polypyrrole films	Sulfite oxidase	Sulfite	Galvanostatic entrapment	High performance	[33]

Table 3 Different biomolecules and their applications in biosensors

Biosensors	Biomolecule	Analyte	Use	References
Glucose biosensors	Glucose oxidase	Glucose	Diagnosis of diabetes	[35]
Paper-based DNA biosensors	DNA strand	DNA complementary strand	Food quality control	[36]
Cytochrome 9450 (CYPs) biosensors	CYPs	Drugs	Pharmaceutical industry	[37]
Fluorescent biosensors	Protein	Different types of molecules	In vivo and in vitro studies	[38]
Optical-fiber biosensor	*Pseudomonas putida*	Biological oxygen demand	Determination of biochemical oxygen demands in rivers	[39]

trode surface due to presence of other species, high loading and poor selectivity. These drawbacks can be overcome by using inorganic substrates in combination with organic substrates.

5 Biomolecules

The performance of any biosensor mainly based on sensitivity and selectivity of biorecognition element used in developing this biosensor. A wide variety of biomolecules have been used for developing biosensors.

The selection of specific type of biomolecule highly depends on the analyte as sensing procedure involves the affinity of these two components with each other. The different biomolecules used as sensing element in biosensors applications are listed in Table 3.

6 Organic–Inorganic Nanohybrids

The manipulation of biosensors in different area of studies increases due to its efficiency and sensitivity. The efficiency of biosensors can be enhanced by using different organic–inorganic hybrids materials for sensing applications. Organic–inorganic hybrid materials are fascinating on a grand scale due to combination of properties originated from both the organic and inorganic components [40]. The resulting hybrid material shows decisive results in the field of biosensors due to enhanced characteristics. Inorganic compounds have certain properties like high chemical and thermal stability which enable them to operate under different operating environment. The incorporation of inorganic materials on the surface of electrode is also

effective. Similarly, different organic materials have some particular characteristics, which are not present in inorganic compounds like high sensitivity and high versatility that enhance selectivity toward analytes [41]. The organic substrates, mostly polymers, exhibit excellent electrochemical properties in addition to their easy deposition on the electrode surface in the form of thin film and can also be readily available for modification with biomolecules. On the other hand, inorganic substrate provides mechanical stability to the sensing platform while using in combination with the polymer. The hybrid materials help to prevent from numerous limitations like high operating temperature, low selectivity, low mechanical strength and stability. The properties could be further enhanced if these organic–inorganic hybrids can be synthesized at nanoscale, which provides unique physical and chemical properties. At nanoscale, the material possesses unique properties due to their large surface-to-volume ratio, which cannot be accomplished by bulk material. The nanomaterials are used to improve sensitivity toward detection of analyte, enlarge the detection range and decrease detection limit. The usage of nanomaterials in biosensor technology causes an increase in detection capability with enhanced specificity and could detect extremely low concentration of analyte. Moreover, nanomaterials exhibit characteristics such as large surface area, high loading capacity and the mass transport of reactants that improve the signal amplification. The Table 4 summarizes few organic–inorganic nanohybrids used in biosensor applications for the detection of specific analytes. The organic–inorganic nanomaterial can be synthesized by several methods, and among these few common methods are described here.

Table 4 Organic–inorganic nanohybrids used in biosensor applications

Organic–inorganic nanohybrids	Organic compound	Inorganic compound	Biomolecule	Analyte	References
TiO_2/CNTs nanohybrids	Carbon nanotubes	TiO_2	Glucose oxidase	Glucose	[47]
TiO_2/MWCNTs nanohybrids	Multiwalled carbon nanotubes	TiO_2	Tyrosinase	Catechol	[48]
Fe_2O_3/CNTs nanohybrids	Carbon nanotubes	Fe_2O_3 nanoparticles	Tyrosinase	Coliforms	[49]
Titania sol–gel nanocomposite	Acetylacetone	Titania	Tyrosinase	Phenolic compounds	[50]
Polypyrrole–chitosan–titanium dioxide	Polypyrrole	TiO_2	Chitosan	Glucose	[51]
Au-NPS/polypyrrole	Polypyrrole	Au	Glucose oxidase	Glucose	[52]
Graphene–metal oxide nanomaterial	Graphene	Metal oxides (CuO, ZnO, NiO, MgO_2, NiO)	Glucose oxidase	Glucose	[53]
Metal oxide–nafion composite films	Nafion	Metal oxide	Glucose oxidase	Glucose	[54]

6.1 In Situ and Ex Situ Method

The organic–inorganic nanohybrids can be synthesized by in situ and ex situ methods, and through these methods, metal nanoparticles are incorporated into polymer matrix. In ex situ approach, metal nanoparticles first prepared and then impregnated into polymer solution, while in the case of in situ method, organic–inorganic hybrid material is generated in such a way that the metal precursor is reduced to metal nanoparticles inside the polymer matrix during the process of synthesis. The in situ method is advantageous due to preparation of hybrids with uniform distribution of metal nanoparticles. The ex situ method is relatively simple, but the product obtains usually exhibit lower level of homogenous dispersion of metal nanoparticles within polymer matrix. Silver–polypyrrole nanocomposites prepared by in situ method used for detection of glucose with the help of enzyme as a biosensing element [42].

6.2 Fabricating of Organic–Inorganic Electrospun Hybrid Nanofibers

Polymer solution is used to prepare polymer-based continuous fibers using electrospinning technique. The process involves application of high electric field to the polymer solution coming out from the tip of electrospinning needle. As a result, deformation of droplet occurs and ejection of charged liquid from the tip of cone accelerating toward the collector that is also a counter electrode, leading the formation of continuous thin film fibers deposited onto the collector. The electrospinning equipment consists of three main components: (a) high-voltage power supply, (b) spinneret and (c) collector. Organic–inorganic nanofibers are prepared with the help of electrospinning method which involved either in situ or ex situ methods [43]. Cellulose acetate fiber is embedded with silver nanoparticles prepared by electrospinning process fiber [44].

6.3 Solid-Phase-Incorporated Reagents

Solid-phase-incorporated reagent involves synthesis of organic–inorganic nanohybrid through immobilization of metal into polymeric matrices through metal reduction. This method mainly used to synthesize the polymer stabilized metal nanoparticles has long lifetime. However, this method is not applicable to all types of polymers or metal nanoparticles. The synthesis of Pt-polymer-stabilized metal nanocluster through solid-phase-incorporated reagent was studied for sensor applications [45].

6.4 Electrochemical Deposition

The electrochemical deposition involves reduction of metal ions in the solution and a subsequent deposition onto conductive polymer substrate. The use of conducting polymer is necessary for effective deposition, and the process is beneficial as different inorganic compounds can be introduced into polymer matrix through electrochemical deposition [25]. An example is preparation of CdS-PPY heterojunction nanowires by electrochemical deposition method in which $CdCl_2$ and elemental sulfur were used as precursors to deposit CdS into the nanopores of the alumina membrane followed by deposition of PPy using its solution in 0.1 M $LiClO_4$ acetonitrile and with applied voltage of 0.85 V [46].

6.5 Seeding Approach

The seeding approach is mainly used to produce organic–inorganic nanohybrids at the nanometric scale. The metal nanoparticles or nanofibers that are initially prepared by a chemical precipitation method are designated as nanoseeds, which help to initiate the polymerization reaction of monomers. Nanoseeds are performed as reactive specie that interacts chemically and efficiently with monomers. Different composite nanofibers were prepared by using seeding approach, e.g., preparation of PPy and PANI nanofibers using different kinds of nanofiber seeds [46].

7 Immobilization Techniques

The immobilization of biomolecule on organic–inorganic substrate with adequate stability, biocompatibility, reproducibility and selectivity is the primary challenge. The biosensing element, depending on their affinity, can be immobilization to the organic or inorganic part of organic–inorganic hybrid substrate. Mostly, the organic substrate used for immobilization of biomolecule is polymers having porous structure. This porous structure provides greater surface area for accommodating biomolecules and supports their entrapment into the porous structure. Another important immobilization method includes sol–gel method that experiences number of benefits, i.e., it can entrap huge amount of biomolecule, thermally stable, low-temperature process and no surface modification required [55].

7.1 Physical Adsorption

The biomolecules can potentially attach on heterogeneous surfaces through van der Waals forces, hydrogen bonding and hydrophobic interactions. This non-covalent adsorption of biomolecule provides random orientation of biomolecules, and attached molecules can plausibly leach from the surface. This type of immobilization method of biomolecule is only suitable for the biosensors that are disposable or used for short-term analysis since the activity of these biosensors reduced due to loss in surface density of biomolecules with time. In one study, T4 bacteriophages and recombinant T4 bacteriophage were physically adsorbed on paper membrane for detection of *Escherichia coli* [56].

7.2 Covalent Bonding

The immobilization of biomolecule in the host matrix could be achieved by using functional groups of enzymes that are not responsible of their catalytic activity. The chemical bonding established between the substrate and functional groups available in amino acids, i.e., carboxylic, thiol, amino and hydroxyl group and solid electrode material [55]. The covalent bonding is much stronger than physical adsorption, and thus, the life, stability and reusability of such biosensors are better.

7.3 Bioactive Linked Entrapment

Bioactive linked entrapment immobilization is mostly used when polymer matrix is used as host for biomolecules. The immobilization of biomolecules through bioactive linked entrapment can be performed through two different approaches. The first approach involves mixing of biomolecule with monomers prior to polymerization reaction such that upon polymerization the biomolecules entrapped in the polymer molecules. The other approach involves covalent attachment of biomolecule with inorganic part of hybrid substrate that is normally difficult and can only be performed at special conditions. An example is trapping of lipase enzyme in organic–inorganic hybrid framework by using bioactive linked entrapment immobilization approach using sol–gel process [57].

7.4 Affinity

In case, if the biomolecule does not have direct affinity to substrate, then an additional molecule as a activated support is used that helps to attach biomolecule to the

substrate. The cellulose-binding domain approach is often used in which cellulose acts as tag molecule having affinity for different types of fusion proteins.

7.5 Crosslinking

Crosslinking between functional monomers and/or between functional monomer and biomolecules affords the formation of mesh structures. The biomolecules such as antigen, antibody and enzyme were embedded in this mesh-structured polymer network. It is important that the activity of biological materials must be retained after chemical crosslinking (Fig. 3).

8 Deposition of Organic–Inorganic Nanohybrids on to the Electrode Surface

An important section of the electrochemical biosensors is the deposition of modified material on the surface of electrode.

In general, drop cast method is used to prepare chemically modified electrodes in which the modifying layer is made up of materials such as nanotubes or nanoparticles

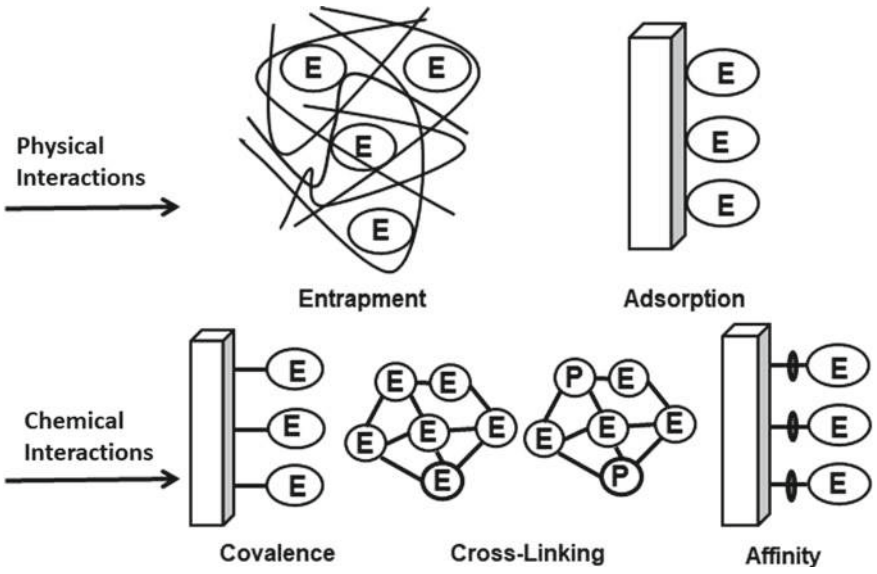

Fig. 3 Schematic representation of different immobilization method using enzyme as an example of biomolecule (E: enzyme, P: inert protein). Adapted with permission from [58]

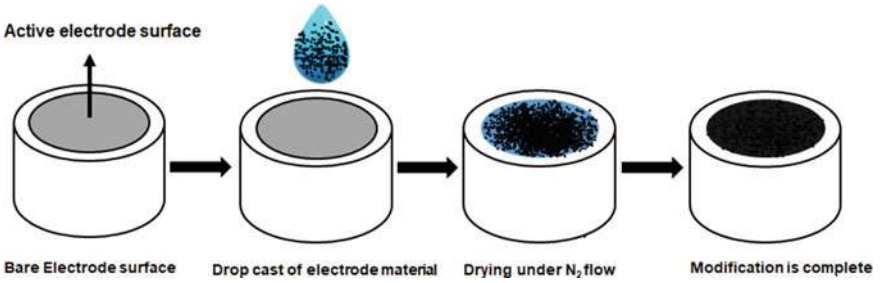

Fig. 4 A facile drop casting approach for deposition of electrode material. Adapted with permission from [59]

and used as electrocatalyst mainly for electrochemical sensing. This method involves transfer of electroactive electrode material by dropping it on the surface of electrode in the dispersion form followed by evaporation of solvent. The advantage of using drop cast method is its simplicity to apply, but limitation involves non-uniform coating and irregular thickness of electrode material on the surface of electrode occur. This method is applicable for on-spot sensing process that need not very high precision. In this process, a dispersion of electrode material use to be prepared in an appropriate solvent followed by ultrasonication for specific time and dialyzed to remove residual species. The obtained dispersion then subjects to centrifugation at specific revolution per minutes (rpm) for certain time. Prior to deposition of active electrode material on the surface of electrode, the electrode surface must be cleaned with alumina powder and water with several times. The cleaned electrode should gently blow under nitrogen stream to remove any moisture. After that, a small amount of suspension in microliters applied over the electrode surface and dried under an infrared lamp. The procedural layout of deposition of electroactive material on the electrode surface through drop cast method is shown in Fig. 4 that is modified version from Ref. [59].

9 Applications of Electrochemical Biosensors

Biosensors are widely used in variety of applications including but not limited to food analysis, monitoring of fermentation process, clinical applications, agriculture, environmental analysis, etc. The biosensors are very sensitive as they possess bioelements, which have high affinity toward target molecules present in given sample. Moreover, the excellent selectivity of bioreceptors makes them a unique class of sensors [22].

9.1 Electrochemical Biosensors for Food Analysis Applications

Biosensors are considered as innovative approach for food quality control procedure as well as attractive tool for food analysis. Biosensors provide accurate information due to rapid and on-site monitoring of test samples, detect the ranges of chemical substances, toxins and food pathogenic bacteria [60]. Electrochemical biosensors are mostly applicable for this analysis due to their well-understood biointeractions and detection mechanism. They are also used to set and verify the nutritional value of food products via confirming the origin and components of food [60]. Electrochemical biosensors based on carbon nanotubes, graphene and metal nanoparticles are used in food analysis. The process involved in electrochemical biosensors is the measure of change takes place during the biochemical reactions on a transducer surface. The change in pH, oxygen consumption, concentration of ions, current or potential difference in food samples can be measured by electrochemical transducer [61, 62].

9.2 Electrochemical Biosensors for Environmental Analysis

Electrochemical biosensors are used in environmental monitoring in effectual manner due to their sensitivity, specificity and ease of operation to detect presence of minute amount of pollutant in given sample.

The process involves interaction of pollutant analyte with the electroactive material of electrode, which originates oxidation or reduction process and display signals. The displayed signals depend on the amount of analyte present in the sample and variation in the amount of oxygen during redox reaction. The electrochemical biosensors also used to test real wastewater samples, determination of chemical species in soil and analysis of gaseous samples to check air pollutants [63, 64]. An example is the DNA biosensors that utilize affinity of complimentary DNA strand with analyte and useful in the determination of low-molecular-weight compounds, i.e., toxins, pollutants and drugs [63].

9.3 Electrochemical Biosensors for Diseases Biomarker Applications

Electrochemical biosensors appeared as an attractive substitute for rapid diagnosis of diseases such as cancer biomarkers, cardiac diseases and Alzheimer's diseases. The detection procedure involves disease-related protein biomarking and DNA mutations present in given sample of diseased person. The biosensing element interacts with DNA copy present in the sample under analysis, which can be computed with the

help of electrochemical transducer. The considerable difference between abnormal test sample and a normal healthy sample could be analyzed with the help of signals.

The presence of abnormal concentration of protein detected through electrochemical biosensors provides prediction about the presence of different types of cancers. The concentration of protein directly related to number of signals appeared in the results each specie separately. The detection of tumor-associated antigens present in human serum through electrochemical antigen biosensor is an example of electrochemical immunosensors for tumors detection.

10 Conclusions and Future Prospective

An affordable healthcare, food quality analysis, precision medicine and environmental monitoring through sensing are a need. The choice of an efficient material comprising desired characteristics is vital to achieve such goals. The number of materials including conducting polymers, metals and carbonaceous materials has characteristic features. The hybrid of organic–inorganic substrate experiencing characteristics of both organic and inorganic substrate is positive gesture toward the advancement of biosensing technology. Organic–inorganic nanohybrid is an efficient host material for immobilization of biomolecule to develop an electrochemical biosensor that could efficiently display results in any form of response such as current, voltage, potential or conductivity. Hybrid materials offer a strategic approach to impart conductivity, stability, mechanical strength and easy fabrication process for immobilization of biomolecules. The organic–inorganic nanohybrid biosensors fulfill the need of time due to combination of organic and inorganic material properties at a single stage. The durability, portability and the performance in term of selectivity and sensitivity of biosensors are still undermined, and to address these challenges are considered as future research trend. The electrode materials such as gold and platinum are mostly utilized to design different biosensors for detection of different types of analytes, but noble metal base sensors are highly expensive. The biosensors could be commonly used in different application condition to availability of high performance and cost-effective materials for their production. The biosensing molecule requires specific environment to remain stable otherwise loss of sensitivity occurs. The biomolecule should be incorporated into host materials, which have high durability as a whole, and resulting electrode material could be applicable for long-term use. The scientist should confer their attention toward developing novel highly efficient and cost-effective materials, improved sensor design and to make it portable for their wade range of application and accessible to community. The parameters such as real sample analysis, sensitivity, accuracy of sensing and reproducibility are useful characteristics for efficient electrochemical biosensors.

References

1. Shakeel A et al (2022) Advanced polymeric/inorganic nanohybrids: an integrated platform for gas sensing applications. Chemosphere 294:133772
2. Gomez J (2021) Analog and digital control of graphene field effect transistor sensors with the Raspberry Pi. University of Washington
3. Javaid M et al (2021) Sensors for daily life: a review. Sens Int 100121
4. Salim GM et al (2015) Optimal light power consumption using LDR sensor. In: 2015 IEEE international symposium on robotics and intelligent sensors (IRIS). IEEE
5. Asal M et al (2018) Recent developments in enzyme, DNA and immuno-based biosensors. Sensors 18(6):1924
6. Gao H et al (2020) Application of microfluidic chip technology in food safety sensing. Sensors 20(6):1792
7. Gheorghiu M (2021) A short review on cell-based biosensing: challenges and breakthroughs in biomedical analysis. J Biomed Res 35(4):255
8. Mandal PK et al (2021) Bacteriophage infection of *Escherichia coli* leads to the formation of membrane vesicles via both explosive cell lysis and membrane blebbing. Microbiology 167(4):001021
9. Aliakbar Ahovan Z et al (2020) Bacteriophage based biosensors: trends, outcomes and challenges. Nanomaterials 10(3):501
10. Grimes CA et al (2002) Wireless magnetoelastic resonance sensors: a critical review. Sensors 2(7):294–313
11. Li S et al (2010) Direct detection of Salmonella typhimurium on fresh produce using phage-based magnetoelastic biosensors. Biosens Bioelectron 26(4):1313–1319
12. Damborský P, Švitel J, Katrlík J (2016) Optical biosensors. Essays Biochem 60(1):91–100
13. Grieshaber D et al (2008) Electrochemical biosensors-sensor principles and architectures. Sensors 8(3):1400–1458
14. Baron R, Saffell J (2017) Amperometric gas sensors as a low cost emerging technology platform for air quality monitoring applications: a review. ACS Sens 2(11):1553–1566
15. Sakata T et al (2007) Stable immobilization of an oligonucleotide probe on a gold substrate using tripodal thiol derivatives. Langmuir 23(5):2269–2272
16. Raymakers J, Haenen K, Maes W (2019) Diamond surface functionalization: from gemstone to photoelectrochemical applications. J Mater Chem C 7(33):10134–10165
17. Migneault I et al (2004) Glutaraldehyde: behavior in aqueous solution, reaction with proteins, and application to enzyme crosslinking. Biotechniques 37(5):790–802
18. Shetti NP et al (2019) Nanostructured titanium oxide hybrids-based electrochemical biosensors for healthcare applications. Colloids Surf B 178:385–394
19. Futera Z, Blumberger J (2018) Adsorption of amino acids on gold: assessing the accuracy of the GolP-CHARMM force field and parametrization of Au–S bonds. J Chem Theory Comput 15(1):613–624
20. Fopase R et al (2020) Strategies, challenges and opportunities of enzyme immobilization on porous silicon for biosensing applications. J Environ Chem Eng 104266
21. Dief EM et al (2020) Covalent linkages of molecules and proteins to Si–H surfaces formed by disulfide reduction. Langmuir 36(49):14999–15009
22. Suni II (2021) Substrate materials for biomolecular immobilization within electrochemical biosensors. Biosensors 11(7):239
23. Aydın EB, Sezgintürk MK (2017) Indium tin oxide (ITO): a promising material in biosensing technology. TrAC Trends Anal Chem 97:309–315
24. Morges W Protein-modified electrodes. The glucose oxidase/polypyrrole system
25. Swamy NK, Sandeep S, Santhosh A (2017) Conductive polymers and their nanohybrid transducers for electrochemical biosensors applications: a brief review. Indian J Adv Chem Sci S2:6–9
26. Rahman M et al (2008) Electrochemical sensors based on organic conjugated polymers. Sensors 8(1):118–141

27. Rahman MA, Won MS, Shim YB (2007) Xanthine sensors based on anodic and cathodic detection of enzymatically generated hydrogen peroxide. Electroanalysis: Int J Devot Fundam Pract Asp Electroanal 19(6):631–637
28. Darain F et al (2007) Superoxide radical sensing using a cytochrome c3 immobilized conducting polymer electrode. Biosens Bioelectron 23(2):161–167
29. Kang X et al (2009) Glucose oxidase–graphene–chitosan modified electrode for direct electrochemistry and glucose sensing. Biosens Bioelectron 25(4):901–905
30. Wang J, Musameh M (2005) Carbon-nanotubes doped polypyrrole glucose biosensor. Anal Chim Acta 539(1–2):209–213
31. He P, Dai L (2004) Aligned carbon nanotube–DNA electrochemical sensors. Chem Commun 3:348–349
32. Baur J et al (2010) Immobilization of biotinylated biomolecules onto electropolymerized poly (pyrrole-nitrilotriacetic acid)–Cu^{2+} film. Electrochem Commun 12(10):1287–1290
33. Ameer Q, Adeloju (SB) Galvanostatic entrapment of sulfite oxidase into ultrathin polypyrrole films for improved amperometric biosensing of sulfite. Electroanalysis: Int J Devot Fundam Pract Asp Electroanal 20(23):2549–2556
34. Deo RP et al (2005) Determination of organophosphate pesticides at a carbon nanotube/organophosphorus hydrolase electrochemical biosensor. Anal Chim Acta 530(2):185–189
35. Karpova EV et al (2019) Noninvasive diabetes monitoring through continuous analysis of sweat using flow-through glucose biosensor. Anal Chem 91(6):3778–3783
36. Bougadi ET, Kalogianni DP (2020) Paper-based DNA biosensor for food authenticity testing. Food Chem 322:126758
37. Schneider E, Clark DS (2013) Cytochrome P450 (CYP) enzymes and the development of CYP biosensors. Biosens Bioelectron 39(1):1–13
38. Wang H, Nakata E, Hamachi I (2009) Recent progress in strategies for the creation of protein-based fluorescent biosensors. ChemBioChem 10(16):2560–2577
39. Chee G-J et al (2000) Optical fiber biosensor for the determination of low biochemical oxygen demand. Biosens Bioelectron 15(7–8):371–376
40. Manatunga DC et al (2020) Recent developments in the use of organic–inorganic nanohybrids for drug delivery. Wiley Interdiscipl Rev: Nanomed Nanobiotechnol 12(3):e1605
41. Wang S et al (2013) Organic/inorganic hybrid sensors: a review. Sens Actuators B Chem 182:467–481
42. Njagi J, Andreescu S (2007) Stable enzyme biosensors based on chemically synthesized Au–polypyrrole nanocomposites. Biosens Bioelectron 23(2):168–175
43. Qiao Z et al (2018) Organic/inorganic nanohybrids formed using electrospun polymer nanofibers as nanoreactors. Coord Chem Rev 372:31–51
44. Son WK et al (2004) Preparation of antimicrobial ultrafine cellulose acetate fibers with silver nanoparticles. Macromol Rapid Commun 25(18):1632–1637
45. Macanás J et al (2006) Preparation and characterization of polymer-stabilized metal nanoparticles for sensor applications. Phys Status Solidi (a) 203(6):1194–1200
46. Park SJ et al (2014) Conducting polymer-based nanohybrid transducers: a potential route to high sensitivity and selectivity sensors. Sensors 14(2):3604–3630
47. Li J et al (2012) Glucose biosensor based on glucose oxidase immobilized on a nanofilm composed of mesoporous hydroxyapatite, titanium dioxide, and modified with multi-walled carbon nanotubes. Microchim Acta 176(1):73–80
48. Fathy SA et al (2018) Tyrosinase biosensor based on multiwall carbon nanotubes-titanium oxide nanocomposite for catechol determination. Desalin Water Treat 130:98–108
49. Cheng Y et al (2009) Amperometric tyrosinase biosensor based on Fe_3O_4 nanoparticles-coated carbon nanotubes nanocomposite for rapid detection of coliforms. Electrochim Acta 54(9):2588–2594
50. Zhang T et al (2003) A sensitive mediator-free tyrosinase biosensor based on an inorganic–organic hybrid titania sol–gel matrix. Anal Chim Acta 489(2):199–206

51. Al-Mokaram A et al (2017) The development of non-enzymatic glucose biosensors based on electrochemically prepared polypyrrole–chitosan–titanium dioxide nanocomposite films. Nanomaterials 7(6):129
52. German N et al (2012) Glucose biosensor based on glucose oxidase and gold nanoparticles of different sizes covered by polypyrrole layer. Colloids Surf A 413:224–230
53. Mohd Yazid SNA et al (2014) A review of glucose biosensors based on graphene/metal oxide nanomaterials. Anal Lett 47(11):1821–1834
54. Choi HN, Kim MA, Lee W-Y (2005) Amperometric glucose biosensor based on sol–gel-derived metal oxide/Nafion composite films. Anal Chim Acta 537(1–2):179–187
55. Bhardwaj T (2014) A review on immobilization techniques of biosensors. Int J Eng Res 3(5)
56. Minikh O et al (2010) Bacteriophage-based biosorbents coupled with bioluminescent ATP assay for rapid concentration and detection of *Escherichia coli*. J Microbiol Methods 82(2):177–183
57. Gupta R, Chaudhury N (2007) Entrapment of biomolecules in sol–gel matrix for applications in biosensors: problems and future prospects. Biosens Bioelectron 22(11):2387–2399
58. Sassolas A, Blum LJ, Leca-Bouvier BD (2012) Immobilization strategies to develop enzymatic biosensors. Biotechnol Adv 30(3):489–511
59. Kumar AKS et al (2020) A mini-review: how reliable is the drop casting technique? Electrochem Commun 121:106867
60. Ivnitski D et al (2000) Application of electrochemical biosensors for detection of food pathogenic bacteria. Electroanalysis: Int J Devot Fundam Pract Asp Electroanal 12(5):317–325
61. Gupta R et al (2021) Advances in nanomaterial-based electrochemical biosensors for the detection of microbial toxins, pathogenic bacteria in food matrices. J Hazard Mater 401:123379
62. Naqvi SAR et al (2021) Nanotechnology: a smart translation of ingredients in the agriculture industry. Aquananotechnology. Elsevier, pp 37–55
63. Marrazza G, Chianella I, Mascini M (1999) Disposable DNA electrochemical biosensors for environmental monitoring. Anal Chim Acta 387(3):297–307
64. Rizwan K et al (2022) MXene-based electrochemical and biosensing platforms to detect toxic elements and pesticides pollutants from environmental matrices. Chemosphere 291:132820

Chapter 9
Organic–Inorganic Nanohybrids Based Sensors for Volatile Organic Compounds

Syed Salman Shafqat, Asma Mukhtar, Syed Rizwan Shafqat, Muhammad Adnan Asghar, Muhammad Rizwan, Dure Najaf Iqbal, and Tahir Rasheed

1 Introduction

In the present era, environmental pollution has become a global issue which has attained attention of researchers to control and monitor the sources of pollution [1–3]. VOCs include aldehydes, aromatic hydrocarbons, polycyclic aromatic hydrocarbon, alcohols, solvents used in paint industry, saturated and unsaturated hydrocarbons, ketones, octanes, chlorinated hydrocarbons, etc. The pollutants in environment appear from many different sources, which include gases evolved from vehicles, wastes and gases discharged from industrial machinery, wastes disposed of by different industries such as refineries, petrochemical industry, fertilizer industry, chemical industry, combustion of coal, leakage of hazardous effluents and from different industrial plants [4]. With no doubt, the industrial revolution has upgraded the quality of life in terms of technology, society, etc., but it has introduced bulk number of contaminants in the environment that are hazardous to human and the ecosystem. All these pollutants exposed to environment by different sources are

S. S. Shafqat (✉) · M. A. Asghar
Department of Chemistry, Division of Science and Technology, University of Education, Lahore, Pakistan
e-mail: salman.shafqat@ue.edu.pk

A. Mukhtar
Department of Chemistry, University of the Punjab, Lahore 5400, Pakistan

S. R. Shafqat
Department of Chemistry, Lahore Garrison University, Lahore 5400, Pakistan

M. Rizwan · D. N. Iqbal
Department of Chemistry, The University of Lahore, Lahore 5400, Pakistan

T. Rasheed (✉)
Interdisciplinary Research Center for Advanced Materials, King Fahd University of Petroleum and Minerals, Dhahran 31261, Saudi Arabia
e-mail: tahir.rasheed@hotmail.com

K. Rizwan et al. (eds.), *Hybrid Nanomaterials*, Materials Horizons: From Nature to Nanomaterials, https://doi.org/10.1007/978-981-19-4538-0_9

affecting the quality of air in outdoor and indoor environment. Not only human activities and industrial revolution create an adverse effect on the environment but natural sources, including forest fires, volcanic eruptions, dust storms, agricultural burning also contribute toward polluting the environment. The environmental pollutants includes variety of harmful solids, liquids, or gases which has reduced the quality of air and caused acute as well as chronic effects on human health from early life [5, 6].

2 Sources of VOCs

Among air pollutants, the one emerging at urgency level for indoor and outdoor pollution is volatile organic compounds (VOCs). VOCs are organic in nature that evaporates frequently due to low boiling point at room temperature which rapidly spreads in the environment and causes the formation of carcinogens. These VOCs cause serious risk to human health such as ENT irritation, aches, unbalancing of body, vomiting and impairment to the kidneys, liver or brain, etc., and cause temporary and permanent hazardous effects on the environment [7–9]. VOCs also causes the generation of ground-level ozone and particles, which leads to smog, and can stimulate diseases in plants, inhibit seed production [10]. Most of the VOCs are available in high concentrations in indoors environment as compared to the outdoors environment. In modern life trends, the living of a human being free of VOCs is unavoidable because these are used as markers in medicinal industry, food processing industry as well as markers of microbial contamination [11–13]. Not only this, VOCs are produced naturally and are present in man-made products such as fragrances, furnishings, cleaners, disinfectants, printers, glues, wood preservatives, aerosol sprays, hobby supplies, dry-cleaned clothing, varnishes, emulsions, solvents, fumigants, preserved fuels and exhausts of vehicles, insecticides, herbicides, pesticide [14–19]. VOCs arising in indoor environment have been shown to be in between 50 and 300 of different types among which aromatic/non-aromatic hydrocarbons, alcohols, aldehydes, ketones, esters, chlorinated and nitrogen-based compounds are common [20–28]. These are inert nonpolar compounds which could pass through membranes causing biotransformation within the body of toxicity level [29].

Since VOCs are present in all the materials used in our daily life and are ten times higher in concentration in our indoor environment as compare to outdoor environment, it is of utmost important to actively monitor VOCs in indoor environments by measuring air quality. The air quality can be monitored at room temperature by different sensing systems, and the higher risk of exposure of VOCs to human has continuously stimulated to upgrade the sensors with advanced detection technologies [30–34].

3 Classification of VOCs

VOCs are hazardous to human health and ecosystem. The VOCs having low boiling point diffuse faster in environment and cause a more serious risk than others. The United States Environmental Protection Agency (EPA) has divided the indoor organic pollutants on the following types based on World Health Organization (WHO) guidelines.

a. **Very Volatile Organic Compounds (VVOCs)**

   These VOCs cover the compounds having boiling point in between 0 and 50–100 °C. Examples include methyl chloride, propane, butane, etc.

b. **Volatile Organic Compounds (VOCs)**

   These VOCs include the compounds having boiling point in between 50 and 260 °C. Examples include toluene, formaldehyde, hexanal, ketone, ethyl alcohol, isopropanol, etc.

c. **Semi-Volatile Organic Compounds (SVOCs)**

   These VOCs include the compounds having boiling point in between 240 and 400 °C. Some common examples include pesticides and fire retardants, etc. [35].

4 Detection of VOCs

Since VOCs are harmful to human health even at very low levels, therefore their monitoring is of utmost important. Several chemical, electrical and chromatographic techniques for detection of VOCs are in practice since last two decades in last years. In earlier stages, the chromatographic technique and mass spectrometry were used as an analytical methodology for identification of VOCs with high accuracy. But due to time consumption, expensive sample preparation procedures, chemical gas sensors designed by chemiresistive material were used as an alternative technique [36]. Carbon allotropes are capable to detect trace-level molecules at room temperature and possess higher surface area. However, these materials have high binding energy with the analyte, lower recovery rate and are less selective [37]. Alternatively, metal oxides (MO_x) have higher recovery rate and are worthy in detecting a large range of analytes at higher conc. The sensing efficiency of metal oxides is observable at higher operating temperature because at this temperature the oxygen adsorbents (required to adsorb VOCs) are generated [38, 39]. In Fig. 1 Different nanostructures of sensing materials are shown.

These materials have ability to drop their efficient properties along with aging and environmental factors which results in declination in response and sensitivity for unwanted gases. Therefore, it is essential to develop a stable and more reliable sensor device which could overcome challenges which include detection of trace-level molecules, outstanding selectivity under humidity, good recovery rate with zero deviation due to temperature and moisture. In this regard, the development of new

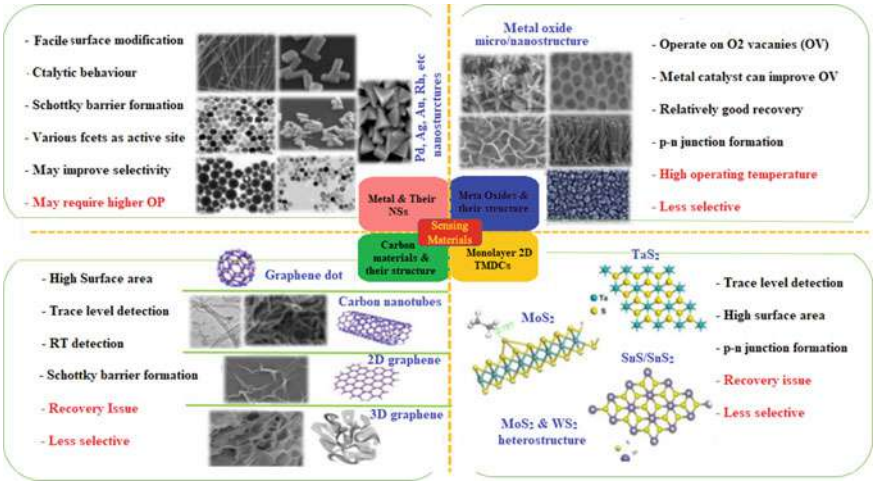

Fig. 1 Nano-micromaterial-based sensors, their merits demerits. This is adopted from an open access article distributed under the Creative Commons Attribution License [40]

sensing technologies having advantages of better sensitivity, fast detection time, low detection limit, easy to operate and suitable for in situ operations is ever needed.

4.1 Electrochemical Sensor

For detection of VOCs, different sensors have been studied. For understanding the detailed working procedure of electrochemical sensor, the electrochemical sensor works on the principle of redox reaction. A sensor is usually made up of a sensing electrode and a transduction electrode which converts the sensed information into an electrical or optical signal [41]. The critical features of a sensor depend on the sensitivity, selectivity, response time, sustainability, limit of detection (LOD) and cost. Based on this fact, the selection of a material during the development of a particular sensor is key point toward sensor performance. Sensitivity is a key feature, which can be defined as the minimum fluctuation of exterior stimulus inducing a noticeable signal variation [42]. Literature survey reveals that a number of materials including carbon nanomaterials, metals as well as metal oxides, etc., hybrid nanoparticles having different sensing properties have been used in chemical sensors.

4.2 Organic–Inorganic Nanohybrid Sensor

A new design for developing VOCs sensing devices was designed by combination of two or more distinguishable materials (usually one being organic and other inorganic) at nanometric scale know as hybrid nanomaterials. These hybrid nanomaterials can be obtained by different combinations of organic polymer with inorganic part. Metal oxides which are inorganic in nature or nanoparticles of metals may combine with organic components which are mostly polymers (conducting in nature) or carbonaceous nanomaterials to attain improved final properties [4, 43–49]. There are different methods used for the designing of the organic–inorganic hybrid nanomaterials; among them, utmost important techniques employed are electrospinning and layer-by-layer (LbL) self-assembly techniques [50–61]. In layer-by-layer (LbL) method, the combination of distinct nanomaterials of opposite charge are layered in the selected substrate, while in electrospinning the distinct nanomaterial present in bulk is converted into nanofibers or these distinct materials get adsorbed in the nanofiber surface in a disperse phase. Both these methodologies are highly favorable because they assemble complex nanoarchitectures which have sky high surface area/volume ratio, appreciative for adsorption of gas molecules over the sensitive layer. For designing a highly promising gas/VOCs sensor, the nature of distinct materials, their ratio in distribution and their synergic interlinkage at the shared junction are basic ingredient [62–64]. When the properties of the distinct materials were studied individually, their hybrid composites resulted in improved performance for sensitivity and selectivity according to the sensor target and the environment. These organic–inorganic nanohybrid-based sensors include conducting polymers, carbon materials and nanoparticles of metal oxides and metals, while their usage depends on their required performance and specific applications. Presently, we will deal with the performance of the organic–inorganic nanohybrid-based sensors for detection of VOCs.

4.3 Sensing of Volatile Organic Compounds

Some recent organic–inorganic nanohybrid-based materials used for sensing of volatile organic compounds will be discussed in the upcoming sections.

4.3.1 Sensor for Alcohols

Reviewing the safety required in chemical and biomedical applications, in-depth research study for sensors of alcohol vapors was performed. It is observed that a chemiresistive sensor designed by nanomaterials is a potent channel with efficient sensing, due to their distinct nanoscale properties and large ratio of surface-to-volume. Based on this fact, nanocomposites of metaloxides were developed within

the carbon allotrope family for sensing ethanol vapors. Among carbon allotrope family, the oxidized single-walled carbon nanohorns (Ox-SWCNH) and metal oxide nanoparticles were dispersed in the polyvinylpyrrolidone PVP matrix with 1:1:1 mass ratios (w/w/w) designing organic–inorganic ternary nanohybrids. These nanohybrids were synthesized by post-condensation method. The sensing films of Ox-SWCNH/SnO_2/PVP nanohybrid was kept at room temperature and was observed that these nanohybrid-based sensors are very sensitive to ethyl alcohol concentrations in the range of less than 1 mg/L in the dry air and showed large sensitivity of ethyl alcohol concentrations ranging from 25 to 50 mg/L. The detection limit for the ternary sensor is 0.3 mg/L, and the response time of sensing layer SWCNH/SnO_2/PVP is about 30–35 s and 90 s which were observed to be its recovery time. [65].

Athawale et al. successfully obtained a hybrid palladium–polyaniline (Pd-PANI) nanocomposite by polymerization (oxidative) to assemble a hybrid-based sensor. This hybrid-based sensor was used to measure the responses of alcohol vapors such as methyl alcohol, ethyl alcohol and isopropyl alcohol. The hybrid nanoparticles were observed to be high in polarity, due to which the manufactured sensor exhibited efficiency for 10 ppm methanol vapors comparative to ethanol and isopropyl alcohol in terms of selectivity and sensitivity [66].

The Pd-PANI nanohybrids responded rapidly and reversibly for methanol vapors due to the fact that methanol vapors induced strong interaction with imine interaction in presence of Pd. This Pd-PANI nanohybrids showed methanol sensing at high sensitivity and selectivity level. The response time for methanol was 8 s which decreased from 8 to 2 s by increasing methanol concentration from 1 to 2000 ppm. Its recovery time was observed to be 9 s. The hybrid Pd–polyaniline nanocomposite reported LOD at 1 ppm. The results obtained revealed that the Pd–Pani nanocomposite appeared to be a proficient sensor [66]. The nanohybrid of Pb(PANI) showed high sensitivity and selectivity for methanol vapors. When Pd was replaced with silver, forming silver/PANI nanohybrid prepared from aniline monomer by means of oxidative polymerization having silver nanoparticles. The nanohybrid showed efficient sensing of ethyl alcohol [67].

A hybrid PANI-silver nanocomposite with thickness of silver ∼15 nm was prepared by mini-emulsion polymerization assisted by ultrasound radiations. This hybrid PANI-silver nanocomposite has been used for detection of ethanol which was recorded by observing changings in conductivity. The efficiency in sensing level and response time of PANI-Ag hybrid sensor was thickness dependent, which could be varied by addition or deletion of the Ag nanoparticles to polyaniline (PANI). This nanocomposite detected ethanol concentration in range of 50–225 ppm and exhibited response time of 2100s. The peak response of PANI-Ag hybrid appeared at 100 ppm [67]. Arshak et al. detected different polar and nonpolar solvents such as propyl alcohol, ethyl alcohol, trichloromethane, hydrocarbons such as methylbenzene and hexane by array-based gas sensors having polyvinyl butyral polymer, MnO_2 and Fe_2O_3 nanocomposite films. The response observed by the sensors was for ethanol and toluene where ethanol exhibited response with 43.27% at 5000 ppm [68]. Polyvinyl butyral polymer combined with nickel oxide and iron oxide with different ratios such as (75% nickel oxide and 25% iron oxide, 50% nickel oxide

and 50% iron oxide, 25% nickel oxide and 75% iron oxide) has been used for identification of ethyl alcohol, dimethyl ketone, toluene and tetrahydrofuran (C_4H_8O) at 25 °C. All the composition was tested along with different VOCs and it was found that the sensors formed by the composition of 75/25% of NiO to Fe_2O_3 combined with PVB nanocomposite exhibited 30 s and 45 s for response and recovery time for CH_3CH_2OH, respectively [68]. For ethanol sensing MoO_3 and PPy hybrid nanocomposites were prepared via vapor polymerization technique. It was observed that individually both PPy and MoO_3 exhibited poor sensing response at 25 °C but improved sensing response was observed when the hybrid of MoO_3–PPy composite was used [68]. Porphyrins have been studied as a sensing material for VOCs detection due to its good response toward sensitivity. Porphyrins combined with metals such as cobalt, nickel forming metalloporphyrins hybridized with metal oxides become functionalized substances which provided absorption sites for VOCs [68].

The Co porphyrin-SnO_2 nanohybrid thin films were prepared by sol–gel technique. The porphyrin is a modified tetraphenylporphyrin which adheres to metal oxide stabilized by a carboxylic group present in it. These hybrid thin films were characterized by SEM. The CoTCPP–SnO_2 sensors were used to detect methanol at temperature of 250 °C (because at this temperature the sensor worked effectively and efficiently), and it was noticed that the sensor exhibited quick and reversible responses toward methanol vapors. After exposure of the sensor with temperature up to 250 °C, the optical characterization of CoTCPP–SnO_2 thin films was performed, and it was observed that the metalloporphyrins are still in it. At higher temperature, the porphyrin in CoTCPP–SnO_2 sensors decomposed thermally and the hybrid CoTCPP–SnO_2 sensors behaved as SnO_2 devices [69]. To detect methanol, Campos et al. used Schottky barrier diodes which were based on electrochemically fabricated PANI/aluminum (Al) nanocomposites. By varying concentration of methanol at room temperature and by varying time intervals, the current–voltage and capacitance of the diodes were observed [68]. An optical sensor has been used for the detection of methanol by Stevens et al. The optical sensor was formed by sol–gel methods by doping a coumarin dye to a surfactant P123 and silica hybrid composite film. The limit of detection for the composite film was 150 ppm for CH_3OH which was detected by observing the changings appearing in fluorescence intensity. The response of methanol vapors was enhanced for the first few sensing cycles only [68]. Surface plasmon resonance (SPR) technique is an optical technique used to study molecular interactions of two different molecules, one being mobile while other one fixed on a thin gold film. Fernandez et al. reported the SPR technique which has been used for detection of ethanol and methanol where gold-polyimide nanohybrid films were manufactured by glow discharge vapor deposition polymerization and were used in optical gas sensors. Usually, individually polyimide film responded poorly for absorption of alcohol vapors, but when polyimide film combines with Au forming, Au-polyimide hybrid nanocomposite showed good response. The spectral range which corresponds to the SPR peak of the gold nanoparticles exhibited effective optical absorption for sensing of methanol and ethanol. The sensing response for CH_3OH appeared at 6000 ppm and for CH_3CH_2OH ethanol appeared

at 6000 ppm [68]. Another method for methanol sensing is the layer-by-layer technique where chitosan carbon nanotube (CH)–CNT nanocomposites have been used by Kumar et al. CH–CNT nanocomposites exhibited good electrical properties as well as chemical properties. The CH–CNT composite is a bionanocomposite which shows tunneling conductance when a gas molecule diffuses in it, resulting in enhanced tunneling conductance by means of chemical and electrical behavior. This chitosan carbon nanotube (CH)–CNT nanocomposite-based transducer showed high sensitivity toward methanol (0–100%) [68]. In pipes and tubes, the flow rate of liquids and gases should be regulated. For this purpose, a flow sensor which is an electronic device has been devised. The (single-walled carbon nanotube) SW.CNT-poly (methyl methacrylate) hybrid nanofibers were designed for a flow sensor by Han et al. These nanohybrids were fabricated in (interdigitated electrodes) IDE by using electrospinning techniques. The SW.CNT-poly(methyl methacrylate) hybrid nanofiber was used for sensing methanol. The detection limit for methanol sensing was observed to be between 600 and 3500 ppm. Nanofiber structures were printed on silver electrodes used in the flow-through sensor design which showed a higher magnitude of sensitivity compared to the nanofiber deposited on a conventional IDE electrode [68]. Figure 2 shows the SEM micrograph of SWCNT-poly(methyl methacrylate) hybrid nanofibers and a comparative study of sensor's responses and sensitivities [68].

In the above discussion, SWCNT was assembled to PMMA forming a hybrid nanocomposite. Here, multi-walled carbon nanotube MWCNT was assembled to PMMA microbeads by using spray-coated layer-by-layer (LBL) techniques. This chemiresistive sensor was used to detect VOCs such as CH_3OH, H_2O, $C_6H_5CH_3$ and $CHCl_3$. This sensing platform was developed by Feller et al. By taking SEM micrograph of MCNT-poly(methyl methacrylate) hybrid, it was found that the hybrid nanocomposite has a crisscross arrangement of multi-walled carbon nanotube linking

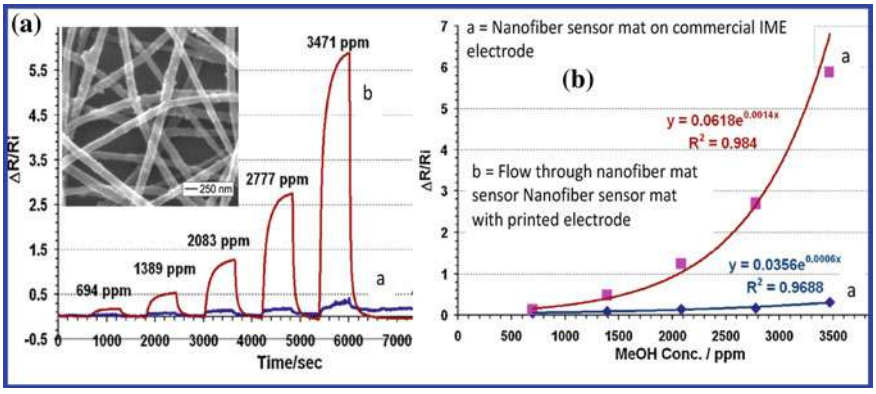

Fig. 2 **a** SEM micrograph of single-walled carbon nanotubes-poly(methyl methacrylate) nanofibers. **a** A comparison of responses of a sensing material for nonflow-through attached to commercial IME electrodes to sensing material of flow-through attached to electrode and **b** comparison of sensitivity of commercial IME as well as printed electrodes. Reprinted with permission from [70]

PMMA. The sensor showed a behavior of adsorption and desorption of analyte when exposed to VOCs and nitrogen, respectively. This behavior observed by the sensor was based on the fact that when VOCs molecules diffuses result in discontinuation of the interlinkages of CNTs. The CNT-CNT junction gap is responsible for electron circulation by tunneling and when gas molecules adsorbs the energy is required for electron circulation [68]. The MWCNT-PMMA hybrid nanocomposite selectively responded to CH_3OH. Other analytes (H_2O, $C_6H_5CH_3$ and $CHCl_3$) concentrations on MWCNT-PMMA response amplitude were also studied. The results obtained showed the efficiency in sensitivity and selectivity that was increased by 2 and 5, respectively, of three-dimensional assemblies of the MWCNT network for methanol with respect to other VOCs [68]. Along with methanol and ethanol, 1-butanol has also been detected. To detect 1-butanol, single-walled carbon nanotubes fabricated with porphyrin (Pr) hybrid served as a sensing material. Lvova et al. used the hybrid nanocomposite in quartz microbalance (QMB) sensors. Two different methods were adopted for fabrication of CNT-Pr hybrid composite.

1. Pyrrole-substituted Py monomers were polymerized by electropolymerization.

   In this polymerization, carboxylic acid (COOH)-functionalized single-walled carbon nanotubes which served as a dopant.
2. Single-walled carbon nanotubes pyrrole-based nanocomposites were synthesized and afterward entrapped in polyporphyrin single-walled carbon nanotubes-COOH films.

Single-walled carbon nanotubes pyrrole-based nanocomposites served as

a. the preconcentrator adsorbing phase and
b. as a coating for QMB design used for detection of sensitivity of 1-butanol.

Their structures are shown in Fig. 3 [68].

For the detection of low concentration levels of 1-butanol using preconcentration procedures, five combination of QMB sensors were fabricated.

i. QMB 1 (polypyrrole/single-walled carbon nanotube –COOH)
ii. QMB 2 (polypyrrole/Ppy-Porph-2/single-walled carbon nanotube –COOH)
iii. QMB 3 (polypyrrole/single-walled carbon nanotube –COOH/single-walled carbon nanotube–tetraphenylporphyrins)
iv. QMB 4 (polypyrrole-Porph-1/ClO_4)
v. QMB 5 (polypyrrole-Porph-2/ClO_4).

Among these, QMB 1, QMB 2, QMB 3 exhibited higher responses of 1-butanol, whereas QMB 4 and QMB 5 exhibited low responses, due to the presence of SWCNTs in QMB 1, QMB 2, QMB 3. The best sensing material among these was QMB3 which exhibited detection range from 46 to 500 ppb of 1-butanol [68]. All the above-mentioned sensors for alcohols have been summarized in Table 1.

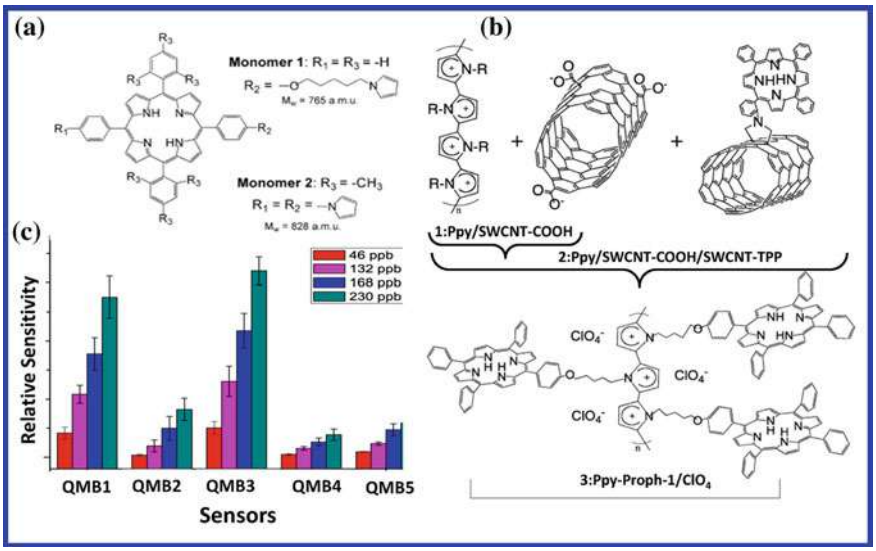

Fig. 3 **a** Structure of tetraphenylporphyrins (TPP) having different monomers 1 and 2 attached. **b** Structure of quartz microbalance (QMB) sensors having polypyrrole backbone attached to H or monomer 2. **c** Comparative study of sensitivities of different QMBs with respect to analyte concentrations [71]

4.3.2 Sensor for Aldehydes

VOCs originating from different sources such as furniture, materials and bonding agents used in buildings, pesticides and different sources are toxic and allergic for humans. Specifically, formaldehyde present in indoor room air even at ppb levels can cause sick building syndrome. To detect aldehydes such as formaldehyde and acetaldehyde at room temperature, Itoh et al. investigated on molybdenum oxide (MoO_3) combined with polymers such as (PNMA) polymer of N-methylaniline, (PoANIS) polymer of o-anisidine and (PANI) polymer of aniline by layered organic–inorganic hybrid films. These hybrids were fabricated by a modified intercalation process. The poly(N-methylaniline) MoO_3 hybrid nanofilm showed enhanced resistivity ($S = 2.8\%$) for aldehyde gases having concentrations of 1–10 ppm. Polyaniline MoO_3 hybrid and poly(o-anisidine) MoO_3 hybrid thin films exhibited efficiency in responses from 25 to 400 ppb at 30 °C for formaldehyde and acetaldehyde. These hybrid layers were characterized by single electron microscopy and X-ray diffraction method [72]. The (PANI)$x$$MoO_3$ hybrid exhibited the sharp response to formaldehyde and a moderate response to acetaldehyde. However, the PoANIS)$x$$MoO_3$ hybrid thin films show equivalent responses toward formaldehyde and acetaldehyde. These responses were observed at several tens ppb level for formaldehyde and acetaldehyde [72]. Among formaldehyde and acetaldehyde, the (PNMA)$x$$MoO_3$ hybrid thin film exhibited sensitivity and selectivity for CH_3CHO. By means of XRD, it was visualized that in the interlayering spaces of (PNMA)$x$$MoO_3$ hybrid composite the

Table 1 Sensors for alcohols with their particular characteristics

Entry	VOCs	Efficacy	Preparation method	Nanohybrids sensor for VOCs	References
01	Methanol	Response time 2–8 s Detection limit of 1 ppm Recovery time 9 s	Oxidative polymerization	Palladium–polyaniline(Pd-PANI)	[58]
02	Methanol	–	Spin-coating technique	CoTCPP–SnO_2	[61]
03	Methanol	–	Electrochemically fabricated	PANI/aluminum (Al)	[60]
04	Methanol	Detection limit of ~150 ppm	Sol–gel method	Mesoporous coumarin 481/dye nonionic surfactant Pluronic P123/silica	[60]
05	Methanol	High sensitivity (0–100%)	–	Chitosan carbon nanotube (CH)-CNT	[60]
06	Methanol	Detection limit 600–3500 ppm	Layer-by-layer (LBL) techniques	SW.CNT-poly(methyl methacrylate) (PMMA)	[60]
07	Methanol	–	Spraycoated layer-by-layer (LBL) techniques	MW.CNT-poly(methyl methacrylate) (PMMA)	[60]
08	Methanol/ethanol	Response at 6000 ppm	Glow discharge vapor deposition polymerization	Au-polyimide	[60]
09	Ethanol	Detection limit 0.3 mg/L Response time 30–35 s Recovery time 90 s	Post-condensation method	Ox-SWCNH/SnO_2/PVP nanohybrid	[57]
10	Ethanol	Detection range 50–225 ppm Response time 2100 s	In situ oxidative polymerization	Silver/PANI	[59]
11	Ethanol	Response 43.27% at 5000 ppm	–	Polyvinyl butyral (PVB), Fe_2O_3/MnO_2	[60]
12	Ethanol	Response time 30 s Recovery time 45 s	–	NiO)/Fe_2O_3 /PVB	[60]
13	Ethanol	–	Vapor polymerization	MoO_3–PPy	[60]

(continued)

Table 1 (continued)

Entry	VOCs	Efficacy	Preparation method	Nanohybrids sensor for VOCs	References
14	1-Butanol	Detection range 46–500 ppb	Electropolymerization	SWCNT-Pr(porphyrin)	[60]

spacing possessed to be of same size as of methyl group, which assisted in adsorption of acetaldehyde molecules. Wang et al. reported a sol–gel method for manufacturing of nanocrystalline antimony-doped tin oxide, of 5 nm thickness, with a copolymer [poly(ethylene-co-butylene)-block-poly-(ethylene oxide] template. For sensing of formaldehyde (10–50 ppm), the sensing materials used antimony-doped tin oxide nanoparticles attached to tubes of alumina with gold (Au) electrodes and platinum (Pt) wires. The hybrid's efficiency was attained at 136 °C which exhibited a sharp response to formaldehyde gas (10%). This sensor showed a sensitivity coefficient of 3.44 and with a limit of detection at 130 ppb [68].

4.3.3 Sensor for Ketones

In the exhaled breath of patients having lung cancer, VOCs such as acetone vapor is present. To detect the acetone in exhaled breath of lung cancer patients, different sensors have been tuned up. Among them, core–shell-structured hybrid materials formed by polymers of [PEDOT] poly(3,4-ethylenedioxythiophene), [PANi] polymer of aniline, [PPy] polymer of pyrrole and magnetic nanoparticles (MNPs) (Fe_3O_4) [73–77]. These hybrid materials were prepared by using polymerized ionic liquid (PILs) which enhanced the formation of poly(3,4-ethylenedioxythiophene) on the magnetic nanoparticle surface. To detect various VOC vapors such as methyl alcohol, ethyl alcohol, dimethyl ketone, benzene and methylbenzene, the hybrid poly(3,4-ethylenedioxythiophene)–PIL-modified Fe_3O_4 was used for sensing of VOCs, and it was analyzed that these hybrid nanoparticles exhibited good response to acetone vapors with high sensitivity up to 1 ppm, i.e., a 38.8% increased sensitivity and reduced noise level. The detection limit estimated as 257 ppb means the sensor exhibited superior sensitivity with a ppb level for detection limit [78]. Acetone can also be detected at ppm level by using Ni and Pd metal nanoparticles covalently assembled on top of poly(3,4-ethylenedioxythiophene-cothiophene-3-acetic acid), poly(EDOT-co-TAA), films. For bridging of Ni and Pd metal nanoparticles to polymer of (3,4-ethylenedioxythiophene-cothiophene-3-acetic acid), 4-aminothiophenol was used. Pictorial representation of the bridge and responses was observed by hybrid nanoparticles. The thickness of both of Ni/Pd-poly(3,4-ethylenedioxythiophene-cothiophene-3-acetic acid) hybrid film showed a different response for acetone toward its sensitivity. It was observed that the responses of 10 ppm level of acetone was observed within 60 s by both Pd/poly(3,4-ethylenedioxythiophene-cothiophene-3-acetic acid) and Ni/[poly(3,4-ethylenedioxythiophene-cothiophene-3-acetic acid)] hybrid films. These two nanohybrid films were used for acetone detection, and it was found that Pd/poly(3,4-ethylenedioxythiophene-cothiophene-3-acetic acid) nanohybrid films are more selective for CH_3COCH_3. All these observations were thickness-dependent as these hybrid films used had the thickness of the ~50 nm [68]. Table 2 shows the efficacy of detectors toward aldehydes and ketones.

Table 2 Sensors for aldehyde and ketones

Entry	VOCs	Efficacy	Preparation method	Nanohybrids sensor for VOCs	References
01	Formaldehyde/acetaldehyde	Responses several tens ppb. superior response to formaldehyde/moderate response to acetaldehyde	Intercalation process	(PANI)$x$$MoO_3$	[62]
02	Formaldehyde/acetaldehyde	Responses at several tens ppb. equal response to formaldehyde/acetaldehyde	Intercalation process	(PoANIS)$x$$MoO_3$	[62]
03	Formaldehyde	Sensitivity coefficient 3.44 Detection limit of 130 ppb	Sol–gel method	Antimony/tin oxide [poly(ethylene-co-butylene)-block-poly-(ethylene oxide] template	[60]
04	Acetone	38.8% higher sensitivity, 11% lower noise level. The detection limit is 257 ppb	–	hybrid PEDOT–PIL-modified Fe_3O_4	[68]
05	Acetone	Response time 60 s at 10 ppm level	Post-condensation method	Pd-poly(EDOT-co-TAA)	[60]

4.3.4 Sensors for Chloroform

Trichloromethane is broadly and most commonly used solvents in different industries including pesticide formulations, in dye industries, rubber industries, as a chemical intermediate in laboratories and industry and as a cleansing agent, etc. The adverse health effects of chloroform include dryness of the mouth and throat, resulting in shortness of breath. Chloroform absorbed into the body via inhalation may cause symptoms including excitement, nausea followed by dizziness. Upon severe exposure of chloroform may be responsible for heart problems, fitting, unconsciousness and in some cases death. Having adverse effects its monitoring and detection is a must. Chloroform has been detected by different sensors. One of the sensors used for chloroform detection is based on quantum dot (QD) hybrid nanoparticles. Quantum dots are made up of cadmium selenide/zinc sulfide sheathed within polystyrene (PS)–polystyrene-co-maleic anhydride. The polystyrene (PS)–polystyrene-co-maleic anhydride polymer were prepared by electrospinning methodology. Difference in electrical conductivity was identified because of the interaction of chloroform molecules with quantum dots and the polystyrene (PS)–polystyrene-co-maleic anhydride side chains. The polymer-based nanofibers exhibited a response time for trichloromethane in <1 s. The sensitivity of sensor for chloroform was found to be more sensitive for chloroform (0.001–0.99%). The polymer-based sensor exhibited 6 month shelf life [68]. The poly(3-hexylthiophene) nanohybrid sensors based on olive oil encapsulated quantum dots of cadmium selenide of 6 nm thickness detected chloroform at 25 °C. This nanohybrid-based sensor showed response for chloroform ranging from 100 to 1200 ppm and exhibited the limit of detection at 100 ppm. On comparative study, it was observed that this sensor was selective for chloroform vapors being detected up to 100 ppm, whereas other solvents such as acetone, propyl alcohol and methylbenzene were detectable at 1000 ppm concentration [68]. Metal-polyaniline-based nanohybrid composites have been used for detection of various VOCs by varying metal ion. Sharma et al. reported cupper polyaniline nanohybrid-based sensors for detection of trichloromethane at ppm level. Comparing pure PANI to Cu-PANI, the Cu-PANI nanohybrid exhibited sensitivity in the range of 1.5–3.5 and showed good and reversible response at a minimum concentration of trichloromethane, i.e., 100 ppm. The mechanism involved for sensing of chloroform included adsorption–desorption of chloroform vapors on a surface of cupper nanoparticles [68].

4.3.5 Sensor for Aliphatic Amines

Aliphatic amines, one of the VOCs, are mandatorily used as intermediates in medicinal, textile and plastic chemical industries. These amines are known to create unpleasant odors, after inhalation may cause severe ENT irritation, tearing, conjunctivitis and corneal edema and when exposed in polluted air it forms carcinogenic nitrosamines. Kim et al. used highly fluorescent organic–inorganic hybrid perovskite nanoparticles as a sensor for the spotting of aliphatic amines. These perovskite

nanoparticles were prepared as stable colloidal solutions with highly crystalline 6 nm-sized nanoparticles which were characterized by transmission electron microscopy (TEM), scanning electron microscopy (SEM) and X-ray diffraction (XRD). The XRD reveals that organic ($CH_3NH_3^+$) and inorganic ($PbBr_3^-$) components in perovskite structure exhibit sharp hydrogen bonding which is responsible for its stabilization.

The detection of aliphatic amines (three different aliphatic amines, monoethyl amine ($EtNH_2$), diethylamine (Et_2NH) and trimethylamine (Et_3N)) by perovskite nanoparticles were based on the fact that the fluorescence signal of perovskite nanoparticle was quenched due to structural changes of $CH_3NH_3PbBr_3$'s crystalline structure upon exposure to aliphatic amines gas. It was observed that there was 11% decrease in PL intensity in <1 s when monoethylamine ($EtNH_2$) was exposed to $CH_3NH_3PbBr_3$ perovskite nanoparticles, whereas the PL intensity was reversibly recovered fully in <1 s and was partially recovered in ~15 s in case of triethyl amine (Et_3N) and diethyl amine (Et_2NH) vapors, respectively. The quenching of fluorescence of $CH_3NH_3PbBr_3$ perovskite nanoparticles by exposure of aliphatic amines was investigated by performing PL spectra measurements, and structural changings in perovskite films were observed by characteristics XRD peaks. These hybrid perovskite nanoparticle-coated films being highly fluorescent are very effective, easily observable by an eye-based aliphatic amine vapor sensor [79]. Ma et al. studied the detection of amines at 25 °C. For this purpose, the interdigitated carbon paste electrodes were deposited with PANI-TiO_2 nanocomposite thin films. The deposition of nanohybrid films on electrode was done by immersion and spincoating methodology. This nanocomposite film of PANI-TiO_2 showed sensitivity for trimethylamine [5.14×10^{-7} mol mL^{-1}], which increased further of 3–5 times of magnitude [68].

Most of the sensors have been used as a sensitive layer on electrodes, resonators, etc., for VOCs detection. For the detection of different VOCs, polysiloxanes containing 3-heptafluorobutanoyl camphorates of metal ions, e.g., Zn(II), Ni(II) and Eu(Ill), forming a hybrid, have been used as s sensitive layers for thickness-shear mode resonators (TSMRs). These sensitive layers were used to selectively detect VOCs, especially those analytes having O and N. The selectivity of nanohybrid composites results from interaction of heteroatom-containing analytes with unsaturated metal complexes. Here, the analyte under observation is pyridine (C_5H_5N) and n-butylamine. Pyridine (C_5H_5N) and n-butylamine were detected with in the concentration range of 20–40 ppb with a limit of detection 1 ppb and were achieved for ($CH_3CH_2CH_2CH_2NH_2$) [68]. Hybrid sensors used for detection of chloroform, and amines are given in Table 3.

4.3.6 Sensors for BTEX

Variety of VOCs have been detected by different sensors. Among VOCs, the hydrocarbons such as benzene, toluene, ethyl benzene and xylene (BTEX) has also been responsible for affecting human health. For sensing of BTEX, different sensing mechanism and hybrid have been studied. Among them, chitosan-coated magnetite nanocomposite hybrid nanomaterials having characteristics such as easy response

Table 3 S ensors used for chloroform and amines

Entry	VOCs	Efficacy	Preparation method	Nanohybrids sensor for VOCs	References
01	Chloroform	Response time of less than 1 s	Electrospinning	Cadmium selenide/zinc sulfide PS–PSMA	[60]
02	Chloroform	Detection limit of 100 ppm	–	CdSe/poly(3-hexylthiophene)	[60]
03	Chloroform	Response ~100 ppm Sensitivity range of 1.5–3.5	–	Cu-PANI	[60]
04	$EtNH_2$	Recovery in <1 s	–	$CH_3NH_3PbBr_3$	[69]
05	Et_2NH	Recovered in ~15 s	–	$CH_3NH_3PbBr_3$	[69]
	Et_3N	Recovered in ~15 s	–	$CH_3NH_3PbBr_3$	[69]
05	Et_3N	–	Spin–coating	PANI-TiO_2	[60]
06	n-Butylamine	Concentration range 20–40 ppb detection limit of 1 ppb	–	Polysiloxanes 3-heptafluorobutanoyl camphorates Zn(II), Ni(II), Eu(Ill),	[60]

time, large surface/volume ratio and simple recovery and reutilization were used for detection of aromatic VOCs [8]. To monitor the VOCs, these chitosan-coated magnetite nanocomposite hybrid nanomaterials based multisensing arrays were utilized [80–82]. The sorbent tubes filled with naphthalenediimide-dopamine (NDI-DA), pyromellitic diimide (PMDI-DA) and perylenediimide-dopamine (PDI-DA)-based magnetite supported organic–inorganic hybrids were used to detect VOCs by adsorption on the surface of tubes. These organic–inorganic hybrids showed different affinities for the adsorption and quantification of the VOCs. PDI-dopamine derivative hybrid nanoparticles (Fe_3O_4NP), filled in sorbent tubes, were used repeatedly up to more than 200 times for the identification and adsorption of benzene, toluene, ethyl benzene and xylene (BTEX) [83]. Two other smaller substituents such as pyromellitic diimide (PMDI) and naphthalene diimide (NDI) were also studied for adsorption and quantification of BTEX [84]. The interaction of these BTEX with nanohybrid particles was then identified by thermal desorption (TD) coupled to gas chromatography (GC) [85]. Porphyrins are interesting functionalizing substances for VOC's sensing materials as they provide various adsorption sites for VOCs to bind, hence enhancing sensitivity and selectivity [86]. A sensor array consists of four single sensors synthesized by functionalizing metal oxide nanoparticles with different kinds of MPPs. The metal oxides fabricated with metal polyporphyrins included ZnO and SnO_2.

The metal polyporphyrins hybridized with metal oxides included cobalt-porphyrin, zinc-porphyrins, nickel-porphyrin. The metal oxide and porphyrins were hybridized and formed four types of sensors which included (i) SnO_2NPs/cobalt-porphyrin, (ii) SnO_2 NPs/zinc-porphyrin, (iii) SnO_2 NPs/nickel-porphyrin and (iv) ZnO NPs/cobalt-porphyrin forming a sensor array. These MOX NP/MPP-based sensors were fabricated by drop-casting the MOX NPs dispersion and MPPs solution onto a MEMS platform [87]. The synthesized device exhibited a limit of detection of 20 ppb for toluene. BTEX were detected by porphyrin-based VOC sensor arrays in range from 1 to 9 ppm. The selectivity for toluene was confirmed using principle component analysis (PCA). The hybrid MOX NP/MPP-based sensors response changed significantly even at low-level concentrations [87]. The sensor detecting methylbenzene at a detection limit of 20 ppb with a greater signal-to-noise ratio of 10 was due to the fact that cobalt-porphyrin hybridized with ZnO NPs (provides adsorption sites) improved the response [86, 88].

There are VOCs such as acrolein, benzene, acrylic acid, etc., which exist in very low concentration in environment, i.e., 0.1 ppm, 1 ppm and 2 ppm, respectively, but have chronic effect upon long-term exposure [72, 89]. Among the broad range of VOCs, the aromatic hydrocarbon such as benzene appeared to be a hazardous VOCs emitted by our daily used items [90]. Benzene is a colorless odorant and is a major element of combustible engines, glues, varnishes, paints, detergents, furniture wax, smoke of tobacco, etc. All these above-mentioned articles are continuously increasing the benzene concentration in ascending mode, so a sensitive, reliable and stable sensor should be adopted for detection of benzene. As described previously macromolecular materials, e.g., porphyrins and metalloporphyrin (MPs) functionalized materials, show superior results for VOCs sensing. A variety of metalloporphyrins have been used for benzene, toluene, ethyl benzene, xylene (BTEX). One of the porphyrins, i.e., iron tetraphenyl porphyrin (FeTPP) has been fabricated with non-covalent single-walled carbon nanotubes (SWNTs). The chemiresistive sensor has exhibited excellent sensing capacity for benzene at the concentration of 1–25 ppm. The sensor having excellent recovery and high stability characteristics makes it important for practical applications. The fabricated SWNT–FeTPP sensor forms a charge transfer complex between SWNT and FeTPP which was characterized by structural (FESEM) as well as electrical (I–V, FET). The sensing behavior of the sensor was revealed by the electron donating capability of benzene. In all the metalloporphyrin, the metal plays a prominent role in increasing the efficiency of the sensor [91, 92]. The fabricated SWNT–FeTPP sensor detected benzene within the range of 1–25 ppm at 25 °C. The SWNT–FeTPP sensor exhibited the sensitivity of benzene of 62% with excellent linearity. The sensors showed response and recovery time in seconds. A comparative sensing behavior of SWNT–TPP (tetraphenyl porphyrin) sensor and the SWNT–FeTPP sensor was performed, and it was revealed that SWNT–FeTPP sensor has a sharp sensing due to metal ion present in center [93]. Solvents such as toluene ($C_6H_5CH_3$) were detected by polyvinyl butyral (PVB), Fe_2O_3 and manganese dioxide (MnO_2) hybrid-based sensors by Arshak et al. The response appeared by the sensors increased with increased solvent vapor concentrations. It was observed that response is dependent on nanocomposite film and its layering.

The polymer polyvinyl butyral showed a response of 19.43% for 5000 ppm concentration of toluene [68]. Nickel oxide combined with iron oxide with ratios such as (75% NiO/25%Fe_2O_3, 50% NiO/50%Fe_2O_3 and 25% NiO/75% Fe_2O_3) and fabricated with polyvinyl butyral nanocomposite films. These nanohybrid films were used for detection of toluene at 25 °C. All the composition was tested along with different VOCs, and it was found that the highest response was displayed for $C_6H_5CH_3$. The quick response and recovery times of all compositions were recorded at 4000 ppm of methyl toluene at 25 °C. The sensors formed by the composition of 75/25% of NiO to Fe_2O_3 combined with PVB nanocomposite exhibited recovery time of 48 s and a response time of 40 s for toluene.

Toluene has also been detected at ppm level by dispersed metal nanoparticles of nickel and palladium over poly(3,4-ethylenedioxythiophene-cothiophene-3-acetic acid) forming a metal hybrid of poly(EDOT-co-TAA) films. The metal nanoparticles and the polymer were interlocked by 4-aminothiophenol. The sensitivity for toluene detection was dependent on the thickness Ni/Pd-poly(3,4-ethylenedioxythiophene-cothiophene-3-acetic acid) hybrid films. The observation showed that 50 nm thickness of Ni/[poly(3,4-ethylenedioxythiophene-cothiophene-3-acetic acid) and Pd/poly(3,4-ethylenedioxythiophene-cothiophene-3-acetic acid) hybrid films had a limit of detection for toluene at 2 ppm and response time of 200 s. Among these two hybrids, the Ni-based hybrid films exhibited selectivity for ethyl benzene [68]. Different sensors and their efficiency for BTE are summarized in Table 4. Another gas sensor was observed for detection of octane and toluene which were based on nanohybrid of multi-walled carbon nanotubes with polyepichlorohydrin and polyetherurethane. It was observed that by introducing small amount of multi-walled carbon nanotube into the polymer enhanced the adsorption capacity for toluene. The limit of detection for methylbenzene and octane was found to be 7.4 and 1.7 ppm, respectively [68].

4.3.7 Single-Walled Sensor Array for Miscellaneous VOCs

Single-walled carbon nanotubes (SWNTs) having properties such as large ratio of surface volume, interesting electronic properties and small structure at nanoscale make them capable for formation of nanohybrid composites. Bases on these properties, single-walled carbon nanotubes (SWNTs) are used frequently for sensor fabrication. One of the major limitations of SWNTs is its selectivity [94–97]. On the other hand, porphyrins are chemically stable having interesting and structural properties optical properties. Central metal ion present in metalloporphyrins has tendency to bind with different analytes [98, 99]. Presently, the metalloporphyrins have been combined with SWNTs to fabricate SWNT–porphyrin hybrid chemiresistor sensor arrays which has been used for detecting volatile organic compounds in the environment [100]. The uniqueness of porphyrin library enhances the capability of developing an independent SWNT–porphyrin hybrid-based sensor array [101]. Different porphyrins, viz. octaethyl porphyrin (OEP), ruthenium OEP (RuOEP), iron OEP (FeOEP), manganese OEP (MnOEP), tetraphenyl porphyrin (TPP), ruthenium TPP

Table 4 Given table summarizes the sensors used for BTEX

Entry	VOCs	Efficacy	Preparation method	Nanohybrids sensor for VOCs	References
01	BTEX		Post condensation method	PMDI-Fe_3O_4/NDI-Fe_3O_4 PDI naphthalenediimide-dopamine-Fe_3O_4	[73, 74]
02	BTEX	Detection limit 20 ppb	–	SnO_2NPs/cobalt-porphyrin SnO_2 NPs/zinc-porphyrin SnO_2 NPs/nickel-porphyrin ZnO NPs/cobalt-porphyrin	[78]
03	BTEX	Limit of detection of benzene 1–25 ppm Sensitivity 62%	–	Iron tetraphenyl porphyrin (FeTPP) SWNTs	[83]
04	Toluene	Limit of detection 5000 ppm	–	Polyvinyl butyral (PVB), Fe_2O_3 and manganese dioxide (MnO_2)	[60]
05	Toluene	Response time 40 s Recovery time 48 s Limit of detection 4000 ppm	–	(NiO)/Fe_2O_3 (75/25, 50/50, 25/75)/PVB	[60]
06	Toluene	Detection limit 2 ppm Response time of 200 s		Ni/poly(EDOT-co-TAA), films	[60]
07	Toluene	Detection limits of 1.7 ppm		MWCNT/polyepichlorohydrin (PECH)/polyetherurethane (PEUT	[60]

(RuTPP) and iron TPP (FeTPP), have been fabricated with SWNTs by solvent casting technique. The characterization of these SWNT–porphyrin hybrid sensor arrays was performed by SEM and AFM. The porphyrin-functionalized SWNT arrays were studied for responses of broad range of VOCs in different concentrations such as dimethyl ketone, ethyl alcohol, methyl alcohol and methyl ethyl ketone and water vapors at room temperature. A dynamic response of the SWNT–OEP hybrid was observed for (methyl ethyl ketone) MEK. The data obtained of a sensor showed 60 and 90% of the maximum response in less than 1 and 7.2 $\pm$ 1.9 min. Similarly, sharp responses were observed for other porphyrin-functionalized SWNT devices for acetone, ethanol (EtOH), methanol (MeOH) and methyl ethyl ketone (MEK) and

water vapors. Furthermore, the OEP-functionalized SWNT device was significantly more sensitive [101].

5 Conclusion

This chapter highlights the diversity of organic–inorganic nanohybrid-based sensors for VOCs. A wide variety of VOCs had detected by different nanohybrid sensors. Over the years, different sensors, some based on metal oxide, some based on polymers, other based on carbon nanotubes, have been extensively used under different temperatures as sensing material for VOCs. Individually, the inorganic metals oxides/metals/carbon nanotubes had limited selectivity and organic polymers had poor conductivity, so continuous synthetic efforts had been poured stewards the development of variety of nanohybrid-based sensors. By combining conducting polymer and metal oxides/metals nanoparticles formed hybrid sensors with unique and interesting physicochemical properties capable to detect VOCs with high sensitivity, high selectivity and quick response in less time. Different sensing performances were observed with different polymers having different metal atoms/metal oxides nanoparticles.

References

1. Sowden M, Mueller U, Blake D (2018) Review of surface particulate monitoring of dust events using geostationary satellite remote sensing. Atmos Environ 183:154–164
2. Bilal M et al (2021) Hydrogen-based catalyst-assisted advanced oxidation processes to mitigate emerging pharmaceutical contaminants. Int J Hydrogen Energy
3. Rizwan K et al (2022) Hydrogen-based sono-hybrid catalytic degradation and mitigation of industrially-originated dye-based pollutants. Int J Hydrogen Energy
4. Shakeel A et al (2022) Advanced polymeric/inorganic nanohybrids: an integrated platform for gas sensing applications. Chemosphere 133772
5. Kelishadi R et al (2009) Lifestyle and environmental factors associated with inflammation, oxidative stress and insulin resistance in children. Atherosclerosis 203(1):311–319
6. Kelishadi R, Poursafa P (2010) Air pollution and non-respiratory health hazards for children. Arch Med Sci: AMS 6(4):483
7. Broza YY et al (2018) Synergy between nanomaterials and volatile organic compounds for non-invasive medical evaluation. Chem Soc Rev 47(13):4781–4859
8. Broza YY, Haick H (2013) Nanomaterial-based sensors for detection of disease by volatile organic compounds. Nanomedicine 8(5):785–806
9. Konvalina G, Haick H (2014) Sensors for breath testing: from nanomaterials to comprehensive disease detection. Acc Chem Res 47(1):66–76
10. Kampa M, Castanas E (2008) Human health effects of air pollution. Environ Pollut 151(2):362–367
11. Turner C (2013) VOC analysis by SIFT-MS, GC-MS, and electronic nose for diagnosing and monitoring disease. Volatile biomarkers: non-invasive diagnosis in physiology and medicine, pp 343–357

12. James D et al (2005) Chemical sensors for electronic nose systems. Microchim Acta 149(1):1–17
13. Gębicki J, Szulczyński B (2018) Discrimination of selected fungi species based on their odour profile using prototypes of electronic nose instruments. Measurement 116:307–313
14. He Z et al (2019) Contributions of different anthropogenic volatile organic compound sources to ozone formation at a receptor site in the Pearl River Delta region and its policy implications. Atmos Chem Phys 19(13):8801–8816
15. Salthammer T (2016) Very volatile organic compounds: an understudied class of indoor air pollutants. Indoor Air 26(1):25–38
16. Al-Dabbous A et al (2019) Oxides of carbon, particulate matters and volatile organic compounds impact on indoor air quality during waterpipe smoking. Int J Environ Sci Technol 16(6):2849–2854
17. Mirzaei A, Leonardi S, Neri G (2016) Detection of hazardous volatile organic compounds (VOCs) by metal oxide nanostructures-based gas sensors: a review. Ceram Int 42(14):15119–15141
18. Liotta L (2010) Catalytic oxidation of volatile organic compounds on supported noble metals. Appl Catal B 100(3–4):403–412
19. Drobek M et al (2015) PVDF-MFI mixed matrix membranes as VOCs adsorbers. Microporous Mesoporous Mater 207:126–133
20. Scirè S, Liotta LF (2012) Supported gold catalysts for the total oxidation of volatile organic compounds. Appl Catal B: Environ 125:222–246
21. Guo Y et al (2019) Influence of fluctuating groundwater table on volatile organic chemical emission flux at a dissolved chlorinated-solvent plume site. Groundw Monit Remediat 39(2):43–52
22. Azzouz I et al (2018) Zinc oxide nano-enabled microfluidic reactor for water purification and its applicability to volatile organic compounds. Microsyst Nanoeng 4(1):1–7
23. Ribes A et al (2007) Development and validation of a method for air-quality and nuisance odors monitoring of volatile organic compounds using multi-sorbent adsorption and gas chromatography/mass spectrometry thermal desorption system. J Chromatogr A 1140(1–2):44–55
24. Churkina G et al (2017) Effect of VOC emissions from vegetation on air quality in Berlin during a heatwave. Environ Sci Technol 51(11):6120–6130
25. Khan FI, Ghoshal AK (2000) Removal of volatile organic compounds from polluted air. J Loss Prev Process Ind 13(6):527–545
26. Lee S et al (2002) Volatile organic compounds (VOCs) in urban atmosphere of Hong Kong. Chemosphere 48(3):375–382
27. Liu Y et al (2008) Source profiles of volatile organic compounds (VOCs) measured in China: Part I. Atmos Environ 42(25):6247–6260
28. Al-Douseri FM, Chen Y, Zhang X-C (2006) THz wave sensing for petroleum industrial applications. Int J Infrared Millimeter Waves 27(4):481–503
29. Barreto G et al (2009) The role of catechols and free radicals in benzene toxicity: an oxidative DNA damage pathway. Environ Mol Mutagen 50(9):771–780
30. Nesheva D et al (2019) Phase characterization and ethanol adsorption in TiO_2 nanotubes anodically grown on Ti6Al4V alloy substrates. J Alloy Compd 798:394–402
31. Zhang R et al (2019) Gold and ZnO-based metal-semiconductor network for highly sensitive room-temperature gas sensing. Sensors 19(18):3815
32. Hermawan A et al (2020) CuO nanoparticles/$Ti_3C_2T_x$ MXene hybrid nanocomposites for detection of toluene gas. ACS Appl Nano Mater 3(5):4755–4766
33. Tian M et al (2019) Layer-by-layer nanocomposites consisting of Co_3O_4 and reduced graphene (rGO) nanosheets for high selectivity ethanol gas sensors. Appl Surf Sci 479:601–607
34. Aroutiounian V (2019) Gas nanosensors made from semiconductor metal oxides. J Contemp Phys (Armen Acad Sci) 54(4):356–367
35. Bhattarai DP et al (2021) Recent progress in metal-organic framework-derived nanostructures in the removal of volatile organic compounds. Molecules 26(16):4948

36. Hübert T et al (2011) Hydrogen sensors—a review. Sens Actuators B Chem 157(2):329–352
37. Yaqoob U, Chung G-S (2016) Highly flexible room temperature NO_2 sensor based on WO_3 nanoparticles loaded MWCNTs-RGO hybrid. In: Oxide-based materials and devices VII. International Society for Optics and Photonics
38. Ji H, Zeng W, Li Y (2019) Gas sensing mechanisms of metal oxide semiconductors: a focus review. Nanoscale 11(47):22664–22684
39. Al-Hashem M, Akbar S, Morris P (2019) Role of oxygen vacancies in nanostructured metal-oxide gas sensors: a review. Sens Actuators B Chem 301:126845
40. Yaqoob U, Younis MI (2021) Chemical gas sensors: recent developments, challenges, and the potential of machine learning—a review. Sensors 21(8):2877
41. Nandasiri MI et al (2016) Adsorption, separation, and catalytic properties of densified metal-organic frameworks. Coord Chem Rev 311:38–52
42. Zhang L-T, Zhou Y, Han S-T (2020) The role of metal–organic framework in electronic sensors. Angew Chem
43. Andre RS et al (2018) Sensitive and selective NH_3 monitoring at room temperature using ZnO ceramic nanofibers decorated with poly (styrene sulfonate). Sensors 18(4):1058
44. Marr I, Moos R (2017) Resistive NOx dosimeter to detect very low NOx concentrations—proof-of-principle and comparison with classical sensing devices. Sens Actuators B: Chem 248:848–855
45. Degler D et al (2016) Structure and chemistry of surface-doped Pt:SnO_2 gas sensing materials. RSC Adv 6(34):28149–28155
46. Wang Y et al (2019) Organic crystalline materials in flexible electronics. Chem Soc Rev 48(6):1492–1530
47. Zhu R, Azzarelli JM, Swager TM (2016) Wireless hazard badges to detect nerve-agent simulants. Angew Chem Int Ed 55(33):9662–9666
48. Zhu H et al (2015) Flow-through microfluidic photoionization detectors for rapid and highly sensitive vapor detection. Lab Chip 15(14):3021–3029
49. Shakeel A et al (2022) Advanced polymeric/inorganic nanohybrids: an integrated platform for gas sensing applications. Chemosphere 294:133772
50. Ghosh R et al (2015) Enhanced ammonia sensing at room temperature with reduced graphene oxide/tin oxide hybrid films. RSC Adv 5(62):50165–50173
51. Bai S et al (2015) Ultrasensitive room temperature NH_3 sensor based on a graphene–polyaniline hybrid loaded on PET thin film. Chem Commun 51(35):7524–7527
52. Patil U et al (2015) Room temperature ammonia sensor based on copper nanoparticle intercalated polyaniline nanocomposite thin films. Appl Surf Sci 339:69–74
53. Meng H et al (2015) Cu_2O nanorods modified by reduced graphene oxide for NH_3 sensing at room temperature. J Mater Chem A 3(3):1174–1181
54. Bandgar D et al (2015) Ultra-sensitive polyaniline–iron oxide nanocomposite room temperature flexible ammonia sensor. RSC Adv 5(84):68964–68971
55. Ye Z et al (2015) The investigation of reduced graphene oxide@ SnO_2–polyaniline composite thin films for ammonia detection at room temperature. J Mater Sci: Mater Electron 26(2):833–841
56. Pang Z et al (2016) A room temperature ammonia gas sensor based on cellulose/TiO_2/PANI composite nanofibers. Colloids Surf A 494:248–255
57. Nirmala R et al (2013) Preparation and characterization of copper oxide particles incorporated polyurethane composite nanofibers by electrospinning. Ceram Int 39(8):9651–9658
58. Pang Z et al (2014) Effect of CSA concentration on the ammonia sensing properties of CSA-doped PA6/PANI composite nanofibers. Sensors 14(11):21453–21465
59. Sanfelice RC et al (2017) Hybrid composite material based on polythiophene derivative nanofibers modified with gold nanoparticles for optoelectronics applications. J Mater Sci 52(4):1919–1929
60. Kondawar SB, Patil PT, Agrawal SP (2014) Chemical vapour sensing properties of electrospun nanofibers of polyaniline/ZnO nanocomposites. Adv Mater Lett 5(7):389–395

61. Pang Z et al (2014) Fabrication of PA6/TiO_2/PANI composite nanofibers by electrospinning–electrospraying for ammonia sensor. Colloids Surf A 461:113–118
62. Zhou L-J et al (2014) Porous nanoplate-assembled CdO/ZnO composite microstructures: a highly sensitive material for ethanol detection. Sens Actuators B Chem 197:370–375
63. Tian L et al (2015) Glucose sensing characterisations of TiO_2/CuO nanofibres synthesised by electrospinning. Mater Res Innov 19(3):160–165
64. Jia G et al (2014) Electrocatalytically active MOF/Graphite oxide hybrid for electrosynthesis of dimethyl carbonate. Electrochim Acta 144:1–6
65. Cobianu C et al (2020) Organic–inorganic ternary nanohybrids of single-walled carbon nanohorns for room temperature chemiresistive ethanol detection. Nanomaterials 10(12):2552
66. Athawale AA, Bhagwat S, Katre PP (2006) Nanocomposite of Pd–polyaniline as a selective methanol sensor. Sens Actuators B Chem 114(1):263–267
67. Choudhury A (2009) Polyaniline/silver nanocomposites: dielectric properties and ethanol vapour sensitivity. Sens Actuators B Chem 138(1):318–325
68. Kaushik A et al (2015) Organic–inorganic hybrid nanocomposite-based gas sensors for environmental monitoring. Chem Rev 115(11):4571–4606
69. Nardis S et al (2004) Preparation and characterization of cobalt porphyrin modified tin dioxide films for sensor applications. Sens Actuators B Chem 103(1–2):339–343
70. Han L, Andrady AL, Ensor DS (2013) Chemical sensing using electrospun polymer/carbon nanotube composite nanofibers with printed-on electrodes. Sens Actuators B Chem 186:52–55
71. Lvova L et al (2012) Carbon nanotubes modified with porphyrin units for gaseous phase chemical sensing. Sens Actuators B Chem 170:163–171
72. Itoh T et al (2008) Preparation of layered organic–inorganic nanohybrid thin films of molybdenum trioxide with polyaniline derivatives for aldehyde gases sensors of several tens ppb level. Sens Actuators B Chem 128(2):512–520
73. Shin S, Jang J (2007) Thiol containing polymer encapsulated magnetic nanoparticles as reusable and efficiently separable adsorbent for heavy metal ions. Chem Commun (41):4230–4232
74. Callaway M et al (2013) Investigation of the toxicity of amine-coated, carboxylcoated and polyaniline-coated FeO magnetic nanoparticles in *Caenorhabditis elegans*. Biosens Bioelectron 4(5)
75. Yuk J, Rose J, Alocilja E (2010) Characterization of polyaniline-coated magnetic nanoparticles for application in a disposable membrane strip biosensor. Eur Phys J Appl Phys 50(1):11401
76. Zhao B, Nan Z (2011) Preparation of stable magnetic nanofluids containing Fe3O4@ PPy nanoparticles by a novel one-pot route. Nanoscale Res Lett 6(1):1–8
77. Tahmasebi E et al (2013) Extraction of three nitrophenols using polypyrrole-coated magnetic nanoparticles based on anion exchange process. J Chromatogr A 1314:15–23
78. Tung TT et al (2015) Core-shell nanostructured hybrid composites for volatile organic compound detection. Int J Nanomed 10(Spec Iss):203
79. Kim S-H et al (2017) Detection of volatile organic compounds (VOCs), aliphatic amines, using highly fluorescent organic-inorganic hybrid perovskite nanoparticles. Dyes Pigm 147:1–5
80. Jalal AH et al (2018) Prospects and challenges of volatile organic compound sensors in human healthcare. ACS Sens 3(7):1246–1263
81. Kim N-H et al (2014) Highly sensitive and selective hydrogen sulfide and toluene sensors using Pd functionalized WO_3 nanofibers for potential diagnosis of halitosis and lung cancer. Sens Actuators B Chem 193:574–581
82. Vishinkin R, Haick H (2015) Nanoscale sensor technologies for disease detection via volatolomics. Small 11(46):6142–6164
83. Gutiérrez MS et al (2018) A very highly efficient magnetic nanomaterial for the removal of PAHs from aqueous media. Small 14(8):1702573
84. Singh D, Baruah JB (2011) Structural study on solvates of dopamine-based cyclic imide derivatives. Cryst Growth Des 11(3):768–777
85. de las Nieves Piña M et al (2019) Influence of the aromatic surface on the capacity of adsorption of VOCs by magnetite supported organic–inorganic hybrids. RSC Adv 9(42):24184–24191

86. D'Amico A et al (2000) Metalloporphyrins as basic material for volatile sensitive sensors. Sens Actuators B Chem 65(1–3):209–215
87. Cho B et al (2018) Fabrication and characterization of VOC sensor array based on SnO_2 and ZnO nanoparticles functionalized by metalloporphyrins. Micro Nano Syst Lett 6(1):1–6
88. Lee K et al (2018) Suspended CoPP-ZnO nanorods integrated with micro-heaters for highly sensitive VOC detection. Sens Actuators B Chem 264:249–254
89. Barro R et al (2009) Analysis of industrial contaminants in indoor air: Part 1. Volatile organic compounds, carbonyl compounds, polycyclic aromatic hydrocarbons and polychlorinated biphenyls. J Chromatogr A 1216(3):540–566
90. Ke M-T et al (2009) A MEMS-based benzene gas sensor with a self-heating WO_3 sensing layer. Sensors 9(4):2895–2906
91. Ehli C et al (2006) Interactions in single wall carbon nanotubes/pyrene/porphyrin nanohybrids. J Am Chem Soc 128(34):11222–11231
92. Kauffman DR, Kuzmych O, Star A (2007) Interactions between single-walled carbon nanotubes and tetraphenyl metalloporphyrins: correlation between spectroscopic and FET measurements. J Phys Chem C 111(9):3539–3543
93. Rushi A et al (2013) Iron tetraphenyl porphyrin functionalized single wall carbon nanotubes for the detection of benzene. Mater Lett 96:38–41
94. Baughman RH, Zakhidov AA, De Heer WA (2002) Carbon nanotubes—the route toward applications. Science 297(5582):787–792
95. Kong J et al (2000) Nanotube molecular wires as chemical sensors. Science 287(5453):622–625
96. Collins PG et al (2000) Extreme oxygen sensitivity of electronic properties of carbon nanotubes. Science 287(5459):1801–1804
97. Snow E et al (2005) Chemical detection with a single-walled carbon nanotube capacitor. Science 307(5717):1942–1945
98. Di Natale C, Monti D, Paolesse R (2010) Chemical sensitivity of porphyrin assemblies. Mater Today 13(7–8):46–52
99. Penza M et al (2010) Metalloporphyrins-modified carbon nanotubes networked films-based chemical sensors for enhanced gas sensitivity. Sens Actuators B Chem 144(2):387–394
100. Biesaga M, Pyrzyńska K, Trojanowicz M (2000) Porphyrins in analytical chemistry. A review. Talanta 51(2):209–224
101. Penza M et al (2011) Carbon nanotube films as a platform to transduce molecular recognition events in metalloporphyrins. Nanotechnology 22(12):125502

Chapter 10
Organic-Inorganic Nanohybrid-Based Sensors for Metal Ions Sensing

Madeeha Batool and Hafiz Muhammad Junaid

1 Introduction

Metal atoms and ions are part and parcel of our lives as these are involved in every biotic as well abiotic component of this world [1]. Due to their influential role in every process of life, their qualitative and quantitative sensing has gained considerable attention. Various types of chemical sensors have been reported for metal on sensing based on their structure, mode of interaction with the targeted analyte, nature of analyte ion and nature of signal produced for a particular analyte [2]. According to the sensing mode, they can be colorimetric, fluorgenic or electrochemical. Chemosensors consist of a chemical system which can selectively bind with the specific analyte and exhibit a detecting signal in the form of energy change [3]. This energy change could be a color change under day light or UV light, a change in fluorescence properties or an electrochemical change, i.e., change in redox potential [4]. On binding of the sensor with the analyte, energy change is produced due to change in electronic structure of both sensor molecule and analyte [5, 6]. Usually, a chemical sensor has chromophoric, fluorophoric or electronegative/electropositive moieties which are responsible for energy change on interaction with analyte and hence develop a sensing signal. Chemosensing is auspicious tool for the qualitative and quantitative determination of various anionic, cationic and neutral species which are biologically, medically and environmentally important [4]. Apart from that, chemosensors are also employed to analyze real samples collected from river water, industrial waste, biological sample for forensic analysis and clinical sample for the determination of different metal ions or any other targeted chemical species.

M. Batool (✉) · H. M. Junaid
School of Chemistry, University of the Punjab, Lahore 54590, Pakistan
e-mail: madeeha.chem@pu.edu.pk

K. Rizwan et al. (eds.), *Hybrid Nanomaterials*, Materials Horizons: From Nature to Nanomaterials, https://doi.org/10.1007/978-981-19-4538-0_10

Metal ion sensing

Metals atoms and ions are essential components of life. I-A and II-A metals, i.e., alkali and alkaline earth metals are highly profuse in biological systems [1] as well as in earth crust. According to a report published by US-Geological Survey in 1924, Sodium (Na), Potassium (K), Calcium (Ca), Magnesium (Mg), Aluminum (Al) and Iron (Fe) are the most abundant elements in our earth crust which are mostly present in the form of oxides and silicates. Al is the one of the three most abundant elements in earth crust comprising 8.3% by weight [4]. Metals are also the key element in living systems. Na and K are important electrolytes in blood and their deficiency elevates the chances of hypertension [7]. Moreover, Na, K, Ca and Mg are necessary for normal cellular function, muscle fitness and bone formation [8]. Fe acts as central metal atom in hemoglobin which is the main constituent of mammalian blood [9]. It is also a co-factor in many enzymes catalyze reactions and is involved in myelination as well [10]. Its deficiency may cause blood diseases [11]. Next to Fe, Zinc (Zn) is the second most abundant d-block metal in the human body [12]. It is essential for various enzymatic system, nervous system signal transmission and gene transcription. However, it is a trace element and its elevated levels may create various abnormalities in normal body functioning [13]. Copper (Cu) is another important metal in our body which acts as an initiator in hemoglobin synthesis and its deficiency leads to cardiovascular abnormalities while excessive concentrations of Cu may lead to Alzheimer's, Parkinson's and Wilson's disease [14, 15]. Mg is analogue to Fe in the chlorophyll molecule, the main integrant of the plant system, photosynthesis, and the food chain [16]. Apart from these, some metals such as Mercury (Hg), Lead (Pb), Arsenic (As) and Chromium (Cr) are extremely toxic to life even in very minute quantities Pollution of these metals is a major environmental threat in under developed countries where there is a weak check and balance over industrial waste management. In their unacceptable levels, these heavy metals are injurious to the environment; however, their accumulation in the bodies of living organisms may cause various chronic and acute diseases. For example, Hg is known for its chronic effect on human health in terms of optic, neural and renal disorders [2, 17]. Pb is among one the most toxic d-block metals [18], which produce adverse effects on mental health like dullness, memory loss and migraine in human beings [19]. As is usually found in the form of arsenite and arsenate ions which lethally affects the human health and leads to cancer and other chronic diseases [20]. Cr has its wide applications in industries such as metallurgies, leather industry, textile industry and refractories [21, 22]. Use of Cr on such a large scale increases the risk of Cr-pollution in air, soil and water. Cr is extremely toxic and carcinogenic in the form of Cr^{6+} [23].

Metals are found everywhere from sediments/rocks to buildings, simple hammers to sophisticated gadgets/instruments and medicines to bio-active materials. Therefore, metal ions detection got considerable attention of researchers belonging to analytical, pharmaceutical, forensic and bio-chemistry. Conservative tools for metal ions sensing, i.e., AAS, ICP-OES and some classical electrochemical techniques, are much costly, time-consuming and require laborious sample preparation [24–26]. Therefore, chemosensors have replaced these instrumental methods now a days.

Chemosensors are cost-effective, time-saving, and their efficiency is comparable or even better than these complex instruments in terms of their detection limits, sensitivity and selectivity [3].

1.1 Organic-Inorganic Hybrids

Organic-inorganic hybrids consist of an organic as well as an inorganic constituent. Organic-inorganic hybrids have been getting the great attention of research and the academic world for the last three decades. These are natural as well as synthetic. These are largely present in nature, i.e., mammalian teeth, bones, shells of molluscs, shellfish's shell, coccoliths, diatoms, etc. [27, 28]. These can be defined as a hetero-structured combination of organic and inorganic moieties in discrete domains [27, 29, 30]. These are produced by bridging inorganic and organic functionalities within the same molecule [31]. Incorporation of organic and inorganic characteristics in the same chemical compound is one of the primogenital dares for a chemist initiated with the commencement of the industrial era. Some of the ancient and well-known organic-inorganic hybrids may be developed for paint industry where Titania particles (TiO_2) suspended in organic solvents or surfactants but, at that time, the term organic-inorganic hybrid was not known [32]. Initially, organic-inorganic hybrids consist of some natural inorganics, i.e., clays, talcs, minerals, etc. added to organic polymers to impart desired chemical properties. However, the word organic-inorganic hybrid has emerged since last few decades. The linking of organic and inorganic components on the same frame work produces a synergistic effect [31] on hybrid's properties as these present thermal and chemical stability like inorganic compounds while diversity in synthetic routes and reactivity are similar to organic compounds [33]. Some key properties of organic-inorganic hybrids are given below as [28, 34]:

- **Synergistic Combination**

  Organic-inorganic hybrids are not a sum of organic and inorganic functionalities, instead, it is a synergistic combination that exhibits marvelous optical, thermal, mechanical, thermal and catalytic properties compared to simple organic and inorganic molecules.
- **Synthesis**

  The major synthetic methods for synthesizing organic-inorganic hybrids include polymerization or insertion of phenomenon of molecular precursors, polymeric precursors or nanoscale species, i.e., metallic salts, nanotubes, nanoparticles, nanoslabs alkoxides, polymeric units, etc. These reactions requires low temperatures (20-300 °C), ordinary pressure and organic or aqueous solvents. These conditions are similar to those typical chemical reactions in organic, organometallic, supramolecular, interclation and polymer chemistry. Their synthesis not only involve simple chemical reactions. Indeed some engineering techniques, i.e.,

micro-emulsion templating, spin coating, electro spinning, dip coating, aerosols processing, etc. are also employed.

- **Texture**

  These can be produced in thin films, thick coatings, fibers, nanopowders, monoliths, foams or any other complex structural design.

- **Tunability**

  Organic-inorganic hybrids are of desired properties can be synthesized. The desired properties could be chemical composition, functional moieties, various scales of sizes and morphologies.

- **Stability**

  Like many inorganic compounds, these hybrids are stable over a wide range of temperature, pH, humidity and other environmental conditions.

Applications of these organic-inorganic hybrids are available in almost every sphere of science, i.e., drug delivery, bio-imaging, sensing devices, optical devices, electrochemistry, photocatalysis, food packaging films, environment and energy [27, 29, 31, 33, 35–37]. Some important applications of these organic-inorganic hybrids are given below as:

- **Bio-Medical**

  Organic-inorganic hybrids are widely used in bio-medical applications. A hybrid "gadolinium-benzyldiethyltriaminepenta acetic acid (Gd-Bz-DTPA) functionalized PAMAM dendrimers" is used in MRI and fluorescence imaging of blood–brain barrier tumor cells [38]. Another hybrid "Folate-conjugated lipid-coated mesoporous silica nanoparticles" employed for targeted sustained drug release/delivery in chemotherapy of cancerous ovarian cells [39]. Various bio-catalysts are based on organic-inorganic hybrids. For example, a hybrid composed of α-chymotrypsin and $Ca_3(PO_4)_2$ speeds up protein digestion [40]. Some organic-inorganic hybrids have also been reported as bio-sensors such as paper-based GOx-$Mn_3(PO_4)_2$ hybrid are known for glucose detection in biological systems [41]. Many bio-active materials are also chemically organic-inorganic hybrids, e.g., polymethacrylate–silica chemical hybrid is a well-known dental filler [42].

- **Electronics**

  Organic-inorganic hybrids are also found their applications in electronics. CH_3 NH_3 $PbBr_3$-based organic/inorganic hybrid is commonly used in LED lights [43]. Another hybrid "pervoskite/cyclohexenylethylamine" is a major component of number of electroluminescent devices [44].

- **Energy and Environment**

  Various solar cells are composed of organic-inorganic hybrids [45]. These hybrids are also used as photocatalysts in a number of photocatalytic reactions. For example N-benzylhexamethylenetetramine bromide/$Cu_2(SCN)_3$-based hybrid [46] and cucurbituril/polyoxometalates [47] are employed as photocatalysts in photocatalytic degradation of tetracycline and organic dyes (methyl orange

and rhodamine B), respectively. Silsesquioxane/polyoxometalates [48] and Calix-3 dye and TiO_2 [49]-based hybrid-based hybrids have also been reported for photocatalytic splitting of water.

- **Optical Devices**

  Organic-inorganic hybrids are also used in optical devices. Hybrids of tungstosilicates with MAAM, VTEOS and TEOS are utilized in photochromic devices [50]. TiO_2/PMMA are the integral part of different devices based on nonlinear optics [51].

- **Miscellaneous Applications**

  Some temperature sensitive organic-inorganic hybrids, i.e., TEOS/APTES-based hybrids used in thermometers [52]. Many organic-inorganic hybrids such as organic polymer/silica-based hybrids used in food packaging [53].

  Applications of organic-inorganic hybrid materials are summarized in Table 1.

1.2 Types of Organic-Inorganic Hybrids

Organic-inorganic hybrids can be classified based on structure and nature of chemical bonding (Fig. 1). Structurally, there are four basic types of organic-inorganic hybrids [33]. Briefly, these are given as under:

a. **Organic intercalated inorganic nanohybrids**: In these hybrids, organic guests are implanted within the layers of inorganic host frame work. For example, hybrids consists of MoO_3 with many guests like poly anilines [54], etc. These hybrids are synthesized by interclation phenomenon in which MoO_3 films were deposited on lanthanum aluminate followed by the process of intercalation into polymeric guests.

b. **Core-shell hybrids**: In these hybrids, inorganic component that is usually a metal oxide acts as core and organic polymeric species forming a shell, for example, surface-modified TiO_2 NPs with amphiphilicterthiophene monomeric units [55]. Such hybrids can be developed by polymerimerization of monomeric units in the presence of metal oxide precursor. The mode of polymerization could be chemical polymerization, oxidative polymerization or electropolymerization.

c. **Organic coating inorganic hybrids**: Different monomers are directly polymerized on the surface of metal oxide in these hybrids. The electrochemical deposition method has made thin films of PANI/TiO2 hybrid. In this technique, metal oxide, i.e., Titania deposits on stainless steel substrate using chemical bath deposition procedure. After that, organic polymer, i.e., PANI deposits by electrode position process [56].

d. **Polymer doped with metal oxide**: These are the composites of inorganic species and conducting polymers, e.g., polyaniline-ZnO conducting nanohybrids [57]. These polymers can be prepared by synthesizing the polymer in

Table 1 Sensing of various metal ions by organic-inorganic hybrids

Hybrid	Species sensed	Technique	Detection signal	LOD	References
Colorimetric Sensors					
Urea conjugated rhodamine/AuNPs	Al^{3+}	Colorimetry	Color change from pink to blue	14.2 nM	[92]
4-(2-Pyridylazo)-resorcinol functionalized ionic microgels	Mn^{2+}, Pb^{2+}, Co^{2+}, Ni^{2+}, Cu^{2+} and Zn^{2+}	Colorimetry	Color change from: Yellow to orange (pH < 11) Yellow to pink (pH > 2)	nM level	[94]
Rhodamine-based modified poly acrylic acid-coated FeNPs (PAA-Rho-FeNPs)	Au^{3+}	Colorimetry	Color change from colorless to pink-purple Increase in FL intensity at 590 nm	0.85 μM	[118]
1,3-alternate calix[4]arene carboxyl acids-modified silver nanoparticles	Cu^{2+}	Colorimetry	Color change from yellow to colorless	2.6×10^{-6} M	[95]
Oxamic acid and p-aminobenzoic acid modified AuNPs	Fe^{3+}	Colorimetry	Color change from red to blue Red shift from 523 to 685 nm	5.3 μM	[65]
Citrate capped AuNPs/CTAB	Hg^{2+}	Colorimetry	Color change from blue to red	11.9 nM	[96]
Immine-based COF/AuNPs	Hg^{2+}	Colorimetry	Color change from colorless to blue	0.75 nM	[97]

(continued)

Table 1 (continued)

Hybrid	Species sensed	Technique	Detection signal	LOD	References
AuNPs modified with methylene blue	Cr^{3+} and Fe^{2+}	Colorimetry	Aggregation formation	23.66 nM(Cr^{3+}) 11.21 nM(Fe^{2+})	[93]
Fluorescent Sensors					
Viologenfuctionalized Tb-phosphonates	Cu^{2+}	Fluorimetry	Quenching of luminescent intensity at 544 nm		[109]
SBA-15 functionalized with 1-(4′-hydroxyphenyl)-4-pyrenyl-2,3-diaza-1,3-butadiene (Py-SBA-15)	Hg^{2+}	Fluorimetry	Fluorescence enhancement at 454 nm	1.7×10^{-7} g/mL 0.85 μM	[114]
Silica/lanthanide complex/MOF (SiO_2@EuTTA@ZIF-8)	Cu^{2+}	Fluorimetry	Decrease in luminescence intensity at 613 nm		[110]
UiO-66-NH2/T-rich FAM labeled DNA	Hg^{2+}	Fluorimetry	Fluorescence enhancement at 518 nm		[113]
Oligosilsesquioxanes/Lanthanide complex Eu(dpa)$_3$@POSS-NH_2	Cu^{2+}	Fluorimetry	Instant luminescent switch off under UV light (254 nm)		[108]
Rhodamine B embedded Ag-SBA-15	Hg^{2+}	Fluorimetry	Decrease in FL intensity at 575 nm	10.54 nM	[116]

(continued)

Table 1 (continued)

Hybrid	Species sensed	Technique	Detection signal	LOD	References
PBHA functionalized POM	Cr^{3+} and Ca^{2+}	Fluorimetry	Decrease in FL intensity for Cr^{3+} and increase in FL intensity for Ca^{2+} at 619 nm	1.423 μM (Cr^{3+}) 0.676 μM (Ca^{2+})	[111]
Polyoxomolybdate/aminopyridine hybrid	Pb^{2+}	Fluorimetry	Emission intensity decrease at 441 nm	6.91 ppb	[117]
Polyhedral oligomericsilsesquioxane	Fe^{2+} and Fe^{3+}	Fluorimetry	PL emission intensity decrease at		[112]
Au nanoparticles (AuNPs) immobilized in poly(N-isopropylacrylamide-co-2-(dimethylamino)ethylmethacrylate) (P(NIPAM-co-DMA)) microgels	Hg^{2+}	Fluorimetry	Enhancement in FL intensity	31 nM	[115]
Electrochemical Sensors					
Bimetallic Au-Pt NPs/Organic nanofibrils (Au-Pt NPs/NFs)	Hg^{2+}	Anodic Striping Voltametery	Pair of redox peaks at 0.522 V and 0.556 V	0.008 ppb	[119]
L-cysteine/Au/TiO_2/GCE	Cu^{2+}	Anodic Striping Voltametery		1 nM	[120]
Fluorogenic Sensors					
Aptamer/MCM-41	As(III)	Flurogenic		0.9 ppb	[121]

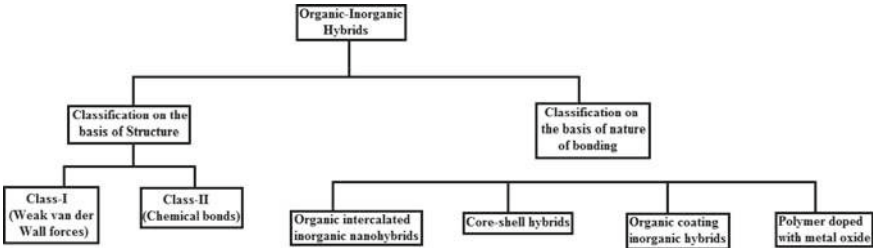

Fig. 1 Classification of organic-inorganic hybrids

the presence of metal oxide or mixing the pure polymer and metal oxide in a proposed composition.

On the basis of nature of chemical bonding, organic-inorganic hybrids are grouped into the following classes.

a. **Class-I**: In hybrids of class-I type, organic and inorganic components of a hybrid are linked with each other through weak van der Waal forces, i.e., hydrogen bonding, hydrophilic-hydrophobic interactions, ionic interactions, etc. Class-I hybrids include organic molecules, i.e., rhodamines, coumarins, porphyrins, etc., entrapped in inorganic networks like silica, alumina, aluminosilicates or metal oxides (TiO_2, ZrO_2).
b. **Class-II**: In these hybrids, organic and inorganic components are bound with each other through electrovalent or covalent bonds. The typical example of such hybrids are organometallic compounds (which contain metal to carbon, metal to oxygen and carbon to oxygen bonds), silica/nylon hybrids, pervoskites, organically modified silica alkoxides, etc.

The commonly used inorganic components include mesoporous silica [58–62] (i.e., SBA-15, SBA-16, MCM-41, etc.), metallic or metal oxide nanoparticles [63–65] (i.e., Fe_3O_4 particles, AuNPs, etc.), quantum dots [27] (i.e., ZnS, CdSe, etc.), rare earths [27] and carbon nanopreparations [27]. There is a broad range of organic components, used for hybrid synthesis. These are [27]: small molecules (i.e., APTMS, APTES, etc.), linear homopolymers (i.e., PVC, PMMA, etc.), block polymers (i.e., PS-b-PMMA), branched polymer (i.e., LDPE, etc.), dendrimers (i.e., poly propylene imine, polyether-copolyester, etc.) and biomolecules (i.e., DNA, peptides, etc.).

1.3 Sensing Applications of Organic-Inorganic Hybrids

A large number of organic-inorganic hybrids have been proposed as sensors for sensing of different physical and chemical species in medicinal, agricultural, industrial and other systems. Some of these are:

i. Gas sensing
ii. Humidity sensing
iii. VOCs sensing
iv. Pesticides sensing
v. Physical parameter sensing.

Gas Sensing: Many organic-inorganic hybrids have reported as gas sensors that are operated at room temperature. An organic-inorganic hybrid-based polythiophene and tungsten oxide (PTP/WO_3) is used for the detection of NO_2 at low temperatures, i.e., less than 90 °C [66]. Another hybrid based on PANI/TiO_2 has been presented for trimethylamine sensing at room temperature [67]. Similarly, PPy/TiO_2 is well known for the detection of ammonia gas even in a concentration as low as 2 ppm [68]. Likewise, PPy/Fe_2O_3 has been introduced as gas sensor as it is sensitive to CO_2, N_2 and O_2 [69].

Humidity Sensing: Humidity control is one of the major parameters to be control in many industries as well as pharmaceutical, medicinal, clinical, forensic, bio-chemical and environmental analytical laboratories. A photopolymerized hybrid based on PPy/TiO_2 NPs has been proposed as humidity sensors [70]. Apart from that, many other organic-inorganic hybrids, i.e., NaPSS/ZnO [71], PANI/WO_3 [72], PPy/Fe_2O_3 [73], etc. have also been reported for this application.

VOCs Sensing: Volatile organic compounds (VOCs) are key indoor air pollutants that are produced from variety of sources, including paints, varnishes, sealants, cleansing agents, tobacco smoke, printers, pharmaceutical and personal care products. Many organic-inorganic hybrids have been found in literature that are sensitive to VOCs and used as sensors for their detection for example PANI/ZnO have shown sensitive and selective response for MeOH, EtOH and CAN [33].

Pesticides Sensing: Pesticides are widely used in agriculture, gardens and households to control pests, herbs, and fungus. Due to their resistive nature, these retain in air and water for a long time and are major contributor in air and water pollution. Organic-inorganic hybrids have also found their applications for pesticide detection [74]. A recent example of this are $MnBr_4(TPA)_2$, $MnBr_4(TEA)_2$ and $MnCl_4(btmdme)_2$ which are sensitive to Ferbam (a pesticide) [75].

Physical parameter Sensing: Organic-inorganic hybrids have also been utilized for the detection of many physical parameters like strain, UV light, etc. [33].

2 Organic-Inorganic Hybrids as Metal Ions Sensors

Although a lot of metallic ion sensors (i.e., Schiff bases, sulfonamides, immidazoles, pyrazoles, coumarines, oxindoles, carbon dots, nanoparticles, etc.) have been reported since last few decades [1, 76–81] but organic/inorganic hybrids attain a special place in various classes of chemosensors. This is because sensors belonging

to all the above-mentioned classes have only one or a few electron deficient or electronegative sites that interact with the target metal ion. In organic-inorganic hybrids, electron deficient and electron rich sites are residing on same molecules. Moreover, coating one component over another or surface modifications makes them ideal for sensing applications. In a nutshell, there are three key striking features which make organic-inorganic hybrids as popular sensors. These are [35, 37]: (i) there is a vast diversity in their structural and functional units (ii) their physico-chemical properties can be tuned by changing or modifying the organic component, inorganic component or both (iii) these can be recycled by suitable chemical action.

2.1 Use of Nanotechnology in Sensing

The development of nanoscale chemical compounds and their applications in sensing studies has been a subject of much concern for chemists due to their tunability in shape and size based on physic-chemical properties, thermal stability, porosity and large surface area [82]. The introduction of nanotechnology in organic-inorganic hybrids improve their sensing properties as nanolevel particle size further add two glorious features: (a) nanostructure auxiliary enhance their surface area which may concentrate the analyte of interest (b) high porosity which ensure the efficient interaction between sensor and analyte. By virtue of these above-mentioned marvelous properties, organic-inorganic nanohybrids have been emerged as more sensitive and selective sensors with regards to other ones.

2.2 Classification of Organic-Inorganic Hybrids Based on Mode of Sensing

The organic-inorganic hybrid sensors those have been reported in literature for the detection of metal ions can be classified in to three classes namely, colorimetric sensors, fluorometric sensors and electrochemical sensors. Figure 2 represents their schematic diagram.

2.2.1 Organic-Inorganic Hybrids as Colorimetric Sensors

Literally, colorimetry is referred to measurement of colors. It could be defined as, "the analytical tool employed to evaluate the concentration of colored species by applying Beer-Lambert law" [83]. A colorimetric sensor is one which produces a quick on-site detection signal for a particular targeted chemical species in the form of an optical change recognized by human eye under diffused light [81, 84]. Swift response,

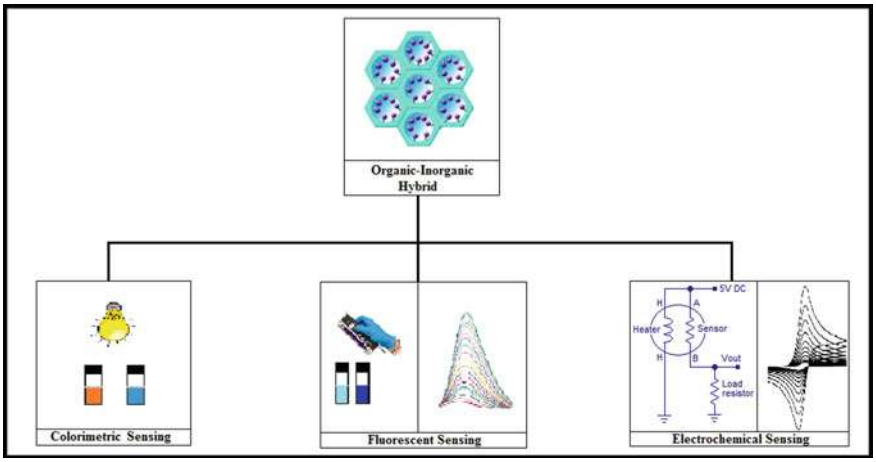

Fig. 2 Classification of organic-inorganic hybrids sensors for metal ions sensing

financially economical and simplicity are some fundamental features of a colorimetric sensor. Various colorimetric metal ions sensors based on different classes, i.e., polyoxometalates [85], silica [86], nanoparticles [87], inorganic nanoclusters [88], Schiff bases [26], Sulfonamides [89], immidazoles [90], pyrazoles [91], carbon dots [81], etc. have been reported. However, the colorimetric metallic sensors based on organic-inorganic hybrid materials are better than other sensors in terms of sensitivity, selectivity, and stability.

These organic-inorganic nanohybrids can colorimetrically sense various types of metal ions and hence can be used as following sensors;

(a) **Essential Metal Colorimetric Sensors**

Al^{3+}

Urea conjugated rhodamine/AuNPs have been reported as naked eye sensors for the detection of tri-positive aluminum ions as this hybrid has exhibited a color change from pink to blue. NMR and IR data revealed that this color change is results due to complex formation between spirolactam carbonyl of hybrid and Al^{3+} ions [92].

Fe^{2+} and Fe^{3+}

It has been observed that an organic-inorganic hybrid "AuNPs modified with methylene blue" produced aggregations upon interaction with ferrous ions. This hybrid has a limitation as it develops a similar visual transition for Cr^{3+} ions under an identical reaction environment [93]. Buduru et al. [65] have introduced oxamic acid and p-aminobenzoic acid modified AuNPs as selective optical sensors for ferric ions which presented a color change from red to blue and a bathochromic shift from 523 to 685 nm in electronic spectrum with an LOD of 5.3 μM.

Cu^{2+}

An organic-inorganic hybrid "4-(2-Pyridylazo)-resorcinol functionalized ionic microgels" has shown an optical transition from yellow to pink for Cu^{2+} ions with a detection limits up to nM level, but it is not selective for Cu^{2+} ions as its produces same color changes for Mn^{2+}, Pb^{2+}, Co^{2+}, $Ni^{2+}$and Zn^{2+} as well [94]. Problem of selectivity of cupric sensing has been resolved by introducing another hybrid "1,3-alternate calix arene carboxyl acids-modified silver nanoparticles" which a naked eye color change from yellow to colorless with a compromised DL value of 2.6 μM [95].

(b) **Toxic Metal Colorimetric Sensors**

Hg^{2+}

Citrate capped AuNPs in CTAB has been presented as colorimetric sensors for Hg(II) ions as this hybrid exhibited a color change form blue to red having and LOD of 11.9 nM. [96] The detection limits have further been improved to 0.75 nM when Immine-based COF/AuNPs reacted with Hg^{2+} ions (color change from color less to blue). Redox reactions are involved behind both of these color changes [97].

Cr^{3+}

Cr(III), a toxic metallic ion, has shown aggregation formation upon reaction with AuNPs modified with methylene blue with a detection limit of 23.66 nM [93].

2.2.2 Organic-Inorganic Hybrids as Fluorometric Sensors

The process of emission of radiation by a substance followed by the absorption of electromagnetic radiations (EMR) is called fluorescence [98]. A fluorescent metal ion sensor contains two main structural features, i.e., metal coordinating group and a fluorophoric group responsible for absorption and emission of EMR [1, 99]. Fluorescent sensors are preferable for scientists and researchers due to their sensitivity, selectivity, rapidity and low detection limits [100]. A large number of fluorescent metal ion sensors based on various chemical classes such as Schiff bases [101], acridines [102], coumarin [103], sulfonamides [104], Rhodamines [105], nanoparticles [106], carbon dots [107], etc. have been reported. Various fluorescent sensors for metal ion based on organic-inorganic hybrids have been discussed below.

(a) Essential Metal Sensors

Cu^{2+}

Oligosilsesquioxanes/Lanthanide complex, i.e., $Eu(dpa)_3$/POSS-NH_2 has exhibited an instant switch off fluorescent at 254 nm for Cu^{2+} ion [108]. Another hybrid "viologenfuctionalized Tb-phosphonate" has shown selective luminescence quenching for Cu^{2+} at 544 nm [109]. Silica/lanthanide complex/MOF (SiO_2@EuTTA@ZIF-8) has also decrease the fluorescence intensity (at 613 nm) for cupric ions [110].

Ca^{2+}

Wu et al. have described a sensitive and selective fluorescent probe "polyhydroxy benzoic acid modified POM" for the detection of Ca^{2+} ions as it exhibits an increase in fluorescence intensity at 619 nm for calcium ions with a detection limit as low as 0.676 μM [111].

Fe^{2+} and Fe^{3+}

Microporous polymers based on polyhedral oligomericsilsesquioxane have been reported as fluorescent chemosensors for ferrous and ferric ions as fluorescent intensity of these hybrids tends to decline upon reaction with Fe^{2+} Fe^{3+} ions. Detection limits of these hybrids for Fe^{2+} and Fe^{3+} are in μM range [112].

(b) **Toxic Metal Sensors**

Hg^{2+}

A hybrid-based fluorescent probe "UiO-66-NH2/T-rich FAM labeled DNA" has selected a fluorescence enhancement for Hg^{2+} at 518 nm [113]. A functionalized silica-based hybrid "SBA-15 functionalized with 1-(4′-hydroxyphenyl)-4-pyrenyl-2,3-diaza-1,3-butadiene (Py-SBA-15)" has been introduced as fluorescent sensing probe for Hg^{2+} detection as this probe has exhibited an increase in fluorescence intensity at 454 nm with an DL value of 0.85 μM for mercury (II) ions [114]. A hybrid based on Au nanoparticles (AuNPs) immobilized in poly(N-isopropylacrylamide-co-2(dimethylamino) ethylmethacrylate) (P(NIPAM-co-DMA)) microgels has displayed fluorescence enhancement for Hg^{2+} with an improved LOD of 31 nM [115]. Another silica-based fluorescent sensor "Rhodamine B embedded Ag-SBA-15" has further decreased the detection limit to 10.54 nM for mercuric ions to with a fluorescence quenching at 575 nm [116].

Pb^{2+}

n organic-inorganic nanohybrid based on polyoxomolybdate/aminopyridine hybrid has been reported for selective fluorescent detection of plumbous ions. This hybrid's fluorescence emission intensity of this hybrid decrease at 441 nm upon interaction with Pb^{2+} ions having an LOD as low as 6.91 ppb. [117]

Cr^{3+}

Wu et al. have presented polyhydroxy benzoic acid modified POM as selective fluorescent probe for the sensing of Cr^{3+} ions as its fluorescence intensity decreased at 619 nm for Cr (III) ions with a detection limit of 1.423 μM [111].

2.3 Organic-Inorganic Hybrid as Electrochemical Sensors

In electrochemical sensing, usually two types of electrodes have been used. A reference electrode and a working electrode. The reference electrode remains at constant potential during an electrochemical measurement. The potential change at working

electrode with respect to reference electrode provides the information about analyte to be studied. The selective and sensitive electrodes got attention of researchers because these electrodes show response for a specific chemical species. Various electrochemical methods have been developed in which such electrodes are being used which selectively respond for specific ionic species. For metal detection, mostly such electrodes are used in voltametric systems.

Many such electrode have been reported which are composed of organic-inorganic hybrid material. Wu et al. have been reported a voltametric electrode based on L-cysteine/Au/TiO_2/GCE for sensitive and selective voltametric determination of Cupric ions with a DL value of 1 nM. Another hybrid probe "Bimetallic Au-Pt NPs/Organic nanofibrils (Au-Pt NPs/NFs)" has been introduced as voltametric electrode for the selective sensing of mercuric ions with LOD of 0.008 ppb.

Metal ion sensing applications of organic-inorganic hybrids are enlisted in Table 1.

3 Mechanism of Metal Ion Sensing by Organic-Inorganic Hybrids

3.1 Complex Formation

A complex is formed as a result of Lewis acid-based interactions between a metal ion and chemical species capable for donating one or more pair of electrons to that metal ion. Such electron donating species are commonly termed as ligands. Ligands could be ionic or neutral molecules. The sensors molecules mostly act as ligand to form a complex with metal ion of interest and hence produce a detection signal.

Niamsa et al. [118] have reported rhodamine-based modified PAA-coated FeNPs (PAA-Rho_2) as colorimetric aurum sensors. This sensor has exhibited a color change from colorless to pink for Au^{3+} ions due to complex formation between hybrid and Au^{3+} ions as shown in Fig. 3. A downfield shift of amide protons from 7.94 ppm to 9.64 ppm on H-NMR spectra suggested some interactions between Au^{3+} ions and carbonyl moieties of spirolactam group. Furthermore, stretching of carbonyl group at 1629 cm^{-1} in IR has also shifted to 1592 cm^{-1} which is an evidence of complexation between Au^{3+} ions and carbonyl moieties of spirolactam group of hybrid. DFT calculations also confirmed this complex formation.

A silica-based organic-inorganic hybrid containing pyrene group (Py-SBA-15) has been presented as a fluorescent sensor for detecting mercuric ions as this hybrid showed fluorescence enhancement at 454 nm. Fluorescence studies revealed that nitrogen lone pair on organic moieties which are coordinated with electron deficient pyrene. Upon interaction with Hg^{2+} ions, these nitrogen lone pairs interacted with Hg^{2+} ions (Fig. 4) creating the electron deficiency on pyrene again which cause fluorescence enhancement [114]

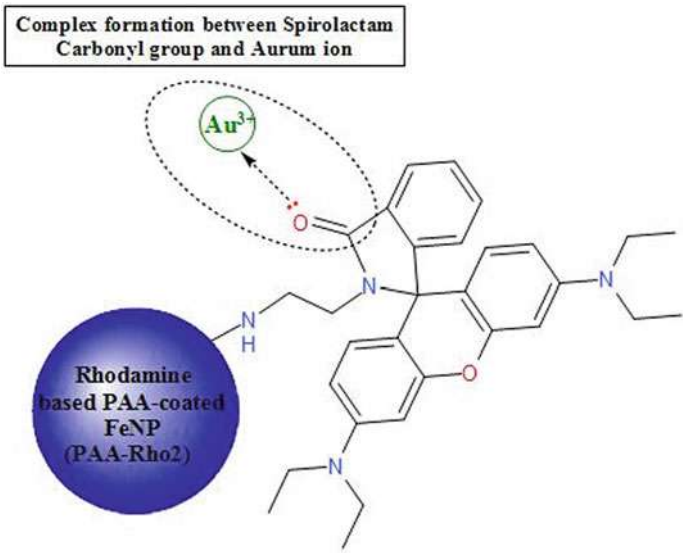

Fig. 3 Complexation between spirolactam carbonyl moieties of PAA-Rho_2 and Au^{3+} ions [118]

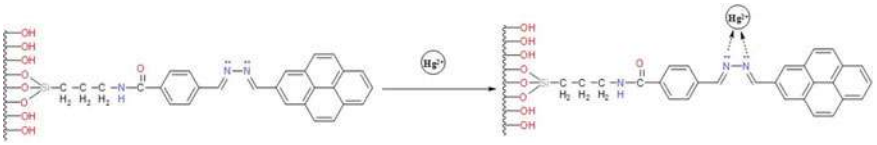

Fig. 4 Complex formation between Hg^{2+} and N-atoms of Py-SBA-15 (Adapted from Ref. [114])

L-cysteine/Au/TiO_2/GCE has been introduced as selective Cu (II) electrochemical sensor in anodic stripping voltametric analysis. Studies demonstrated a complexation mechanism for this selective sensing as L-cysteine coordinated with Cu^{2+} ions by N-atom of amino ($–NH_2$) group and O-atom of carboxyl group (–COOH) [120].

3.2 Redox Reaction

Oxidation–reduction reactions are collectively termed as redox reactions. These reactions are characterized by the loss of electron from one of the reactants and gain of that electron by another reactant. The reaction between metal ions and a sensor molecule usually involves the transfer of electron form moieties on the sensor molecule to the metal ion. A visual transition from blue to red has been observed upon AuNPs/CTAB nanohybrid interaction with Hg^{2+} ions. Citrate ions present on the surface of AuNPs

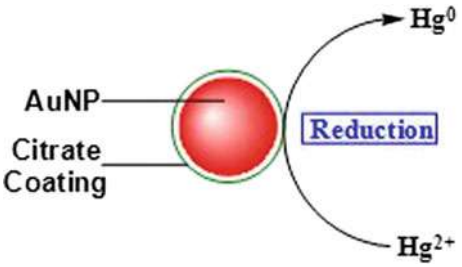

Fig. 5 Reduction of Hg^{2+} by citrate capped AuNPs [96]

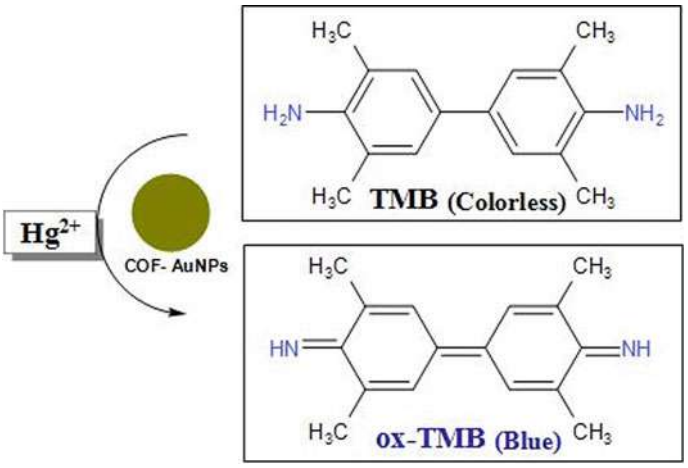

Fig. 6 Oxidation of TMB by Hg^{2+} in the presence of COF-AuNPs [97]

reduced Hg^{2+} to Hg^0 (Fig. 5) and Hg deposited on the surface of AuNPs as Hg-Au alloy [96].

COF-AuNPs have shown a colorless to blue optical change for Hg^{2+} in the presence of TMB. COF-AuNPs catalyzes the oxidation of TMB by Hg^{2+} ions as shown in Fig. 6 [97].

3.3 Cation Exchange

Ion exchange phenomenon is widely applicable in many analytical applications. Upon interaction with ion of interest, some metal ion sensors exchange certain cation present in their structure with targeted ion and produce a detection signal due to this cation exchange process. A fluorescent probe "polyoxomolybdate/amino pyridine hybrid" [117] has tended to quench fluorescence intensity upon addition of plumbous ions. A cation exchange mechanism between central atoms of polyoxomolybdate

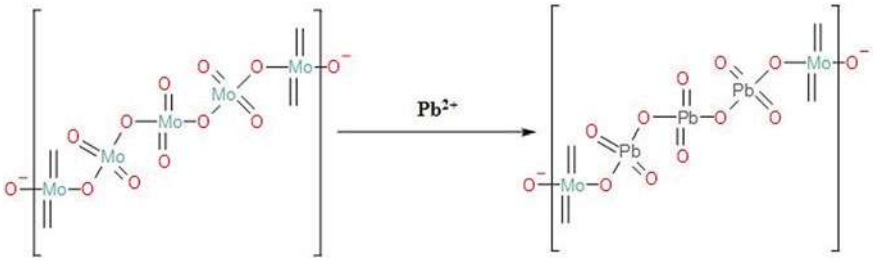

Fig. 7 Cation exchange between central atoms of POM and analyte [117]

(POM) and analyte of interest has been proposed for this fluorescence quenching as described in Fig. 7.

3.4 Intramolecular Energy Transfer

Transfer of energy from one part of a molecule to another part of molecule upon interaction with electromagnetic radiations or any chemical species is known as intramolecular energy transfer. In some fluorescent systems based on organic-inorganic hybrids, a transfer of energy from inorganic fluorescent centers to organic photochromic centers cause change in fluorescent properties of the system. These fluorescent changes, i.e., intramolecular energy transfer in hybrid molecule, happened upon hybrid with metal ion interaction. Yang et al. [109] have described the luminance quenching of Viologen functionalized Tb-phosphonates upon interaction with Cu^{2+} ions at 544 nm as a result of reduction in energy transfer from organic moieties to Tb^{3+} ions within hybrid structure due to interactions between analyte of interest and P-OH groups or terminal water molecules.

4 Performance Evaluation

Performance efficiency of a sensor can be evaluated on the basis of its limit of detection for particular analyte of interest [122]. Lower the detection limit of a sensor for a specific metal ion, more efficient will be the sensor [123]. A comparison of some organic-inorganic hybrids-based sensors for various metal ions with pure organic or inorganic sensors is given in Table 2.

Urea conjugated rhodamine/AuNPs have exhibited an LOD of 14.2 nM [92] for Al^{3+} which much lower than 0.39 μM [124], 0.38 μM [125] and 0.3 μM [88] presented by a Schiff base, CDs and Au-nanocluster-based sensors, respectively.

Similarly, an organic-inorganic hybrid "L-cysteine/Au/TiO_2/GCE" have been employed for the determination of Cu^{2+} electrochemically by anodic stripping

Table 2 Comparison of performance efficiency of organic-inorganic hybrids and other sensors

Metal ion	Sensor	Nature of sensor	Sensing technique	LOD	References
Al^{3+}	Urea conjugated rhodamine/AuNPs	Org.–inorg. Hybrid	Colorimetry	14.2 nM	[92]
	N,N'-Bis (salicylidene)-1,4-diaminobenzene (a Schiff base)	Organic	Fluorimetry	0.39 μM	[124]
	Methylene-bis-acrylamide/p-phenylenediamine derived CDs	Organic	Colorimetry	0.38 μM	[125]
	Gold nanoclusters	Inorganic	Fluorimetry	0.3 μM	[88]
Cu^{2+}	L-cysteine/Au/TiO_2/GCE	Org.–inorg. Hybrid	Anodic stripping voltametry	1 nM	[120]
	2,2′-((1E,1′E)-(((Hexylazanediyl)bis (4,1-phenylene)) bis (methanylylidene)) bis(azanylylidene))bis (4-methylphenol) (a Schiff base)	Organic	Colorimetry	18.9 nM	[126]
	AuNPs	Inorganic	Raman spectroscopy	500 nM	[127]
Hg^{2+}	Rhodamine B embedded Ag-SBA-15	Org.–inorg. Hybrid	Fluorimetry	10.54 nM	[116]
	1, 10-phenanthroline-based Schiff base	Organic	Fluorimetry	22.2 nM	[26]
	AgNPs	Inorganic	Colorimetry	0.85 μM	[87]
Cr^{3+}	AuNPs modified with methylene blue	Org.–inorg. Hybrid	Colorimetry	23.66 nM	[93]
	2,3-dimethyl-4-(2-oxo-1,2-diphenylethylideneamino)-1-phenyl-1,2-dihydropyrazol-5-one (a Schiff base)	Organic	Colorimetry	0.12 μM	[128]
	N-doped CNPs	Inorganic	Fluorimetry	0.15 μM	[129]

voltammetry with a DL value of 1 nM [120] which is significantly lower than 18.9 nM [126] and 0.3 μM [127] reported for a colorimetric Schiff base cupric sensor and Raman active AuNPs-based cupric sensor, respectively.

Likewise, LOD comparison of a hybrid sensor for Hg (II) ions "Rhodamine B embedded Ag-SBA-15" (LOD = 10.54 nM) [116] with an organic, i.e., Schiff base-based mercuric sensors (LOD = 22.2 nM) [26] and an inorganic, i.e., AgNPs-based Hg^{2+} sensors (LOD = 0.85 μM) [87] is an evident of superiority of organic-inorganic nanohybrid-based sensors in terms of sensitivity.

An LOD of 23.66 nM has been calculated for Cr^{3+} sensing colorimetric probe "AuNPs modified with methylene blue" [93] which is significantly lower than 0.12 μM [128] and 0.15 μM [129] observed for a Schiff base and a N-doped-CNPs sensor, respectively.

5 Conclusion and Future Directions

Organic-inorganic nanohybrids are fascinating for researchers to detect various metal ions as these sensors are tunable, coast effective and green in nature. Moreover, their low detection limits compared to other sensor classes is evidence of their efficiency in terms of sensitivity. This chapter covers the sensing of metal ions utilizing organic-inorganic hybrids-based sensors. However, there is still an empty space in this field for sensing some biologically and environmentally important metal ions like Cd, As, Pb, etc.

References

1. Carter KP, Young AM, Palmer AE (2014) Fluorescent sensors for measuring metal ions in living systems. Chem Rev 114(8):4564–4601
2. Roy A, Nandi M, Roy P (2021) Dual chemosensors for metal ions: a comprehensive review. TrAC Trends Anal Chem 116204
3. Junaid HM et al (2020) Naked eye chemosensing of anions by Schiff bases. Crit Rev Anal Chem 1–18
4. Kaur B, Kaur N, Kumar S (2018) Colorimetric metal ion sensors–a comprehensive review of the years 2011–2016. Coord Chem Rev 358:13–69
5. Prodi L (2005) Luminescent chemosensors: from molecules to nanoparticles. New J Chem 29(1):20–31
6. Kaur N, Kumar S (2011) Colorimetric metal ion sensors. Tetrahedron (Oxford. Print) 67(48)
7. Geleijnse JM, Kok FJ, Grobbee DE (2004) Impact of dietary and lifestyle factors on the prevalence of hypertension in Western populations. Eur J Public Health 14(3):235–239
8. Nielsen FH, Lukaski HC (2006) Update on the relationship between magnesium and exercise
9. Gao G-Y et al (2015) A reversible fluorescent chemosensor for iron ions based on 1H-imidazo [4, 5-b] phenazine derivative. Sens Actuators, B Chem 213:501–507
10. Tang X et al (2018) A relay identification fluorescence probe for Fe^{3+} and phosphate anion and its applications. Spectrochim Acta Part A Mol Biomol Spectrosc 191:172–179
11. Liu S-R, Wu S-P (2012) New water-soluble highly selective fluorescent chemosensor for Fe (III) ions and its application to living cell imaging. Sens Actuators, B Chem 171:1110–1116

12. Fraker PJ, King LE (2004) Reprogramming of the immune system during zinc deficiency. Annu Rev Nutr 24:277–298
13. Bush AI (2000) Metals and neuroscience. Curr Opin Chem Biol 4(2):184–191
14. Lee SY et al (2016) Simultaneous detection of Cu^{2+} and Cr^{3+} by a simple Schiff-base colorimetric chemosensor bearing NBD (7-nitrobenzo-2-oxa-1, 3-diazolyl) and julolidine moieties. Tetrahedron 72(35):5563–5570
15. Martínez R et al (2008) Bis (indolyl) methane derivatives as highly selective colourimetric and ratiometric fluorescent molecular chemosensors for Cu^{2+} cations. Tetrahedron 64(9):2184–2191
16. Chen ZC et al (2018) Functional dissection and transport mechanism of magnesium in plants. In: Seminars in cell & developmental biology. Elsevier
17. Rice KM et al (2014) Environmental mercury and its toxic effects. J Prev Med Public Health 47(2):74
18. Tchounwou P et al (2012) Heavy metal toxicity and the environment. Mol Clin Environ Toxicol 101:133–164
19. Feleafel M, Mirdad Z (2013) Hazard and effects of pollution by lead on vegetable crops. J Agric Environ Ethics 26(3):547–567
20. Hughes MF (2002) Arsenic toxicity and potential mechanisms of action. Toxicol Lett 133(1):1–16
21. Zhao J et al (2001) Effects of chromate and chromate conversion coatings on corrosion of aluminum alloy 2024–T3. Surf Coat Technol 140(1):51–57
22. Kogel JE et al (2006) Industrial minerals & rocks: commodities, markets, and uses. SME
23. Hingston J et al (2001) Leaching of chromated copper arsenate wood preservatives: a review. Environ Pollut 111(1):53–66
24. Quang DT, Kim JS (2010) Fluoro-and chromogenic chemodosimeters for heavy metal ion detection in solution and biospecimens. Chem Rev 110(10):6280–6301
25. Batool M et al (2020) Metal ion detection by carbon dots—a review. Crit Rev Anal Chem 1–12
26. Berhanu AL et al (2019) A review of the applications of Schiff bases as optical chemical sensors. TrAC, Trends Anal Chem 116:74–91
27. Zhao N et al (2018) Versatile types of organic/inorganic nanohybrids: from strategic design to biomedical applications. Chem Rev 119(3):1666–1762
28. Faustini M et al (2018) History of organic-inorganic hybrid materials: prehistory, art, science, and advanced applications. Adv Func Mater 28(27):1704158
29. Park D-H et al (2013) Polymer–inorganic supramolecular nanohybrids for red, white, green, and blue applications. Prog Polym Sci 38(10–11):1442–1486
30. Shakeel A et al (2022) Advanced polymeric/inorganic nanohybrids: An integrated platform for gas sensing applications. Chemosphere 133772
31. Walcarius A (2001) Electrochemical applications of silica-based organic− inorganic hybrid materials. Chem Mater 13(10):3351–3372
32. Judeinstein P, Sanchez C (1996) Hybrid organic-inorganic materials: a land of multidisciplinarity. J Mater Chem 6(4):511–525
33. Wang S et al (2013) Organic/inorganic hybrid sensors: a review. Sens Actuators, B Chem 182:467–481
34. Yao H-B, Gao M-R, Yu S-H (2010) Small organic molecule templating synthesis of organic-inorganic hybrid materials: their nanostructures and properties. Nanoscale 2(3):322–334
35. Sun Z et al (2016) Multifunctional optical sensing probes based on organic-inorganic hybrid composites. J Mater Chem B 4(31):5194–5216
36. Kumar P, Deep A, Kim K-H (2015) Metal organic frameworks for sensing applications. TrAC, Trends Anal Chem 73:39–53
37. Shu Y et al (2021) Encapsulation of luminescent guests to construct luminescent metal-organic frameworks for chemical sensing. ACS sensors 6(3):641–658
38. Sarin H et al (2008) Effective transvascular delivery of nanoparticles across the blood-brain tumor barrier into malignant glioma cells. J Transl Med 6(1):1–15

39. Samanta S, Pradhan L, Bahadur D (2018) Mesoporous lipid-silica nanohybrids for folate-targeted drug-resistant ovarian cancer. New J Chem 42(4):2804–2814
40. Yin Y et al (2015) An enzyme–inorganic hybrid nanoflower based immobilized enzyme reactor with enhanced enzymatic activity. J Mater Chem B 3(11):2295–2300
41. Li W et al (2018) Efficient in situ growth of enzyme-inorganic hybrids on paper strips for the visual detection of glucose. Biosens Bioelectron 99:603–611
42. Wei Y et al (1998) Novel organic-inorganic chemical hybrid fillers for dental composite materials. J Appl Polym Sci 70(9):1689–1699
43. Kim YH et al (2015) Multicolored organic/inorganic hybrid perovskite light-emitting diodes. Adv Mater 27(7):1248–1254
44. Hattori T et al (1996) Highly efficient electroluminescence from a heterostructure device combined with emissive layered-perovskite and an electron-transporting organic compound. Chem Phys Lett 254(1–2):103–108
45. Liu Q et al (2012) Highly efficient crystalline silicon/Zonyl fluorosurfactant-treated organic heterojunction solar cells. Appl Phys Lett 100(18):183901
46. Qiao X, Wang C, Niu Y (2020) N-Benzyl HMTA induced self-assembly of organic-inorganic hybrid materials for efficient photocatalytic degradation of tetracycline. J Hazard Mater 391:122121
47. Lü J et al (2012) Photochromic hybrid materials of cucurbituril and polyoxometalates as photocatalysts under visible light. Chem Commun 48(5):669–671
48. Prabu R et al (2018) Non-covalent polyhedral oligomeric silsesquioxane-polyoxometalates as inorganic-organic-inorganic hybrid materials for visible-light photocatalytic splitting of water. Inorg Chem Front 5(10):2666–2677
49. Huang J-F et al (2019) Facile synthesis of porous hybrid materials based on Calix-3 dye and TiO_2 for high photocatalytic water splitting performance with excellent stability. J Mater Chem A 7(7):2993–2999
50. Huang Y et al (2006) Synthesis and photochromism of a novel organic-inorganic hybrid film embedded with polyoxomatalates. Mater Chem Phys 97(2–3):431–436
51. Yuwono AH et al (2003) Transparent nanohybrids of nanocrystalline TiO_2 in PMMA with unique nonlinear optical behavior. J Mater Chem 13(6):1475–1479
52. Brites C et al (2013) Thermometry at the nanoscale using lanthanide-containing organic-inorganic hybrid materials. J Lumin 133:230–232
53. Iotti M et al (2009) Organic-inorganic hybrid coatings for the modification of barrier properties of poly (lactic acid) films for food packaging applications. J Polym Environ 17(1):10–19
54. Itoh T et al (2007) Preparation and characterization of a layered molybdenum trioxide with poly (o-anisidine) hybrid thin film and its aldehydic gases sensing properties. Bull Chem Soc Jpn 80(5):1011–1016
55. Kimura M et al (2012) Sensing of vaporous organic compounds by TiO2 porous films covered with polythiophene layers. Adv Func Mater 22(3):469–476
56. Dhawale D et al (2008) Room temperature liquefied petroleum gas (LPG) sensor based on p-polyaniline/n-TiO_2 heterojunction. Sens Actuators, B Chem 134(2):988–992
57. Khan AA, Khalid M (2010) Synthesis of nano-sized ZnO and polyaniline-zinc oxide composite: characterization, stability in terms of DC electrical conductivity retention and application in ammonia vapor detection. J Appl Polym Sci 117(3):1601–1607
58. Du X, Qiao SZ (2015) Dendritic silica particles with center-radial pore channels: promising platforms for catalysis and biomedical applications. Small 11(4):392–413
59. Yang P, Gai S, Lin J (2012) Functionalized mesoporous silica materials for controlled drug delivery. Chem Soc Rev 41(9):3679–3698
60. Li Z et al (2012) Mesoporous silica nanoparticles in biomedical applications. Chem Soc Rev 41(7):2590–2605
61. Wu S-H, Mou C-Y, Lin H-P (2013) Synthesis of mesoporous silica nanoparticles. Chem Soc Rev 42(9):3862–3875
62. Atabaev TS et al (2013) Mesoporous silica with fibrous morphology: a multifunctional core–shell platform for biomedical applications. Nanotechnology 24(34):345603

63. Ge F et al (2012) Effective removal of heavy metal ions Cd^{2+}, Zn^{2+}, Pb^{2+}, Cu^{2+} from aqueous solution by polymer-modified magnetic nanoparticles. J Hazard Mater 211:366–372
64. Liu J et al (2011) Magnetic nanocomposites with mesoporous structures: synthesis and applications. Small 7(4):425–443
65. Buduru P, SRR BC (2016) Oxamic acid and p-aminobenzoic acid functionalized gold nanoparticles as a probe for colorimetric detection of Fe^{3+} ion. Sens Actuators, B: Chem 237:935–943
66. GUO X-Z et al (2012) Low-temperature NO_2 sensors based on polythiophene/WO_3 organic-inorganic hybrids. Trans Nonferrous Met Soc China 22(2):380–385
67. Ma X et al (2006) Preparation of polyaniline–TiO_2 composite film with in situ polymerization approach and its gas-sensitivity at room temperature. Mater Chem Phys 98(2–3):241–247
68. Wu Y, Xing S, Fu J (2010) Examining the use of TiO_2 to enhance the NH3 sensitivity of polypyrrole films. J Appl Polym Sci 118(6):3351–3356
69. Tandon R et al (2006) Gas and humidity response of iron oxide—polypyrrole nanocomposites. Sens Actuators, B Chem 114(2):768–773
70. Su P-G, Huang L-N (2007) Humidity sensors based on TiO_2 nanoparticles/polypyrrole composite thin films. Sens Actuators, B Chem 123(1):501–507
71. Li Y, Yang M, She Y (2004) Humidity sensors using in situ synthesized sodium polystyrenesulfonate/ZnO nanocomposites. Talanta 62(4):707–712
72. Parvatikar N et al (2006) Electrical and humidity sensing properties of polyaniline/WO3 composites. Sens Actuators, B Chem 114(2):599–603
73. Suri K et al (2002) Gas and humidity sensors based on iron oxide–polypyrrole nanocomposites. Sens Actuators, B Chem 81(2–3):277–282
74. Rizwan K et al (2022) MXene-based electrochemical and biosensing platforms to detect toxic elements and pesticides pollutants from environmental matrices. Chemosphere 291:132820
75. Chen S et al (2019) Organic-inorganic manganese (II) halide hybrids based paper sensor for the fluorometric determination of pesticide ferbam. Sens Actuators, B Chem 297:126701
76. Chen X et al (2012) Fluorescent chemosensors based on spiroring-opening of xanthenes and related derivatives. Chem Rev 112(3):1910–1956
77. Kim HN et al (2008) A new trend in rhodamine-based chemosensors: application of spirolactam ring-opening to sensing ions. Chem Soc Rev 37(8):1465–1472
78. Cheng T et al (2008) A highly sensitive and selective OFF-ON fluorescent sensor for cadmium in aqueous solution and living cell. J Am Chem Soc 130(48):16160–16161
79. Kar C et al (2013) NIR-and FRET-based sensing of Cu^{2+} and S^{2-} in physiological conditions and in live cells. Inorg Chem 52(2):743–752
80. Sun Z et al (2015) A novel piperazine-bis (rhodamine-B)-based chemosensor for highly sensitive and selective naked-eye detection of Cu^{2+} and its application as an INHIBIT logic device. J Lumin 167:156–162
81. Junaid HM, Solangi AR, Batool M (2021) Carbon dots as naked eye sensors. Analyst 146(8):2463–2474
82. Asefa T, Duncan CT, Sharma KK (2009) Recent advances in nanostructured chemosensors and biosensors. Analyst 134(10):1980–1990
83. Lindon JC, Tranter GE, Koppenaal D (2016) Encyclopedia of spectroscopy and spectrometry. Academic Press
84. VS AP et al (2017) Colorimetric sensors for rapid detection of various analytes. Mater Sci Eng C 78:1231–1245
85. Sabarinathan C et al (2021) Polyoxometalate based ionic crystal: dual applications in selective colorimetric sensor for hydrated $ZnCl_2$ and antimicrobial activity. New J Chem 45(12):5576–5588
86. Thirumalai M, Maheswari MA (2021) Mesoporous silica monolith based colorimetric probes for Co^{2+} ions. Mater Lett 130142
87. Firdaus ML et al (2017) Colorimetric detection of mercury (II) ion in aqueous solution using silver nanoparticles. Anal Sci 33(7):831–837

88. Mu X et al (2014) One-pot synthesis of tyrosine-stabilized fluorescent gold nanoclusters and their application as turn-on sensors for Al^{3+} ions and turn-off sensors for Fe^{3+} ions. Anal Methods 6(16):6445–6451
89. Goh H et al (2017) Dipodal colorimetric sensor for Ag+ and its resultant complex for iodide sensing using a cation displacement approach in water. Tetrahedron Lett 58(11):1040–1045
90. Satapathy R, Wu Y-H, Lin H-C (2012) Novel thieno-imidazole based probe for colorimetric detection of Hg^{2+} and fluorescence turn-on response of Zn^{2+}. Org Lett 14(10):2564–2567
91. Nayak N et al (2018) Remarkable colorimetric sensing behavior of pyrazole-based chemosensor towards Cu (ii) ion detection: synthesis, characterization and theoretical investigations. RSC Adv 8(32):18023–18029
92. Kaur R et al (2019) Colorimetric sensor for detection of trace level Al (III) in aqueous medium based on organic-inorganic nanohybrid. Chem Phys Lett 722:140–145
93. Salimi F et al (2018) Colorimetric sensor of detection of Cr (III) and Fe (II) ions in aqueous solutions using gold nanoparticles modified with methylene blue. Optik 158:813–825
94. Zhou X, Nie J, Du B (2015) 4-(2-Pyridylazo)-resorcinol functionalized thermosensitive ionic microgels for optical detection of heavy metal ions at nanomolar level. ACS Appl Mater Interfaces 7(39):21966–21974
95. Nsengiyuma G et al (2016) Self-assembly of 1, 3-alternate calix [4] arene carboxyl acids-modified silver nanoparticles for colorimetric Cu^{2+} sensing. Sens Actuators, B Chem 236:675–681
96. Sun X et al (2018) Colorimetric sensing of mercury (II) ion based on anti-aggregation of gold nanoparticles in the presence of hexadecyl trimethyl ammonium bromide. Sens Actuators, B Chem 260:998–1003
97. Li W et al (2019) Fabrication of a covalent organic framework and its gold nanoparticle hybrids as stable mimetic peroxidase for sensitive and selective colorimetric detection of mercury in water samples. Talanta 204:224–228
98. Lakowicz JR (2013) Principles of fluorescence spectroscopy. Springer science & business media
99. Formica M et al (2012) New fluorescent chemosensors for metal ions in solution. Coord Chem Rev 256(1–2):170–192
100. Jeong Y, Yoon J (2012) Recent progress on fluorescent chemosensors for metal ions. Inorg Chim Acta 381:2–14
101. Reimann MJ et al (2019) Water-soluble sulfonate Schiff-base ligands as fluorescent detectors for metal ions in drinking water and biological systems. ACS Omega 4(2):2874–2882
102. Wang C et al (2018) Acridine-based fluorescence chemosensors for selective sensing of Fe^{3+} and Ni^{2+} ions. Spectrochim Acta Part A Mol Biomol Spectrosc 199:403–411
103. Zhu G et al (2019) A novel coumarin-based fluorescence chemosensor for Al^{3+} and its application in cell imaging. Spectrochim Acta Part A Mol Biomol Spectrosc 210:105–110
104. Mondal S et al (2015) Fluorescence sensing and intracellular imaging of Al^{3+} ions by using naphthalene based sulfonamide chemosensor: structure, computation and biological studies. RSC Adv 5(90):73626–73638
105. Bhalla V et al (2013) Rhodamine based fluorescence turn-on chemosensor for nanomolar detection of Fe^{3+} ions. Sens Actuators, B Chem 178:228–232
106. Guo Y et al (2015) Fluorescent carbon nanoparticles for the fluorescent detection of metal ions. Biosens Bioelectron 63:61–71
107. Yarur F, Macairan J-R, Naccache R (2019) Ratiometric detection of heavy metal ions using fluorescent carbon dots. Environ Sci Nano 6(4):1121–1130
108. Xu Q, Li Z, Li H (2016) Water-Soluble luminescent hybrid composites consisting of oligosilsesquioxanes and lanthanide complexes and their sensing ability for Cu^{2+}. Chem Eur J 22(9):3037–3043
109. Yang W et al (2016) Photochromic terbium phosphonates with photomodulated luminescence and metal ion sensitive detection. Chem Eur J 22(43):15451–15457
110. Liu C, Yan B (2015) Highly effective chemosensor of a luminescent silica@ lanthanide complex@ MOF heterostructured composite for metal ion sensing. RSC Adv 5(123):101982–101988

111. Wu H et al (2019) A PHBA-functionalized organic-inorganic hybrid polyoxometalate as a luminescent probe for selectively sensing chromium and calcium in aqueous solution. Dyes Pigm 171:107696
112. Mohamed MG et al (2021) Ultrastable luminescent hybrid microporous polymers based on polyhedral oligomeric silsesquioxane for CO_2 uptake and metal ion sensing. Microporous Mesoporous Mater 311:110695
113. Wu LL et al (2016) A metal–organic framework/DNA hybrid system as a novel fluorescent biosensor for mercury (II) ion detection. Chem Eur J 22(2):477–480
114. Wang Y et al (2010) A highly selective regenerable optical sensor for detection of mercury (II) ion in water using organic-inorganic hybrid nanomaterials containing pyrene. New J Chem 34(9):1946–1953
115. Tang Y et al (2016) A turn-on fluorescent probe for Hg^{2+} detection by using gold nanoparticle-based hybrid microgels. Sens Actuators, B Chem 228:767–773
116. Chockala B et al (2017) Organic-inorganic hybrid fluorescent sensor thin films of rhodamine B embedded Ag-SBA15 for selective recognition of Hg (II) ions in water. Chin Chem Lett 28(7):1399–1405
117. Song X-X et al (2018) The selectively fluorescent sensing detection and adsorptive removal of Pb^{2+} with a stable [δ-Mo_8O_{26}]-based hybrid. J Colloid Interface Sci 532:598–604
118. Niamsa N et al (2013) Hybrid organic-inorganic nanomaterial sensors for selective detection of Au^{3+} using rhodamine-based modified polyacrylic acid (PAA)-coated FeNPs. Polym Chem 4(10):3039–3046
119. Gong J et al (2010) Stripping voltammetric detection of mercury (II) based on a bimetallic Au− Pt inorganic− organic hybrid nanocomposite modified glassy carbon electrode. Anal Chem 82(2):567–573
120. Wu J et al (2018) Organic-inorganic-hybrid-enhancement electrochemical sensor for determination of Cu (II) in river water. Electroanalysis 30(8):1820–1827
121. Oroval M et al (2017) Selective fluorogenic sensing of As (III) using aptamer-capped nanomaterials. ACS Appl Mater Interfaces 9(13):11332–11336
122. Isaac IO et al (2018) Novel acridine-based thiosemicarbazones as 'turn-on'chemosensors for selective recognition of fluoride anion: a spectroscopic and theoretical study. Roy Soc Open Sci 5(7):180646
123. Patra L et al (2020) A selective fluorogenic chemosensor for visual detection of chemical warfare reagent mimic diethylchlorophosphate. J Photochem Photobiol, A 388:112188
124. Wang Q, Wen X, Fan Z (2018) A Schiff base fluorescent chemsensor for the double detection of Al^{3+} and PPi through aggregation induced emission in environmental physiology. J Photochem Photobiol, A 358:92–99
125. Li C et al (2018) A carbon dots/rutin system for colorimetric and fluorimetric dual mode detection of Al^{3+} in aqueous solution. Analyst 143(22):5467–5473
126. Parsaee Z et al (2018) A novel high performance nano chemosensor for copper (II) ion based on an ultrasound-assisted synthesized diphenylamine-based Schiff base: design, fabrication and density functional theory calculations. Ultrason Sonochem 41:337–349
127. Ly NH, Seo C, Joo S-W (2016) Detection of copper (II) ions using glycine on hydrazine-adsorbed gold nanoparticles via Raman spectroscopy. Sensors 16(11):1785
128. Kumawat LK et al (2016) Novel synthesized antipyrine derivative based "Naked eye" colorimetric chemosensors for Al^{3+} and Cr^{3+}. Sens Actuators, B Chem 231:847–859
129. Li P et al (2017) An efficient "off–on" carbon nanoparticle-based fluorescent sensor for recognition of chromium (VI) and ascorbic acid based on the inner filter effect. J Mater Chem B 5(16):2979–2988

Chapter 11
Organic-Inorganic Nanohybrids-Based Sensors for Gases, Humidity, UV and Others

Sohail Shahzad, Komal Rizwan, and Muhammad Zubair

Abbreviations

anti-EpCAM	Epithelial cell adhesion molecule antibodies
CLCuKoV-Bur	Cotton leaf curl
CV	Crystal violet
Gr	Graphene
GCE	Glassy carbon electrode
l-Dopa Khokran virus-Burewala strain	l-3,4-dihydroxyphenylalanine
MWCNTs	Multi-walled carbon nanotubes
NRs	Nanorods
PDI	Polycrystalline perylene diimide
PANI	Polyaniline
PDDA	Poly(diallyldimethylammonium chloride)
R6G	Rhodamine 6 G
RH	Relative humidity
SWCNT-COOH	Carboxylated single-wall carbon nanotubes
SWCN	Single-walled carbon nanotube

S. Shahzad · K. Rizwan (✉)
Department of Chemistry, University of Sahiwal, Sahiwal 57000, Pakistan
e-mail: komal.rizwan45@yahoo.com

M. Zubair
Department of Chemistry, Government College University Faisalabad, Faisalabad 38000, Pakistan

K. Rizwan et al. (eds.), *Hybrid Nanomaterials*, Materials Horizons: From Nature to Nanomaterials, https://doi.org/10.1007/978-981-19-4538-0_11

1 Introduction

Nanotechnology is concerned with those materials which possess chemical and physical characteristics at nanoscale. Nanosensors are used to collect information at nanoscale and then transformed it into useful data for analysis. At least, one dimension of 100 nm is present in nanosensors. Nanosensors allow scientists to create new generation technologies. Nanosensors can be synthesized through to down, bottom up and self-assembly approaches. Nanohybrids are novel conjugates made up of organic and inorganic materials. Nanohybrids possess unique functionalities with enhanced physical and chemical properties. Nanohybrids possess highly porous framework, great catalytic potential and electrical potential. These materials have played great role in different fields of life particularly in mitigation of environmental pollutants [1–5]. Nanohybrids have been widely used to synthesize nanosensors [6, 7]. Nanohybrids of polymeric materials with the inorganic materials overcome the defects of polymer/material oxides and increased their response, sensitivity and stability. Polymeric nanohybrids with inorganic materials (metals, metal oxides, metal oxide semiconductors) are famous class of sensing materials for sensing of different environmental pollutants such as gases, pesticides, pharmaceuticals and dyes. Applications of organic inorganic nanohybrids for sensing and detection of various toxic gases, humidity, UV light and biosensing have been discussed in this chapter. We have also discussed the future perspective of nanohybrid-based nanosensors.

2 Organic-Inorganic Nanohybrids-Based Sensors for Sensing of Gases

Industrial revolution has increased the air pollution. Toxic gases like CO_2, CO, NO_2, SO_2 and H_2S are responsible to cause nausea, weight loss, dizziness, cancer and skin burning. Concentration of every gas which is present in our environment and breathed by humans without any side effect is represented as TLV (threshold limit value). These values are given in ppm. Effects of various toxic gases on health of human beings and their threshold limit values are given in Fig. 1. Continuous emission of gases in environment is responsible to cause global warming, depletion of ozone and acid rain. Gases may be introduced in atmosphere through natural and man-made sources. Eruption of volcanoes, thundering, cloud lightning, wood fire and live stocks are various natural sources responsible to introduce toxic gases in environment while ships, cars, aeroplanes, factories, domestic and agriculture activities are considered as main man-made sources (Fig. 2).

Conventional techniques for sensing toxic gases in environment have various drawbacks; therefore, there is extreme need of developing nanosensors to sense the toxic gases and ultimately controlling air pollution. Scientists have synthesized different nanosensors by using various organic-inorganic nanohybrids and various transduction elements to sense gases. Tsai et al. prepared the hybrid organic/inorganic

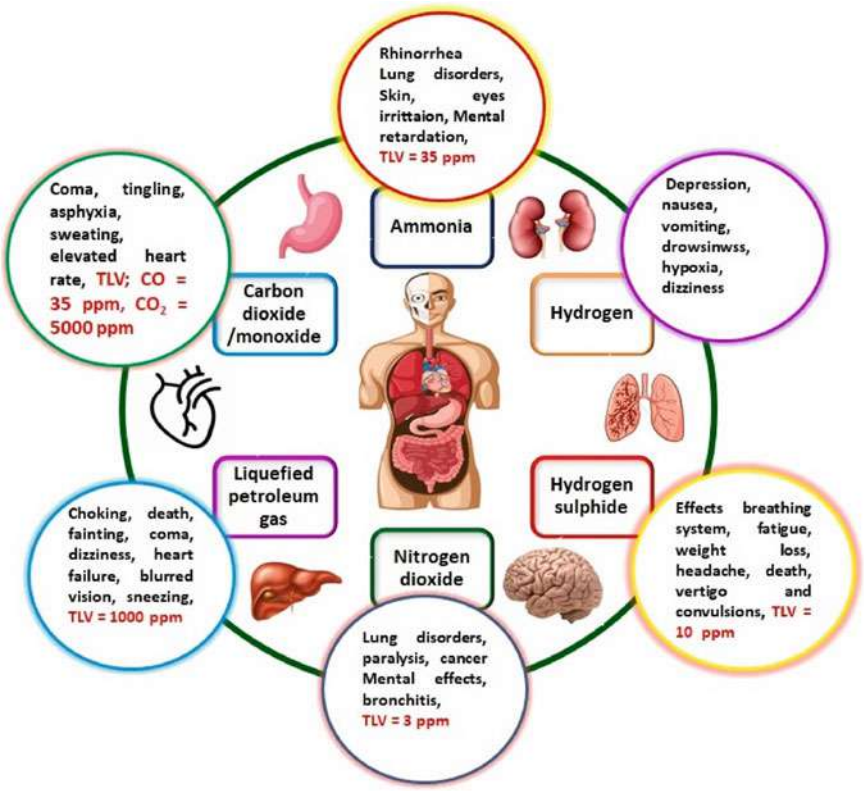

Fig. 1 Presentation of health effects of toxic gases on human beings. TLV is abbreviation for threshold limit value. Reprinted with permission from [14]

nanostructures-based carbon monoxide (CO) gas-detecting sensors by coating a membrane of polycrystalline perylene diimide (PDI) on ZnO nanorods (NRs). The successful application of coating of organic PDI membrane on ZnO NRs and formation of hybrid membrane on the sensing device were evaluated using various techniques including SEM, HRTEM, XRD, Raman spectroscopy, energy dispersive spectrometer and confocal laser scanning microscopy. The results indicated that addition of PDI on ZnO NRs effectively enhances interactions with CO gas, and ultimately, gas-sensing stability was increased, which led to enhance gas-sensing applications of CO. These hybrid PDI/ZnO organic/inorganic nanostructure materials have advantages of their compact size, low preparation cost, simple mode of fabrication and device stability and can be used in future gas-sensing applications [8]. Moon et al. reported the synthesis of a nanohybrid chemiresistive gas sensor functional at room temperature using zinc oxide nanorods and reduced graphene oxide (rGO) on a polydimethylsiloxane (PDMS) substrate which is elastic, stress-absorbable and three-dimensional (3D) micropatterned in nature. The synthesized nanohybrids have shown good mechanical strength (tensile strain of 20%), ultrasensitivity in the range

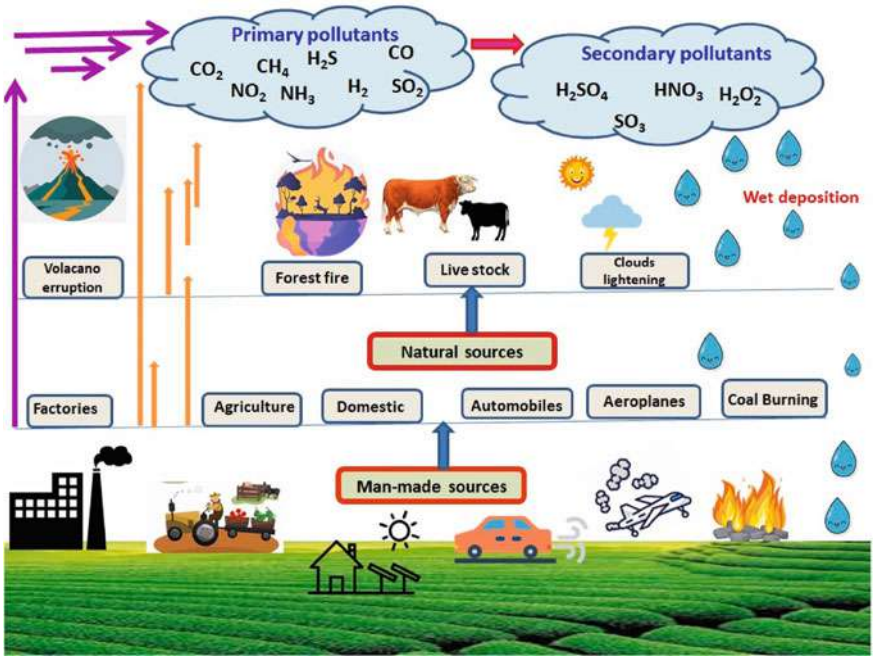

Fig. 2 Natural and man-made sources responsible for introduction of toxic gases in our environment. Reprinted with permission from [14]

of 40 ppb of NO_2 due to huge area of sensing and greater selectivity of NO_2 in comparison with SO_2, while the reduced graphene oxide eradicated the requirement of heating. Additionally, sensor also showed prompt response, excellent recovery times and higher reproducibility compared with reduced graphene oxide sensor [9]. Rapid and extremely sensitive carbon dioxide gas sensors were developed by simple vacuum thermal evaporation technique using porous silicon and molybdenum trioxide nanohybrid materials over microporous silicon as substrate. These nanohybrid sensors showed an outstanding sensitivity for CO_2 (15% at 150 ppm of CO_2), decent repeatability and quick response time of 8 s at 100 ppm concentration of CO_2 at a temperature of 250 °C. The lower limit of detection was calculated as 50 ppm. These properties make these sensors as promising materials for practical CO_2-sensing applications [10]. Sivakumar et al. fabricated the SnO_2 nanoparticles (NPs) decorated with various concentrations (0–5 wt. %) of reduced graphene oxide hybrids for gas-sensing applications. Similarly, some other gas sensors based on pure SnO_2 and composite SnO_2/rGO were also fabricated and evaluated for NO_2 and CO_2 gas sensing. The results indicated that due to synergistic effects of both SnO_2 and rGO, composite nanohybrid materials exhibited increased selectivity and repeatability along with high response (88.9), fast response (12 s) and recovery time (34 s) toward NO_2 gas [11]. Room temperature hydrogen gas (H_2) sensor was developed using hybrid nanostructures comprising graphene nanosheets (GNS) and silver sulfide (Ag_2S)

by employing microwave-assisted hydrothermal technique [12]. The SEM images displayed the rice-shaped Ag_2S nanoparticles impregnated onto graphene surfaces. The results indicated that synthesized hybrid materials (GNS-Ag_2S) showed better H_2 gas-sensing efficiency compared to pure Ag_2S nanoparticles. The GNS-Ag_2S-based hybrid materials exhibited maximum response of 45.5% for 150 ppm exposure of H_2 gas at room temperature. Hybrid materials (GNS-Ag_2S) showed 19 s of sensing response and recovery time of 31 s toward H_2 gas. Fast response time and better sensitivity of the prepared sensor were due to synergetic effect between GNS and Ag_2S hybrids. Gupta et al. have reported the synthesis of gas sensors based on pristine single walled carbon nanotubes (SWNT) and hybrid nanostructures-based SnO_2 functionalized SWNT for gas-sensing applications of NO_2 and NH_3 [13]. The responses of both sensors were compared toward NO_2 and NH_3 gases at their concentrations ranging from 2 to 20 ppm. In addition to this, adsorption kinetic studies were also performed for both types of sensors to evaluate their sensitivity toward NO_2 and NH_3 gases. Carbon nanotube (CNT) network electrical model and dependence on concentration of gas were also investigated. Langmuir adsorption model was applied to evaluate the change in conductivity with varying concentration of gas. Langmuir constants which are indicative of absorption capacity showed an increase in their values for functionalized SWNT as compared to pristine. This increase in surface absorption kinetics may be credited due to modification of SWNT with a functional group. Efficiency of organic-inorganic nanohybrids-based sensors for detection of different gases has been presented in detail in Table 1.

3 Organic-Inorganic Nanohybrids-Based Biosensors

A sensor generally consists of receptor (biological element), and a transducer plus readout system, while receptor in biosensors is composed of a biological element and it is made immovable and fixed onto converter in various ways. Working principle of biosensor has been presented in Fig. 3. Biosensors are used to sense the changes in biological-based processes and convert biological signal into electrical signal. Combination of biologically sensitive element and transducer shall convert biological material in respective electrical signal, and transducer output may be either in form of current or voltage. If output is obtained in form of current, then further it must be converted in voltage for further processing. Biosensors are used in wide applications in different fields of life (Fig. 4).

Sensitive flexible biosensors were developed using 3D layered silver nanoflowers (AgNFs)/graphene nanohybrids by rapid electrodeposition and transfer method [27]. Flexible eco-friendly graphene films are not only suitable for Ag atom absorption, but also provide a growth platform for the formation of AgNFs nanostructures and finally to serve as nano-spacer to formulate layered nanohybrids based on both AgNFs and graphene. These proposed flexible biosensors can be used for the detection of rhodamine 6 G, DNA and lysozyme molecules. Jalil et al. fabricated facile, eco-friendly, ultrasensitive and electrochemical nanohybrid biosensor

Table 1 Organic-inorganic nanohybrids-based sensors for sensing of gases

Nanohybrids-based nanosensors	Target gas	Sensitivity/Max. response	Linear Range/conc. checked	LOD	References
PDI/ZnO NRs	CO	–	–	–	[8]
RGO/ZnO NRs/PDMS	NO_2	–	–	40 ppb	[9]
p-Si/α-MoO_3	CO_2	15% at 150 ppm CO_2	–	50 ppm	[10]
SnO_2/rGO	NO_2	88.9	100–500 ppm	-	[11]
Ag_2S/GNS	H_2	45.5% for 150 ppm	50–150 ppm	–	[12]
SWCN/SnO_2	NO_2 and NH_3	–	2–20 ppm	–	[13]
CuO/rGO	NO_2	400.8% for 5 ppm	–	50 ppb	[15]
rGO/AuNP	H_2O_2	0.0641 μA μM^{-1} cm^{-2}	–	6.55 μM	[16]
CuO/rGO nanopellets	H_2O_2	84.39 μA mM^{-1} cm^{-2}	–	–	[17]
rGO/AgNP/TiO_2	H_2O_2		0.1–10 mM	20 μM	[18]
$CuCo_2O_4$/rGO	H_2O_2	320.3 μA mM^{-1} cm^{-2}	30–5010 μM	80 nM	[19]
TCN(II)–KOH-rGO	N_2O	1–16 ppm	–	1 ppm	[20]
ZnO/SiO2/rGO	1-propanol	–	150–450 ppm	156.8 ppm	[21]
rGO/Fe_3O_4/Cu_2O	H_2S		500 pM-100 μM	230 pM	[22]
NiO/rGO	CO_2 and acetone	83 counts /ppm	0–500 ppm		[23]
AgNPs/NPC/rGO/GCE	H_2O_2	493 μA mM^{-1} cm^{-2}	25–15,000 μM	1.4 μM	[24]
$MnFe_2O_4$/rGO	H_2O_2	–	0.1–4.0 mM	0.528 nM	[25]
Pd/rGO	H_2	–	–	–	[26]

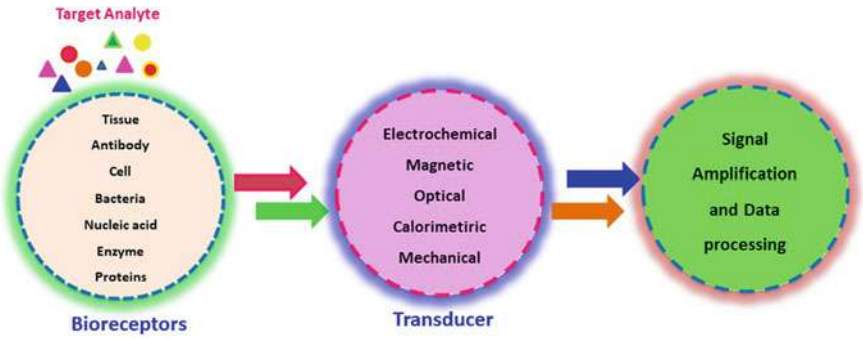

Fig. 3 General representation of working principle of biosensor

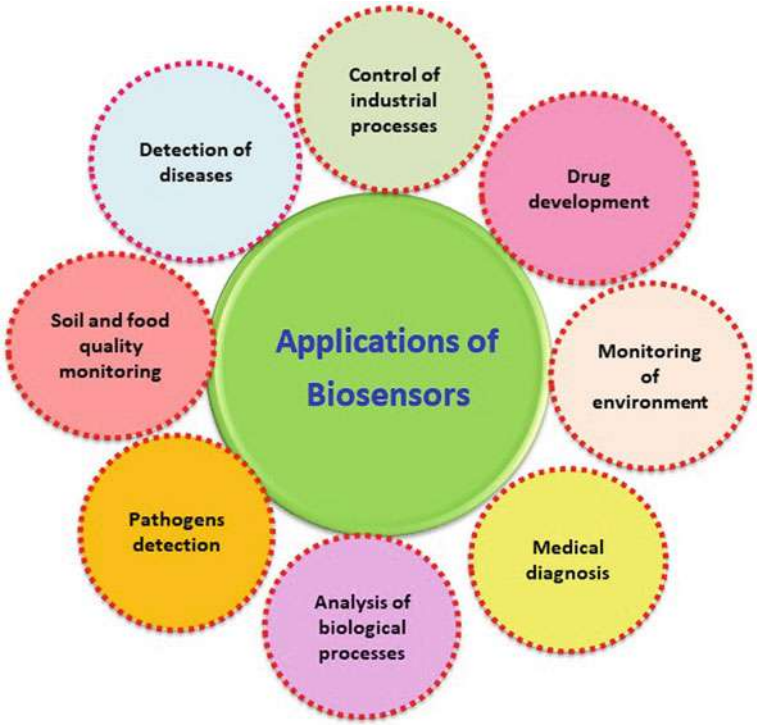

Fig. 4 Applications of biosensors in various fields

using molybdenum disulfide and reduced graphene oxide by biomolecular-assisted synthetic method. l-cysteine was used for reduction of graphene oxide to get reduced graphene oxide. Synthesized nanohybrid showed enhanced electrochemical properties by depositing electrophoretically onto indium tin oxide-coated glass substrate. The synthesized molybdenum disulfide, reduced graphene oxide and indium tin

oxide-based biosensor can detect epithelial cell adhesion molecule antibodies, which are specific to cancer biomarker, from 0.001 to 20 ng mL^{-1} concentration with limit of detection of 44.22 fg mL^{-1}. This outstanding performance of biosensor was attributed due to effective immobilization of antibodies on molybdenum disulfide and reduced graphene oxide surface, thus providing excellent specificity for epithelial cell adhesion molecule antigen. Final results indicated that fabricated biosensor has decent stability, selectivity and reproducibility and can be used for early detection of cancer biomarker [28]. A biosensor based on gold urchin (GU) surface and single walled carbon nanotube (SWCN) was developed for early-stage diagnosing of gastric cancer with high accuracy [29]. Synthesized hybrid biosensor forms a high-performance sensing platform which is called as dimicroelectrode junction (DMEJ). Biomarker for gastric cancer is a transcription factor, SRY-box containing gene-17. The results indicated that hybrid material has improved electric flow and showing the capture DNA attachment by reaching 1 aM limit of detection. Thus, the formulated SWCN-GU constructed DMEJ surface may be used for evaluation and diagnosing of gastric cancer progression. Development of a novel microchip-based biosensor has been reported using 3D copper nanostructures/graphene (CuNs-GO) nanohybrid by a biological synthetic approach for the efficient detection of major worldwide cotton infecting virus, i.e., cotton leaf curl Khokran virus-Burewala strain (CLCuKoV-Bur) [30]. Conduction and metallic character were imparted to (CuNs-GO) nanohybrid by both graphene sheets and copper nanoparticles (decorated on graphene sheets) of 10–15 nm size. This (CuNs-GO) nanohybrid has surface potential of +38 mV to serve as active interface of microchips and thus permits positive attaching of virus DNA. These hybridization procedures result in alteration in transporting electron between graphene sheets and consequently reduction in electrical (conductance) properties of devices. The prepared sensor showed excellent sensitivity with 200 pM limit of detection. Further studies on specificity patterns using various other viruses showed that sensor has minor response production ability, which is just 10–20% of signal, for other non-complementary DNAs which include cotton leaf curl Multan betasatellite, cotton leaf curl Multan alphasatellite and maize insect resistance1-cystein protease genes. Thus, the developed sensors can successfully be applied in virus-infected cotton fields for direct and simple observing of the virus infectivity level. Chen and co-workers formulated the synthesis of novel 3D graphene/gold–platinum–palladium nanoflower sensing platform for efficient sensing applications of circulating tumor DNA (ctDNA) (a biomarker for early diagnosis of cancer). The technique has many advantages including that it can detect low levels of ctDNA and amplification effectiveness along with great specificity for discerning single-nucleotide mismatches. Thus, the synthesized electrochemical biosensor exhibited great specificity and excellent execution in human serum assays and thus can potentially be used in clinical and diagnostic applications for efficient ctDNA detection [31].

Kumar and others fabricated a biosensor based on copper nanoparticle(CuNP) supported on reduced graphene oxide (rGO) for sensing and detection of dopamine and uric acid from human blood samples employing an easy and economical method. The fabricate (CuNP/rGO) sensor was characterized by various spectroscopic techniques including UV-Vis, Raman, atomic force, FTIR, and SEM and XRD

techniques. Efficiency of the fabricated sensor was assessed using cyclic voltammetry and electrochemical impedance spectroscopy [32]. Biosensing applications of organic-inorganic nanohybrids-based sensors have been presented in detail in Table 2.

4 Organic-Inorganic Nanohybrids-Based Sensors for Sensing of Toxic Organic Pollutants

A highly sensitive electrochemical device was developed to monitor toxicity levels of 2,4,6-trichlorophenol, polystyrene nanoplastics and bisphenol AF from water samples by using nanocomposites from tungsten disulfide nanosheets/hydroxylated multi-walled carbon nanotubes (WS_2/MWCNTs-OH) (Fig. 5). The sensor was prepared by modification of low-cost, disposable and energy-efficient screen-printed carbon electrode. Various types of characterizations including morphology, structure and electrochemical properties were evaluated by SEM, TEM, XRD and spectroscopic techniques including energy dispersive and electrochemical impedance. Viability of cells and electrochemical signals were monitored by cell line obtained from kidney of grass carp fish. Results indicated better sensitivity of WS_2/MWCNTs-OH-based sensor due to lower detection values as compared to MTT assay (IC_{50} for 2,4,6-trichlorophenol is 169.96 μM, for bisphenol AF is 21.88 μM and for polystyrene nanoplastics is 123.01 μg mL^{-1}). In addition to this, practical application of WS_2/MWCNTs-OH-based sensor was also assessed in chemical wastewater samples for its application in monitoring of environmental toxicity [48].

Atta et al. designed a sensitive electrochemical sensor comprising nanoparticles of gold, carbon nanotubes, nafion and 15-crown-5 ether to detect hydrazine hydrate from water samples [49]. Carbon nanotubes provide large surface area, while gold nanoparticles provide excellent electrical conduction properties. Similarly, nafion has large selectivity for cations which accelerates preconcentration of hydrazine hydrate and crown ether provides excellent binding capability and stable supramolecular complexes. Thus, each component of sensor imparted unique properties and overall a synergistic effect to composite for enhancement of current signal. The nanocomposite surface provided enormous electroactive surface; thus, conversion of hydrazine hydrate is more preferred over the synthesized sensor surface with value of oxidation potential +135 mV compared to +630 mV over glassy carbon/carbon nanotube electrode. Additionally, amperometric measurement of hydrazine hydrate was also accomplished from concentration range of 0.005–200 μM with LOD of 0.132 nM. A highly accurate and delicate sensor was prepared by Verma and his team using nanocomposite based on the reduced graphene oxide and molybdenum trioxide nanoparticles for detection of bisphenol A (BPA) [50]. Molybdenum trioxide nanoparticles were prepared in situ at low temperature by one-pot hydrothermal process onto the surface of reduced graphene oxide. Electrochemical behavior was

Table 2 Potential role of organic-inorganic nanohybrids for biosensing

Organic-inorganic nanohybrids	Target	Sensitivity/Max. response	Linear range/conc	LOD	References
AgNFs/graphene	R6 G, CV, lysozyme and DNA	–	–	10^{-15} M (R6 G), 10^{-13} M (CV)	[27]
MoS_2/rGO	Anti-EpCAM (cancer biomarker)	0.104 mA $ng^{-1}mLcm^{-2}$	0.001–20 ng mL^{-1}	44.22 fg mL^{-1}	[28]
CWCT/GU	SOX-17 (gastric cancer biomarker)	–	1 aM–10 fM	1 aM	[29]
CuNs-GO	CLCuKoV-Bur (cotton virus)	–	–	200 pM	[30]
Gr/AuPtPd	CtDNA (cancer biomarker)	-	0.01–500 pM	0.13 pM	[31]
CuNP/rGO	Dopamine and uric acid	–	–	–	[32]
AgNP/CQDs/rGO	Dopamine	–	0.1–300 μM	1.59 nM	[33]
Au-rGO composite on carbon strip with a specific antibody	Plasmodium vivax	–	–	~40 *vivax* infected Red Blood Cells (*Pv* iRBCs)/10 μL blood sample	[34]
Ag/TiO_2/rGO	CA 15-3 (breast cancer biomarker)	–	0.1–300 UmL^{-1}	0.07 UmL^{-1}	[35]
α-Fe_2O_3/rGO	Dopamine	–	1.0×10^{-8} to 9.0×10^{-4} mol/L)	3.26 nM	[36]
rGO/AuNP	ProGRP	–	–	0.136 fg/mL	[37]
rGO/AuNP	microRNA-122 biomarker	–	10 μM–10 pM	1.73 pM	[38]

(continued)

Table 2 (continued)

Organic-inorganic nanohybrids	Target	Sensitivity/Max. response	Linear range/conc	LOD	References
rGO/AuNP	Uric acid and ascorbic acid	0.31 $\mu A\ cm^{-2}\ \mu M^{-1}$ (uric acid)	10–500 $\mu mol\ dm^{-3}$ (uric acid)	3.6 μM (uric acid)	[39]
AuNP/AMBI/rGO	Progesterone	–	0.9×10^{-9} to 27×10^{-6} mol L^{-1}	0.28×10^{-9} mol L^{-1}	[40]
Cu/rGO-BP	Glucose	480 $\mu A\ cm^{-2}\ mM^{-1}$	2–25 mM	11 μM	[41]
2-D-TiC-rGO	Furazolidone	19.63 $\mu A\ \mu M^{-1}\ cm^{-2}$	0.01–111 μM	2 nM	[42]
MnO/Mn_3O_4/rGO	H_2O_2	274.15 $\mu A\ mM^{-1}\ cm^{-2}$	0.004 to 17 mM	0.1 μM	[43]
CeO_2/rGO-GCE	uric acid and tryptophan	–	0.1–20.0 μM	13.2 nM (uric acid)	[44]
AuNPs/rGO	Pyocyanin biomarker		1–100 μM	0.27 μM (PBS) 1.34 μm (human saliva) 2.3 μM (urine)	[45]
Apt/PANi–RGO–G*NPs/Au	DYS14 DNA aptamer sequence of Y-chromosome	–	1.0×10^{-16}–1.0×10^{-8} M	4.26×10^{-17} M	[46]
SWCNT-COOH/Nd_2O_3-SiO	*L*-DOPA	–	2–52 $\mu mol\ L^{-1}$	–	[47]

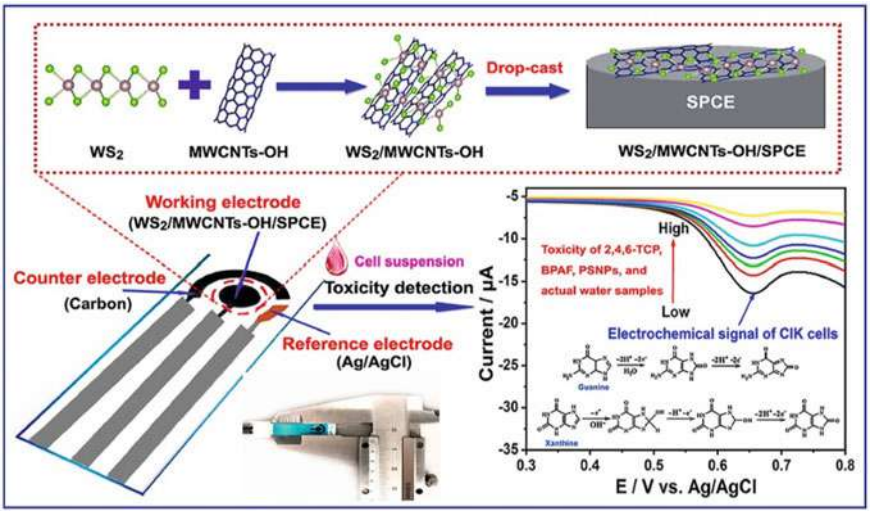

Fig. 5 Tungsten disulfide nanosheets/hydroxylated multi-walled carbon nanotubes-based electrochemical sensor for sensing of toxicity of 2,4,6-trichlorophenol, polystyrene nanoplastics and bisphenol AF in aqueous matrices. Published with permission from [48]

increased due to synergistic effects of both components. The 2D structure and chemical functionality of reduced graphene oxide deliver larger active surface area, while molybdenum trioxide nanoparticles provide enhanced conductivity, thus providing an outstanding platform for BPA detection. The prepared sensor showed good selectivity for BPA and high sensitivity of 13.96 μA with linearity range of 0.76 × 10^{-9} μM–0.820 μM, and limit of detection was calculated as 0.12 nM. Thus, the sensor can potentially be used in food industry for the detection of BPA. Wang and his co-workers prepared an electrochemical novel highly sensitive sensor from nanoparticles of gold, MoS_2 nanoflowers and ionic liquid functionalized graphene nanocomposite for BPA sensing from environmental water samples. It was concluded that sensor exhibited high activity for BPA, great sensitivity, selectivity and stability with linear range of 0.05–4.0 μM and LOD of 0.028 μM. The prepared sensor was also effectively applied for the detection of BPA from lake samples, and acceptable recoveries ranged from 95.7 to 105.4% [51].

In another study, a novel sensitive and highly selective electrochemical modified glassy carbon electrode (GCE) sensor was fabricated using a (CS/GQD/$NiMoO_4$) nanocomposite of chitosan (CS), graphene quantum dots (GQD) and nickel molybdate ($NiMoO_4$) for the detection of diazinon [52]. The sensor was prepared by a simple method of covalent immobilization of polymer and nanoparticle due to presence of functional groups on the surface of GCE. The results under optimized parameters indicated two linearity ranges between 0.1 and 330 μM and LOD of 30 nM. Finally, the prepared sensor showed high stability, reproducibility and selectivity for sensing applications of diazinon.

Gopi et al. reported the one-pot synthesis of a colloidal gel based on molybdenum bismuth vanadate ($MoBiVO_4$) and then further increased its charge transfer property by mixing with graphene oxide (GO) using sonochemical technique [53]. Synthesized $MoBiVO_4$/GO composite was used for the modification of glassy carbon electrode (GCE) and finally used to detect 2, 4, 6-trichlorophenol (TCP), which is an environmental pollutant. Thus, the modified $MoBiVO_4$/GO/GCE exhibited a enhanced response as compared to simple GCE electrode due to increased electron channeling property of GO together with $MoBiVO_4$. Further, the prepared GO/$MoBiVO_4$/GCE-based sensor showed LOD of 0.4 nM and greater sensitivity of 2.49 $\mu A\ \mu M^{-1}\ cm^{-2}$ with wide linearity range of 0.199–17.83 μM for TCP, which indicates its potential use in detection of TCP. Table 3 presents role of various organic-inorganic nanohybrids-based sensors for sensing of toxic organic pollutants.

5 Organic-Inorganic Nanohybrids-Based Sensors for Sensing of Humidity and UV

Sensing of humidity is important in various fields such as in agriculture for storage of seeds, food industry, electronic industry, biomedical field and monitoring of environment. Humidity sensors used the phenomena of alteration in physical features of sensitive element when directly exposed to humid environment because of adsorption and de-sorption of water. Different units like relative humidity (RH), PPM and dew/frost points are used to determine humidity. Different materials like polymers, polymer electrolytes, different composites and hybrids of polymers with inorganic materials have been reported for sensing of humidity. Nanohybrids of organic-inorganic materials are also reported for humidity sensing. They are found promising candidates for humidity sensing because of their great sensitivity toward external stimulus.

A humidity sensor was developed by Lin et al., using nanocomposite material based on various weight percentages of graphene doped by empty spheres of zirconium dioxide (Gr/HS-ZrO_2) by hydrothermal method [62]. Characterization was accomplished by TEM, XRD, EDX and Raman spectroscopy. Similarly, electrical properties of prepared Gr/HS-ZrO_2 nanocomposite were measured on the basis of variation in humidity on nanocomposite. The results indicated that Gr/HS-ZrO_2 nanocomposite incorporating 1 wt % graphene showed exceptional humidity detection applications as evident from high and rapid sensing response (11 s) and excellent recovery times (30 s). Thus, proposed sensor can potentially be used to monitor atmospheric humidity. Khan et al. designed the preparation of a stable, extremely sensitive humidity sensor which can work at room temperature using a polymer polyvinylpyrrolidone (PVP) and tungsten trioxide (WO_3) an inorganic compound by ultrasonication method. Synthesized PVP/WO_3 sensor was characterized by FTIR, XRD and HRTEM. It was concluded from results that sensor incorporating 20 wt % of WO_3 exhibited better response of 44.73 nF/%RH, short

Table 3 Potential role of different organic-inorganic nanohybrids for sensing of toxic organic pollutants

Organic-inorganic nanohybrids	Target	Sensitivity/Max. response	Linear Range/conc	LOD	References
WS_2/MWCNTs-OH	2,4,6-trichlorophenol, bisphenol AF, polystyrene-based nanoplastics	–	–	–	[48]
CNT/NF/CW/Au_{nano}	Hydrazine hydrate	–	0.005–200 μM	0.132 nM	[49]
rGO/ MoO_3Nps	BPA	13.96 μA	0.76 × 10^{-9} μM-0.820 μM	0.12 nM	[50]
AuNPs/MoS_2-NFs/IL-graphene	BPA	–	0.05–4.0 μM	0.028 μM	[51]
CS/GQD/$NiMoO_4$	diazinon	–	0.1 and 330 μM	30 nM	[52]
GO/$MoBiVO_4$/GCE	2,4,6-trichlorophenol	2.49 μA μM^{-1} cm^{-2}	0.199–17.83 μM	0.4 nM	[53]
TA/GO/AuNP	Ascorbic acid	19.30 μA·mM^{-1}	–	–	[54]
$ZnFe_2O_4$/PANI/rGO	p-nitrophenol	36.898 mA mM^{-1} cm^{-2}	1–100 μmol/L		[55]
$MnCo_2O_4$/GO	4-nitrophenol	6.868 μA μM^{-1} cm^{-2}	0.5–151.5 μM	0.012 μM	[56]
RGO/DHB/$Co(OH)_2$)	Hydrazine	1446.82 μA mM^{-1} cm^{-2}	5–1700 μM	0.165 μM	[57]
Gr/CuO/Cu_2O	Glucose	845 and 1108 μA cm^2 mM^{-1}	–	0.25 μM	[58]
PDDA/rGO/PANI	Triethylamine	–	2–100 ppm	74 ppb	[59]
MoS_2/rGO/MWCNTs/CB	Chloramphenicol	3.581 μA μM^{-1} cm^{-2}	–	–	[60]
V_2Se_9/rGO/GCE	2,4,6-trichlorophenol	22 μA μM^{-1} cm^{-2}	0.001–1150 μM	35.07 nM	[61]

response of 10 s, recovery time of 15 s and hysteresis value of 1.3% with excellent stability and repeatability. Results of nanocomposite PVP/WO_3-based sensor were also compared with pure PVP and WO_3 material-based sensors [63]. A very simple one-pot method was applied by Tsai et al., [64] for the synthesis of a ternary nanocomposite film based on platinum (Pt) nanoparticles, polythiophene and reduced graphene oxide (Pt/polythiophene/rGO) for designing of a highly sensitive, flexible and novel humidity sensor. In the first step, 2-thiophene methanol (2-TPM) was reacted with $PtCl_4^{2-}$ ions, releasing electrons which reduced simultaneously $PtCl_4^{2-}$ ions to Pt nanoparticles and GO to RGO by an oxidative polymerization procedure. The results indicated that Pt/polythiophene/RGO-based film incorporating 30 mg of Pt and 0.1 g of rGO displayed the highest sensitivity, flexibility and long-term stability. Additionally, this humidity sensor also presented an acceptable linearity and working humidity's ranges, a low hysteresis, a short recovery time and low temperature dependence. Humidity sensing mechanism was also explained by complex impedance spectra and thus revealed that (H_3O^+) ions dominate conductance process. Kalim et al. designed the preparation of efficient and cost-effective humidity sensor by using a simple spray coating of multilayers of carbon nanotubes and zinc oxide (CNTs/ZnO) and carbon nanotubes, zinc oxide and silver (CNTs/ZnO/Ag) on cellulose. In the initial step, all the conductive inks including CNTs, ZnO and Ag nanoparticles were sonicated for 15 min in each case and then sprayed over conducting cellulose polymer substrate. The surface studies established the presence of CNTs and cellulose conducting networks and also the layers of ZnO and Ag nanoparticles. The overall results of sensing measurements exhibited that CNTs/ZnO/Ag nanocomposite showed low resistance and improved current as compared to CNTs/ZnO nanocomposite [65]. Sensing of UV is important to prevent human beings from lethal diseases.

Tsai et al. fabricated the hybrid organic/inorganic photo sensing nanocomposites for UV light detection applications by depositing a membrane of polycrystalline perylene diimide (PDI) on ZnO nanorods (NRs). The results concluded that addition of PDI on ZnO NRs effectively increases the CO gas binding capability and also gas-sensing stability, thus overall enhancing CO gas-sensing applications. These hybrid PDI/ZnO organic/inorganic nanostructure material impulse responses were measured, and the results indicated that these hybrid materials can effectively increase the UV light absorption efficiency by the addition of PDI on ZnO NRs surface. Due to their various advantages including their compact size, low preparation cost, simple mode of fabrication and device stability, these can be used in future for portable hazardous UV light-sensing applications [8]. Table 4 presents the potential role of organic-inorganic-based nanosensors for sensing of humidity and UV.

6 Challenges and Future Perspectives

In this chapter, we have reviewed applications of various organic-inorganic nanohybrids in sensing of gases, organic molecules, humidity and UV. Various organic

Table 4 Different organic-inorganic nanohybrids-based sensors for sensing of humidity and UV

Organic-inorganic nanohybrids	Target	Sensing/response	Rapid response (sec)	Recovery time (s)	References
Gr/HS-ZrO_2	Humidity	S = 1740	11	30 s	[62]
PVP/WO_3	Humidity	44.73 nF/%RH	10	15	[63]
Pt/polythiophene/RGO	Humidity	0.0474 sensitivity	73	–	[64]
CNTs/ZnO and CNTs/ZnO/Ag sprayed on cellulose	Humidity	–	–	–	[65]
chitosan-CeO_2-CdO	Humidity	5–95% RH	1 s	1 s	[66]
Guar gum xanthate/CuS	Humidity	10–80% RH	–	–	[67]
PDI/ZnO NRs	UV light	Significant response	–	–	[8]
Cellulose/ZnO	UV light	Significant response	–	–	[68]

materials (CNTS, PVP, chitosan, cellulose, rGO, polythiophene, Gr, SWCN, etc.) hybridized with various inorganic materials (metals, metal oxides, etc.) have been discussed for their promising detection and sensing potential for various gases and other described pollutants. These nanohybrids are potent for sensing in low limits of detection ranging from ppb to ppm with quick response and less recovery time, wide linear range and great sensitivity as described in Tables 1, 2, 3 and 4. The sensors designed from nanomaterials are beneficial due to small in size and easily portable to various detecting fields. Conclusively, these materials found promising for environmental monitoring, but still limitations exist which are important to solve for further development of nanohybrids-based sensors. Economic routes should be introduced for designing of sensors at commercial scale applications. Nanohybrid materials must be stable at various conditions, and they should have also the capability to be used for numerous times.

References

1. Rizwan K, Rasheed T, Bilal M (2022) 10—Nano-biodegradation of polymers. In: HMN Iqbal, M Bilal, TA Nguyen, G Yasin (Eds) Biodegradation and biodeterioration at the nanoscale. Elsevier, pp 213–238
2. Shakeel A, Rizwan K, Farooq U, Iqbal S, Altaf AA (2022) Advanced polymeric/inorganic nanohybrids: an integrated platform for gas sensing applications. Chemosphere 133772
3. Kausar F, Bagheri AR, Rasheed T, Bilal M, Rizwan K, Nguyen TA, Iqbal HMN (2022) Chapter 7—nanomaterials for removal of heavy metals from wastewater. In: A Denizli, N Ali, M Bilal, A Khan, TA Nguyen (Eds) Nano-Biosorbents for decontamination of water, air, and soil pollution. Elsevier, pp 135–161
4. Rasheed T, Hussain T, Anwar MT, Ali J, Rizwan K, Bilal M, Alshammari FH, Alwadai N, Almuslem AS (2021) Hybrid nanofluids as renewable and sustainable colloidal suspensions

for potential photovoltaic/thermal and solar energy applications. Front Chem 9(802)
5. Rizwan K, Bilal M, Slimani Y, Show PL, Rtimi S, Roy A, Iqbal HMN (2022) Hydrogen-based sono-hybrid catalytic degradation and mitigation of industrially-originated dye-based pollutants. Int J Hydrogen Energy
6. Rasheed T, Rizwan K (2022) Metal-organic frameworks based hybrid nanocomposites as state-of–the-art analytical tools for electrochemical sensing applications. Biosens Bioelectron 199:113867
7. Rizwan K, Rahdar A, Bilal M, Iqbal HMN (2022) MXene-based electrochemical and biosensing platforms to detect toxic elements and pesticides pollutants from environmental matrices. Chemosphere 291:132820
8. Tsai Y-S, Tsai SC, Kuo CC, Chan WL, Lin WH, Wu YS, Lin YS, Li MH, Kuo M-Y, Chen H (2021) Organic/inorganic hybrid nanostructures of polycrystalline perylene diimide decorated ZnO nanorods highly enhanced dual sensing performance of UV light/CO gas sensors. Results Phys 24:104173
9. Moon D-B, Bag A, Lee H-B, Meeseepong M, Lee D-H, Lee N-E (2021) A stretchable, room-temperature operable, chemiresistive gas sensor using nanohybrids of reduced graphene oxide and zinc oxide nanorods. Sens Actuators, B: Chem 130373
10. Thomas T, Kumar Y, Ramón JAR, Agarwal V, Guzmán SS, Reshmi R, Pushpan S, Loredo SL, Sanal K (2021) Porous silicon/α-MoO_3 nanohybrid based fast and highly sensitive CO_2 gas sensors. Vacuum 184:109983
11. Sivakumar R, Krishnamoorthi K, Vadivel S, Govindasamy S (2021) Progress towards a novel NO_2 gas sensor based on SnO_2/RGO hybrid sensors by a facial hydrothermal approach. Diam Relat Mater 116:108418
12. Parveen RA, Rakkesh RA, Durgalakshmi D, Balakumar S (2021) Graphene-Ag_2S hybrid nanostructures: a hybrid gas sensor for room temperature hydrogen sensing application. Mater Lett 130470
13. Gupta S, Anand A, Kumar R (2021) Study of adsorption kinetics of pristine and SnO_2 functionalized carbon nanotubes as environment gas sensors for NO_2 and NH_3 gases. Mater Today Proc
14. Shakeel A, Rizwan K, Farooq U, Iqbal S, Altaf AA (2022) Advanced polymeric/inorganic nanohybrids: an integrated platform for gas sensing applications. Chemosphere 294:133772
15. Bai H, Guo H, Wang J, Dong Y, Liu B, Xie Z, Guo F, Chen D, Zhang R, Zheng Y (2021) A room-temperature NO_2 gas sensor based on CuO nanoflakes modified with rGO nanosheets. Sens Actuators, B Chem 337:129783
16. Patella B, Buscetta M, Di Vincenzo S, Ferraro M, Aiello G, Sunseri C, Pace E, Inguanta R, Cipollina C (2021) Electrochemical sensor based on rGO/Au nanoparticles for monitoring H_2O_2 released by human macrophages. Sens Actuators, B Chem 327:128901
17. Lohar G, Pore O, Fulari A (2021) Electrochemical behavior of CuO/rGO nanopellets for flexible supercapacitor, non-enzymatic glucose, and H_2O_2 sensing application. Ceram Int 47(12):16674–16687
18. Li L, Zhai L, Liu H, Li B, Li M, Wang B (2021) A novel H_2O_2 photoelectrochemical sensor based on ternary RGO/Ag-TiO_2 nanotube arrays nanocomposite. Electrochim Acta 374:137851
19. Jiang L, Zhao Y, Zhao P, Zhou S, Ji Z, Huo D, Zhong D, Hou C (2021) Electrochemical sensor based on reduced graphene oxide supported dumbbell-shaped $CuCo_2O_4$ for real-time monitoring of H_2O_2 released from cells. Microchem J 160:105521
20. Ramu A, Umar A, Gopi S, Algadi H, Albargi H, Ibrahim AA, Alsaiari MA, Wang Y, Choi D (2021) Tetracyanonickelate (II)/KOH/reduced graphene oxide fabricated carbon felt for mediated electron transfer type electrochemical sensor for efficient detection of N_2O gas at room temperature. Environ Res 111591
21. Samadi S, Nouroozshad M, Zakaria SA (2021) ZnO@ SiO_2/rGO core/shell nanocomposite: a superior sensitive, selective and reproducible performance for 1-propanol gas sensor at room temperature. Mater Chem Phys 124884
22. Gu W, Zheng W, Liu H, Zhao Y (2021) Electroactive Cu_2O nanocubes engineered electrochemical sensor for H_2S detection. Anal Chim Acta 1150:338216

23. Shanavas S, Ahamad T, Alshehri SM, Acevedo R, Anbarasan PM (2021) A facile microwave route for fabrication of NiO/rGO hybrid sensor with efficient CO_2 and acetone gas sensing performance using clad modified fiber optic method. Optik 226:165970
24. Zhang Y, Liu Y-Q, Chu W, Bai Y (2021) ZIF-8-derived N-doped porous carbon coated reduced graphene oxide as ultrasensitive platform and its application for electrochemical sensing. J Alloy Compd 857:157604
25. Zhao X, Li Z, Chen C, Xie L, Zhu Z, Zhao H, Lan M (2021) MnFe2O4 nanoparticles-decorated graphene nanosheets used as an efficient peroxidase minic enable the electrochemical detection of hydrogen peroxide with a low detection limit. Microchem J 166:106240
26. Hashtroudi H, Kumar R, Savu R, Moshkalev S, Kawamura G, Matsuda A, Shafiei M (2021) Hydrogen gas sensing properties of microwave-assisted 2D Hybrid Pd/rGO: effect of temperature, humidity and UV illumination. Int J Hydrogen Energy 46(10):7653–7665
27. Lv K, Wei Q, Zhu T, Zhao X, Li Z, Xu Y, Chen S, Li Z, Fan X, Lu W (2021) Sensitive flexible biosensor based on the three-dimensional layered AgNFs@ graphene nanohybrids. Sens Actuators, B Chem 336:129737
28. Jalil O, Pandey CM, Kumar D (2021) Highly sensitive electrochemical detection of cancer biomarker based on anti-EpCAM conjugated molybdenum disulfide grafted reduced graphene oxide nanohybrid. Bioelectrochemistry 138:107733
29. Yu Z, Gopinath SC, Lakshmipriya T, Anbu P (2021) Single-walled carbon nanotube-gold urchin nanohybrid for identifying gastric cancer on dimicroelectrodes junction. J Taiwan Inst Chem Eng 121:108–114
30. Rafiq A, Taj A, Haider S, Tahir MA, Zia R, Moschou D, Iqbal MJ, Khan WS, Mansoor S, Bajwa SZ (2021) Biologically prepared copper-graphene nanohybrid as the interface of microchips for sensitive detection of crop viruses. J Market Res 12:727–738
31. Chen M, Wu D, Tu S, Yang C, Chen D, Xu Y (2021) CRISPR/Cas9 cleavage triggered ESDR for circulating tumor DNA detection based on a 3D graphene/AuPtPd nanoflower biosensor. Biosens Bioelectron 173:112821
32. Kumar NS, Al-Ghurabi EH, Asif M, Boumaza M (2021) Retrieving and morphological portrayal of Cu-nanoparticle impregnated reduced graphene oxide (CuNP@ rGO) electrochemical bio-sensor. Sens Actuators, A 329:112826
33. Han G, Cai J, Liu C, Ren J, Wang X, Yang J, Wang X (2021) Highly sensitive electrochemical sensor based on xylan-based Ag@ CQDs-rGO nanocomposite for dopamine detection. Appl Surf Sci 541:148566
34. Singh S, Chatterjee M, Chatterjee K, Arun RK, Chanda N (2021) Design of a point-of-care device for electrochemical detection of P. vivax infected-malaria using antibody functionalized rGO-gold nanocomposite. Sens Actuators B: Chem 327:128860
35. Shawky AM, El-Tohamy M (2021) Signal amplification strategy of label-free ultrasenstive electrochemical immunosensor based ternary Ag/TiO_2/rGO nanocomposites for detecting breast cancer biomarker CA 15-3. Mater Chem Phys 124983
36. Liu J, Sun L, Li G, Hu J, He Q (2021) Ultrasensitive detection of dopamine via electrochemical route on spindle-like α-Fe_2O_3 Mesocrystals/rGO modified GCE. Mater Res Bull 133:111050
37. Liu Y, Si S, Dong S, Ji B, Li H, Liu S (2021) Ultrasensitive electrochemical immunosensor for ProGRP detection based on 3D-rGO@ Au nanocomposite. Microchem J 106644
38. Kasturi S, Eom Y, Torati SR, Kim C (2021) Highly sensitive electrochemical biosensor based on naturally reduced rGO/Au nanocomposite for the detection of miRNA-122 biomarker. J Ind Eng Chem 93:186–195
39. Mazzara F, Patella B, Aiello G, O'Riordan A, Torino C, Vilasi A, Inguanta R (2021) Electrochemical detection of uric acid and ascorbic acid using r-GO/NPs based sensors. Electrochim Acta 388:138652
40. Zhao X, Zheng L, Yan Y, Cao R, Zhang J (2021) An electrocatalytic active AuNPs/5-Amino-2-mercaptobenzimidazole/rGO/SPCE composite electrode for ultrasensitive detection of progesterone. J Electroanal Chem 882:115023
41. Zhu T, Wang X, Chang W, Zhang Y, Maruyama T, Luo L, Zhao X (2021) Green fabrication of Cu/rGO decorated SWCNT buckypaper as a flexible electrode for glucose detection. Mater Sci Eng, C 120:111757

42. Rajakumaran R, Anupriya J, Chen S-M (2021) 2D-Titanium carbide MXene/RGO composite modified electrode for selective detection of carcinogenic residue furazolidone in food and biological samples. Mater Lett 297:129979
43. Li Y, Tang L, Deng D, He H, Yan X, Wang J, Luo L (2021) Hetero-structured MnO-Mn_3O_4@rGO composites: synthesis and nonenzymatic detection of H_2O_2. Mater Sci Eng, C 118:111443
44. Wu B, Xiao L, Zhang M, Yang C, Li Q, Li G, He Q, Liu J (2021) Facile synthesis of dendritic-like CeO_2/rGO composite and application for detection of uric acid and tryptophan simultaneously. J Solid State Chem 296:122023
45. Rashid JIA, Kannan V, Ahmad MH, Mon AA, Taufik S, Miskon A, Ong KK, Yusof NA (2021) An electrochemical sensor based on gold nanoparticles-functionalized reduced graphene oxide screen printed electrode for the detection of pyocyanin biomarker in Pseudomonas aeruginosa infection. Mater Sci Eng C 120:111625
46. Malmir M, Arjomandi J, Khosroshahi AG, Moradi M, Shi H (2021) Label-free E-DNA biosensor based on PANi-RGO-G* NPs for detection of cell-free fetal DNA in maternal blood and fetal gender determination in early pregnancy. Biosens Bioelectron 113356
47. Đurđić S, Stanković V, Vlahović F, Ognjanović M, Kalcher K, Manojlović D, Mutić J, Stanković DM (2021) Carboxylated single-wall carbon nanotubes decorated with SiO_2 coated-Nd_2O_3 nanoparticles as an electrochemical sensor for L-DOPA detection. Microchem J 168:106416
48. Wu G, Zheng H, Xing Y, Wang C, Yuan X, Zhu X (2021) A sensitive electrochemical sensor for environmental toxicity monitoring based on tungsten disulfide nanosheets/hydroxylated carbon nanotubes nanocomposite. Chemosphere 131602
49. Atta NF, Galal A, El-Gohary AR (2021) An innovative design of hydrazine hydrate electrochemical sensor based on decoration of crown ether/Nafion/carbon nanotubes composite with gold nanoparticles. J Electroanal Chem 888:115165
50. Verma D, Yadav AK, Mukherjee MD, Solanki PR (2021) Fabrication of a sensitive electrochemical sensor platform using reduced graphene oxide-molybdenum trioxide nanocomposite for BPA detection: an endocrine disruptor. J Environ Chem Eng 9(4):105504
51. Wang Y, Liang Y, Zhang S, Wang T, Zhuang X, Tian C, Luan F, Ni S-Q, Fu X (2021) Enhanced electrochemical sensor based on gold nanoparticles and MoS_2 nanoflowers decorated ionic liquid-functionalized graphene for sensitive detection of bisphenol A in environmental water. Microchem J 161:105769
52. Ghiasi T, Ahmadi S, Ahmadi E, Olyai MRTB, Khodadadi Z (2021) Novel electrochemical sensor based on modified glassy carbon electrode with graphene quantum dots, chitosan and nickel molybdate nanocomposites for diazinon and optimal design by the Taguchi method. Microchem J 160:105628
53. Gopi PK, Ravikumar CH, Chen S-M, Chen T-W, Ali MA, Al-Hemaid FM, El-Shikh MS, Alnakhli A (2021) Tailoring of bismuth vanadate impregnated on molybdenum/graphene oxide sheets for sensitive detection of environmental pollutants 2, 4, 6 trichlorophenol. Ecotoxicol Environ Saf 211:111934
54. Chen W-L, Dai Y-M, Huang B-S, Lai G-H, Tsai M-H (2021) Preparation and electrochemical sensor application of tetra aniline/graphene oxide/gold nanoparticle composites. Colloids Surf A Physicochemical Eng Aspects 127110
55. Wei W, Yang S, Hu H, Li H, Jiang Z (2021) Hierarchically grown $ZnFe_2O_4$-decorated polyaniline-coupled-graphene nanosheets as a novel electrocatalyst for selective detecting p-nitrophenol. Microchem J 160:105777
56. Manjula N, Chen S-M (2021) Simple strategy synthesis of manganese cobalt oxide anchored on graphene oxide composite as an efficient electrocatalyst for hazardous 4-nitrophenol detection in toxic tannery waste. Microchem J 106514
57. Mohiuddin AK, Ahmed MS, Roy N, Jeon S (2021) Electrochemical determination of hydrazine in surface water on $Co(OH)_2$ nanoparticles immobilized on functionalized graphene interface. Appl Surf Sci 540:148346
58. Cuara E, Sierra U, Mercado A, Barriga-Castro ED, Cortés A, Gallardo-Vega C, Valle-Orta M, Fernández S (2021) Synthesis of copper oxides-graphene composites for glucose sensing. Carbon Trends 4:100050

59. Wang Z, Chang J, Hu Q, Zhi H, Feng L (2021) A novel wearable TEA sensor based on PDDA-functionalized graphene/polyaniline composite self-powered by a triboelectric nanogenerator. Sens Actuators B: Chem 130308
60. Gao S, Zhang Y, Yang Z, Fei T, Liu S, Zhang T (2021) Electrochemical chloramphenicol sensors-based on trace MoS_2 modified carbon nanomaterials: insight into carbon supports. J Alloy Compd 872:159687
61. Hwa K-Y, Ganguly A, Santhan A, Sharma TSK (2021) Vanadium selenide decorated reduced graphene oxide nanocomposite: a co-active catalyst for the detection of 2, 4, 6–Trichlorophenol. Chemosphere 282:130874
62. Lin W-D, Hong R-Y, Chuang M-H, Wu R-J, Chavali R-J (2021) Enhanced performance of humidity sensor based on Gr/hollow sphere ZrO_2 nanocomposites. Sens Actuators A: Phys 112872
63. Khan HU, Tariq M, Shah M, Ullah S, Ahsan AR, Rahim A, Iqbal J, Pasricha R, Ismail I (2021) Designing and development of polyvinylpyrrolidone-tungsten trioxide (PVP-WO_3) nanocomposite conducting film for highly sensitive, stable, and room temperature humidity sensing. Mater Sci Semicond Process 134:106053
64. Tsai M-S, Su P-G, Lu C-J (2020) Fabrication of a highly sensitive flexible humidity sensor based on Pt/polythiophene/reduced graphene oxide ternary nanocomposite films using a simple one-pot method. Sens Actuators, B Chem 324:128728
65. Kalim B, Ansar MT, Ullah Z, Abbas SK, Riaz S, Siddiqi SA, Atiq S (2020) CNTs/ZnO and CNTs/ZnO/Ag multilayers spray coated on cellulose fiber for use as an efficient humidity sensor. Ceram Int 46(16):25593–25597
66. Chani MTS (2022) Fabrication and characterization of chitosan-CeO_2-CdO nanocomposite based impedimetric humidity sensors. Int J Biol Macromol 194:377–383
67. Le T-A, Zouheir M, Nikiforow K, Khatib M, Zohar O, Haick H, Huynh T-P (2022) Synthesis, characterization, and humidity-responsiveness of guar gum xanthate and its nanocomposite with copper sulfide covellite. Int J Biol Macromol 206:105–114
68. Mun S, Kim HC, Ko H-U, Zhai L, Kim JW, Kim J (2017) Flexible cellulose and ZnO hybrid nanocomposite and its UV sensing characteristics. Sci Technol Adv Mater 18(1):437–446

Chapter 12
Application of Organic-Inorganic Nanohybrids in Wastewater Treatment

Azka Abdur Rehman, Zaeem Bin Babar, Shahid Munir, Mashhood Urfi, Sumaira Kanwal, Muhammad Naeem Ashraf, and Komal Rizwan

1 Introduction

Organic-inorganic nanohybrids possess large surface areas, higher number of pores, and channels in between the edges and planes giving remarkable aspect ratios, low masses and higher volumes, and remarkable mechanical strengths. Above all, there is an edge of designing and fabrication of nanohybrids according to the desired application while playing with the key features of the parent materials and furthermore their synergy with each other. There are multiple categories of water pollutants raising exponential threats to the ecosystem and eventually to public health. The most common water pollutants include pharmaceutical waste (e.g., paracetamol, steroids, diclofenac, and antibiotics.) [26], heavy metals (Cr, Zn, Hg, Cu, Pb, Cd, and Zn.) [52] pesticides [56], dyes [78, 107], waterborne pathogens [73], and radionuclides [38]. This chapter is structured to emphasize the sources, toxicity, and challenges associated with toxic pharmaceutical wastes, heavy metals, and pesticides in wastewater and potential of organic and inorganic nanohybrids in adsorptive and photocatalytic remediation of these pollutants. Main sources of pharmaceutical

A. A. Rehman · Z. B. Babar · S. Munir · M. Urfi
Institute of Energy and Environmental Engineering, University of the Punjab, Lahore, Pakistan

Z. B. Babar
Institute of Environmental Sciences and Engineering (IESE), School of Civil and Environmental Engineering (SCEE), National University of Sciences and Technology (NUST), Islamabad, Pakistan

S. Kanwal
Department of Environmental Sciences, University of Narowal, Narowal, Pakistan

M. N. Ashraf
W2Systems, Brisbane, CA 94005, USA

K. Rizwan (✉)
Department of Chemistry, University of Sahiwal, Sahiwal 57000, Pakistan
e-mail: komal.rizwan45@yahoo.com

K. Rizwan et al. (eds.), *Hybrid Nanomaterials*, Materials Horizons: From Nature to Nanomaterials, https://doi.org/10.1007/978-981-19-4538-0_12

based wastes includes pharmaceutical industrial, medical, and domestic effluents [48], whereas heavy metal sources may include natural contamination and anthropogenic activities. Natural sources of heavy metals are metallic crusts leaching, sedimentation and re-deposition, soil erosion, and metallic evaporation from water surfaces to the ground and soil. Generation of heavy metal contamination is inevitable in anthropogenic activities such as ore smelting, electroplating, petrochemical industrial waste, and mining. [91]. The major source of pesticides is agricultural activity from start of crop planting to its production and storage [24]. After contamination of water, these pollutants travel from several sources to humans including aquatic life to agricultural plants. These pollutants are causing major threats to humans in several ways. Figure 1 presents the toxic repercussions of pharmaceutical, metals, and pesticide-based pollutants on public health. Such emerging threats are bringing novel diseases and gene mutations in humans and animals. This needs to be addressed appropriately with effective remediation techniques and methods. Researchers have proposed several promising materials that shows potential of maximum removal of water contamination with zero footprint. Organic-inorganic nanohybrids are one such

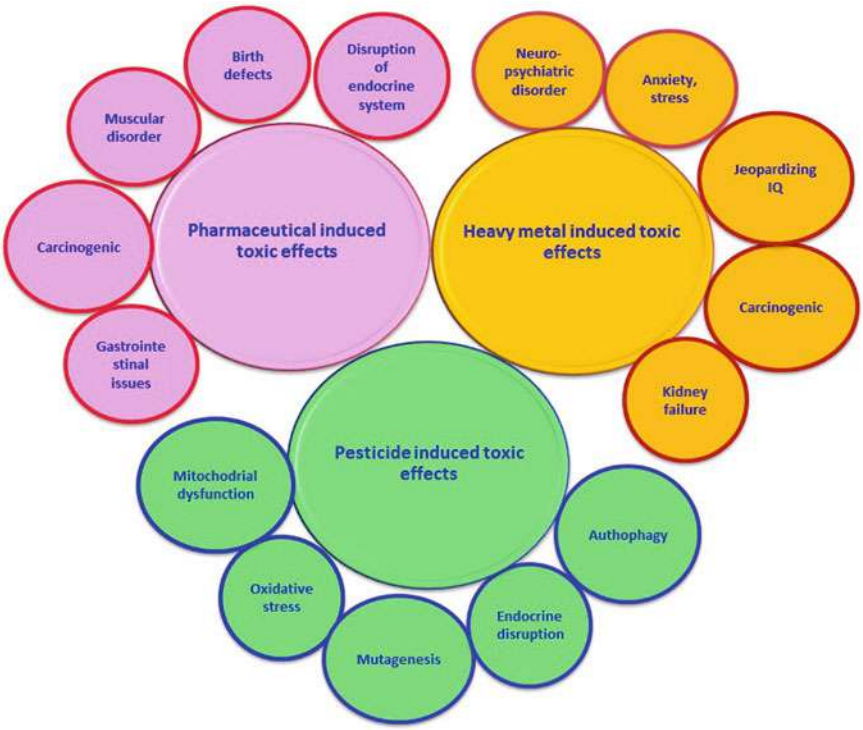

Fig. 1 Toxic repercussions of pharmaceutical, noxious metals, and pesticide-based pollutants on human health

category to attain maximum level of pollutant mitigation with least environmental impact [8, 72, 116].

2 Potential Role of Organic-Inorganic Nanohybrids for Removal of Pollutants from Wastewater

2.1 Organic-Inorganic Nanohybrids for Removal of Pharmaceuticals

Adsorptive and photocatalytic removal of pharmaceuticals from wastewaters are the most favorable technologies. The graphical representation of both these removal processes is shown in Fig. 2.

2.1.1 Adsorptive Removal of Pharmaceuticals

Current global scenario depicts an exponential growth in pharmaceutical and medical fields, owing to sustainable human health. However, such rapid growth of pharmaceutical industry is adversely impacting the natural environment. The negative consequences of untreated pharmaceutical waste have caused serious threats to public health. An increased concentration of pharmaceutical compounds in wastewaters

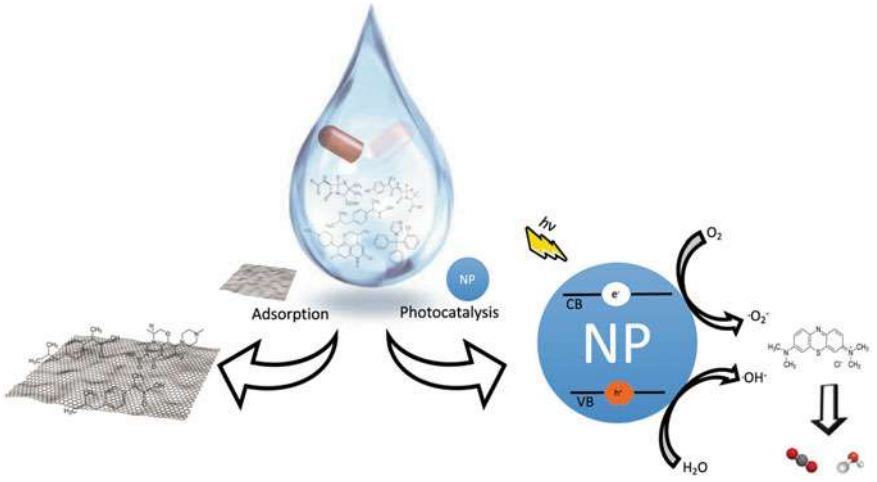

Fig. 2 Representation of adsorptive and photocatalytic removal mechanism of pharmaceuticals. This is adopted from an open access article distributed under the Creative Commons Attribution License [23]

has resulted in an emergent call to explore the effective ways to eradicate pharmaceutical compounds from wastewater [12]. Organic-inorganic nanohybrid materials have shown a promising role in adsorption, the most reliable way of pollutant removal from wastewater so far. These nanohybrids have tunable surfaces, high adsorption capacities, hydrophobicity, and high mechanical strength. Such characteristics of organic-inorganic nanohybrids make them suitable candidates for effective adsorptive treatment of several pharmaceutical pollutants in wastewater (Table 1). These adsorbents also tend to embark several cycles of regeneration and effective re-adsorption [90, 96].

Graphene-based organic-inorganic nanohybrids showed the maximum adsorption capacities [88, 90, 96] for effective abatement of pharmaceutical pollutants. The superior adsorption capability (282.9 mg g^{-1}) of magnetic chitosan-grafted graphene oxide composite may be due to presence of –COOH and –OH functional moieties on rough surfaces of graphene oxide [96]. This combination resulted in massive electrostatic forces of attraction and π-π electron interactions. Nevertheless, adjustment of the reaction conditions such as pH and less ionic strength has played major part in the enhanced adsorption process. Fe_3O_4@graphene (Fe_3O_4@G)-based magnetic nanocomposite showed higher adsorption capacity (423 mg g^{-1}) for oxytetracycline (OTC), which is attributed to the successful linking of Fe_3O_4 on GO basal planes [115]. These linkages helped to prevent the agglomeration of Fe_3O_4 and to enormously increase the π-π and cation-π interactions leading to such a high rate of antibiotic removal from wastewater. Most of the carbonaceous organic-inorganic nanohybrids shows difficulty in the regeneration of adsorbent, and hence, this increases the cost of adsorbent regeneration followed by reuse and complexity of the process. Magnetic separation has overcome this issue by providing easy separation of adsorbate magnetically that reduces the cost and complication associated with adsorbent regeneration and reuse.

High surface area is supposed to provide more attachment sites for adsorbates and hence an increased adsorption capacity. For instance, magnetic chitosan-grafted graphene oxide (MCGO) showed higher BET specific surface area of 388.3 m^2 g^{-1} and significant adsorption capacity (282.9 mg g^{-1}) of ciprofloxacin in comparison with many other nanomaterials [96]. This behavior in graphene oxide might be linked to high hydrophobicity and presence of substantial number of functional groups having oxygen located on the adsorbent surface. However, there is evidence of magnetic agglomeration that caused the surface area of graphene oxide (1685.7 m^2g^{-1}) to reduce when in the combined form of MCGO. Similarly, MnO_2/graphene nanocomposite [88] exhibited less than one third of the surface area of MCGO, i.e., 106 m^2g^{-1} and offers a substantial adsorption capacity 1(98 mg g^{-1}), although less than that but still a significant value compared to the whole lot of other subclass materials. Such kind of enhanced adsorption capacities have direct correlation with the superior adsorption characteristic of the metallic induction in the structure of adsorbent [90, 115]. Considering the surface area exhibited by Fe_2O_3 nanoparticles (11.6 m^2/g), this is hard to explain its own contribution to the adsorption capacity. However, addition of these metallic nanomaterials into the matrixes of carbonaceous

Table 1 Adsorptive potential of organic-inorganic nanohybrids for removal of pharmaceuticals

Adsorbent category	Organic-inorganic nanohybrid-based adsorbent	Adsorbate	Adsorption conditions	Adsorbent dose	Surface area m^2/g	Adsorption capacity (mg/g)	Regeneration cycles	References
Carbonaceous and metal oxides-based clay minerals	Magnetic chitosan-grafted graphene oxide composite	Ciprofloxacin	pH 5	300 mg/L	388.3	282.9	4	[96]
	Graphene oxide/MOF	Naproxen (NAP) and Ketoprofen (KTP)	pH 7, 6 h	50 mg/L	–	155 and 120	4	[82]
	Magnetically modified graphene nanoplatelets	Antibiotic amoxicillin	pH 5	5 mg/L	543.2	106.38	4	[70]
	Graphene oxide supported nZVI/copper bimetallic-nanoparticles (BNPs)	Tetracyclines (TCs)	pH 5–7, 15 min	100 mg/L	130	201.9	5	[90]
	MnO_2/graphene	Tetracycline (TC)	pH 5, 1500 min	50 mg/L	106	198	–	[88]
	Fe_3O_4@graphene (Fe_3O_4@G) magnetic	Oxytetracycline (OTC)	pH 7	60 mg/L	–	423	–	[115]
	Graphitic carbon nitride modified by molybdenum trioxide (g-C_3N_4/MoO_3)	Diclofenac	pH 6, 35–45 °C	1 g/L	–	162	4	[75]
	Organosilane-grafted sepiolites (3-ami-nopropyltriethoxysilane (APTES), 3 chloropropyltriethoxysilane (CPTES), triethoxy(octyl)silane (OTES))	Atenolol, ranitidine, carbamazepine	pH 6–9, 20 °C, 24 h	1.6 g/L	–	–	–	[94]

(continued)

Table 1 (continued)

Adsorbent category	Organic-inorganic nanohybrid-based adsorbent	Adsorbate	Adsorption conditions	Adsorbent dose	Surface area m^2/g	Adsorption capacity (mg/g)	Regeneration cycles	References
	Organoclay derivatives with benzyldimethyltetradecylammonium (BDTA) cationic and polyoxyethylene(20)oleyl-ether (Brij-O20) non-ionic surfactants	Atenolol, codeine, doxepin, diclofenac, Metoprolol, ibuprofen trimethoprim, bezafibrate, oxazepam, salicylic acid, carbamazepine, sulfamethoxazole,	pH 7.8, 25 °C	2 g/L	–	–	–	[69]
Chitosan	$NiFe_2O_4$-COF-chitosan-terephthalaldehyde	Tetracycline (TC), cefotaxime (CTX)	pH 8, pH 4, 40 h	5.4 mg	107.33	388.52, 309.26	6	[60]
	Nanotitanium oxide/chitosan/nano-bentonite (NBent-$NTiO_2$-Chit)	Levofloxacin, ceftriaxone	pH 4, pH 5, 20–60 °C 10 min	60 mg	16.385	90	–	[63]
	ZIF-8/chitosan	Tetracycline	pH 8–9, 20–80 °C	400 mg/L	221.4	495.04	–	[117]

nanomaterials effects the hydrophobicity and promotes inclusion of many other functional groups on the surface of mix matrix. Synergistically, organic-inorganic hybrids exhibit enhanced adsorption capacity and of course better regeneration and recycling of the adsorbent.

Clay mineral-based organic-inorganic nanohybrid adsorbents showed great affinities for pharmaceutical compounds in wastewater due to their high surface areas and charged character. Organo-modified clay minerals (Ethoxy-silanes, octyl-silanes, etc.) have higher affinity for neutral and anionic pharmaceutical compounds due to their hydrophobic functionalization. Surface grafting of sepiolites by such organosilanes that induced octyl, γ-aminopropyl, 3-chloropropyl, and triphenyl moieties for adsorptive removal of atenolol, ranitidine, carbamazepine from wastewater [94]. Zeta potential and pH equilibrium showed that removal mechanism has been caused by the interactions of electronegative and electropositive atoms, π-π interactions, and organic–organic (alkyl compounds) hydrophobic interactions. An effective adsorbent has been presented by derivatives of Na^+ ion exchanged clay (montmorillonite) and benzyldimethyltetradecylammonium (BDTA) cationic and polyoxyethylene(20)oleyl-ether 9 non-ionic polymers. Electrical charge and zeta potential demonstrated that electrostatic interaction dominated the several other interaction mechanisms to remove several pharmaceutical pollutants including atenolol, salicylic acid, oxazepam, codeine, etc.

2.1.2 Photocatalytic Degradation and Removal of Pharmaceuticals

In case of organic-inorganic nanohybrids, at least one adsorbent and one semiconductor synergically remove pollutants. The adsorbent component adsorbs the pollutant and the semiconductor induces photocatalytic degradation of pollutants by allowing the pollutant to react with oxygen produced by photons which get absorbed by the semiconductor catalyst surface [23, 25, 67]. Table 2 shows a variety of organic-inorganic nanohybrids for the removal of different pharmaceutical compounds under UV source followed by their adsorption onto the surface.

Nanohybrid of TiO_2 with various carbon-based materials (reduced-graphene oxide, g-C_3N_4, carbon, mesoporous carbon, and multi-walled carbon nanotubes) for effective removal of carbamazepine, ibuprofen, sulfamethoxazole, acetaminophen, ciprofloxacin, tetracycline, and pharmaceutical wastewater, etc., was studied previously [61, 71, 79]. Remediation rates have been really impressive, for instance, graphitized mesoporous carbon (GMC)-doped TiO_2 mineralized the 100% ciprofloxacin in 1.5 h in the wastewater sample [118]. It was observed that 50% of ciprofloxacin was removed in dark period that is referred to the effective adsorption by mesoporous carbon. While in UV radiation, graphitic carbon not only enabled remarkable charge transfer to promote rapid photocatalytic degradation but also helped to reduce recombination effect of electrons and holes. A serious limitation in photocatalytic remediation of pollutants is the cost of light source that provides bandgap energy to electrons, so they could leave valence band and enter conduction band to proceed for the photocatalysis process. Carbon-based organic-inorganic

Table 2 Photocatalytic potential of organic-inorganic nanohybrids for degradation and removal of pharmaceuticals

Organic-inorganic nanohybrid-based photocatalyst	Pharmaceuticals	Light source	Degradation potential (%)	Decay time	References
TiO_2-reduced graphene oxide (rGO)-coated side-glowing optical fibers (SOFs)	Carbamazepine, ibuprofen, sulfamethoxazole	UV and visible light irradiation	54, 81, 92	180 min	[61]
Graphene/titanium dioxide nanotubes	Acetaminophen	UV, 14 W	96	3 h	[23]
Carbon-doped TiO_2	Acetaminophen	440–490 nm, 5 W	94	5.0×10^{-3} min^{-1}	[19]
Magnetic ZnFe-CLDH/RGO composites	Paracetamol	Solar light (>300 nm), 500 W	95	420 min	[121]
Co_3O_4 nanoparticles modified g-C_3N_4 composites (Co_3O_4-g- C_3N_4)	Diclofenac sodium (DCF)	Visible light, >420 nm, 300 W	100	30 min	[84]
g- C_3N_4/TiO_2/Fe_3O_4@SiO_2 heterojunction	Ibuprofen (NSAID)	Visible light, 64 W	98	15 min	[54]
TiO_2–2.7% rGO SOFs	Ibuprofen (NSAID)	High-pressure UV, 160 W Low-pressure UV, 39 W Visible, 40 W	81, 41, 18	30 min	[41]
Graphitized mesoporous carbon (GMC)-TiO_2	Ciprofloxacin	UV, 254 nm, 14 W	100	1.5 h	[118]
MWCNT/TiO_2	Tetracycline, pharmaceutical wastewater	UV, 240 nm, 12 W	83	300 min	[3]
TiO_2 on polyvinylidene fluoride (PVDF) dual layer hollow fiber membranes	Diclofenac (NSAID), trimethoprim, warfarin, carbamazepine, metoprolol, gemfibrozil, iopromide	Low-pressure UV, 254 nm, 40 W	–	–	[71]
MgO/ZnO/graphene	Sulfamethoxazole	UVA (30 W)	–	–	[65]
Ag_3PO_4/GO film	Norfloxacin	Vis light (250 W)	–	–	[44]

nanohybrids demonstrated extraordinary performance with low-power lamps [3, 14, 19, 23]. For instance, carbon-doped TiO_2 degraded 94% of the acetaminophen with 5 W lamp [19]. Other efficiency reducing factors such as recombination effect and charge carrier transfer rate and time have been addressed by these nanohybrid systems. Semiconductor doping in organic structures helped to reduce the bandgap which lead to lower energy consumption and effective photocatalytic activity [23]. Light source posed direct impact on photocatalytic degradation rate of pharmaceutical compounds [14]. Ibuprofen was degraded using TiO_2–2.7% rGO/SOFs as an organic-inorganic nanohybrid photocatalyst. It could only degrade 81%, 41%, and 18% in the presence of high-pressure UV lamp (160), low-pressure UV lamp (39 W), and visible light source (40 W), respectively [41]. Most of the researchers have experimented the photocatalytic degradation under UV light which is an expensive light source, and it requires additional photo-reactors for commercial applications. However, numerous scientists presented their findings using visible light [54, 62, 85] which is of course not as effective as UV light, but it shows mineralization rate of pharmaceutical compounds comparable to low-power UV lamps.

Photocatalytic degradation normally breaks down the organic structures of pharmaceutical substances and forms water-soluble minerals that are less harmful for environment than the parent molecules. If pharmaceutical compounds which are to be degraded contain stable aromatic ring structure (diclofenac, steroids, and pyridine), there is high chance that those long-chained ring structures would be breaking down into smaller ones which further converts into phenolic compounds [11]. Phenolic compounds themselves are considered as pollutants and offer adverse effects in wastewater and ecosystem [11]. Even some of the pharmaceutical compounds such as paracetamol produce acids, after degradation [110]. Another environment unfriendly prospect of photocatalytic degradation arises by the instability in the structure of photocatalyst that could cause solubility of ions in water and would become reason of more damage to the whole aquatic life. Such potential concerns are important to be considered, while structuring the photocatalyst, their parent compounds, and design of reaction system for proper degradation of the pharmaceutical waste. Organic-inorganic nanohybrid systems are best suited in this scenario to address the above-mentioned potential threats.

2.2 Organic-Inorganic Nanohybrids for Removal of Heavy Metals

Heavy metals possess characteristics of non-biodegradability, high density, and chemical stability in wastewater. The main sources of their contamination in water environment include untreated industrial disposal (textile, electroplating, tanning, chemical, and metal processing plants) and domestic effluent streams [120]. They become part of food chain and eventually reach humans and other living species via water bodies and agricultural route. Removal of such toxic elements from wastewater

is essential to prevent their toxic effects on environment and public health. Therefore, it is necessary to properly treat wastewater before its release to the aquatic systems. This section focuses on potential of organic-inorganic nanohybrids for adsorptive and photocatalytic removal of heavy metals.

2.2.1 Adsorptive Removal of Heavy Metals

In adsorption process, adsorbate(s) tends to attach to the surface of the adsorbent via physical or chemical interactions. Physical adsorption typically refers to the weak bonding of adsorbent and adsorbate, that is usually reversible and endothermic in nature, while chemisorption is exothermic and refers to the strong and irreversible chemical interactions between an adsorbent and adsorbate(s) [35]. Adsorption process gives high efficiency, working feasibility, operational ease, no sludge production, better regeneration, and recyclability in the efficient treatment of heavy metals [55]. Adsorption capacity generally depends on the structural features of adsorbent including specific surface area, pore distribution with respect to size, chemical functionalities (active sites), and intrinsic reactivity of molecules toward the adsorbate. Additionally, adsorption depends on solution's pH, adsorbent dose, temperature, contact time, and contaminant concentration [27, 29]. Figure 3 demonstrates prime factors which influence the adsorptive removal of heavy metals.

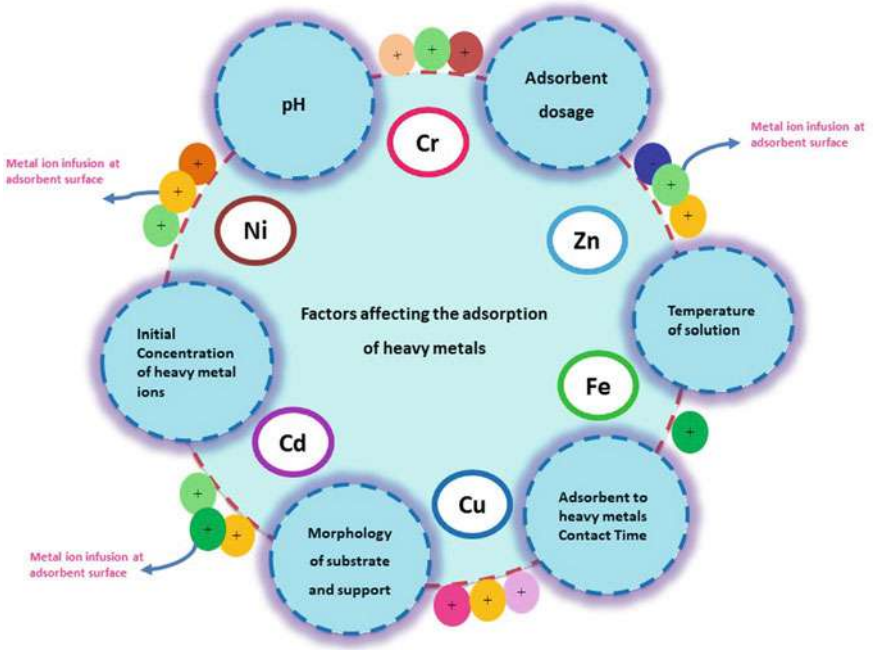

Fig. 3 Factors affecting the adsorptive removal of (positively charged) heavy metals

Carbon-based nanohybrids are based on activated carbon, biochar, carbon nanotube (single and multi-walled carbon nanotubes, magnetized multi-walled carbon nanotubes), fullerene, graphene quantum dots, graphene, and other materials associated with graphene (graphene oxide, reduced graphene oxide, graphene hydrogel, etc.) [34]. However, these hybrids require high cost and time of production, therefore, research efforts are mainly focused on the low cost and relatively fast synthesis of efficient nanohybrids. Activated carbon modified with inorganic constituents has demonstrated excellent adsorption capacities. Activated carbon intercalated with nanoclay and thiolated graphene oxide exhibited 208 mg g^{-1} of adsorption capacity for Pb (II) [66]. This nanohybrid adsorbent showed an appreciable surface area (1296 m^2g^{-1}) owing to the inherent substantial surface properties of activated carbon along with its synergy with constituting nanomaterials. Magnesium silicate impregnated onto palm-shell waste activated carbon exhibited excellent adsorption capacities for Cu (II), Zn (II), Al (III), Fe (II), Mn (II), and As (V) (Table 3) [15]. Magnesium silicates played prime role in heavy metals adsorption. The perfect nanostructures of carbon nanotubes, graphene, and reduced graphene oxide offer chemical stability, extraordinary mechanical and thermal stability, reasonable surface area, and well-defined pores and channels. Additionally, their modifications with inorganic materials lead to enhanced adsorption capacities. For the case of Cr (VI), poly(m-phenylenediamine)-coated Fe_3O_4/o-MWCNTs nanoparticles (PmPD/Fe_3O_4/o-MWCNTs) have shown extraordinary adsorption capacity (346 mg g^{-1}) [93].

Metal oxides-based nanohybrids are excellent of nanohybrids constitute metal oxides in their hybrid structures along with organic constituents. They are cost-effective, eco-friendly, and have high heavy metal removal efficiency and selectivity [53]. Magnetite/graphene oxide hybrid (MGO) showed high adsorption capacity at low concentration of heavy metals [20]. Organic nanomaterials/polymers help in mitigating the problems associated with metal oxide nanomaterials (as stand-alone adsorbents) such as chemical instability, biocompatibility, and aggregation for large-scale utilization [28]. Metal oxide-based organic-inorganic nanohybrids exhibited better dispersion in aqueous medium and reduces aggregation due to electrostatic repulsion [99, 112].

Silica and clay mineral-based nanohybrids have shown promising results regarding heavy metal eradication from treating wastewater (Table 3). The abundantly exploited clay minerals (i.e., montmorillonite [21, 68], bentonite [68], kaolinite, diatomite, zeolite, and sand) exhibited synergistic effect in hybrid form with organic nanomaterials and polymers for adsorption of heavy metals. This phenomenon is associated with the intrinsic negatively charged surface of clay minerals that resulted in enhanced electrostatic interaction with charged heavy metals.

2.2.2 Photocatalytic Removal of Heavy Metals

A photocatalyst (typically a semiconductor) is characterized by its valance band (VB) which is filled with electrons and conduction band (CB). Two types of light sources can be used (depending on the type of catalyst used), i.e., UV (300–388 nm)

Table 3 Adsorptive potential of organic-inorganic nanohybrid for removal of heavy metals

Adsorbent category	Adsorbent subcategory	Organic-inorganic nanohybrid-based adsorbents	Heavy metals	Adsorption conditions	Adsorbent dose	Adsorption capacity (mg/g)	Regeneration cycles	References
Carbonaceous nanomaterial	Activated carbon	Activated carbon/nanoclay/thiolated graphene oxide (AC/NC/ TGO) n	Pb (II)	pH 5, 40 min	0.5 g/L	208	–	[66]
		Iron oxide/activated carbon (Fe_3O_4/AC)	Cr (VI), Cu (II), Cd (II)	pH 2 Cr (VI) @ pH 6 Cu (II) @ pH 3 for Cd (II), 51 ℃, 3 h	5 g/L	2.39, 2.14, 2.47	–	[40]
		Magnetic chlorinated biochar (Fe-Cl/ biochar)	Hg^o	140 ℃, 0.011 s	0.09 mg/m^3	2.14	–	[101]
		Phosphoric acid activated carbon	Cu (II)	pH 5, 7.5 min	1–4 g/L	21.4	7	[98]
		Thiol-functionalized activated carbon	Cu (II), Pb (II), Cd (II), Ni (II)	pH 5	80 mg/40 mL	87.7, 238.1, 96.2, and 52.4	–	[57]

(continued)

Table 3 (continued)

Adsorbent category	Adsorbent subcategory	Organic-inorganic nanohybrid-based adsorbents	Heavy metals	Adsorption conditions	Adsorbent dose	Adsorption capacity (mg/g)	Regeneration cycles	References
		Magnesium silicate impregnated onto palm-shell waste activated carbon (PPAC)	Cu (II), Zn (II), Al (III), Fe (II), Mn (II), As (V)	pH 2–6, 25 ℃, 24 h	100 mg/L	369, 373, 244, 234, 562, 191	3	[15]
	Carbon nanotubes	Poly(m-phenylenediamine)-coated Fe_3O_4/o-MWCNTs nanoparticles (PmPD/Fe_3O_4/o-MWCNTs)	Cr (VI)	pH 2	–	346	5	[93]
	Graphene and graphene related materials (Graphene oxide, reduced graphene oxide, graphene hydrogels)	Graphene oxide-NiFe layered double hydroxide (GO-NiFe LDH)	Cr (VI)	pH 6–7, 30 ℃	–	53.6	4	[119]
		Partially reduced graphene oxide-Fe_3O_4	Pb (II)	pH 6, 10 min	0 mg/L	373.14	–	[30]
		Reduced graphene oxide grafted by 4-sulfophenylazo groups (RGOS)	Pb (II), Cu (II), Ni (II), Cd (II), Cr (III)	10 min	100 mg/L	689, 59, 66, 267, 191	–	[111]

(continued)

Table 3 (continued)

Adsorbent category	Adsorbent subcategory	Organic-inorganic nanohybrid-based adsorbents	Heavy metals	Adsorption conditions	Adsorbent dose	Adsorption capacity (mg/g)	Regeneration cycles	References
		Hydrogel beads from graphene oxide/sodium alginate (GO/SA)	Mn (II)	pH 8.9	750 mg/L	56.49	8	[106]
		Activated carbon/ nanoclay/ thiolated graphene oxide (AC/NC/ TGO) n	Pb (II)	pH 5, 40 min	0.5 g/L	208	-	[66]
		Graphene oxide/Fe_3O_4	Pb (II)	50 ℃	0.3 g/L	114.9		[66]
		3D-reduced graphene oxide/sodium alginate double network (GAD) beads	Sb (III)	pH 6, 25 ℃, 4 h	400 mg/L	7.67	5	[105]
		Chitosan / polyvinyl alcohol/graphene oxide (CH-g-PVA/GO) hydrogel	Pb (II)	2 h	5 mg/L	16.2	-	[42]
Metal oxide-based-nanomaterials	Iron oxides (Goethite, magnetite, hematite, hydrous iron oxides, zerovalent iron)	Biochar-supported goethite	Pb (II)	25–35 ℃,10 h	10–150 mg/L	103.04	5	[112]
		Goethite (α-FeOOH)/reduced graphene oxide (rGO)	Pb (II)	pH 5	0.10 g/L	277.78	-	[28]
		Porous Fe_2O_3 nanocubes-impregnated porous graphene aerogel (PGA/P– Fe_2O_3)	As (III), As (V)	pH 6.9, 35 ℃,	0.1–0.6 g/L	60.81, 76.71	-	[108]
		Magnetite/graphene oxide hybrid (MGO)	Zn (II), Ni (II), Cr (VI)	pH 7, 30 ℃	1 g/L	333, 250, 200	-	[20]
	Zinc oxide	Zinc oxide–graphene nanocomposite (ZnO–Gr)	Ni (II)	pH 8.2, 25 and 35 °C	30 mg/L	66.7	-	[32]

(continued)

Table 3 (continued)

Adsorbent category	Adsorbent subcategory	Organic-inorganic nanohybrid-based adsorbents	Heavy metals	Adsorption conditions	Adsorbent dose	Adsorption capacity (mg/g)	Regeneration cycles	References
	Magnesium oxide	Magnesium oxide-rice husk biochar composite	Cd (II)	pH 5, 25 °C	1 g/L	18.1	-	[99]
Silica/zeolite-based nanomaterials	Silicon	Nanoporous silica (NP) modified with thiol moiety [NPSi-SH]	Mg (II), Ca (II), Mn (II), Cr (III), Fe (III), Co (II), Ni (II), Cu (II), Zn (II), Cd (II), Hg (II), Pb (II)	pH 7, 5–10 min	-	0.075, 0.100, 0.150, 0.275, 0.400, 0.250, 0.150, 0.800, 0.200, 0.300, 0.475, 0.175 mmol/g	-	[1]
		Silica functionalized by pyridinecarboximidamides	Cu (II), Co (II), Ni (II)	pH 5–7, 30–35 °C	0.1 g/L	65.79, 42.74, 57.80	-	[4]

(continued)

Table 3 (continued)

Adsorbent category	Adsorbent subcategory	Organic-inorganic nanohybrid-based adsorbents	Heavy metals	Adsorption conditions	Adsorbent dose	Adsorption capacity (mg/g)	Regeneration cycles	References
		Magnetic mesoporous silica modified with poly (1-vinylimidazole) oligomer	Hg (II)	pH 7, 25 °C	-	346	5	[83]
	Zeolite	Cu-exchanged zeolite A (Cu-ZEA)	As (III)	pH 6–6.5	–	–	–	[50]
		Zeolite-reduced graphene oxide (ZrGO)	As (III)	pH 8, 30 min	100 µg/L	49.23 µg/g	–	[89]
		Polyaniline/zeolite (PANI/Zeolite)	Cr (VI)	pH 6, 30 °C, 10 min	5 mg/L	0.4	–	[86]
		Polypyrrole/thiol-functionalized Beta/MCM-41 (PPy/SH-Beta/MCM-41)	Hg (II)	pH 8, 45 °C, 10 min	2.2 g/L	163.93	6	[43]
Clay mineral based	Montmorillonite/ bentonite	Cysteine-montmorillonite	Cd (II), Hg (II), Pb (II), Co (II), Zn (II), Ni (II), Cu (II)	25 °C, 24 h	100 g/L	0.225, 0.229, 0.231, 0.219, 0.235, 0.228, 0.242 mmol/g	–	[21]
		Alginate-montmorillonite/polyaniline	Cr (VI)	pH 2–9, 5–60 s	50 mg/L	29.89	3	[68]

(continued)

Table 3 (continued)

Adsorbent category	Adsorbent subcategory	Organic-inorganic nanohybrid-based adsorbents	Heavy metals	Adsorption conditions	Adsorbent dose	Adsorption capacity (mg/g)	Regeneration cycles	References
		Humic acid-immobilized-amine-modified polyacrylamide/bentonite composite (HA-Am-PAA-B)	Cu (II), Zn (II), Co (II)	pH 5, 9 and 8, 2 h	100 mg/L	106.2, 96.1, 52.9	3	[7]

or visible light (380–520 nm). Initially, when photons from light source strike the valance band of catalyst, they excite the electrons. By receiving sufficient energy that is either equal or greater than the bandgap energy between VB and CB, electrons jump to CB from VB leaving a hole or positive charge in the VB. Afterward, any of the following three reactions can be possible; (i) evolution of heat after recombination of electrons and holes, (ii) they could subsequently get trapped in metastable surface states, (iii) if there is some electron acceptor or donor adsorbed on the surface of the catalyst, they react with them and commence redox reaction on the double layer surface of charged particles [14]. The reaction mechanism in the photodegradation of heavy metals commences from the photoelectrochemical generation of electrons and holes when light beam strikes the surface of catalyst. Such kind of reaction generates reactive oxygen species. These reactive oxygen species react with the adsorbed heavy metals onto the surface of photocatalyst and reduces it into less toxic form.

Photocatalytic degradation generally depends upon pH, initial metal ion concentration, mass of photocatalyst, presence of electron or hole scavenger, and intensity of light. Photocatalytic degradation of heavy metals transforms them into less hazardous substances such as Cr (VI) is thermodynamically stable and toxic but after degradation, and it turns into Cr(III) which has less detrimental effects than Cr(VI) [64]. Similarly, As(III) and Pb(II) are more toxic than As(V) and Pb(IV), respectively [29]. Iron cross-linked alginate hydrogel beads showed complete transformation of the total Cr(VI) and As(III) into Cr(III) and As(V) at pH 3 within 60 min, respectively. About 70% of Cr(VI) and 85% As(III) owe their degradation to the light irradiated photocatalysis, while rest of the removal in initial dark periods owed to the adsorption occurred in the reaction system. This reaction system showed complete redox reaction. Irrespective of the fact that Cr (VI) caused an inhibitory effect to the oxidation of As (III) which has been controlled by adjusting the Fe (II) ionic concentration in the reaction system. pH plays vital role in redox followed by photocatalytic degradation of heavy metals, and low pH accelerates metal reduction due to its control over the surface charge and adsorption of the pollutant. TiO_2/Alg/FeNPs demonstrated remarkable remediation of Pb(II), Cr(III), and Cu(II) up to 99% in pH sensitive environment. Furthermore, recent studies have focused on the simple and fast methods to manufacture efficient nanocomposites for the photocatalytic treatment of toxic metals. For instance, [46] synthesized α-Fe_2O_3/g-C_3N_4 nanocomposite using Z-scheme in which α-Fe_2O_3 nanoparticles were homogeneously diffused on g-C_3N_4 nanosheet and subsequently analyzed it for the abatement of Hg(II) from wastewater [46]. In previously reported preparation schemes for the synthesis of Fe_2O_3/g-C_3N_4 nanocomposite, co-calcination [31], hydrothermal [51], and wet impregnation [92] were commonly utilized processes. Calcination, hydrothermal method, and wet impregnation process are complicated because of involvement of several sub-steps, and thus, they are extremely time-consuming. It was found that in the presence of visible light and using formic acid (votive donor), the efficiency of Fe_2O_3/g-C_3N_4 nanocomposite for the eradication of Hg(II) from wastewater increased from 41.1% to 90% by varying Fe_2O_3 content from 1 to 6% in a time span of 60 min, respectively. Additionally, the rate of removal of Hg(II) via photocatalysis for α-Fe_2O_3/g-C_3N_4 nanohybrid with 6% content was increased

by 4.6 and 6.8 times than those found out for the individual α-Fe_2O_3 and g-C_3N_4, respectively. Table 4 shows the photocatalytic potential of various organic-inorganic nanohybrids for degradation of heavy metals.

Table 4 Photocatalytic potential of various organic-inorganic nanohybrids for degradation of heavy metals

Organic-inorganic nanohybrid-based photocatalysts	Heavy metals	Light source	Degradation efficacy (%)	Decay time	References
PW_{12}/CN@Bi_2WO_6 composite	Cr(VI)	Simulated xenon	98.7%	90 min	[103]
Microdisk-like g-C_3N_4/diatomite composites (g-C_3N_4/DE)	Cr(VI)	Visible light	0.0740	1 min	[37]
Cellulose acetate (CA) /chitosan/single walled CNTs (SWCNTs/ferrite/TiO_2	Cr(VI), As(V)	UV lamp	95%	60 min	[109]
Ag/UiO-66-NH_2	Cr(VI)	Visible light	90%	30 min	[114]
$ZnIn_2S_4$ nanosheets with MOF molding heterostructure	Cr(VI)	Visible light	100%	30 min	[39]
Electrospun polymer nanofibers coated with TiO_2 hollow spheres	Cr(VI), As(III)	Visible light	99%, 83%	120 min	[13]
Mesoporous imprinted tetracycline, POPD-$CoFe_2O_4$ heterojunction photocatalyst	Cu(II)	Visible light	100%	–	[36]
Iron (III) cross-linking alginate hydrogel beads (Fe-SA)	Cr(VI), As(III)	Visible light	100%	150 min	[113]
Mesoporous α-Fe_2O_3/g-C_3N_4 heterojunction	Hg(II)	Visible light	90%	60 min	[46]
TiO_2/Alg/FeNPs beads	Cr(III), Cu(II), Pb(II)	UV light	98.6%, 98.4%, 99.5%	120 min	[47]
Chitosan/Ag	Cu(II), Pb(II) & Cd(II)	Natural sunlight	10^{-4} and 1.5×10^{-4} mol dm^{-3} s^{-1}	240 min	[5]

2.3 *Application of Organic-Inorganic Nanohybrids for Removal of Pesticides*

Pesticides are commonly used as disinfectants and biological agents to control the pests, weeds, insects, mice, etc. However, the production of pesticides is a major environmental and health concern [95]. They contaminate the ground water, surface water, and landfill leachate. One of the most common categories of highly toxic pesticides is organophosphorus pesticides (OPPs) such as diazinon, phosalone, profenofos, and methidathion. [49].

2.3.1 Adsorptive Removal of Pesticides

Previously, various materials including activated carbon, metal organic framework, clay materials, graphene, biomass materials, and agricultural residues were utilized for treating pesticides in wastewater [74, 79, 80]. Currently, organic-inorganic nanohybrids are gaining attention to remove pollutants (i.e., pesticides) from wastewater due their low costs, high removal efficiencies, and regeneration abilities. A nanohybrid of zirconium-based MOF and graphene oxide (UiO-67/GO) proved excellent adsorbent with enhanced adsorption capability (482.69 mg g^{-1}) to remove glyphosate from wastewater. Presence of Zr-OH functional moiety (FTIR peak @1380 cm^{-1}) on surface of nanohybrid was responsible for the adsorption of glyphosate and FTIR analysis showed the presence of new bonds (Zr-OP, P = O, and P−O at 941, 1157, and 1075 cm^{-1}, respectively), thus confirming the adsorption of glyphosate on surface of nanohybrid. This significant adsorption may be attributed to synergistic features of both MOF and graphene oxide such as high porosity, large surface, and nanochannels among frameworks. Hence, the fabricated UiO-67/GO may be considered as a next generation adsorbent for the abatement of different pesticides present in wastewater [104]. The Fe_3O_4/SiO_2/GO-PEA nanohybrid exhibited maximum adsorption potential (32.6 mgg^{-1}) for a mixture of organophosphorus pesticides including chlorpyrifos, parathion, and malathion. Excellent adsorptive removal was attributed to enhanced surface properties (large surface area and porosity). Additionally, the presence of carbonyl and amine-based functional moieties facilitates the interaction between nanohybrid and pesticide molecules. The electrostatic forces between surface of nanohybrid (having various functional moieties) and pesticides are also responsible for adsorption phenomena. The convenient separation of as-synthesized nanohybrid from aqueous solution under magnetic forces and desorption was obtained within 15 min. Nanohybrid was highly stable as its adsorption potential remained unchanged even after 10 cycles of reuse. Furthermore, Fe_3O_4@SiO_2@GO-PEA was used to treat the samples from Vaal River and Dam in South Africa and great adsorption potential (<86.9%) was observed. This supports the applications of fabricated nanohybrids in real-world samples [97]. Magnetic multi-walled carbon nanotubes (M-M)/metal organic framework (ZIF-8)-based nanohybrid (M-M/ZIF-8) was utilized to study the treatment

of eight pollutants (OPPs) present in wastewater and soil. The adsorption capacity of eight OPPs including triazophos, diazinon, phosalone, profenofos, methidathion, ethoprop, sulfotep, and isazofos was found 3.12, 2.59, 3.80, 3.89, 2.34, 2.18, 2.84, and 3.00 mg g^{-1}, respectively. The adsorption of OPPS is completed approximately in 15 min. Coordination polymerization was dominant mechanism for the deposition of ZIF-8 particles on the surface of the magnetic multi-walled carbon nanotubes (MWCNTs). The effective removal of OPPs by M-M/ZIF-8 via adsorption might be partly related to its high surface area (127.95 m^2g^{-1}) and pore volume (0.564 cm^3g^{-1}). In addition, the presence of various functional moieties (characteristic peaks at 578, 1550, 1420, 900–1330, 421, and 995 cm^{-1} for Fe–O stretching vibration, MWCNTs, imidazole stretching, imidazole planes, Zn–N stretching, and C–N stretching vibration, respectively) might be responsible for adsorption of OPP. Hence, M-M-ZIF-8 proved to be effective nanohybrid for treating OPPs from wastewater [58]. Table 5 shows the adsorptive potential of various organic-inorganic nanohybids for removal of pesticides.

2.3.2 Photocatalytic Degradation of Pesticides

PANI/SnO_2-based nanohybrids have been synthesized for the catalytic removal of dichlorodiphenyltrichloroethane (DDT) from wastewater. For DDT, the microwave-aided degradation efficiency of PANI/SnO_2-50/50 was found to be approximately 87% with degradation time of less than 12 min. The important parameters including DDT concentration and microwave power were investigated. The degradation efficiency of PANI/SnO_2-50/50 decreased by 22% with an increase in DDT concentration from 100 to 500 mg L^{-1}. Whereas, with an increase in microwave power from 300 W to 1100 V, the degradation efficiency increased by 61%. Radical generation experiments confirmed the formation of radicals (i.e., OH and O^{2-}) responsible for effective catalytic removal of DDT. Recycling capability of PANI/SnO_2-50/50 was proved to be significant, and 81% removal of DDT was achieved after utilizing the nanohybrid for third cycle. This highlighted the tremendous reusability and stability of PANI/SnO_2-50/50 nanohybrid. Therefore, this nanohybrid proved to be efficient in treating organic pollutants [77].

Dehghan and colleagues synthesized the rGO/Fe_3O_4/ZnO (GFZ) for oxidative removal of metalaxyl. The fabricated nanohybrid effectively degraded the metalaxyl in synthetic aqueous sample (92%) and agriculture runoff samples (58.3%) in presence of visible light within 120 min.

The production of radicals (OH and O^{2-}) and their roles to remove Metalaxyl was confirmed using scavenging studies. The degradation rate of Metalaxyl in the presence of butanol scavenger was maximum as compared to other scavengers including silver nitrate and benzoquinone. Hence, OH radicals seemed to be primarily involved in the degradation process. The reusability of GZF was studied for consecutive 5 runs and negligible change in degradation efficiency was observed. Thus, it exhibited good usability characteristics. Therefore, GFZ seemed to be an effective and a practical photocatalyst demonstrating an excellent degradation of pesticides from wastewater

Table 5 Organic-inorganic nanohybrids for adsorptive and photocatalytic removal of pesticides from aqueous matrices

Organic-inorganic nanohybrids	Pesticides	Removal phenomenon	Adsorption capacity (mg g^{-1})	Surface area (m^2g^{-1}) and Pore volume (cm^3 g^{-1})	Photocatalytic degradation (%)	Irradiation source	Degradation time (min)	References
Metal organic framework (UiO-67)/graphene oxide (GO)	Glyphosate	Adsorption	482.7	–	–	–	–	[105]
Fe_3O_4@SiO_2@ graphene oxide (GO)-Phenylethylamine (PEA)	Organophosphorus pesticides (OPPs)	Adsorption	32.2	133 and 0.48	–	–	15	[97]
Magnetic multi-walled carbon nanotubes (M-M)/metal organic framework (ZIF-8)	Organophosphorus pesticides (OPPs)	Adsorption	2.18–3.89	127.95 and 0.564	-	-	15	[58]
Polyaniline (PANI)/SnO_2	DDT	Photocatalysis	–	–	97	Microwave	12	[77]
Reduced graphene oxide (rGO)/Fe_3O_4/ZnO (GFZ)	Metalaxyl	Photocatalysis	–	–	92	Visible	120	[18]

under visible light source [18]. Table 5 presents photocatalytic potentials of various organic-inorganic nanohybids for treating pesticides.

3 Conclusions

Globally, water pollution is one the most emerging issues. The wastewater containing heavy metals, pesticides, radionuclides, pharmaceuticals, etc., are released from variety of anthropogenic sources such as industries, medical facilities, and domestic effluents. These water pollutants are potentially carcinogenic. In the above chapter, recent applications of organic-inorganic nanohybrids to treat the wastewater with a focus on effective treatment of pharmaceutical contaminants, heavy metals, and pesticides via adsorption and photocatalysis were discussed. Graphene-based organic-inorganic nanohybrids, magnesium silicate impregnated onto palm-shell waste activated carbon (PPAC), and metal organic framework (UiO-67)/graphene oxide (GO) were found to have the maximum adsorption capacities regarding adsorptive treatment of a variety of pharmaceutical impurities, heavy metals, and pesticides, respectively. For example, high adsorption capacities (120–423 mgg^{-1}) of nanohybrids based on graphene for treating pharmaceutical pollutants were mainly due to high porosity, active sites, and surface properties as evident from their substantial surface areas (106–543.2 m^2g^{-1}). Photocatalytic removal rates of nanohybrids of TiO_2 with various carbon-based materials, $ZnIn_2S_4$ nanosheets with MOF, and Polyaniline (PANI)/SnO_2 for pharmaceuticals pollutants, heavy metals, and pesticides were found to be excellent, respectively. For instance, 100% ciprofloxacin was removed from wastewater using mesoporous carbon-doped TiO_2 in 1.5 h. Also, the nanohybrid of $ZnIn_2S_4$ nanosheets with MOF demonstrated 100% removal of Cr(VI) in 30 min. These high removal rates are predominantly associated with the resultant composition of a nanohybrid which facilities in lowering bandgap energy and generation of surface groups. Other critical parameters in photocatalysis are pH, light source, catalyst dose, and initial concentration of pollutant. Another interesting property of such nanohybrids is the synergic removal of pollutants via both adsorption and photocatalysis. However, it generally depends on the intrinsic characteristics of parent compounds used for the manufacturing of such nanohybrids. Thus, organic-inorganic nanohybrids can be considered as an emerging class of materials exhibiting significant prospects in effective and efficient eradication of pollutants from wastewater with minimal environmental impact.

References

1. Abdel-Fattah TM, Haggag SMS, Mahmoud ME (2011) Heavy metal ions extraction from aqueous media using nanoporous silica. Chem Eng J 175:117–123. https://doi.org/10.1016/j.cej.2011.09.068

2. Abdullah N, Yosuf N, Lau WJ, Jaafar J (2019) Recent trends of heavy metal removal from water/wastewater by membrane technologies. J Ind Eng Chem
3. Ahmadi M, Motlagh HR, Jaafarzadeh N et al (2017) Enhanced photocatalytic degradation of tetracycline and real pharmaceutical wastewater using MWCNT/TiO_2 nano-composite. J Environ Manage
4. Aksamitowski P, Wieszczycka K, Filipowiak K (2019) Silica functionalized by pyridinecarboximidamides as a novel sorbent of heavy metals ions. Sep Sci Technol
5. Al-Sherbini ASA, Ghannam HEA, El-Ghanam GMA et al (2019) Utilization of chitosan/Ag bionanocomposites as eco-friendly photocatalytic reactor for Bactericidal effect and heavy metals removal. Heliyon 5:e01980. https://doi.org/10.1016/j.heliyon.2019.e01980
6. Alharbi NS, Hu B, Hayat T et al (2020) Efficient elimination of environmental pollutants through sorption-reduction and photocatalytic degradation using nanomaterials. Front Chem Sci Eng
7. Anirudhan TS, Suchithra PS (2010) Heavy metals uptake from aqueous solutions and industrial wastewaters by humic acid-immobilized polymer/bentonite composite: Kinetics and equilibrium modeling. Chem Eng J 156:146–156. https://doi.org/10.1016/J.CEJ.2009.10.011
8. Anjum M, Miandad R, Waqas M, Barakat MA (2019) Remediation of wastewater using various nano-materials. Arab J Chem
9. Arman NZ, Salmiati S, Aris A, Salim MRMM (2021) A review on emerging pollutants in the water environment: existences. Health Effects Treat Process
10. Balali-Mood M, Naseri K, Tahergorabi Z et al (2021) Toxic mechanisms of five heavy metals: mercury, lead, chromium, cadmium, and arsenic. Front Pharmacol 12:1–19. https://doi.org/10.3389/fphar.2021.643972
11. Banaschik R, Jablonowski H, Bednarski PJ, Kolb JF (2018) Degradation and intermediates of diclofenac as instructive example for decomposition of recalcitrant pharmaceuticals by hydroxyl radicals generated with pulsed corona plasma in water. J Hazard Mater 342:651–660. https://doi.org/10.1016/J.JHAZMAT.2017.08.058
12. Bilal M, Rizwan K, Adeel M, Iqbal HMN (2021) Hydrogen-based catalyst-assisted advanced oxidation processes to mitigate emerging pharmaceutical contaminants. Int J Hydrogen Energy
13. Cai J, Li H (2020) Electrospun polymer nanofibers coated with TiO2 hollow spheres catalyze for high synergistic photo-conversion of Cr(VI) and As(III) using visible light. Chem Eng J 398:125644. https://doi.org/10.1016/J.CEJ.2020.125644
14. Chen D, M. Sivakumar, Ray AK (2008) Heterogeneous photocatalysis in environmental remediation. Asia Pacific J Chem Eng
15. Choong CE, Lee G, Jang M et al (2018) One step hydrothermal synthesis of magnesium silicate impregnated palm shell waste activated carbon for copper ion removal. Metals (Basel) 8.https://doi.org/10.3390/met8100741
16. Corra L (2009) Children and noise—children's health and the environment. World Heal Organ 1–67
17. Dąbrowski A, Hubicki Z, Robens E (2004) Selective removal of the heavy metal ions from waters and industrial wastewaters by ion-exchange method. Chemosphere
18. Dehghan S, Jafari AJ, FarzadKia M et al (2019) Visible-light-driven photocatalytic degradation of metalaxyl by reduced graphene oxide/Fe_3O_4/ZnO ternary nanohybrid: influential factors, mechanism and toxicity bioassay. J Photochem Photobiol A Chem 375:280–292. https://doi.org/10.1016/j.jphotochem.2019.01.024
19. de Luna MDG, Te LJC, Gotostos MJN, Lu MC (2016) Photocatalytic oxidation of acetaminophen using carbon self-doped titanium dioxide. Sustain Environ Res 26:161–167. https://doi.org/10.1016/j.serj.2016.02.001
20. El-Fawal EM, Saad L, Moustafa YM (2020) Computational DFT study of magnetite/graphene oxide nanoadsorbent: Interfacial chemical behavior and remediation performance of heavy metal hydrates from aqueous system. Water Environ Res
21. El Adraa K, Georgelin T, Lambert JF et al (2017) Cysteine-montmorillonite composites for heavy metal cation complexation: a combined experimental and theoretical study. Chem Eng J 314:406–417. https://doi.org/10.1016/j.cej.2016.11.160

22. Faisal M, Saquib Q, Alatar AA, Al-Khedhairy AA (2020) Cellular and molecular phytotoxicity of heavy metals
23. Fanourakis SK, Peña-Bahamonde J, Bandara PC, Rodrigues DF (2020) Nano-based adsorbent and photocatalyst use for pharmaceutical contaminant removal during indirect potable water reuse. NPJ Clean Water 3. https://doi.org/10.1038/s41545-019-0048-8
24. Felsot AS, Racke KD, Hamilton DJ Disposal and degradation of pesticide waste
25. Fernández-Castro P, Vallejo M, Román MFS, Ortiz I (2015) Insight on the fundamentals of advanced oxidation processes. Role and review of the determination methods of reactive oxygen species. J Chem Technol Biotechnol
26. Gan J, Li X, Rizwan K et al (2021) Covalent organic frameworks-based smart materials for mitigation of pharmaceutical pollutants from aqueous solution. Chemosphere
27. Gao X, Meng X (2021) Photocatalysis for heavy metal treatment: a review. Processes 9.https://doi.org/10.3390/pr9101729
28. Gordon-Nuñez F, Vaca-Escobar K, Villacís-García M et al (2019) Applicability of goethite/reduced graphene oxide nanocomposites to remove lead from wastewater. https://doi.org/10.3390/nano9111580
29. Guan X, Du J, Meng X et al (2012) Application of titanium dioxide in arsenic removal from water: a review. J Hazard Mater 215–216:1–16. https://doi.org/10.1016/J.JHAZMAT.2012.02.069
30. Guo T, Bulin C, Li B et al (2018) Efficient removal of aqueous Pb(II) using partially reduced graphene oxide-Fe_3O_4. Adsorpt Sci Technol 36:1031–1048. https://doi.org/10.1177/0263617417744402
31. Guo T, Wang K, Zhang G, Wu X (2019) A novel α-Fe_2O_3@g-C_3N_4 catalyst: synthesis derived from Fe-based MOF and its superior photo-Fenton performance. Appl Surf Sci 469:331–339
32. Hadadian M, Goharshadi EK, Fard MM, Ahmadzadeh H (2018) Synergistic effect of graphene nanosheets and zinc oxide nanoparticles for effective adsorption of Ni (II) ions from aqueous solutions. Appl Phys A
33. Hall DW, Sandrin JA, McBride RE (1990) An overview of solvent extraction treatment technologies
34. Hasdi ND (2020) Reviewing methods to prepare activated carbon from various sources. Nanoscale Res Lett 14:1–17
35. Hashemian S, Ardakani MK, Salehifar H (2013) Kinetics and thermodynamics of adsorption methylene blue onto tea waste/$CuFe_2O_4$ composite. Am J Anal Chem 04:1–7. https://doi.org/10.4236/ajac.2013.47a001
36. He F, Lu Z, Song M et al (2019) Selective reduction of Cu^{2+} with simultaneous degradation of tetracycline by the dual channels ion imprinted POPD-$CoFe_2O_4$ heterojunction photocatalyst. Chem Eng J 360:750–761. https://doi.org/10.1016/J.CEJ.2018.12.034
37. He H, Li J, Yu C, Luo Z (2019) Surface decoration of microdisk-like g-C_3N_4/diatomite with Ag/AgCl nanoparticles for application in Cr(VI) reduction. Sustain Mater Technol 22:e00127. https://doi.org/10.1016/J.SUSMAT.2019.E00127
38. Hossain F (2020) Natural and anthropogenic radionuclides in water and wastewater: Sources, treatments and recoveries. J Environ Radioact
39. Hussain MB, Azhar U, Loussala HM, Razaq R (2020) Synergetic effect of ZnIn2S4 nanosheets with metal-organic framework molding heterostructure for efficient visible- light driven photocatalytic reduction of Cr(VI). Arab J Chem 13:5939–5948. https://doi.org/10.1016/j.arabjc.2020.04.029
40. Jain M, Yadav M, Kohout T et al (2018) Development of iron oxide/activated carbon nanoparticle composite for the removal of Cr(VI), Cu(II) and Cd(II) ions from aqueous solution. Water Resour Ind 20:54–74. https://doi.org/10.1016/J.WRI.2018.10.001
41. Jallouli N, Pastrana-Martínez LM, Rubeiro AR (2018) Heterogeneous photocatalytic degradation of ibuprofen in ultrapure water, municipal and pharmaceutical industry wastewaters using a TiO_2/UV-LED system. Chem Eng J
42. Jasim LS, Irhayyim SH (2021) Adsorption and removal studies of heavy metal Pb(II) on their water solution on adsorbent surface of vinyl alcohol/chitosan-graphene oxide. IOP Conf Ser Earth Environ Sci 790https://doi.org/10.1088/1755-1315/790/1/012063

43. Javadian H, Taghavi M (2014) Application of novel Polypyrrole/thiol-functionalized zeolite Beta/MCM-41 type mesoporous silica nanocomposite for adsorption of Hg^{2+} from aqueous solution and industrial wastewater: Kinetic, isotherm and thermodynamic studies. Appl Surf Sci 289:487–494. https://doi.org/10.1016/j.apsusc.2013.11.020
44. Ji B, Yang Z, Fi L, Ma L (2020) Immobilized Ag_3PO_4/GO on 3D nickel foam and its photocatalytic degradation of norfloxacin antibiotic under visible light
45. Joo SH, Tansel B (2015) Novel technologies for reverse osmosis concentrate treatment: a review. J Environ Manage
46. Kadi MW, Mohamed RM, Ismail AA, Bahnemann DW (2020) Performance of mesoporous α-Fe_2O_3/g-C_3N_4 heterojunction for photoreduction of Hg(II) under visible light illumination. Ceram Int 46:23098–23106. https://doi.org/10.1016/J.CERAMINT.2020.06.087
47. Kanakaraju D, Rusydah bt Mohamad Shahdad N, Lim YC, Pace A (2019) Concurrent removal of Cr(III), Cu(II), and Pb(II) ions from water by multifunctional TiO_2/Alg/FeNPs beads. Sustain Chem Pharm 14:100176. https://doi.org/10.1016/J.SCP.2019.100176
48. Kaval İ, Behçet L, Çakilcioğlu U (2015) Survey of wild food plants for human consumption in Geçitli (Hakkari, Turkey). Indian J Tradit Knowl 14:183–190
49. Kenneth D Katz (2020) Organophosphate toxicity. In: Medscape Logo. https://emedicine.medscape.com/article/167726-overview. Accessed 31 Dec 2021
50. Khatamian M, Khodakarampoor N, Saket-Oskoui M (2017) Efficient removal of arsenic using graphene-zeolite based composites. J Colloid Interface Sci 498:433–441. https://doi.org/10.1016/j.jcis.2017.03.052
51. Khurram R, Nisa ZU, Javed A, Wang Z, Hussien MA (2022) Synthesis and characterization of an α-Fe_2O_3-decorated g-C_3N_4 heterostructure for the photocatalytic removal of MO. Molecules 27:1442
52. Kinuthia GK, Ngure V, Beti D et al (2020) Levels of heavy metals in wastewater and soil samples from open drainage channels in Nairobi, Kenya: community health implication. Sci Rep 10:1–13. https://doi.org/10.1038/s41598-020-65359-5
53. Kumar A, Joshi H, Kumar A (2020) Remediation of arsenic by metal/ metal oxide based nanocomposites/nanohybrids: contamination scenario in groundwater, practical challenges, and future perspectives. Sep Purif Rev
54. Kumar A, Khan M, Zeng X, Lo IMC (2018) Development of g-C3N4/TiO_2/Fe_3O_4@SiO_2 heterojunction via sol-gel route: a magnetically recyclable direct contact Z-scheme nanophotocatalyst for enhanced photocatalytic removal of ibuprofen from real sewage effluent under visible light. Chem Eng J
55. Kumar R, Rauwel P, Rauwel E (2021) Nanoadsorbants for the removal of heavy metals from contaminated water: current scenario and future directions. Processes 9https://doi.org/10.3390/pr9081379
56. Le TDH, Scharmüller A, Kattwinkel M (2017) Contribution of waste water treatment plants to pesticide toxicity in agriculture catchments
57. Li J, Xing X, Li J et al (2018) Preparation of thiol-functionalized activated carbon from sewage sludge with coal blending for heavy metal removal from contaminated water. Environ Pollut 234:677–683. https://doi.org/10.1016/J.ENVPOL.2017.11.102
58. Liu G, Li L, Huang X et al (2018) Adsorption and removal of organophosphorus pesticides from environmental water and soil samples by using magnetic multi-walled carbon nanotubes @ organic framework ZIF-8. J Mater Sci 53:10772–10783. https://doi.org/10.1007/s10853-018-2352-y
59. Liu S, Wang S, Jiang Y, Zhao Z, Jiang G, Sun Z (2019) Synthesis of Fe_2O_3 loaded porous g-C_3N_4 photocatalyst for photocatalytic reduction of dinitrogen to ammonia. Chem Eng J 373:572–579. https://doi.org/10.1016/j.cej.2019.05.021
60. Li Z, Liu Y, Zou S, et al (2020) Removal and adsorption mechanism of tetracycline and cefotaxime contaminants in water by $NiFe_2O_4$-COF-chitosan-terephthalaldehyde nanocomposites film. Chem Eng J
61. Lin L, Wang H, Xu P (2017) Immobilized TiO_2-reduced graphene oxide nanocomposites on optical fibers as high performance photocatalysts for degradation of pharmaceuticals. Chem Eng J

62. Lu X, Che W, Hu X et al (2019) The facile fabrication of novel visible-light-driven Z-scheme $CuInS_2/Bi_2WO_6$ heterojunction with intimate interface contact by in situ hydrothermal growth strategy for extraordinary photocatalytic performance. Chem Eng J 356:819–829. https://doi.org/10.1016/J.CEJ.2018.09.087
63. Mahmoud ME, El-Ghanam AM, Mohamed RH, Saad SR (2020) Enhanced adsorption of levofloxacin and ceftriaxone antibiotics from water by assembled composite of nanotitanium oxide/chitosan/nano-bentonite. Mater Sci Eng C
64. Mccarron P, Harvey I, Brogan R, Peters TJ (2000) Chromium waste : interview study. 320
65. Moradi S, Hayati F, Kakavandi B, Bashardoust P (2020) Performance and reaction mechanism of MgO/ZnO/Graphene ternary nanocomposite in coupling with LED and ultrasound waves for the degradation of sulfamethoxazole and pharmaceutical wastewater. Sep Purif Technol
66. Mousavi SM, Hashemi SA, Amani AM et al (2018) Pb(II) removal from synthetic wastewater using Kombucha Scoby and graphene oxide/Fe_3O_4. Phys Chem Res 6:759–771. https://doi.org/10.22036/pcr.2018.133392.1490
67. Nosaka Y, Nosaka AY (2017) Generation and detection of reactive oxygen species in photocatalysis. Am Chem Soc
68. Olad A, Farshi Azhar F (2014) A study on the adsorption of chromium (VI) from aqueous solutions on the alginate-montmorillonite/polyaniline nanocomposite. Desalin Water Treat 52:2548–2559. https://doi.org/10.1080/19443994.2013.794711
69. Oliveira T, MohammedBoussafir, Fougère L et al (2020) Use of a clay mineral and its nonionic and cationic organoclay derivatives for the removal of pharmaceuticals from rural wastewater effluents. Chemosphere
70. ÖzgeKerkez-Kuyumcu, SenaBayazit Ş, AbdelSalam M (2016) Antibiotic amoxicillin removal from aqueous solution using magnetically modified graphene nanoplatelets. J Ind Eng Chem
71. Paredes L, Murgolo S, Dzinun H, Othman MHD (2019) Application of immobilized TiO_2 on PVDF dual layer hollow fibre membrane to improve the photocatalytic removal of pharmaceuticals in different water matrices. Appl Cataysis
72. Rahman MA, Habib ML, Chisty AH (2022) Organic–inorganic polymer hybrids for water and wastewater treatment. In: Inorganic-organic composites for water and wastewater treatment
73. Ramírez-Castillo FY, Loera-Muro A, Jacques M et al (2015) Waterborne pathogens: detection methods and challenges. Pathogens 4:307–334. https://doi.org/10.3390/pathogens4020307
74. Rasheed T, Rizwan K, Bilal M, Sher F, Iqbal HMN (2021) Tailored functional materials as robust candidates to mitigate pesticides in aqueous matrices–a review. Chemosphere 282:131056. https://doi.org/10.1016/j.chemosphere.2021.131056
75. Rashid J, Saleemi F, Akram B et al (2021) Facile synthesis of g-C_3N_4/MoO_3 nanohybrid for efficient removal of aqueous diclofenac sodium. Nanomaterials 11:1–17. https://doi.org/10.3390/nano11061564
76. Renu, Agarwal M, Singh K (2017) Heavy metal removal from wastewater using various adsorbents: a review. J Water Reuse Salination
77. Riaz U, Zia J (2020) Microwave-assisted rapid degradation of DDT using nanohybrids of PANI with SnO_2 derived from Psidium Guajava extract. Environ Pollut 259:113917. https://doi.org/10.1016/j.envpol.2020.113917
78. Rizwan K, Rahdar A, Bilal M, Iqbal HMN (2022) MXene-based electrochemical and biosensing platforms to detect toxic elements and pesticides pollutants from environmental matrices. Chemosphere 291:132820. https://doi.org/10.1016/j.chemosphere.2021.132820
79. Rizwan K, Bilal M, Slimani Y, Show PL, Rtimi S, Roy A, Iqbal HMN (2022) Hydrogen-based sono-hybrid catalytic degradation and mitigation of industrially-originated dye-based pollutants. Int J Hydrogen Energy
80. Saleh IA, Zouari N, Al-Ghouti MA (2020) Removal of pesticides from water and wastewater: Chemical, physical and biological treatment approaches. Environ Technol Innov 19:101026. https://doi.org/10.1016/j.eti.2020.101026
81. Samiey B, Cheng CH, Wu J (2014) Organic-inorganic hybrid polymers as adsorbents for removal of heavy metal ions from solutions: a review. Materials (Basel) 7:673–726. https://doi.org/10.3390/ma7020673

82. Sarker M, Song JY, Jhung SH (2018) Adsorptive removal of anti-inflammatory drugs from water using graphene oxide/metal-organic framework composites. Chem Eng J
83. Shan C, Ma Z, Tong M, Ni J (2015) Removal of Hg(II) by poly(1-vinylimidazole)-grafted Fe_3O_4@SiO_2 magnetic nanoparticles. Water Res 69:252–260. https://doi.org/10.1016/J.WATRES.2014.11.030
84. Shao H, Zhao X, Wang Y et al (2017) Synergetic activation of peroxymonosulfate by Co_3O_4 modified g-C_3N_4 for enhanced degradation of diclofenac sodium under visible light irradiation. Appl Catal
85. Sheydaei M, Shiadeh HRK, Ayoubi-Feiz B, Ezzati R (2018) Preparation of nano N-TiO_2/graphene oxide/titan grid sheets for visible light assisted photocatalytic ozonation of cefixime. Chem Eng J 353:138–146. https://doi.org/10.1016/J.CEJ.2018.07.089
86. Shyaa AA, Hasan OA, Abbas AM (2015) Synthesis and characterization of polyaniline/zeolite nanocomposite for the removal of chromium(VI) from aqueous solution. J Saudi Chem Soc 19:101–107. https://doi.org/10.1016/j.jscs.2012.01.001
87. Singh A, Basu S (2020) Synthesis of mesoporous magnetic Fe_2O_3/g-C_3N_4 monoliths for Rhodamine B removal. Microporous Mesoporous Mater 303:110299. https://doi.org/10.1016/j.micromeso.2020.110299
88. Song Z, Ma Y-L, Li C (2019) The residual tetracycline in pharmaceutical wastewater was effectively removed by using MnO_2/graphene nanocomposite. Sci Total Environ
89. Soni R, Shukla DP (2019) Synthesis of fly ash based zeolite-reduced graphene oxide composite and its evaluation as an adsorbent for arsenic removal. Chemosphere 219:504–509. https://doi.org/10.1016/J.CHEMOSPHERE.2018.11.203
90. Tabrizian P, Ma W, Bakr A, Rahaman MS (2019) pH-sensitive and magnetically separable Fe/Cu bimetallic nanoparticles supported by graphene oxide (GO) for high-efficiency removal of tetracyclines. J Colloid Interface Sci
91. Tchounwou PB, Yedjou CG, Patlolla AK, Sutton DJ (2012) Molecular, clinical and environmental toxicicology volume 3: environmental Toxicology. Mol Clin Environ Toxicol 101:133–164. https://doi.org/10.1007/978-3-7643-8340-4
92. Theerthagiri J, Senthil RA, Priya A, Madhavan J, Michael RJV, Ashokkumar M (2014) Photocatalytic and photoelectrochemical studies of visible-light active α-Fe_2O_3–g-C_3N_4 nanocomposites. RSC Adv 4:38222–38229
93. Tian Z, Yang B, Cui G et al (2015) Synthesis of poly(m-phenylenediamine)/iron oxide/acid oxidized multi-wall carbon nanotubes for removal of hexavalent chromium. RSC Adv
94. Undabeytia T, Madrid F, Vázquez J, Pérez-Martínez JI (2019) Grafted sepiolites for the removal of pharmaceuticals in water treatment. Clays Clay Miner
95. US EPA (2021) Why we use pesticides. https://www.epa.gov/safepestcontrol/why-we-use-pesticides. Accessed 31 Dec 2021
96. Wang F, Yang B, Wang H et al (2016) Removal of ciprofloxacin from aqueous solution by a magnetic chitosan grafted graphene oxide composite. J Mol Liq
97. Wanjeri VWO, Sheppard CJ, Prinsloo ARE et al (2018) Isotherm and kinetic investigations on the adsorption of organophosphorus pesticides on graphene oxide based silica coated magnetic nanoparticles functionalized with 2-phenylethylamine. J Environ Chem Eng 6:1333–1346. https://doi.org/10.1016/j.jece.2018.01.064
98. Wu L, Wan W, Shang Z et al (2018) Surface modification of phosphoric acid activated carbon by using non-thermal plasma for enhancement of Cu(II) adsorption from aqueous solutions. Sep Purif Technol 197:156–169. https://doi.org/10.1016/J.SEPPUR.2018.01.007
99. Xiang J, Lin Q, Guo J, Liu Q (2018) Enhanced adsorption of Cd(II) from aqueous solution by a magnesium oxide–rice husk biochar composite. Environ Sci Pollut Res
100. Xiao D, Dai K, Qu Y, Yin Y, Chen H (2015) Hydrothermal synthesis of α-Fe2O3/g-C3N4 composite and its efficient photocatalytic reduction of Cr(VI) under visible light. Appl Surface Sci 358(A):181–187. https://doi.org/10.1016/j.apsusc.2015.09.042
101. Xu Y, Luo G, He S et al (2019) Efficient removal of elemental mercury by magnetic chlorinated biochars derived from co-pyrolysis of $Fe(NO_3)_3$-laden wood and polyvinyl chloride waste. Fuel

102. Yang L, Hu W, Chang Z et al (2021) Electrochemical recovery and high value-added reutilization of heavy metal ions from wastewater: Recent advances and future trends. Environ Int 152:106512. https://doi.org/10.1016/J.ENVINT.2021.106512
103. Yang R, Zhong S, Zhang L, Liu B (2020) PW_{12}/CN@Bi_2WO_6 composite photocatalyst prepared based on organic-inorganic hybrid system for removing pollutants in water. Sep Purif Technol 235:116270. https://doi.org/10.1016/J.SEPPUR.2019.116270
104. Yang T, Li F, Zhou X et al (2019) Impact of nitrogen fertilizer, greenhouse, and crop species on yield-scaled nitrous oxide emission from vegetable crops: a meta-analysis. Ecol Indic 105:717–726. https://doi.org/10.1016/j.ecolind.2019.02.001
105. Yang X, Zhou T, Deng R et al (2021) Removal of Sb(III) by 3D-reduced graphene oxide/sodium alginate double-network composites from an aqueous batch and fixed-bed system. Sci Rep 11:1–17. https://doi.org/10.1038/s41598-021-01788-0
106. Yang X, Zhou T, Ren B et al (2018) Removal of Mn (II) by sodium alginate/graphene oxide composite double-network hydrogel beads from aqueous solutions. Sci Rep 8:1–16. https://doi.org/10.1038/s41598-018-29133-y
107. Yaseen DA, Scholz M (2019) Textile dye wastewater characteristics and constituents of synthetic effluents: a critical review. Springer, Berlin Heidelberg
108. Yu X, Wei Y, Liu C et al (2019) Ultrafast and deep removal of arsenic in high-concentration wastewater: a superior bulk adsorbent of porous Fe_2O_3 nanocubes-impregnated graphene aerogel. Chemosphere
109. ZabihiSahebi A, Koushkbaghi S, Pishnamazi M et al (2019) Synthesis of cellulose acetate/chitosan/SWCNT/Fe_3O_4/TiO_2 composite nanofibers for the removal of Cr(VI), As(V), Methylene blue and Congo red from aqueous solutions. Int J Biol Macromol 140:1296–1304. https://doi.org/10.1016/J.IJBIOMAC.2019.08.214
110. Zavala MÁL, Lara CRJ (2018) Degradation of paracetamol and its oxidation products in surface water by electrochemical oxidation. Environ Eng Sci 35
111. Zhang C-Z, Chen B, Bai Y, Xie J (2018) A new functionalized reduced graphene oxide adsorbent for removing heavy metal ions in water via coordination and ion exchange. Sep Sci Technol
112. Zhang S, Du Q, Sun Y, Yang F (2020) Fabrication of L-cysteine stabilized α-FeOOH nanocomposite on porous hydrophilic biochar as an effective adsorbent for Pb^{2+} removal. Sci Total Environ
113. Zhang W, Liu F, Sun Y et al (2019) Simultaneous redox conversion and sequestration of chromate(VI) and arsenite(III) by iron(III)-alginate based photocatalysis. Appl Catal B Environ 259:118046. https://doi.org/10.1016/J.APCATB.2019.118046
114. Zhang W, Wang L, Zhang J (2019b) Preparation of Ag/UiO-66-NH_2 and its application in photocatalytic reduction of Cr(VI) under visible light. Res Chem Intermed
115. Zhang Y, Jiao Z, Hu Y et al (2016) Removal of tetracycline and oxytetracycline from water by magnetic Fe_3O_4@graphene. Environ Sci Pollut Res
116. Zhao N, Yan L, Zhao X et al (2018) Versatile types of organic/inorganic nanohybrids: from strategic design to biomedical applications
117. Zhao R, Ma T, Zhao S et al (2020) Uniform and stable immobilization of metal-organic frameworks into chitosan matrix for enhanced tetracycline removal from water. Chem Eng J
118. Zheng X, Xu S, Wang Y et al (2018) Enhanced degradation of ciprofloxacin by graphitized mesoporous carbon (GMC)-TiO_2 nanocomposite: Strong synergy of adsorption-photocatalysis and antibiotics degradation mechanism. J Colloid Interface Sci
119. Zheng Y, Cheng B, You W et al (2019) 3D hierarchical graphene oxide-NiFe LDH composite with enhanced adsorption affinity to Congo red, methyl orange and Cr(VI) ions. J Hazard Mater 369:214–225. https://doi.org/10.1016/J.JHAZMAT.2019.02.013
120. Zhou Q, Yang N, Li Y et al (2020) Total concentrations and sources of heavy metal pollution in global river and lake water bodies from 1972 to 2017. Glob Ecol Conserv 22:e00925. https://doi.org/10.1016/J.GECCO.2020.E00925
121. Zhu J, Zhu Z, Zhang H, Lu H (2018) Calcined layered double hydroxides/reduced graphene oxide composites with improved photocatalytic degradation of paracetamol and efficient oxidation-adsorption of As(III). Appl Catal

Chapter 13
Organic–Inorganic Nanohybrids for the Removal of Environmental Pollutants

Zaeem Bin Babar, Ariha Shahi, Abdul Rauf, Hamed Sattar, and Komal Rizwan

1 Introduction

Due to rapid industrial expansions, urban developments, and excessive and uncontrolled utilization of natural resources, environment is being consistently damaged [89]. The industrial activities associated with the manufacturing of chemicals, fertilizers, paper and pulp, etc., are discharging huge amounts of contaminated water, volatile organic compounds (VOCs), and gases and therefore, polluting and degrading the quality of soil and water bodies and atmosphere, respectively. Generally, both organic and inorganic contaminants are present in wastewater. The pollutants such as dyes, pesticides, VOCs, and phenolic substances are typically organic, whereas substances such as heavy metals and salts have inorganic nature [1]. Generally, treatment methods of wastewater are divided into three major categories: (a) chemical, (b) physical, and (c) biological processes as shown in Fig. 1. Commonly known methods include membrane separation, ion-exchange, adsorption, chemical precipitation, photocatalysis, aerobic and anaerobic processes, and Fenton's oxidation [47, 76]. Adsorption is an effective method in treating wastewater by employing a variety of adsorbents which are of low cost, convenient to use, and can be regenerative [76]. Also, photocatalysis employing semiconductors remove pollutants by converting them into CO_2, H_2O, and mineral acids in the presence of light source (i.e., ultraviolet, visible) [66]. For the case of air pollutants such as VOCs, CO_2, NO_x,

Z. B. Babar · A. Shahi · A. Rauf · H. Sattar
Institute of Energy and Environmental Engineering, University of the Punjab, Lahore, Pakistan

Z. B. Babar
Institute of Environmental Sciences and Engineering (IESE), School of Civil and Environmental Engineering (SCEE), National University of Sciences and Technology (NUST), Islamabad, Pakistan

K. Rizwan (✉)
Department of Chemistry, University of Sahiwal, Sahiwal, Pakistan
e-mail: komal.rizwan45@yahoo.com

K. Rizwan et al. (eds.), *Hybrid Nanomaterials*, Materials Horizons: From Nature to Nanomaterials, https://doi.org/10.1007/978-981-19-4538-0_13

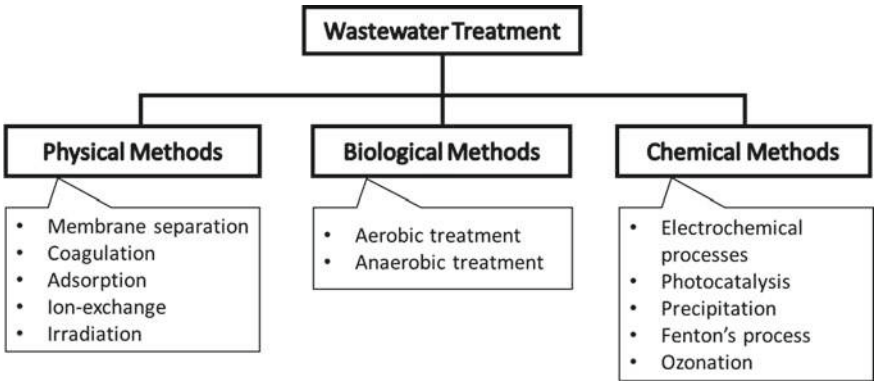

Fig. 1 Treatment methods for wastewater for the removal of contaminants

CH_4, the respective control and treatment strategies are highlighted in Table 1. Over the last decade, the development and subsequent application of organic–inorganic hybrids in the removal of contaminants (dyes, gases, VOCs etc.) from environment is gaining a lot of attention. Organic–inorganic hybrids are single-phase materials and fabricated by the combination of organic and inorganic materials via molecular interactions between the functional groups of respective materials [91]. Additionally, they not only offer superior properties than their individual constituents but also reduce their individualistic limitations. In organic–inorganic hybrid, organic component adds a variety of functional groups, versatility, and reactivity, whereas inorganic component provides advantages of thermal stability and reliability. This contributes to the high selectivity of organic–inorganic hybrid toward a target contaminant with increased removal efficiency [41]. In this chapter, removal of various dyes, VOCs, and gases via adsorption and photocatalytic degradation processes (Fig. 2) using a variety of recently developed organic–inorganic hybrids has been presented in detail.

Table 1 Summary of control and treatment strategies for various air pollutants

Air pollutants	Control and treatment strategies	References
CO_2	Increased forestation / Post-combustion CO_2 capture	[34, 86]
CO	CO formation could be prevented through efficient or complete combustion of fuels in all the regimes	[35]
SO_2	Precombustion sulfur removal by washing, post-combustion removal by SO_2 scrubbers, coal gasification	[55, 57]
VOCs	Removal of VOCs through adsorption and photocatalysis	[17]
CH_4	Processing and management of digestive products, reduction of 65% of CH_4 emissions are possible through gas leak prevention during coal mining as well as oil and gas production	[5, 12, 69]
NO_x (NO_2, N_2O)	Prevention of thermal NO_x through low-temperature combustion technologies, management of animal waste	[52, 79]

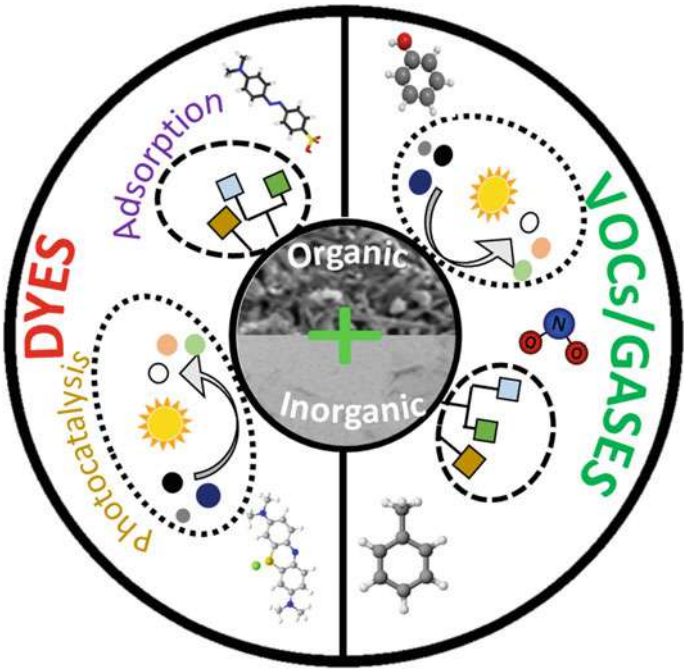

Fig. 2 Organic–inorganic nanohybrids for adsorptive and photocatalytic removal of different environmental pollutants

2 Environmental Pollutants; Sources and Toxic Health Effects

Figure 3 demonstrates the various sources of environmental pollutants including dyes, VOCs, and gases. Additionally, the sources and the associated detrimental effects of dyes, VOCs, and gases on public health and ecosystem have been explained in this section.

2.1 Dyes

A dye is a colored soluble compound, which is linked to the substrate via physical and/or chemical interaction between the groups of dye and substrate [15]. A dye is classified into two main groups based on (a) chromogens, for instance, acridine, anthraquinone, azo, azine, diphenylmethane, thiazine indigoid, xanthene, etc., and (b) their nature for specific applications, for example, acidic, basic, direct, disperse, etc. [15]. The major sources of dyes comprise textile, tannery, cosmetic and food, and pharmaceutical industries [45]. However, dyes are majorly used in the textile

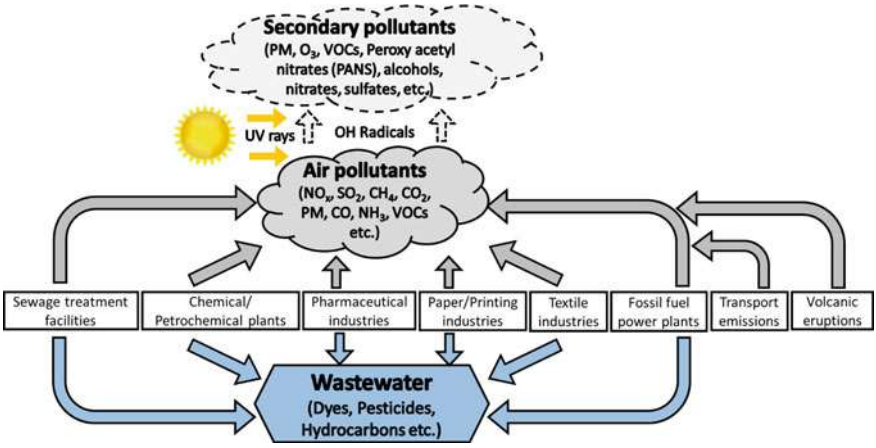

Fig. 3 A variety of sources of wastewater (dyes, pesticides, etc.) and air pollutants (both primary and secondary)

and leather production facilities to apply color to products such as fabric stuff such as cloth, bed covers, denim, rugs, and curtains. The worldwide yearly production of dyes is approximately 700,000 tons. Examples of the most common dyes (based on chromogens) used in textile sector are azo, anthraquinone, and phthalocyanine dyes [11]. Therefore, owing to mega-scale manufacturing of dyes in the view of their variety of applications, they have penetrated in the environmental segments of water bodies and soil [50]. They are also known as environmental micropollutants as they are primarily found samples of water, particulates, sediments, and aquatic organisms [67]. These dyes pose a substantial impact on the quality of water bodies (surface and ground water). Additionally, they are responsible for augmenting chemical and biological oxygen demands (COD and BOD). Furthermore, they undermine the processes of photosynthesis and diminish plant growth. Finally, they become part of food chain, and their subsequent accumulation results in toxic, carcinogenic, and mutagenic effects among humans [26]. Methylene blue is classified as a thiazene dye and commonly found in the effluents released from laundry, textile, paper, and printing industries [23]. It is also known to have negative impacts on central nervous system [70]. Rhodamine B belongs to xanthene class of dyes and is typical present in the effluents of sewage treatment plants [10]. It causes oxidative stress which can damage cells in cerebellum and brain stem tissue [64].

2.2 Volatile Organic Compounds and Gases

Volatile organic compounds (VOCs) have high volatility and vaporize easily under ambient conditions. Therefore, they have high vapor pressures. Primarily, they are composed of carbon, hydrogen, oxygen, nitrogen, sulfur, and chlorine. Examples

of common VOCs are acetone, ethanol, benzene, toluene, xylene, carbon tetrachloride, etc. [13]. VOCs and gases including CO_2, CO, SO_2, and NO_x are emitted from multiple sources such as petrochemical plants, textile units, cement manufacturing industries, fossil fuel-based power plants, vehicular emissions, biomass burnings, and brick kilns [42]. The sources of VOCs and gases and their health and environmental impacts are summarized in Table 2. Briefly, in high concentrations, they have detrimental effects on human health and cause irritations, allergic skin reactions, severe upper and lower respiratory problems, and genetic disorders [19, 24]. For example, benzene causes leukemia, skin cancer, and Alzheimer's and Parkinson's disease [9]. Additionally, VOCs have vital part in enhancing reduced visibility by forming secondary particles. In the presence of UV light from sun, VOCs react with atmospheric OH radicals and O_3 in the presence of NO_x, SO_2, and NH_3 to form a wide range of chemical compounds in both gas and particle phases [3, 4, 30, 83]. Additionally, they induce photochemical smog, deteriorate soil quality, and instigate O_3 disparity [13].

3 Application of Organic–Inorganic Nanohybrids for Removal of Dyes

3.1 Adsorptive Removal of Dyes

Over the last few years, a variety of organic–inorganic nanohybrids have been developed, characterized and applied to treat contaminants such as dyes from synthetic and industrial wastewater. Table 3 summarizes the role of various organic–inorganic nanohybrids for adsorptive removal of dye. We have reported the dye selectivity and respective adsorption capacities of listed organic–inorganic nanohybrids including CNW-graft-PAA/LDH hydrogel [48], P_2Mo_{18}/MIL-101(Cr) [18], 10%CuO-BC [75], and BW(Ni)0.5 [80]. In general, the above-mentioned organic–inorganic nanohybrids exhibited appreciable adsorption capacities for a variety of dyes in the broad range of approximately 22.42–1399 mg g^{-1}. It is an established fact that adsorption capacity depends on various characteristics of adsorbent including pore volume, surface area, and types of chemical functionalities. Typically, high specific surface area and pore volume promote adsorption due to presence of large number of active sites. For instance, for the adsorptive removal of Methylene blue, P_2Mo_{18}/MIL-101(Cr) showed a relatively higher adsorption capability of 312 mg g^{-1} [18] than 22.42 mg g^{-1} obtained for CNW-graft-PAA/LDH hydrogel [48]. This high adsorption capacity of P_2Mo_{18}/MIL-101(Cr) for Methylene blue might be due to sufficiently higher surface area of 800.42 m^2 g^{-1} than 2.02 m^2 g^{-1} obtained for CNW-graft-PAA/LDH hydrogel. However, in addition to the surface area, types of chemical functional available on adsorbent's surface and respective composition play a vital part in the enhanced adsorption capacity of a specific adsorbent. For example, although P_2Mo_{18}/MIL-101(Cr) possessed higher surface area (800.42 m^2 g^{-1}) than

Table 2 Summary of sources and associated health and environmental impacts of various air pollutants

Air pollutants	Type	Sources	Impact on human health and environment	References
CO_2	Primary pollutant	Combustion of fossil fuels in power plants, automobiles, deforestation, soil degradation	Primary greenhouse gas, causes global warming, indirect cause of respiratory diseases via CO production	[34, 86]
CO	Primary pollutant	Smoking, motor vehicles operation, incomplete burning of fuels and biomasses in power plants	Involves in ground-level ozone formation. Causes fatigue, headaches, and dizziness	[35]
SO_2	Primary pollutant	Combustion of high sulfur coal and other fuels in powerplants or locomotives	Acid rain, respiratory problems including respiratory tract infection and inflammation	[55, 57]
VOCs	Primary pollutant	Burning of fossil fuels in powerplants, engines, furnaces, and fireplaces The propellants, solvents, household cleaning products containing benzene or other hydrocarbons	Benzene is carcinogenic, similarly different VOC compounds cause different health effects to the eyes, brain cells, and lungs	[17]
CH_4	Primary pollutant	Municipal landfills, coal mining, oil and gas production and distribution, agriculture, livestock farming, combustion of biogas	Greenhouse gas has a global warming potential 28–36 times more than that of CO_2	[5, 12, 69]
NO_x (NO_2, N_2O)	Primary pollutant	Combustion of coal, motor vehicles operations, biogas production, wastewater containing N-based organic materials, fertilizers	Acid rain, smog formation, NO_2 increases mortality rate through cancer and heart diseases, causes chronic lung diseases N_2O is a far more dangerous greenhouse gas than CO_2 and CH_4, only its concentration in the atmosphere is lower than the other two	[52, 79]

Table 3 Summary of synthesis, surface characteristics, adsorption capacity, regenerative abilities of organic–inorganic nanohybrids for the adsorptive removal of dyes from wastewater

Organic–inorganic nanohybrids	Organic component	Inorganic component	Preparation method	Surface characteristics			Dye selectivity	Adsorption capacity (mg g^{-1})	Regeneration/ desorption cycles	References
				BET		FTIR				
				Pore diameter (nm) and volume (cm^3 g^{-1})	Surface area (m^2 g^{-1})	Wavelength (cm^{-1}) and functional groups				
Cellulose nanowhisker-graft-poly (acrylic acid)/LDH	Cellulose nanowhiskers (CNWs)	Mg/Al-CO_3-layered double hydroxide (LDH)	Hydrolysis of cotton linter to form CNWs. Then modification of CNWs was performed through graft polymerization using acrylic acid in the presence of Mg/Al-CO_3–LDH	6.84 and –	2.02	• 3400 (board band) for OH group • 2900 for CH stretching vibrations • 1000–1300 for CO stretching vibrations • 1635 for bending of H_2O molecules • 1363 (strong peak) for CO_3^{2-} group • Around 800 (multiple peaks) for metal–oxygen vibrations • 3100–3400 for OH vibrational mode • 1704 for carbonyl vibrational mode • 1556 for symmetrical vibrations of carboxylate group • 1460 for asymmetrical vibrations of carboxylate group • 1350 (minor peak) for asymmetrical stretching of carbonate group	Fuchsine	25.9	Removal efficiencies for dyes sustained up till 03 adsorption–desorption cycles	[48]
							Janus green	25.77		
							Malachite green	26.10		
							Crystal violet	23.14		
							Methylene blue	22.42		

(continued)

Table 3 (continued)

Organic–inorganic nanohybrids	Organic component	Inorganic component	Preparation method	Surface characteristics			Dye selectivity	Adsorption capacity (mg g^{-1})	Regeneration/ desorption cycles	References
				BET		FTIR				
				Pore diameter (nm) and volume (cm^3 g^{-1})	Surface area (m^2 g^{-1})	Wavelength (cm^{-1}) and functional groups				
P_2Mo_{18}/MIL-101(Cr)	Terephthalic acid	Wells–Dawson-type polyoxometalate (P_2Mo_{18}) and $Cr(NO_3)_3.9H_2O$	It was prepared using by the reaction of $(NH_4)_6P_2Mo_{18}O_{62}$ (Wells–Dawson-type polyoxometalate commonly known as P_2Mo_{18}), $Cr(NO_3)_3.9H_2O$ and terephthalic acid under hydrothermal conditions	2.56 and 0.513	800.42	• At 1076 for stretching of PO bonds • At 935 for terminal bands of MoN • At 906 and 763 for inter- and intrabridges of Mo − O − Mo, respectively • At 1600 and 1402 high intensity peaks for asymmetric and symmetric vibrations of carbonyl groups • 600–1600 bands representing benzene • At 750 representing CH group • At 578 stretching of CrO	Methylene blue	312.0	Removal efficiencies for Methylene blue was found to be approximately 94% up till 06 adsorption–desorption cycles	[18]

(continued)

Table 3 (continued)

Organic–inorganic nanohybrids	Organic component	Inorganic component	Preparation method	Surface characteristics			Dye selectivity	Adsorption capacity (mg g^{-1})	Regeneration/desorption cycles	References
				BET		FTIR				
				Pore diameter (nm) and volume (cm^3 g^{-1})	Surface area (m^2 g^{-1})	Wavelength (cm^{-1}) and functional groups				
Copper oxide/biochar (CuO/BC)	Copper oxide (CuO)	Biochar (BC) obtained from pyrolysis of Hickory woodchips at 600 °C	It was prepared by modifying BC using CuO through environmental friendly ball milling of CuO particles with BC	– and 0.111	296.5	• At 3407, 1580, and 478, peaks can be linked to the stretching of O−H and N−H groups, aromatic groups, and C−O bending, respectively • At 1089 and 1429, peaks corresponds to C−O and phenolic O−H, respectively • At about 871 and 754, peaks can be ascribed to aromatic C−H bending • At 2371 and 2329, peaks correspond to asymmetrical stretching vibration of C−H bonds, respectively • At 485, sharp vibration peak of the Cu(II)−O bond was observed for 10%-CuO/BC sample	Reactive red (RR 120)	1399	-	[75]

(continued)

Table 3 (continued)

Organic–inorganic nanohybrids	Organic component	Inorganic component	Preparation method	Surface characteristics			Dye selectivity	Adsorption capacity (mg g^{-1})	Regeneration/ desorption cycles	References
				BET		FTIR				
				Pore diameter (nm) and volume (cm^3 g^{-1})	Surface area (m^2 g^{-1})	Wavelength (cm^{-1}) and functional groups				
Magnetic activated wakame biochar	Nickle chloride solution	Wakame Biochar	In a single step, impregnation of nickel on wakame biochar and subsequent activation with KOH at 800 °C was performed	12.12 and 0.451	744.2	• Between 3300–3500, OH stretching band for alcohol or phenol group • At 1634 and 1586, peaks represent vibration of the primary amine (NH) group • At 1404, peak is attributed to nitro compounds (N−O) group • Between 1050 and 1200, peaks for stretching vibrations of alcohols, carboxylic acids and ethers • Around 600, the vibration peaks below 600 cm^{-1} can be considered as stretching vibrations caused hollow metallic compounds	Methylene blue	479.49	A high adsorption capacity of 117.58 mg/g for Methylene blue was found after 05 cycles regeneration cycles in which desorption was performed using magnetic separator	[80]

BW(Ni)0.5 (744.2 $m^2\ g^{-1}$); however, for the adsorptive removal of Methylene blue, P_2Mo_{18}/MIL-101(Cr) demonstrated lower adsorption capacity of 312 mg g^{-1} than 479.49 mg g^{-1} reported for BW(Ni)0.5. This might be due to difference in composition and functionalities on the surface of respective adsorbents. The availability of negatively charged OH, NH, and NO functional groups in BW(Ni)0.5 might be responsible for the relatively higher adsorption capacity (479.49 mg g^{-1}) of cationic Methylene blue dye [80] than P_2Mo_{18}/MIL-101(Cr) (312 mg g^{-1}), which only possessed OH group as evident from the its respective FTIR spectrum. It is clear from Table 3, that CNW-graft-PAA/LDH hydrogel seems to be more versatile with respect to treating a variety of dyes including Fuchsine, Janus green, Malachite green, Crystal violet, and Methylene blue with reasonable adsorption capacities of 25.9 mg g^{-1}, 25.77 mg g^{-1}, 26.10 mg g^{-1}, 23.14 mg g^{-1}, and 22.42 mg g^{-1}, respectively. Apparently, most of the research studies (as explained above) focused on the removal of a single representative dye. However, to further evaluate the practical versatility and effectiveness of the above-mentioned organic–inorganic nanohybrids in terms of dye selectivity, it is important to test them for the treating a variety of industrially relevant dyes.

3.2 Photocatalytic Degradation of Dyes

This section describes the detailed potential of various organic–inorganic nanohybrids for photocatalytic removal of dyes. As evident (Table 4), the dye degradation efficiency and degradation time were found to be in the approximate range of 90–99% and 34–240 min, respectively for all the reported organic–inorganic nanohybrids, irrespective of the dye concentration, light source, and photocatalyst dosage. However, parameters such as dye concentration, light source, and photocatalyst dosage are critical regarding economics and widescale usage for industrial wastewater treatment. From practical standpoint and performance evaluation, photocatalyst possessing high percent degradation of dye per unit dosage of photocatalyst (i.e., organic–inorganic nanohybrid) with low degradation time against high dye concentration will be preferred. For the case of reported nanohybrids, the percent degradation of dye per mg of polyaniline-titanium oxide/reduced graphene oxide [32], MIL-101 Fe/PANI/Pd [22], zinc oxide/cellulose nanocrystals [39] was 1.8. 36.8, and 2.4, respectively. Hence, it was the highest (36.8) for MIL-101 Fe/PANI/Pd with percent degradation efficiency and dosage of 92% and 2.5 mg, respectively. Additionally, it is worthwhile to mention that MIL-101 Fe/PANI/Pd exhibited significantly lower degradation time of 34 min than 90, 150, and 240 min required by polyaniline-titanium oxide/reduced graphene oxide, zinc oxide/cellulose nanocrystals, and polycarbazole (PCz)-tin oxide (SnO_2) [2] to achieve the percent degradation of 90.5, 95, and 93.02/99.13% (Rhodium B/Methylene blue), respectively. Thus, MIL-101 Fe/PANI/Pd can be considered as the most efficient photocatalyst among other aforementioned catalysts. This high degradation performance of MIL-101 Fe/PANI/Pd might be due to its inherent composition in which MIL-101 Fe,

Table 4 Summary of synthesis, surface characteristics, photocatalytic degradation efficiencies, and regenerative abilities of organic–inorganic nanohybrids for the photocatalytic removal of dyes from wastewater

Organic–inorganic nanohybrid	Organic component	Inorganic component	Preparation method	Surface characteristics		Dye selectivity	Photocatalytic studies			Regeneration	References
				BET	FTIR						
				Surface area ($m^2\ g^{-1}$)	Wavelength (cm^{-1}) and functional groups		Dye concentration (mg L^{-1}) and light source	Dosage (mg)	Degradation (%) and degradation time (min)		
Polyaniline-titanium oxide/reduced graphene oxide (PANI-TiO_2/rGO)	Polyaniline (PANI)	Titanium oxide and reduced graphene oxide (rGO)	Initially, rGO was functionalized with TiO_2 by hydrothermal treatment followed by oxidative polymerization with aniline	116.8	• At 1217 and 2918, peaks were attributed to C–N and C–H stretching of PANI • At 1396 and 1046, peaks corresponded to C–N stretching and bending vibrations of C–H group • At 1629, peak referred to the graphene-based skeletal vibration • Around 1000, wide peaks were associated with stretching and bending of Ti–O–Ti	Rhodium B	4.79 and visible	50	90.5 and 90	Negligible change in removal efficiency till 04 regeneration cycles	[32]

(continued)

Table 4 (continued)

Organic–inorganic nanohybrid	Organic component	Inorganic component	Preparation method	Surface characteristics		Dye selectivity	Photocatalytic studies			Regeneration	References
				BET	FTIR						
				Surface area ($m^2\ g^{-1}$)	Wavelength (cm^{-1}) and functional groups		Dye concentration (mg L^{-1}) and light source	Dosage (mg)	Degradation (%) and degradation time (min)		
MIL-101 Fe/PANI/Pd	Polyaniline (PANI)	Pd, MIL-101 Fe	It was prepared by functionalizing MIL-101 Fe by PANI followed by grafting of Pd	28.03	• At 1600–1400, the broad peaks were associated with asymmetrical and symmetrical stretching of the carboxylate in the MIL-101 • At 540, the vibrations were linked to the Fe–O • At 1133, the band was attributed to carboxylate group with stretchings of C–C and C–H • At 1477, peak was related to C=C stretching of PANI with aromatic rings of quinonoid and benzenoid • At 798, C-H and C=C groups in benzenoid were found • At 1303, band was attributed to C–N of secondary amines	Rhodium B	25 and visible	2.5	92 and 34	–	[22]

(continued)

Table 4 (continued)

Organic–inorganic nanohybrid	Organic component	Inorganic component	Preparation method	Surface characteristics		Dye selectivity	Photocatalytic studies			Regeneration	References
				BET	FTIR						
				Surface area ($m^2\ g^{-1}$)	Wavelength (cm^{-1}) and functional groups		Dye concentration (mg L^{-1}) and light source	Dosage (mg)	Degradation (%) and degradation time (min)		
Zinc oxide/cellulose nanocrystals (ZnO/CNCs)	Cellulose nanocrystals (CNCs)	Zinc oxide (ZnO)	Initially, CNCs were extracted from Nypa fruticans trunk (NFT) using hydrolysis by HCl. Then, via precipitation ZnO nanoparticles were integrated to CNCs	74.8	• At 3375 and 1380, bands were associated with hydroxyl groups • At 1630 and 1060, peaks might be attributed to O–H bending C–O–C stretching of pyranose and glucose • At 440, peak was linked to stretching of Zn–O • At 1721, the C=O stretching with decreased band intensity as compared to CNC might be due to strong interaction between O-atoms of carbonyl and ZnO	Methylene blue	31.9 and UV	40	95 and 150	–	[39]

(continued)

Table 4 (continued)

Organic–inorganic nanohybrid	Organic component	Inorganic component	Preparation method	Surface characteristics		Dye selectivity	Photocatalytic studies			Regeneration	References
				BET	FTIR						
				Surface area ($m^2\ g^{-1}$)	Wavelength (cm^{-1}) and functional groups		Dye concentration (mg L^{-1}) and light source	Dosage (mg)	Degradation (%) and degradation time (min)		
Polycarbazole (PCz)-tin oxide (SnO_2) (PCT)	Polycarbazole (PCz)	Tin oxide (SnO_2)	In the first step, PCz was prepared via polymerization of carbazole monomer. Then, PCz was polymerized with SnO_2	7.9	• At 440, peak was linked to stretching of Zn–O • At 1721, the C=O stretching with decreased band intensity as compared to CNC might be due to strong interaction between O-atoms of carbonyl and ZnO	Rhodium B	0.48 and sunlight	–	93.02 and 240	Negligible change in the degradation behavior till 4 cycles	[2]
						Methylene blue	3.2 and sunlight	–	240		

polyaniline, and Pd mutually interacted in an energetically favorable manner. This might have promoted the splitting of electron–hole pairs and facilitated interfacial transfer between polyaniline and MIL-101 Fe supported by Pd. Additionally, the presence of specific surface functional group (i.e., Fe–O) and good surface area (28.03 $m^2\ g^{-1}$) might enhanced the photocatalytic activity of MIL-101 Fe/PANI/Pd.

4 Potential of Organic–Inorganic Nanohybrids for Removal of Gases and VOCs

Organic–inorganic nanohybrids play great role for removal of various gases [59]. Among the pollutants mentioned in Table 2, most of the emissions can be prevented or controlled to the maximum levels (such as CH_4, SO_2, NO_x), except for CO_2 and VOCs that require remedial techniques. In this section, the potential of organic–inorganic nanohybrids for the removal of CO_2 and VOCs has been discussed.

4.1 Mitigation Technologies

Various CO_2 capturing methods from gas streams have been investigated in several studies. These include (1) capture before combustion, (2) capture after combustion, and (3) oxy-fuel combustion. In general, the capture after combustion is commonly used due to its economic feasibility [74]. Additionally, it can be conveniently retrofitted in already existing combustion units. For the case of capturing before combustion and oxy-fuel combustion, retrofitting requires a lot of financial resources and thus are considered expensive. Common technologies for capturing CO_2 after combustion are adsorption, absorption, membrane separation, etc. Among aforementioned technologies, amine scrubbing via absorption is the most mature and practical method. However, it requires a lot of energy for amine regeneration. As per National Energy Technology Laboratory, USA, for the case of subcritical coal-based power unit, the amine scrubbing technology increases power cost by 85% [20]. Other disadvantages associated with amine-based absorption include increased chances of corrosion and the cost associated with amine make-up allowed researchers to explore other methods such as adsorption and membrane technology. Several methods have been used to mitigate VOCs over the years; some of those methods are mentioned below:

- *Recovery* through adsorption, membrane separation, condensation
- *Destruction* through ozone catalytic oxidation, photocatalytic degradation, incineration, biological degradation.

However, a single method for recovery or destruction of VOCs is not efficient enough; therefore, the synergic effect of multiple treatments has been considered

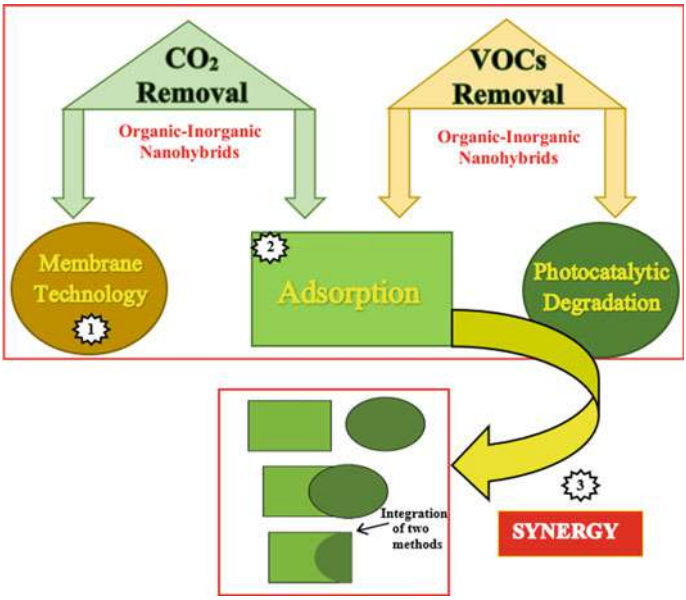

Fig. 4 Adopted technologies for the removal of CO_2 and VOCs

a rather attractive option (Fig. 4). Among all the other methods, a combination of adsorption and photocatalysis is considered one of the most efficient technologies because it consumes lower energy, exhibits higher removal efficiency, and has proved to be the most environment friendly [90]. In this integration, the increase in photocatalytic degradation performance can be seen as a result of the enrichment of VOCs from gas to a solid phase. Moreover, photocatalyst oxidized VOCs to CO_2 and H_2O at room temperature, thereby regenerating the adsorbent for uninterrupted VOC removal [14].

4.2 Membrane-Based CO_2 Separation

Membrane-based separation process for capturing CO_2 is an environmental friendly, easy to handle, and less costly method than conventional amine-based absorption process as per IPCC report (2006). Since in this method no chemical reaction is involved, it has minimal impact on environment in comparison with amine-based absorption process. Additionally, there is no cost associated with regeneration; thus, it is more economical process than amine-based absorption [74].

4.2.1 Mixed Matrix Membranes (MMMs); Polymer–Inorganic Nanohybrids

The typical characteristics of polymeric membranes (Pebax® and Polyactive®) include working at relatively lower temperatures and good temperature stability and strength in comparison with ceramic membranes. Generally, flue gases have high flow rates. Therefore, for effective CO_2 capturing, extremely large surface area is a major requirement for membranes. On the other hand, development of ceramic membranes with extensive surface areas is a major challenge. For the case of polymeric membranes, the manufacturing cost is far lower than ceramic membranes which is primarily due to abundance of raw materials for their development. Hence, employing polymer-based membranes is a viable option for capturing CO_2 from flue gas [46]. However, as highlighted above, the only limitation of polymer-based membranes for CO_2 capture is material characteristics which can be modified via chemical treatments and/or altering membrane properties via blending with other substances. In this context, developing new membranes such as a combination of both organic and inorganic constituents [typically known as mixed matrix membranes (MMMs)] is a promising opportunity. In these membranes, polymeric substances are consistently mixed in a dispersed inorganic filler. Such membranes have the tendency to overcome limitation as explained above. Common examples of inorganic fillers include silica, metal oxides, zeolites, and metal–organic frameworks (MOFs). They enhance the performance of the resultant membranes by inclusion of their own intrinsic properties and introduction of a variety of functional groups along with excellent chemical and mechanical strength. Some of the polymer–inorganic nanohybrid combinations are shown in Fig. 5 and Table 5.

Polyhedral oligomeric silsesquioxane (POSS) is an eccentric class of Si-based inorganic nanostructure components having a 3D cage-like structure with formula $(RSiO_{1.5})_n$ $(n \geq 6)$, which are novel fillers for polymer matrices with excellent properties. POSS exhibits some unique properties in the formation of POSS-polymer hybrid membranes compared to other inorganic fillers. Mostly, the inorganic nanoscale agents have a limitation of size distribution that cause hindrance in their dispersion inside polymer matrices. POSS molecules, on the other hand, can disperse effectively throughout the matrix, even on a molecular level, due to their definite structure and size, therefore, resulting in providing excellent properties to nanohybrid membranes in terms of thermal as well as mechanical stability and resistance to oxidation. Moreover, R in $(RSiO_{1.5})_n$ $(n \geq 6)$ represents organic functional groups that can act as active sites, therefore enhancing the affinity of the nanohybrid membrane toward CO_2, resulting in high CO_2 selectivity [77].

Metal–organic frameworks, a major class of molecular sieves, consist of inorganic metallic clusters and organic links. These organic linkers and metal nodes hold together the entire MOF structure via coordination bonds, providing active binding sites for CO_2, increasing the chemical interaction of nanohybrid membranes. Moreover, MOFs remarkably reduce energy consumption for CO_2 separation [6].

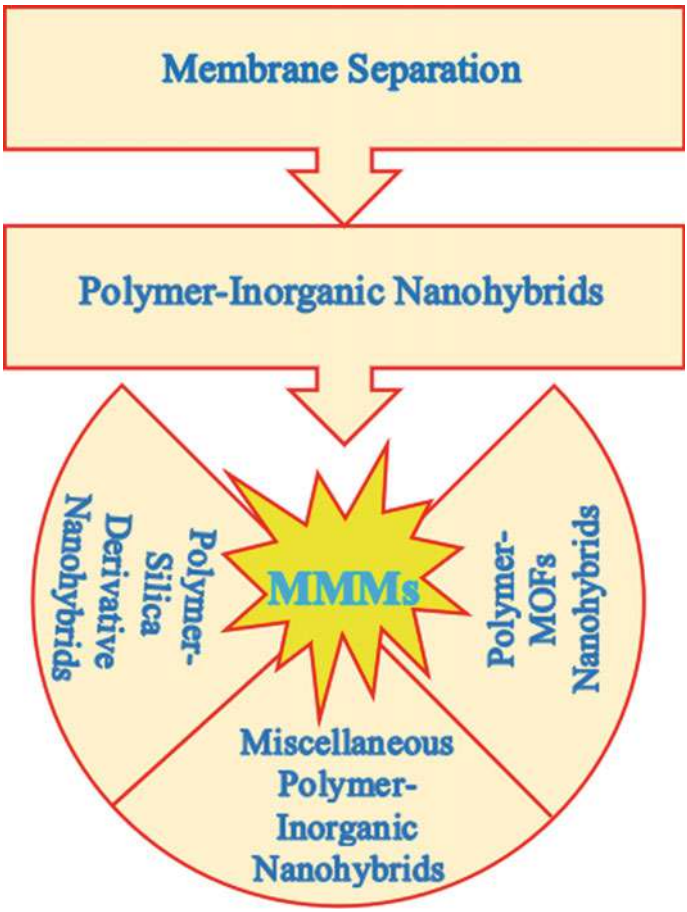

Fig. 5 Adopted types of organic–inorganic nanohybrid combinations for MMMs

4.2.2 Adsorption-Based CO_2 Capture

Among other sorption methods, the solid adsorption method is more efficient as it possesses advantages such as low energy consumption, high adsorption potential, good performance of regeneration, no risk of corrosion, simple operation. Therefore, it exhibits good application potential in gas separation. Solid adsorption occurs when a fluid makes contact with a solid surface; it results in the enrichment of material or increased density of the fluid in an interface compared to other phases. Solid adsorption includes solid–gas and solid–liquid interfaces. The utilization of organic–inorganic nanohybrid materials as solid adsorbents provides improved adsorption performance as they exhibit the best properties of both species (organic and inorganic) combined (Fig. 6; Table 6). Some of the categories of these nanohybrid adsorbents have been mentioned below.

Table 5 Polymer–inorganic nanohybrids for CO_2 capture through MMMs

MMMs origin	Species	Inorganic species	Conditions	CO_2 permeation (Barrer)	Selectivity	References
Polymer-silica-derivative nanohybrids	Pebax 1657	Halloysite nanotubes	25 °C, 1 bar	80.4	290 (CO_2/N_2)	[82]
	PEG	POSS-NH_2	30 °C	1566.8	Moderate	[27]
	Pebax 1657	Siloxane–alumina	Room temperature	1765	28 (CO_2/N_2)	
	Pebax 1657	Porous organosilicon nanotube	30 °C, 2 bar (dry)	164	25 (CO_2/CH_4)	[78]
	Pebax 1657	Porous organosilicon nanotube	30 °C, 2 bar (humidified)	972	29 (CO_2/CH_4)	
	Pebax 1657	POSS-acid	35 °C, 2 bar	127	8.8 (CO_2/H_2)	[87]
Polymer-MOFs nanohybrids	Pebax 1657	UiO-66-NH_2	20 °C, 3 bar (dry)	85	82 (CO_2/N_2)	[61]
	Pebax 1657	UiO-66-NH_2	20 °C, 1 bar (humidified)	130	72 (CO_2/N_2)	
Miscellaneous polymer–inorganic nanohybrids	Pebax 1657	Fe_3O_4-GO	25 °C, 2 bar	538	75 (CO_2/N_2)	[88]
	Pebax 1657	MXene	30 °C, 2 bar	148	63 (CO_2/N_2)	

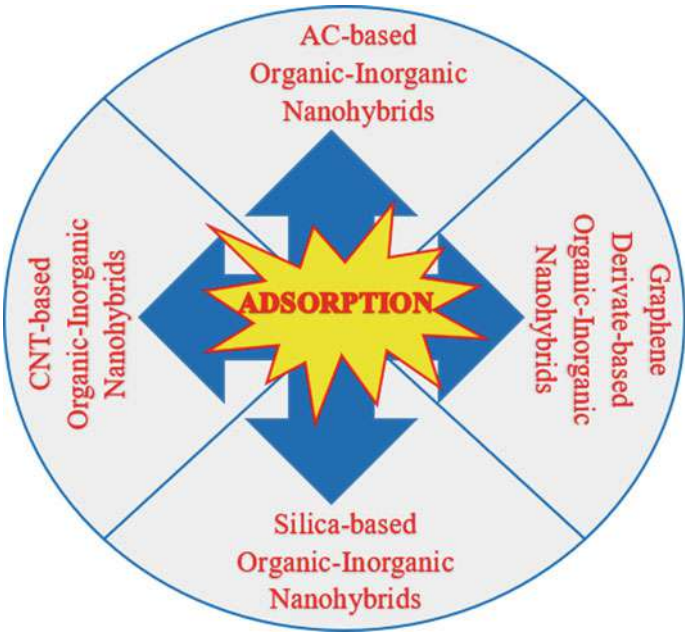

Fig. 6 Adopted organic–inorganic nanohybrids for CO_2 adsorption

Activated carbon has always been considered a good adsorbent due to its lower price, developed pore structure, mature preparation technology, large surface area and hydrophobicity that makes it especially attractive for post-combustion CO_2 capture. AC-based CO_2 adsorption is mainly physical, resulting in the temperature sensitivity of the adsorbent. This issue can be resolved by the formation of AC-based organic–inorganic nanohybrids with MgO, CuO, NiO, and so on. The addition of other materials in AC-based adsorbents can enhance the performance as well as selectivity, due to the combined effect of AC and additives. CO_2, being of acidic nature, exhibits great affinity toward basic materials, due to which the introduction of metallic oxides to AC can extraordinarily enhance the adsorption capacity of the material. During acid–base interaction between the gas molecules and surface of the adsorbent, the metal oxides, having base characteristics, donate their electrons to CO_2. This combination of AC-MO nanohybrid materials improves surface properties and promotes CO_2 interaction of AC [31].

Graphene, consisting of 2D carbon atoms in a hexagonal honeycomb lattice, and its oxidized form, GO, have both been extensively being used as adsorbents for the past few years. Graphene and its derivatives are employed in adsorption applications because they have superior thermal as well as mechanical properties and large theoretical specific surface area, but due to strong van der Waals forces, graphene sheets have the propensity to form aggregations resulting in the decrease of surface area. The adsorption capacity of any material strongly depends upon pore characteristics and surface area; therefore, surface modification or introduction of

Table 6 AC-based organic–inorganic nanohybrid adsorbents

Adsorbent origin	Organic species	Inorganic specie	Adsorbent synthesis	Adsorption conditions	CO_2 Adsorption capacity (mmol g^{-1})	Regeneration/ stability	References
AC-inorganic-based nanohybrids	AC	CuO nanoparticles	Wet impregnation	25 °C, 1 bar	6.72	Stable with no performance loss for multiple cycles	[8]
	H_3PO_4-modified AC	Al_2O_3	Co-impregnation	30 °C, 1 bar	18.87	Stable for 10 cycles, low energy requirement	[44]
		MgO	Co-impregnation	30 °C, 1 bar	18.85		
		Cu_2O	Co-impregnation	30 °C, 1 bar	21.52		
		NiO	Co-impregnation	30 °C, 1 bar	20.67		
Graphene/GO-inorganic nanohybrids	GO (CNF derived)	Fe_3O_4	Colloidal blending	27 °C, 20 bar	2.0	Good with a low-temperature requirement	[53]
	GO (graphite derived)	Fe_3O_4	Chemical method	27 °C, 20 bar	2.3	Good with a low-temperature requirement	
	Graphene	TEPA-functionalized Si aerogel	Wet impregnation and freeze drying	90 °C, 0.15 bar	4.9	Stable for 10 cycles	[73]
	GO	TiO_2	Colloidal blending	25 °C, 1 bar	35.806	–	[40]
	Graphene	TEPA-functionalized Si aerogel and SBA-15 (mesoporous silica sieve)	Wet impregnation and freeze drying	25–120 °C	6.02	Stable for 10 cycles	Wang et al. (2019b)

(continued)

Table 6 (continued)

Adsorbent origin	Organic species	Inorganic specie	Adsorbent synthesis	Adsorption conditions	CO_2 Adsorption capacity (mmol g^{-1})	Regeneration/ stability	References
CNT-inorganic nanohybrids	MWCNT	HNO_3 and H_2SO_4	Chemical treatment	25 °C, 1 bar	0.3274	–	[38]
	MWCNT	ZnO and SiO_2	Chemical method	0 °C, 1 bar	1.32	–	[21]
	PEI-functionalized CNT	Nanozeolite and Cd cations	Colloidal blending	25 °C, 20 bar	3.7	–	[56]
	N-doped CNT	K_2CO_3	Chemical activation	0 °C, 1 bar	4.5	Short regeneration cycle, low energy requirement	[72]
Silica–organic nanohybrids	Phenolic resin (AC source)	H-ZSM-5	Thermal method	25 °C, 1 bar	2.3	–	[84]
	AC	Zeolite 13X (honeycomb monolith)	Hydrothermal method	25 °C, 2.4 bar	2.63	–	[49]
	Phenolic resin (AC source)	Zeolite NaUSY	Hydrothermal method	25 °C, 1 bar	3.21	–	[85]

additives in G/GO structures can alleviate this problem. GO is more reactive than graphene because of the presence of oxygen functional groups such as hydroxyl and epoxy groups on the surface, and carboxylic and ketone groups at the edges that allow the addition of other materials. That is why GO is a favorable candidate to support metal oxides. In GO-MO nanohybrids, acid–base interaction between CO_2 and metal oxides increases the chemical interaction between adsorbent and adsorbate.

Carbon nanotubes (CNTs), which exist in form of either single or multiwalled carbon nanotubes (MWCNTs), display cylindrical morphology and have been extensively used for CO_2 adsorption due to their hollow morphology, thermal stability, mechanical strength, and wide surface area [63]. Unfunctionalized CNTs have lower adsorption capacity, which is why the introduction of inorganic additives to enhance its sorption capacity has been a potential area of investigation for many years now. The introduction of MOFs or metallic oxide can enhance the adsorption capacity of CNTs due to acid–base electron transfer/reaction between CO_2 and metallic species as discussed before.

Silica-based minerals and compounds (such as mesoporous silica, MCM-41, zeolites), being non-toxic non-metallic nanomaterials, are broadly used as nanofillers during adsorption processes due to their high mechanical strength, easy dispersion, high-temperature resistance, and good chemical stability [33]. However, these materials (especially zeolites), when exposed to moisture, tend to encounter a substantial drop in adsorption capacity. Therefore, the addition of water-repellent components such as graphene and activated carbons in zeolites and other Si-based materials could result in improved hydrophobicity, thereby improving the adsorption capacity of the nanohybrid.

4.3 Adsorption–Photocatalysis Synergic VOC Removal

Photocatalytic degradation has been extensively adopted VOC removal technology due to ease of its operation at room temperature and non-selectiveness. In this process, a semiconductor is illuminated, and as a result, photoexcited electrons and holes (in a vacant conduction band) are formed that react with the VOCs adsorbed on the surface of the photocatalyst and oxidize them into CO_2 and H_2O. Due to their electronic configuration, semiconductors can provide photo-induced charges for the redox process. Titanium oxide (TiO_2) is the most extensively used semiconductor as compared to other semiconductors (such as ZnO, ZnS, Fe_2O_3, CdS) due to its chemical as well as physical stability, resistance to corrosion, lower cost, and non-toxicity [68]. At low concentrations (ppb-ppm), the conventional semiconductors have a very low tendency to adsorb VOC. Moreover, generally, the photocatalysts are unstable and prone to agglomeration. *Carbon*, having a large surface area and porous structure, has a great tendency to support distribution as well as fixation of the nanosized photocatalysts [36]. Moreover, carbon-based materials, having black color, represent high adsorption potential and fast electron transfer that keeps the VOC molecules in the vicinity of active sites of the reaction, improve visible light adsorption tendency,

promote the radical formation, and prevent by-product formation as well as inactivation of photocatalysts. In absence of these carbon-based materials, the by-products of photocatalysis are conveniently aggregated on the surface of the photocatalyst and its catalytic efficiency is reduced as a result [65]. Some of the carbon–semiconductor nanohybrids for the integrated adsorption–photocatalysis process are given in Table 7.

Activated carbon fibers (ACFs) ensure the VOC molecules' flow toward the site of adsorption by providing a special adsorption force field, leading to high adsorption potential and capacity [7]. However, being hydrophobic, ACFs could only remove weak polar or non-polar VOCs such as formaldehyde, toluene, and styrene. To improve adsorption–photocatalysis performance, acid treatment could be performed to ACFs before application in the integration process. The acid treatment results in the addition of more functional groups on ACFs surface and larger pore size which is helpful in the interaction between ACFs and photocatalyst. CNTs comprise peculiar hollow structure that provides stability to the nanoparticles of photocatalyst and longer residence time to VOC molecules on the material. Moreover, depending upon the diameter and helicity of the tube, CNT could either be metallic, semimetallic, or semiconducting due to which CNT acts as an electron-transfer channel in synergic VOC removal [29].

Graphene material holds many advantages compared to other carbon materials such as fast thermal and electrical conductivity, high UV–visible light-transmittance rate corrosion resistance and good mechanical properties. The photogenerated electrons behave as massless Dirac fermions causing enhanced performance of photocatalysis [43].

However, a single layer of graphene tends to aggregate due to van der Waals force, its zero-bandgap makes graphene conductor rather than semiconductor, which makes dispersion of metal oxides on graphene as well adsorption of VOCs very difficult. To overcome this problem, some modifications have been applied to graphene over the years such as N-doping and Si-modified graphene. Some of the key factors other than nanohybrid properties that affect the synergic VOC removal efficiencies of the adsorption–photocatalysis integration method are humidity, temperature and concentration of VOC that is to be removed. All these factors have an inverse relation with the adsorption–photocatalysis synergic efficiencies, as shown in Fig. 7.

5 Regeneration, Stability, and Reproducibility of Nanohybrids

For practical and economic considerations in industrial wastewater treatment, the regeneration of adsorbent is critical. There are different ways to reuse and regenerate adsorbents. Generally, the regeneration methods depend on nature of adsorbents and adsorbate. For instance, $P_2Mo_{18}O_{62}$/MIL-101(Cr) is insoluble in water, and thus, it

Table 7 Organic–inorganic nanohybrids for integrated adsorption–photocatalysis process

Nanohybrids' origin	Organic species	Inorganic species	BET surface area (m^2/g)	VOC	Initial concentration (ppm)	Adsorption efficiency (%)	Photocatalytic efficiency (%)	References
AC-inorganic	ACFs	TiO_2	441.3	Toluene	460	97	81	
	ACFs	TiO_2	1020.6	Formaldehyde	0.8	14.6	83.6	
	ACFs	Au/TiO_2	–	Styrene	25 ± 1.5	–	91	[62]
CNT-inorganic	MWCNT	MnO_2	93	Formaldehyde	10	–	43	[37]
Graphene–inorganic	N-doped graphene	Fe_2O_3	–	Acetaldehyde	810	–	55	[71]
Graphene–inorganic	rGO	TiO_2	105.1	Formaldehyde	0.5	–	88.3	[81]
	rGO	TiO_2	208.1	Methanol	4000 ± 200	80 mg/g catalyst	–	[54]

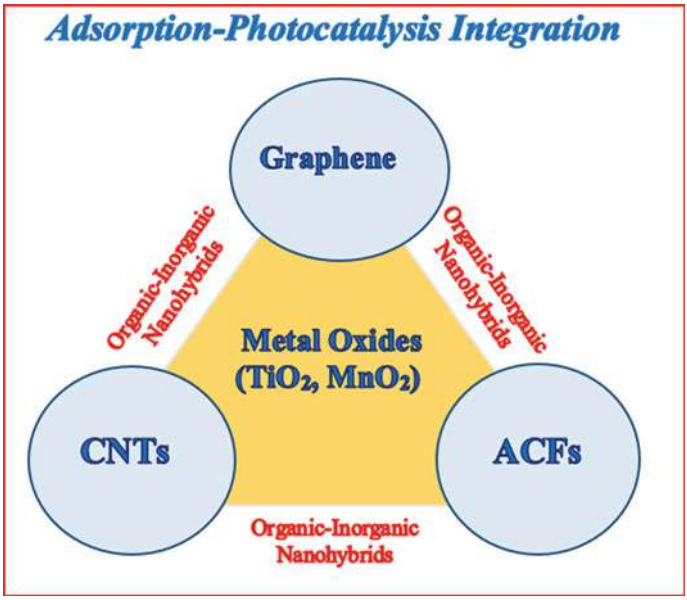

Fig. 7 Adopted organic–inorganic nanohybrid combinations for synergic adsorption–photocatalysis process

can be conveniently extracted from aqueous solution via centrifugation. Additionally, it can be simply regenerated by washing with 1:1 solution of water and ethanol. Also, $BW(Ni)_{0.5}$ can be easily separated from aqueous solution by applying magnetic field since nickel is uniformly distributed on the surface of biochar. In general, the organic inorganic nanohybrids studied in this chapter for the adsorptive and catalytic removal of dyes demonstrated significant recycling/regenerative capabilities with effective recycling/regeneration cycles in the range of 3–6, till removal efficiencies of dyes were sustained as presented in Tables 3, 4 and 6 respectively. For the adsorptive removal of CO_2, regeneration of respective organic inorganic nanohybrids was effective up to maximum of 10 cycles.

6 Conclusion and Future Perspectives

In this chapter, various organic inorganic nanohybrids developed and characterized in very recent years for the removal of various dyes (Methylene blue, Rhodium B, etc.), pesticides (CCPs), and VOCs (i.e., formaldehyde, toluene) and gases (CO_2) via adsorption and photocatalytic degradation were analyzed with respect to their synthesis methods, characterization, adsorption capacity, degradation efficiency, and regenerative capability. For the dyes, the maximum adsorption capacity and photocatalytic efficiency were found to be 1399 mg g^{-1} and 92% for the removal of Reactive

Red dye (RR 120) and Rhodium B (Initial concentration of 25 mg L^{-1}) by copper oxide/biochar (CuO/BC) and MIL-101 Fe/PANI/Pd, respectively as compared to other reported nanohybrids. For the removal of glyphosate and DDT (typical pesticides), UiO-67/GO and PANI/SnO_2 demonstrated maximum adsorption capacity and photocatalytic degradation of 483.7 and 97%, respectively. These appreciable high removal efficiencies via adsorption or photocatalytic degradation seemed to be associated with surface properties such as abundant specific functional groups and surface areas of adsorbents and photocatalysts. For the removal of CO_2, GO-TiO_2 nanohybrid showed the maximum adsorption capacity of 35.806 mmol g^{-1} under the ambient conditions of 25 °C and 1 bar as compared to other nanohybrids. Toluene (VOC) was effectively removed using ACF-TiO_2 nanohybrid for integrated adsorption and photocatalysis and exhibited significant adsorption and photocatalytic efficiency of 97% and 81%, respectively. For all reported nanohybrids, the regeneration was found to be effective in the range of 3–10 cycles without any substantial change in their removal efficiencies.

Despite of the considerable recent advancements in the development of a wide variety of organic inorganic nanohybrids and their applications in environmental remediation, following are the important recommendations regarding future studies:

- Most of the studies investigated the removal efficiency of a specific organic–inorganic nanohybrid utilizing synthetic wastewater containing a single model contaminant. However, from practical stand point, actual wastewater containing a variety of dyes/pesticides should be used for testing the adsorption capacity and/or photocatalytic removal efficiency of a nanohybrid.
- Additionally in most cases, batch studies were performed to evaluate the adsorptive and photocatalytic removal efficiency of nanohybrid. However, these performance evaluations should be made in continuous flow mode mimicking the actual industrial operation using lab-scale pilot studies.
- Also, a limited number of studies focused on the regeneration capabilities of a specific nanohybrid. Secondly, regeneration of nanohybrids has not been thoroughly investigated. In this context, future studies can further explore the efficacy of various regenerating agent, innovative regeneration methodology, effect of regeneration time, etc.
- Lastly, life cycle analysis (LCA) and detailed economic feasibility can also be incorporated to analyze the fate and financial status of utilizing certain nanohybrids in the view of practical considerations.

References

1. Ahmed J, Thakur A, Goya A (2021) Industrial wastewater and its toxic effects. In: Shah MP (ed) Biological treatment of industrial wastewater. Royal Society of Chemistry
2. Ali MM, Williams DJ, Banu MS (2020) Enhanced photocatalytic activity of annealed polycarbazole-tinoxide nanocomposite against RhB and MB dyes under UV and natural

sunlight irradiations. J Polym Res 27:338. https://doi.org/10.1007/s10965-020-02165-7
3. Bin BZ, Park J-H, Kang J, Lim H-J (2016) Characterization of a smog chamber for studying formation and physicochemical properties of secondary organic aerosol. Aerosol Air Qual Res 16:3102–3113. https://doi.org/10.4209/aaqr.2015.10.0580
4. Bin BZ, Park JH, Lim HJ (2017) Influence of NH_3 on secondary organic aerosols from the ozonolysis and photooxidation of A-pinene in a flow reactor. Atmos Environ 164:71–84. https://doi.org/10.1016/j.atmosenv.2017.05.034
5. Baillie J, Risk D, Atherton E et al (2019) Methane emissions from conventional and unconventional oil and gas production sites in southeastern Saskatchewan, Canada. Environ Res Commun 1:011003. https://doi.org/10.1088/2515-7620/ab01f2
6. Ban Y, Zhao M, Yang W (2020) Metal-organic framework-based CO_2 capture: from precise material design to high-efficiency membranes. Front Chem Sci Eng 14:188–215. https://doi.org/10.1007/s11705-019-1872-6
7. Baur GB, Beswick O, Spring J et al (2015) Activated carbon fibers for efficient VOC removal from diluted streams: the role of surface functionalities. Adsorption 21:255–264. https://doi.org/10.1007/s10450-015-9667-7
8. Boruban C, Esenturk EN (2018) Activated carbon-supported CuO nanoparticles: a hybrid material for carbon dioxide adsorption. J Nanoparticle Res 20:59. https://doi.org/10.1007/s11051-018-4139-0
9. Cheng S, Zhang J, Wang Y et al (2019) Global research trends in health effects of volatile organic compounds during the last 16 years: a bibliometric analysis. Aerosol Air Qual Res 19:1834–1843. https://doi.org/10.4209/aaqr.2019.06.0327
10. Chiang TL, Wang YC, Ding WH (2012) Trace determination of rhodamine B and rhodamine 6G dyes in aqueous samples by solid-phase extraction and high-performance liquid chromatography coupled with fluorescence detection. J Chin Chem Soc 59:515–519. https://doi.org/10.1002/jccs.201100318
11. Dixit S, Yadav A, Dwivedi PD, Das M (2015) Toxic hazards of leather industry and technologies to combat threat: a review. J Clean Prod 87:39–49. https://doi.org/10.1016/j.jclepro.2014.10.017
12. Flores-Jiménez DE, Carbajal N, Algara-Siller M et al (2019) Atmospheric dispersion of methane emissions from sugarcane burning in Mexico. Environ Pollut 250:922–933. https://doi.org/10.1016/j.envpol.2019.04.025
13. Gelles T, Krishnamurthy A, Adebayo B et al (2020) Abatement of gaseous volatile organic compounds: a material perspective. Catal Today 350:3–18. https://doi.org/10.1016/j.cattod.2019.06.017
14. Geng Q, Tang S, Wang L, Zhang Y (2010) Investigation into adsorption and photocatalytic degradation of gaseous benzene in an annular fluidized bed photocatalytic reactor. Environ Technol (United Kingdom) 49:4446–4652. https://doi.org/10.1080/09593330.2014.954005
15. Gürses A, Açıkyıldız M, Güneş K, Gürses, M.S. (2016) Dyes and pigments: their structure and properties. In: Dyes and pigments.SpringerBriefs in Molecular Science. Springer, Cham
16. Gusain R, Gupta K, Joshi P, Khatri OP (2019) Adsorptive removal and photocatalytic degradation of organic pollutants using metal oxides and their composites: a comprehensive review. Adv Colloid Interface Sci 272:102009. https://doi.org/10.1016/j.cis.2019.102009
17. Harb P, Locoge N, Thevenet F (2020) Treatment of household product emissions in indoor air: real scale assessment of the removal processes. Chem Eng J 380:122525. https://doi.org/10.1016/j.cej.2019.122525
18. Hoseini AA, Farhadi S, Zabardasti A, Siadatnasab F (2020) An organic-inorganic hybrid nanomaterial composed of a Dowson-type $(NH_4)_6P_2Mo_{18}O_{62}$ heteropolyanion and a metal-organic framework: synthesis, characterization, and application as an effective adsorbent for the removal of organic dyes. RSC Adv 10:40005–40018. https://doi.org/10.1039/d0ra07042d
19. Hua X, Wu YJ, Zhang X et al (2018) Analysis on ambient volatile organic compounds and their human gene targets. Aerosol Air Qual Res 18:2654–2665. https://doi.org/10.4209/aaqr.2018.08.0320

20. James R, Zoelle A, Keairns D et al (2019) Cost and performance baseline for fossil energy plants, volume 1: bituminous coal and natural gas to electricity
21. Jena KK, Panda AP, Verma S et al (2019) MWCNTs-ZnO-SiO_2 mesoporous nano-hybrid materials for CO_2 capture. J Alloys Compd 800:279–285. https://doi.org/10.1016/j.jallcom.2019.06.011
22. Karami K, Beram SM, Siadatnasab F et al (2021) An investigation on MIL-101 Fe/PANI/Pd nanohybrid as a novel photocatalyst based on MIL-101(Fe) metal–organic frameworks removing methylene blue dye. J Mol Struct 1231:130007. https://doi.org/10.1016/j.molstruc.2021.130007
23. Khan MR, Khan MA, Alothman ZA et al (2014) Quantitative determination of methylene blue in environmental samples by solid-phase extraction and ultra-performance liquid chromatography-tandem mass spectrometry: a green approach. RSC Adv 4:34037–34044. https://doi.org/10.1039/c4ra03504f
24. Kwon JW, Park HW, Kim WJ et al (2018) Exposure to volatile organic compounds and airway inflammation. Environ Heal A Glob Access Sci Source 17:1–8. https://doi.org/10.1186/s12940-018-0410-1
25. Lee GH, Choi KC (2020) Adverse effects of pesticides on the functions of immune system. Comp Biochem Physiol Part-C Toxicol Pharmacol 235:108789. https://doi.org/10.1016/j.cbpc.2020.108789
26. Lellis B, Fávaro-Polonio CZ, Pamphile JA, Polonio JC (2019) Effects of textile dyes on health and the environment and bioremediation potential of living organisms. Biotechnol Res Innov 3:275–290. https://doi.org/10.1016/j.biori.2019.09.001
27. Li S, Jiang X, Yang X et al (2019) Nanoporous framework "reservoir" maximizing low-molecular-weight enhancer impregnation into CO_2-philic membranes for highly-efficient CO_2 capture. J Memb Sci 570–571:278–285. https://doi.org/10.1016/j.memsci.2018.10.068
28. Li W, Wu R, Duan J et al (2016) Impact of prechlorination on organophosphorus pesticides during drinking water treatment: Removal and transformation to toxic oxon byproducts. Water Res 105:1–10. https://doi.org/10.1016/j.watres.2016.08.052
29. Li Z, Gao B, Chen GZ et al (2011) Carbon nanotube/titanium dioxide (CNT/TiO_2) core-shell nanocomposites with tailored shell thickness, CNT content and photocatalytic/photoelectrocatalytic properties. Appl Catal B Environ 110:50–57. https://doi.org/10.1016/j.apcatb.2011.08.023
30. Link MF, Kim J, Park G et al (2017) Elevated production of NH_4NO_3 from the photochemical processing of vehicle exhaust: implications for air quality in the Seoul Metropolitan Region. Atmos Environ 156:95–101. https://doi.org/10.1016/j.atmosenv.2017.02.031
31. Liu Z, Green WH (2013) Experimental investigation of sorbent for warm CO_2 capture by pressure swing adsorption. Ind Eng Chem Res 52:9665–9673. https://doi.org/10.1021/ie303534u
32. Ma J, Dai J, Duan Y et al (2020) Fabrication of PANI-TiO_2/rGO hybrid composites for enhanced photocatalysis of pollutant removal and hydrogen production. Renew Energy 156:1008–1018. https://doi.org/10.1016/j.renene.2020.04.104
33. Ma M, Li H, Xiong Y, Dong F (2021) Rational design, synthesis, and application of silica/graphene-based nanocomposite: a review. Mater Des 198:109367. https://doi.org/10.1016/j.matdes.2020.109367
34. Manan ZA, Mohd Nawi WNR, Wan Alwi SR, Klemeš JJ (2017) Advances in process integration research for CO_2 emission reduction—a review. J Clean Prod 167:1–13. https://doi.org/10.1016/j.jclepro.2017.08.138
35. Manning AJ, Ryall DB, Derwent RG et al (2003) Estimating European emissions of ozone-depleting and greenhouse gases using observations and a modeling back-attribution technique. J Geophys Res Atmos 108:4405. https://doi.org/10.1029/2002jd002312
36. Mcevoy JG (2014) Carbon-enhanced photocatalysts for visible light induced detoxification and disinfection. University of Ottawa, Canada
37. Miao J-L, Li C-B, Liu H-H, Zhang X-X (2017) MnO_2/MWCNTs nanocomposites as highly efficient catalyst for indoor formaldehyde removal. J Nanosci Nanotechnol 18:3982–3990. https://doi.org/10.1166/jnn.2018.15216

38. Mukhtar A, Mellon N, Saqib S et al (2020) CO_2/CH_4 adsorption over functionalized multi-walled carbon nanotubes; an experimental study, isotherms analysis, mechanism, and thermodynamics. Microporous Mesoporous Mater 294:109883. https://doi.org/10.1016/j.micromeso.2019.109883
39. Nang An V, Van TTT, Nhan HTC et al (2020) Investigating methylene blue adsorption and photocatalytic activity of ZnO/CNC nanohybrids. J Nanomater 2020. https://doi.org/10.1155/2020/6185976
40. Nazari Kudahi S, Noorpoor AR, Mahmoodi NM (2019) Adsorption performance indicator for power plant CO_2 capture on graphene oxide/TiO_2 nanocomposite. Iran J Chem Chem Eng 38:293–307
41. Ng NT, Kamaruddin AF, Wan Ibrahim WA et al (2018) Advances in organic–inorganic hybrid sorbents for the extraction of organic and inorganic pollutants in different types of food and environmental samples. J Sep Sci 41:195–208. https://doi.org/10.1002/jssc.201700689
42. Nielsen P (2021) WHO global air quality guidelines. Bonn, Germany
43. Novoselov KS, Geim A (2007) The rise of graphene. Nat Mater 63:183–191
44. Nowrouzi M, Younesi H, Bahramifar N (2018) Superior CO_2 capture performance on biomass-derived carbon/metal oxides nanocomposites from Persian ironwood by H_3PO_4 activation. Fuel 223:99–114. https://doi.org/10.1016/j.fuel.2018.03.035
45. Qamar SA, Ashiq M, Jahangeer M, Riasat A, Bilal M (2020) Chitosan-based hybrid materials as adsorbents for textile dyes—a review. Case Stud Chem Environ Eng 2:100021. https://doi.org/10.1016/j.cscee.2020.100021
46. Ramasubramanian K, Ho WSW (2011) Recent developments on membranes for post-combustion carbon capture. Curr Opin Chem Eng 1:47–54. https://doi.org/10.1016/j.coche.2011.08.002
47. Rani M, Shanker U, Jassal V (2017) Recent strategies for removal and degradation of persistent & toxic organochlorine pesticides using nanoparticles: a review. J Environ Manage 190:208–222. https://doi.org/10.1016/j.jenvman.2016.12.068
48. Razani S, Dadkhah Tehrani A (2019) Development of new organic-inorganic, hybrid bionanocomposite from cellulose nanowhisker and Mg/Al-CO_3-LDH for enhanced dye removal. Int J Biol Macromol 133:892–901. https://doi.org/10.1016/j.ijbiomac.2019.04.149
49. Regufe MJ, Ferreira AFP, Loureiro JM et al (2018) New hybrid composite honeycomb monolith with 13X zeolite and activated carbon for CO_2 capture. Adsorption 24:249–265. https://doi.org/10.1007/s10450-018-9938-1
50. Rizwan K, Bilal M, Slimani Y, Show PL, Rtimi S, Roy A, Iqbal HMN (2022) Hydrogen-based sono-hybrid catalytic degradation and mitigation of industrially-originated dye-based pollutants. Int J Hydrogen Energy. https://doi.org/10.1016/j.ijhydene.2022.03.188
51. Rhodes CJ (2018) Pollinator decline—an ecological calamity in the making? Sci Prog 101:121–160. https://doi.org/10.3184/003685018X15202512854527
52. Riddick SN, Mauzerall DL, Celia M et al (2019) Methane emissions from oil and gas platforms in the Bohai Sea, China. Environ Pollut 19:9787–9796. https://doi.org/10.1016/j.envpol.2020.114486
53. Rodríguez-García S, Santiago R, López-Díaz D et al (2019) Role of the structure of graphene oxide sheets on the CO_2 adsorption properties of nanocomposites based on graphene oxide and polyaniline or Fe_3O_4-nanoparticles. ACS Sustain Chem Eng 7:12464–12473. https://doi.org/10.1021/acssuschemeng.9b02035
54. Roso M, Boaretti C, Pelizzo MG et al (2017) Nanostructured photocatalysts based on different oxidized graphenes for VOCs removal. Ind Eng Chem Res 56:9980–9992. https://doi.org/10.1021/acs.iecr.7b02526
55. Sadare OO, Masitha M, Yoro KO, Daramola MO (2018) Removal of sulfur (e.g DBT) from petroleum distillates using activated carbon in a continuous packed-bed adsorption column. In: Proceedings of the World Congress on Engineering and Computer Science 2018 (WCECS 2018), vol II, San Francisco, USA, 23–25 Oct 2018, pp 509–513
56. Salehi S, Anbia M, Hosseiny AH, Sepehrian M (2018) Enhancement of CO_2 adsorption on polyethylenimine functionalized multiwalled carbon nanotubes/Cd-nanozeolite composites. J Mol Struct 1173:792–800. https://doi.org/10.1016/j.molstruc.2018.07.056

57. Saygın M, Gonca T, Öztürk Ö et al (2017) To investigate the effects of air pollution (PM_{10} and SO_2) on the respiratory diseases asthma and chronic obstructive pulmonary disease. Turkish Thorac J 18:33–39. https://doi.org/10.5152/TurkThoracJ.2017.16016
58. Shah R (2020) Pesticides and human health. In: Emerging contaminants. IntechOpen, pp 1–22
59. Shakeel A, Rizwan K, Farooq U, Iqbal S, Altaf AA (2022) Advanced polymeric/inorganic nanohybrids: an integrated platform for gas sensing applications. Chemosphere 294:133772. https://doi.org/10.1016/j.chemosphere.2022.133772
60. Sharma A, Kumar V, Shahzad B et al (2019) Worldwide pesticide usage and its impacts on ecosystem. SN Appl Sci 1:1–16. https://doi.org/10.1007/s42452-019-1485-1
61. Shen J, Liu G, Huang K et al (2016) UiO-66-polyether block amide mixed matrix membranes for CO_2 separation. J Memb Sci 513:155–165. https://doi.org/10.1016/j.memsci.2016.04.045
62. Shi J, Chen J, Li G et al (2017) Fabrication of Au/TiO_2 nanowires@carbon fiber paper ternary composite for visible-light photocatalytic degradation of gaseous styrene. Catal Today 281:621–629. https://doi.org/10.1016/j.cattod.2016.06.026
63. Smart SK, Cassady AI, Lu GQ, Martin DJ (2006) The biocompatibility of carbon nanotubes. Carbon NY 44:1034–1047. https://doi.org/10.1016/j.carbon.2005.10.011
64. Sulistina DR, Martini S (2020) The effect of rhodamine b on the cerebellum and brainstem tissue of *Rattus norvegicus*. J Public health Res 9:101–104. https://doi.org/10.4081/jphr.2020.1812
65. Sunkara B, Zhan J, He J et al (2010) Nanoscale zerovalent iron supported on uniform carbon microspheres for the in situ remediation of chlorinated hydrocarbons. ACS Appl Mater Interfaces 2:2854–2862. https://doi.org/10.1021/am1005282
66. Tahir MB, Sohaib M, Sagir M, Rafique M (2022) Role of nanotechnology in photocatalysis. Encycl Smart Mater 578–589. https://doi.org/10.1016/b978-0-12-815732-9.00006-1
67. Tkaczyk A, Mitrowska K, Posyniak A (2020) Synthetic organic dyes as contaminants of the aquatic environment and their implications for ecosystems: a review. Sci Total Environ 717:137222. https://doi.org/10.1016/j.scitotenv.2020.137222
68. Tseng TK, Lin YS, Chen YJ, Chu H (2010) A review of photocatalysts prepared by sol-gel method for VOCs removal. Int J Mol Sci 11:2336–2361. https://doi.org/10.3390/ijms11062336
69. Turner AJ, Frankenberg C, Kort EA (2019) Interpreting contemporary trends in atmospheric methane. Proc Natl Acad Sci U S A 116:2805–2813. https://doi.org/10.1073/pnas.1814297116
70. Vutskits L, Briner A, Klauser P et al (2008) Adverse effects of methylene blue on the central nervous system. Anesthesiology 108:684–692. https://doi.org/10.1097/ALN.0b013e3181684be4
71. Wang H, Raziq F, Qu Y et al (2015) Role of quaternary N in N-doped graphene-Fe_2O_3 nanocomposites as efficient photocatalysts for CO_2 reduction and acetaldehyde degradation. RSC Adv 00:85061–85064. https://doi.org/10.1039/c5ra17882g
72. Wang H, Xu C, Zhou Y et al (2019) Fabrication of hierarchical N-doped carbon nanotubes for CO_2 adsorption. NANO 14:1950072. https://doi.org/10.1142/S1793292019500723
73. Wang W, Motuzas J, Zhao XS, Diniz da Costa JC (2019) 2D/3D amine functionalised sorbents containing graphene silica aerogel and mesoporous silica with improved CO_2 sorption. Sep Purif Technol 222:381–389. https://doi.org/10.1016/j.seppur.2019.04.050
74. Wang Y, Zhao L, Otto A et al (2017) A review of post-combustion CO_2 capture technologies from coal-fired power plants. Energy Procedia 114:650–665. https://doi.org/10.1016/j.egypro.2017.03.1209
75. Wei X, Wang X, Gao B et al (2020) Facile ball-milling synthesis of CuO/biochar nanocomposites for efficient removal of reactive red 120. ACS Omega 5:5748–5755. https://doi.org/10.1021/acsomega.9b03787
76. Xu L, Wang J (2017) The application of graphene-based materials for the removal of heavy metals and radionuclides from water and wastewater. Crit Rev Environ Sci Technol 47:1042–1105. https://doi.org/10.1080/10643389.2017.1342514
77. Yang L, Tian Z, Zhang X et al (2017) Enhanced CO_2 selectivities by incorporating CO_2-philic PEG-POSS into polymers of intrinsic microporosity membrane. J Memb Sci 543:69–78. https://doi.org/10.1016/j.memsci.2017.08.050

78. Yang L, Zhang S, Wu H et al (2019) Porous organosilicon nanotubes in pebax-based mixed-matrix membranes for biogas purification. J Memb Sci 573:301–308. https://doi.org/10.1016/j.memsci.2018.12.018
79. Yang T, Li F, Zhou X et al (2019) Impact of nitrogen fertilizer, greenhouse, and crop species on yield-scaled nitrous oxide emission from vegetable crops: a meta-analysis. Ecol Indic 105:717–726. https://doi.org/10.1016/j.ecolind.2019.02.001
80. Yao X, Ji L, Guo J et al (2020) Magnetic activated biochar nanocomposites derived from wakame and its application in methylene blue adsorption. Bioresour Technol 302:122842. https://doi.org/10.1016/j.biortech.2020.122842
81. Yu L, Wang L, Sun X, Ye D (2018) Enhanced photocatalytic activity of rGO/TiO_2 for the decomposition of formaldehyde under visible light irradiation. J Environ Sci (China) 73:138–146. https://doi.org/10.1016/j.jes.2018.01.022
82. Zhang Y, Shen Y, Hou J et al (2018) Ultraselective pebax membranes enabled by templated microphase separation. ACS Appl Mater Interfaces 10:20006–20013. https://doi.org/10.1021/acsami.8b03787
83. Zhao D, Schmitt SH, Wang M et al (2018) Effects of NO_x and SO_2 on the secondary organic aerosol formation from photooxidation of α-pinene and limonene. Atmos Chem Phys 18:1611–1628. https://doi.org/10.5194/acp-2017-294
84. Zhao Q, Wu F, Men Y et al (2019) CO_2 capture using a novel hybrid monolith (H-ZSM5/activated carbon) as adsorbent by combined vacuum and electric swing adsorption (VESA). Chem Eng J 358:707–717. https://doi.org/10.1016/j.cej.2018.09.196
85. Zhao Q, Wu F, Xie K et al (2018) Synthesis of a novel hybrid adsorbent which combines activated carbon and zeolite NaUSY for CO_2 capture by electric swing adsorption (ESA). Chem Eng J 336:659–668. https://doi.org/10.1016/j.cej.2017.11.167
86. Zheng X, Streimikiene D, Balezentis T et al (2019) A review of greenhouse gas emission profiles, dynamics, and climate change mitigation efforts across the key climate change players. J Clean Prod 234:1113–1133. https://doi.org/10.1016/j.jclepro.2019.06.140
87. Zhu B, Liu J, Wang S et al (2019) Mixed matrix membranes containing well-designed composite microcapsules for CO_2 separation. J Memb Sci 572:650–657. https://doi.org/10.1016/j.memsci.2018.11.039
88. Zhu W, Qin Y, Wang Z et al (2019) Incorporating the magnetic alignment of GO composites into Pebax matrix for gas separation. J Energy Chem 31:1–10. https://doi.org/10.1016/j.jechem.2018.04.013
89. Zia J, Riaz U (2021) Photocatalytic degradation of water pollutants using conducting polymer-based nanohybrids: a review on recent trends and future prospects. J Mol Liq 340:117162. https://doi.org/10.1016/j.molliq.2021.117162
90. Zou W, Gao B, Ok YS, Dong L (2019) Integrated adsorption and photocatalytic degradation of volatile organic compounds (VOCs) using carbon-based nanocomposites: a critical review. Chemosphere 218:845–859. https://doi.org/10.1016/j.chemosphere.2018.11.175
91. Zvonkina I, Soucek M (2016) Inorganic-organic hybrid coatings: common and new approaches. Curr Opin Chem Eng 11:123–127. https://doi.org/10.1016/j.coche.2016.01.008

Chapter 14
Tungstate-Based Nanohybrid Materials for Wastewater Treatment

Junaid Munawar, Ehsan Ullah Rashid, Shahid Nawaz, Sayed Ali Abbas Sherazi, Muhammad Ali, Abbas Rahdar, Komal Rizwan, and Muhammad Bilal

1 Introduction

Environmental issues associated with metal pollution continue to pose a serious threat to our health and economy. It is crucial to remove hazardous metals from industrial wastewater. Various methods are available for this purpose, such as reverse osmosis, ultra-filtration, chemical precipitation, solvent extraction, ion exchange, electrodialysis, and adsorption [7, 14, 33, 50]. Water containing metal ions can be treated with ion exchange, and it has been documented to be an important and cost-effective method. Wastewater from domestic areas is called sewage that contains (99.9%) water; rest of the part contains several types of solids, organic, and inorganic compounds [65]. The most appropriate technology for wastewater purification is using a semiconductor, which has various benefits such as no usage of chemicals, UV light, and complete mineralization of befouling agents. These processes are considered green and cost-effective [26, 80]**.** When suitable light energy is irradiated to semiconductors, holes are formed in valance bands by the excitation of electrons

J. Munawar
College of Chemistry, Beijing University of Chemical Technology, Beijing 100029, China

E. U. Rashid · S. A. A. Sherazi · M. Ali
Department of Chemistry, University of Agriculture, Faisalabad 38040, Pakistan

S. Nawaz
Department of Chemistry, The University of Lahore, Lahore, Pakistan

A. Rahdar
Department of Physics, University of Zabol, P. O. Box. 98613, 35856 Zabol, Iran

K. Rizwan
Department of Chemistry, University of Sahiwal, Sahiwal 57000, Pakistan

M. Bilal (✉)
School of Life Science and Food Engineering, Huaiyin Institute of Technology, Huaian, China
e-mail: bilaluaf@hyit.edu.cn

K. Rizwan et al. (eds.), *Hybrid Nanomaterials*, Materials Horizons: From Nature to Nanomaterials, https://doi.org/10.1007/978-981-19-4538-0_14

into the conduction band. These charge carriers undergo interfacial charge transfer and adsorption to initiate redox processes or recombine by releasing excessive energy as heat [74]. For efficient photocatalysis potential of the conduction band and valance band, their edges must be adequate for the generation of superoxide and hydroxyl radicals.

Titania and ZnO are witnessed as worldwide interest because of their unmatched opto-electronic and physiochemical properties. It was demonstrated in 1972 that titanium dioxide (TiO_2) could be used as a photoanode for splitting water excited by ultraviolet light [20]. Because TiO_2 has chemical stability, long durability and nontoxicity, it is among the most extensively studied semiconductor as a photocatalyst [8]. TiO_2 photocatalysts have a narrow bandgap of *3.2 eV so that they can only absorb ultraviolet (UV) light, which only represents a small fraction of solar light (*5%), thereby hardly harvesting the remaining sunlight [37]. These are a few WO_3 [32], Bi_2WO_6 [44], ZnO [35], Bi_2O_3 [31], and NiO-based semiconductors [42]. Thus, they are widely used as photocatalysts for environmental treatment and water splitting by the solar. Metal nanoparticles and oxides have been demonstrated to be awesome impetuses in oxidation responses [59, 88]. The recent development of the ternary tungstate-based oxide complex has offered the potential candidate for efficient photocatalysis [46]. It can be noted that tungsten-based materials can degrade organic pollutants into less harmful by-products, thereby assisting in environmental remediation. Due to its multifunctional characteristics, WO_3 has a lot of applications in the fields of electro-chromium, photo-chromium, sensors, solar devices, photocatalysis, and splitting of water. Various articles are available for photocatalysis with TiO_2, but only a few articles deal with tungsten-based materials [34]. The performance of these amended materials in practical applications is still unsatisfactory, and it has yet to be established worldwide.

A photocatalyst must have an edge sufficiently negative for the photo-reduction reaction. At the same time, it must have an edge sufficiently positive for the photo-oxidation reaction [10]. Researchers have paid a lot of attention to advanced oxidation processes for wastewater over the last several decades [6, 62, 86]. Advanced oxidation processes (AOPs) are a cutting-edge technology for removing maximum organic content, hazardous pollutants, and other contaminants from wastewater. Figure 1 shows some of the metal tungstate materials used to treat wastewater. The main goal of this section is to give a rapid reference for researchers working on wastewater treatment by using tungstate metals for photocatalytic decay, AOPs, and so on. This chapter focuses on tungstate metals-based composites for dye degradation and hybrid AOPs for industrial wastewater treatment.

2 Waste and Their Sources

In the era of industrialization, there are many alarming pollutants such as synthetic dyes [61], sewage and debris in runoff water coming from textiles, leather accessories, food packing materials, furniture, pharmaceuticals, plastics, and various other

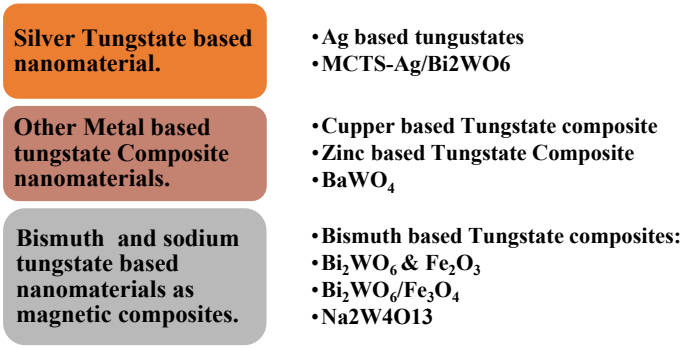

Fig. 1 Metal tungstate composites for the remediation of wastewater

industries. Their effect is not only polluting water but also an alarming hazard to the environment [64]. From the agriculture runoff which is composed of insecticides, neonicotinoid-based pesticides [66], herbicides (atrazine), and fertilizers due to their excessive use when it rains, the agriculture flow carries to the neighboring water bodies because many pollutants are in water flow and then pollute the water assets [41]. The leather tannery waste contains a high concentration of sulfate, extremely colored compounds, sodium chloride, numerous organic and inorganic compounds, and poisonous metallic compounds. These pollutants undergo oxidation, and many colloidal substances can be decayed [2]. Anthropogenic activities have a great contribution to environmental pollution. It can be estimated in this way that nearly 7 lakh tons of various dyes are generated annually. Figure 2 shows different sources are responsible for the contamination of fresh water. Most organic dyes even in low quantities (0.001 mg/L) are injurious [11] to humans and may cause serious health problems. Several colors are found in sub-surface and surface water, which contribute to various water ailments such as extreme respiratory tract irritation, mucous membrane irritation, dermatitis, and nasal septum perforation. Wastewater and its sources have several methodologies such as reverse osmosis and bio-filtration [1], adsorption [27], photo-chemical, and coagulation [63], which has been used for the treatment of wastewater. Removing organic pollutants from runoff water is a significant issue worldwide [4]. The excellent treatment and effectiveness of photocatalysis of TiO_2 by coupling with ozonation (treatment by ozone) by UV irradiation has recently gained a lot of attention. Therefore, this chapter will focus on various types of metal tungstate composite nanomaterial for developing novel strategies to enhance the photocatalytic performance of MWO_4-based materials for the treatment of wastewater.

Fig. 2 Wastewater and their sources

3 Metal-Based Tungstate Nanocomposites

3.1 Silver-Based Tungstate Composites

Silver tungstate (Ag_2WO_4) has versatile properties useful for water splitting, gas sensing, optical fibers, and catalysts [3, 58]. Metal-oxide nanoparticles, e.g., TiO_2, WO_3, and ZnO, have been widely employed to degrade bacteria, viruses, and hazardous pollutants using UV radiation. The photodecomposition of methylene blue using visible light was studied. There are three distinct crystal phases of Ag_2WO_4: the orthorhombic, hexagonal, and cubic phases. The orthorhombic phase is the most stable among all these crystals. Figure 3 shows the process of synthesizing silver

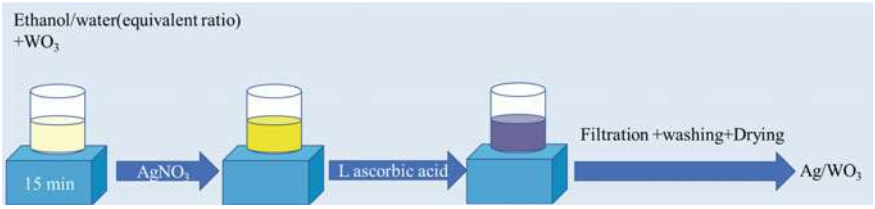

Fig. 3 Synthesis of silver tungstate composite

tungstate composite. The diverse shapes and structures of silver tungstate are fabricated by distinct processes, including hydrothermal synthesis, ion-exchange routes, micro-emulsions, and precipitation [3, 73].

Dye Degradation Mechanism on Ag/WO_3 Under Visible-Light Irradiation

A literature review indicates that the work functions of WO_3 and Ag are 5.7 eV and 4.26 eV, respectively. When Ag comes into contact with WO_3, there is the accessibility of electron transfer from Ag to WO_3's CB, resulting in Fermi level equilibration. In this way, a deflexed energy band forms at the Ag/WO_3 interface due to the accumulation of excess electrons on the surface of WO_3. As a result of the deflexed energy band in the space charge region, as-excited electrons are rapidly transferred from WO_3 to Ag nanoparticles, which reduces the recombination of electron–hole pairs generated. Due to the low level of CB in WO_3, which is more positive than the given potential for the single-electron reduction of O_2, the multi-electron reduction of O_2 will move electrons accumulated on Ag nanoparticles to surface-adsorbed oxygen molecules, thus forming H_2O_2 [12]. When visible light irradiates, the VB electrons transfer into the CB. Hence, at the surface of WO_3, holes (h^+) and electrons (e^-) are generated. Oxygen vacancy defects then trap the photo-generated electrons. After that, the holes react with hydroxide ions; therefore, the electrons react with dissolved oxygen to generate the $OH^{\cdot}$ radicals, which destroy the MB dye and turn it into harmless gases, such as carbon dioxide and water. A further reaction between hydrogen peroxide and electrons leads to more $OH^{\cdot}$, which speeds up the decomposition of dye [47]. The mechanism of the reaction is shown below.

$$Ag/WO_3 + \text{visiblelight} \rightarrow h^+(\text{hole}) + e(\text{electron})$$
$$h^+ + H_2O \rightarrow H^+ + Oh$$
$$h^+ + OH \rightarrow OH^{\cdot}$$
$$e^- + O_2 \rightarrow O_2^{\cdot}$$
$$O_2^{\cdot} + e^- + 2H^+ \rightarrow H_2O_2$$
$$O_2^{\cdot} + H_2O_2 \rightarrow OH^{\cdot} + OH + O_2$$
$$OH^{\cdot} + \text{dye} \rightarrow \text{nontoxic products} + CO_2 \uparrow$$
$$O_2^{\cdot} + \text{dye} \rightarrow \text{nontoxic products} + CO_2 \uparrow$$

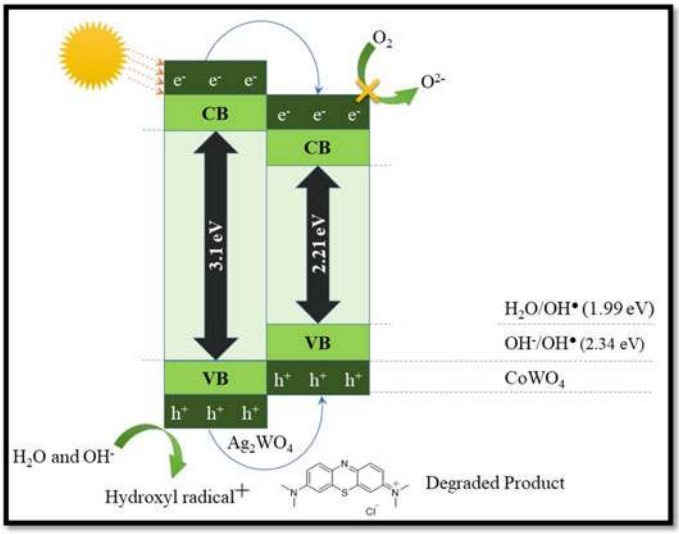

Fig. 4 Photo-degradation process by Ag_2WO_4 and $CoWO_4$

Figure 4 shows the general mechanism of $AgWO_3$ for the degradation of pollutants. As a result, the Ag/WO_3 photocatalyst exhibits excellent stability and recyclability, photocatalytic activity, and antibacterial properties, making them more feasible in various applications, such as water purification and surface sterilization under bright and dark light.

3.1.1 MCTS-Ag/Bi_2WO_6

Contaminated surface and groundwater reduce water resources [60]. Heavy metals have become serious threats to the environment and human health due to their non-biodegradable nature and slow accumulation throughout the food chain. In the past thousand years, copper has been one of the most important heavy metals used by humans; however, high concentrations can be harmful to human health. Currently, environmental water is contaminated with excessive levels of residual copper due to industrialization, and these industrial effluents come from pulp mills, metal plating baths, and paper [79]. Copper exists as Cu0, Cu (I), Cu (II), and Cu (III) in the environment, but Cu (II) is the major concern in aqueous solutions. It is toxic to aquatic organisms even when present at extremely low levels. Among the traditional ways to remove Cu (II) from water and wastewater are adsorption, electrochemical precipitation, ion exchange, and membrane ultra-filtration [30]. Adsorption technique can effectively remove contaminants from the environment. For removing Cu (II), there are many types of adsorbents. However, chitosan carbon nanotubes (CTS)

are particularly attractive due to their biodegradability, biocompatibility, renewability, and chemical properties (polycation, hydrogel, reactive groups such as OH, NH_2) [15].

The visible-light responsive photocatalyst VBi2WO6 is an important bismuth-based photocatalyst that has been extensively used to remove heavy metals. To prepare Bi2WO6, hydrothermal process was used for the photocatalytic reduction of Cr (VI) [36]. In order to remove Cr(VI), a heterojunction of Co_3O_4/Ag/Bi_2WO_6 was fabricated [72]. In this experiment [75], Bi_2WO_6 was utilized as a photocatalyst combined with chitosan to increase adsorption capacity. A higher adsorption capacity was observed for the MCTS-Ag/Bi_2WO_6 under illumination. In the presence of MCTS and Ag/Bi_2WO_6, there was a synergistic effect on Cu(II) absorption. If the light is more powerful, the bandgap of Ag/Bi_2WO_6 may excite an electron from the valence band into the condition band, which would reduce Cu(II) to Cu and lower the reactive energy for adsorption. After MCTS adsorbed Cu(II), eNH_2^+ of MCTS was transformed into eNH_3^+, which inhibited proton–hole recombination. Even after 120 min, only adsorption of Cu(II) by MCTS did not reduce Cu(II) concentrations in the dark. In this experiment, MCTS-Ag/Bi_2WO_6 adsorption of Cu(II) reached the maximum (687 mg/g) when illuminated. This showed that illumination could increase the adsorption of Cu(II) [82].

3.2 Copper-Based Tungstate Composites ($CuWO_4$)

Environmental contamination is a worldwide concern with water pollution being a major contributor. The textile sectors are the most polluting industrial sectors for wastewater production, using a considerable quantity of water. Because sulfhydryl groups are components of many essential enzymes, bismuth has the effect of denaturing and destroying the function of these enzymes. The photocatalytic degradation of natural toxins by semiconductors is gaining popularity as a preferred technique for the corruption of natural waste due to its efficiency and low cost. Electrons reach the conduction band by oxidizing and reducing impurities and forming holes in the valence band. As a result, experts have recently become interested in photocatalysts that are brightly visible light determined.

$CuWO_4$ has received attention as a potential material for sunlight-based oxidation [82]. Furthermore, not much attention had been paid to the breakdown of pollutants in aqueous solution by $CuWO_4$ chains. The wolframite type has a monoclinic structure shared by transition metal tungstates. Moreover, the transition is associated with the fourth period of the periodic table ($ZnWO_4$, $NiWO_4$, $CoWO_4$, $FeWO_4$, and $MnWO_4$) [23]. $CuWO_4$ is the most notable exception since it solidifies at ambient temperature with a triclinic structure. The second-order John–Teller (SOJT) effect of $CuWO_4$ crystals has a triclinic structure [29]. $CuWO_4$ is an n-type semiconductor that has a 2.25 eV indirect band gap. The band gap is highly influenced by the octahedral structure of WO_6 and CuO_6 and how they are coupled. Effect of $CuWO_4$ [22] is used for the disintegration of orange G (OG), amido black (AB) dyes, and methylene blue

under solar irradiation in aqueous solutions. Within 120 min, the decay efficiency of the three dyes was as follows: MB > AB > OG. Nanoparticles and nanochains constructed from nanoparticles are among the photocatalytic materials with the types of samples that were synthesized by using a solvothermal process. The decay of dye can be explained by the following mechanism.

$$\mathrm{CuWO_4} \xrightarrow{hv} \mathrm{e_{CB}^- + h_{VB}^+}$$
$$\mathrm{OH^- + h_{VB}^+ \rightarrow OH^{\cdot}}$$
$$\mathrm{O_2 + e_{CB}^- \rightarrow O_2^{\cdot}}$$
$$\mathrm{H_2O + O_2^- \rightarrow OH^{\cdot} + OH^-}$$
$$\mathrm{O_2^{-\cdot} + dye \rightarrow CO_2 + H_2O}$$
$$\mathrm{OH^{\cdot} + dye \rightarrow CO_2 + H_2O}$$

3.3 Zinc-Based Tungstate Composites ($ZnWo_2$)

As a result of its broad temperature range (0.3–1050 K) and significant isotropic negative thermal expansion, Zr(IV) tungstate has been studied extensively. Titanium dioxide (TiO_2) and zinc oxide (ZnO) nanostructures have been widely used as photocatalysts, although the wolframite structure of $ZnWO_4$ performs better efficiency for the mitigation of wastewater [55]. It has been seen as a viable alternative due to its excellent photocatalytic activity, chemical stability, lack of toxicity, inexpensive cost, and band gap energy of 3.7 eV. Modifying, ZnWO4 photocatalyst performance by manipulating its geometry, such as a rod [18], hollow [89], mesoporous [21], and core−shell [85] structure, has been a major focus of many studies on semiconductor photocatalyst ZnWO4. As an alternative for TiO_2 and ZnO in photocatalysis, $ZnWO_4$ has been widely studied to remove water pollution, decontaminate heavy metals, and remove other solids and gaseous pollutants [77]. The brass and nickel wastewater samples were collected and promptly filtered via a Millipore cellulose membrane filter from the respective industries in Moradabad, UP India, respectively (0.45 mm pore size). The pH of the model solution was adjusted to using concentrated HNO_3, and the prescribed pre-concentration technique (column operation) was followed. Atomic absorption spectroscopy (AAS) was used to measure the ion concentrations of Cu(II), Zn(II) and Ni(II). Heterostructured $ZnWO_4$ photocatalysts, such as $CdS/Zn_{1-x}Cd_xWO_4$ [76], $BiOI/ZnWO_4$ [17], and $LAS/ZnO/ZnWO_4$ [78], have been described. Ion-doped $ZnWO_4$ semiconductor materials, including F: $ZnWO_4$ [21], Cd: $ZnWO_4$ [81], and B: $ZnWO_4$ [43], have been effectively produced so far. With no need for a template, $Zn_{1-x}Cd_xWO_4$ nanorods have been manufactured. To degrade MO in sewage, $Zn_{1x}Cd_xWO_4$ nanostructures outperform the pure $ZnWO_4$ in photocatalytic activity. Many characterizations were carried out to better understand the underlying causes of the doped $ZnWO_4$ nano-architectures, which enhanced the

photocatalytic activity [77]. Metal-ion selectivity and excellent chemical, thermal stability of Zr(IV) tungstate were favorable features for treating wastewater.

3.4 Barium-Based Tungstate Composite ($BaWO_4$)

Photocatalytically, technology is among the greatest water treatment methodologies, since it is an eco-friendly and cost-effective [64] method for purifying wastewater. It eliminates all kinds of inorganic and organic pollutants and impurities. The heaviest member of the alkaline earth tungstate family is barium tungstate ($BaWO_4$). $BaWO_4$ crystallizes in the tetragonal type of structure under ambient circumstances, like many other ABX_4-type compounds (space group [*SG*]: I41/a, No. 88, Z = 4). Due to its outstanding magnetic properties, photoluminescence, and electrical conductivity, $BaWO_4$ is being studied extensively. LEDs [5], humidity sensors, scintillator detectors [69], optic filters, microwave dielectrics, photocatalysts [70], phosphors, and solid-state lasers are some of the applications of $BaWO_4$-based materials. Many studies on the fabrication and characterization of metal tungstate have recently been published, including co-precipitation, hydrothermal synthesis, solid-state reaction, molten salt synthesis [55], pulsed laser deposition method, electrochemical process, polymeric precursor method, solvothermal synthesis [90], and DNA-templated synthesis [57].

Organic dyes are one of the most hazardous toxins found in industrial effluent. Organic dyes are utilized in various industries, including medicines, paper, cosmetics, leather, electronics, textiles, and plastics. In the following, it has been stated that the textile sector merely uses synthetic dyes (i.e., 80%) for printing. Many dyes contain non-biodegradable compounds. Methods have been run down for degradation based on physical, chemical, and biological ways. However, due to their costly nature, they are not suitable on a large scale. Therefore, alternative methods have been developed via green chemicals which are feasible [53, 54]. Rhodamine B (RHB) was discovered to be the most significant xanthene class basic dye. It is a well-known water tracer fluorescent and widely employed as a dye in the textile industry. Organic contaminants (such as methyl orange and rhodamine B) can be removed from water using $BaWO_4$ nanoparticles as photocatalysts.

3.5 Bismuth-Based Tungstate Composites (Bi_2WO_6)

As one of the most researched visible-light-driven photocatalysts, bismuth tungstate (BWO), a ternary metal oxide, has been credited with a broad spectrum light response and the absence of secondary contamination after use [19, 39]. A standard solid-state procedure was employed to initially synthesize BWO, and ultrasound-induced aggregation, micro-emulsions, calcinations, precipitation, and the hydro/solvothermal process are only a few of the methods used till now to synthesize BWO [13]. BWO,

with a wide range of structures and morphologies, has distinct characteristics [45]. Because of this, one of the latest aspects has been the creation of controlled structures and morphologies to improve the photocatalytic activity of BWO. Conduction band (CB) and valance band (VB) of nanostructured BWO include photoexcited electrons (e^-) and holes (h^+) that are crucial for environmental application photocatalysis. (CB) e^- may directly reduce inorganic contaminants such as bromated or interact with soluble molecular oxygen to generate superoxide radical entities that can participate in the oxidation of organic contaminants [84]. Colorful dyes can be oxidized with the help of the high oxidation properties of VB h^+. Dye waste from printing, dyeing, and other businesses is found in large quantities across the world's water resources, which has resulted in a significant pollution problem. The photodegradation of organic dyes by nanostructured BWO photocatalysts is very effective [40]. It has been shown that BWO is an excellent photocatalyst for the oxidation of benzylic alcohols under visible light. The benzylic alcohols were converted to aldehydes by sunlight produced h^+ and $^{\cdot}O_2$ over flower-like BWO. The absence of $^{\cdot}OH$ radicals, a lack of oxidation capacity, and greater adsorption of benzylic alcohols than aldehydes were all factors that led to this [87]. It was recently reported [9] that a BWO/$CdWO_4$ (BCW) 3D hierarchical heterostructure may selectively catalyze the hydroxylation of benzophenone in the presence of oxygen as the oxidant. This hierarchical heterostructure's increased light absorption and charge carrier separation led to excellent photocatalytic activity [83].

3.5.1 Bi_2WO_6 and Fe_2O_3

Water contamination caused by leftover medicines is a big issue worldwide. Photocatalysis mediated by bismuth tungstate has been effective for the withdrawal of these organic compounds from water by controlling their morphology [83]. Because of its nontoxic nature, suitable band gap energy, and simplicity of synthesis, Bi_2WO_6 (bismuth tungstate) is an efficient visible-light active photocatalyst [24]. It has been extensively used to remove a broad range of organic contaminants from wastewater, notably colors. However, it has lately received a lot of interest for its use in the degradation of medicine pollutants. The construction of Bi_2WO_6-based photocatalysts with improved photocatalytic capabilities by controlling morphology, doping, and heterojunction development is emphasized. Serious notice has been taken for the processes and potential deterioration routes for antimicrobial medicines in wastewater [82]. For future research directions, issues that need greater focus and inquiry on using Bi_2WO_6-based photocatalysts for pharmaceutical waste removal from wastewater particularly in real-life applications are described.

There has been a lot of effort to produce catalysts that are active to visible light to make greater use of solar radiation in nature. Photocatalysts containing bismuth, particularly Bi_2WO_6, are photocatalytically active to visible light and exhibit potential photocatalytic productivity to various pollutants and azo dyes on interaction with visible light [25, 26]. Magnetic ferrites of many types, like $CoFe_2O_4$, $NiFe_2O_4$, and

Fe_2O_4, were coupled with various photocatalysts to create magnetic ferrite composites [28]. Doping with magnetic materials in many situations reduces the photocatalytic activities of the original catalysts by reducing the number of active sites accessible for interaction. To make magnetic composites that sustain the photoactivity of the native catalyst while still having outstanding magnetic characteristics, new strategies are needed. Magnetite is an excellent magnetic material commonly utilized in catalysis due to its low cost and feasibility of manufacturing [49]. Aside from its ultra-high-density magnetic feature, Fe_3O_4 has been employed as a Fenton-like heterogeneous catalyst which is involved in the oxidation process of organic molecules [51].

H_2O_2 is a common oxidizing agent that is extensively employed for the treatment of wastewater. Rhodamine B (RhB) can be utilized to imitate non-biodegradable, hazardous chemical molecules that contain numerous benzene rings [71]. Visible light (>400 nm) was used to assess the photocatalytic performance of the magnetic composite to RhB in the existence of H_2O_2. The functions of Bi_2WO_6, Fe_3O_4, and H_2O_2 and the reaction process were thoroughly explored. The effects of H_2O_2 concentration and solution pH on photocatalytic efficiency have been investigated. The degradation process was also explored thoroughly. The suggested technique was useful in developing a wastewater treatment system that uses visible light and an electromagnetic photo-Fenton coupling oxidation system. The degradation process was also investigated in H_2O_2 which may react with photo-generated electrons to form hydroxyl radicals as an electron capture agent (OHs) [16]. Hydrogen peroxide may interact with Bi_2WO_6/Fe_3O_4 composite and affects its photocatalytic ability. Bi_2WO_6 and their composites, such as C/Fe–Bi_2WO_6, Fe_3O_4/Bi_2WO_6-carbon, and Co_3O_4/Bi_2WO_6, are shown to have greater photocatalytical degradation efficiency with the help of H_2O_2. Doping of Bi_2WO_6 with Fe_3O_4 to create magnetic Bi_2WO_6/Fe_3O_4 composites and degradation processes combined with Bi_2WO_6/Fe_3O_4 in the presence of H_2O_2 [51, 52].

3.5.2 Bi_2WO_6/Fe_3O_4

Song et al. [56] described *s*eparation and purification technology for water purification by applying Fe_3O_4 magnetic nanoparticles. Auxiliary portrayals revealed that three types of Fe_3O_4 attractive nanoparticles with various normal sizes were blended, with a normal molecule size of 355 nm, 12 nm, and 8 nm reported and NPs prepared with co-precipitation approach and co-precipitation merging a surface decoration process, respectively [83]. These NPs were created to clean wastewater that contained metal ions such as Ni(II), Cr(VI), Cd(II), and Cu(II). It was revealed that decreasing the molecule size or increasing the surface zone increased the adsorption range of Fe_3O_4 particles. pH, the measure of an adsorbent, and temperature are all factors that influence the adsorption of metal particles. The results showed that the pH and temperature of the wastewater had a significant impact on the component. The amount of adsorption can be achieved in the shortest amount of time. Similar work has been

done by Wang and coworkers for the degradation of methylene blue under the UV source (Wang et al. 2009).

3.6 Sodium-Based Tungstate Composite (Na_2W4O_{13})

$Na_2W_4O_{13}$ has been discovered to have several advantageous properties, including ionic conduction and luminescence behaviors. In one dimensional nanostructure, it is supposed to be more active than in film form or granule. Furthermore, in the existence of ultraviolet light exposure and sacrificial agents, $Na_2W_4O_{13}$ splits water into hydrogen and oxygen with a band gap energy of 3.1 eV. Because of its high band gap, the value of $Na_2W_4O_{13}$ as a visible photocatalyst is restricted and tailoring the band gap energy of $Na_2W_4O_{13}$ for visible-light harvesting with increased potency is required. For their prospective uses in sunlight-driven photocatalysis, band gap semiconductor material alterations through doping with anions or cations have received considerable interest. Traditional biological wastewater treatment technologies, such as physical and chemical treatment procedures, cannot successfully address the vast variety of pollutants contained in wastewater due to their high robustness in the chemical environment and limited biodegradability.

Photocatalytic efficiency of Sn^{2+} and N^{3-} doped $Na_2W_4O_{13}$ was studied to degrade the dyes, and stable photocatalytic materials must be prepared that absorb light in the visible range. The degradation of dangerous environmental contaminants 4-chlorophenol and rhodamine B is hard to disintegrate under irradiation of visible light. It was investigated in the attendance of newly produced layered tungstate ($Na_2W_4O_{13}$) with doped analogues. It has been investigated that the ion-exchange approach using an aqueous route is useful for removing harmful metal ions from nuclear effluents and industrial wastewater. The elimination of these hazardous metal ions from aqueous systems is critical for human health and environmental safety. Consequently, an effort is made to remove the hazardous Pb^{2+} by $Na_2W_4O_{13}$ from Pb $(NO_3)_2$ aqueous solution. The resulting chemical is ash-colored and known as $SnWO_4$. The pristine $Na_2W_4O_{13}$ can be prepared by the sol–gel method at a low temperature. $Na_2W_4O_{13}$ and $SnCl_2$ acidic solution (1:2 M ratios) were stirred at room temperature. The substance was filtered and rinsed multiple times with water following the ion-exchange process and then dried in the air. Un-reacted urea can be removed using deionized water. This procedure can also be done using double distilled water. The concentration of un-exchanged Pb^{2+} in filtrate can be determined using atomic absorption spectroscopy (AAS) [67, 68]. Heavy metal ion-containing wastewater is a major environmental issue. Adsorption is a widely used approach in wastewater treatment that relies on the physical interaction of metal particles and sorbents. Because of their unique exceptional structural features, tungstate metals are good sorbents for removing heavy metal ions from wastewater [48].

4 Conclusion

Nanotechnology has enormous promise in driving water and wastewater remediation to increase processing products and the contention of water adaptability. The presentation covered all the features and mechanisms of prospective tungstate metals-based materials that permit different applications. It also explained the strengths and drawbacks of existing techniques for future research. Many methods have been developed for the treatment of wastewater. Those conventional methods for the treatment of wastewater are not enough to fulfill the need of today's freshwater because they are energy-consuming, not biodegradable, and not efficient to remove all kinds of pollutants. Although, there is a need for novel, eco-friendly, and economic methods for water/wastewater remediation. Therefore, photocatalytic degradation has proven the most cost-effective and tremendous method for the degradation of several dyes like methylene blue and other organic dyes that are carcinogenic. TiO_2 can be used as a photocatalyst, but it has a large band gap. Thus, a suitable candidate for the catalyst is WO_3 for degradation processes. It is doped with different metals like silver and copper which reduces its band gap; therefore, it enhances photocatalytical activity in the visible region. Different composites like Bi_2WO_6, Fe_3O_4/Bi_2WO_6, $CuWO_4$, $BaWO_4$, and $Na_2W_4O_{13}$ showed high activity toward degradation of different effluents present in the wastewater. These advanced organic processes (AOPs) are more efficient and environmentally friendly for the production of CO_2 and clean water with low expenditure and can be used multiple times.

References

1. Ahuchaogu AA, Chukwu OJ, Obike A, Igara CE, Nnorom IC, Echeme JBO (2018) Reverse osmosis technology, its applications and nano-enabled membrane. Int J Adv Res Chem Sci 5(2):20–26
2. Akan J, Moses E, Ogugbuaja V, Abah J (2007) Assessment of tannery industrial effluents from Kano metropolis, Kano State, Nigeria. J Appl Sci 7(19):2788–2793
3. Ayappan C, Palanivel B, Jayaraman V, Maiyalagan T, Mani A (2019) One-step hydrothermal synthesis of $CaWO_4/\alpha$-Ag_2WO_4 heterojunction: an efficient photocatalyst for removal of organic contaminants. Mater Sci Semicond Process 104:104693
4. Adams VD (2017) Water and wastewater examination manual. Routledge, London
5. Ameta A, Ameta R, Ahuja M (2013) Photocatalytic degradation of methylene blue over ferric tungstate. Sci Revs Chem Commun 3(3):172–180
6. Ahmad W, Khan A, Ali N, Khan S, Uddin S, Malik S, Ali N, Khan H, Khan H, Bilal M (2021) Photocatalytic degradation of crystal violet dye under sunlight by chitosan-encapsulated ternary metal selenide microspheres. Environ Sci Pollution Res 28(7):8074–8087
7. Ali N, Bilal M, Khan A, Ali F, Yang Y, Malik S, Din SU, Iqbal HM (2021) Deployment of metal-organic frameworks as robust materials for sustainable catalysis and remediation of pollutants in environmental settings. Chemosphere 129605
8. Chen H, Nanayakkara CE, Grassian VH (2012) Titanium dioxide photocatalysis in atmospheric chemistry. Chem Rev 112(11):5919–5948
9. Chen P, Chen L, Zeng Y, Ding F, Jiang X, Liu N, Au C-T, Yin S-F (2018) Three-dimension hierarchical heterostructure of $CdWO_4$ microrods decorated with Bi2WO6 nanoplates for high-selectivity photocatalytic benzene hydroxylation to phenol. Appl Catal B 234:311–317

10. Chenot C, Robiette R, Collin S (2019) First evidence of the cysteine and glutathione conjugates of 3-sulfanylpentan-1-ol in hop (*Humulus lupulus* L.). J Agric Food Chem 67(14):4002–4010
11. de Luna LA, da Silva TH, Nogueira RFP, Kummrow F, Umbuzeiro GA (2014) Aquatic toxicity of dyes before and after photo-Fenton treatment. J Hazard Mater 276:332–338
12. Dong P, Yang B, Liu C, Xu F, Xi X, Hou G, Shao R (2017) Highly enhanced photocatalytic activity of WO_3 thin films loaded with Pt–Ag bimetallic alloy nanoparticles. RSC Adv 7(2):947–956
13. Dong S, Ding X, Guo T, Yue X, Han X, Sun J (2017) Self-assembled hollow sphere shaped Bi_2WO_6/RGO composites for efficient sunlight-driven photocatalytic degradation of organic pollutants. Chem Eng J 316:778–789
14. Dzumbira W, Ali N, Duanmu C, Yang Y, Khan A, Ali F, Bilal M, Iqbal H (2021) Separation and remediation of environmental pollutants using metal–organic framework-based tailored materials. Environ Sci Poll Res 1–21
15. Elwakeel KZ (2009) Removal of reactive black 5 from aqueous solutions using magnetic chitosan resins. J Hazard Mater 167(1–3):383–392
16. Gulkaya I, Surucu GA, Dilek FB (2006) Importance of H_2O_2/Fe^{2+} ratio in Fenton's treatment of a carpet dyeing wastewater. J Hazard Mater 136(3):763–769
17. Geng Y, Ma J, Hou Z, Li N, Wang L (2019) Enhanced photocatalytic activity of $ZnWO_4$/BiOI composites under visible-light irradiation. J Nanosci Nanotechnol 19(12):7771–7776
18. Hojamberdiev M, Zhu G, Xu Y (2010) Template-free synthesis of $ZnWO_4$ powders via hydrothermal process in a wide pH range. Mater Res Bull 45(12):1934–1940
19. Hou J, Cao S, Wu Y, Liang F, Sun Y, Lin Z, Sun L (2017) Simultaneously efficient light absorption and charge transport of phosphate and oxygen-vacancy confined in bismuth tungstate atomic layers triggering robust solar CO_2 reduction. Nano Energy 32:359–366
20. Hou Y, Li X, Zhao Q, Chen G, Raston CL (2012) Role of hydroxyl radicals and mechanism of *Escherichia coli* inactivation on Ag/AgBr/TiO_2 nanotube array electrode under visible light irradiation. Environ Sci Technol 46(7):4042–4050
21. Huang G, Zhu Y (2007) Enhanced photocatalytic activity of $ZnWO_4$ catalyst via fluorine doping. J Phys Chem C 111(32):11952–11958
22. Hang TTM, Vy NHT, Hanh NT, Pham T-D (2021) Facile synthesis of copper tungstate ($CuWO_4$) for novel photocatalytic degradation of tetracycline under visible light. Sustain Chem Pharmacy 21:100407
23. He H, Cao L, He Z, Lu J (2014) Surface characterisations and photocatalytic property of MWO_4 ($M = Fe^{2+}$, Co^{2+}, Ni^{2+}) nanoparticles. Int J Nano Biomater 5(2–3):113–124
24. Hou L, Hua H, Gan L, Liu Y, Yuan C, Liu S (2015) Hydrothermal synthesis of visible-light-driven hierarchical Bi3. 84W0. 16O6. 24 photocatalysts toward efficient degradation of methyl orange. J Nanoparticle Res 17(4):1–10
25. Hsini A, Naciri Y, Laabd M, Bouziani A, Navío J, Puga F et al (2021) Development of a novel PANI@ WO_3 hybrid composite and its application as a promising adsorbent for Cr (VI) ions removal. J Environ Chem Eng 105885
26. Huang J, Xue P, Wang S, Han S, Lin L, Chen X, Wang Z (2022) Fabrication of zirconium-based metal-organic frameworks@ tungsten trioxide (UiO-66-NH_2@ WO_3) heterostructure on carbon cloth for efficient photocatalytic removal of tetracycline antibiotic under visible light. J Colloid Interface Sci 606:1509–1523
27. Iqbal MZ, Pal P, Shoaib M, Abdala AA (2017) Efficient removal of different basic dyes using graphene. Desalin Water Treat 68:226–235
28. Keerthana S, Yuvakkumar R, Kumar PS, Ravi G, Hong S, Velauthapillai D (2021) Investigation of PEG directed Sb_2WO_6 for dyes removal from wastewater. Chemosphere 132677
29. Kuzmin A, Kalinko A, Evarestov R (2013) Ab initio LCAO study of the atomic, electronic and magnetic structures and the lattice dynamics of triclinic $CuWO_4$. Acta Mater 61(1):371–378
30. Kamble S, Marathe K (2005) Membrane characteristics and fouling study in MEUF for the removal of chromate anions from aqueous streams. Sep Sci Technol 40(15):3051–3070
31. Ke J, Liu J, Sun H, Zhang H, Duan X, Liang P, Li X, Tade MO, Liu S, Wang S (2017) Facile assembly of $Bi_2O_3/Bi_2S_3/MoS_2$ np heterojunction with layered n-Bi_2O_3 and p-MoS_2 for enhanced photocatalytic water oxidation and pollutant degradation. Appl Catal B 200:47–55

32. Ke J, Zhou H, Liu J, Duan X, Zhang H, Liu S, Wang S (2018) Crystal transformation of 2D tungstic acid H_2WO_4 to WO_3 for enhanced photocatalytic water oxidation. J Colloid Interface Sci 514:576–583
33. Khan A, Rahman S, Malik S, Ali N, Yang Y, Zhou C et al (2021) Functionalized polymeric nanomaterials for environmental remediation. In: Handbook of functionalized nanomaterials. Elsevier, Amsterdam, pp 3–28
34. Kumar P, Verma S, Korošin NČ, Žener B, Štangar UL (2021) Increasing the photocatalytic efficiency of $ZnWO_4$ by synthesizing a $Bi_2WO_6/ZnWO_4$ composite photocatalyst. Catal Today
35. Kumar SG, Rao KK (2015) Zinc oxide based photocatalysis: tailoring surface-bulk structure and related interfacial charge carrier dynamics for better environmental applications. RSC Adv 5(5):3306–3351
36. Li J, Shi Q, Chen Y, Song M (2017) Hydrothermal synthesis of Bi_2WO_6 and photocatalytic reduction of aqueous Cr(VI) under visible light irradiation. 100(1):012030
37. Li X, Jiang Y, Cheng W, Li Y, Xu X, Lin K (2015) Mesoporous TiO2/carbon beads: One-pot preparation and their application in visible-light-induced photodegradation. Nano-Micro Lett 7(3):243–254
38. Li X, Li J, Bai J, Dong Y, Li L, Zhou B (2016) The inhibition effect of tert-butyl alcohol on the TiO_2 nano assays photoelectrocatalytic degradation of different organics and its mechanism. Nano-Micro Lett 8(3):221–231
39. Liang L, Lei F, Gao S, Sun Y, Jiao X, Wu J, Qamar S, Xie Y (2015) Single unit cell bismuth tungstate layers realizing robust solar CO_2 reduction to methanol. Angew Chem Int Ed 54(47):13971–13974
40. Liang L, Tursun Y, Nulahong A, Dilinuer T, Tunishaguli A, Gao G, Abulikemu A, Okitsu K (2017) Preparation and sonophotocatalytic performance of hierarchical Bi_2WO_6 structures and effects of various factors on the rate of Rhodamine B degradation. Ultrason Sonochem 39:93–100
41. Lingamdinne LP, Koduru JR, Karri RR (2019) A comprehensive review of applications of magnetic graphene oxide based nanocomposites for sustainable water purification. J Environ Manage 231:622–634
42. Liu J, Li Y, Ke J, Wang S, Wang L, Xiao H (2018) Black NiO-TiO_2 nanorods for solar photocatalysis: recognition of electronic structure and reaction mechanism. Appl Catal B 224:705–714
43. Liu Z, Tian J, Zeng D, Yu C, Zhu L, Huang W, Yang K, Li D (2017) A facile microwave-hydrothermal method to fabricate B doped $ZnWO_4$ nanorods with high crystalline and highly efficient photocatalytic activity. Mater Res Bull 94:298–306
44. Luo S, Ke J, Yuan M, Zhang Q, Xie P, Deng L, Wang S (2018) CuInS2 quantum dots embedded in Bi_2WO_6 nanoflowers for enhanced visible light photocatalytic removal of contaminants. Appl Catal B 221:215–222
45. Ma D, Wu J, Gao M, Xin Y, Ma T, Sun Y (2016) Fabrication of Z-scheme g-C3N4/RGO/Bi2WO6 photocatalyst with enhanced visible-light photocatalytic activity. Chem Eng J 290:136–146
46. Mal P, Bera G, Rambabu P, Turpu G, Chakraborty B, Ramaniah LM, Singh R, Sen P, Das P (2016) Electronic, magnetic and spectroscopic properties of doped $Mn_{(1-x)}A_xWO_4$ (A= Co, Cu, Ni and Fe) multiferroic: an experimental and DFT study. J Phys Condens Matter 29(7):075901
47. Matalkeh M, Nasrallah GK, Shurrab FM, Al- ES, Mohammed W, Elzatahry A, Saoud KM (2022) Visible light photocatalytic activity of Ag/WO_3 nanoparticles and its antibacterial activity under ambient light and in the dark. Results Eng 13:100313
48. Marschall R, Soldat J, Wark M (2013) Enhanced photocatalytic hydrogen generation from barium tantalate composites. Photochem Photobiol Sci 12(4):671–677
49. Mishra P, Patnaik S, Parida K (2019) An overview of recent progress on noble metal modified magnetic Fe_3O_4 for photocatalytic pollutant degradation and H_2 evolution. Catal Sci Technol 9(4):916–941

50. Muhammad Z, Ali F, Sajjad M, Ali N, Bilal M., Shaik MR, Adil S, Sharaf M, Awwad EM, Khan M (2021) Zirconium-doped chromium IV oxide nanocomposites: synthesis, characterization, and photocatalysis towards the degradation of organic dyes. Catalysts 11(1):117
51. Oliveira FK, Santiago AA, Catto AC, da Silva LF, Tranquilin RL, Longo E, Motta FV, Bomio MR (2021) Cerium molybdate nanocrystals: Microstructural, optical and gas-sensing properties. J Alloys Compounds 857:157562
52. Palanisamy G, Bhuvaneswari K, Bharathi G, Pazhanivel T, Grace AN, Pasha SK (2021) Construction of magnetically recoverable ZnS–WO_3–$CoFe_2O_4$ nanohybrid enriched photocatalyst for the degradation of MB dye under visible light irradiation. Chemosphere 273:129687
53. Quyen VT, Kim J, Park P-M, Huong PT, Viet NM, Thang PQ (2021) Enhanced the visible light photocatalytic decomposition of antibiotic pollutant in wastewater by using Cu doped WO_3. J Environ Chem Eng 9(1):104737
54. Samuel O, Othman MHD, Kamaludin R, Sinsamphanh O, Abdullah H, Puteh MH, Kurniawan TA (2021) WO_3–based photocatalysts: a review on synthesis, performance enhancement and photocatalytic memory for environmental applications. Ceramics Int
55. Siriwong P, Thongtem T, Phuruangrat A, Thongtem S (2011) Hydrothermal synthesis, characterization, and optical properties of wolframite $ZnWO_4$ nanorods. CrystEngComm 13(5):1564–1569
56. Song T-H, Li J-Y, Gao Y-J (2021) Preparation of Bi_2WO_6/Fe_3O_4 composite and photocatalytic degradation of bisphenol A. Sci Adv Mater 13(3):381–386
57. Stambouli HB, Guenfoud F, Benomara A, Mokhtari M, Sönmez- M (2021) Synthesis of $FeWO_4$ heterogeneous composite by the sol–gel process: enhanced photocatalytic activity on malachite green. React Kinet Mech Catal 133(1):563–578
58. Shahed GV, Taherian Z, Khataee A, Meshkani F, Orooji Y (2020) Samarium-impregnated nickel catalysts over SBA-15 in steam reforming of CH_4 process. J Ind Eng Chem 86:73–80
59. Shang Y, Cheng X, Shi R, Ma Q, Wang Y, Yang P (2020) Synthesis and comparative investigation of adsorption capability and photocatalytic activities of WO_3 and $W_{18}O_{49}$. Mater Sci Eng, B 262:114724
60. Shao P, Yu S, Duan X, Yang L, Shi H, Ding L, Tian J, Yang L, Luo X, Wang S (2020) Potential difference driving electron transfer via defective carbon nanotubes toward selective oxidation of organic micropollutants. Environ Sci Technol 54(13):8464–8472
61. Sharma V, McKone HT, Markow PG (2011) A global perspective on the history, use, and identification of synthetic food dyes. J Chem Educ 88(1):24–28
62. Sheikh ZA, Ali N, Ali F, Ali A, Shabir G, Bilal M (2021) Fabrication, morphological, structural and electrochemical characterization of sulfonated polyimide/clay-based hybrid nanocomposite membranes for energy application. J Polym Res 28(3):1–12
63. Tetteh EK, Rathilal S (2019) Application of organic coagulants in water and wastewater treatment. Org Polym
64. Tahir MB, Nabi G, Rafique M, Khalid N (2017) Nanostructured-based WO_3 photocatalysts: recent development, activity enhancement, perspectives and applications for wastewater treatment. Int J Environ Sci Technol 14(11):2519–2542
65. Templeton MR, Butler D (2011) Introduction to wastewater treatment. Bookboon
66. Tian Y, Wang Y, Sheng Z, Li T, Li X (2016) A colorimetric detection method of pesticide acetamiprid by fine-tuning aptamer length. Anal Biochem 513:87–92
67. Thilagavathi T, Venugopal D, Marnadu R, Chandrasekaran J, Thangaraju D, Palanivel B, Hamdy MS, Shkir M, Ali HE (2021) WO_3/$CoWO_4$ nanocomposite synthesis using a facile co-precipitation method for enhanced photocatalytic applications. J Phys Chem Solids 154:110066
68. Toste CT (2021) Development of a new biophotocatalytic system for biofuel production
69. Veresnikova A, Lubsandorzhiev B, Barabanov I, Grabmayr P, Greiner D, Jochum J, Knapp M et al (2009) Fast scintillation light from $CaMoO_4$ crystals. Nucl Instrum Methods Phys Res Sect A Accel Spectrometers Detectors Assoc Equip 603(3):529–531
70. Vidya S, Solomon S, Thomas J (2013) Synthesis, characterization, and low temperature sintering of nanostructured BaWO4 for optical and LTCC applications. Adv Condensed Matter Phys

71. Vinu R, Madras G (2010) Environmental remediation by photocatalysis. J Indian Inst Sci 90(2):189–230
72. Wan J, Xue P, Wang R, Liu L, Liu E, Bai X, Fan J, Hu X (2019) Synergistic effects in simultaneous photocatalytic removal of Cr(VI) and tetracycline hydrochloride by Z-scheme $Co_3O_4/Ag/Bi_2WO_6$ heterojunction. Appl Surf Sci 483:677–687
73. Wang B-Y, Zhang G-Y, Cui G-W, Xu Y-Y, Liu Y, Xing C-Y (2019) Controllable fabrication of α-Ag_2 WO_4 nanorod-clusters with superior simulated sunlight photocatalytic performance. Inorg Chem Front 6(1):209–219
74. Wang H, Liu W, He X, Zhang P, Zhang X, Xie Y (2020) An excitonic perspective on low-dimensional semiconductors for photocatalysis. J Am Chem Soc 142(33):14007–14022
75. Wu Q-S, Cui Y, Yang L-M, Zhang G-Y, Gao D-Z (2015) Facile in-situ photocatalysis of Ag/Bi_2WO_6 heterostructure with obviously enhanced performance. Sep Purif Technol 142:168–175
76. Wu Y, Luo N, Xie R (2020) Enhanced visible light photocatalytic performance of $CdS/Zn_{1-x}Cd_xWO_4$ composites prepared by a facile protocol. Ceram Int 46(9):14114–14123
77. Wu Y, Luo N, Xie R (2020) Rodlike Cadmium-incorporated zinc tungstate nanoarchitecture fabricated by a facile and template-free strategy as a photocatalyst for the effective degradation of organic pollutants in sewage. ACS Omega 5(38):24318–24328
78. Wu Y, Tie J, Chen C, Luo N, Yang D, Hu W, Liu X (2019) Synthesis of LAS/ZnO/$ZnWO_4$ 3D rod-like heterojunctions with efficient photocatalytic performance: synergistic effects of highly active site exposure and low carrier recombination. Ceram Int 45(11):13656–13663
79. Wuana RA, Okieimen FE (2011) Heavy metals in contaminated soils: a review of sources, chemistry, risks and best available strategies for remediation. International Scholarly Research Notices
80. Yadav P, Shrivastava V, Nagarajan R (2021) Carbon and nitrogen co-doped WO_3 as sonocatalyst. Solid State Sci 115:106588
81. Ye D, Li D, Zhang W, Sun M, Hu Y, Zhang Y, Fu X (2008) A new photocatalyst $CdWO_4$ prepared with a hydrothermal method. J Phys Chem C 112(44):17351–17356
82. Yang L, Peng Y, Qian C, Xing G, He J, Zhao C, Lai B (2021) Enhanced adsorption/photocatalytic removal of Cu(II) from wastewater by a novel magnetic chitosan@ bismuth tungstate coated by silver (MCTS-Ag/Bi_2WO_6) composite. Chemosphere 263:128120
83. Yi H, Qin L, Huang D, Zeng G, Lai C, Liu X, Li B, Wang H, Zhou C, Huang F, Liu S,Guo X (2019) Nano-structured bismuth tungstate with controlled morphology: fabrication, modification, environmental application and mechanism insight. Chem Eng J 358:480–496
84. Yu L, Ruan S, Xu X, Zou R, Hu J (2017) One-dimensional nanomaterial-assembled macroscopic membranes for water treatment. Nano Today 17:79–95
85. Zhang K, Lin L, Hussain S, Han S (2018) Core–shell $NiCo_2O_4$@ $ZnWO_4$ nanosheets arrays electrode material deposited at carbon-cloth for flexible electrochemical supercapacitors. J Mater Sci Mater Electron 29(15):12871–12877
86. Zeb S, Ali N, Ali Z, Bilal M, Adalat B, Hussain S, Gul S, Ali F, Ahmad R, Khan S, Iqbal HM (2020) Silica-based nanomaterials as designer adsorbents to mitigate emerging organic contaminants from water matrices. J Water Process Eng 38:101675
87. Zhang Y, Xu Y-J (2013) Bi_2WO_6: a highly chemoselective visible light photocatalyst toward aerobic oxidation of benzylic alcohols in water. RSC Adv
88. Zhang Z, Zhang C, Zheng H, Xu H (2019) Plasmon-driven catalysis on molecules and nanomaterials. Acc Chem Res 52(9):2506–2515
89. Zhu J, Liu M, Tang Y, Sun T, Ding J, Han L, Wang M (2017) Facile photochemical synthesis of $ZnWO_4$/Ag yolk-shell microspheres with enhanced visible-light photocatalytic activity. Mater Lett 190:60–63
90. Zhang C, Shen E, Wang E, Kang Z, Gao L, Hu C, Xu L (2006) One-step solvothermal synthesis of high ordered $BaWO_4$ and $BaMoO_4$ nanostructures. Mater Chem Phys 96(2–3):240–243
91. Zhu B, Hu Y, Kennedy S, Milne N, Morris G, Jin W, Gray S, Duke M (2011) Dual function filtration and catalytic breakdown of organic pollutants in wastewater using ozonation with titania and alumina membranes. J Membrane Sci 378(1–2):61–72

Chapter 15
Organic–Inorganic nanohybrids in Dye-Sensitized Solar Cells

Osama Majeed Butt, Muhammad Zaffar, Muhammad Shakeel Ahmad, Komal Rizwan, Adnan Daud Khan, and Muhammad Saad Rehan

1 Introduction

Renewable energy sector is growing at a much faster pace than ever before, and there is a need for much better harnessing systems for renewable energies. Thus, research in the renewable energy technologies is needed to have efficient and reliable energy generation systems [1]. Different renewable energy resources are the solar, wind, hydro, tidal, biomass, and geothermal energy. Hydropower has been immensely utilized globally for the production of electricity. The main issue with hydropower is that it needs huge water reservoirs. Similarly, the global potential of wind is approximately 1.3×10^{12} KW; however, wind also has major drawbacks. Firstly, it is not a stable source, and secondly not every region is blessed with sufficient wind to meet the energy demands of the community. Unlike the wind and hydropower sources, solar energy is available in abundance. Global solar potential is approximately 174,000 TW per day which can easily meet the global energy demand. In addition to this, the pattern of availability of the solar energy to the human beings

O. M. Butt (✉)
Institute of Electrical, Electronics and Computer Engineering, University of the Punjab, Lahore, Pakistan
e-mail: osama.ee@pu.edu.pk

O. M. Butt · M. S. Ahmad
UM Power Energy Dedicated Advanced Center, University of Malaya, Kuala Lumpur, Malaysia

M. Zaffar
Institute of Energy and Environmental Engineering, University of the Punjab, Lahore, Pakistan

K. Rizwan (✉)
Department of Chemistry, University of Sahiwal, Sahiwal, Pakistan
e-mail: komal.rizwan45@yahoo.com

A. D. Khan · M. S. Rehan
Center for Advanced Studies in Energy (CAS-E), University of Engineering and Technology, Peshawar, Pakistan

K. Rizwan et al. (eds.), *Hybrid Nanomaterials*, Materials Horizons: From Nature to Nanomaterials, https://doi.org/10.1007/978-981-19-4538-0_15

is exactly according to the requirements, i.e., sun shines with immense intensity in summers and at noon times during which the maximum energy is consumed. Almost every region on earth receives sunshine; therefore, it can be said that solar energy is the only form of energy from which every region on earth can benefit. Besides this, it is cleaner and more sustainable than other forms of energies. The investigations on solar energy started back in the decade of 1970s, and since then, it has been a key area of investigation [2]. Many regarded it as the solution for reducing the use of fossil and other not-so-clean fuels. As a result, solar energy has been the object of optimistic predictions to replace all the current not-so-clean means of energy production eventually. Given the afore mentioned, it can be said that the only promising renewable resource has the potential to cater the issues generated by excessive use of fossil fuels.

To harness solar energy, photovoltaic (PV) devices are commonly used. These devices convert solar energy to electric current through photovoltaic effect. Among the PV devices, much development has been made in the solar cells. The history of solar energy dates to seventh century B.C. Charles Fritts, in 1883, developed the first ever solar cell by depositing a layer of gold on selenium. This cell had an achieved an efficiency of 1%. Later, Albert Einstein in 1905 explained in detail the phenomenon of conversion of light into electricity. Bell Laboratories had the honor of introducing the modern solar cell in 1954. To date solar cells have progressed a lot. Many different types of solar cells have been developed. Most notable among them are single crystalline silicon solar, thin film, multi-crystalline silicon solar cells, and III–V generation solar cells. The most developed type of solar cells is the crystalline silicon solar cells. Studies showed that the maximum efficiency they have attained is up to 27.6%. Two types of crystalline solar cells exist, one is the single crystalline, and the other one is the multi-crystalline. Multi-crystalline silicon solar cells are cheaper than single crystalline ones. As far as the efficiency is concerned, the single crystalline cells have higher efficiency. Currently, different governments are providing subsidies to promote the renewable energy sources.

Another type of solar cells is the thin film solar cells. The major advantage of these cells is that they require lesser materials. Examples of these cells include amorphous silicon, CdTE solar cells, dye-sensitized solar cells, and CIGS solar cells, etc. Fabrication techniques and availability of the materials are the key issues which need attention in the context of their mass scale production. Keeping the view, the current research trends and technological advancements, it can be said that in the future the roll-to-roll production, stability, and transportation issues have to be tackled so that they can be deployed at large scales. Therefore, the cells which are easy to process and do not require specialized environments such as high vacuum are expected to capture the markets in future. Similarly, the cells whose materials are abundantly available are expected to dominate as compared to those who require rare-earth elements. Among the different types of solar cells, many investigations are underway on the dye-sensitized solar cells (DSSCSs) because they have demonstrated remarkable efficiencies and are easy to synthesize [3–5]. Michael Gratzel first invented them in 1985. So far efficiency of greater than 10% has been achieved. Moreover, the production cost of these cells is also low. Another plus point of these cells is that they can

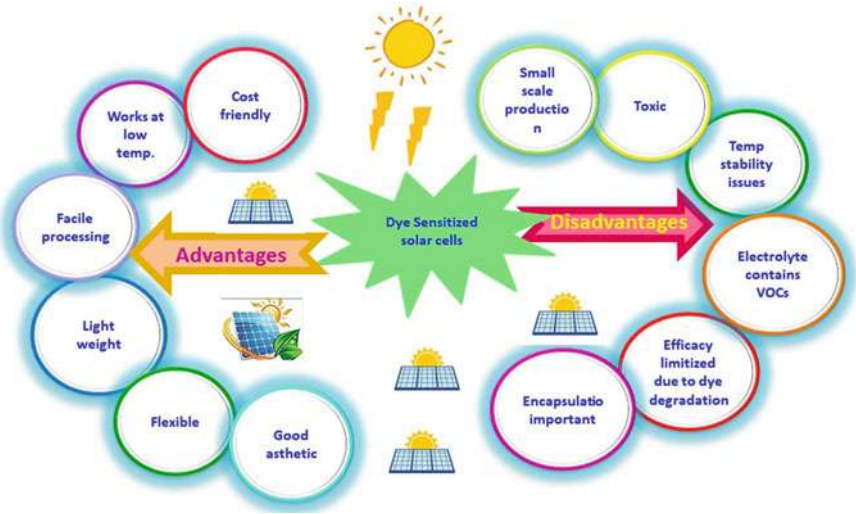

Fig. 1 Advantages and disadvantages of dye-sensitized solar cells

work under low light conditions [5]. Advantages and disadvantages of dye-sensitized solar cells are presented in Fig. 1.

2 Basic Architecture of DSSC

There are four main components of a DSSC including (a) Working electrode, (b) Photosensitizer or dye, (c) Redox mediator, and (d) Counter electrode. The functions and role of each component are discussed below.

2.1 ITO/FTO Coated Glass

The transparent conductive substrate should exhibit a transparency of 80% to allow maximum light to pass through, and it should be electrically conductive for efficient charge transfer. The most used substrates in DSSCS include fluorine-doped SnO_2 (FTO) or indium-doped SnO_2 (ITO). These substrates are developed by coating films of FTO or ITO on soda-lime glass. The coating plays a very important role in the collection of current and therefore is also known as current collector. As far as the performance is concerned, the ITO coated glass has higher conductivity and transparency than the FTO coated glass [2].

2.2 Working Electrode

Electrode is developed by depositing a thin layer of oxide semiconductors on FTO or ITO coated glass. These semiconductors can be *n*-type such as SnO_2, Nb_2O_5, TiO_2, and ZnO or *p*-type such as nickel oxide. Generally, anatase phase of TiO_2 is used because it is less toxic, easily available, and less expensive. The TiO_2 band gap is 3.2 eV. Different binding materials as polyethylene glycol can be used in the preparation of TiO_2. Coating techniques such as doctor blading and screen printing are used. The size of nanoparticles used ranges from 15 to 30 nm, while the thickness of coating is 15–20 um. The different crystalline phases of TiO_2 include rutile phase, anatase, and brookite as shown in Fig. 2. Anatase and rutile phases have tetragonal structures, while brookite possesses orthorhombic geometry. The most stable form of TiO_2 is rutile. Upon increasing temperatures, transformation from amorphous to anatase to rutile phases occurs in TiO_2. Different techniques used for the preparation of TiO_2 include sol–gel method, hydrothermal method, synthesis through ultrasonic irradiation, hydrothermal method assisted by microwaves, and sputtering. In order to achieve nanoparticles with improved crystallinity and large surface area, sol–gel method is the most effective technique for the preparation of TiO_2. In this technique,

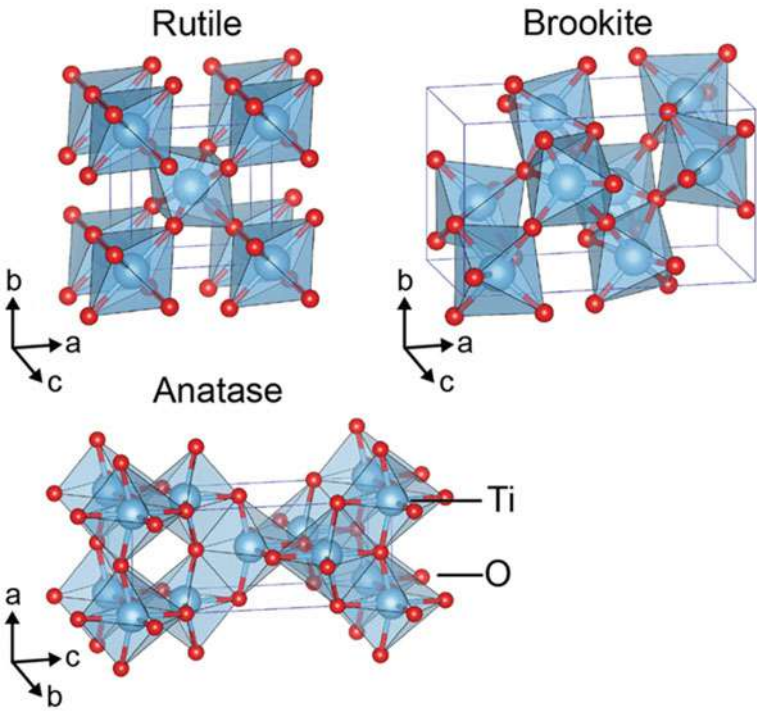

Fig. 2 Different phase of TiO_2. Adapted from [8]

the alkoxide precursors are used which subsequently calcined. Calcination changes the TiO_2 phase from anatase to rutile. The intermediate phase, i.e., mix anatase and rutile phase, can also be produced. TiO_2 has proven superior performance than other semiconductors. Studies suggest that the band gap of ZnO is closer to TiO_2 and it also has a higher carrier mobility. But ZnO suffers from higher instability and charge recombination. In this context, different researchers have made attempts to modify the shape and size of ZnO to achieve comparable performance to TiO_2. The main problem with Titania is that it absorbs a certain portion of light in UV range [6]. Therefore, to increase the light absorption by Titania, the electrode is immersed in a dye solution. The dye solution is developed by mixing a photosensitizer in a solvent. Due to highly porous structure TiO_2, many dye molecules covalently bond themselves with TiO_2. This increases the light absorption by TiO_2. Nowadays flexible substrates are also being used. These substrates are developed by coating TiO_2 layer on polymeric films [6]. Flexible substrates have dual benefits. They add to the flexibility of cell and increase the light trapping efficiency of the cell. However, the polymeric films cannot be heated above 200 °C; i.e., TiO_2 remains incompletely calcined. Therefore, polymeric substrates have lower efficiencies. Another reason is the poor adhesion between TiO_2 and substrate [7]. Mechanical pressing has been presented as an alternative to calcination process. A flexible DSSC with an efficiency of 8.1% was reported [6].

2.3 Photosensitizer or Dye

The dye absorbs the maximum sunlight. It should possess the following feature.

- The dye should be luminescent.
- It should be able to absorb light in UV–Vis and NIR regions.
- It should be water repellant to ensure the stability of the cell in the long run.
- It should not aggregate on TiO_2. For this purpose, co-absorbents can be used.
- It should be able to resist light and heat.

The dye is a crucial element of a DSSC as it contributes to the maximum light absorption. This has aroused the interests of scientists in exploring new dye materials which can absorb maximum light. Generally, ruthenium (Ru) dye is used, but it is very costly and is not abundantly available [9]. Therefore, the possible alternatives of Ru dye are under consideration. In this context, organic dyes are the potential candidates. In 2008, indoline has been used as organic dye with a cell efficiency of 9.8%. The increase in efficiency of solar cells from 2% in 1976 to greater than 10% can be justified to the use of new light capturing dyes. In the past decades, metal complexes and metal free organic dyes were also used. A metal complex is composed of the metal ion in the center along with a ligand which has at least one anchoring group. These complexes absorb visible light because of transfer of charges through metal ligand. Some of the metal ligands were even used in the past as standard dyes for DSSCS. As the research on the dyes progressed, their working in the NIR region

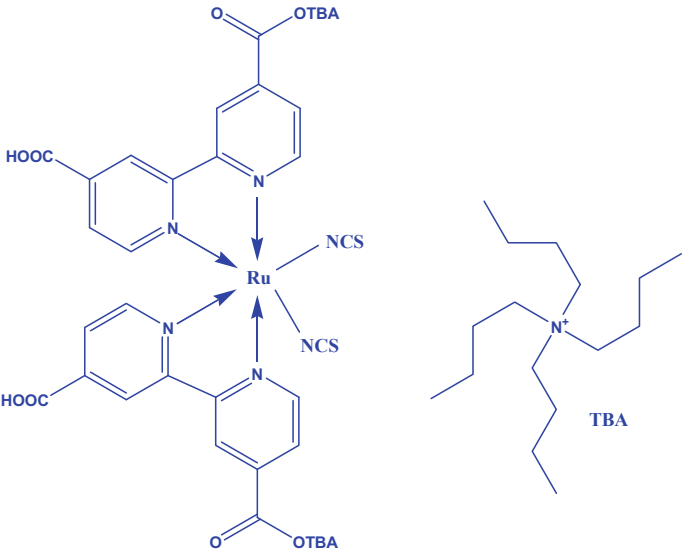

Fig. 3 Structure of N719 dye

got improved by using Ru complexes in the dyes. A classical example of this type of dye is N719 dye shown in Fig. 3, which contained Ru complex, and the efficiency of the cell using this dye was reported to be 10.4%. Along with the synthetic dyes, some researchers have also reported the use of natural dyes in DSSCS. Authors report some novel dye materials by incorporating non-polar groups into the organic structures. Such dyes have achieved an efficiency of 8.60%. Dyes based on cyanide groups have achieved efficiency of 7.6%. Dyes based on the flower extracts are quite inefficient despite of adding the sugar content in them.

2.4 Electrolyte

The electrolyte of a DSSC is composed of solvent additives, cations, a redox couple, and ionic liquids. The main properties of the electrolyte include: It should be noncorrosive to cell components, is resistant to high temp and chemicals, has capability to regenerate the oxidized dye, must establish a good electrical contact between the electrodes, and its absorption spectra should not overlap with that of the dye [10]. Table 1 shows the commonly used liquid dyes and their benefits.

Counter Electrode (CE)

The counter electrode performs several important functions: (a) In the reduction of electrolyte, the counter electrode acts as a catalyst. Thus, CE assists in the regeneration of the electrolyte, (b) Collection of current from the external circuit, (c) Plays a

Table 1 Commonly used liquid dyes in DSSC

S. No.	Name of dye	Properties
1.	Iodide/tri-iodide	Highly efficient but causes corrosion in counter electrode and because of its volatility it causes dye desorption and hence results in poor stability of the cell
2.	Acetonitrile (ACN), *N*-methyl pyrrolidine (NMP), solvent mixtures, such as ACN/Valero nitrile	The dielectric constants of these liquids are very high
3.	4-tert-butylpyridine (TBP)	TBP can change the conduction band and helps in the recombination of charge carriers

very important role in the reflection of un-absorbed light from the working electrode, thereby increasing the efficiency of the cell.

The most commonly used counter electrode is platinum-based, but due to its high cost and lesser abundance, many other materials such as carbon, carbonyl sulfide, $CoNi_{0.25}$, Au/GNP, alloy CEs like FeSe and have also been investigated by different researchers. Carbon-based electrodes have high surface area but are unable to reflect light [7]. Similarly, graphite has also been used as a counter electrode, but platinum is still the first choice of researchers due to its reflective properties. Sputtering and chemical vapor deposition are the most used techniques for the preparation of counter electrode. Nickel-based counter electrodes have also achieved remarkable efficiency of 8%. Cobalt sulfide films when used as counter electrodes have also shown effective results. Carbon nanotubes are also a potential candidate as counter electrode because of ordered structure which enables the fast transfer of electrolyte into the electrode. Polymeric materials with high conductivity are also under use these days with the reported efficiency of around 6%.

2.5 Working Principle of a DSSC

The photosensitizer absorbs the sunlight resulting in which its electrons get excited. The working range of the dye is around 700 nm corresponding to a photon with an energy of almost 1.72 eV. The excited electron enters the conduction band of Titania which leaves the dye oxidized. The injected electrons travel through the working electrode to the external circuit and reaches the counter electrode. Upon reaching the counter electrode, their interaction with the redox mediator turns it in into a reduced state. The reduced redox mediator finally reduces the oxidized sensitizer. This results in the regeneration of the electrolyte and completion of the circuit.

3 Organic/Inorganic Hybrids as Efficient Counter Electrode

Dye-sensitized solar cell's photovoltaic performance greatly depends upon the counter electrode as electron gathers from the external circuit to catalyze reduction of electrolyte. It also influences the stability of device and its cost [11]. Electrodes prepared with different methodologies have variety of applications; i.e., gold sputtered micro electrodes were prepared for electrochemical DNA detection. This leads to variety of application of applications for the improvements in electrodes [12]. CE in DSSCs acts as catalyst and helps to complete process the regeneration of oxidized redox couple at cathode by accepting electron from anode and helps in regeneration of oxidized dye through reduced redox couple by accepting electron by transferring electron to oxidized redox couple at counter electrode surface and to oxidize dye in dye-sensitized solar cell at solid state through ionic transport [13]. It collects electrons from external circuit and returns them to the main cell process circulation, and it also reflects un-absorbed sunlight back to the cell like a mirror for re-utilization. It enhances the efficiency of the cell. Features of efficient counter electrodes are presented in Fig. 4. Preparation of counter electrodes can be performed through various methods, and it depends on the type of electrode and their precursor materials Fig. 5.

Characterization of counter electrodes is very important and is done through the following methods of solar cell device testing:

- Photovoltaic measurements, i.e., current density–voltage curve
- Voltammetry (cyclic)

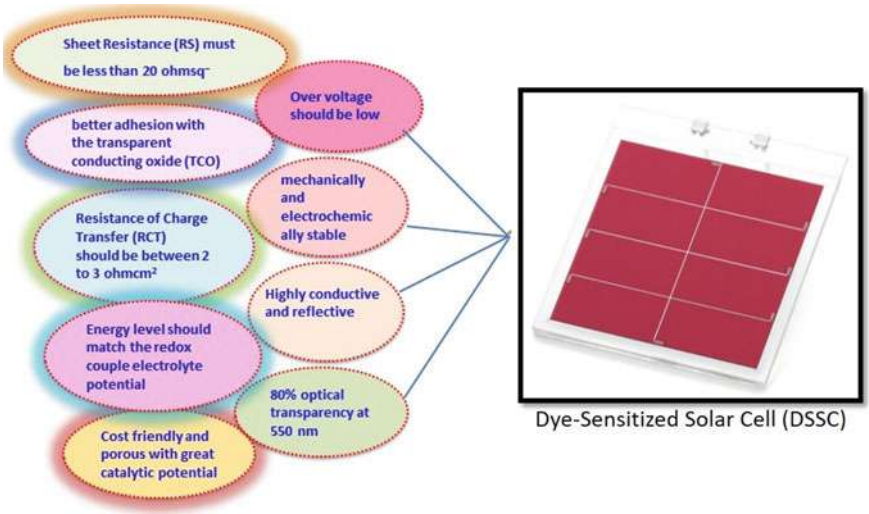

Fig. 4 Features of efficient counter electrodes

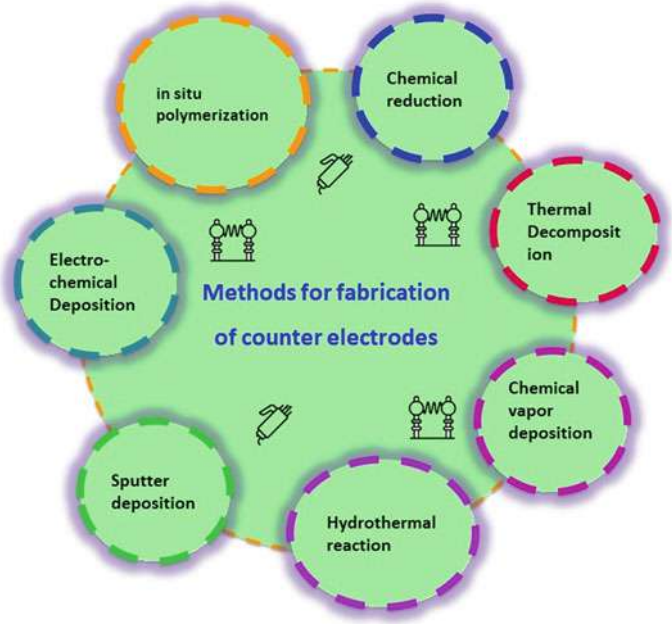

Fig. 5 Various methods for fabrication of counter electrodes

- Spectroscopy of electrochemical impedance
- Modulated photocurrent intensity and photo voltage spectroscopy.

3.1 Novel Flexible Counter Electrodes

Manufacturing of counter electrodes are completed via depositing a C on nanowires during layering of metal and polymer substrate of polyacrylate [14]. The metal nanowire materials contain one layer of copper and silver nanowires (CuNWs and AgNWs); moreover, a double layer of same materials CuNWs/AgNWs and AgNWs/CuNWs has been tested. A paste is made by mixture of black carbon and graphite after which this paste is applied to the metal nanowires polymer that is working as a substrate by spray casting, drop casting, or doctor blading. For the process of as-synthesized, the average diameter of silver nanowires (AgNWs) is 25–35 mm and for copper nanowires (CuNWs) is 20–30 nm, while the average lengths of both are 10–20 μm and 20–30 μm, respectively. The dispersion in isopropanol is done in proportion of 5 mg/ml and 2 mg/ml and between CuNWs and AgNWs, respectively. Copper nanowires (CuNWs) and silver nanowires (AgNWs) were dispersed in isopropanol with the quantity of 5 mg/ml and 2 mg/ml. After that using Meyer rod method, AgNW disperse solution coated on substrates of glass (76.2 mm × 25.4 mm) which were ultrasonically cleaned during the process. The spray coating was done

on copper CuNW dispersion was on a glass substrate that is pre-cleaned by using air brush at 0.4 mega Pascal pressure and at a 10 cm distance. After that, these substrates were air dried, and films of metallic nanowire are obtained. Similarly, by following the above process in sequence, the double layer NW metal was formed. Then, the formed NWs coatings were passed through the acrylate monomer at 1 wt% DMPA for polymerization. After that, a newly formed polymer with a thickness of 120 μm obtained. Then, it passes through an ultraviolet curing for 90 s and converted from a substrate to a transparent modified metal/polymer.

Doctor blading, drop casting, and spray coating techniques are used to fabricate carbon paste on nanowire polymer composite substrate [15]. We have obtained water-based carbon paste through doctor blading. Ethanol-based carbon paste is being fabricated on metal nanofilms during the spray coating. A maximum power consumption efficiency is achieved 4.39% from a counter electrode that is made up of carbon layer, and the drop casting method is used to deposit the silver nanowires (AgNW) polymer substrate. While on the other hand, a CE made up with an improved copper nanowire (CuNW) layer achieves 4.01% cell efficiency. The counter electrodes can achieve more efficiency by improving the preparation.

3.2 Graphene and Transition Metal as Counter Electrodes

In the recent few decades, focus of energy generation was diverted toward PV technology to develop an ecofriendly, promising, and urged solar cells (SCs). However, comparatively higher cost of production, uncertain nature, and least efficient productions of solar cells are major footraces in SCs commercialization. So, the materials of two dimensions (2DMs) are appreciated as they have been exploited to overcome the problems of high production cost, lesser catalytic activity, rate of charge separation, and to upgrade the solar cells' electrochemical efficiency. The investigation enunciates on (a) graphene's electrochemical activity and di-chalcogenides of transition metal (TMDCs) as HTL in SCs and (b) checking the counter electrode (CE) affordability and efficiency based on the graphene once TMDCs are analyzed for dye-sensitized solar cell (DSSC) [16–18]. This analysis provides a relative study of 2DMs as HTL and CE for production of most efficient and inexpensive photovoltaic devices. Several blends of materials encompassing graphene, molybdenum disulfide (MoS_2), tungsten disulfide (WS_2), reduced graphene oxide (rGO), graphene oxide (GO) as HTL, as well as counter electrode substances inside photovoltaic cells were under consideration and were being studied. Several approaches are being briefly conferred with a view to develop the SCs efficiency by exploiting TMDCs and grapheme-based CEs and HTL [19]. This analysis emphasizes upon the current development in the emerging cheap and immensely effective PV instruments by utilizing 2DMs. The conducted research indicates the PSS: GO/PEDOT shows 13.1% power conversion efficiency (PCE) if made in various modifications. Furthermore, the statistical analysis reveals that such efficiency of cell could be increased via improving the layer's thickness, which provides a path for the development of more efficient and effective

SC which can be used for future marketing applications. Every solar cell is made up of a semiconductor PN-junction producing some amount of current which directly relates to sunlight as electron–hole pairs are generated due to sunlight. The following equation will define the efficiency of SC.

$$\eta = V_{\mathrm{oc}} I_{\mathrm{sc}} \frac{\mathrm{FF}}{P_{\mathrm{inp}}}$$

Fill factor of SC can be calculated by

$$\mathrm{FF} = V_{\mathrm{m}} / V_{\mathrm{oc}} I_{\mathrm{sc}},$$

About 85% of the world's energy needs depend on fossil fuels, i.e., coal and natural gas. Various modifications are made in the equipment and certain conditions for storage of renewable energy to meet the present-day needs of solar cells, fuel cell, photo-electrochemical cell, batteries, and super-capacitor [20]. At present circumstances, fuels are depleting day by day, so the attentions of researchers been diverse toward renewable energy, photovoltaic devices (PV) are under focus for developments to improve efficiency and to develop the materials that can harvest light energy from all the spectrums of light, and their behavior should be environment-friendly.

3.3 NiO NWs with Carbon Shell Counter Electrodes

To enhance an object's catalytic activity, increasing the surface area active is important via the electrolyte direct contact. In electrochemical applications, large surface area of nanowires makes them an optimistic building block for catalysts. The coating of nickel oxide (NiO) was acquired by dissolving the molten solution of nickel in the same silicon nanowire compounds aligned vertically with a shell of carbon (SiNW/C). By the combination of carbon shell with NiO and silicon nanowire arrays, the current study is targeted at achieving the catalytic activity's synergic effect [13]. It has also revealed in this study that the nanomaterial obtained in the results shows a very good electro-catalytic activity and also is effective for dye-sensitive sun cells (DSSCs) as a counter electrode. Energy dispersive spectroscopy, X-ray diffraction, and X-ray photoelectron spectroscopy were used to find the composition of the material. The techniques of transmission electron microscopy and scanning electron microscopy were employed to examine the micro and nano structures of the materials. Maximum power conversion efficiency of the DSSC composed of the NiO @ SiNW/C calculator electrode was 9.49%, and it was significantly higher than that of the DSSC composed on the Pt counting electrode. A cobalt based on hydroxyapatite (Co_3O_4 @ nHAP) is comparatively more environment-friendly nanomaterial, and nano-hydroxyapatite (nHAP) is an auspicious substance for process of catalysis due to its durability of metal or complexes, made of radiation of ultraviolet and ability of calcination.

Produced cobalt-based nanomaterial (Co_3O_4 @ nHAP) is then specified as shown in Fig. 6 by the various characterization methods like EDX, mapping, XRD, FTIR, and FESEM. The ions obtained from cobalt were determined to get merged into the hydroxyapatite. Nanomaterials composed of Co_3O_4 @ nHAP have been employed as a catalyst to reduce Rhodamine B (Rh B) and 2-nitrophenol (2-NP), and Co_3O_4 @ nHAP nanomaterial type has been tested in dye-sensitive solar cells (DSSC) as a counter electrode for the first time. The powerful conversion of nanomaterials of Co_3O_4 @ nHAP at 12 min was determined as 97.8% for 2-NP and for Rh B 86.7% at 15 min and as *I–V* cycles between 97.8%, to 85.8% when 2-NP reuse activity was performed, respectively. When Co_3O_4 @nHAP/CNT and Co_3O_4 @nHAP were placed as opposite electrodes on DSSC, they were found more efficient on power conversion; these nanomaterials also shorten the layer thickness of DSSC. So, it is documented that PCE of manufactured DSSC is improved as well as layer thickness is reduced to 0.05% and 0.36%, respectively [21].

Up conversion nanoparticles (UCNPs) which are highly stable both thermally and photo-chemically have revealed their usages in photovoltaic (PV) dye-synthesized solar cells (DSSCs). The UCNPs based on lanthanides have shown in the near-infrared range (NIR) a flexible absorption and has a high transmission capacity from high altitude (NIR) photons of light to become photon waves of low wavelength (visible light). Here, we broadly deliberate the emergent use of UCNPs in DSSCs. We strive to clarify important concepts of body that UCNPs successfully acquire devolution. Graphene, contact with plasmatic NP, crystal structure, morphology, and mesoporous shell of TiO_2, significantly affects the DSSCs entire energy conversion efficiency. 1D nanostructures such as fiber, tubes, and rods mostly improve

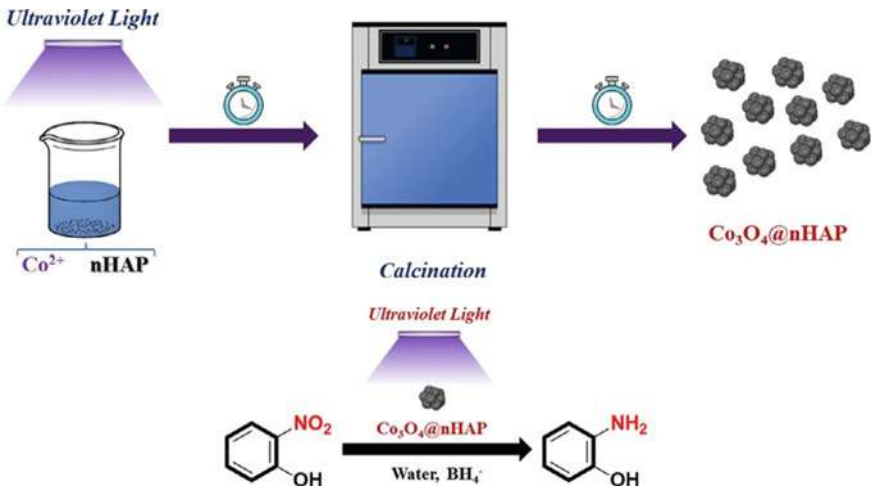

Fig. 6 Manufacturing of nanomaterial Co_3O_4@nHA. Scheme for degradation with **Co_3O_4**@nHAP catalyst of 2-nitrophenol to 2-aminophenol. Organic–inorganic nanoparticles counter electrodes. Reprinted with permission from [21]

revenue efficiency by providing DSSCs with specific modes of transport. In addition, dye loading can be increased greatly by a certain surface area with a mesoporous structure that, in turn, increases efficiency of photovoltaic current. Furthermore, we describe different influential factors efficient emission and photovoltaic current of built-in cells. We again described the various lattice of handling and its physiochemical features used by implementation of active DSSCs. In this study, we have highlighted UCNPs and described their very high performance that shows improvement in photovoltaic current and their trending developments in device planned for DSSCs. The investigation provides a useful guide that focuses on lanthanide-doped UCNPs for integration of objects as well construction of an opto-electronic system. This analysis comes to a conclusion by examining the electron transport parameters Jsc, Voc, FF, and power conversion efficiency (g). Up conversion of nanoparticles has made the light harvesting more efficient. So, DSSCs can be expanded by considering electron transport structures. A new type of [PdClL] complex and immobilize nanomaterials based on carbon [graphene oxide (GO) and multi-wall carbon nanotubes (MWCNTs)] were built on a basic composite path and categorized by FT-IR, ^{13}C NMR, 1H NMR, SEM–EDX, XRD, and EIS-MS analyses techniques. Built-in MWCNTs are supported [PdClL] (M1) and GO-supported [PdClL] (M2) nanomaterials of organic/inorganic hybrid performed on tri-iodide to iodide to reduce reactions like counter electrodes (CEs) in photovoltaics (dye-sensitive sun cells, DSSCs). Nanomaterials which are combined (M1 and M2) as CE-free Pt comparisons platinum, nanotube of carbon, and power conversion efficiency (PCEs) of counter electrodes (M1 and M2) have been developed with the additive [PdClL]. PCE for M1 and M2 noted as 1.88% and 0.81%, respectively. Moreover, performance has shown the relative efficiency (ηrel) of z42% of MWCNTs based on [PdClL] (M1), and z18% on GO-supported [PdClL] (M2) CEs on CEs of platinum are adjusted at 100% [22]. The results in this report indicate that many hybrid nanomaterials having a process of immobilization are inexpensively made and used as platinum-free electrodes in DSSC cells.

3.4 In Situ Carbon Template Synthesis

For the In situ preparation of ruthenium N dopped and template free mesoporous carbon (Ru–N-TMC), firstly this carbonized product was made using precursors of ruthenium (III) acetylacetonate [Ru(acac)$_3$] and poly(butyl acrylate)-ß-polyacrylonitrile (PBA-ß-PAN) block copolymer. After stabilization, then carbonization was performed for 30 min at 900 °C within nitrogen conditions [23]. Ru–N-TMC compound was synthesized for the bifacial window solar cell. It has shown a mean visible transmittance of 42.25% and resistance of lower charge transfer of 0.55 in comparison with 1.00 of platinum. It has shown better efficiency of power conversion (PCE) of 11.42% to 11.16% in case of Pt. It has in front and rear illumination PCE of 10.13% and 8.64%, respectively. This proves its efficiency in bifacial counter electrode. High performance of catalyst was attributed to its large surface

area and presence of numerous sites for activity and charge transfer. In situ synthesis of Co/Co1P1N3 was performed with nanoscale porous metal organic framework for usage in the dye-sensitized solar cell counter electrode. ZIF-67 metal organic framework was used as precursor material to adsorb triphenylphosphine (PPh_3). In this way, phosphorus, nitrogen carbon-rich cobalt anchored complex was achieved with pyrolysis at 900 °C. The prepared counter electrode outperformed the conventional Pt in power conversion efficiency (PCE) with 8.51% (Co/Co1P1N3) to 7.88% (Pt). It was concluded that CO-P coordination improves the catalytic efficiency.

4 Organic/Inorganic Hybrids as Efficient Photo Anode

DSSC photo anode significantly affects the dye-sensitized solar cell's (DSSC) performance owing to dye (sensitizer) filling and the driving of electron produce by exciting from the sensitizer dye to the external load. Among the numerous semiconductors of varied band gap, TiO_2 gives away better efficiency due to its low-cost, non-toxicity, rich availability, biocompatibility, and substantial surface area to load the dye is excellent in effect. Photo anode in DSSC to enhance the solar cell efficiency must contain the low resistance of charge transfer and large current density.

4.1 Photo anodes Mixed of MgO–ZnO

Dye-sensitized solar cell (DSSC) photo anodes can be manufactured by addition of different amount of MgO nano powder to ZnO nano powder (0–9 wt%) with a changed misty powder mingling and crushing process. The addition of 1% by weight MgO can attain max Jsc (4.00 mA/cm^2) and max photovoltaic transformation effectiveness (1.03%) that were 39% and 27% improved than ZnO DSSCs which was taken as reference, respectively, for the MgO/ZnO DSSC. When a minor volume of MgO was supplementary, the electron carriage ratio or electron injection efficiency into the photo anodes was better. However, after adding a huge amount of MgO, the electron carriers produced through light were dropped due to this efficiency drop in dye-sensitized solar cell (DSSC). With a small amount of MgO, the electron carriers produced through light increased due to this enhance in efficiency in dye-sensitized solar cell (DSSC) [24]. By adding MgO, MgO/ZnO DSSC open-circuit voltage (*Voc)* first rises a little but after specific amount to some extent drops. At the same time, efficiency and short-circuit current density indicate an equivalent tendency of increasing initial and formerly decrease that was reverse to the alteration of *Rs* with the rise of MgO attentions. Fill factor is relatively not associated to the MgO adding along with the series resistant and displays a leaning like to the modification of shunt resistant (*Rsh*) by the rising MgO amount. The MgO/ZnO DSSC motley through 1 wt% of MgO makes the greatest in photovoltaic effects part, like the *Jsc* (mA/cm^2) as well as efficiency (1.03%) indicates a rise of 39%

and 27%, correspondingly comparing with ZnO DSSC. If a minor MgO volume was supplementary, then the electron carriage ratio or electron injection efficiency into the photo anodes was better. Also, as per the *Rs* drops, the carriage degree of electron or the electron addition efficiency in the photo anode is improved, as well as the *Jsc* and *Voc*. When a high amount of MgO is put in, the anode's specific surface area drops because of the accumulation of MgO nano elements that formerly affect a little in dye adsorption to produce electron. Meanwhile, an increase of Rs joined through the local accumulation of MgO sources, the check in transport of electron and recombining ratio of hole and electron rises, that therefore reduces the quantity of photo produces carriers and concludes in the reduction of current density (*Jsc*) and open-circuit voltage (*Voc*). At a distance stated before, the MgO adding to the ZnO coating produces uneven defects mainly cracks in the layer that develop the source for the creation of recombination hubs, that not even increase a recombination of electron and the hole as well as too openly encouraging the asymmetrical deviations of shunt resistance and fill factor. However, due to this varying *Voc* and fill factor do not change considerably, the efficiency is majorly depending upon current density (*Jsc*). So it is concluded that optimize amount of MgO–ZnO can regulator the electron charge transfers procedure and increase ZnO DSSC efficiency [24].

4.2 Ni-Doped TiO_2 Nanoparticles DSSC Photo Anode

The photo anode in DSSC to enhance the solar cell efficiency must contain the low resistance of charge transfer and large current density. For this purpose, nanostructured doped TiO_2 was used, nickel as a transition metal ion doped in TiO_2, enhancing the DSSC efficiency showed in analysis. With different ratio of nickel nitrate 0.0 to 0.2 M (0.0 M: NT-0; 0.025 M: NT-1; 0.05 M: NT-2; 0.1 M: NT-3; 0.2 M: NT-4), nickel-doped TiO_2 can be produced through sol–gel method. The produce nickel-doped TiO_2 compositional, morphology, crystal structure, electrical characteristics, and optical checked by the different characterization techniques. From this photo anode DSSCs were manufactured in which photo anodes are (NT-0 to NT-4) sensitize dyes (N719), electrolyte (LIL/I) and with counter electrode coated with platinum (Pt). It is found that 72.8-Ω resistance for charge transfer was established which is a very low value of resistance calculated from the electrochemical impedance spectroscopic techniques. Ni-doped TiO_2 (NT-4) photo anode DSSC inclusive light to electrical conversion efficiency was about 3.60%. It is comparatively better than the other un-doped cells [25].

The average crystallite size measured by XRD is to be different as 10.54–5.37 nm by amassed Ni molar application after 0.0–0.2 M. The anatase phase of TiO_2 is checked by Raman techniques of the manufactured nanoparticles. Raman shift was found on 144 cm^{-1}, forming a larger wavenumber area to Ni ions, indicating the effective absorption of Ni into TiO_2 matrixes. FESEM observed spherical shaped of particles with accumulation in different areas, and non-important deviations were found in the morphology though enhancing nickel (Ni) ratio (0.0 to 0.2 M). Presence

of Ti, O, and Ni elements in the samples prepared was confirmed by EDS. In the pure TiO_2 light absorption spectra was observed at 412 nm, while the absorption spectra shifted from ultraviolet to visible spectra by increasing doping concentration of Ni. By increasing the nickel doping amount 0 to 0.2 M, there was decrease in band gap values from 3.0 to 2.21 eV. The PL release strength of the Ni doped in TiO_2 material was decreased comparable to pure TiO_2 that showed the incorporation of Ni ions in TiO_2 that goes to the decrease of charge recombination. From above analysis, it was clear that the electron reduction lifetime which is 72.82 ms, efficiency of the charge collection (i.e., 99.87%), Jsc (10.15 mA/cm^2), and the overall DSSC efficiency (which is 3.60%) manufactured from 0.2 M amount (NT-4) have great transport of charge carrier as compared with other solar cells. So, this concludes that dye-sensitized solar cells (DSSC) made from nickel ratio of 0.2 M (NT-4) photo anode develop active one devices in contrast to different solar cell [25].

4.3 Nickel–Zinc Co-doped TiO_2 Photo Anode DSSCS

The efficiency of performance of dye-sensitized solar cell (DSSC) can be enhanced via the incorporation of Ni and Zn co-doped TiO_2 thin layer as a photo anode layer inside the cell. With spin coating techniques, nickel and zinc were coated on TiO_2 in different ratio above fluorine-doped tin oxide (FTO) substance. Similar mercurochrome organic dye were developed to use for sensitizer dye with TiO_2 Dye-sensitized solar cells photo anode. The photosensitive belongings to pure NZT-20, NZT-40, NZT-60, NZT-80, and TiO_2 hindering coating are arranged through a photo anode of Ni and Zn-doped TiO_2 by varying amounts of doping investigated. In this regard, the band gap values were 3.83, 3.78, 3.82, and 3.83 eV for photo anode of Ni and Zn doped with TiO_2 applications of NZT-20 to NZT-80 individually. CTR and IC [i.e., interfacial capacitances and charge transfer resistance (CTR)] electrochemical impedance spectroscopy can imply DSSCs. Charge transfer capacitance values and resistance values of every models can be calculated from EIS measurements. The NZT-80 model takes an in-height rate of capacitance and resistance and therefore marks the photovoltaic dye-sensitized solar cells working efficiency. The sample of NZT-80 provides 61% rise of efficacy (performance) like associated with its pure TiO_2 (no co-doping with Ni–Zn) by blocking layer incorporated photo anode [26].

4.4 Photo Anode Al-Doped ZnO DSSC

The production of vertically allied (Al) aluminum doped with ZnO (ZnO:Al) NW thin films deposits on FTO and being used as photo anode for DSSCs. Precise Al films ($\sim$3, $\sim$6 and $\sim$10 nm) were coated onto produced ZnO through chemical method nanowire film by method of electron beam vaporization. The produced films were formerly imperiled to different amounts of Al ($\sim$0.98 at.%, 1.94 at.% and

∼2.89 at.%) incorporated into the ZnO nanowires by rapid thermal annealing. The films optical, microstructural, and compositional analysis can be checked by the growing of extremely transparent and well-aligned nanowires of ZnO:Al with a hexagonal crystal assembly. The photo anode of basic DSSC can be manufactured from zinc oxide nano wire and thin film zinc oxide aluminum wire. In these DSSC cell with photo anode, N3 dye as a photosensitizer can be used which is commercially available, for electrolyte solution iodide/tri-iodide and counter electrode was glass-coated FTO. Short-circuit current substantially rises, observation showed that for the pristine ZnO nanowire film-based DSSC, it increases from 1.3 to 4.4 mA cm^{-2} and 2.89% for ZnO:Al nanowire film-based DSSC, and 0.13–0.49% overall power conversion efficiency increase was observed for the ZnO:Al thin film-based DSSC [27].

4.5 *Europium and Terbium Lanthanide with TiO_2 Photo Anode DSSC*

Recently, terbium (Tb^{3+}) and europium (Eu^{3+}) which are ions of rare-earth incorporation in TiO_2 photo anodes in DSSCs effects were observed. Eu^{3+} ions were organized at the locations of cation of Ti^{4+} present in the matrix, while ions of Tb^{3+} compensated the inhabitance of site, supportive phase of anatase remains unchanged while not producing any form of new malformations showed by X-ray photoelectron spectroscopy (XPS). Moreover, an efficient interfacial charge transfer by photo-produced electron transfer estimations indicates the TiO_2 co-doped (3.1 ns kET) compared to pure TiO_2 (kET = 2.6 ns). DSSCs made on Eu^{3+}/Tb^{3+}-based DSSC TiO_2 co-doped showed better performance having 9.11% efficiency as compared to the pure TiO_2 of 7.20% efficiency and the entirely Tb^{3+} (7.10%) or Eu^{3+} (8.01%) doped samples that was recognized with the combined influence of quicker transportation of electron and extended lifetime of electron in the co-doped TiO_2 film. Efficiency of Eu^{3+}/Tb^{3+} co-doping DSSCs is an alternate method to additionally enhance performance for advancing the DSSCs toward commercial usage [28].

4.6 *Mg-Doped ZnO Photo Anode DSSC*

Dye-sensitized solar cell (DSSC) having a Mg-doped Zn thin films photo anode with natural dye rose myrtle (*Rhodomyrtus tomentosa*) was investigated. By utilizing scanning electron microscopy (SEM), UV–visible near infrared (UV–Vis NIR) spectrophotometer, energy dispersive spectroscopy (EDS), and X-ray diffractometer (XRD) at 400–550 °C annealing temperature effect on the films of photo anode were thoroughly investigated. Wurtzite hexagonal having a crystallite size of 25 nm of all given samples checked by XRD. The particles with irregular shape were present on

the surface structure of the Mg-doped ZnO thin film confirmed by scanning electron microscope images. When annealing temperature is raised, a bigger particle size increases as well as increasing the smaller band gap energy.

A very strong absorption spectra of Rhodomyrtus tomentosa sensitizer dye was observed in the visible light region. When Mg–ZnO photo anode annealed at 500 °C, 3.53% highest efficiency was observed. Effectively a DSSC device via photo anode of Mg-doped ZnO thin film and *Rhodomyrtus tomentosa* natural dye as the dye sensitizer was manufactured. SEM discovered the particles with irregular shapes of thin film surface Mg-doped ZnO with help of scanning electron microscope. Particle size increased with increasing the annealing temperature and also with annealing temperature band gap, energy slightly increased. We conclude that annealing temperature has a significant effect and the maximum efficiency at the annealing temperature of 500 °C was achieved [29].

4.7 Cobalt-RGO CO-doped TiO_2 Photo Anode DSSC

TiO_2 has a very common electron transportation material to transport the electrons produce by photo light to external load from DSSC since a long time. But, enhancing the TiO_2 electrical conductivity and its properties stabilizing is one of the major tasks to increase DSSC performance. At this point, graphene oxide cobalt-reduced co-doped TiO_2 nanoparticles were fabricated with an altered sol–gel process that organized the constituent part size together and a lessened band gap of small particles in nano size as measured with XRD and ultraviolet visible spectra. Morphological characterization of the newly manufactured nano composites was observed using SEM and TEM in-depth, whereas the photovoltaic parameters were examined by EIS Nyquist curves, J–V curves, and instance photon to the current conversing efficiency (IPCE) absorption spectrum. Improved Jsc of 12.83 mA cm^{-2}, Voc of 0.618 V as well as PCE, and $\eta = 5.24\%$ of DSSCs were found through Co/rGO co-doped TiO_2 created photo anode as compared to pure TiO_2 (efficiency is 3.71%), TiO_2 doped with cobalt (efficiency 4.09%), and TiO_2 doped with rGO (efficiency of 4.43%) created dye-sensitized solar cells. Enormous enhancement in performance, were qualified for improved use of radiations in visible region (41% greater PEC was observed in Co/rGO co-doped TiO_2), better adsorption dye and enrichment of charge transferal characteristics by conquering the resistances of electron transference. The rGO fusion enhanced the transfer of electrons that compensate the recombination loss, thus improving the DS solar cell's Jsc. rGO synergetic function along with transition metal aided at holding the nano-assembly integral structure which increases photo-generated carriers [30].

4.8 Mg-Doping of ZnO Photo Anode DSSC

DSSCs or dye-sensitized solar cells founded of ZnO image anodes need, notwithstanding huge studies, insulated after cells based on TiO_2, that is because of normally minor open-circuit voltages V and the FF (fill factor) right here, and DSSCs have been geared up by Mg-doped ZnO (MZO) photo anodes grounded on nano debris, skinny movies or ZnO–MZO core–shell-type nanoparticles with variable Mg-ratio. The cells had been calculated in thorough image electrochemical and picture luminescence assessments. It became particular that V changed into meaningfully improved by using Mg-doping. A pure effect of the Mg-attention also becomes exposed on the bearing and recombination of electrons in MZO, critical to a higher mobile overall performance at little and lesser mobile efficiency at large amount of Mg in Mg/ZnO. Nanoparticles with pure ZnO core and Mg/ZO shell vacant a method to poorer have an impact on of stepped forward delivery competition in Mg/ZnO and to take advantage of at the considerably better V [31].

4.9 La with TiO_2 Photo Anode DSSC

By dip coating process commonly known as sol–gel TiO_2, TiO_2/La–TiO_2 La–TiO_2 and La–TiO_2/TiO_2 were produced. Using the XRD technique, the produced film's characteristics parameters phase, particle size, density of dislocation line, and distance of inter-planner and lattice were found. Anatase phase is found for all the films which is a good property required for solar cell. A large grain size is observed for La-doped TiO_2/TiO_2. Further UV–Vis spectroscopy is applied to check the optical properties of the films; majorly the checked properties are band gap, absorbance, dielectric constants, refractive index, extinction coefficient, and transmittance. In the UV–Vis spectroscopy analysis, low band gap and high transmittance in visible range were found for La-doped TiO_2/TiO_2 film that makes it a very attractive ones for DSSCs. So, from these electrodes, DSSCs were produced within which electrolyte is iodide/tri-iodide and using N719 dye. Very Voc ~ 0.74 V, FF ~ 0.73, Jsc 6.57 mA/cm^2, and 3.53% of efficiency were found for 1% La–TiO_2/TiO_2 as compared to other ones. 3.53% very high efficiency rate is chiefly is due to advances in charge transfer rate, less band gap energy value, and weak rate of recombination [32].

4.10 Nitrogen-Doped TiO_2/Graphene Nanofibers Photo anode DSSC

To optimize the performance of dye-sensitized solar cell (DSSC) photo anode is a critical part. This research work uses hydrothermal technique for nitrogen doping on electro spinning's produced nano fiber graphenes TiO_2. By doctor blade coating

method photo anode of a nitrogen-graphene co-doped TiO_2 was produced, after that. Nitrogen and graphene doping into compound nanofibers were confirmed by micro morphological technique with satisfactory morphology and distribution. Nitrogen doping increases the dye-sensitized solar cell response to light energy, confirmed by data produced from UV light spectroscopy and monochromatic light conversion performance. 26% higher efficiency from un-doped was obtained, and the overall efficiency that is 5.1% using solar simulator J–V curve was obtained. So, we conclude that composite fiber co-doped will be a favorable route for further application and future work [33].

4.11 Cu/S with TiO_2 Photo anode DSSC

Novel sol–gel course becomes followed aimed at the production of un-doped and Cu/S co-doped TiO_2 NPs through steady at ease material 0.05% of non-metallic sulfur and numerous amount material from 0.1 to 0.5% of steel Cu. Creations of TiO_2 anatase crystalline segment were determined from the XRD effects through crystallite length smaller than 11 nm for all of manufactured samples. Ultraviolet visible light (UV–Vis) evaluation discovered which co-doped by copper/sulfur changed the TiO_2 optical properties and protracted adsorption inside the seen sunny location using purple change in band gap energies. EDAX evaluation showed the pureness of Cu/S co-doped TiO_2 nanoparticles, similarly a glaring existence for copper, sulfur, oxygen atoms, and titanium in stoichiometric amount. By photovoltaic extents, below simulated sun irradiation, the based DSSCs totally on Cu/S co-doped TiO_2 with 0.3% Cu along with 0.5% S have showed the high-quality PCE of 10.44% through notably stepped forward short-circuit current density (Jsc) of twenty-two.05 mA/cm^2. This more wanted power conversion efficiency is attributed to the correct particle length, greater floor vicinity, and high dye adsorption with consequently advanced short-circuit contemporary density (Jsc). By assessment, the un-doped TiO_2 NPs-based DSSC has shown 6.37% PCE along with 14.85 mA/cm^2 Jsc [34].

In this have a look at, un-doped and copper/sulfur co-doped TiO_2 particles of nano size have been correctly ready through sol–gel approach and in a DSSC hired as photo anode. Morphological, optical, and structural characterizations of nanoparticles which were synthesized had been executed. In every example, XRD analysis revealed anatase crystalline stage creation of TiO_2 having crystallite sizes much fewer than eleven nm. FE-SEM calculation presented the even division of elements throughout the material samples, and EDAX analysis deep-rooted purity as well as existence of copper, sulfur, titanium, and oxygen in stoichiometric ratio in nanoparticles of optimized Cu/S co-doped TiO_2. Ultraviolet visible spectroscopy discovered Cu/S co-doping into the TiO_2 lattice changed the aforementioned band hole energy to lower values and stretched its absorption inside seen variety of spectrum of the sun. The photovoltaic performance of the DSSC fabricated using 0.3 at.% Cu/S co-doped TiO_2 nanoparticles becomes located to be superior to the opposite fabricated DSSCs. The 0.3 at.% Cu/S co-doped DSSC has displayed the first-class PCE

of 10.44% approximately 63.8% enhancements within the PCE comparative to un-doped DSSC. This advanced overall efficiency is owning to the desirable mixture of S and Cu, suitable size of the particle, higher floor vicinity, good sized band hole discount, extended dye loading, higher Jsc, and as a result advanced PCE [34].

4.12 Titanim-Doped Hydroxyapatites Photo anodes for DSSC

A comprehensive look on composition based on photo anode Nd^{3+} (Neodymium)-doped Nd–TiO_2 (Titania) for acquiring progressed efficiency in distinct forms of sun strengthconversion cell, i.e., the Quantum Dot (QD) sensitized solar cells (abbreviated as QDSC), dye sensitized solar cell (DSSC) and picture-electrochemical cells (percent). The complete categorization of the morphological, dielectric homes, and optical research of Titania (Nd-TiO_2) along with distinct doping amount were accomplished. Urbach electricity investigation and XPS verified more through the dielectric studies mounted a vital vacancies role in the advanced electrical residences of doped TiO_2 in evaluation with that of un-doped TiO_2. Efficiency of photovoltaic equipment (DSSC and QDSC) and p.c water excruciating devices has been analyzed by using the CdS-QD sensitized Nd-TiO_2 photo anodes and N719 dye. More advantageous of light energy conversion performance of ≈30% for QDSC and ≈60% for dye-sensitized solar cell was found with Nd (0.4 mol percent)-TiO_2 photo anodes in assessment along with un-doped TiO_2 photo anodes. In addition, the percentage H_2O breaking of CdS (QDs) sensitization showed the photo current density Jsc of (1.8 mA-cm^2 at 1.23 V vs. RHE), that is 3.0 instances greater than un-doped TiO_2, whereas N719 photo anode of DSSC exhibited the present-day density of (0.7 mA-cm^2 at 1.23 V vs. RHE) that was two instances better than un-doped TiO_2. The effects recognized the fact that improved doping awareness of Nd (0.4 mol percent)-TiO_2 is popular for all of the classes of solar electricity conversion equipment [35].

5 Organic/Inorganic Hybrids-Based Quasi-solid Electrolyte

The electrolyte is an essential part of a DSSC. A good electrolyte carries the following essential features. It is very important to bring the oxidized dye back to ground state. The electrolyte must assist in this process. The loss of electrolyte by evaporation, leakage, or other factors must be prevented, especially in case of liquid electrolytes. The electrolyte must have long-term stability. The electrolyte should have low absorption of the light falling in the visible regime.

5.1 Classification of Electrolytes Used in DSSCS

Based on the physical states, the electrolytes of a DSSC can be classified as solid, quasi-solid, and liquid. Liquid electrolytes have been extensively applied in DSSCS.

5.1.1 Liquid State Electrolytes

Iodide/tri-iodide redox couple in an organic matrix is the most used liquid electrolyte in DSSCs and has achieved a remarkable performance with an overall efficiency of the cell around 11.1% [1]. However, there are some serious drawbacks of using liquid electrolyte such as: Liquid electrolytes have a serious problem of leakage of toxic solvent. The leakage of toxic solvents leads to the environmental contamination. As a result of evaporation of volatile iodine ions, the concentration of charge carriers gets reduced which leads to an overall increased resistance of the cell [36].

5.1.2 Solid-State Electrolytes

As an alternate to the liquid electrolytes, solid-state electrolytes have also been investigated. There are two types of solid-state electrolyte DSSCS. The first one uses hole transport materials, while the second one uses redox couple as medium in solid-state electrolyte.

Hole Transport Materials as Solid-State Electrolytes

HTM materials have been widely used as electrolytes in a DSSC. In recent years, copper-based inorganic HTMS have been extensively investigated. CuBr, CuSCN, or CuI or have been used in fabricating DSSCs. They can be cast from solution or can be deposited under vacuum. For instance, DSSC based on CuI has achieved an efficiency of 2.4%. However, the stability issues are yet to be resolved. Therefore, organic HTMS must be investigated. As compared to the inorganic HTM materials, the organic HTMS are preferred because of their low cost, easy processing, and abundance. The first DSSC with organic HTM was reported in 1998 with an efficiency of 0.74%. In this cell, the organic HTM 2,2′,7,7′-tetrakis (*N*,*N*-di-*p* methoxy phenylamine) 9,9′-spirobifluorene (OMeTAD) was used. The addition of Ag ions in the dye solution enhanced the efficiency to 3.2% due to improved dye adsorption. In general, the performance of DSSCS with HTMS as solid-state electrolytes is lesser than those with liquid electrolytes due to following major reasons: (a) Solid-state electrolytes possess low conductivities, (b) Charge recombination from TiO_2 to HTM is very high, (c) Contact between the dye molecules and HTM is not effectively established due to incomplete penetration of HTM into mesoporous TiO_2.

Solid-State Electrolytes Comprising Redox Couple

To address the issues discussed in the previous section, solid-state electrolytes composed of the redox couples were introduced. A few examples of such DSSCS are listed below:

- An electrolyte which used iodide/tri-iodide redox couple was prepared by incorporating TiO_2 nanoparticle into polyethylene oxide (PEO) with the device efficiency of 4.2%.
- Plastic crystal electrolyte made up of iodide/tri-iodide redox couple was prepared resulting in the cell efficiency of 6.5%.
- In another study, a single crystal solid-state electrolyte based on $LiIC_6H_{10}N_2O_2$ [$LiI(HPN)_2$] and iodide/tri-iodide was prepared.

Quasi-solid Electrolytes

To cater to the disadvantages of solid and liquid and electrolytes, both are combined, resulting in the formation of a quasi-solid electrolyte, also known as gel electrolyte. A gel electrolyte has the following unique features:

- The ionic conductivity should be higher under ambient conditions.
- The interfacial contact with TiO_2 should be well established.
- High stability is also necessary.
- Effective penetration into the TiO_2 layer.

Types of Quasi-solid Electrolyte

A quasi-solid electrolyte is formed by mixing sufficient amount of liquid electrolyte in an organic monomer or polymer matrix. This mixing can be either physical or chemical. Physical mixtures are generally termed as thermoplastic gels while chemical mixtures as thermosetting gels. The following sections review the performance of these two types of electrolytes.

Composite Polymer Electrolyte

Composite polymer electrolytes are prepared by mixing inorganic materials in liquid polymer electrolytes. These were first introduced in 1998. The inorganic nanoparticles act as a geletor material leading to the improved properties of the liquid polymer electrolyte. Fillers such as SiO_2, Al_2O_3, $LiAlO_2$, and TiO_2 have widely promoted by different researchers.

- Special focus these days in on using the **TiO_2 nanoparticles** in liquid polymer electrolytes. This is due to the fact that TiO_2 nanoparticles aid in improving the mechanical properties as well. In a study conducted by Liu and Wu, it was found that when TiO_2 nanoparticles are mixed with acrylic acid grafted polyethylene, the tensile strength of the composite polymer showed a significant increase. This improved mechanical strength is due to a strong interaction between the TiO_2

phase and carboxylic group. Based on this behavior, it can be said that addition of TiO_2 nanoparticles in polymeric membrane such as P(EO-EC) can result in a strong interaction between the titania phase and carbonate and oxide groups, hence an improved mechanical property.

TiO_2 also strongly affects the ionic conductivity of the polymer electrolytes, especially the semi-crystalline polymer. As a result of inclusion of TiO_2 nanoparticles, the crystallization of the polymer is suppressing, and amorphous phase increases due to which the ionic conductivity increases.

- **SiO_2** has also been investigated as gelator material in a polymer matrix. It helps in solidification of liquid polymer matrix. A DSSC with quasi-solid electrolyte with an efficiency of 6.1% has been reported. In this cell, SiO_2 nanoparticles were added to Lil-C_2H_5OH electrolyte.
- Similarly, **Al_2O_3 nanoparticles** are also used in the synthesis of quasi-solid electrolytes. By mixing of poly((1-(4-ethenylphenyl) methyl)-3-butylimidazolium iodide (MPII) and MPII-modified Al_2O_3 nanoparticles, a DSSC was prepared, and this cell showed efficiency of 7.6%.
- Some recent studies have demonstrated a better performance of DSSC synthesized with **nano-clay-based polymer electrolytes.** Nano-clay minerals in general have a high ionic conductivity which make them a suitable candidate as a gelating material in liquid polymer electrolytes. They also exhibit excellent rheological properties. DSSC based on such electrolytes has achieved an efficiency of 10%.
- Incorporation of **carbon nanomaterials** helps in the solidification of the liquid polymer and improves the ionic conductivity. Literature suggests that varying the percent content of the carbon nanomaterial in the composite can alter the physical state of the electrolyte as well.

Quasi-solid Ionic Liquid Electrolytes

Ionic liquids are salts with melting points below 100 °C. They are also termed as liquids containing organic ions that can undergo several structural changes. Due to this inherent property, several salts can be used to achieve a desired property for a particular application. Ionic liquids are increasingly being used in DSSC applications for making quasi-solid electrolytes. These electrolytes for DSSCS are developed by dissolving a polymer matrix with appropriate amounts of ionic liquid electrolyte and an iodide source. Additives such as plasticizers and co-polymers are also employed. They are also known as polymer gel electrolytes. Benefits of these electrolytes are listed below:

- The volatility of such electrolytes is negligible.
- The thermo electrochemical stability is significantly high.
- Slight modifications in the anionic or cationic component can lead to changed physical and chemical properties. This can help in tuning their properties for applications in solar cells.

Recent works related to quasi-solid ionic liquid electrolytes are discussed below:

- A DSSC based on ionic liquid polymer gel consisting of 1-propyl-3-methylimidazolium iodide (PMImI) and poly (vinylidene fluoridecohexafluoropropylene) (PVDF-HFP) has demonstrated an efficiency of 5.3%.
- Another similar work reported a DSSC based on electrolyte 1-propyl-2,3-dimethylimidazolium iodide (C8H15IN2) and PVDFHFP (5 wt%) with an overall efficiency of 6.1%.
- Ionic liquid 1,2-dimethyl-3-propylimidazoli-um iodide when mixed with potassium iodide (KI) and polyethylene oxide (PEO) in an optimized ratio resulted in cell efficiency of 5.87%.
- Quasi-solid electrolyte developed using EMImI ionic liquid along with polyethylene glycol showed an efficiency of 7.13%.
- An electrolyte developed using using PVP and $HOOC(CH_2)nCOOH$ resulted in cell efficiency of 5.2%.
- Some researchers have also reported graphene oxide-based electrolytes. A DSSC based on poly(1-butyl-3-vinylimidazolium bis(trifluoromethanesulfonyl)imide), 1-propyl-3-methylimidazolium iodide, and graphene oxide electrolyte depicted the power conversion efficiency around 4.83%. Results also show that the amount of graphene oxide significantly impacts the ionic conductivity of electrolyte. The cell has also shown higher long-term stability than that with graphene oxide.
- Some researchers also prove the efficacy of mixing poly-ionic liquid in ionic liquids in developing quasi-solid electrolytes. IL/[PBVIm][TFSI] gel electrolyte has also resulted in an efficiency of 4.4% of the device.

Thermoplastic Gel Electrolyte (TPGE)

The TPGE contains gelator and liquid electrolyte. The liquid electrolyte consists of organic solvent, redox couple, additive, or IL electrolyte system. Following are few examples of such types of DSSCS:

- The first thermoplastic polymer gel-based DSSC used electrolyte which was composed of NaI, poly(acrylonitrile) (PAcN), EC, can, and PC. However, its efficiency was lower in comparison with liquid electrolytes-based DSSCS.
- Another research group developed the TPGE containing poly (vinylidenefluoride-*co*-hexafluoropropylene) (PVDF–HFP) mixed with MePN-based liquid electrolyte containing 1,2-dimethyl-3-propyl imidazolium iodide and iodide. The performance of this cell was similar to another cell using the same liquid electrolyte.
- A DSSC with an efficiency of 6.1% was developed by using TPGE based on 1,3:2,4-di-*O*-dimethylbenzylidene-D-sorbitol/MePN.
- An electrolyte with a gelator, an ionic liquid, iodide, and 1-alkyl-3-methylimidazolium iodide was reported resulting in the cell efficiency of 5%.

Here, it is important to mention that the properties of the thermoplastic gel electrolytes strongly depend on temperature. When the temperature increases, the phase

of the gel changes from gel to sol. As a result of this, the conduction mechanism also changes which changes the performance of the DSSC.

Thermosetting Gel Electrolyte (TSGE)

TPGES generally suffers from the chemical instability. Therefore, environmentally stable electrolytes should be considered. Among them, the thermosetting gel electrolytes are a good option. These electrolytes undergo thermally irreversible changes and are therefore known as thermosetting electrolytes. Although they appear to be solid but due to the presence of liquid electrolyte, they are treated as quasi-solid electrolytes [37].

- A technique known as photo-induced polymerization is employed in the synthesis of TSEGS. In a study by Hayase group, chemically cross-linked polymers were demonstrated by using this process.
- Formation of cross-linking structures of quasi-solid electrolytes can result in an increased efficiency. Reports suggest that cross-linked structures are created after illumination under UV light by adding the PEG and PEGDA monomer into TiO_2 films.
- In a study conducted by Komya et al., oligomers with three polymerizable groups were used as gel electrolyte precursors. Increased Voc of this cell was reported along with the cell efficiency of 8.1%.
- Another electrolyte was reported in which cross-linked gel electrolyte precursors were injected into a DSSC. Then, the gelation was carried out by heating the cell at 80C. Heating favored the creation of a three-dimensional network of polymer resulting in creation of TSGE. This device showed on overall efficiency of 7.72%.
- PAA–PEG networks have the capacity to adsorb large quantity of electrolyte. Electrolytes based on this network depicted high stability and an efficiency of 6.10%. Adding a third component PPY increased the cell efficiency to 7.0%.
- Phase inversion method has also been reported for the synthesis of membrane electrolytes. In this method, ultrathin porous membranes are soaked in organic electrolytes to create ultrathin membrane electrolytes. 8.35% efficient DSSCS with membrane electrolytes have been reported.
- A research group had recently employed copolymers, amino-acid cross-linkers, and amide cross-linkers, and the resulting device was 9.48% efficient.
- Porous co-polymers have also been developed which had demonstrated an efficiency of 9.10%.
- Studies also showed that encapsulation can also improve the stability of TSEG electrolytes-based DSSCS. Encapsulation of TiO_2 resulted in cross-linking polymerization on the surface of TiO_2.
- Surface-induced cross-linking polymerization of MMA and 1,6-hexanediol diacrylate (HDDA) on the surfaces of TiO_2 particles resulted in the formation of nano porous network polymer.
- Some studies showed that by adding graphene into PAA-PEG, conducting gel electrolytes can be synthesized. Comparable efficiencies are achieved by adding graphene, graphene oxide, or graphite.

- Another TSEG was reported which used ureasil as precursor and liquid electrolyte composed of iodide salts. The device efficiency achieved was 5–6% along with the long-term stability [38].
- Similarly, a novel TSGE based on poly (acrylic acid)-poly (ethylene glycol) (PAA–PEG) hybrid and liquid electrolyte for fabricating a DSSC has also been reported [39]. This type of electrolyte has the following advantages:
  - The creation of 3D network structures in hydrogel results in an outstanding stability of the hydrogel.
  - Strong interaction between hydrophilic groups in PAA and absorbed aqueous solution can be achieved.

If we compare the electrical parameters of these types of DSSCS, the current density of such cells is lower, while the open-circuit voltage is higher. Lower mobility of electrolyte components results in decreased current density, while the polymer chains on TiO_2 surface suppress the dark current resulting in high open-circuit voltage.

6 Techno-Economic Analysis

Cost and efficiency are essential for any solar cell. A cell which is highly efficient may not be suitable for mass scale production due to high production cost and lesser availability of materials. Similarly, the cheaper and easy to produce cells may not be efficient. Therefore, these two aspects must be dealt simultaneously.

Easy fabrication techniques make the DSSCS as promising candidates for large-scale production. However, due to issues associated with the long-term stability and efficiency, the path to their commercialization is not easy. Issues like leakage and highly volatile solvents can be overcome by employing quasi-solid-state electrolyte. Following are the main challenges associated with the organic/inorganic hybrid-based DSSCS:

- The contact between the electrolyte and the semiconductor should be maximized, and it is the first challenge to be addressed. Much research is still required on the electrolyte–semiconductor interface. This issue can be tackled with the advanced techniques such as photo-induced polymerization.
- Another concern is that the selection of monomers should be made in a way that they can interact with TiO_2 nanoparticles. This improved interaction will lead to high conduction of the charge carriers at the TiO_2/electrolyte interface.

Having overcome these challenges, the stability of QS-DSSC can further be improved.

7 Conclusion

The DSSCS based on quasi-solid electrolytes so far has proven long-term stability as compared to the traditional DSSCS. If we look into the performance of the cell is concerned, they are less efficient in comparison with DSSC based on liquid electrolytes. Studies suggest that the properties of QS-DSSC are strongly dependent on the optimization and selection materials and additives used in the polymerization. Therefore, the right selection of materials and environment-friendly manufacturing processes can lead to better performance and a promising future of QS-DSSCS.

References

1. Carella A, Borbone F, Centore R (2018) Research progress on photosensitizers for DSSC. Front Chem 481
2. Mahmood A (2015) Recent research progress on quasi-solid-state electrolytes for dye-sensitized solar cells. J Energy Chem 24(6):686–692
3. Pandey AK et al (2018) Improved electron density through hetero-junction binary sensitized TiO_2/CdTe/D719 system as photoanode for dye sensitized solar cell. Phys E 101:139–143
4. Rehman Q et al (2019) Super absorption of solar energy using a plasmonic nanoparticle based CdTe solar cell. RSC Adv 9(59):34207–34213
5. Butt MTZ et al (2022) Performance evaluation methods of DSSCs. In: Dye-sensitized solar cells. Elsevier, pp 91–101
6. Ahmad M, Pandey A, Rahim N (2018) Effect of germanium on the TiO_2 photoanode for dye sensitized solar cell applications. A potential sintering aid. In: IOP conference series: materials science and engineering. IOP Publishing
7. Ahmad MS et al (2020) Pt-TCO free Sn–Ag–Cu ternary alloy as cost effective counter electrode layer for dye sensitized solar cell. Optik 206:164317
8. Haggerty JES et al (2017) High-fraction brookite films from amorphous precursors. Sci Rep 7(1):15232–15232
9. Ahmad MS, Pandey A, Rahim NA (2017) Towards the plasmonic effect of Zn nanoparticles on TiO_2 monolayer photoanode for dye sensitized solar cell applications. Mater Lett 195:62–65
10. ur Rehman S et al (2020) Synthesis of polyvinyl acetate/graphene nanocomposite and its application as an electrolyte in dye sensitized solar cells. Optik 202:163591
11. Wu J et al (2017) Counter electrodes in dye-sensitized solar cells. Chem Soc Rev 46(19):5975–6023
12. Martínez-Muíño A et al (2020) Origin of the electrocatalytic activity in carbon nanotube fiber counter-electrodes for solar-energy conversion. Nanoscale Adv 2(10):4400–4409
13. Zhou D et al (2021) A rational design of an efficient counter electrode with the $Co/Co_1P_1N_3$ atomic interface for promoting catalytic performance. Mater Chem Front 5(7):3085–3092
14. Han Q et al (2020) Flexible counter electrodes with a composite carbon/metal nanowire/polymer structure for use in dye-sensitized solar cells. Sol Energy 208:469–479
15. Malara F et al (2011) Flexible carbon nanotube-based composite plates as efficient monolithic counter electrodes for dye solar cells. ACS Appl Mater Interfaces 3(9):3625–3632
16. Iqbal MZ et al (2020) Role of graphene and transition metal dichalcogenides as hole transport layer and counter electrode in solar cells. Int J Energy Res 44(3):1464–1487
17. Wu M, Ma T (2014) Recent progress of counter electrode catalysts in dye-sensitized solar cells. J Phys Chem C 118(30):16727–16742
18. Butt OM et al, Development of dye sensitized solar cell by characterizing polymeric counter electrodes 2nd International Conference n Advanced Research in Applied Science & Engineering, 7 - 29 March, 2020, Oxford, United Kingdom

19. Nhari LM, El-Shishtawy RM, Asiri AM (2021) Recent progress in organic hole transport materials for energy applications. Dyes Pigm 193:109465
20. Iqbal MZ et al (2020) Recent developments in graphene based novel structures for efficient and durable fuel cells. Mater Res Bull 122:110674
21. Dayan S (2021) Performance improvement of Co_3O_4@ nHAP hybrid nanomaterial in the UV light-supported degradation of organic pollutants and photovoltaics as counter electrode. J Mol Struct 1238:130390
22. Dayan S (2020) Immobilized palladium complex into carbon-based nanomaterials: as catalyst for counter-electrode in the photovoltaics. J Mol Struct 1217:128444
23. Aftabuzzaman M, Lu C, Kim HK (2020) Recent progress on nanostructured carbon-based counter/back electrodes for high-performance dye-sensitized and perovskite solar cells. Nanoscale 12(34):17590–17648
24. Chen H-Y et al (2021) Performance analysis of dye-sensitized solar cells with various MgO–ZnO mixed photoanodes prepared by wet powder mixing and grinding. J Mod Opt 68(21):1240–1250
25. Raguram T, Rajni K (2021) Effect of Ni doping on the characterization of TiO_2 nanoparticles for DSSC applications. J Mater Sci Mater Electron 32(13):18264–18281
26. Bramhankar T et al (2020) Effect of Nickel-Zinc Co-doped TiO_2 blocking layer on performance of DSSCs. J Alloy Compd 817:152810
27. Bhattacharyya S, Mallick Z, Gayen R (2020) Vertically aligned Al-doped ZnO nanowire arrays as efficient photoanode for dye-sensitized solar cells. J Electron Mater 49(6):3860–3868
28. Akman E et al (2020) Europium and terbium lanthanide ions co-doping in TiO_2 photoanode to synchronously improve light-harvesting and open-circuit voltage for high-efficiency dye-sensitized solar cells. Sol Energy 202:227–237
29. Siregar N et al (2021) Fabrication of dye-sensitized solar cells (DSSC) using Mg-doped ZnO as photoanode and extract of rose myrtle (*Rhodomyrtus tomentosa*) as natural dye. Int J Photoenergy
30. Rahmatabadi D et al (2021) DIC-based experimental study of fracture toughness through R-curve tests in a multi-layered Al–Mg (LZ91) composite fabricated by ARB. J Alloy Compd 883:160843
31. Ringleb A et al (2021) Influence of Mg-doping on the characteristics of ZnO photoanodes in dye-sensitized solar cells. Phys Chem Chem Phys 23(14):8393–8402
32. Bao W et al (2021) Tb^{3+}/Eu^{3+} co-doped $Al_2O_3–B_2O_3–SrO$ glass ceramics: preparation, structure and luminescence properties. Opt Mater 122:111772
33. Gao N et al (2020) Nitrogen doped TiO_2/Graphene nanofibers as DSSCs photoanode. Mater Chem Phys 255:123542
34. Gupta A et al (2020) Novel synergistic combination of Cu/S co-doped TiO_2 nanoparticles incorporated as photoanode in dye sensitized solar cell. Sol Energy 203:296–303
35. Katta VS et al (2021) Vacancies induced enhancement in neodymium doped titania photoanodes based sensitized solar cells and photo-electrochemical cells. Sol Energy Mater Sol Cells 220:110843
36. Bella F, Bongiovanni R (2013) Photoinduced polymerization: an innovative, powerful and environmentally friendly technique for the preparation of polymer electrolytes for dye-sensitized solar cells. J Photochem Photobiol C Photochem Rev 16:1–21
37. Lan Z et al (2010) Application of thermosetting organic solvent free polymer gel electrolyte in quasi-solid-state dye-sensitized solar cell. J Appl Polym Sci 116(3):1329–1333
38. Makris T et al (2011) A quasi solid-state dye-sensitized solar cell made of polypyrrole counter electrodes. Electrochim Acta 56(5):2004–2008
39. Wu J et al (2008) Progress on the electrolytes for dye-sensitized solar cells. Pure Appl Chem 80(11):2241–2258

Chapter 16
Organic–Inorganic Nanohybrids in Supercapacitors

Muhammad Abbas, Syed Fahad Bin Haque, Yafen Tian, John P. Ferraris, and Kenneth J. Balkus Jr.

1 Introduction

The need for energy storage is becoming increasingly important for diverse areas such as renewable energy, electric vehicles, grid reliability, and consumer electronics. These applications require long-lasting and economical systems that can store and deliver energy on demand [21, 88, 92]. Supercapacitors hold great promise for fulfilling these needs. There are three types of supercapacitors: electrochemical double-layer capacitors (EDLC), pseudocapacitors (PC), and hybrid supercapacitors (HSC). EDLCs store energy electrostatically at the electrode/electrolyte boundary resulting in high power and cyclability. PCs store energy from surface redox reactions on the electrode, affording high energy. HSCs combine the advantages of EDLCs and PCs. The nature of the interface between the pseudocapacitive and double-layer components in hybrids as well as its accessibility affect the ultimate performance. A discussion of the EDLC/PC interface using select examples will be presented in this chapter. Materials for EDLC include activated carbons (ACs), carbon nanotubes (CNTs), graphene, turbostratic carbons with different morphologies including carbon nanofibers (CNFs), and templated carbons (TCs). The PC component will be primarily limited to redox-active transition metal oxides, nitrides, sulfides, and carbides (TMeX, X=O, N, S, C) [15, 27, 81].

Figure 1 shows a Ragone plot comparing the energy density and power density of different types of energy storage devices [86]. The target region in this plot is the upper right-hand quadrant, representing high energy and high power [1, 7]. If the energy density of supercapacitors can be improved, the combined advantages of

Muhammad Abbas and Syed Fahad Bin Haque contributed equally.

M. Abbas · S. F. B. Haque · Y. Tian · J. P. Ferraris · K. J. Balkus Jr. (✉)
Department of Chemistry and Biochemistry, The University of Texas at Dallas, 800 West Campbell Rd, Richardson, TX 75080, USA
e-mail: balkus@utdallas.edu

K. Rizwan et al. (eds.), *Hybrid Nanomaterials*, Materials Horizons: From Nature to Nanomaterials, https://doi.org/10.1007/978-981-19-4538-0_16

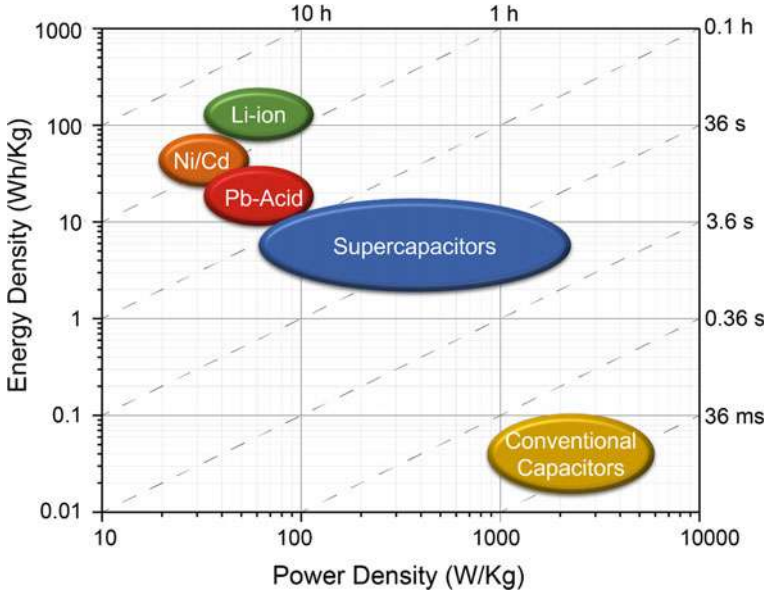

Fig. 1 Ragone plot showing power density versus energy density for various energy storage devices

batteries and capacitors will be realized. This is more likely to be achieved through hybrid supercapacitors and more specifically nanohybrid supercapacitors.

In the 1950s, General Electric explored porous carbon materials (EDLC) to improve conventional capacitors [11]. Later, RuO_2 (PC) was shown to have high capacitance due to its redox chemistry [103]. This concept has been expanded to other redox-active transition metal oxides, nitrides, sulfides, and carbides (TMeX, X=O, N, S, C) [6]. Conway demystified the difference between batteries and supercapacitors [20]. In supercapacitors, the energy is stored either as a Helmholtz electrical double-layer and/or through near-surface faradic reactions. In contrast, a battery stores energy through redox or intercalation involving the electrolyte and the bulk of the electrode material [3].

Figure 2 shows three types of supercapacitors along with corresponding idealized cyclic voltammograms. The EDLC (Fig. 2a) stores charge at the interface between the electrolyte and the electrode. This nanoscale charge separation is that Helmholtz double layer. No chemical redox reaction or phase change occurs [38, 43]. The resulting cyclic voltammogram appears box-like, as only electrostatic interaction occurs. EDLCs have a relatively high-power density and long cycle life but low energy density related to lower capacitance (Eq. (2), vide infra) compared to other types of supercapacitors and batteries. In contrast, PCs store their energy through surface or near-surface faradic redox reactions which increases their energy density (Fig. 2b). Since pseudocapacitive materials are often insulating, they have a lower power density compared to EDLC. The redox reactions often manifest themselves as peaks in the CV especially in three-electrode experiments. In a hybrid supercapacitor

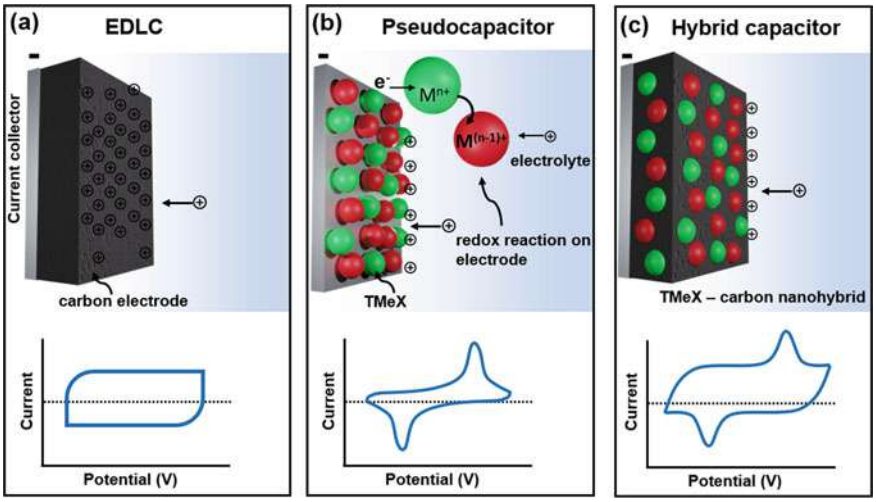

Fig. 2 Schematic representation of supercapacitor types and corresponding cyclic voltammograms: **a** EDLC; **b** pseudocapacitor; **c** hybrid capacitor electrodes

(HSC), both EDLC and pseudocapacitive materials are combined (Fig. 2c), and their cyclic voltammograms frequently exhibit the electrochemical signatures of both components. Ideally, this combination should result in high energy density and power density electrode materials [90, 104].

The Kiviat diagram in Fig. 3 highlights important properties of the different types of supercapacitors as well as Li-ion batteries, illustrating the advantages and disadvantages of each. Batteries exhibit high energy densities with modest power. In contrast, EDLCs exhibit high power with lower energy density. The energy density

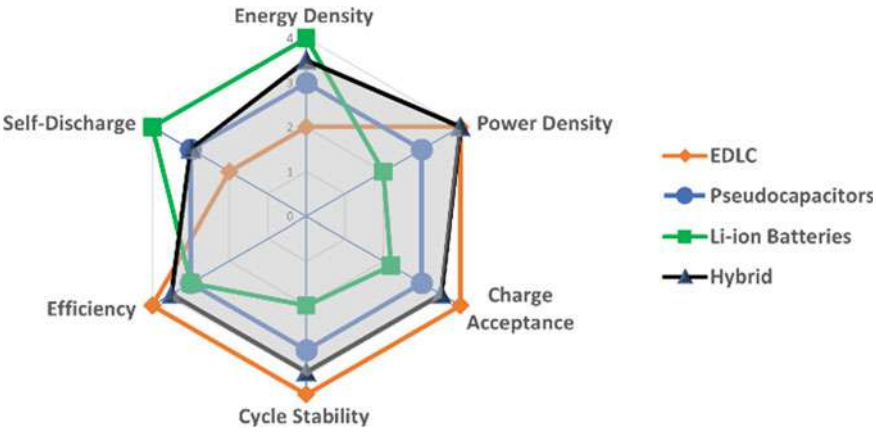

Fig. 3 Kiviat diagram comparing properties of select energy storage devices

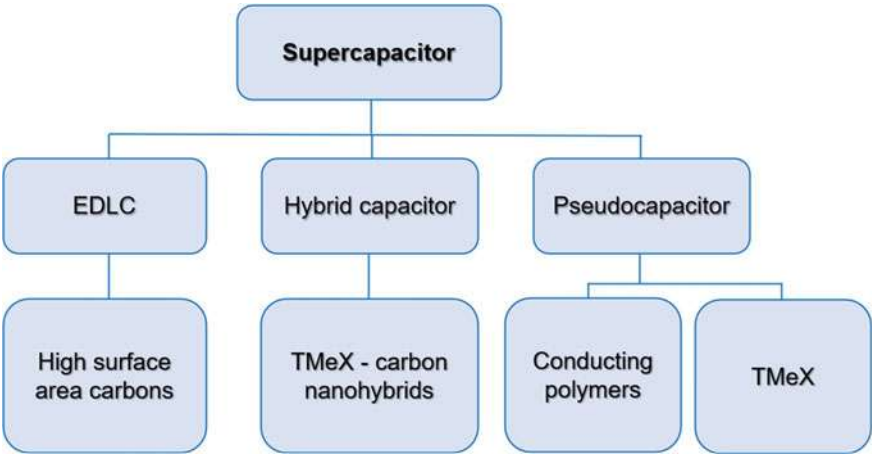

Fig. 4 Types of supercapacitors and electrode materials

can be increased with hybrid supercapacitors (HSCs), which combine the properties of EDLCs and PCs. From this diagram, the hybrid supercapacitors (shaded area) are promising energy storage systems as they display improved charge acceptance, higher efficiencies, and cycle stabilities compared to batteries.

The most common types of supercapacitors with their representative electrode materials are shown in Fig. 4. EDLCs typically employ high surface area porous carbon materials [71]. Pseudocapacitors are based on TMeXs or conducting polymers [86]. In hybrid supercapacitors, both EDLC and TMeX are combined to achieve high power and energy density [71]. Conducting polymers have been prepared on carbons for supercapacitors [31, 46, 79, 80, 123]. Carbon-coated conducting polymers like polyaniline (PANI) and polypyrrole (PPy) have also been prepared for supercapacitor electrode materials [56]. Nevertheless, the theoretical capacitances of conducting polymers are lower than TMeXs and will not be discussed further in this chapter [58]. Rather we will focus on the combination of TMeXs with multiple types of carbon materials [20, 23, 98, 107, 108, 117].

Several electrochemical characterization techniques are used to assess the performance of a hybrid electrode material for supercapacitors. The most common methods include cyclic voltammetry (CV), galvanostatic charging/discharging (GCD) and electrochemical impedance spectroscopy (EIS). CV measures the current response to a linear sweep in potential between two points and provides a range of information including signatures of redox reactions and double-layer capacitance [22, 69]. GCD shows the change in potential with time at a constant current input and output, and provides information on capacitance, power density, and energy density [9]. Electrochemical impedance spectroscopy (Nyquist and Bode plots) gives the response of different elements of the cell to frequency and potential [45, 66].

When GCD is used to calculate the specific capacitance, power density and energy density, the following equations (Eqs. (1)–(4)) are used.

$$C_{\text{cell}} = \frac{I\,\Delta t}{m\,\Delta V} \tag{1}$$

$$C_{\text{electrode}} = 4C_{\text{cell}} \tag{2}$$

"C_{cell}" is the specific cell capacitance in farads per gram (F g^{-1}), "$C_{\text{electrode}}$" is the gravimetric capacitance of just the working electrode, "Δt" is the time of discharge in seconds, "I/m" is the current in amperes divided by the total electrode mass in grams which implies the current density, and "ΔV" is the voltage window in volts,

$$E = \frac{1}{2} \times \frac{C_{\text{cell}}\,\Delta V^2}{3600} \times 1000 \tag{3}$$

$$P = \frac{E}{\Delta t} \times 3600 \tag{4}$$

Here, "E" is energy density in Wh/kg and "P" is power density in W/kg.

Cyclic voltammetry can also be used to calculate specific cell capacitance using the equation below

$$C_{\text{cell}} = \frac{A}{2} \times \frac{1}{m\nu\,\Delta V} \tag{5}$$

where "A" is the area under the CV curve, "m" is the mass of both electrodes, "ν" is the scan rate and "ΔV" is the voltage window. Using the capacitance from here, energy density and power density can also be calculated from Eqs. (3) and (4) [19, 65].

The electrochemical performance of nanohybrids designed for energy storage is studied by fabricating electrodes into cells in a two or three-electrode configuration. In a two-electrode cell, one of the electrodes acts as the working electrode and the other one as a both counter and a reference electrode. This gives the capacitance of the cell. Whereas in three-electrode settings, counter and reference electrodes are physically different and standard reference electrodes can be used. Two-electrode cells such as coin cells or spiral wound cells are the most common commercial types [67, 94].

2 Interfaces in Organic–Inorganic Nanohybrids

Hybrid electrode materials are mixtures of at least two different components that synergistically combine their properties [106]. Generally, studies on hybrids focus on composition versus performance. However, an understanding of the interface between the individual components is critical to design high energy/power supercapacitors. Nanohybrid composites can maximize this interface due to their enhanced surface area [8]. Nanohybrid composites can be classified by the type of interface between carbon and TMeX. This includes physical mixtures, core–shell hybrids,

Fig. 5 Classification of organic (black)–inorganic (red) hybrid based on their interface

in situ dispersion, 1D and 2D hybrids as well as intimate contact (Fig. 5). This classification allows for a correlation between composite type and performance. From left to right in Fig. 5, interfacial contact increases.

Since most TMeXs are insulators, combining them with conductive carbons improves charge transport [76, 77]. The nanohybrid electrodes can be fabricated using numerous types of carbonaceous materials including activated carbons (ACs), carbide-derived carbons (CDCs), carbon nanofibers (CNFs), templated carbon nanostructures (TCNs), carbon nanotubes (CNTs) and graphene [51, 85, 89, 110]. The degree of interaction between such carbons and TMeXs is defined as the interaction quotient (IQ, unitless number) in Fig. 6a. The type of carbon will dictate the interface and contact that occurs with the TMeX. Physical mixtures will have the lowest degree of interaction between carbon and TMeX. Electrospun composite fibers can be core–shell or in situ dispersion. Core–shell fibers can be prepared physically (coaxial spinneret) or by spinning solutions with chemically phase separated domains. Simply combining the TMeX in the polymer precursor solution creates

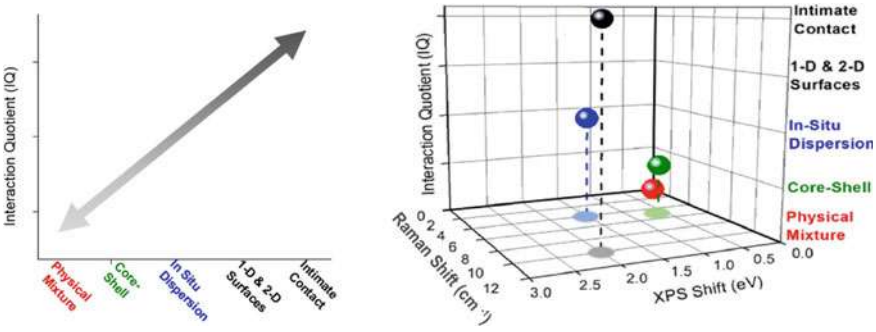

Fig. 6 **a** Interaction quotient versus hybrid electrode configuration. **b** Interaction quotient versus TMeX Raman shift versus TMeX XPS shift

in situ dispersions in the e-spun fiber. 1D carbons such as carbon nanotubes (CNTs) or 2D carbons like graphene may have high conductivity and stronger interaction if TMeX nanoparticles are grown from the carbon surface. Templated carbons generally mean the carbons coat the TMeX nanoparticles. This intimate contact provides the highest interaction quotient. However, this does not necessarily afford the best performance, since there must be a balance between interfacial contact and porosity for electrolyte accessibility. Spectroscopic characterization of the different types of nanohybrids can provide a quantitative measure of interfacial contact. For example, the 3D plot in Fig. 6b shows the Raman shifts for TMeXs vs the x-ray photoelectron spectral shifts vs the IQ. The greatest shifts are observed for the composites with the greatest interfacial contact. A deeper fundamental understanding of the interactions between the components in hybrid devices is necessary to fully realize the potential of these composite materials. Ultimately, the performance of HSCs can be correlated with the degree of interaction between carbon and TMeX. The interaction quotient (IQ) will affect the charge transfer capabilities of the electrode. This attribute, in conjunction with the pore structure and surface area of the carbons and the TMeXs, will ultimately control the performance of HSCs [26].

2.1 Physical Mixtures

The interface in physical mixtures depends on the degree of dispersion, particle wetting and void space. Generally, there are only weak van der Waals interactions between the carbon and TMeX or none at all [16, 85]. The physical mixture is the easiest to prepare but has the lowest degree of contact between carbon and TMeX. Selected examples are summarized in Table 1. This includes, nanohybrids with different carbons such as Co–W–S@N, S-codoped carbon [68], $Ti_3C_2T_x$/rGO [125], Ni, Co–OH/rGO [63], MnO_2/graphene [122], GO/$La_2Ti_2O_7$ [60], AC/$MnCo_2O_4$ [44], Co_3O_4/carbon aerogel [57], Co_2MnO_4/$Co_2(OH)_3Cl$ acetylene black [40], CoS/N-doped carbon dots-acetylene black [39], $NiCo_2O_4$/CN [2], $Ni(OH)_2$/graphene [9], and WS_2/CT [33].

A physical mixture of rGO and titanium carbide ($Ti_3C_2T_x$/RGO) was prepared to make stretchable electrodes for supercapacitors [125]. The XPS data showed no shifts in comparison to bulk $Ti_3C_2T_x$ [30], indicating minimal interaction between the carbon and TMeX, consistent with the low capacitance. Similarly, a composite of porous carbon and binary metal chalcogenide was prepared by carbonization of phosphotungstic acid (PTA) and a zeolitic imidazolate framework (ZIF-67) [68]. The XPS spectrum in Fig. 7b shows Co $2p_{3/2}$ and $2p_{1/2}$ peaks at 781.9 and 798.4 eV indicating that it is primarily present as Co^{2+} with binding energy the same as bulk CoS_2 [53]. The XPS spectrum in Fig. 7c shows 32.74 and 34.91 eV peaks for tungsten, which could be assigned to W^{4+} the same as reported for bulk WS_2 [84]. Since the binding energies of both Co and W do not shift from the bulk TMeX, the interaction at the interface must be weak (Fig. 6).

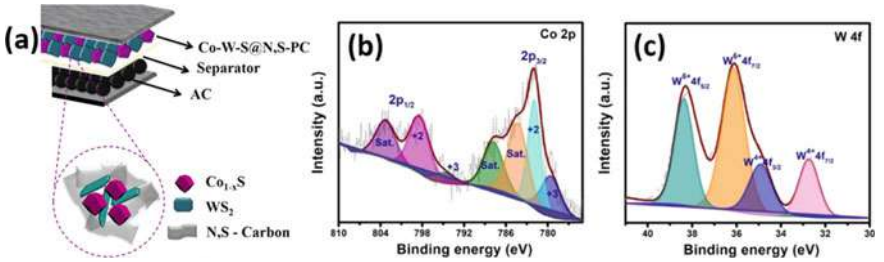

Fig. 7 **a** Cartoon represents Co–W–S and porous carbon mixture; high-resolution XPS spectra of **b** Co 2p and **c** W 4f [68]. Adopted with permission from the American Chemical Society

In a similar study, Co_3O_4@NiO was synthesized on CNT yarn and coated with graphene [124]. The XPS of the CNT/Co_3O_4@NiO before and after graphene coating was unchanged indicating no strong interactions. Huang and coworkers prepared metal oxide nanoparticles (Fe_3O_4, $CoFe_2O_4$, $NiFe_2O_4$) mixed with rGO aerogels with a capacity of 388 mAh g^{-1} at 5 A g^{-1} [37]. The XPS binding energy of Ni $2p_{3/2}$ appears at 855 eV which is same as the bulk TMeX [82]. Similarly, the mixture of lanthanum titanate ($La_2Ti_2O_7$, LTO) and graphene oxide (GO) was studied [60]. The XPS spectrum of this mixture shows La $3d_{5/2}$ and $3d_{3/2}$ peaks at 835.6 and 852.5 eV, corresponding to the bulk $La_2Ti_2O_7$ particles [35]. Some other examples are listed in Table 1, without XPS or Raman data for the TMeX, none of which exhibits

Table 1 Selected examples of physical mixtures nanohybrids

Material	Electrolyte	C_s (F g^{-1})	Energy density (Wh kg^{-1})
Co–W–S@N, S-carbon [68]	3 M KOH	1001 at 2 A g^{-1}	32.9
$Ti_3C_2T_x$/rGO [125]	1 M H_2SO_4	115 at 1 A g^{-1}	–
Ni, Co–OH/rGO [63]	6 M KOH	1316 at 0.5 A g^{-1}	56.1
MnO_2/graphene [122]	2 M KOH	1227 at 0.5 A g^{-1}	19.6
GO/$La_2Ti_2O_7$ [60]	1 M H_2SO_4/sucrose	900.6 at 1 A g^{-1}	94.0
AC/$MnCo_2O_4$ [44]	2 M KOH	121.68 at 30 A g^{-1}	3.71
Co_3O_4/carbon aerogel [57]	PVA-KOH	180.8 at 1 A g^{-1}	10.44
Co_2MnO_4/$Co_2(OH)_3Cl$ acetylene black [40]	2 M KOH	779 at 1 A g^{-1}	27.8
CoS/CDs-acetylene black [39]	3 M KOH	697 at 1 A g^{-1}	36.6
$NiCo_2O_4$/CN [2]	6 M KOH	547 at 1 A g^{-1}	–
$Ni(OH)_2$/graphene [9]	1 M KOH	690 at 1.4 A g^{-1}	29
WS_2/CT [33]	3 M KOH	10 at 1 A g^{-1}	–

exceptional performance. To improve interfacial interaction, alternative fabrication techniques are required and will be discussed in subsequent sections.

2.2 Core–Shell Materials

The dispersion of TMeXs in polymer precursor solutions could lead to improved particle wetting and interfacial contact. Electrospinning is a popular method for preparing polymer derived carbon nanofiber composites [98, 113]. The electrospinning experiment involves a reservoir containing a polymer/TMeX solution, and a grounded conducting collector. By applying a high voltage, the precursor solution is charged and ejected forming a fiber that deposits as a non-woven mat on the collector [42]. Core–shell nanofibers can be fabricated mechanically with concentric spinnerets or chemically using polymer blends that phase separates [113]. Typical polymers include polyacrylonitrile (PAN), polyamides, polyimides (PI), poly(methyl methacrylate) (PMMA), poly(vinyl pyrrolidone) (PVP), poly(vinyl acetate) (PVAc), poly(vinyl alcohol) (PVA), poly(ethylene oxide) (PEO), poly(vinyl chloride) (PVC), polystyrene (PS), and conducting polymers [54]. In one configuration, the polymers are fed through the outer shell of a concentric (coaxial) spinneret while a solution of TMeX (either with or without a sacrificial polymer carrier) is fed through the core [119]. Upon carbonization, the outer polymer is converted to a carbon shell while the core contains TMeX as shown in Fig. 8. In this case, the conductive carbon is the outer shell while the typically insulating TMeX is in the core. In another configuration, the TMeX could be coated on the outside however, this is less common because of difficulties making electrical contact.

Core–shell nanohybrids can also be fabricated chemically by electrospinning immiscible polymer blends, such as polyacrylonitrile blended with polystyrene (PAN: PS), which was successful for the encapsulation of metal oxides in CNFs [24]. In this case, the PS formed channels in the PAN fiber as shown in Fig. 8d. Upon carbonization, the PS decomposes leaving hollow channels. Both techniques can be used with heteropolyacids (HPA), which possess $\geq$12 metal ions per cluster, to increase transition metal oxide (TMeX) loading even further. The encapsulated TMeX can be accessed via the porosity generated by porogens and/or activation. There is a variety of sacrificial polymers such as polystyrene (PS), poly(methyl methacrylate) (PMMA), etc. that will form ordered porosity by electrospinning the blends. The miscibility parameters of the polymers can be used to select polymer combinations that may phase separate into core–shell structures upon electrospinning [41, 72, 73]. Another iteration of core–shell fibers is to first prepare hollow fibers, then load the TMeX in channels. For example, PAN-PVP hollow carbon nanofibers were prepared and then loaded with $NiCo_2O_4$ nanoparticles [100]. XPS spectra for Ni $2p_{3/2}$ and $2p_{1/2}$ gave peaks at 853.03 and 871.05 eV as compared to bulk at 853.5 and 872.6 eV. Similarly, Co 2p pair of spin–orbit peaks ($2p_{3/2}$ and $2p_{1/2}$) for Co^{2+} and Co^{3+} shifts by 0.5 eV to a lower binding energy [18]. These data suggest that there is a

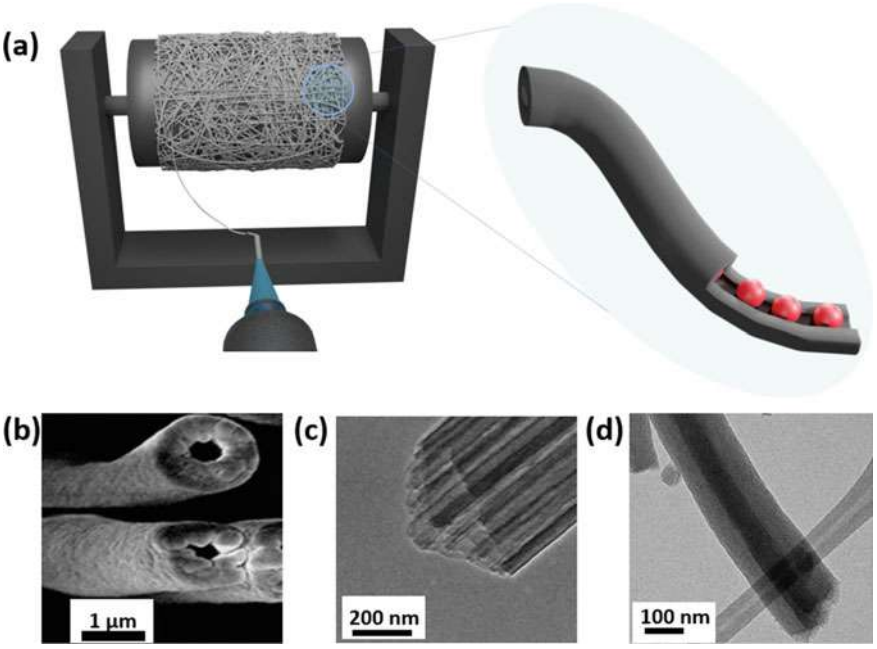

Fig. 8 **a** Cartoon for electrospinning and TMeX-carbon core–shell nanohybrid. **b** SEM image of PAN hollow fibers [4]. **c** TEM image of PAN-PS multichannel hollow nanofibers [75]. **d** TEM image of PAN-PS carbonized fibers with tungsten oxide nanorod core [24]. Figures are reprinted with permission from the American Chemical Society (8b), [75] (8c), and [24] (8d)

moderate interaction between the CNFs and TMeX. This interface results in a capacitance of 2992 F g^{-1} at 5 A g^{-1} and an energy density of 93.7 Wh kg^{-1} compared to 1264 F g^{-1} for the bulk TMeX [18]. Selected examples are summarized in Table 2, which includes TMeX nanohybrids with different carbons, e.g., $NiCo_2O_4$@CNFs

Table 2 Selected examples of core–shell nanohybrids

Material	Electrolyte	C_s (F g^{-1})	Energy density (Wh kg^{-1})
$NiCo_2O_4$@CNFs [100]	2 M KOH	2992 at 5 A g^{-1}	93.7
MnO_2@PAA/PPy [61]	1 M Na_2SO_4	580 at 5 A g^{-1}	–
Double-layer HCs@MoS_2 [62]	3 M KOH	399.4 at 0.5 A g^{-1}	–
TiO_2 NFs@Au@MnO_2 [36]	1 M Na_2SO_4	224 at 0.5 A g^{-1}	19.8
MnO_2/CNT [99]	1 M Na_2SO_4	250 mF cm^{-2}	88.8 mWh cm^{-2}
ZnO@C nanocables [116]	PVA/LiCl	1260.9 at 0.05 mA cm^{-2}	0.04 mWh cm^{-3}
NiMn-LDH@$NiCoP_2O_7$ with activated carbon [74]	KOH	142.1 at 10 mA cm^{-2}	56.15

[100], MnO_2/C NRs/AgNPs [28], MnO_2@PAA/PPy [61], double-layer HCs@MoS_2 [62], $CuCo_2S_4$@NiMn-LDH//AC [55], $NiCo_2O_4$@HfC_{NWs}/carbon cloth [118], and NiMn-LDH@ $NiCoP_2O_7$ with activated carbon [74].

2.3 *In Situ Dispersion*

Although the core–shell configuration improves the interfacial contact area over physical mixtures, this interaction can be increased through in situ dispersion. In this case, the electrospinning solution is prepared by mixing the TMeX nanoparticles with a precursor polymer. The resulting electrospun nanohybrid contains a uniform dispersion of TMeX when carbonize [114]. Since in situ dispersion is random, some TMeX particles are located in the bulk, and on the surface. For example, polyacrylonitrile and PAN-based copolymers were electrospun with V_2O_5 nanoparticles and carbonized [112]. As the PAN is carbonized, ammonia is released, resulting in the formation of VN. The XPS spectrum shows a modest shift to lower binding energy relative to the bulk [29]. Further activation of CNFs with CO_2 results in V_2O_3 nanoparticles embedded in the porous carbon network. Similar shifts in binding energy were also observed for V_2O_3.

Another approach to in situ dispersion would be to electrospin a mixture of TMeX precursor and polymer. For example, a mixture of cobalt (III) acetylacetonate, polyacrylonitrile (PAN), and polymethacrylic acid (PMAA) was electrospun followed by carbonization [65]. Figure 9a shows the dispersion of Co_3O_4 particles is not uniform in the absence of PMAA. In the case of the PAN/PMAA blend, PMAA shepherds the cobalt ions resulting in a more uniform dispersion and particle size

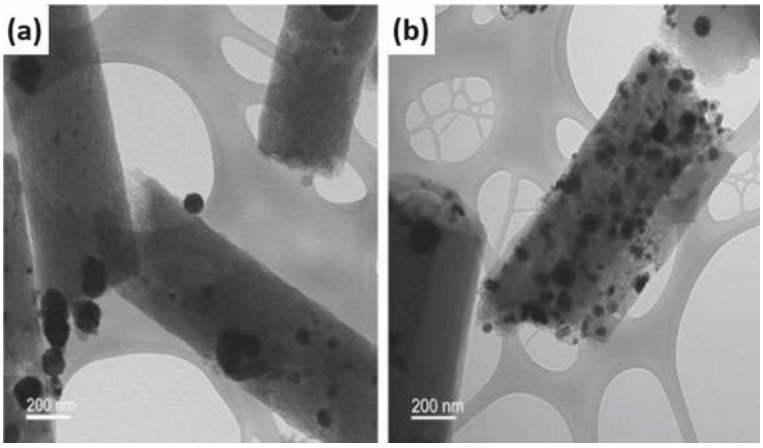

Fig. 9 TEM of carbonized **a** PAN-Co, and **b** PAN-PMAA-Co fibers [65]. Reprinted with permission from IOP publishing

Table 3 Selected examples of in situ dispersion nanohybrids

Material	Electrolyte	C_s (F g^{-1})	Energy density (Wh kg^{-1})
Mn–V–O@C nanofibers [83]	1 M K_2SO_4	668.5 F g^{-1} at 1 A g^{-1}	37.77
Co_3O_4–Cu NCNWs [32]	6 M KOH	1242 at 2 mV/s	44
NiO/CNFs [50]	6 M KOH	850 F g^{-1} at 2 A g^{-1}	–
PAN-PMAA–Co_3O_4 [65]	1 M Na_2SO_4	125 F g^{-1} at 1 A g^{-1}	8.9
FeO_x@C–CNF [87]	1 M H_2SO_4	332.4 F g^{-1} at 0.5 A g^{-1}	45.2
PPPMn10–CNF [115]	6 M KOH	188 at 1 mV/s	20.5
$NiCo_2O_4$@NC [49]	6 M KOH	2000.6 F g^{-1} at 1 A g^{-1}	61.2
$NiCo_2S_4$/CF [64]	Sodium polyacrylate-KOH gel	1169 F g^{-1} at 1 A g^{-1}	28.8
Co–Co_3O_4@CNT-NC [127]	6 M KOH	823.4 at 1 A g^{-1}	46.7

(Fig. 9b). Symmetric coin cells using 1 M Na_2SO_4 as the electrolyte resulted in a specific capacitance of 68 F g^{-1}, while the capacitance of PAN-PMAA-Co_3O_4 almost doubled to 125 F g^{-1} at 5 mV s^{-1} for PAN-Co. The increased capacitance in PAN-PMAA-Co_3O_4 can be attributed to a smaller, more uniform particle size resulting in improved interfacial contact in the composite. Some other representing examples of in situ dispersion type interfaces are mentioned in Table 3.

2.4 1D and 2D Materials

TMeXs have been grown on high surface area carbons such as CNTs and graphene to produce 1D and 2D hybrid supercapacitors. The carbons can be oxidized with nitric acid or HNO_3/H_2SO_4 to introduce functional groups such as COOH and OH [59, 93, 102]. These functional groups can bind metal ions from which TMeXs can be grown. Since the TMeXs are bound to the 1D and 2D surfaces, the IQ of these interfaces is greater than that found in physical mixtures or in situ dispersions. For example, MnO_2 nanowires (MNW) and V_2O_5 nanowires (VNW) were separately prepared on reduced graphene oxide (rGO) [78]. In this case, the Mn^{2+} and V^{5+} were bound to the oxygen functional groups of graphene oxide. Upon hydrothermal synthesis, metal oxide nanowires were formed and GO converted to rGO as shown in Fig. 10a. The TEM images showing the TMeX nanowires grown on rGO are shown in Fig. 10b. The XPS spectra show the Mn $2p_{3/2}$ and Mn $2p_{1/2}$ peaks at 642.2 and 653.5 eV which is shifted to lower binding energy relative to MnO_2 [91]. Similarly, V_2O_5 nanowires

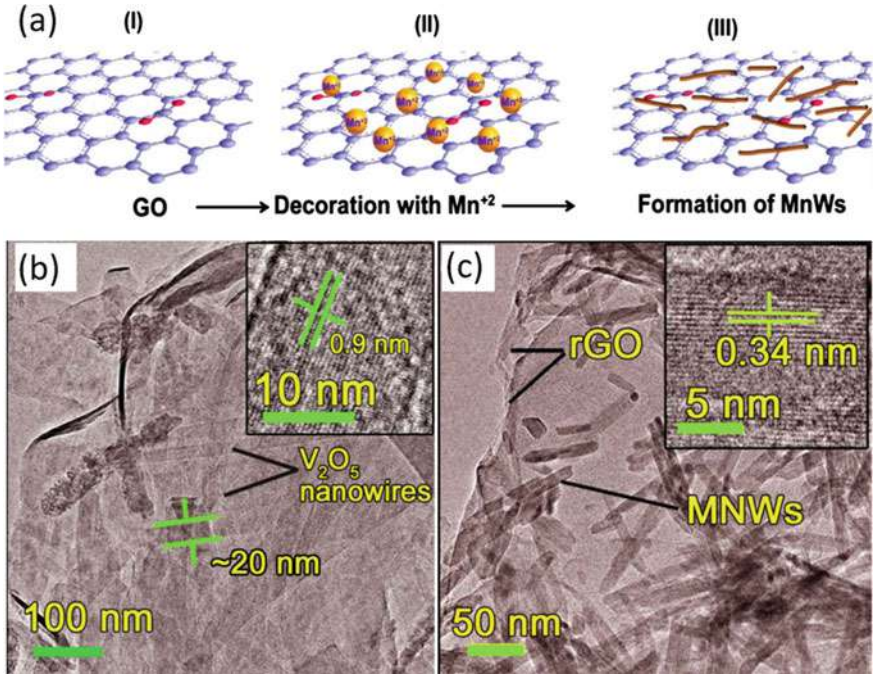

Fig. 10 **a** Graphical representation of MNW-rGO composite synthesis. **b** TEM image of VNW-rGO. **c** TEM image of MNW-rGO [78]. Adapted with permission from Elsevier

grown on rGO show a V $2p_{3/2}$ at 516.3 eV which is also shifted (~1 eV) from the bulk [105]. These shifts are consistent with stronger interfacial contact with the rGO.

The overall current response for the EDLC and TMeX components can be described as diffusion-controlled charge (Q_d) and surface capacitive charge (Q_s) determined by the Trasatti method [5, 17]. The total volumetric charge (Q_t) is the sum of Q_s and Q_d which varies with sweep rate (v). An approximate value for Q_s is given for all scan rates (Fig. 11a) and Q_d can be estimated for any given scan rate. Figure 11b shows that at a sweep rate of 5 mV/s, most of the charge is from the surface capacitance in the MNW electrode. In the VNW electrode, the charge contributions are approximately equal. The hybrid cell, which is a combination of an VNW-rGO anode and a MNW-rGO cathode, ~70% of the total charge can be ascribed to Q_d. The HSCs exhibits much higher Q_d, compared to both VNW-rGO and MNW-rGO separately. These results show that in this hybrid, both the carbon and the TMeX contribute to charge storage.

In addition to XPS, Raman spectroscopy can also be used to characterize interfaces based on interactions between carbon and TMeX. For example, MoS_2 was grown on rGO, then coated with PANI by in situ polymerization. The Raman spectrum shows D and G bands at 1326 and 1595 cm^{-1} as well as the in plane $E_{2g}{}^1$ and out of plane A_{1g} modes of MoS_2 at 375 and 408 cm^{-1}. These TMeX bands are shifted by

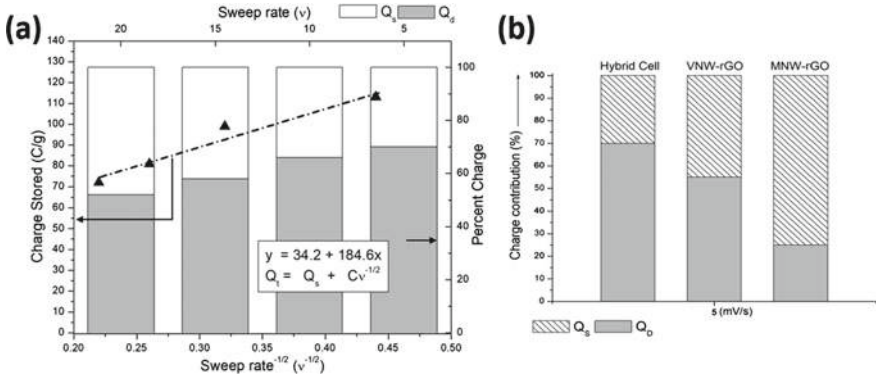

Fig. 11 **a** Charge stored versus inverse square root of the sweep rate relationship in the hybrid cell. **b** Surface (Q_s) and diffusion (Q_d) charge contribution at 5 mV/s for hybrid cell, VNW-rGO and, MNW-rGO

8 cm^{-1} consistent with the 2D interfacial interaction of MoS_2 on rGO [48]. Carbon nanotubes (CNTs) can also be surface engineered with functional groups that bind metal ions [25]. For example, $NiMoO_4$ was grown on amine-functionalized CNTs by hydrothermal methods [101]. Using a three-electrode system with 2 M KOH aqueous electrolyte a specific capacitance of 612 F g^{-1} was reported. The nanohybrid was an improvement over the pure $NiMoO_4$ which exhibited a capacitance of 343.71 F g^{-1}. In another example, CNTs were combined with rGO by first depositing cobalt on GO followed by growth of CNTs from the supported cobalt as shown in TEM images in Fig. 12 [10]. XPS analysis shows a binding energy for the Co $2p_{3/2}$ at 780.3 eV which is shifted from a binding energy of 778 eV which is normally observed for

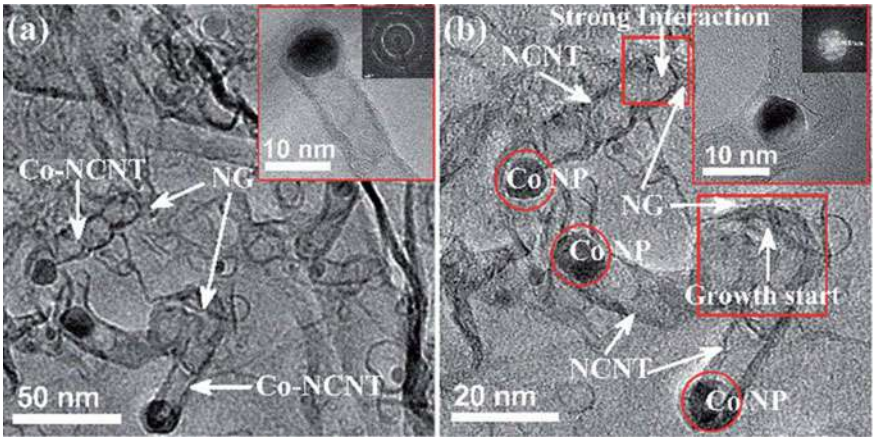

Fig. 12 3D NG/Co–NCNT nanohybrid **a** TEM and **b** HR-TEM images [10]. Reprinted with permission from the Royal Society of Chemistry

Table 4 Selected examples of 1D and 2D nanohybrids

Material	Electrolyte	C_s (F g^{-1})	Energy density (Wh kg^{-1})
Bi_2O_3/CNFs [109]	2 M KOH	2656 at 1 A g^{-1}	85.3
MnCoO-rGO [126]	3 M KOH	2749 at 0.5 A g^{-1}	35.5
Co_3O_4/C@CNFs [70]	2 M KOH	1623 at 1 A g^{-1}	36.6
MoS_2/rGO [52]	1 M H_2SO_4	1224 at 1 A g^{-1}	22.3
Gr–CeO_2–Pt [47]	6 M KOH	600 at 5 A g^{-1}	21.4
RuO_2/g–C_3N_4@rGO [121]	6 M KOH	704.3 at 0.5 A g^{-1}	2.5
CoS_2-rGO [34]	2 M KOH	1417 at 2 A g^{-1}	35.6
MnO_2/CNT [95]	0.5 M Na_2SO_4	1250 at 1 A g^{-1}	33.5
$Mn_{0.1}Ni_{0.9}MoO_4$/rGO [120]	Alkaline PVA	688.9 at 0.5 A g^{-1}	49.2
3D NG/Co-NCNT [10]	6 M KOH	2568 at 2 A g^{-1}	88.4
$NiMoO_4$-CNTs [101]	6 M KOH	611.69 at 1 A g^{-1}	20.4

the bulk metal. The presence of the metal is confirmed by XRD, so the shift must reflect a strong support interaction for this 1D/2D interface. This is manifested by the nanohybrid's capacitance of 2568 F g^{-1} at 2 A g^{-1}, which is over 2X better than the physical mixture. Selected examples of 1D and 2D nanohybrids are given in the Table 4.

2.5 Intimate Contact Materials

The complete coverage of TMeX with carbon results in a very intimate interaction. This is generally achieved by growing the carbon on the TMeX, either by CVD or thermal decomposition of an organic coating [96, 97]. In the 1D/2D interface, the TMeX is typically grown on carbon such that TMeX is partially in contact with carbon. The growth of carbon on the TMeX would afford a greater interconnected area. For example, La-catalyzed acetylene-steam chemical vapor deposition resulted in a templated carbon [12–14]. The templated carbon exhibits conductivity (10^5–10^6 S/m) two orders of magnitude higher than related carbon molecular sieves. Mechanistically, the metal oxide or hydroxide forms a metal acetylide on the surface which can react with water to form graphitic carbon, regenerating the metal hydroxide. This is illustrated in Fig. 13a for $Y(OH)_3$ [12]. The interface between the templated carbon and Y_2O_3 was characterized using X-ray photoelectron spectroscopy (XPS) and Raman spectroscopy. Figure 13b shows the Raman spectrum ($A_g + F_g$ band) for Y_2O_3, templated carbon (TC)-coated Y_2O_3 and the physical mixture of templated carbon and Y_2O_3. The TC-coated Y_2O_3 exhibits a 10 cm^{-1} shift relative to Y_2O_3, while the physical mixture exhibits no shift. When carbon is grown directly on the Y_2O_3 surface, charge transfer occurs. Therefore, Raman spectroscopy provides a

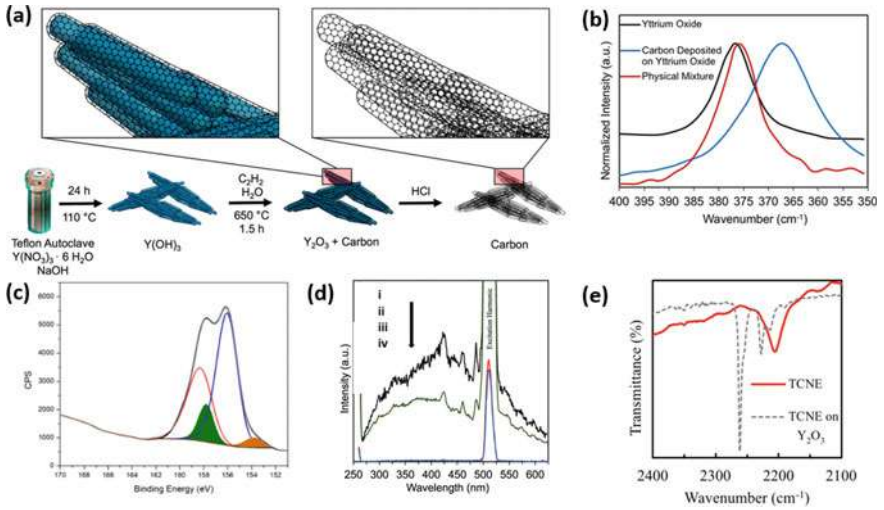

Fig. 13 **a** The synthesis route for $Y(OH)_3$ templated carbon microspindles. **b** Raman spectra of the A_g/T_g peak for Y_2O_3, TC deposited on Y_2O_3, and the physical mixture of TC and Y_2O_3. **c** XPS of carbon deposited on Y_2O_3. **d** Solid-state fluorescence spectra of 8-HQ adsorbed on (i) Y_2O_3, (ii) the physical mixture of TC and Y_2O_3, (iii) Y-templated carbon, and (iv) TC without 8-HQ. **e** IR-spectra of the TCNE probe and TCNE deposited on Y_2O_3 [12]. Adapted with permission from the American Chemical Society

sensitive tool for probing the interfaces. The deconvoluted XPS Y-3d spectrum of TC-coated Y_2O_3 is shown in Fig. 13c. The shifted smaller peaks show binding energies similar to yttrium carbide, the shift indicates there is a strong interaction with carbon. The physical mixture of yttrium oxide and the TC provides the weakest interface and shows no difference from the pure metal oxide. In contrast, the TC-coated yttrium oxide shows two new peaks (shaded) for the $3d_{3/2}$ and the $3d_{5/2}$ bands. This is what would be expected for charge transfer from carbon to the yttrium oxide indicating intimate contact. In addition to direct spectroscopic characterization of the nanohybrids, small probe molecules can be used to evaluate access to the carbon and/or TMeX surface. For example, the fluorescent probe 8-hydroxyquinoline (8-HQ) was employed to determine the access to the Y_2O_3/carbon interfaces. Figure 13d shows that the yttrium catalyzed carbon is not fluorescent. In contrast, the 8-HQ adsorbed on pure Y_2O_3 turns on fluorescence and the physical mixture exhibits attenuated fluorescence. Additionally, another small molecule probe tetracyanoethylene (TCNE) coordinates to the TMeX through the nitriles. Figure 13e shows a shift in the nitrile stretching frequency upon coordination to Y_2O_3. However, there is no interaction with the TC-coated Y_2O_3 indicating the interface is not accessible by this small (~6 Å) probe molecule. While yttrium oxide is not electrochemically active in the range of commonly used electrolytes, its use in the formation of templated carbon provides an opportunity to investigate models of hybrid nanostructures with intimate contact interfaces. In cases where metal oxides are redox-active, researchers will be able to

Table 5 Selected examples of intimate contact nanohybrids

Material	Electrolyte	C_s (F g^{-1})	Energy density (Wh kg^{-1})
Y_2O_3-TC [12]	EMIM-TFSI	137.2 at 10 mV/s	57.4
La_2O_3-TC [111]	EMIM-TFSI	128.1 at 10 mV/s	55.0
MnO_2/C NRs/AgNPs[28]	3 M KOH	628 at 1 A g^{-1}	48.3
FeO_x@C–CNF[87]	1 M H_2SO_4	332.4 at 0.5 A g^{-1}	45.2

correlate the strength of the interfacial interactions with changes in electrochemical performance [12].

In addition to CVD, organic molecules can coat the TMeX affording an intimate contact with the carbon. For example, a nanohybrid of MnO_2/carbon/Ag nanorods was prepared by heating MnO_2 nanorods and glucose solution at 160°C in an autoclave [28]. Mn 2*p* spectrum shows peaks at 641.7 and 653.5 eV for $2p_{3/2}$ and $2p_{1/2}$ which is shifted toward lower energy by 0.7 eV in comparison to bulk MnO_2 [91]. This nanohybrid exhibited a specific capacitance of 628 at 1 A g^{-1} and an energy density of 48.3 Wh kg^{-1} in asymmetric supercapacitor. Selected examples of intimate contact nanohybrids are given in Table 5.

It is also possible to get more than one type of interface in the same nanohybrid. For example, carbon-coated iron oxide particles were prepared inside carbon nanofibers (FeO_x@C–CNF) [87]. In this case, β-cyclodextrin (β-CD) was annealed with a Fe complex to make the carbon-coated FeO_x nanoparticles. The TEM images in Fig. 14 show the particles are uniformly dispersed in the CNFs. Thus, there are both in situ dispersion and intimate contact type interfaces. The XPS spectrum shows the Fe $2p_{3/2}$ binding energy for Fe_3O_4 at 710.8 eV. A shoulder at 709.6 eV was speculated to be FeO (not detected by XRD), however, an ~1 eV shift would also be consistent with an intimate contact interface. The electrochemical behavior of FeO_x@C–CNF in 1 M H_2SO_4 showed a specific capacitance of 332.4 F g^{-1} at 0.5 A g^{-1}. The contribution from EDLC was determined to be 59.5% versus 40.5% for PC at 1 mV s^{-1}.

3 Conclusion

The role of the interfaces in nanohybrid supercapacitors is not well understood but must be for the systematic design of future energy storage systems. The current research in nanohybrid supercapacitors often focuses on materials as opposed to the carbon-TMeX interface. Five different types of interfaces and combinations thereof have been described in this chapter. The interaction quotient (IQ), a qualitative measure of the interfacial contact, increases from physical mixtures to intimate contact materials, and provides a useful concept for classifying the nanohybrids. While the IQ is a major contributing factor to electron transfer, the electrode performance will still depend on several other parameters including the nature of

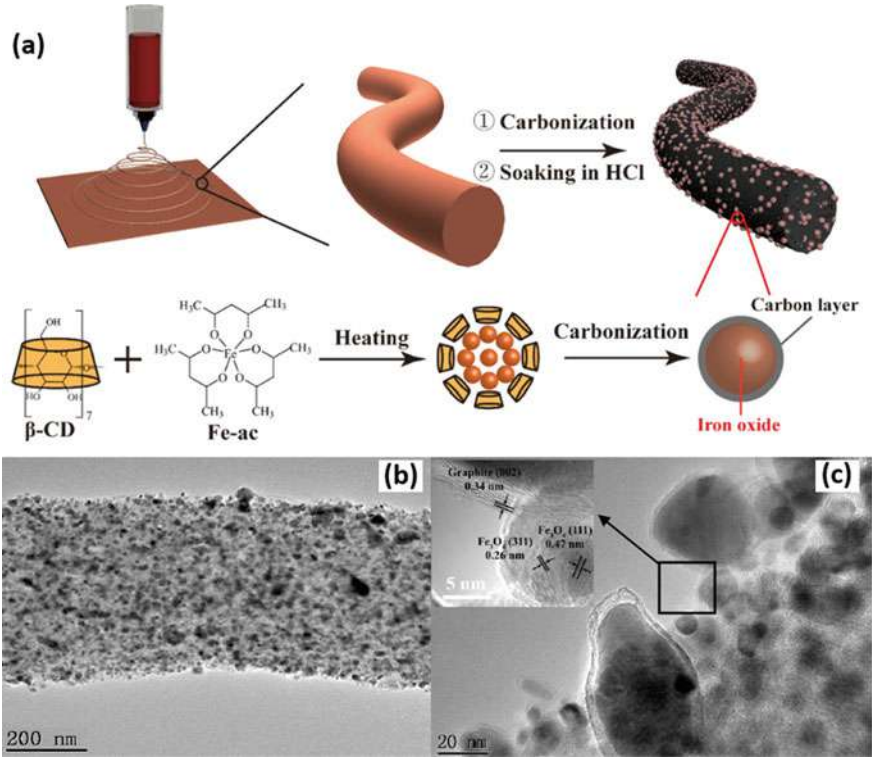

Fig. 14 **a** Graphical presentation of synthesis of FeO_x@C–CNF **b** TEM **c** high-resolution TEM of composite [87]. Reprinted with permission from the American Chemical Society

materials, their composition, porosity, and cell engineering. Several analytical techniques including XPS and Raman spectroscopy which clearly show evidence of carbon-TMeX interactions, have been highlighted. Additionally, the use of probe molecules confirms the type of interface, and provides information about its accessibility. Researchers are encouraged to consider the type of interface in their design of future nanohybrid electrode materials.

References

1. Abeykoon NC, Mahmood SF, Yang DJ, Ferraris JP (2019) Electrospun poly (acrylonitrile-co-itaconic acid) as a porous carbon precursor for high performance supercapacitor: study of the porosity induced by in situ porogen activity of itaconic acid. Nanotechnology 30(43):435401
2. Abouali S, Garakani MA, Xu Z-L, Kim J-K (2016) $NiCo_2O_4$/CNT nanocomposites as bi-functional electrodes for Li ion batteries and supercapacitors. Carbon 102:262–272
3. Afif A, Rahman SMH, Azad AT, Zaini J, Islan MA, Azad AK (2019) Advanced materials and technologies for hybrid supercapacitors for energy storage—a review. J Energy Storage

25:100852
4. Anka FH, Balkus KJ Jr (2013) Novel nanofiltration hollow fiber membrane produced via electrospinning. Ind Eng Chem Res 52(9):3473–3480
5. Ardizzone S, Fregonara G, Trasatti S (1990) "Inner" and "outer" active surface of RuO_2 electrodes. Electrochim Acta 35(1):263–267
6. Augustyn V, Simon P, Dunn B (2014) Pseudocapacitive oxide materials for high-rate electrochemical energy storage. Energy Environ Sci 7(5):1597–1614
7. Babu B, Simon P, Balducci A (2020) Fast charging materials for high power applications. Adv Energy Mater 10(29):2001128
8. Bach-Toledo L, Hryniewicz BM, Marchesi LF, Dall'Antonia LH, Vidotti M, Wolfart F (2020) Conducting polymers and composites nanowires for energy devices: a brief review. Mater Sci Energy Technol 3:78–90
9. Baig MM, Gul IH, Baig SM, Shahzad F (2021) The complementary advanced characterization and electrochemical techniques for electrode materials for supercapacitors. J Energy Storage 44:103370
10. Balamurugan J, Thanh TD, Kim NH, Lee JH (2016) Facile synthesis of 3D hierarchical N-doped graphene nanosheet/cobalt encapsulated carbon nanotubes for high energy density asymmetric supercapacitors. J Mater Chem A 4(24):9555–9565
11. Becker HI (1957) Low voltage electrolytic capacitor. US Patent No. US2800616A
12. Brown AT, Agrawal VS, Wunch MA, Lin J, Thomas MC, Ferraris JP, Chabal YJ, Balkus KJ Jr (2021) Yttrium oxide-catalyzed formation of electrically conductive carbon for supercapacitors. ACS Appl Energy Mater 4(11):12499–12507
13. Brown AT, Lin J, Vizuet JP, Thomas MC, Balkus KJ (2021) Graphene-like carbon from calcium hydroxide. ACS Omega 6(46):31066–31076
14. Brown AT, Thomas MC, Chabal YJ, Balkus KJ Jr (2019) Nanocast carbon microsphere flowers from a lanthanum-based template. Mater Lett 234:224–227
15. Chatterjee DP, Nandi AK (2021) A review on the recent advances in hybrid supercapacitors. J Mater Chem A 9(29):15880–15918
16. Chen L, Yan R, Oschatz M, Jiang L, Antonietti M, Xiao K (2020) Ultrathin 2D graphitic carbon nitride on metal films: underpotential sodium deposition in Adlayers for sodium-ion batteries. Angew Chem Int Ed 59(23):9067–9073
17. Chen Z, Augustyn V, Jia X, Xiao Q, Dunn B, Lu Y (2012) High-performance sodium-ion pseudocapacitors based on hierarchically porous nanowire composites. ACS Nano 6(5):4319–4327
18. Cheng J, Lu Y, Qiu K, Yan H, Xu J, Han L, Liu X, Luo J, Kim J-K, Luo Y (2015) Hierarchical core/shell $NiCo_2O_4$@ $NiCo_2O_4$ nanocactus arrays with dual-functionalities for high performance supercapacitors and Li-ion batteries. Sci Rep 5(1):1–12
19. Conway BE (2013) Electrochemical supercapacitors: scientific fundamentals and technological applications. Springer Science and Business Media
20. Conway BE (1991) Transition from "supercapacitor" to "battery" behavior in electrochemical energy storage. J Electrochem Soc 138(6):1539
21. El-Kady MF, Shao Y, Kaner RB (2016) Graphene for batteries, supercapacitors and beyond. Nat Rev Mater 1(7):1–14
22. Elgrishi N, Rountree KJ, McCarthy BD, Rountree ES, Eisenhart TT, Dempsey JL (2018) A practical beginner's guide to cyclic voltammetry. J Chem Educ 95(2):197–206
23. Faraji S, Ani FN (2015) The development supercapacitor from activated carbon by electroless plating—a review. Renew Sustain Energy Rev 42:823–834
24. García JA (2021) Electrochemical performance of polymer derived carbon nanofibers and tungsten compound/carbon composites. Ph.D. dissertation. The University of Texas at Dallas
25. Gerber I, Oubenali M, Bacsa R, Durand J, Gonçalves A, Pereira MFR, Jolibois F, Perrin L, Poteau R, Serp P (2011) Theoretical and experimental studies on the carbon-nanotube surface oxidation by nitric acid: interplay between functionalization and vacancy enlargement. Chem A Eur J 17(41):11467–11477

26. Goodenough JB, Abruna HD, Buchanan MV (2007) Basic research needs for electrical energy storage. Report of the basic energy sciences workshop on electrical energy storage. DOESC (USDOE Office of Science (SC)), 2–4 Apr 2007
27. Gu T-H, Kwon NH, Lee K-G, Jin X, Hwang S-J (2020) 2D inorganic nanosheets as versatile building blocks for hybrid electrode materials for supercapacitor. Coord Chem Rev 421:213439
28. Guan Y, Guo Z, Che H, Mu J, Zhang X, Zhang Z, Wang G, Bai Y, Xie H (2018) Core/shell nanorods of MnO_2/carbon embedded with Ag nanoparticles as high-performance electrode materials for supercapacitors. Chem Eng J 331:23–30
29. Haasch RT, Lee T-Y, Gall D, Greene JE, Petrov I (2000) Epitaxial VN (001) grown and analyzed in situ by XPS and UPS. I. Analysis of As-deposited layers. Surf Sci Spectra 7(3):221–232
30. Halim J, Cook KM, Naguib M, Eklund P, Gogotsi Y, Rosen J, Barsoum MW (2016) X-ray photoelectron spectroscopy of select multi-layered transition metal carbides (MXenes). Appl Surf Sci 362:406–417
31. Haq AU, Lim J, Yun JM, Lee WJ, Han TH, Kim SO (2013) Direct growth of polyaniline chains from N-doped sites of carbon nanotubes. Small 9(22):3829–3833
32. Harilal M, Vidyadharan B, Misnon II, Anilkumar GM, Lowe A, Ismail J, Yusoff MM, Jose R (2017) One-dimensional assembly of conductive and capacitive metal oxide electrodes for high-performance asymmetric supercapacitors. ACS Appl Mater Interfaces 9(12):10730–10742
33. Hu B, Qin X, Asiri AM, Alamry KA, Al-Youbi AO, Sun X (2013) WS_2 nanoparticles–encapsulated amorphous carbon tubes: a novel electrode material for supercapacitors with a high rate capability. Electrochem Commun 28:75–78
34. Hu B, Li H, Liu A, Yue C, Guo Z, Mu J, Zhang X, Che H (2020) Construction of 2D–2D plate-on-sheet cobalt sulfide-reduced graphene oxide nanocomposites for enhanced energy storage properties in supercapacitors. ACS Appl Energy Mater 4(1):88–97
35. Hu J, Sun M, Cai X, Zhai C, Zhang J, Zhu M (2017) Two dimensional perovskite $La_2Ti_2O_7$ nanosheet as Pt catalyst support for photo-assisted methanol oxidation reaction. J Taiwan Inst Chem Eng 80:231–238
36. Huang D, Lu Z, Xu Q, Liu X, Yi W, Gao J, Chen Z, Wang X, Fu X (2022) Nanoflowers@Au@MnO_2 core-shell composite based on modified Ti foil for flexible supercapacitor electrode. Electrochim Acta 139866
37. Huang H, Wang X, Tervoort E, Zeng G, Liu T, Chen X, Sologubenko A, Niederberger M (2018) Nano-sized structurally disordered metal oxide composite aerogels as high-power anodes in hybrid supercapacitors. ACS Nano 12(3):2753–2763
38. Jayawickramage RAP, Balkus KJ, Ferraris JP (2019) Binder free carbon nanofiber electrodes derived from polyacrylonitrile-lignin blends for high performance supercapacitors. Nanotechnology 30(35):355402
39. Ji Z, Li N, Xie M, Shen X, Dai W, Liu K, Xu K, Zhu G (2020) High-performance hybrid supercapacitor realized by nitrogen-doped carbon dots modified cobalt sulfide and reduced graphene oxide. Electrochim Acta 334:135632
40. Jing M, Hou H, Yang Y, Zhu Y, Wu Z, Ji X (2015) Electrochemically alternating voltage tuned Co hydroxide chloride for an asymmetric supercapacitor. Electrochim Acta 165:198–205
41. Jo E, Yeo J, Kim DK, Oh JS, Hong CK (2014) Preparation of well-controlled porous carbon nanofiber materials by varying the compatibility of polymer blends. Polym Int 63(8):1471–1477
42. Jung J-W, Lee C-L, Yu S, Kim I-D (2016) Electrospun nanofibers as a platform for advanced secondary batteries: a comprehensive review. J Mater Chem A 4(3):703–750
43. Jung K-H, Kim SJ, Son YJ, Ferraris JP (2019) Fabrication of carbon nanofiber electrodes using poly (acrylonitrile-co-vinylimidazole) and their energy storage performance. Carbon Lett 29(2):177–182
44. Kesavan KS, Surya K, Michael MS (2018) High powered hybrid supercapacitor with microporous activated carbon. Solid State Ionics 321:15–22

45. Ko JS, Lai C-H, Long JW, Rolison DR, Dunn B, Nelson Weker J (2020) Differentiating double-layer, psuedocapacitance, and battery-like mechanisms by analyzing impedance measurements in three dimensions. ACS Appl Mater Interfaces 12(12):14071–14078
46. Kotal M, Thakur AK, Bhowmick AK (2013) Polyaniline–carbon nanofiber composite by a chemical grafting approach and its supercapacitor application. ACS Appl Mater Interfaces 5(17):8374–8386
47. Kumar R, Agrawal A, Nagarale RK, Sharma A (2016) High performance supercapacitors from novel metal-doped ceria-decorated aminated graphene. J Phys Chem C 120(6):3107–3116
48. Li H, Zhang Q, Yap CCR, Tay BK, Edwin THT, Olivier A, Baillargeat D (2012) From bulk to monolayer MoS_2: evolution of Raman scattering. Adv Func Mater 22(7):1385–1390
49. Li J, Liu Y, Zhan D, Zou Y, Xu F, Sun L, Xiang C, Zhang J (2021) Electrospinning synthesis of $NiCo_2O_4$ embedded N-doped carbon for high-performance supercapacitors. J Energy Storage 39:102665
50. Li Q, Guo J, Xu D, Guo J, Ou X, Hu Y, Qi H, Yan F (2018) Electrospun N-doped porous carbon nanofibers incorporated with NiO nanoparticles as free-standing film electrodes for high-performance supercapacitors and CO_2 capture. Small 14(15):1704203
51. Li S, Zhou X, Chen Z, Herbert FC, Jayawickramage R, Panangala SD (2020) Hierarchical porous carbon arising from metal–organic framework-encapsulated bacteria and its energy storage potential. ACS Appl Mater Interfaces 12(10):11884–11889
52. Li X, Zhang C, Xin S, Yang Z, Li Y, Zhang D, Yao P (2016) Facile synthesis of MoS_2/reduced graphene oxide@polyaniline for high-performance supercapacitors. ACS Appl Mater Interfaces 8(33):21373–21380
53. Li Y, Yin J, An L, Lu M, Sun K, Zhao Y, Gao D, Cheng F, Xi P (2018) FeS_2/CoS_2 interface nanosheets as efficient bifunctional electrocatalyst for overall water splitting. Small 14(26):1801070
54. Liang J, Zhao H, Yue L, Fan G, Li T, Lu S, Chen G, Gao S, Asiri AM, Sun X (2020) Recent advances in electrospun nanofibers for supercapacitors. J Mater Chem A 8(33):16747–16789
55. Lin J, Jia H, Liang H, Chen S, Cai Y, Qi J, Qu C, Cao J, Fei W, Feng J (2018) Hierarchical $CuCo_2S_4$@NiMn-layered double hydroxide core–shell hybrid arrays as electrodes for supercapacitors. Chem Eng J 336:562–569
56. Liu T, Finn L, Yu M, Wang H, Zhai T, Lu X, Tong Y, Li Y (2014) Polyaniline and polypyrrole pseudocapacitor electrodes with excellent cycling stability. Nano Lett 14(5):2522–2527
57. Liu W, Li X, Zhu M, He X (2015) High-performance all-solid state asymmetric supercapacitor based on Co_3O_4 nanowires and carbon aerogel. J Power Sources 282:179–186
58. Lokhande VC, Lokhande AC, Lokhande CD, Kim JH, Ji T (2016) Supercapacitive composite metal oxide electrodes formed with carbon, metal oxides and conducting polymers. J Alloy Compd 682:381–403
59. Lu L, Xu T, Chen W, Lee JM, Luo Z, Jung IH, Park HI, Kim SO, Yu L (2013) The role of N-doped multiwall carbon nanotubes in achieving highly efficient polymer bulk heterojunction solar cells. Nano Lett 13(6):2365–2369
60. Lu M, Cao Y, Xue Y, Qiu W (2021) Preparation of graphene oxide/$La_2Ti_2O_7$ composites with enhanced electrochemical performances for supercapacitors. ACS Omega 6(42):27994–28003
61. Lu X, Shen C, Zhang Z, Barrios E, Zhai L (2018) Core–shell composite fibers for high-performance flexible supercapacitor electrodes. ACS Appl Mater Interfaces 10(4):4041–4049
62. Luan X, Zhu K, Zhang X, Yang P (2022) MoS_2 nanosheets coupled with double-layered hollow carbon spheres towards superior electrochemical activity. Electrochim Acta 139929
63. Ma H, He J, Xiong D-B, Wu J, Li Q, Dravid V, Zhao Y (2016) Nickel cobalt hydroxide@reduced graphene oxide hybrid nanolayers for high performance asymmetric supercapacitors with remarkable cycling stability. ACS Appl Mater Interfaces 8(3):1992–2000
64. Ma Z, Sun Z, Jiang H, Li F, Wang Q, Qu F (2020) Nanoporous electrospun $NiCo_2S_4$ embedded in carbon fiber as an excellent electrode for high-rate supercapacitors. Appl Surf Sci 533:147521

65. Malekpour S, Balkus KJ, Ferraris JP (2021) Hybrid supercapacitors using electrodes from fibers comprising polymer blend–metal oxide composites with polymethacrylic acid as chelating agent. Nanotechnology 32(32):325401
66. Mei B-A, Munteshari O, Lau J, Dunn B, Pilon L (2018) Physical interpretations of Nyquist plots for EDLC electrodes and devices. J Phys Chem C 122(1):194–206
67. Miller JR (2016) Engineering electrochemical capacitor applications. J Power Sources 326:726–735
68. Mohamed AM, Abo El Naga AO, Zaki T, Hassan HB, Allam NK (2020) Bimetallic Co–W–S chalcogenides confined in N, S-codoped porous carbon matrix derived from metal–organic frameworks for highly stable electrochemical supercapacitors. ACS Appl Energy Mater 3(8):8064–8074
69. Morales DM, Risch M (2021) Seven steps to reliable cyclic voltammetry measurements for the determination of double layer capacitance. J Phys Energy 3(3):34013
70. Mukhiya T, Ojha GP, Dahal B, Kim T, Chhetri K, Lee M, Chae S-H, Muthurasu A, Tiwari AP, Kim HY (2020) Designed assembly of porous cobalt oxide/carbon nanotentacles on electrospun hollow carbon nanofibers network for supercapacitor. ACS Appl Energy Mater 3(4):3435–3444
71. Panangala SD, Karunaweera C, Jayawickramage R, Balkus KJ Jr, Ferraris JP (2019) Aromatic polyimides containing diaminobenzoic acid as in situ porogen for electrochemical supercapacitors. ACS Appl Polym Mater 1(11):3203–3209
72. Panapitiya NP, Wijenayake SN, Huang Y, Bushdiecker D, Nguyen D, Ratanawanate C, Kalaw GJ, Gilpin CJ, Musselman IH, Balkus KJ Jr (2014) Stabilization of immiscible polymer blends using structure directing metal organic frameworks (MOFs). Polymer 55(8):2028–2034
73. Panapitiya NP, Wijenayake SN, Nguyen DD, Huang Y, Musselman IH, Balkus KJ Jr, Ferraris JP (2015) Gas separation membranes derived from high-performance immiscible polymer blends compatibilized with small molecules. ACS Appl Mater Interfaces 7(33):18618–18627
74. Patil SJ, Chodankar NR, Pujari RB, Han Y-K, Lee DW (2020) Core-shell hetero-nanostructured 1D transition metal polyphosphates decorated 2D bimetallic layered double hydroxide for sustainable hybrid supercapacitor. J Power Sources 466:228286
75. Perananthan S (2017) Preparation of free standing carbon nanofiber electrodes for supercapacitor applications. Doctoral dissertation
76. Perera SD, Liyanage AD, Nijem N, Ferraris JP, Chabal YJ, Balkus KJ Jr (2013) Vanadium oxide nanowire–graphene binder free nanocomposite paper electrodes for supercapacitors: a facile green approach. J Power Sources 230:130–137
77. Perera SD, Patel B, Nijem N, Roodenko K, Seitz O, Ferraris JP, Chabal YJ, Balkus KJ Jr (2011) Vanadium oxide nanowire–carbon nanotube binder-free flexible electrodes for supercapacitors. Adv Energy Mater 1(5):936–945
78. Perera SD, Rudolph M, Mariano RG, Nijem N, Ferraris JP, Chabal YJ, Balkus KJ Jr (2013) Manganese oxide nanorod–graphene/vanadium oxide nanowire–graphene binder-free paper electrodes for metal oxide hybrid supercapacitors. Nano Energy 2(5):966–975
79. Rudge A, Davey J, Raistrick I, Gottesfeld S, Ferraris JP (1994) Conducting polymers as active materials in electrochemical capacitors. J Power Sources 47(1–2):89–107
80. Rudge A, Raistrick I, Gottesfeld S, Ferraris JP (1994) A study of the electrochemical properties of conducting polymers for application in electrochemical capacitors. Electrochim Acta 39(2):273–287
81. Ruiyi L, Keyang H, Yongqiang Y, Haiyan Z, Zaijun L (2021) Atomically dispersed RuO_2-tryptophan functionalized graphene quantum dot-graphene hybrid with double Schottky heterojunctions for high performance flexible supercapacitors. Chem Eng J, 130893
82. Sakamoto K, Hayashi F, Sato K, Hirano M, Ohtsu N (2020) XPS spectral analysis for a multiple oxide comprising NiO, TiO_2, and $NiTiO_3$. Appl Surf Sci 526:146729
83. Samir M, Ahmed N, Ramadan M, Allam NK (2019) Electrospun mesoporous Mn–V–O@C nanofibers for high-performance asymmetric supercapacitor devices with high stability. ACS Sustain Chem Eng 7(15):13471–13480

84. Scarfiello R, Mazzotta E, Altamura D, Nobile C, Mastria R, Rella S, Giannini C, Cozzoli PD, Rizzo A, Malitesta C (2021) An insight into chemistry and structure of colloidal 2D-WS_2 nanoflakes: combined XPS and XRD study. Nanomaterials 11(8):1969
85. Shao H, Wu Y-C, Lin Z, Taberna P-L, Simon P (2020) Nanoporous carbon for electrochemical capacitive energy storage. Chem Soc Rev 49(10):3005–3039
86. Shao Y, El-Kady MF, Sun J, Li Y, Zhang Q, Zhu M, Wang H, Dunn B, Kaner RB (2018) Design and mechanisms of asymmetric supercapacitors. Chem Rev 118(18):9233–9280
87. Shi W, Hu B, Zhang H, Li J, Yang J, Liu J (2020) Carbon-encapsulated iron oxide nanoparticles in self-supporting carbon nanofiber for high-performance supercapacitor in acid electrolyte with superior stability. ACS Appl Energy Mater 3(12):12652–12661
88. Simon P, Gogotsi Y (2020) Perspectives for electrochemical capacitors and related devices. Nat Mater 19(11):1151–1163
89. Simon P, Taberna P-L, Béguin F (2013) In: Béguin F, Şackowiak EF (eds) Electrical double-layer capacitors and carbons for EDLCs
90. Stoller MD, Park S, Zhu Y, An J, Ruoff RS (2008) Graphene-based ultracapacitors. Nano Lett 8(10):3498–3502
91. Stranick MA (1999) MnO_2 by XPS. Surf Sci Spectra 6(1):31–38
92. Sun H, Zhang Y, Zhang J, Sun X, Peng H (2017) Energy harvesting and storage in 1D devices. Nat Rev Mater 2(6):1–12
93. Sun S, Lang J, Wang R, Kong L, Li X, Yan X (2014) Identifying pseudocapacitance of in an ionic liquid and its application in asymmetric supercapacitors. J Mater Chem A 2(35):14550–14556
94. Talaie E, Bonnick P, Sun X, Pang Q, Liang X, Nazar LF (2017) Methods and protocols for electrochemical energy storage materials research. Chem Mater 29(1):90–105
95. Tan X, Liu S, Guo Q, Zhang J, Liang S, He M, Luo J (2020) Synthesis and characterisation of amorphous MnO_2/CNT via solid-state microwave for high-performance supercapacitors. Int J Energy Res 44(6):4556–4567
96. Tian Y, Zhu X, Abbas M, Tague D, Wunch M, Ferraris J, Balkus K (2022) Magnesium Hydroxide Templated Hierarchical Porous Carbon Nanosheets as Electrodes for High-Energy-Density Supercapacitors. ACS Applied Energy Materials, 5(6), 6805-6813. https://doi.org/10.1021/acsaem.2c00417
97. Tian Y, Zhu X, Abbas M, Tague D, Ferraris J, Balkus K (2022) Two-Dimensional Hexagonal-Shaped Mesoporous Carbon Sheets for Supercapacitors. ACS Omega. https://doi.org/10.1021/acsomega.2c01149
98. Tiwari AP, Mukhiya T, Muthurasu A, Chhetri K, Lee M, Dahal B, Lohani PC, Kim H-Y (2021) A review of electrospun carbon nanofiber-based negative electrode materials for supercapacitors. Electrochem 2(2):236–250
99. Tiwari P, Janas D, Chandra R (2021) Self-standing MoS_2/CNT and MnO_2/CNT one dimensional core shell heterostructures for asymmetric supercapacitor application. Carbon 177:291–303
100. Tomboc GM, Kim H (2019) Derivation of both EDLC and pseudocapacitance characteristics based on synergistic mixture of $NiCo_2O_4$ and hollow carbon nanofiber: an efficient electrode towards high energy density supercapacitor. Electrochim Acta 318:392–404
101. Tomboc GM, Kim H (2019) Highly porous tailored onto amine functionalized CNT as advanced nanocomposite electrocatalyst for supercapacitor application. J Mater Sci Mater Electron 30(10):9558–9571
102. Tomboc GM, Tesfaye Gadisa B, Jun M, Chaudhari NK, Kim H, Lee K (2020) Carbon transition-metal oxide electrodes: understanding the role of surface engineering for high energy density supercapacitors. Chem Asian J 15(11):1628–1647
103. Trasatti S, Buzzanca G (1971) Ruthenium dioxide: a new interesting electrode material. Solid state structure and electrochemical behaviour. J Electroanal Chem Interfacial Electrochem 29(2):A1–A5
104. Vangari M, Pryor T, Jiang L (2013) Supercapacitors: review of materials and fabrication methods. J Energy Eng 139(2):72–79

105. Verhoeven JAT, Van Doveren H (1980) XPS studies on Ba, BaO and the oxidation of Ba. Appl Surf Sci 5(4):361–373
106. Vlad A, Singh N, Rolland J, Melinte S, Ajayan PM, Gohy J-F (2014) Hybrid supercapacitor-battery materials for fast electrochemical charge storage. Sci Rep 4(1):1–7
107. Wang J-G, Kang F, Wei B (2015) Engineering of MnO_2-based nanocomposites for high-performance supercapacitors. Prog Mater Sci 74:51–124
108. Wang X, Yushin G (2015) Chemical vapor deposition and atomic layer deposition for advanced lithium ion batteries and supercapacitors. Energy Environ Sci 8(7):1889–1904
109. Wang Y, Zhou J, Chen K, Zhao W, Tao K, Han L (2021) Metal-organic framework-derived Bi_2O_3/C and $NiCo_2S_4$ hollow nanofibers for asymmetric supercapacitors. ACS Appl Nano Mater 4(11):11895–11906
110. Wang Z, Perananthan S, Panangala SD, Ferraris JP, Balkus KJ (2018) Wrinkled mesoporous silica supported lanthanum oxide as a template for porous carbon. J Nanosci Nanotechnol 18(1):414–418
111. Wang Z, Perera WA, Perananthan S, Ferraris JP, Balkus KJ Jr (2018) Lanthanum hydroxide nanorod-templated graphitic hollow carbon nanorods for supercapacitors. ACS Omega 3(10):13913–13918
112. Wunch MA (2020) Preparation of functionalized graphenes and their performance for corrosion resistance and synthesis of vanadium nitride carbon nanofiber mats and their application for asymmetric supercapacitor electrodes. Ph.D. dissertation. The University of Texas at Dallas
113. Xue J, Wu T, Dai Y, Xia Y (2019) Electrospinning and electrospun nanofibers: methods, materials, and applications. Chem Rev 119(8):5298–5415
114. Yang C-H, Hsiao Y-C, Lin L-Y (2021) Novel in situ synthesis of freestanding carbonized ZIF67/polymer nanofiber electrodes for supercapacitors via electrospinning and pyrolysis techniques. ACS Appl Mater Interfaces 13(35):41637–41648
115. Yang C-M, Kim B-H (2018) Highly conductive pitch-based carbon nanofiber/MnO_2 composites for high-capacitance supercapacitors. J Alloy Compd 749:441–447
116. Yang P, Xiao X, Li Y, Ding Y, Qiang P, Tan X, Mai W, Lin Z, Wu W, Li T (2013) Hydrogenated ZnO core–shell nanocables for flexible supercapacitors and self-powered systems. ACS Nano 7(3):2617–2626
117. Yang Z, Tian J, Yin Z, Cui C, Qian W, Wei F (2019) Carbon nanotube-and graphene-based nanomaterials and applications in high-voltage supercapacitor: a review. Carbon 141:467–480
118. Yin X, Li H, Fu Y, Yuan R, Lu J (2020) Hierarchical core-shell structure of $NiCo_2O_4$ nanosheets@HfC nanowires networks for high performance flexible solid-state hybrid supercapacitor. Chem Eng J 392:124820
119. Yu B, Gele A, Wang L (2018) Iron oxide/lignin-based hollow carbon nanofibers nanocomposite as an application electrode materials for supercapacitors. Int J Biol Macromol 118:478–484
120. Yuan J, Yao D, Jiang L, Tao Y, Che J, He G, Chen H (2020) Mn-doped $NiMoO_4$ mesoporous nanorods/reduced graphene oxide composite for high-performance all-solid-state supercapacitor. ACS Appl Energy Mater 3(2):1794–1803
121. Zhang J, Ding J, Li C, Li B, Li D, Liu Z (2017) Fabrication of novel ternary three-dimensional RuO_2/graphitic-C_3N_4@ reduced graphene oxide aerogel composites for supercapacitors. ACS Sustain Chem Eng 5(6):4982–4991
122. Zhang M, Zheng H, Zhu H, Xu Z, Liu R, Chen J, Song Q, Song X, Wu J, Zhang C (2020) Graphene-wrapped MnO_2 achieved by ultrasonic-assisted synthesis applicable for hybrid high-energy supercapacitors. Vacuum 176:109315
123. Zhao H, Yang J, Lin T, Lü Q, Chen G (2015) Nanocomposites of sulfonic polyaniline nanoarrays on graphene nanosheets with an improved supercapacitor performance. Chem A Eur J 21(2):682–690
124. Zhou Q, Chen X, Su F, Lyu X, Miao M (2020) Sandwich-structured transition metal oxide/graphene/carbon nanotube composite yarn electrodes for flexible two-ply yarn supercapacitors. Ind Eng Chem Res 59(13):5752–5759

125. Zhou Y, Maleski K, Anasori B, Thostenson JO, Pang Y, Feng Y, Zeng K, Parker CB, Zauscher S, Gogotsi Y (2020) $Ti_3C_2T_x$ MXene-reduced graphene oxide composite electrodes for stretchable supercapacitors. ACS Nano 14(3):3576–3586
126. Zhu Y, Zhang C, Tang S, Huang H, Wang S, Luo Q, Du Y (2019) Graphene-anchored mesoporous Mn–Co oxide battery-like materials for ultrahigh performance hybrid supercapacitors. ACS Appl Energy Mater 2(10):7546–7553
127. Zou Y, Cai C, Xiang C, Huang P, Chu H, She Z, Xu F, Sun L, Kraatz H-B (2018) Simple synthesis of core-shell structure of Co–Co_3O_4@ carbon-nanotube-incorporated nitrogen-doped carbon for high-performance supercapacitor. Electrochim Acta 261:537–547

Chapter 17
Organic–Inorganic Nanohybrids in Flexible Electronic Devices

Rabia Akhtar, Ameer Fawad Zahoor, Asim Mansha, Sajjad Ahmad, Muhammad Irfan, Kulsoom Ghulam Ali, and Bushra Parveen

1 Introduction

Nanomaterials (NMs) play a vital role in medicinal, cosmetic as well as in chemical industries. Besides this, their extensive use in batteries, fuel, and solar cells makes them a prominent candidate for electronic devices. This wide range of applications of nanomaterials is due to their distinctive thermo-physical, mechanical, and optical properties. However, in the past few decades, a lot of effort has been devoted to increase the efficacy of these nanomaterials by inserting single-particle nanomaterials in an appropriate matrix [1]. Organic–inorganic nanohybrids have received significant consideration in this regard.

Organic–inorganic nanohybrids are made up of two different components typically polymers/biomolecules as an organic part and metals/metal oxides (Pt, Pd, Ni, Ru, Au, Ag, ZnO, Al_2O_3, SiO_2, and TiO_2) as an inorganic part (Fig. 1). The contrasting properties of these components enhance the characteristics of resulting hybrid molecules. More often organic components which are used to synthesize these nanohybrids are biocompatible, easily molded, and act as solid support for inorganic material resultantly, enhancing the electronic, magnetic, and catalytic properties of the inorganic material [2]. Organic–inorganic nanohybrids have a lot of applications in physics [3], polymer chemistry [4], and organic and inorganic chemistry [5]. The first type of these hybrid composites is prepared by dispersing Prussian blue

R. Akhtar · A. F. Zahoor (✉) · A. Mansha · K. G. Ali · B. Parveen
Department of Chemistry, Government College University Faisalabad, Faisalabad 38000, Pakistan
e-mail: fawad.zahoor@gcuf.edu.pk

S. Ahmad
Department of Chemistry, University of Engineering and Technology Lahore, Faisalabad Campus, Faisalabad 38000, Pakistan

M. Irfan
Department of Pharmaceutics, Government College University Faisalabad, Faisalabad 38000, Pakistan

K. Rizwan et al. (eds.), *Hybrid Nanomaterials*, Materials Horizons: From Nature to Nanomaterials, https://doi.org/10.1007/978-981-19-4538-0_17

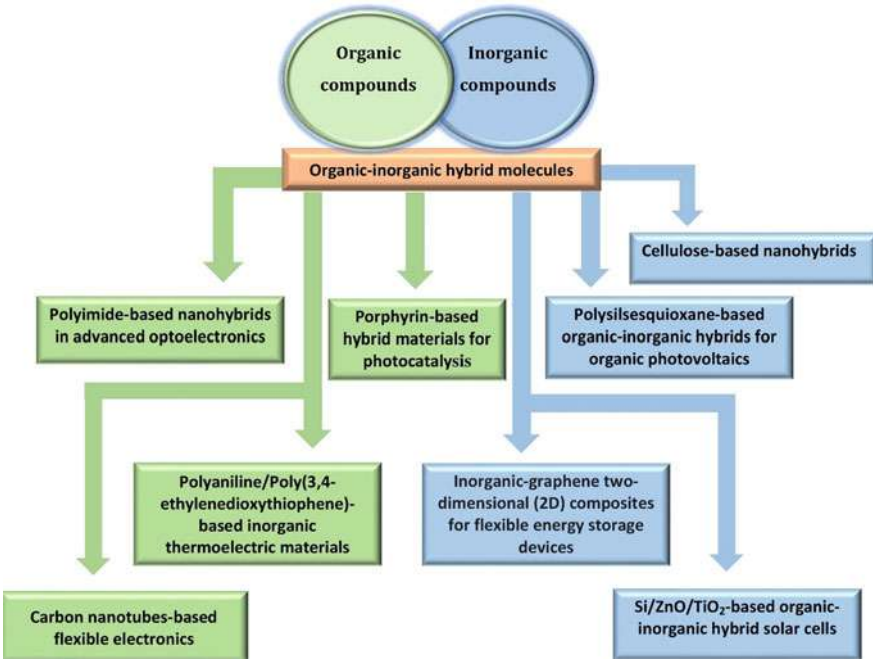

Fig. 1 Various organic–inorganic nanohybrids

(iron(III) hexacyanoferrate) in organic solvents. However, the concept of preparation and utilization of organic–inorganic hybrids in nanotechnology and life sciences has been advanced in 1980s [6].

Flexible electronic devices have been widely used in energy storage and sensor systems due to their flexibility and biocompatibility. Moreover, their easy fabrication and lightweight properties have raised their demand for medical devices and portable electronics [7, 8]. Currently, different flexible electronic devices are made up of organic–inorganic compounds, e.g., carbon materials [9], metal oxides [10], and polymers [11] which significantly improve the efficacy of these devices. However, the growing use of these flexible devices in our daily life gives a considerable challenge to scientists for making advancements in these devices regarding materials and fabrication.

2 Classification of Organic–Inorganic Nanohybrids

According to the nature of organic–inorganic material, these hybrids can be classified into two groups.

Class I

In class I hybrid compounds, weak physical interaction is present. Organic and inorganic materials are immersed with each other by van der Waals, electrostatic forces, or hydrogen bonding. Specific functional groups on organic and inorganic surfaces restrict the separation of these components in an inhomogeneous phase [12]. Different metal oxides embedded with a thin layer of nanostructures surrounded by polymer matrix belong to this class of compounds which have wide applications in biosensors [13], photocatalysis [14], and optoelectronics [15].

Class II

Class II hybrid materials are composed of chemical bonding of organic and inorganic compounds. Two different functional groups such as metal to carbon links and alkoxy groups are present on the building blocks of this class [16]. Perovskites, metal–organic frameworks (MOF), and bimetallic organophosphate oxides are the prominent examples of class II hybrids which are widely used in batteries [17], filtration [18], and hydrophilic and hydrophobic materials [16].

3 Synthesis of Organic–Inorganic Nanohybrids

3.1 Sol–Gel and Solvothermal Approaches

Among a variety of synthetic approaches for the preparation of organic–inorganic hybrid materials, sol–gel is a quite simple and low-temperature process that forms a colloidal suspension of the inorganic component in an organic solvent. These components are trapped within organic solvent via hydrogen bonds or van der Waals interactions [19]. Compounds synthesized via this approach are efficiently used in electrolytes, biosensors, corrosion protection, etc. Similar to the sol–gel protocol, organic–inorganic hybrids can also be synthesized by solvothermal method. This technique uses solubility of the organic and inorganic compounds in a solvent at high temperature (100–1000 °C) and pressure (1–10,000 atm), following crystallization of nanostructure from the solvent [20].

3.2 (Self) Assembly Approach

Conversion of a disordered system's components to an ordered pattern via local or non-covalent interactions between its components is called the self-assembly method. To control hybrid materials on a meso-, or nanoscopic scale, this spontaneous self-assembly approach can be used to induce unique physical and chemical characteristics to the hybrid molecules. This versatile synthetic method is often represented as legochemistry and finds extensive applications in biosensors and biomedical sciences, etc. [21].

3.3 Supramolecular Template Approach

The supramolecular template method is a quick and easy approach for preparing organic–inorganic nanohybrids within the pores of a microporous membrane or template. This methodology typically involves the usage of inorganic material with preorganized nanostructures and assembling of organic matrix on the surface of the inorganic solid [22].

3.4 Combination Approach

This integrative synthesis of organic–inorganic nanohybrids combines all the above-discussed synthetic approaches and involves micro-modeling methods which allow the development of hierarchically organized nanomaterials [23].

4 Applications of Organic/Inorganic Nanohybrids

4.1 Inorganic-Graphene Two-Dimensional (2D) Composites for Flexible Energy Storage Devices

Graphene which is made up of hexagonally arranged carbon atoms is a transparent material. It finds extensive applications in electronics due to its unique characteristics such as high thermal and electrical conductivity and high flexibility and resistance. However, its inert behavior toward functionalization is a major drawback that limits its use. Till now, a lot of data has been published for the preparation of graphene derivatives with different organic and inorganic scaffolds. Particular attention has been made to synthesizing inorganic-graphene derivatives due to the compatibility of inorganic materials with graphene [24]. More often, these hybrids can be prepared by using graphene oxide (synthesized by oxidizing graphite with ozone/strong acid)

as a substrate on which the oxygenated functional group imparts distinctive characteristics in the graphene oxide (GO). This polar oxygen group enhances the functionalization property of graphene and increases its dispersion in different types of solvents [25, 26]. This phenomenon makes it a good candidate for the construction of conductive thin film electrodes (obtained via depositing GO stable dispersion on different materials). Moreover, the electrochemical efficacy of graphene oxide can be enhanced in energy storage devices by these polar groups which easily absorb electrolyte ions and capture various electrochemical active species. For the preparation of inorganic-graphene derivatives, chemical vapor deposition (CVD) approach is used. For example, carbon nanotube [27] and cadmium selenide [28] can be grown on graphene via this approach. To attain two-dimensional hybrid molecules, integrate inorganic composites such as metal oxides on the surface of graphene by simply mixing both materials with subsequent heat treatment [29]. In another approach, metal-reduced graphene oxide (rGO) hybrid materials are obtained by using an anode made up of graphene oxide on which metal ions are reduced photochemically [30].

4.2 Inorganic-Graphene Two-Dimensional Composites for Flexible Supercapacitors

Flexible electrochemical capacitors have gained significant importance in electronic papers, implantable medical devices, etc., because of their mechanical stability and flexibility in all bending states [31]. Besides these characteristics chemical stability, high conductivities, and large surface areas should be the significant features of these devices. To impart these properties in devices, two-dimensional graphene-based thin films play an important role. However, the efficacy of these films is depriving day by day as a result of certain drawbacks such as aggregation and restacking of graphene in fabrication. Literature study reveals that various inorganic-graphene 2D hybrid materials significantly decrease the aggregation process and increase the electrolyte ions transportation [32, 33]. Few examples which highlight the importance of inorganic-graphene 2D hybrids are presented here:

Carbon nanotubes linked with reduced graphene oxide were developed by Jung et al. which can transport a volumetric capacitance of 165 F cm^{-3} [34]. Similarly, flexible capacitors based upon β-$Ni(OH)_2$-graphene thin films were synthesized by Xie et al. and can show 660.8 F cm^{-3} volumetric capacitance [35]. An ultrathin two-dimensional manganese dioxide-based graphene hybrid [36], molybdenum disulfide-graphene materials [37], and graphite oxide films [38] are the other examples of inorganic-graphene hybrids that can be used efficiently for flexible supercapacitors.

4.3 Inorganic-Graphene Two-Dimensional Composites for Flexible Lithium-Ion Batteries

The main difference between electrochemical capacitors (ECs) and batteries is their energy densities which are 4–10 Wh kg^{-1} in the case of ECs and 30–150 Wh kg^{-1} for batteries. When electricity is supplied to the battery, an oxidation–reduction reaction takes place which transforms reactants of high energy into low energy products. The free energy difference is considered as the electric energy supplied to external circuit. To increase the power densities of batteries especially lithium-ion batteries which are extensively used in laptops and mobiles, two-dimensional nanomaterials play a significant role due to their high surface area and shortened lithium-ion transport path. Several 2D nanohybrids have been synthesized in this regard in which graphene-inorganic hybrids are placed at a prominent position which not only enhance electrical conductivity but also prevent the accumulation of supported materials. Some highlighted examples include

- Wang et al. reported SiNW@G-rGO electrodes which show capacitance of ≈1600 mAh g^{-1} at the current density of 2.1 A g^{-1} [39].
- Zhao et al. synthesized graphite (EG)-based paper with Co_3O_4 nanoparticles as an anode which exhibits reversible capacity: 103 mAh g^{-1} at a current density of 1000 mA g^{-1} [40].
- Li et al. synthesized three-dimensional interconnected $LiFePO_4$-graphene (GF) as cathode and $Li_4Ti_5O_{12}$-GF as an anode which show discharge capacity and energy density 143 mAh g^{-1} at 0.2 C and 110 Wh kg^{-1}, respectively [41].
- Xiong et al. reported two-dimensional $ZnMn_2O_4$-graphene (ZMO-G) as anode and $LiFePO_4$ (LFPO) nanosheet as a cathode which display capacitance 69 mAh g^{-1} at 5 C and 58 mAh g^{-1} at 10 C rates [42].

4.4 Inorganic-Graphene Two-Dimensional Composites for Flexible Lithium-Sulfur Batteries

Increasing demand for high energy storage devices, lithium-sulfur batteries insert a valuable place in electrical gadgets. These batteries provided 2567 Wh kg^{-1} energy densities which are 8 times greater than C/$LiCoO_2$ batteries (387 Wh kg^{-1}) [43]. Moreover, sulfur shows environmentally friendly behavior and is available at a low cost. Besides these significant characteristics, their use is limited due to certain drawbacks such as:

- Electrical conductivity is low in these batteries, therefore utilizing less active sulfur and showing poor rate capability.
- Quick decay of capacity in these batteries which destroys the structural stability of cathodes and anodes is a major disadvantage. This happens due to the volume change between sulfur and lithium sulfide.

- Deposition of Li_2S_2/Li_2S layer on the surface of the electrodes blocks the ions transportation; resultantly, these batteries display poor Coulombic efficiency and low cyclic capacity [44, 45].

To overcome these problems, sulfur is implanted in conducting polymers [46] and porous carbon materials [47] by adopting different protocols. Two-dimensional sulfur-graphene materials have prime importance in this regard due to efficient capability of graphene to capture polysulfides (which deposit Li_2S_2/Li_2S layer) increasing the electrical conductivity of the electrodes. A number of graphene-based sulfur electrodes have been developed by various researchers which can display capacitance of $\approx$1000 mAh g^{-1}. For example,

- Sulfur electrode loaded on a graphene current collector—reported by Zhou et al. [48]
- Graphene-based layered structure with sulfur impregnation—reported by Yang et al. [49]
- Self-supporting graphene-sulfur paper electrode—reported by Jin et al. [50].

4.5 Inorganic-Graphene Two-Dimensional Composites for Flexible Sodium-Ion Batteries

0.86 gA h^{-1} electrochemical equivalent, −2.71 V redox potential, and inexhaustible sodium resources make sodium a suitable candidate for replacement of lithium-ion batteries which (lithium) is rare and thereof expensive for portable devices. On the other side, graphene hybrids play a vital role in sodium-ion batteries which assist sodium-ion transportation and show the highest reversible capacitance of $\approx$400 mAh g^{-1} when the current density is 100 mA g^{-1} as reported by Zhang et al. This electrochemical efficacy was attained by constructing Sb-rGO as anode and $Na_3V_2(PO_4)_3$-rGO as a cathode [51]. Similarly, electrodes made up of MoS_2, and rGO flakes exhibit a capacitance of 240 mAh g^{-1} when the current density is 25 mA g^{-1} [52].

4.6 Carbon Nanotubes in Flexible Electronic Devices

Carbon nanotubes first described by Iijima [53] are made up of graphene sheets and can be characterized as single-walled, double-walled, or multi-walled according to the wrapping of the graphene sheets. The excellent flexible nature of carbon nanotubes, great charge carrier ability, and ultrathin structure of these nanotubes make them a suitable candidate for flexible electronic devices. Besides these unique characteristics, a large effort has been focused to functionalize CNTs with different organic and inorganic materials [54]. For instance, Lipomi et al. synthesized polydimethylsiloxane (PDMS)-based single-walled carbon nanotubes (SWCNTs) to construct

such types of conductors which provide stable conductivity even after 10,000 cycles of stretching with 25% strains [55]. Peng et al. modified CNTs with manganese dioxide and used them to construct planar supercapacitor with excellent performance [36]. Later on, Kim et al. used SWCNT/zinc tin oxide (ZTO) hybrid materials to attain the fastest ring oscillator [56]. Lee et al. provided 4.1% power conversion efficiency (PCE) of solar cells by dispersing boron-doped multi-walled carbon nanotubes on fullerene-polymer active layer [57]. On the other side, Chaudhary et al. suggested that incorporating SWCNTs at the appropriate position in polymer-fullerene solar cells provided 4.9% PCE [58].

4.7 Porphyrin-Based Hybrid Materials for Photocatalytic Applications

Porphyrins and their hybrids have emerged as important building blocks for various electronic devices due to their significant photophysical, photochemical, electrochemical, and optoelectronic properties [59]. Moreover, these hybrids find extensive applications in solar panels because of the good absorption abilities of porphyrins. A variety of methods have been described to form porphyrin nanohybrids in various literature reports. For example:

- Surfactant-assisted self-assembly (SAS) method [60]
- Sonication-assisted assembly method [61]
- Ionic self-assembly [62]
- Vaporization–condensation–recrystallization (VCR) organization [63]
- Coordination polymerization [64]
- Reprecipitation [65–67].

In recent years, photocatalytic applications of porphyrins are broadly studied, and it was found that as-obtained porphyrins do not perform well charge-transfer functions. To solve this problem, different organic–inorganic nanohybrids have been designed enhancing solar energy conversion properties in resulting hybrid materials. Metal-porphyrin hybrid composites especially those made up of platinum and gold are on the top of the list in this regard because of the excellent optical and electric characteristics of the metallic nanoparticles. Some highlighted examples are presented in Table 1.

Table 1 Metal/metal oxide-porphyrin nanohybrids

S. No.	Nanohybrids	References
1.	Pt-porphyrin nanohybrids	Wang et al. [68]
2.	Zn(II) and Sn(IV)-porphyrin nanohybrids	Tian et al. [69]
3.	Au-porphyrin nanohybrids	Kotiaho et al. [70]
4.	TiO_2-porphyrin nanohybrids	Huang et al. [71]
5.	Pt/TiO_2-porphyrin nanohybrids	Hasobe et al. [72]

4.8 Polyimide-Based Nanohybrids in Advanced Optoelectronics

Polyimides having imide groups have been widely used as high-performance plastics owing to their significant thermal stability and excellent chemical and mechanical properties. A major part of these polymers is utilized in microelectronics, fuel cells, spacecraft, and heat-resistant materials [73]. In contrast, on a commercial scale, the usage of these polymers is limited because these polymers require high processing temperature, and their solubility in organic solvents is poor. The rigid, semicrystalline, and planar hetero-aromatic skeleton of these polymers, high dielectric constant, and strong absorption in the UV–Vis region are the major drawbacks of polyimides that limit their use [74].

To overcome these problems, functionalization of polyimides (Table 2) with different organic/inorganic materials is an effective technique to attain unique characteristics in resulting nanohybrids such as:

- Controlled thermo-optical property
- High polarizing property
- High thermal conductivity.

Table 2 Metal oxide-polyimide nanohybrids

S. No.	Nanohybrids	Properties	References
1.	Zinc oxide-polyimide nanohybrids	High thermal conductivity	Yorifuji and Ando [75]
2.	Silicon dioxide-polyimide nanohybrids	High thermal stability and high transparency	Gao et al. [76] Qiu et al. [77]
3.	Polyimide films having silver nanoparticles	High thermal diffusivity	Yorifuji and Ando [78]
4.	Sulfur-containing polyimide-Titanium dioxide nanohybrids	High refractive index	Liu et al. [79]

4.9 Cellulose-Based Nanohybrids

Cellulose which is made up of glucose units through glycosidic linkage when combined with metals or metal oxides provides a vast opportunity to attain flexible electronic materials. Cellulose nanocrystals themselves induce unique characteristics in capacitors and many other electronic devices such as fast charging capability, and excellent power density as a result of their high strength and flexible nature. There is a significant role of fast charging devices in energy storage processes which save energy and release it during the acceleration process. Considering the importance of cellulose nanocrystals and their hybrids, a lot of data has been reported on their synthesis by a different era of chemists. For example, Chu et al. combined the intrinsic properties of photonic cellulose nanocrystals with plasmonic silver [80] and gold nanoparticles [81] by self-coassembly of substrates which put a great impact on ultrasensitive spectroscopies and data storage devices. By decoration of gold nanoparticles with cellulose nanocrystals grafted on graphene sheets, resulting hybrids were obtained with excellent catalytic activity as reported by Wang et al. [82]. Similarly, incorporation of different metal oxides such as zinc oxide, silicon dioxide, titanium dioxide, and aluminum oxide/iron(III) oxide on cellulose nanocrystals gave hybrid materials with significant thermal stability as described by Goikuria et al. [83]. Later on, by the research group of Martakov [84] and Xue et al. [85], cellulose nanocrystals with TiO_2 were synthesized to achieve promising catalytic properties in desired nanohybrid materials.

4.10 Polysilsesquioxane-Based Organic–Inorganic Hybrids for Organic Photovoltaics

In the past few years, considerable attention has been devoted to the construction of organo-silicon hybrids (e.g., siloxane, silsesquioxanes, and silicones) with organic semiconductors to improve the efficacy of these semiconductors in various electronic devices such as organic light-emitting diodes, fuel cells, organic field-effect transistors, and optical and thermoelectric devices [86–88]. Among various organo-silicon structures, the polysilsesquioxane family has a significant place due to the functional tenability, rigidity, and thermal stability of the silica core. Polyhedral oligomeric silsesquioxane (POSS), a subfamily of polysilsesquioxane, has different reactive sites (1–8) at silicon peaks that can be incorporated in a variety of dendrimers and hyperbranched polymers to construct hybrid materials for electronic devices [89]. In 2004, Sellinger and Laine [90] significantly used POSS inserted hybrid materials in organic light-emitting diodes (OLEDs). From then, various advancements in the functionalization of silsesquioxane with conjugated polymers have been reported for enhancing quantum efficiencies, brightness, solubility, and color stability of the

resulting hybrids. Besides this, silsesquioxanes are tailored onto light-emitting conjugated polymers to increase the lifetime of devices by decreasing the energy trapping and aggregation processes [91, 92].

4.11 Organic–Inorganic Hybrids for Flexible Thermoelectric Devices

A lot of research has been focused on the construction of thermoelectric materials due to the increasing demand for thermoelectric devices which convert waste heat into electricity. Different examples around us depict that a little amount of energy is utilized of the total process while the remaining is wasted in the environment. Such as ~34% of energy is effectively used by the combustion of fossil fuel [93] and ~25% of energy is utilized for vehicles by the combustion of fuel [94]. For the usage of remaining waste heat for different purposes, thermoelectric materials play a significant part. Since the discovery of bismuth telluride and lead telluride-based thermoelectric materials in 1950, various data has been reported to construct advanced thermoelectric materials as compared to the traditional materials which were expansive and made up of toxic elements [95]. To improve the efficacy of flexible thermoelectric devices, different organic/inorganic hybrid materials have been used in which thermoelectric characteristics of various polymers, e.g., polyaniline (PANI), poly(3,4-ethylenedioxythiophene) (PEDOT), etc., are combined with high electrical conductive inorganic and carbon materials.

4.12 Polyaniline-Based Inorganic Thermoelectric Materials

Despite the significant conducting properties of polyaniline, its lower power factor (10^{-6} W/mK) as compared to inorganic materials has diverted the attention of scientists to synthesize various polyaniline-based inorganic materials. Some of these types of literature examples are highlighted in Table 3.

Table 3 PANI-inorganic nanocomposites

S. No.	Nanohybrids	References
1.	Polyaniline-TiO_2 hybrid materials	Debnath et al. [96]
2.	Polyaniline-NiO hybrid materials	Sarkar et al. [97]
3.	Polyaniline-reduced graphene oxide hybrid materials	Islam et al. [98]
4.	Polyaniline-Bi_2Te_3 hybrid materials	Toshima et al. [99]
5.	Polyaniline-Pt and Au hybrid materials	Toshima et al. [100]

4.13 Poly(3,4-Ethylenedioxythiophene) (PEDOT)-Inorganic Thermoelectric Nanomaterials

Despite some salient features of poly(3,4-ethylenedioxythiophene) polymer such as excellent electrical conductivity, environmental and thermal stability, low thermal conductivity, and low density, their limited use in electrical devices is due to their poor solvent solubility. Therefore, they are often used with polystyrene sulfonate (PSS). To improve the characteristics of PEDOT:PSS, these polymers are combined with different metals and organic materials.

Some examples are given below:

- PEDOT:PSS protected silver, gold, and palladium nanoparticles [101]
- PEDOT:PSS with gallium zinc oxide nanoparticles [102]
- PEDOT:PSS films having poly(*N*-vinyl-2-pyrrolidone)-based germanium dioxide nanoparticles [103]
- PEDOT:PSS-stannous sulfide nanocomposites [104]
- PEDOT:PSS-SnSe nanomaterials [105]
- PEDOT-PbTe nanotubes [106]
- PEDOT:PSS-SiO_2 nanomaterials [107]
- PEDOT:PSS-Bi_2S_3 nanomaterials [108].

5 Organic–Inorganic Materials for Solar Cells

Solar cells are well-known semiconductors used to convert solar energy into electricity. They are worked on a similar principle as computer memory cards and are usually made up of silicon. Silicon-based solar cells belong to the first generation of solar cells and give 18–25% power conversion efficiencies. However, to make up the low cost with high power conversion efficiencies, second (copper indium gallium selenide solar cells) and third generations of solar cells (organic, organic–inorganic, and dye-sensitized solar cells) are manufactured (Fig. 2). Nowadays, organic–inorganic solar cells that belong to the third generation place a prominent position in the market because of their hybrid characteristics, e.g., stability, excellent carrier mobility (adopted from inorganic part), efficient solution processability, and improved light absorption properties (adopted from organic part) [109, 110]. Some of the examples of these types of solar cells are listed here.

5.1 Silicon-Based Organic–Inorganic Hybrid Solar Cells

Silicon has been widely used in different types of solar cells, and hybrid molecules made up of silicon usually show 10% power conversion efficiencies [111]. An example of organic–inorganic hybrid material synthesized by the combination of

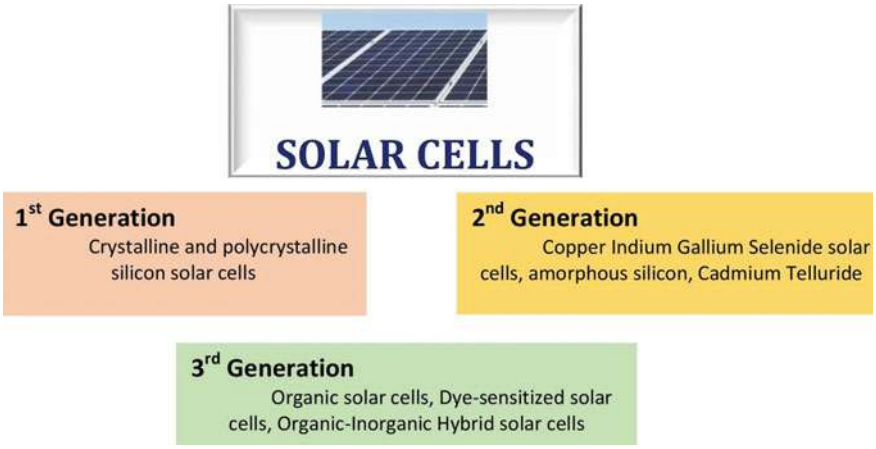

Fig. 2 Classification of solar cells

PEDOT:PSS films and silicon displays the highest power conversion efficiency (PCE) 11.3% [112].

5.2 Zinc Oxide-Based Organic–Inorganic Hybrid Solar Cells

Zinc oxide is stable in air, shows excellent light transmittance property, and thereof has been used with organic molecules in solar cells [113]. Solar cells which are constructed by using zinc oxide-based graphene sheets display PCE of 1.55% [114]. However, by the usage of ZnO-plastic sheets-based hybrid materials in solar cells, 3.11% PCE can be obtained [115]. By combining poly(3-hexylthiophene) with zinc oxide and antimony trisulphide, the resulting hybrid solar cell shows 2.4% PCE [116]. On the other hand, zinc oxide nanowires increase PCE to 2.9% [117].

5.3 Titanium Dioxide-Based Organic–Inorganic Hybrid Solar Cells

Titanium dioxide has become popular in photovoltaic because of its stability in chemical environments and non-toxic nature. Besides this, it is available in market at a low cost and gives significant photoelectric conversion efficiency. TiO_2 nanowires, nanocrystals, and nanorods exhibit excellent photocatalytic activity and have been used in dye-sensitized and heteroconjuction solar cells. An overview of these types of hybrids is depicted in Table 4.

Table 4 TiO_2-based hybrid solar cells

S. No.	Nanohybrids	Power conversion efficiency	References
1.	TiO_2-PEDOT nanohybrid	0.09%	Dehaudt et al. [118]
2.	Poly 2-methoxy-5-(2 ethylhexyloxy)-1,4-phenylenevinylene (MEH-PPV)-TiO_2	0.038–0.063%	Atienzar et al. [119]
3.	TiO_2-poly(octylthiophene) nanohybrid	0.048% (when brookite mesoporous material used) and 0.74% (when anatase mesoporous material used)	Lancelle-Beltran et al. [120]
4.	Manganese-doped TiO_2-phenylC61-butyric acid methyl ester:Poly(3-hexylthiophene) hybrid	2.44%	Alparslan et al. [121]
5.	F8T2/SFT2-TiO_2 hybrid materials	0.05% (in case of F8T2) and 0.01% (in case of SFT2)	Jo et al. [122]

6 Conclusion

Day by day, the increasing demand for flexible electronics attracts our attention to construct these types of gadgets with excellent performance. For the construction of these devices, organic–inorganic hybrid materials play a significant role which imparts distinctive characteristics of both organic and inorganic materials in required electrical devices such as chemical stability, high conductivities, and large surface areas. Therefore, extensive effort has been made by the researchers to synthesize these types of nanocomposites in the past few years. In this chapter, we highlighted some of these organic–inorganic nanohybrids and their applications in various flexible electronic devices. Hopefully, this data provides facile information for the researchers to put more effort in this field for the enhancement of electrical conductivity of flexible electronic devices at a low cost.

References

1. Baig N, Kammakakam I, Falath W (2021) Nanomaterials: a review of synthesis methods, properties, recent progress, and challenges. Mater Adv 2(6):1821–1871
2. Sanchez C, Julián B, Belleville P, Popall M (2005) Applications of hybrid organic–inorganic nanocomposites. J Mater Chem 15(35–36):3559–3592
3. Wang MS, Xu G, Zhang ZJ, Guo GC (2010) Inorganic-organic hybrid photochromic materials. Chem Commun 46(3):361–376

4. Kango S, Kalia S, Celli A, Njuguna J, Habibi Y, Kumar R (2013) Surface modification of inorganic nanoparticles for development of organic–inorganic nanocomposites—a review. Prog Polym Sci 38(8):1232–1261
5. Furukawa H, Cordova KE, O'Keeffe M, Yaghi OM (2013) The chemistry and applications of metal-organic frameworks. Science 341(6149):1230444
6. Faustini M, Nicole L, Ruiz-Hitzky E, Sanchez C (2018) History of organic–inorganic hybrid materials: prehistory, art, science, and advanced applications. Adv Func Mater 28(27):1704158
7. Lee SH, Jeong CK, Hwang GT, Lee KJ (2015) Self-powered flexible inorganic electronic system. Nano Energy 14:111–125
8. Fan FR, Tang W, Wang ZL (2016) Flexible nanogenerators for energy harvesting and self-powered electronics. Adv Mater 28(22):4283–4305
9. Wang L, Jackman JA, Ng WB, Cho NJ (2016) Flexible, graphene-coated biocomposite for highly sensitive, real-time molecular detection. Adv Funct Mater 26(47):8623–8630
10. Zhu L, Wang L, Xue F, Chen L, Fu J, Feng X, Li T, Wang ZL (2017) Piezo-phototronic effect enhanced flexible solar cells based on *n*-ZnO/*p*-SnS core-shell nanowire array. Adv Sci 4(1):1600185
11. Oh JY, Kim S, Baik HK, Jeong U (2016) Conducting polymer dough for deformable electronics. Adv Mater 28(22):4455–4461
12. Sanchez C, Soler-Illia GDA, Ribot F, Lalot T, Mayer CR, Cabuil V (2001) Designed hybrid organic–inorganic nanocomposites from functional nanobuilding blocks. Chem Mater 13(10):3061–3083
13. Viter R, Savchuk M, Iatsunskyi I, Pietralik Z, Starodub N, Shpyrka N, Ramanaviciene A, Ramanavicius A (2018) Analytical, thermodynamical and kinetic characteristics of photoluminescence immunosensor for the determination of Ochratoxin A. Biosens Bioelectron 99:237–243
14. Pavlenko M, Coy EL, Jancelewicz M, Załęski K, Smyntyna V, Jurga S, Iatsunskyi I (2016) Enhancement of optical and mechanical properties of Si nanopillars by ALD TiO_2 coating. RSC Adv 6(99):97070–97076
15. Sessolo M, Bolink HJ (2011) Hybrid organic–inorganic light-emitting diodes. Adv Mater 23(16):1829–1845
16. Judeinstein P, Sanchez C (1996) Hybrid organic–inorganic materials: a land of multidisciplinarity. J Mater Chem 6(4):511–525
17. Sun C, Liu J, Gong Y, Wilkinson DP, Zhang J (2017) Recent advances in all- solid-state rechargeable lithium batteries. Nano Energy 33:363–386
18. Arkas M, Allabashi R, Tsiourvas D, Mattausch EM, Perfler R (2006) Organic/inorganic hybrid filters based on dendritic and cyclodextrin "nanosponges" for the removal of organic pollutants from water. Environ Sci Technol 40(8):2771–2777
19. Manocha LM, Yasuda E, Tanabe Y, Manocha S, Vashistha D (2000) Sol–gel processing of carbidic glasses. Bull Mater Sci 23(1):1–4
20. Forster PM, Thomas PM, Cheetham AK (2002) Biphasic solvothermal synthesis: a new approach for hybrid inorganic-organic materials. Chem Mater 14(1):17–20
21. Shen M, Shi X (2010) Dendrimer-based organic/inorganic hybrid nanoparticles in biomedical applications. Nanoscale 2(9):1596–1610
22. Fattahi P, Yang G, Kim G, Abidian MR (2014) A review of organic and inorganic biomaterials for neural interfaces. Adv Mater 26(12):1846–1885
23. Xue J, Wu T, Dai Y, Xia Y (2019) Electrospinning and electrospun nanofibers: Methods, materials, and applications. Chem Rev 119(8):5298–5415
24. Gao N, Fang X (2015) Synthesis and development of graphene-inorganic semiconductor nanocomposites. Chem Rev 115(16):8294–8343
25. Chen D, Feng H, Li J (2012) Graphene oxide: preparation, functionalization, and electrochemical applications. Chem Rev 112(11):6027–6053
26. Paredes JI, Villar-Rodil S, Martínez-Alonso A, Tascon JMD (2008) Graphene oxide dispersions in organic solvents. Langmuir 24(19):10560–10564

27. Zhao MQ, Liu XF, Zhang Q, Tian GL, Huang JQ, Zhu W, Wei F (2012) Graphene/single-walled carbon nanotube hybrids: one-step catalytic growth and applications for high-rate Li-S batteries. ACS Nano 6(12):10759–10769
28. Kim YT, Shin HW, Ko YS, Ahn TK, Kwon YU (2013) Synthesis of a CdSe-graphene hybrid composed of CdSe quantum dot arrays directly grown on CVD-graphene and its ultrafast carrier dynamics. Nanoscale 5(4):1483–1488
29. Zhang LS, Jiang LY, Yan HJ, Wang WD, Wang W, Song WG, Guo YG, Wan LJ (2010) Mono dispersed SnO_2 nanoparticles on both sides of single layer graphene sheets as anode materials in Li-ion batteries. J Mater Chem 20(26):5462–5467
30. Pasricha R, Gupta S, Joshi AG, Bahadur N, Haranath D, Sood KN, Singh S, Singh S (2012) Directed nanoparticle reduction on graphene. Mater Today 15(3):118–125
31. Bae S, Kim H, Lee Y, Xu X, Park JS, Zheng Y, Iijima S (2010) Roll-to-roll production of 30-inch graphene films for transparent electrodes. Nat Nanotechnol 5(8):574–578
32. Shao Y, El-Kady MF, Wang LJ, Zhang Q, Li Y, Wang H, Mousavi MF, Kaner RB (2015) Graphene-based materials for flexible supercapacitors. Chem Soc Rev 44(11):3639–3665
33. Mao M, Hu J, Liu H (2015) Graphene-based materials for flexible electrochemical energy storage. Int J Energy Res 39(6):727–740
34. Jung N, Kwon S, Lee D, Yoon DM, Park YM, Benayad A, Choi Y, Park JS (2013) Synthesis of chemically bonded graphene/carbon nanotube composites and their application in large volumetric capacitance supercapacitors. Adv Mater 25(47):6854–6858
35. Xie J, Sun X, Zhang N, Xu K, Zhou M, Xie Y (2013) Layer-by-layer β-$Ni(OH)_2$/graphene nanohybrids for ultraflexible all-solid-state thin-film supercapacitors with high electrochemical performance. Nano Energy 2(1):65–74
36. Peng L, Peng X, Liu B, Wu C, Xie Y, Yu G (2013) Ultrathin two-dimensional MnO_2/graphene hybrid nanostructures for high-performance, flexible planar supercapacitors. Nano Lett 13(5):2151–2157
37. Bissett MA, Kinloch IA, Dryfe RA (2015) Characterization of MoS_2-graphene composites for high-performance coin cell supercapacitors. ACS Appl Mater Interfaces 7(31):17388–17398
38. El-Kady MF, Kaner RB (2013) Scalable fabrication of high-power graphene micro-supercapacitors for flexible and on-chip energy storage. Nat Commun 4(1):1–9
39. Wang B, Li X, Zhang X, Luo B, Jin M, Liang M, Dayeh SA, Picraux ST, Zhi L (2013) Adaptable silicon-carbon nanocables sandwiched between reduced graphene oxide sheets as lithium ion battery anodes. ACS Nano 7(2):1437–1445
40. Zhao Y, Ma C, Li Y, Chen H, Shao Z (2015) Self-adhesive Co_3O_4/expanded graphite paper as high-performance flexible anode for Li-ion batteries. Carbon 95:494–496
41. Li N, Chen Z, Ren W, Li F, Cheng HM (2012) Flexible graphene-based lithium ion batteries with ultrafast charge and discharge rates. Proc Natl Acad Sci 109(43):17360–17365
42. Xiong P, Peng L, Chen D, Zhao Y, Wang X, Yu G (2015) Two-dimensional nanosheets based Li-ion full batteries with high rate capability and flexibility. Nano Energy 12:816–823
43. Manthiram A, Fu Y, Chung SH, Zu C, Su YS (2014) Rechargeable lithium-sulfur batteries. Chem Rev 114(23):11751–11787
44. Manthiram A, Chung SH, Zu C (2015) Lithium-sulfur batteries: progress and prospects. Adv Mater 27(12):1980–2006
45. Ji X, Nazar LF (2010) Advances in Li-S batteries. J Mater Chem 20(44):9821–9826
46. Yin L, Wang J, Yang J, Nuli Y (2011) A novel pyrolyzed polyacrylonitrile-sulfur@MWCNT composite cathode material for high-rate rechargeable lithium/sulfur batteries. J Mater Chem 21(19):6807–6810
47. Li Z, Zhang J, Lou XW (2015) Hollow carbon nanofibers filled with MnO_2 nanosheets as efficient sulfur hosts for lithium-sulfur batteries. Angew Chem 127(44):13078–13082
48. Zhou G, Pei S, Li L, Wang DW, Wang S, Huang K, Cheng HM et al (2014) Batteries: a graphene-pure-sulfur sandwich structure for ultrafast, long-life lithium-sulfur batteries. Adv Mater 26(4):664–664
49. Yang X, Zhang L, Zhang F, Huang Y, Chen Y (2014) Sulfur-infiltrated graphene-based layered porous carbon cathodes for high-performance lithium-sulfur batteries. ACS Nano 8(5):5208–5215

50. Jin J, Wen Z, Ma G, Lu Y, Cui Y, Wu M, Liang X, Wu X (2013) Flexible self- supporting graphene-sulfur paper for lithium sulfur batteries. RSC Adv 3(8):2558–2560
51. Zhang W, Liu Y, Chen C, Li Z, Huang Y, Hu X (2015) Flexible and binder-free electrodes of Sb/rGO and Na_3V_2 $(PO_4)_3$/rGO nanocomposites for sodium-ion batteries. Small 11(31):3822–3829
52. David L, Bhandavat R, Singh G (2014) MoS_2/graphene composite paper for sodium-ion battery electrodes. ACS Nano 8(2):1759–1770
53. Iijima S (1991) Helical microtubules of graphitic carbon. Nature 354(6348):56–58
54. Peng LM (2018) A new stage for flexible nanotube devices. Nat Electron 1(3):158–159
55. Lipomi DJ, Vosgueritchian M, Tee BC, Hellstrom SL, Lee JA, Fox CH, Bao Z (2011) Skin-like pressure and strain sensors based on transparent elastic films of carbon nanotubes. Nat Nanotechnol 6(12):788–792
56. Kim B, Jang S, Geier ML, Prabhumirashi PL, Hersam MC, Dodabalapur A (2014) High-speed, inkjet-printed carbon nanotube/zinc tin oxide hybrid complementary ring oscillators. Nano Lett 14(6):3683–3687
57. Lee JM, Park JS, Lee SH, Kim H, Yoo S, Kim SO (2011) Selective electron-or hole-transport enhancement in bulk-heterojunction organic solar cells with N- or B-doped carbon nanotubes. Adv Mater 23(5):629–633
58. Chaudhary S, Lu H, Müller AM, Bardeen CJ, Ozkan M (2007) Hierarchical placement and associated optoelectronic impact of carbon nanotubes in polymer-fullerene solar cells. Nano Lett 7(7):1973–1979
59. Drain CM, Varotto A, Radivojevic I (2009) Self-organized porphyrinic materials. Chem Rev 109(5):1630–1658
60. Guo P, Chen P, Liu M (2012) Porphyrin assemblies via a surfactant-assisted method: from nanospheres to nanofibers with tunable length. Langmuir 28(44):15482–15490
61. Atula SD (2008) Sonication-assisted supramolecular nanorods of meso-diaryl-substituted porphyrins. Chem Commun 6:724–726
62. Wang Z, Medforth CJ, Shelnutt JA (2004) Porphyrin nanotubes by ionic self-assembly. J Am Chem Soc 126(49):15954–15955
63. Yoon SM, Hwang IC, Kim KS, Choi HC (2009) Synthesis of single-crystal tetra (4-pyridyl) porphyrin rectangular nanotubes in the vapor phase. Angew Chem Int Ed 48(14):2506–2509
64. Wang Z, Lybarger LE, Wang W, Medforth CJ, Miller JE, Shelnutt JA (2008) Monodisperse porphyrin nanospheres synthesized by coordination polymerization. Nanotechnology 19(39):395604
65. Lee SJ, Hupp JT, Nguyen ST (2008) Growth of narrowly dispersed porphyrin nanowires and their hierarchical assembly into macroscopic columns. J Am Chem Soc 130(30):9632–9633
66. Lee SJ, Malliakas CD, Kanatzidis MG, Hupp JT, Nguyen ST (2008) Amphiphilic porphyrin nanocrystals: Morphology tuning and hierarchical assembly. Adv Mater 20(18):3543–3549
67. Hu JS, Guo YG, Liang HP, Wan LJ, Jiang L (2005) Three-dimensional self-organization of supramolecular self-assembled porphyrin hollow hexagonal nanoprisms. J Am Chem Soc 127(48):17090–17095
68. Wang Z, Li Z, Medforth CJ, Shelnutt JA (2007) Self-assembly and self-metallization of porphyrin nanosheets. J Am Chem Soc 129(9):2440–2441
69. Tian Y, Martin KE, Shelnutt JYT, Evans L, Busani T, Miller JE, Medforth CJ, Shelnutt JA (2011) Morphological families of self-assembled porphyrin structures and their photosensitization of hydrogen generation. Chem Commun 47(21):6069–6071
70. Kotiaho A, Lahtinen RM, Tkachenko NV, Efimov A, Kira A, Imahori H, Lemmetyinen H (2007) Gold nanoparticle enhanced charge transfer in thin film assemblies of porphyrin-fullerene dyads. Langmuir 23(26):13117–13125
71. Huang CC, Parasuraman PS, Tsai HC, Jhu JJ, Imae T (2014) Synthesis and characterization of porphyrin-TiO_2 core-shell nanoparticles as visible light photocatalyst. RSC Adv 4(13):6540–6544

72. Hasobe T, Sakai H, Mase K, Ohkubo K, Fukuzumi S (2013) Remarkable enhancement of photocatalytic hydrogen evolution efficiency utilizing an internal cavity of supramolecular porphyrin hexagonal nanocylinders under visible-light irradiation. J Phys Chem C 117(9):4441–4449
73. Nam KH, Choi HK, Yeo H, You NH, Ku BC, Yu J (2018) Molecular design and property prediction of sterically confined polyimides for thermally stable and transparent materials. Polymers 10(6):630
74. Eastmond GC, Paprotny J, Pethrick RA, Santamaria-Mendia F (2006) A comparison of poly (ether imide) s with 3-phthalimide and 4-phthalimide units: synthesis, characterization, and physical properties. Macromolecules 39(22):7534–7548
75. Yorifuji D, Ando S (2011) Enhanced thermal conductivity over percolation threshold in polyimide blend films containing ZnO nano-pyramidal particles: advantage of vertical double percolation structure. J Mater Chem 21(12):4402–4407
76. Gao H, Yorifuji D, Jiang Z, Ando S (2014) Thermal and optical properties of hyperbranched fluorinated polyimide/mesoporous SiO_2 nanocomposites exhibiting high transparency and reduced thermo-optical coefficients. Polymer 55(12):2848–2855
77. Qiu F, Da Z, Yang D, Cao G, Li P (2008) The synthesis and electro-optic properties of polyimide/silica hybrids containing the benzothiazole chromophore. Dyes Pigm 77(3):564–569
78. Yorifuji D, Ando S (2010) Enhanced thermal diffusivity by vertical double percolation structures in polyimide blend films containing silver nanoparticles. Macromol Chem Phys 211(19):2118–2124
79. Liu JG, Nakamura Y, Ogura T, Shibasaki Y, Ando S, Ueda M (2008) Optically transparent sulfur-containing polyimide-TiO_2 nanocomposite films with high refractive index and negative pattern formation from poly (amic acid)-TiO_2 nanocomposite film. Chem Mater 20(1):273–281
80. Chu G, Yin H, Jiang H, Qu D, Shi Y, Ding D, Xu Y (2016) Ultrafast optical modulation of rationally engineered photonic-plasmonic coupling in self-assembled nanocrystalline cellulose/silver hybrid material. J Phys Chem C 120(48):27541–27547
81. Chu G, Wang X, Yin H, Shi Y, Jiang H, Chen T, Gao J, Qu D, Xu Y, Ding D (2015) Free-standing optically switchable chiral plasmonic photonic crystal based on self-assembled cellulose nanorods and gold nanoparticles. ACS Appl Mater Interfaces 7(39):21797–21806
82. Wang Y, Zhang H, Lin X, Chen S, Jiang Z, Wang J, Huang J, Zhang F, Li H (2018) Naked Au nanoparticles monodispersed onto multifunctional cellulose nanocrystal-graphene hybrid sheets: towards efficient and sustainable heterogeneous catalysts. New J Chem 42(3):2197–2203
83. Goikuria U, Larranaga A, Vilas JL, Lizundia E (2017) Thermal stability increase in metallic nanoparticles-loaded cellulose nanocrystal nanocomposites. Carbohyd Polym 171:193–201
84. Martakov IS, Torlopov MA, Mikhaylov VI, Krivoshapkina EF, Silant'ev VE, Krivoshapkin PV (2018) Interaction of cellulose nanocrystals with titanium dioxide and peculiarities of hybrid structures formation. J Sol-Gel Sci Technol 88(1):13–21
85. Xue J, Song F, Yin XW, Zhang ZL, Liu Y, Wang XL, Wang YZ (2017) Cellulose nanocrystal-templated synthesis of mesoporous TiO_2 with dominantly exposed (001) facets for efficient catalysis. ACS Sustain Chem Eng 5(5):3721–3725
86. Tchinda AJ, Ngameni E, Kenfack IT, Walcarius A (2009) One-step preparation of thiol-functionalized porous clay heterostructures: application to Hg(II) binding and characterization of mass transport issues. Chem Mater 21(18):4111–4121
87. Arkhireeva A, Hay JN, Oware W (2005) A versatile route to silsesquioxane nanoparticles from organically modified silane precursors. J Non-Cryst Solids 351(19–20):1688–1695
88. Shea KJ, Loy DA (2001) Bridged polysilsesquioxanes. Molecular-engineered hybrid organic–inorganic materials. Chem Mater 13(10):3306–3319
89. Leu CM, Chang YT, Wei KH (2003) Polyimide-side-chain tethered polyhedral oligomeric silsesquioxane nanocomposites for low-dielectric film applications. Chem Mater 15(19):3721–3727

90. Sellinger A, Tamaki R, Laine RM, Ueno K, Tanabe H, Williams E, Jabbour GE (2004) Solution processable nanocomposites based on silsesquioxane cores for use in organic light emitting diodes (OLEDs). MRS Online Proc Lib (OPL) 847
91. Xiao S, Nguyen M, Gong X, Cao Y, Wu H, Moses D, Heeger AJ (2003) Stabilization of semiconducting polymers with silsesquioxane. Adv Func Mater 13(1):25–29
92. Chan KL, Sonar P, Sellinger A (2009) Cubic silsesquioxanes for use in solution processable organic light emitting diodes (OLED). J Mater Chem 19(48):9103–9120
93. Ovik R, Long BD, Barma MC, Riaz M, Sabri MFM, Said SM, Saidur R (2016) A review on nanostructures of high-temperature thermoelectric materials for waste heat recovery. Renew Sustain Energy Rev 64:635–659
94. Yang J, Stabler FR (2009) Automotive applications of thermoelectric materials. J Electron Mater 38(7):1245
95. He J, Tritt TM (2017) Advances in thermoelectric materials research: looking back and moving forward. Science, 357(6358):eaak9997
96. Debnath A, Deb K, Sarkar K, Saha B (2020) Improved thermoelectric performance in TiO_2 incorporated polyaniline: a polymer-based hybrid material for thermoelectric generators. J Electron Mater 49(8):5028–5036
97. Sarkar K, Debnath A, Deb K, Bera A, Saha B (2019) Effect of NiO incorporation in charge transport of polyaniline: improved polymer based thermoelectric generator. Energy 177:203–210
98. Islam R, Chan-Yu-King R, Brun JF, Gors C, Addad A, Depriester M, Roussel F et al (2014) Transport and thermoelectric properties of polyaniline/reduced graphene oxide nanocomposites. Nanotechnology 25(47):475705
99. Toshima N, Imai M, Ichikawa S (2011) Organic–inorganic nanohybrids as novel thermoelectric materials: hybrids of polyaniline and bismuth(III) telluride nanoparticles. J Electron Mater 40(5):898–902
100. Toshima N (2013) Metal nanoparticles for energy conversion. Pure Appl Chem 85(2):437–451
101. Hata S, Omura T, Oshima K, Du Y, Shiraishi Y, Toshima N (2017) Novel Preparation of Poly (3, 4-ethylenedioxythiophene)-poly (styrenesulfonate)-protected noble metal nanoparticles as organic–inorganic hybrid thermoelectric materials. Bull Soc Photogr Imaging 27:13–18
102. Hata S, Taguchi K, Oshima K, Du Y, Shiraishi Y, Toshima N (2019) Preparation of Ga–ZnO nanoparticles using microwave and ultrasonic irradiation, and the application of poly(3,4-ethylenedioxythiophene)-poly (styrenesulfonate) hybrid thermoelectric films. ChemistrySelect 4(22):6800–6804
103. Shiraishi Y, Hata S, Okawauchi Y, Oshima K, Anno H, Toshima N (2017) Improved thermoelectric behavior of poly(3,4-ethylenedioxythiophene)-poly(styrenesulfonate) using poly(*n*-vinyl-2-pyrrolidone)-coated GeO_2 nanoparticles. Chem Lett 46(7):933–936
104. Cheng X, Wang L, Wang X, Chen G (2018) Flexible films of poly(3,4-ethylenedioxythiophene): poly(styrenesulfonate)/SnS nanobelt thermoelectric composites. Compos Sci Technol 155:247–251
105. Ju H, Kim J (2016) Chemically exfoliated SnSe nanosheets and their SnSe/poly(3,4-ethylenedioxythiophene): poly(styrenesulfonate) composite films for polymer based thermoelectric applications. ACS Nano 10(6):5730–5739
106. Wang Y, Cai K, Yao X (2011) Facile fabrication and thermoelectric properties of PbTe-modified poly(3,4-ethylenedioxythiophene) nanotubes. ACS Appl Mater Interfaces 3(4):1163–1166
107. Liu E, Liu C, Zhu Z, Xu J, Jiang F, Wang T, Li C (2017) Preparation of poly(3,4-ethylenedioxythiophene): poly(4-styrenesulfonate)/silicon dioxide nanoparticles composite films with large thermoelectric power factor. J Compos Mater 52:621–627
108. Wang YY, Cai KF, Yao X (2012) One-pot fabrication and enhanced thermoelectric properties of poly(3,4-ethylenedioxythiophene)-Bi_2S_3 nanocomposites. J Nanopart Res 14(5):1–7
109. Green MA, Emery K, King DL, Igari S, Warta W (2001) Solar cell efficiency tables (version 18). Prog Photovolt 9(4):287–293

110. He M, Qiu F, Lin Z (2013) Toward high-performance organic–inorganic hybrid solar cells: bringing conjugated polymers and inorganic nanocrystals in close contact. J Phys Chem Lett 4(11):1788–1796
111. Kalita G, Adhikari S, Aryal HR, Afre R, Soga T, Sharon M, Umeno M (2009) Silicon nanowire array/polymer hybrid solar cell incorporating carbon nanotubes. J Phys D Appl Phys 42(11):115104
112. Liu Q, Ono M, Tang Z, Ishikawa R, Ueno K, Shirai H (2012) Highly efficient crystalline silicon/zonyl fluorosurfactant-treated organic heterojunction solar cells. Appl Phys Lett 100(18):183901
113. Huang J, Yin Z, Zheng Q (2011) Applications of ZnO in organic and hybrid solar cells. Energy Environ Sci 4(10):3861–3877
114. Shin KS, Jo H, Shin HJ, Choi WM, Choi JY, Kim SW (2012) High quality graphene-semiconducting oxide heterostructure for inverted organic photovoltaics. J Mater Chem 22(26):13032–13038
115. Shin KS, Park HJ, Kumar B, Kim KK, Ihn SG, Kim SW (2011) Low- temperature growth and characterization of ZnO thin films for flexible inverted organic solar cells. J Mater Chem 21(33):12274–12279
116. Liu CP, Wang HE, Ng TW, Chen ZH, Zhang WF, Yan C, Jha SK (2012) Hybrid photovoltaic cells based on ZnO/Sb_2S_3/P3HT heterojunctions. Phys Status Solidi (b) 249(3):627–633
117. Liu CP, Chen ZH, Wang HE, Jha SK, Zhang WJ, Bello I, Zapien JA (2012) Enhanced performance by incorporation of zinc oxide nanowire array for organic–inorganic hybrid solar cells. Appl Phys Lett 100(24):243102
118. Dehaudt J, Beouch L, Peralta S, Plesse C, Aubert PH, Chevrot C, Goubard F (2011) Facile route to prepare film of poly(3,4-ethylene dioxythiophene)-TiO_2 nanohybrid for solar cell application. Thin Solid Films 519(6):1876–1881
119. Atienzar P, Ishwara T, Horie M, Durrant JR, Nelson J (2009) Hybrid polymer-metal oxide solar cells by in situ chemical polymerization. J Mater Chem 19(30):5377–5380
120. Lancelle-Beltran E, Prené P, Boscher C, Belleville P, Buvat P, Lambert S, Guillet F, Marcel C, Sanchez C (2008) Solid-state organic/inorganic hybrid solar cells based on poly (octylthiophene) and dye-sensitized nanobrookite and nanoanatase TiO_2 electrodes. Eur J Inorg Chem 2008(6):903–910
121. Alparslan Z, Kösemen A, Örnek O, Yerli Y, San SE (2011) TiO_2-based organic hybrid solar cells with Mn^{+2} doping. Int J Photoenergy
122. Jo J, Vak D, Noh YY, Kim SS, Lim B, Kim DY (2008) Effect of photo- and thermo-oxidative degradation on the performance of hybrid photovoltaic cells with a fluorene-based copolymer and nanocrystalline TiO_2. J Mater Chem 18(6):654–659

Chapter 18
Organic–Inorganic Nanohybrids for Light Harvesting Application

Syed Muhammad Ali Trimzi, Muhammad Wajahat Ali, Ataf Ali Altaf, and Samia Kausar

1 Solar Energy and Light Harvestation

Sunlight is the radiative light and heat from the sun that may be gathered in a number of ways, such as solar power generation, solar thermal, e.g., solar water heating, and solar architecture. Sunlight is the visible solar energy that reaches the Earth's surface. Nearly half of the radiation absorbed at Earth's surface is visible radiation which are the most plentiful source of energy is in the form of sunlight. It determines the amount of net primary output on the planet by boosting high-energy chemical processes that would otherwise go unnoticed [1]. Solar energy is expected to contribute a major portion of the world's energy demands over the next century; thus, researchers triggered to understand how to capture, transport, and store it effectively. Lot of research is going on to investigate and optimize both the effective collection of photon at a reactive site as well as the transmission of excitation energy in order to efficiently use energy gathered from sunshine to induce photochemical processes or to manufacture solar fuels. This would enable the creation of molecular "circuits" that can control, sort, and respond to excitation energy in complex ways [2].

Solar energy is one of the most appealing alternative energy sources. It is interesting to know that more solar energy reaches the Earth's surface in a minute as compare to the entire population of human beings uses it in a single year. The capacity to capture even a smaller percentage of this solar energy and to convert it into useable energy would be a highly appealing and maybe full answer to our ever-increasing energy demands. The current knowledge about the structure and the operation of conversion of solar energy by photosynthetic organisms into chemical energy has unlocked the doors to new potentials for developing novel solar devices

S. M. A. Trimzi · M. W. Ali · A. A. Altaf (✉)
Department of Chemistry, University of Okara, Okara, Pakistan
e-mail: atafali_altaf@yahoo.com

S. Kausar
Department of Chemistry, University of Gujrat, Hafiz Hayat Campus, Gujrat 50700, Pakistan

K. Rizwan et al. (eds.), *Hybrid Nanomaterials*, Materials Horizons: From Nature to Nanomaterials, https://doi.org/10.1007/978-981-19-4538-0_18

Fig. 1 Solar energy output of a photovoltaic system

(Fig. 1) either by mimicking biology or by combining mechanical and biological systems in hybrid devices [3].

These efforts have been supported by significant advancement in the use of x-ray crystallography to discover the structure of proteins involved in photosynthesis. Many of these, such as pigment positions and alignments, as well as their bonding inside protein frameworks, are now known with greater than 5 Å precision [4]. This understanding is crucial for deciphering spectroscopic data collected on these structures with precision and accuracy. Because many of the processes in photosynthesis, such as light harvesting and charge separation, are carried out by protein complexes smaller than 100 nm, assembling them into hybrid devices necessitates nano-scale control and agility, as well as the development of ways to probe interactions within such small constructs. These possibilities have been opened up by the chemical production of nanostructures and their biological conjugation, as well as the ongoing advancement of nanotechnology techniques [2].

2 Materials for Light Harvesting Applications

Using light-capturing materials, photochemical reactions convert sunlight into chemical energy. The complexes and pigments present in plants as well as some photosynthetic microbes for light harvestation serve as inspiration for the development of light harvesting materials [5]. The active antenna complexes observed in photosynthetic organisms have stirred synthetic light collecting materials which emulate light absorption equipment in the biological systems. Synthetic light harvesting materials include dendrimer, porphyrin array and assemblies, organic gels, bio- and synthetic peptides, organic–inorganic hybrid compounds, and semiconductor materials like non-oxides, oxynitrides, and oxysulfides. Synthetic and bio-synthetic light harvesting materials can help with photovoltaic, photocatalysis, and photopolymerization.

2.1 Dendrimers

The development of supramolecular molecules which may operate like antenna complexes in synthetic photosynthetic-related applications has been a major emphasis since the late 1990s most of them are artificially generated antennas termed as dendrimers (Fig. 2) [6, 7]. Dendritic molecular structures for light harvestation are designed to feature a large number of donor chromophores which are light collecting in nature and convey energy to a dendrimer's energy "sink." When the number of terminal groups functioning as donor chromophores doubles, then the distance between terminal groups and energy acceptor core also doubles, reducing their energy transfer effectiveness. Dendrimers can include a huge amount of chromophoric compounds like coumarin-related donor chromophores, in highly ordered arrays to promote efficient energy transfer. Dendrimer molecules' cores (energy acceptors) can be modified using porphyrins, fullerenes, and metal complexes. A perylene-based core and the dendrimer branches made out of coumarin units have been found to achieve near 99% of energy transfer efficiencies in some dendrimer systems.

A light harvesting complex is made up of chromophores, which are complex component proteins that are sometimes part of a larger giant complex of a photosystem, which is the functional unit of photosynthesis. Plants and photosynthetic

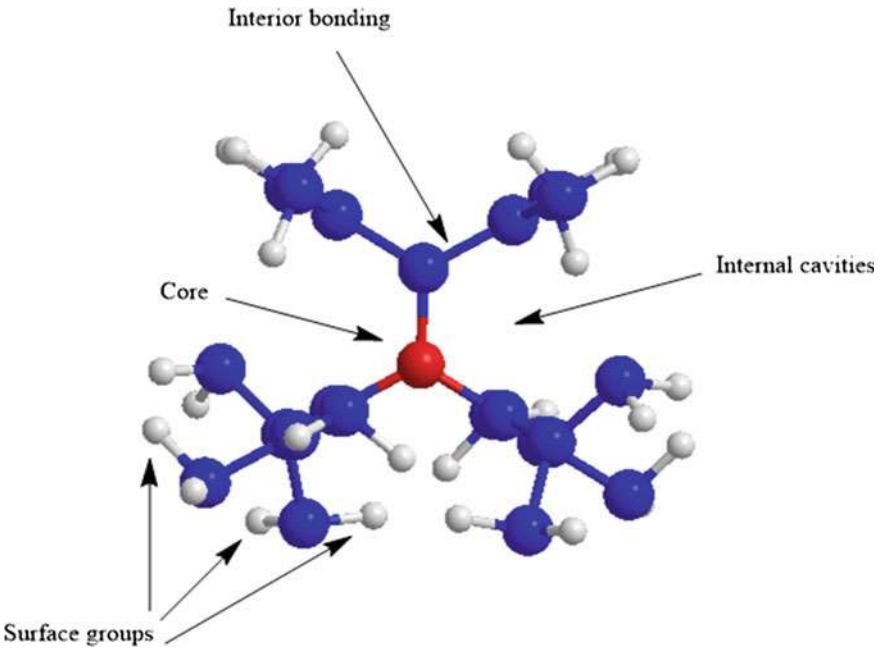

Fig. 2 Basic structure of dendrimers

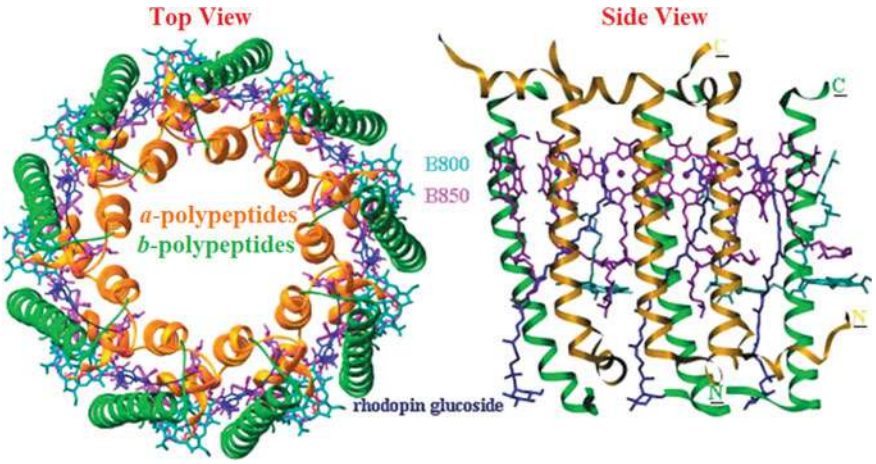

Fig. 3 Structure of the LH2 complex from *Rps. acidophila* strain 10,050, Reproduced with permission from [9] (Copyright 2001 American Chemical Society)

microorganisms use it to gather much of the incoming light than the photosynthetic reaction center as shown in Fig. 3 [8].

2.2 Biomaterials

Proteins in natural light harvesting complexes self-assemble with operational donor chromophores to enhance light harvestation and transfer of energy during photosynthetic processes. Synthetic peptides with optoelectronic properties are probable to be designed to imitate this phenomenon present in natural light harvesting complexes. PPC proteins not only enhance arrangement of chromophores through light harvesting but they also actively participate in the photophysical subtleties of photosynthesis. Certain biomimetic-based artificially generated light harvesting complexes along with proteins and peptides assemble themselves in such a way that chromophores in complex are positioned for maximum light harvestation. Peptide-based self-assemblies and polypeptides modified with porphyrin rings have been fabricated to do both charge separation and light harvestation. Other peptide-based donor and acceptor chromophoric conjugates rely on the self-assembly of amyloid fibrils into a beta sheet to finely adjust the chromophores for efficient light harvesting. One form of biological material employed in the artificial light harvesting-based systems is synthetic peptides and proteins [10]. Triad molecules having porphyrin for light harvestation and charge separation and porphyrin, carotenoid, and fullerene-based triad and porphyrin, ferrocene, and fullerene are shown in Fig. 4 [11].

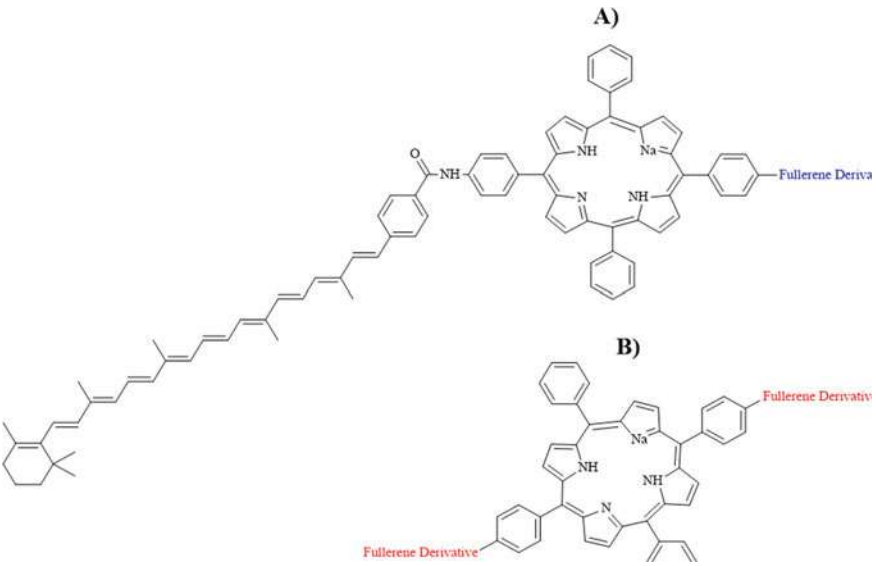

Fig. 4 Triad molecules having porphyrin for light harvestation and charge separation: **a** Porphyrin, carotenoid, and fullerene-based triad, **b** porphyrin, ferrocene and fullerene

2.3 Organic and Inorganic Hybrids (OIHs)

The interface of organic–inorganic molecules is a critical characteristic which affects the efficacy of the light harvesting devices due to incorporation of materials like organic–inorganic hybrid perovskites and metal–organic frameworks (MOFs). Lead-halide perovskite materials have excellent photophysical properties and can be used in optoelectronic applications. In general, halide-based perovskite materials have good optical absorption properties and facilitate charge transfer, indicating that they most probably can be used for photovoltaic-related and solar energy conversion. MOFs with solar light collecting capabilities may be made using a variety of synthetic approaches, such as using porphyrin-containing strut or metallo-porphyrins as the fundamental organic building blocks. MOFs can also be activated and functionalized by incorporating photosensitive ruthenium or osmium complexes within the structure, or by utilizing quantum dots to modify the surface. Basic classification of organic–inorganic hybrids is shown in Fig. 5 [12].

2.4 Nanohybrids

A nanohybrid is the chemical bonding of two nanoparticles, whereas a nanocomposite is the incorporation of a nanomaterial to a matrix, such as a polymer, which is not a nanomaterial in and of itself [13, 14]. There are two main classes of nanohybrids as

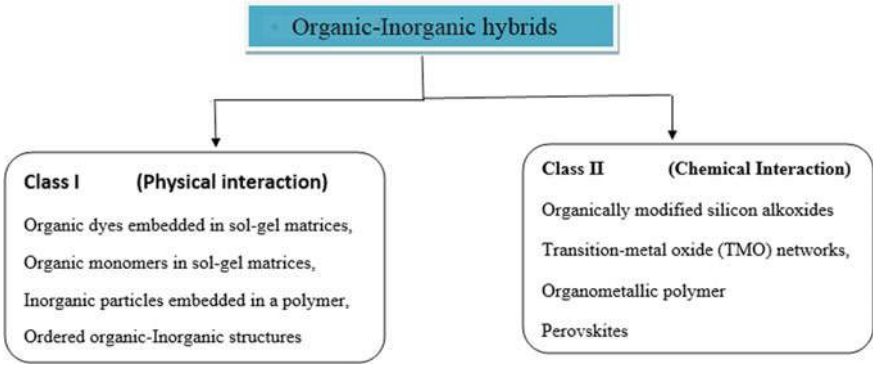

Fig. 5 Basic classification of OIHs

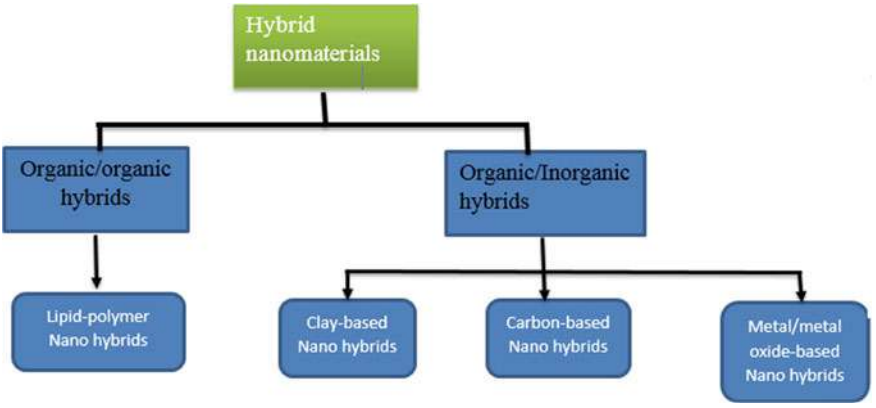

Fig. 6 Basic classification of nanohybrid materials

organic–inorganic hybrids and organic–organic nanohybrids as shown in Fig. 6 [15]. As the basic components of organic–organic NHs, basic carbon nanomaterials such as single-walled and multi-walled nanotubes (SWNTs and MWNTs), fullerenes, and graphene sheets are coupled with other carbonaceous units to form hierarchical structures. Metal/metal NHs, clay-based NHs, and carbon-based NHs are the three forms of organic/inorganic hybrids [13].

2.5 Organic/Inorganic Nanohybrids (OINHs)

OINHs are nanocomposites with finely blended organic (biological) and inorganic networks. On the other hand, O-I hybrid nanomaterials are more likely to have well-structured assemblies at the molecular scale, with minimum one element at

nanoscales, both an organic or inorganic element (100 nm) [16]. Surprisingly, the final characteristics of OINHs nanomaterials might be attributed to either the sum of the individual intact molecules or the considerable synergy created by the nanohybrid interface. The architectural style, design, consistency, morphological, and chemical characteristics of O-I hybrid nanomaterials are impacted not only by the synthesized circumstances, such as the preparation methods, pH, temperature, contact time, and so on, but also by the number and proportion of organic and inorganic networks. O-I hybrid nanoparticles hold a lot of promise for developing high-performance customized components for a wide range of applications [17].

2.5.1 Types of Organic/Inorganic NHs

Organic/inorganic NHs have two types of classes which based on bonding [16]. Hybrid systems in which the organic and inorganic components interact by weak interactions, such as van der Waals, hydrogen bonds, or electrostatic bonds, are classified as Class I, as shown in Fig. 7. Hybrid materials in which the organic and inorganic components are joined by covalent or iono-covalent chemical bonds are classified as Class II. Of course, many hybrid materials have both strongly and weakly bound organo-mineral interfaces, but due to the significance of strong chemical bonds on the final hybrid material's characteristics, this type of hybrid will also be categorized as Class II [18].

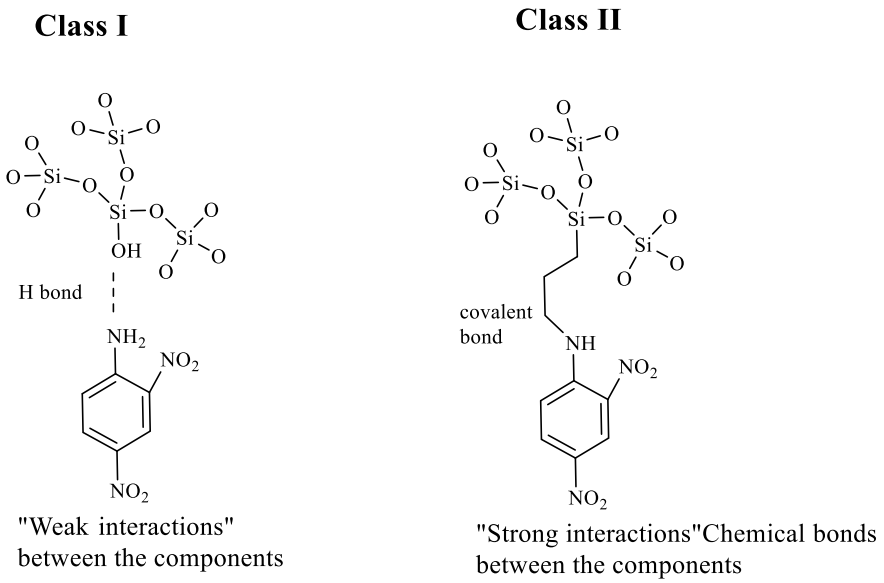

Fig. 7 Classification of OINHs

3 Applications of OINHs for Light Harvesting

3.1 Development of PP-TiO_2 Light Harvesting OINHs for Photocatalysis

As per reports of Prasenjit et al., light harvesting nanohybrids are more efficient for photovoltaic and photocatalysis applications due to the synergetic effect of numerous parameters such as surface area, hierarchical structure, rapid photo-induced charge separation, and comparably delayed charge recombination. The suggested PPTiO_2 light harvesting nanohybrid is particularly effective for methylene blue degradation in the presence of Cu (II) ion species that are engaged in the decomposition process. When H_2O_2 is present, the generation of OH increases when exposed to solar light, which improves the photocatalytic activity of (Cu) PP-TiO_2 for MB degradation. This finding supports the theory that reactive oxygen species (ROS) are involved in MB breakdown. According to research, when N_2 bubbles in the solution, the photodegradation efficiency of (Cu) PP-TiO_2 is lowered. According to the findings, O_2 works primarily as an electron trap during photocatalytic processes, causing O_2 radicals to form. The sensitizer (PP) injects electrons into TiO_2's conduction band (CB) under visible light irradiation, and CB electrons transfer to MB via reactive oxygen species, causing MB to degrade (ROS). Photocatalyst photocorrosion and photochemical stability are particularly important factors to consider when assessing their application performance, as they can significantly reduce the cost of the process during photocatalytic operations. Recycling tests were carried out under repeated irradiation to further evaluate the photocatalytic activity of the generated nanohybrids. The photocatalytic activity of many nanohybrids is shown in Fig. 8 over time. The results reveal that after four cycles, the photodegradation efficiency of the CuPP-TiO_2 rate does not change much, indicating that the catalyst is the most stable under

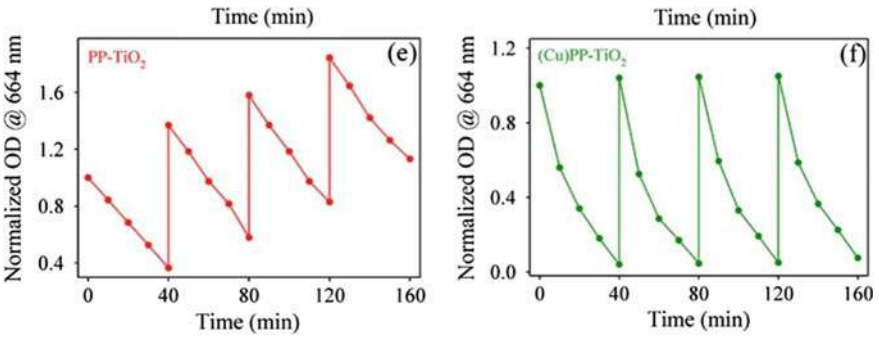

Fig. 8 CuPP-TiO_2 degradation of methylene blue under sunlight irradiation (shown by the red line); MB Degradation by PP-TiO_2 under visible light exposure (represented by green line), Reproduced with permission from [19] (Copyright 2017 Elsevier)

MB photodegradation. The photocatalytic activity, on the other hand, dropped by 30% after four cycles (PP-TiO_2) [19].

The (Cu)PP-TiO_2 nanohybrids particularly effective photocatalysis might be attributed to the extra structural stability provided by the copper ion within the PP moiety. The findings further show that CuPP-TiO_2 is a highly stable photocatalyst that may be used in practical applications [20]. The photocurrent generated by a solar cell is affected by the light harvesting ability of a sensitizer, which is a fundamental characteristic that controls the ability of solar energy capture. Photodegradation of the model organic contaminant MB during visible light irradiation was used to assess the photocatalytic activity of the nanohybrids. As illustrated in following equation, MB creates the colorless product leuco-methylene blue (LMB) [21] during the photocatalytic process.

$$2\text{MB} + 2e^- + H^+ \rightarrow \text{MB} + \text{LMB}$$

Because of the efficient energy or charge transfer mechanism, inorganic–organic semiconductor hybrid nanostructures remain a frontier field of research for designing optoelectronic, photovoltaic, and light harvesting devices.

3.2 Integration of Porphyrin Molecules into QD Doped PVK Nanoparticles for Energy Transfer

Sadananda et al. reported that inorganic–organic semiconducting nanocrystals ($Cd_{0.52}Zn_{0.48}S$) are enclosed in semiconducting organic poly (9-vinylcarbazole) [PVK] nanoparticles with the 5- (4-aminophenyl)-10,15,20-triphenyl-21,23H-porphyrin (APTPP) molecule. A steady-state and time-resolved spectroscopic research reveals a cascade energy transfer from the host PVK nanoparticle to the QD and prophyrin molecule. By integrating porphyrin molecules into QD doped PVK nanoparticles, energy transfer improves from 68 to 86%. Because of the great efficiency of cascade energy transfer, novel porphyrin and quantum dot-based functional polymer nanoparticles may be designed for use in efficient light harvesting systems and other photodriven devices. Absorption and emission spectrum of alloy QD ($Cd_{0.52}Zn_{0.48}S$) is shown in Fig. 9.

In an inorganic–organic hybrid system, CdTe QDs operate as an antenna, transferring exaction to a Nile red acceptor encapsulated in PMMA polymer nanoparticles. PVK [poly (9-vinylcarbazole)] is a non-conjugated semiconducting molecule that can encapsulate porphyrin molecules, hydrophobic dyes, and other small organic molecules in aqueous media, making it a useful non-conjugated semiconducting molecule for creating stable nanoparticles in aqueous media. Because of their excellent electrochemical structural, photophysical, and self-assembly capabilities, porphyrin molecules have been discovered to be employed for effective photodynamic therapeutic and light harvesting applications.

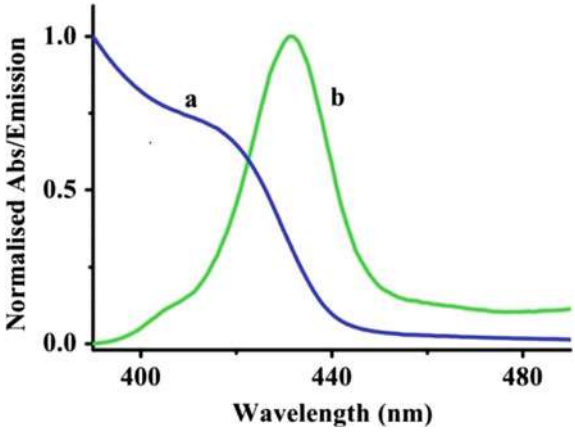

Fig. 9 Absorption and emission spectrum of alloy QD ($Cd_{0.52}Zn_{0.48}S$). Reproduced with permission from [22] (Copyright 2016 Elsevier)

PVK nanoparticles were made using the re-precipitation process previously described. PVK were dissolved in dried THF to sustain a 1.0 mg/ml PVK concentration. Before ultrasonic assisted treatment for 15 min, a 500 mL volume of this THF solution was forcefully agitated for 10–15 min in 10 mL double distilled water. The outcome was an aqueous solution of PVK nanoparticles. To keep the PVK nanoparticles from aging, THF was removed from the aqueous phase by partial vacuum evaporation for 1 h and then filtered through a 0.2 mm filter paper. Prepare a three- to four-day PVK nanoparticles aqueous solution.

The QDs doped PVK nanoparticles were generated with the same re-precipitation method as the QDs doped PVK nanoparticles. In this case, the THF solutions of QDs and PVK were thoroughly mixed to keep the 3.5 mM concentration of QDs and the 1.0 mg/ml concentration of PVK, and then ultra-sonicated for 5 min to obtain a clear mixed solution [23]. After that, the THF solution was quickly introduced into double distilled water with vigorous shaking for 10–15 min, followed by ultrasonication, vacuum evaporation, and filtration through 0.2 mm filter paper as per standard procedures. Finally, a PVK NP solution doped with QDs was created. UV–Vis Spectra of PVK nanoparticles and QDs doped PVK NP is shown in Fig. 10 [22]

3.3 Photodegradation of Azo Dyes Through Polyoxometalates (POMs)

Anne Dolbeeq et al. reported the photocatalytic azo dye degradation utilizing polyoxometalate-based materials [24]. The latest advances in the polyoxometalates (POMs) and their assemblies that meet numerous requirements are discussed. A summary of primary POM-based azo dye degradation processes shown in Fig. 11. Switch ability by visible light is one of these characteristics of the POMs, as it is the capability of photoreduction which is multi-electronic followed by reversible

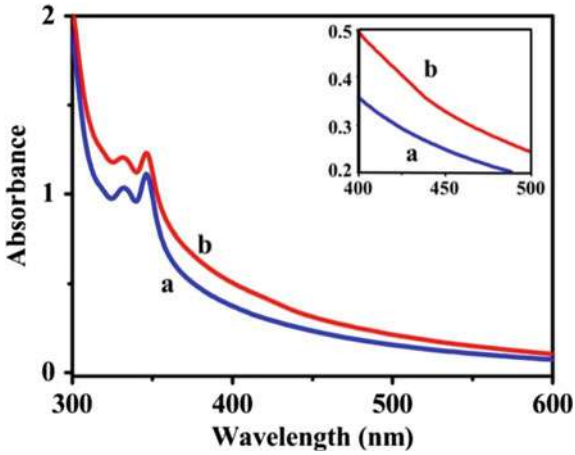

Fig. 10 UV–Vis Spectra of **a** PVK nanoparticles, **b** QDs doped PVK NP. Reproduce with permission from [22] (Copyright 2016 Elsevier)

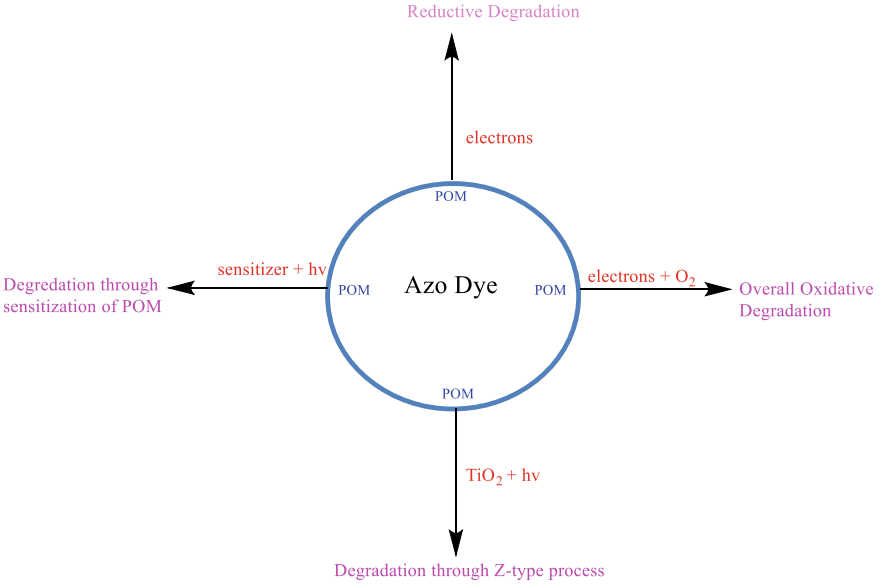

Fig. 11 Summary of primary POM-based azo dye degradation processes

electron exchange with the substrate, heterogenization without loss of attributes and cost effectiveness. This method is unique, and it has been proven to introduce new pathways for researching degradation of organic pollutants which includes azo dyes, that are near to green chemistry breakthroughs [25].

As per reports of Anne Dolbeeq et al. with a few exceptions, the majority of the instances in the following are based on a well-established chemical strategy including the intermediate synthesis of one-electron reduced POM (POM red). Exposing a

selected POM to radiation at its oxygen to metal charge transfer (OMCT) bands in the presence of an electron donor (substrate S) results in the formation of POM_{red} (reduced form) [24] and S is oxidized simultaneously according to a well-known reaction scheme:

S-POM precomplexation as:

$$POM + S \rightarrow (POM - S)(K) \tag{1}$$

Photo-based excitation of the POMS complex as:

$$(POM - S)(\lambda \leq 400\,nm) \rightarrow (POM - S)^* \tag{2}$$

Charge transfer and photoreduction of the POM:

$$(POM - S)^* \rightarrow (POM_{red}) + S^+ \tag{3}$$

Re-oxidation (re-generation) of the POM upon exposure to di-oxygen:

$$POM_{red} + O_2 \rightarrow POM + O^{2-} \tag{4}$$

Formation of the hydroperoxyl radical in acidic medium:

$$O^{2-} + H^+ \rightarrow HO^{2-} \tag{5}$$

The process results in the buildup of POM_{red}, which are well-characterized blue POM complexes, in the lack of an electron acceptor. When the one-electron reduced form of the POM is generated, there is no re-oxidation via H^+. It is been suggested that the energized POM (POM*) can react with organic substrate indirectly via OH^- in accordance with:

$$POM^* + H_2O \rightarrow POM_{red} + OH^- + H^+ \tag{6}$$

4 Conclusion

Some advanced research organic–inorganic nanohybrid materials for light harvesting applications was focused in this chapter. Lot of research was being carried out on materials use to convert light energy into useful output. Various synthetic scaffolds were investigated like dendrimer, porphyrin array and assemblies, organic gels, bio-based and synthetic peptides, organic–inorganic hybrid compounds to achieve the maximum light harvesting efficacies. The organic–inorganic interface was investigated owing to its synergy effect of many factors like surface area, hierarchical structure, and rapid photo-induced charge separation and relatively slow charge

recombination. Recent work on PP-TiO_2 materials as light harvesting OINHs for photocatalysis was reported. Photodegradation efficiency for the CuPP-TiO_2 rate show significant cycle stability after four cycles suggesting the catalyst's greatest stability for MB photodegrading. Porphyrin molecules were integrated into QD doped PVK nanoparticles for energy transfer. By integrating porphyrin molecules into QD doped PVK nanoparticles, energy transfer improves from 68 to 86%. High efficiency of cascade energy transfer, novel porphyrin may be designed for use in efficient light harvesting systems and other photo-driven devices. The polyoxometalates (POMs) were investigated to light degradation of azo dyes owing to switch ability by visible light followed by reversible electron exchange with a substrate, heterogenization without loss of attributes and cost effectiveness.

References

1. Jiang Y, McNeill JJCR (2017) Light-harvesting and amplified energy transfer in conjugated polymer nanoparticles. 117(2):838–859
2. Kundu S, Patra AJCr (2017) Nanoscale strategies for light harvesting. 117(2):712–757
3. Shrotriya V et al (2006) Efficient light harvesting in multiple-device stacked structure for polymer solar cells. 88(6):064104
4. Scholes GD et al (2011) Lessons from nature about solar light harvesting. 3(10):763–774
5. Mayr T et al (2009) Light harvesting as a simple and versatile way to enhance brightness of luminescent sensors. 81(15):6541–6545
6. Astruc D, Boisselier E, Ornelas CJCr (2010) Dendrimers designed for functions: from physical, photophysical, and supramolecular properties to applications in sensing, catalysis, molecular electronics, photonics, and nanomedicine. 110(4):1857–1959
7. Jain K et al (2010) Dendrimer toxicity: Let's meet the challenge. 394(1–2):122–142
8. Fassioli F et al (2014) Photosynthetic light harvesting: excitons and coherence. 11(92):20130901
9. van Grondelle R, Novoderezhkin V (2001) Dynamics of excitation energy transfer in the LH1 and LH2 light-harvesting complexes of photosynthetic bacteria. Biochemistry 40(50):15057–15068
10. Ihssen J et al (2014) Light harvesting proteins for solar fuel generation in bioengineered photoelectrochemical cells. 15(4):374–384
11. Hashimoto H et al (2015) Natural and artificial light-harvesting systems utilizing the functions of carotenoids. 25:46–70
12. Silina YE et al (2020) Application of organic-inorganic hybrids in chemical analysis, bio-and environmental monitoring. 10(4):1458
13. García MC, Uberman PM (2019) Nanohybrid filler-based drug-delivery system. Nanocarriers for drug delivery. Elsevier, pp 43–79
14. Shakeel A et al (2022) Advanced polymeric/inorganic nanohybrids: an integrated platform for gas sensing applications. Chemosphere 294:133772
15. Aich N et al (2014) A critical review of nanohybrids: synthesis, applications and environmental implications. 11(6):609–623
16. Semenova D, Silina YEJN (2019) The role of nanoanalytics in the development of organic-inorganic nanohybrids—seeing nanomaterials as they are. 9(12):1673
17. Liu C-H et al (2012) Making organic-inorganic nanocomposites via selective dispersion of PS-tethered SiO_2 particles in polystyrene-block-polymethylmethacrylate copolymer
18. Faustini M et al (2018) History of organic–inorganic hybrid materials: prehistory, art, science, and advanced applications. 28(27):1704158

19. Kar P et al (2017) Can a light harvesting material be always common in photocatalytic and photovoltaic applications? 200:70–77
20. Kar P et al (2014) Impact of metal ions in porphyrin-based applied materials for visible-light photocatalysis: key information from ultrafast electronic spectroscopy. 20(33):10475–10483
21. Kar P et al (2015) Nano surface engineering of Mn_2O_3 for potential light-harvesting application. 3(31):8200–8211
22. Mandal S et al (2016) A ternary system of quantum dot–Porphyrin–Semiconducting organic nanoparticles for light harvesting. 222:76–83
23. Bhattacharyya S et al (2012) Energy/hole transfer phenomena in hybrid α-Sexithiophene (α-STH) nanoparticle–CdTe quantum-dot nanocomposites. 13(18):4155–4162
24. Dolbecq A et al (2012) Polyoxometalate-based materials for efficient solar and visible light harvesting: application to the photocatalytic degradation of azo dyes. 22(47):24509–24521
25. Dong H et al (2020) Self-assembly hydrothermal synthesis of Silverton-type polyoxometalate-based photocatalysts for enhanced degradation. 2020. 36(16):4454–4464

Chapter 19
Organic–Inorganic Nanohybrids as Thermoelectric Materials

Muhammad Ayyaz, Noor-ul-Huda Altaf, Mohsin Khan, Ambreen Ashar, Sehrish Maqsood, Muhammad Yasin Naz, and Shazia Shukrullah

1 Introduction

Energy production and sustainability are fundamental concerns for human beings. Global population growth, food shortage, and economic disparities are all also major challenges, but these challenges could be resolved by enough sustainability of energy. Leading world governments have recently placed a greater emphasis on reducing the threat of climate variations caused by fossil fuels combustion, and it is therefore crucial to assess the efficiency of the current energy production systems. It has been reported that 63% of global energy usage is wasted in heat form [1]. As a result, it is crucial to advance solutions for energy conversion techniques from that wasted heat into useful forms of energy like electricity. If we could generate electricity from this wasted heat, we could reduce our reliance on fossil fuels while also lowering global temperatures. Thermoelectric devices have attained great intention for several decades due to their unique characteristics including fast operation, no moving parts, high reliability, and low environmental impact [2].

Organic/inorganic hybrid-based thermoelectric materials (TEMs) have capability to directly convert heat into electricity, therefore these are considered as auspicious materials for energy harvesting and cooling technological applications. In 1821, Thomas Johann Seebeck discovered that Seebeck effect can produce voltage gradient in thermoelectric junctions in the presence of temperature gradient. Similarly, in 1834, Jean Charles Athanase Peltier contemplated that a thermoelectric junction

M. Ayyaz · N. U. H. Altaf · S. Maqsood · M. Y. Naz · S. Shukrullah
Department of Physics, University of Agriculture, Faisalabad 38040, Pakistan

M. Khan
Center of Excellence in Solid State Physics, University of the Punjab, Lahore 54590, Pakistan

A. Ashar (✉)
Department of Chemistry, University of Agriculture, Faisalabad 38040, Pakistan
e-mail: ambreenashar2013@gmail.com

K. Rizwan et al. (eds.), *Hybrid Nanomaterials*, Materials Horizons: From Nature to Nanomaterials, https://doi.org/10.1007/978-981-19-4538-0_19

could generate a temperature gradient across the junction due to an electrical current flowing through it (the Peltier effect) [3, 4].

Solid-state thermoelectric devices can be employed in various applications, including refrigeration, waste heat recovery, temperature sensing, and air-conditioning. The efficiency of these thermoelectric devices is controlled by various parameters such as thermal stability, electrical conductivity, type of material, thermal conductance, and Seebeck coefficient [5]. The Seebeck effect quantification in a specific material is governed by the Seebeck coefficient (α) and by open circuit voltage (V_{OC}) of thermoelectric material imperiled to temperature gradient. Generally, V_{OC} units lie between $\mu\,VK^{-1}$ to $m\,VK^{-1}$. The overall efficacy of thermoelectric materials to transform heat into electricity is measured by a unitless figure of merit ZT, given as

$$ZT = \frac{\sigma T \alpha^2}{\kappa}$$

where κ and σ denote the thermal conductivity and electrical conductivity, respectively [6].

Since, a huge portion of energy generated by current technologies is wasted in the form of errant heat energy, for example, in electrical power production and transportation systems. In these systems, the use of thermoelectric devices provides direct conversion of this wasted heat energy into electrical power, offering a promising way to enhance the fuel efficacy of conventional and emerging energy systems [7]. In recent few years, thermoelectric innovations have received widespread acclaim around the world. The thermoelectric generators directly produce electrical energy from heat with low pollution and high reliability [8]. Researchers have recently concentrated on doped thermoelectric materials with appropriate *n*-type or *p*-type dopants and synthesis of nanohybrids by mixing inorganic and organic elements to improve their efficacy.

Organic–inorganic nanohybrids are a new type of functional hybrid nanomaterials that have many novel characteristics, such as high catalytic activity and stimulating optical properties. They not only retain the therapeutic benefits of each factor, such as lower σ and S for organic materials and high for inorganic materials, but these also have unique interfacial chemistry. The electrical and morphological characteristics and surface interfacial chemistry of these TEMs are all important in their applications. These features of TEMs can be rationally engineered using well-established synthetic methods. Organic–inorganic nanomaterials with these exceptional properties can increase the value of ZT while also improving compatibility, resulting in improved stability and activity in thermoelectric devices. Organic–inorganic thermoelectric nanohybrids may boost the efficacy of the solar cells through heat control and sunlight harvesting [9].

Conventionally prepared thermoelectric semiconductors are costly, difficult to handle, and have a low reliability, which prevents them from being widely used in commercial thermoelectric devices. Compared to traditional energy production systems, the regular thermoelectric module (leg-type) design with no moving parts

has a significant benefit (e.g., turbines, compressors, and engines). Thermoelectric nanohybrids have high energy densities/weight and unit volume, which make them perfectly suitable for mobile distribution systems. In comparison to conventional TEMs, nanohybrids doped with inorganic–organic materials have lower thermal conductivity and high Seebeck coefficient and electric conductivity, facile synthesis, processing and are light weight [10]. We prepared a list of nanohybrids that have been described and addressed thermoelectric devices in this chapter.

2 Scientific Mechanisms of Organic/Inorganic Nanohybrid Thermoelectrics

2.1 Theory of Percolation

The theory of percolation was used first time to study physical processes in disordered systems toward the beginning of global connectedness. The percolation threshold (also named as "geometric percolation transition") states that: the minor phase particles (i.e., fillers) get contacted to each other, forming continuous clusters that spread all over the system. The physical features of heterogeneous multicomponent systems are well explained by this percolation theory (or phases) [11]. As the concentration approaches the threshold limit, the physical characteristics of the composites, such as thermal or electrical conductivity, undergo severe nonlinear variations, as illustrated in Fig. 1. Percolation relations with power laws of $\sigma \propto (f_v - f_c)^t$ for $f_v > f_c$ and $(\sigma \propto (f_c - f_v)^{-s})$ for $f_v < f_c$ can be used to demonstrate the transport features of the systems near the insulating-conductive transitions, where "f_v" is the volumetric ratio of secondary phase (conductive), f_c denotes the threshold percolation limit, "t" denotes the crucial exponent in the conduction phase, while

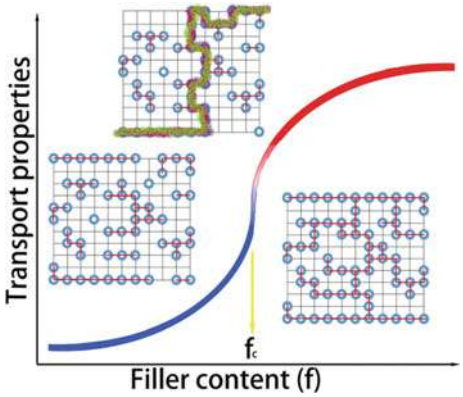

Fig. 1 Percolation approach and nonlinear variations in the transport characteristics of composite hybrids (blue line with dashes) around threshold percolation limit (f_c). The insets depict the fillers phase transition of in the microstructures of composites near percolation (shown by dark patches). Adapted from [17]

"*s*" denotes the critical exponent in organic and inorganic quasi-disordered structured thermoelectrics that have already shown atomic level or molecule percolation phenomenon of thermal and electric conductivity [12]. Digenite (Cu_xS), for example, has a liquid-like mobility and rapid ion conduction. Cu-ions are randomly placed among the tightly bounded S-ions at high temperatures and jump to different places via vacant interstices. In a percolation system, the conductive media are copper vacancies (i.e., empty interstices). There are six S-atoms and 18 interstices in each sulfur hexagonal unit cell (6-Cu_xS). The conductive minor phase (f_v) content can be computed using a simple stiff model as $(18 - 6x)/24$. A 60% increase in the ZT value can be achieved nearby threshold percolation limit (f_c ~0.3) in the conductive phase [13]. The addition of locally percolated highly conductive WTe_2 pellets to $WTe_2/CoSb_3$ inorganic composites increased the composite's electrical conductivity, and the noticeable bipolar peak of pure $CoSb_3$ was swiftly suppressed. As a result of the compositing process, the power factor was increased about 59 times of immaculate $CoSb_3$ power factor [14]. Han et al. used latex technology to prepare organic polyaniline–poly(vinylacetate) (PANI–PVAc) nanocomposites [15]. The electric properties (thermoelectric, thermoresistive, and piezoresistive nature) and the PANI–PVAc ratio matched the percolation design for superficial and structural alterations well. For sensor applications, composites containing 10–30 wt% PANI demonstrated good thermostability and adequate electrical conductivities of the polymer matrix. In organic/inorganic hybrids, this effect is important because it influences the model by material designing and optimization of microstructures, compositions, and performance [16].

2.2 Interface and Grain Boundaries Effects

Seebeck coefficient, thermal conductivity, and electric conductivity are three major thermoelectric features that are interconnected. Decoupling certain characteristics, such as band engineering and phonon engineering, has taken a lot of effort [18, 19]. Phonon production is used to boost up the values of ZT factor of thermoelectric materials as the thermal conductivity of lattices is substantially phonon dependent. The introduction of nanoscale precipitates, atomic-level lattice disorder, and meso-level grain boundaries may disperse phonons by differing mean-free pathways, increasing the ZT values and reducing the lattice thermal conductivity [20]. With several layers synthesized by spin coating on glass plate, Andrei et al. investigated the size dependency of electric conductivity in PEDOT:PSS thermoelectrics. The thickness of the layers influenced the electrical conductivity greatly. This mechanism could be ascribed to a sequence of processes at two distinct scales: percolation between the conjugated chain restructuring and grains and was studied by UV/Vis, XPS, AFM, and Raman analysis [21]. Most of the organic/inorganic thermoelectrics are prepared using similar techniques in order to achieve higher ZT values and lower thermal conductivity near percolation's threshold limit. On other hand, the interface

between the inorganic and organic phases is not well defined which results in higher resistivity value with reduced the predicted effects [22].

2.3 Energy Filter Effects/Superlattice Effects

Typically, the connection of thermal and electrical transport makes it difficult to modify phonon characteristics separately without compromising electronic transport. In accordance with the effect of quantum confinement, Hicks et al. [23] reported in 1993 that an elevated density states near Fermi level can boost up power factor of a thermoelectric superlattice. Another electron-transmitting/phonon-blocking superlattice can take advantage of the acoustic disparity between the layers to decrease the thermal conductivity of lattices. Inorganic/inorganic superlattice structures, such as Bi_2Te_3/Sb_2Te_3 and $PbSe_{0.98}Te_{0.02}/PbTe$, were then prepared [24]. ZT values ranged around 1.5–2.0 at ambient temperature were achieved using these effects. Experiments showed that the structure caused a considerable increment in Seebeck coefficient value and a continuous drop in the thermal conductivity when the superlattice thickness was increased. Inorganic/organic nanohybrid superlattice structures, such as micro-level composite materials following the percolation phenomenon, can potentially reveal hybrid features obtained synergistically from both the host and the guest. Intermixed polymers (conjugates), and coated inorganic materials on the other hand, can result in unique thermal and electrical features [17]. Such as, Kanatzidis et al. [25], used polyaniline (PANI) encapsulation in MoS_2 to create a nanoscale molecular composite with remarkable charge-transport characteristics. Wan et al. [26] used electrochemical intercalation and solvent exchange to create $TiS_2[(HA)_x$-$(DMSO)_w]$ inorganic/organic superlattices as illustrated in Fig. 2. The mixing of inorganic component TiS_2 results in power factor enhancement of hybrid inorganic/organic superlattices. In phonon transport scattering, the interaction between organic and inorganic layers is crucial. In $[(HA)_{0.08}(H_2O)_{0.22}(DMSO)_{0.03}]TiS_2$, a ZT in-plane value of 0.28 was reported near 100 °C owing to the considerable decrease in thermal conductivity. The 2D materials (such as MoS_2, phosphine, and hexagonal boron nitride) have risen popularity since the successful exfoliation of monolayer graphene. The layer strength of 2D materials in heterojunctions based upon Vander Waals heterojunctions, for example, graphene/BN/graphene, graphene/phosphene/graphene, and silicone/transition metal sulfide, can be modified to control the transport barrier of electrons [27]. Consequently, the thermal conductivity of the vertical heterojunction in the plane direction will be substantially lower than that of the covalently linked interface [28]. This suggests that the use of Vander Waals heterojunctions to enhance the thermoelectric efficiency of materials is a viable option. Organic/inorganic dipole–dipole heterojunction superlattices are more important for research because the cross-linkage of organic molecular layers can efficiently dissociate the interactions between atomic layers [29]. By

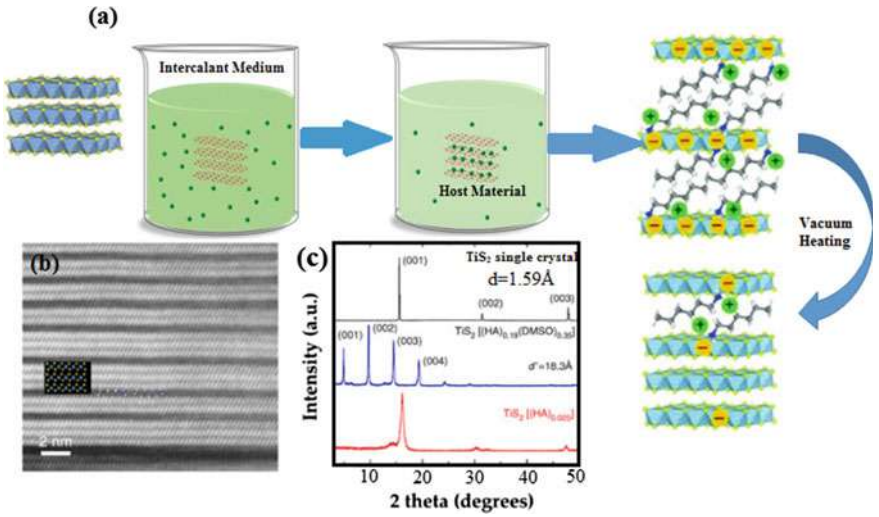

Fig. 2 **a** Illustration of the electrochemical intercalation procedure, **b** STEM micrograph of $TiS_2(HA)_{0.025}$, **c** XRD diffractograms of TiS_2 single crystal and its associated superlattices. This figure is modified from [31]

electrochemical molecular embedding, Wang et al. [30] effectively synthesized inorganic/organic superlattices including SnSe/CTAB, BP/CTAB (hexadecyltrimethylammonium bromide), and Bi_2Se_3. These generic synthesis pathways and ideas can be used to thermoelectric research in the future, resulting in significant improvements in ZT values.

The energy-filtering effect is categorized also as a superlattice effect, which explains why the Seebeck coefficient rises in 0–3-type thermoelectric nanohybrids. At 300 °C, an *n*-type composite film (CuAgSe/Ag/Ag_2Se) has a power factor value of 2231.49 mW m^{-1} K^{-2}. The energy barriers lie nearby the CuAgSe/Ag, Ag_2Se/Ag, and Ag_2Se/CuAgSe interfaces. The Schottky barrier is formed by the overlapped bandgap energy of the two thermoelectric semiconductors and the metallic silver nanoparticles. Low-energy carriers are prevented in the composites, whereas high-energy carriers are allowed to jump through the interfaces. This provides an ultrahigh value of power factor due to the cohabitation of a high carrier concentration with a good Seebeck coefficient [32].

3 Organic and Inorganic Nanohybrids as Thermoelectric Materials

Since the last decade, a new candidate hybrid organic and inorganic material has been used in the area of thermoelectrics because of their great potential to improve thermoelectric efficacy by combining the effects of higher Seebeck coefficient and lower thermal conductivity in organic materials and higher electric conductivity in inorganic materials [33]. Accordingly, the organic and inorganic materials are combined to take advantage of the former's high power factor and latter's poor thermal conductivity simultaneously. The result is known as hybrid type, and it consists primarily of an inorganic additive (the metal-based compounds) doped into an organic matrix. When inorganic and organic thermoelectrics are physically combined to produce nanohybrids, the resulting parameters of hybrid are termed as Seebeck coefficient (δ) and the electric conductivity (σ) of the nanohybrids. The value of σ and δ can be computed using the Eqs. (1–2) [34]:

$$\sigma_{\text{hybrid}} = (1-x)\sigma_{\text{organic}} + x\sigma_{\text{inorganic}} \tag{1}$$

$$\delta_{\text{hybrid}} = \frac{(1-x)\delta_{\text{organic}}\sigma_{\text{organic}} + x\delta_{\text{inorganic}}\sigma_{\text{inorganic}}}{(1-x)\sigma_{\text{organic}} + x\sigma_{\text{inorganic}}} \tag{2}$$

where $\sigma_{\text{inorganic}}$, σ_{organic}, $\delta_{\text{inorganic}}$, and δ_{organic} are the Seebeck coefficient and electric conductivity of inorganic and organic constituents, respectively, which are assumed constant under zero-band stretching. Variable x represents an inorganic constituent in inorganic/organic nanohybrids.

For example, intrinsic PA is basically nonmetallic. It is converted into a metallic state after getting substituted with I_2, as substitution level increases, its conductivity value also increases. Poly(alkyl thiophene) [35], polypyrrole [36], and polyphenylene [37] are examples of conductive organic polymer materials that have been prepared and used in LEDs, batteries, and other applications due to their exceptional electrical, optical, and mechanical properties. Thermoelectric features of some nanohybrids are listed in Table 1. The reported TE nanohybrids are explored in further detail below.

Organic/inorganic nanohybrids can be screen-printed as reliable thermoelectric modules to produce energy from the temperature differential between the ambient air and the human body [51]. As a result, these hybrid thermoelectric nanostructures can be used in wearable devices as green power sources. The PEDOT polymer has gained interest due to its remarkable properties such as high optical transparency, high electrical conductivity, low mass density, environmental stability, low thermal conductivity, good flexibility, ease of handling, and great thermal stability.

Pure PEDOT and doped PEDOT are used to prepare most of the nanohybrids. PEDOT/PbTe [43], PEDOT:PSS/Te [52], PEDOT:PSS/Bi_2Te_3 [53], PEDOT:PSS/graphite [54], and PEDOT:PSS/$Ca_3Co_4O_9$ [55] are some of the thermoelectric inorganic materials that have been incorporated into PEDOT matrix to prepare PEDOT hybrid nanostructures.

Table 1 Thermoelectric feature of some organic–inorganic nanohybrids

Nanohybrids	Nanohybrids	Electrical conductivity ($S\ m^{-1}$)	ZT ($W/m/K^2$)	Seebeck coefficient ($\mu\ V\ K^{-1}$)	Thermal conductivity ($W\ m^{-1}\ K^{-1}$)	Refs.
PEDOT:PSS	Bi_2Te_3	6000–15,000	0.08	60–150	~0.558	[38]
-	$Ca_3Co_4O_9$	–	0.1×10^{-4}	136	11.4	[39]
	Graphite	4.03	2.2×10^{-3}	23.3	0.29	[40]
PANI–PVAc		Increases from 10^{-7} to 4	Increases from 1.2×10^{-7} to 1.2×10^{-6}	−2.5	0.4–0.5	[41]
PLA/$Bi_{0.5}Sb_{1.5}Te_3$	Bi_2Te_3/Sb_2Te_3	–	0.011	200	–	[42]
PANI	MoS2				–	
PEDOT	PbTe	0.064		1204	–	[43]
PANI-	Au NPs	330		15	–	[44]
polyaniline	RGO-CdS-		1.97		–	[45]
–	CNT	2228	0.19	116	5	[46]
PEDOT:Tos		67	0.25	220	0.37	[47]
PANI	$Bi_{0.5}Se_{1.5}Te_3$ (93–99 wt%)	–	–	15	–	[48]
PEOT:PSS	Te nanorods	1930	~0.10	163	0.22–0.30	[49]
PANI/	MWCNT	~6000	–	~30	~0.5	[50]

Wang et al. [43] used PEDOT polymerization medium to add PbTe nanoparticles whose diameter was about 50 nm and then cold-press the obtained material into pellets at 10 MPa. The electric conductivity of pure PEDOT is remarkably low as 0.064 S m^{-1}. The electric conductivity of the composites raises to a value of 0.616 S m^{-1} when the PbTe concentration is increased to a value of 43.90 wt% (because the electric conductivity of PbTe particles is greater), although it is still lower than that of PbTe (8.2 S m^{-1}). With increased PbTe content, the Seebeck coefficient value drops. Due to the lower value of positive Seebeck coefficient of pure PbTe, its value decreases from 4088 (pure PEDOT) to 1204 μ V K^{-1} (a sample with 43.90 wt% PbTe) with increase in PbTe content. As PEDOT:PSS composite has higher electric conductivity and lower thermal conductivity values, thus mixing technique of inorganic materials with higher Seebeck coefficients, the thermoelectric characteristics of PEDOT:PSS/inorganic nanohybrids can be enhanced.

Toshima et al. [56] used a simple technique to prepare Bi_2Te_3 nanoparticles, using inexpensive starting materials like $BiCl_3$ and $TeCl_4$, and then prepared nanohybrid materials using these nanoparticles and conducting polyaniline. Polyaniline with an emeraldine base structure was synthesized and dried under vacuum for 12 h at 50 °C. The emeraldine form of Bi_2Te_3 nanoparticles and polyaniline were physically combined, and the solution was combined with camphorsulfonic acid in *m*-cresol. The PANI film has the similar order of electric conductivity as the hybrid film made by casting the aforesaid mixes (physical mixing technique), but greater Seebeck coefficient value.

As a result, the power factor of above nanohybrid films is almost 50 times that of the PANI film. It was not clear that, why these hybrid films made with physical combination have higher power factor and Seebeck coefficient values than those made with a solution mixture [56]. Toshima [57] successfully hybridized Au and Pt nanoparticles with PANI. They mixed up PANI with PVP-coated Au and Pt nanoparticles fabricated using a standard alcohol reduction process in the presence of PVP to develop a hybrid material with a twofold increased ZT values of thermoelectrics.

Graphene is also a popular nanofiller because of its greater surface area and aspect ratio [58]. Graphene synthesis is easier and cheaper than SWNT synthesis, which makes the final thermoelectric materials more practical [59].

PANI-Au NPs hybrid materials were synthesized by Toshima et al. [44] by in situ reduction of $HAuCl_4$ with aniline and subsequently oxidizing the remaining aniline with ammonium peroxodisulfate. At 323 K, the nanohybrid demonstrated increased electric conductivities of up to 330 S cm^{-1} and Seebeck coefficient of 15 μ V m K^{-2}.

Zhang et al. [38] fabricated nanohybrid thermoelectrics by impregnating PEDOT:PSS emulsions into Bi_2Te_3 nanoparticles. It was possible to achieve the highest value of power factor of 130 W^{-1} m^{-1} K^{-2}. ZT was estimated to be 0.08 for 90% *p*-type Bi_2Te_3 and 10% PEDOT:PSS, which is around 1/10 of Bi_2Te_3 and greater than PEDOT:PSS [38].

To fabricate the RGO-CdS-polyaniline ternary organic–inorganic nanohybrid thermoelectrics, More et al. [45] employed a straightforward in situ thermoelectric technique. The energy band configuration between CdS quantum dots, graphene oxide and PANI increased the *P*-type electric conductivity by decreasing thermal

conductivity, indicating the filtering effect of synergetic energy. The power factor and electric conductivity of RGO/CdS/PANI nanohybrids were improved when the filler content (RGO-CdS) was increased. With a ZT value of 1.97, the nanohybrid (with 0.4 wt% filler; G4) exhibits moderate thermal conductivity but good electric conductivity.

Organic semiconductors were made from a-CNT webs substituted with n-type and p-type molecular dopant materials by An et al. [46]. By annealing CNT (oxygen desorption from p-CNT) webs with benzyl viologen, the maximum value of power factor was attained, resulting in the *n*-type TE material. For the non-annealed BV-doped CNT web, the *n*-type thermoelectric power factor value was higher than the power factor of 1901 μ W m K^{-2} (*p*-type). As a result, their thermoelectric features for *n*-type CNT webs at 300 K were observed near 2228 S cm^{-1}, −116 μ V K^{-1}, 5 W m^{-1} K^{-1}, and 0.19 ZT. They also fabricated a *p*-type thermoelectric by substitution of *p*-CNT web into 10 mM of F_4TCNQ, which helped to regulate the strong electronic affinity. With a Seebeck coefficient of 50 μ V K^{-1}, an electric conductivity of 3000 S cm^{-1}, a ZT of 0.11, and a thermal conductivity of 6 W m^{-1} K^{-1} were achieved. The greatest power factor value for the *p*-type thermoelectric was found near 2252 μ W m K^{-2}.

4 Fabrication Techniques and Future Challenges

Synthesis procedure and parameters play crucial role in the fabrication of high-performance and reliable thermoelectric nanohybrids and devices with good electrical and optical transport features. Several synthesis techniques (as displayed in Fig. 3) are currently in use and are elaborated in the sections below.

4.1 Electrospinning Technique

Starting with molten polymers or a solution, electrospinning method is utilized to prepare ultrapure fiber materials with higher surface/volume ratio and adjustable structures. The chemical composition and particle size distribution of electrospun fibers are uniform. In this method, a fluid drop on the spinneret tip is subjected to an electric field. A syringe-type pump is utilized to discharge the mixture through the needle at a controlled speed, and the collector is affixed near the tip. The tip and the collector are connected by a high voltage, which causes the solvent to evaporate and continuous fiber materials to fabricate [60, 61]. Because of their low density, higher surface-to-volume ratio, and flexibility, the nanofibers of electrospun polymers have been studied in nanocatalysis and various biomedical applications. Electrospinning was utilized by Dalton et al. to prepare n-type and p-type carbon fibers from PAN and lignin mixtures [62]. Meanwhile, inorganic fibers with some flexibility, such as Mg_2Si, [17], $NaCo_2O_4$, [17], and PbTe [63], have also been produced effectively.

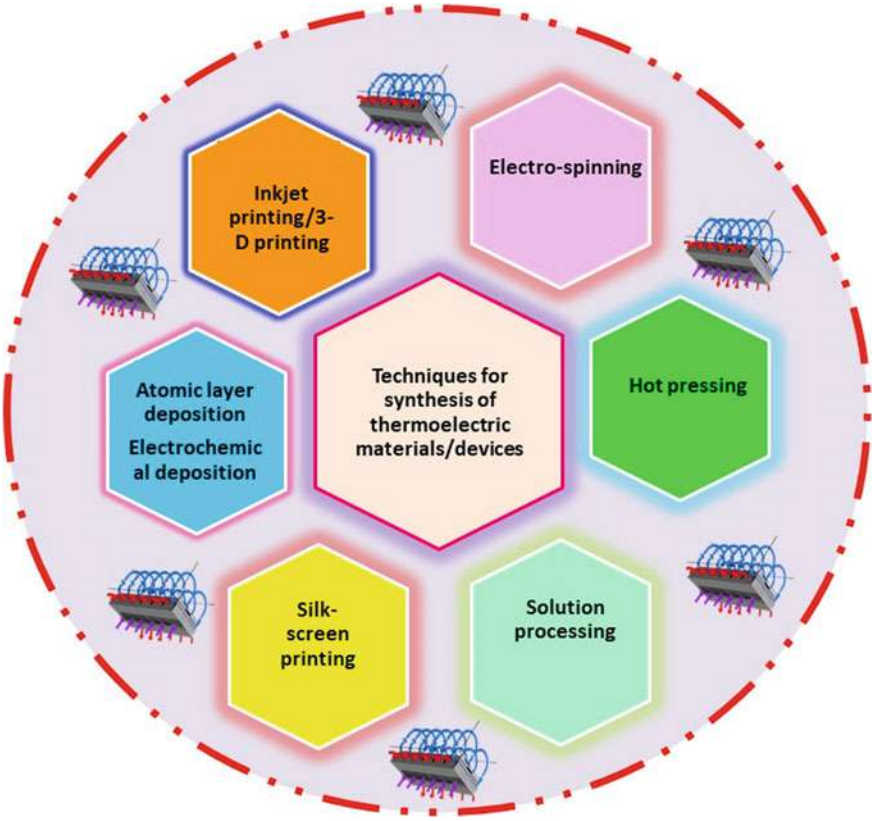

Fig. 3 Techniques for synthesis of thermoelectric materials/devices

The interfaces and grain boundaries in thermoelectric fibers can disperse phonons, reducing the value of thermal conductivity and improving the transport characteristics of the fibers. However, obtaining fiber composites with good thermoelectric characteristics remains a challenge. Wang et al. [64] used in situ polymerization and electrospinning procedures to prepare polyaniline (PANI) and CNT composite nanofiber materials. Strong chemical interactions cause PANI and CNTs backbone chains to align themselves along the fiber axis. Higher backbone chain arrangement minimizes the *p–p* conjugated imperfections, enhances the effective degree of delocalization of electrons, and thus increases PANI's carrier mobility, resulting in a twofold increase in the power factor value in a leaning way [64]. This suggests that the electrospinning technique can be used to fabricate a flexible and reliable nanocomposite with good thermoelectric performance by increasing the order of the backbone chain structure. When the temperature difference is 200 °C, very reliable fibers comprising *p*- and *n*-junctions created by this technique can gather ecological heat in the desired through-thickness direction, with an output power of 8.6 W/m^2.

4.2 Hot Pressing

A uni-axial pressure is provided to the powder compacted system that is inserted in an alloy or graphite mold during the hot pressing process. Previously, in powder metallurgy, this procedure was invented and used to create high-temperature ceramic materials and alloys of high density at lower sintering temperatures [65]. For the manufacture of thermoelectric nanocomposites, hot pressing has recently become a comparatively emerging process [61, 66, 67]. Mostly, dense inorganic–organic hybrids can be fabricated with a simple DIY hot pressing equipment due to the thermoplasticity of polymer-based matrix. Kim et al. [68] used hot pressing to prepare n-type carbon bucky paper at 60 °C in 6 MPa for 3 min that contains CNTs and a PVDF composite. Brush-printing and hot pressing of epoxy/$Bi_{0.5}Sb_{1.5}Te_3$ films with high arrangement on polyimide substrates were used [69]. The steady temperature differential of a prototype flexible thermoelectric cooler with epoxy/$Bi_{0.5}Sb_{1.5}Te_3$ films reached to 6 °C with an operational current flow of 60 mA. The spark plasma sintering (SPS) is a highly proficient sintering process that permits quick sample annealing at low temperatures [70–72] and is particularly well suited to the fabrication of thermoelectric nanohybrids. Ge et al. used SPS process at a temperature of 100 °C to synthesize a PEDOT:PSS/Cu_2SnSe_3 nanocomposite polymer bulk [73]. After SPS, the polymer-powdered sample was converted into a homogenous polymer bulk, and the prepared material had significantly better characteristics as compared to the materials processed with a cold-press. The specimen containing 33 wt% of nanomaterials showed greater ZT value among all of the examined specimens (0.04 @ 45 °C), which is found 20 times greater in comparison to the 0.002 value estimated for pristine PEDOT:PSS bulk specimen.

4.3 Solution Processing

Conventional solution formulation techniques are very appropriate for fabrication of superconductors having organic matrix. Among these techniques, hydrothermal fabrication is a significant way to synthesize inorganic filler materials with no aggregating effect. The solution of inorganic fillers is mixed up with organic dielectric materials and then placed on a vacuumized or pre-cleaned glass slide, followed by quick dehydration using air to fabricate inorganic–organic thermal composite films [74]. Such as Miao and colleagues [75] employed hydrothermal technique to generate highly conductive reduced graphene material (RGO); after that, they produced RGO/Te nanoscale composite bilayer films on a filter substrate composed of glass fiber utilizing drop coating technique. The obtained findings indicate that the films have the highest power factor value of 80 mW/mK^2. Lin et al. [76] introduced cuprous selenide nanopowders to mix up the solvents at ambient temperature and stirred the obtained mixture for 10 min. Using this procedure, they successfully prepared Cu_2Se ink. A homogeneous layer was created onto glass substrate

through straightforward spin coating procedure, and its maximum power achieved 0.62 mW $(mK^2)^{-1}$. After continuous repeating of bending 10^3 times, nearly 90% of the thermodynamic efficiency may possibly be achieved.

4.4 Silk-Screen Printing or Paste Processing

For many years, screen printing technology has been used to synthesize the thermoelectric nanohybrids, thin-film hybrid materials, and devices. Due to its low cost, ease of operation, scalability, and ability to print curved surfaces, screen printing has gained popularity as an efficient manufacturing technique for preparation of thermoelectric nanohybrids, thin films, and devices [77, 78]. Most of the time, the solution treatment of beaker containing organic and inorganic components results in the formation of the organic–inorganic composite adhesive used in screen printing applications. The biological composite paste must meet certain viscosity requirements in order to get a better diffusion impact on the material during printing, according to the manufacturer. Other difficulties incorporate anti-oxidation mechanism during the curing and printing processes, as well as post-treatment of the fiber glass paste after it has been printed. Many different types of thermal composite films, including those made of Bi_2Te_3 and PbTe-based materials, have been produced by screen printing [79–81]. A composite film of PANI/Te was synthesized by screen printing Te nanorods with the conductive PANI, and a ZT factor value of 0.220 was achieved at 110 °C. According to Wang et al. at DT = 40 °C, the highest output voltage and power of the prototype device with ten legs of PANI/Te-Ag components were 29.90 mV and 0.730 mW, respectively, and the highest output power was 0.730 mW [82]. Varghese et al. applied screen printing to prepare flexible Bi_2Te_3 films and systems for use in medical applications. The paste was created using a wet-chemical method that was stimulated by microwaves. Temperature-sensitive thermally conductive films were displayed onto a polyimide substrate, which was then cold compacted before being annealed (the process is shown in Fig. 4). With the printed films in place, the thermoelectric device has a power density of 4 $mWcm^{-2}$ of surface area at DT = 60 °C. Screen printing technology is a scalable and low-cost process which has a wide range of potential applications, including the fabrication of adjustable thermoelectric harvested energy and cooling devices [77].

4.5 Layer Deposition Method

Generally, the main purpose of conventional coating technique is to place external substances on the surface to obtain multilayer films. In the deposition procedures of thermodynamic inorganic–organic composite materials, the organic parts are generally utilized as materials to work as electrode, and natural compounds are placed on the organic materials surface to produce 2–2 composite system. Furthermore,

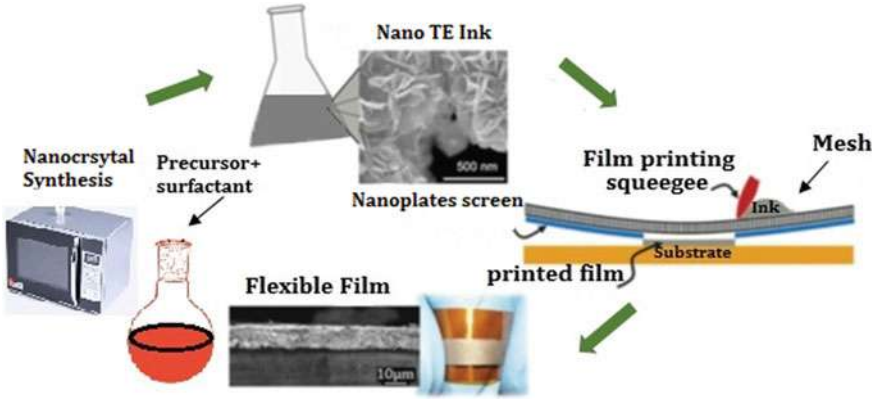

Fig. 4 Illustration of overall synthesis procedure of flexible and reliable thermoelectric films, such as nano-ink processing, nanocrystal processing, screen printing on a flexible substrate, and sintered thin films. Figure adapted from [77]

organic small molecule (OSM) substances can be placed layer after layer with organic materials to make metamaterial structures [83–85]. Although numerous layer deposition methods may be employed to deposit inorganic substances, including physical thermal evaporation, pulsed laser deposition. Additionally, there are two conventional approaches to implement commercialized layer-by-layer coating for inorganic/organic composite materials, as follows.

4.5.1 Electrochemical Deposition Technique

When negative and positive ions in an electrochemical solution are produced under the influence of an applied electric field (E), redox processes take place on electrode surface, which result in the formation of thin-film layers. Because of its low initial investment and great efficiency, this approach is well suited for industrial production and has attained great attention for its use in the fabrication of thermoelectrics [86–88]. The fact that electrochemical deposition can only take place on conductive substrate makes it a viable option for the preparation of organic–inorganic hybrid films. For example, electrochemical deposition of inorganic thermoelectrics on organic conducting polymers (ICP) to be used as an operating electrode is a feasible option for the fabrication of organic–inorganic composite films. Culebras et al. created thin Te/PEDOT films by electrochemically producing Te on the PEDOT operating electrode using a conventional electrochemical deposition technique [89]. A greater value of power factor (320 mW (m K^2)$^{-1}$) was achieved due to an increase in the Seebeck coefficient of the films, which improved from 9 to 230 mV K^{-1} after deposition. The high porosity of the Te polycrystalline film, on the other hand, resulted in a considerable rise in the electric resistivity of the sample. In the future,

it will be a very difficult task to increasing the electrochemical properties of films using electrochemical deposition.

4.5.2 ALD/MLD

Atomic layer deposition, which is identical to chemical vapor deposition (CVD), may deposit compounds on substrate layer by layer with a monoatomic thickness. This approach can be used to regulate the thickness of the material being deposited on an atomic scale and to deposit it in a conformal manner since the material reactions that take place during atomic layer deposition are similar to sequential, self-limiting surface reactions [90–93]. Recently, the ALD methodology has been used in synthesis of inorganic thermoelectric materials such as Bi_2Te_3, Sb_2Te_3, Bi_2Se_3, ZnO, and TiO_2, which have been published in the research [94–96]. There are less limits on the substrate due to the fact that the ALD process may be conducted at a constant voltage and low temperature, and this technology may be extremely competitive in the field of fabrication of flexible reliable materials. The introduction of inorganic thermoelectrics with fiber materials is being pursued in order to increase their application in reusable flexible thermoelectric materials [97]. Similar to ALD, molecular layer deposition (MLD) deposits thin films in molecular units by using consecutive, self-limiting processes of deposition. It is possible to use a combined ALD and MLD technique to substitute metal oxides and organic materials on a substrate in order to obtain a uniform organic–inorganic network of superlattices, instead of conventional deposition of inorganic source on organic substrates. The contact between the oxide and organic components can disperse much more phonons or cause confinement effects, both of which increase the thermoelectric characteristics of the material [83]. In a study, Karttunen and colleagues employed ALD/MLD to synthesize ZnO-organic superlattice thin-film thermoelectrics on fiber cotton substrates. The prepared films were highly flexible and exhibit low thermal conductivity compared with pure ZnO film [98]. It is expected that ALD and MLD techniques will perform significant roles in the development of adjustable thermoelectric nanohybrids and structures in the foreseeable future.

4.6 Inkjet Printing Technique

In the past few years, inkjet printing technology has been incorporated in the fabrication of electrical devices such as OLED, PCB due to its novel features of digitized processes, additive, and non-contact. This category also includes the simple spin-spray technique, which is one of the most effective strategies for rapidly developing homogeneous thermoelectric films of relatively complicated composition [99]. Inkjet printing can be separated into two forms based on different working principles: First one is continuous inkjet printing, and other one is drop-on-demand inkjet printing.

The latter has increasingly gained significance in the market. At the moment, there are two forms of drop-on-demand inkjet technology: piezoelectric inkjet technique and thermal inkjet technique. The technology of thermal inkjet printing creates vapor bubbles within the ink by rapid heating. This usually occurs above the ink's boiling point. It is more suited to water-based inks than organic solvents as heat is required for evaporation [100]. The piezo-inkjet printer uses the effect called inverse piezoelectric effect in order to shrink ink via a piezoelectric part which is adjusted by an electrical signal from the nozzle to the ink to be squashed away and finally pattern is formed by expelled onto the substrate. After solving the challenges of thermoelectric inks, this technology minimizes energy usage, increases machine service life, and overcomes ink material restrictions [101, 102]. While ensuring that the ink has good thermoelectric efficiency, it is also important to consider the ink's printability, which faces a significant challenge in designing of thermoelectric nanohybrid systems and is also critical to realize the high-quality thermoelectric inkjet printing. This happens due to (1) the intrinsic complexity of the thermoelectric nanohybrids systems that cause dynamic variation in thermoelectric characteristics and ink's fluid properties, which are caused by the proportion and type of hybrids; (2) to cover the printable and post-treatment necessities of thermoelectric inks, they frequently contain additives such as thickeners, stabilizers, binders, and surfactants, which finally add to the ink system's complexity [103, 104]. Some literature on inkjet printing of thermoelectrics, such as Bi_2Te_3, carbon nanotubes, graphene, and polymers, [105–107] have focused on the regulation of thermoelectric ink printing efficiency. Chen et al. [105] synthesized Bi_2Te_3 TE nanowires before dispersing them in DI water in an ultrasonic bath in order to create a jettable ink that was then printed onto a substrate (glass). The film's Seebeck coefficient was measured around 140 μ V K^{-1}, which was same as that of bulk Bi_2Te_3. Kato et al. [108] investigated how to make a coatable ink with PEDOT:PSS, $Bi_{0.4}$ $Sb_{1.6}Te_3$, using PEDOT:PSS, $Bi_{0.4}$ $Sb_{1.6}Te_3$, with an organic additive (PAA). Chen et al. [109] used inkjet printing to apply Bi_2Te_3 and $Bi_{0.5}Sb_{1.5}Te_3$ nanowires to polyimide to create a highly flexible TEG.

The greatest power factors for the $Bi_{0.5}Sb_{1.5}Te_3$ and Bi_2Te_3 films after annealing at 450 °C were 180 $\mu W/m^{-1}$ K^{-2} and 110 $\mu W/m^{-1}$ K^{-2}, respectively. At DT = 32 °C, the generator's power reached 130 nW, and it kept performing after repeating the bending experiments 50 times along a radius of curvature of 10 mm. Inkjet printing will be able to make high-efficient, low-cost, expandable, miniaturized, and flexible TEGs in near future, if thermoelectric inks of long-lasting stability, acceptable fluid characteristics, and outstanding thermoelectric features can be achieved.

4.7 3D Printing

The 3D printing technology, which comprises fused deposition molding (FDM), laminated object manufacture (LOM), stereolithography apparatus (SLA), and selective laser sintering (SLS), has obtained a lot of interest in recent years as an "additive manufacturing technique". The 3D printing has been utilized to build thermoelectrics

due to its benefits of quick prototyping, printability of complicated entities, high material usage, and flexible product design. By combining SLA technology with a $Bi_{0.5}Sb_{1.5}Te_3$/photosensitizer composite, He et al. created an organic–inorganic composite thermoelectrics having a very low thermal conductivity value with a value of ZT factor up to 0.12 [110]. Kim et al. synthesized a Bi_2Te_3-based thermoelectric ink with chalcogenidometallate ions of Sb_2Te_3 as a binder material, then used an extrusion-based 3D printer to build thermoelectric devices [111]. They obtained values of ZT factor 0.9 (*p*-type) and 0.6 (*n*-type) for the synthesized thermoelectric materials with various forms (*p*-type). At 40 °C, the cylindrical TEG synthesized by 3D printing shows a power density value of 1.40 mW/cm^2. Wang et al. used extrusion synthesis to create a composite thermoelectric wire for FDM-based 3D printer utilizing $Bi_{0.5}Sb_{1.5}Te_3$ as filler and polylactic acid (PLA) as the matrix [42]. The content of the fillers and matrix could be tailored to control the thermoelectric characteristics and flexibility of the composite wires. These findings suggest that 3D printing technique has very high potential in the area of thermoelectrics and might be used in rapid fabrication flexible thermoelectric nanohybrids and devices [112].

5 Thermoelectric Devices Based on Organic–Inorganic Nanohybrids

Thermoelectric-based devices use heat to generate electricity. This is a compact solid-state device that can be employed for power production, refrigeration, and power conversion. TE devices typically have a surface area of a few cm^2 and a thickness of a few mm. The thermoelectric device that generates energy from a temperature gradient is known as thermoelectric generator, and when used for cooling purposes, they are known as thermoelectric coolers. To construct such thermoelectric devices, a staking configuration of thermocouples is connected thermally in parallel or electrically in series [113].

5.1 Thermoelectric Power Generator (TEG)

Thermoelectric generators are solid-state, fuel-free, and dependable devices that use Seebeck effect to directly transform waste heat into electrical power. TEG devices utilize the Seebeck effect [114]. The Seebeck effect is used in a TEG by connecting one *p*-type and one *n*-type semiconductor thermally in parallel and electrically in series**.** Conductive tabs are attached to the components through a low melting temperature solder joining the *p*–*n* pairs (PbSn or BiSn). The TEG converts thermal energy into electrical energy when a temperature difference arises between its two connections according to theory of Seebeck effect.

When electricity is produced between the hot and cold junctions across the terminals, the Peltier effect occurs. To put it another way, the heat retrieved from hot source must scatter through the module's semiconductor n and p components, and then to the cold source, that is usually the air [115]. The ZT value is defined as Seebeck coefficients and power factor for a material's total efficacy in conversion of heat to electrical energy.

$$ZT = \frac{\alpha^2 \sigma T}{K}$$

where T, κ, α, and σ denote the thermal conductivity, electrical conductivity, Seebeck coefficient, and absolute temperature, respectively. Here, the overall thermal conductivity is measured as $k = k_{\text{ph}} + k_e$, where k_{ph} and k_e denote the heat transferred by phonons and electrons, respectively.

An electrical crystal and a phonon glass should be the optimal TE materials to maximize σ and κ. Because both phonons and charge carriers transfer heat, the materials that are good at conducting electricity are usually good at conducting the heat [116]. Also, because of the inverse link between electrical conductivity and Seebeck coefficient, designing organic semiconductors for TE applications is more difficult, because maximizing one condition often has a negative impact on the other. If no temperature data is known for a specific material, the power factor (PF) of TE hybrid materials is expressed by equation [117],

$$\text{PF} = \alpha^2 \sigma$$

Various semiconductor and conductive materials are employed in thermocouples based on Seebeck effect. TEGs are extensively applied in a variety of applications due to their appealing features, which include low maintenance, energy efficiency, and a long lifespan. In recent few years, they have become a popular topic in the energy-harvesting field, with applications incorporating size dependence, supplied power, and raw materials [118]. Inorganic crystalline semiconductors have dominated the thermoelectric material domains, but their use has been limited due to their high cost, inherent toxicity, and fragility. In contrast to organic thermoelectrics, they are made up of abundant and less harmful components. Organic materials can also be treated in solution, allowing them to be coated over large areas with low-cost printing technology including roll-to-roll printing, inkjet printing, gravure printing, and so on, resulting in more cost-effective TEG that is more suitable to recover heat at low working temperatures. It is important that organic thermoelectrics are low cost, mechanical flexible, eco-friendly and have lower thermal and electrical conductivity than inorganic semiconductors. Due to ease of fabrication and material abundance mark, organic semiconductor technology is worth researching for thermoelectric applications [102].

5.2 Thermoelectric Cooler (TEC)

The thermoelectric cooler (TEC) operates according to Peltier effect and transforms electric energy into heat energy. When a voltage is applied to a PN junction, the heat retrieved from hot source is scattered into *p* and *n*-junctions of semiconductor and is finally shifted to the cold source which is usually the atmosphere [119]. Numerous of applications where TE coolers have been used such as beverage cooler, rail road, car, and submarine. Unfortunately, TECs have a limited lifespan, which may be determined by measuring the change in their AC resistance. The AC resistance increases as a TEC becomes "old" or worn out. New high-performance TE cooling materials are being intensively pursued [120]. TEC has governed increased attention in the literature that is Hu et al. enhanced electrical conductivity of the prepared inorganic hybrid film made up of nickel nanowires and measured optical power factor near 24.3 $\mu Wm^{-1} K^{-2}$ [121]. Xie et al. showed that high temperature is usually caused by heat generation in the batteries which is impaired by high charging and discharging rate [122]. Results found that thermoelectric thin film has enormous potential in the TECs, and temperature control is also important for TECs.

5.3 Environmental Thermoelectric (TE) Sensors

Thermoelectric sensors instigate the use of different heating powers measured volume flow rate in micro-channels. It connects wireless communication system with a network of active and advanced sensors. Using TEGs for self-powering, TE sensors based on catalyst combustor have realized the monitoring of different chemical gases. It helps in reducing maintenance tasks and expenses while also avoids the use of batteries and lowers the pollution from chemical compounds emitted by them. This technology, in combination with TEGs, has been widely used in different fields including industry, Building Energy Management (BEM), residential and commercial smart buildings. Sensors are important in modern industry because they can continuously monitor a variety of industrial or environmental variables. Flexible thermoelectric devices may now not only self-energize by the environmental thermal energy, but also monitor variations in the atmosphere, such as blood pressure and body temperature of humans. This is possible due to advancement of various polymer-based thermoelectric composites in recent years. Hou and colleagues [123] synthesized a simple flexible human touch sensor based on graphene's TE properties.

The sensors are self-powered by its own thermoelectric conversion effect and can detect cooling or local temperature and pressure to trace the position of person's touch, suggesting that it could have a unique application value in the design of electronic skin. However, despite their efficiency, the cost and weight of these devices are very considerable. These organic TE hybrids were used as thermoelectric sensors as an alternative. One self-powered TE sensor was created using oxidized MWCNTs and an ethylene-octene copolymer. With increase in oxygen-containing functional

moieties on surface of MWCNTs, the thermoelectric power was increased. Organic vapor influenced the resistance of the MWCNT/EOC hybrid material, with average increase of 0.05, 3.6, 1.1, and 0.05 S after exposure to ethanol, heptane, and toluene-saturated vapor, respectively. These devices are useful for inexpensive gas detection and monitoring [124].

6 Conclusion

In conclusion, this chapter highlighted a number of significant advancements in organic/inorganic thermoelectric nanohybrids. These organic/inorganic nanohybrids exhibit excellent performance due to consecutive development of conductive polymers from last few decades. These inorganic/organic thermoelectric nanohybrids, on the other hand, perform lower than their fully inorganic counterparts. The significance of nanolevel interfaces in organic/inorganic thermoelectric nanocomposites has been highlighted in experimental research, but a complete insight of carriers transport at the organic/inorganic interface in these hybrids has resumed elusive. Other carriers transport mechanisms, such as energy filtering and modulation doping, could be applied to boost up the thermoelectric efficacy of hybrid inorganic/organic nanocomposites by increasing the Seebeck coefficient and electric conductivity while reducing the thermal conductivity. The carriers transport interface should be justified at the nanolevel. Recently, various superlattices of organic/inorganic thermoelectric nanohybrids have been prepared, including hybrid thiophene/SiGe superlattice, the hybrid TiS_2/[(hexylammonium)$_x$(H_2O)$_y$(DMSO)$_z$] superlattice, PEDOT:PSS/Si heterostructures, and (Zn, Al)O/hydroquinone superlattices. As a result of organic intercalation, the ZT values of these superlattice nanohybrids were greatly improved (better than their intrinsic inorganic counterparts). This was attributed to a large reduction in heat conductivity and an increment in electrical conductivity. These ideas can be applied to organic/inorganic thermoelectric nanohybrids to boost up the electrical conductivity and Seebeck coefficient of hybrids simultaneously.

References

1. Fan Z et al (2021) Recent developments in flexible thermoelectrics: from materials to devices. Renew Sustain Energy Rev 137:110448
2. Soleimani Z et al (2021) A comprehensive review on the output voltage/power of wearable thermoelectric generators concerning their geometry and thermoelectric materials. Nano Energy 89:106325
3. Nyandang AN et al (2021) Power generation using thermoelectric power generator with parabolic solar dish concentrator. In: Journal of physics: conference series. IOP Publishing
4. Kemerink M et al (2021) Organic and hybrid thermoelectrics. AIP Publishing LLC, p 260401
5. Jangra V, Maity S, Vishnoi P (2021) A review on the development of conjugated polymer-based textile thermoelectric generator. J Ind Text 1528083721996732

6. Cowen LM et al (2017) Organic materials for thermoelectric energy generation. ECS J Solid State Sci Technol 6(3):N3080
7. Yao B et al (2022) Thermal management of electronics and thermoelectric power generation from waste heat enabled by flexible Kevlar@ SiC thermal conductive materials with liquid-crystalline orientation. Energy Convers Manage 251:114957
8. Singh VP et al (2021) Thermoelectric energy harvesting using cement-based composites: a review. Mater Today Energ 21:100714
9. Yang J et al (2021) PEDOT: PSS/PVA/Te ternary composite fibers toward flexible thermoelectric generator. Compos Commun 27:100855
10. Prunet G et al (2021) A review on conductive polymers and their hybrids for flexible and wearable thermoelectric applications. Mater Today Phys 18:100402
11. Hansen CM (2021) Electron transport and performance degradation in next generation photovoltaic technologies. University of California, Davis
12. Kralj-Iglič V et al (2021) Socratic lectures: 4th international minisymposium, Ljubljana, 11–12 Dec 2020: peer reviewed proceedings
13. Wang L, Aslani F (2021) Mechanical properties, electrical resistivity and piezoresistivity of carbon fibre-based self-sensing cementitious composites. Ceram Int 47(6):7864–7879
14. Banerjee P et al (2021) Effect of particle-size distribution and pressure-induced densification on the microstructure and properties of printable thermoelectric composites and high energy density flexible devices. Nano Energy 89:106482
15. Han S, Chen S, Jiao F (2021) Insulating polymers for flexible thermoelectric composites: a multi-perspective review. Compos Commun 28:100914
16. Dhakal KN et al (2022) Electrically conductive and piezoresistive polymer nanocomposites using multiwalled carbon nanotubes in a flexible copolyester: Spectroscopic, morphological, mechanical and electrical properties. Nano-Struct Nano-Objects 29:100806
17. Jiang Q et al (2020) Recent advances, design guidelines, and prospects of flexible organic/inorganic thermoelectric composites. Mater Adv 1(5):1038–1054
18. Zhang Q et al (2022) Enhancing the room temperature thermoelectric performance of n-type Bismuth-telluride-based polycrystalline materials by low-angle grain boundaries. Mater Today Phys 22:100573
19. Zhu T et al (2017) Compromise and synergy in high-efficiency thermoelectric materials. Adv Mater 29(14):1605884
20. Sarkar D, Das S, Biswas K (2021) Valence band convergence and nanostructured phonon scattering trigger high thermoelectric performance in SnTe. Appl Phys Lett 119(25):253901
21. Foster MJ (2021) Modeling conductive properties of highly aligned single-walled carbon nanotube and graphene thin films. Wright State University
22. Xie M et al (2021) Achievements and prospects of thermoelectric and hybrid energy harvesters for wearable electronic applications. Thin film and flexible thermoelectric generators, devices and sensors, pp 3–40
23. Hicks LD et al (1993) Effect of quantum-well structures on the thermoelectric figure of merit. Phys Rev B 47(19):12727
24. Nandihalli N (2021) Thermoelectric films and periodic structures and spin Seebeck effect systems: facets of performance optimization. arXiv preprint arXiv:2109.08179
25. Kanatzidis MG et al (1993) New intercalation compounds of conjugated polymers. Encapsulation of polyaniline in molybdenum disulfide. Chem Mater 5(5):595–596
26. Wan C et al (2016) Flexible thermoelectric foil for wearable energy harvesting. Nano Energy 30:840–845
27. Yin S, Wan C, Koumoto K (2022) High thermoelectric performance in flexible TiS2/organic superlattices. J Ceram Soc Jpn 130(2):211–218
28. Ma H et al (2021) Strategies for enhancing thermal conductivity of polymer-based thermal interface materials: a review. J Mater Sci 56(2):1064–1086
29. Ranjan P et al (2018) Decoration of inorganic nanostructures by metallic nanoparticles to induce fluorescence, enhance solubility, and tune band gap. J Phys Chem C 122(12):6748–6759

30. Wang C et al (2018) Monolayer atomic crystal molecular superlattices. Nature 555(7695):231–236
31. Wan C et al (2017) Ultrahigh thermoelectric power factor in flexible hybrid inorganic-organic superlattice. Nat Commun 8(1):1–9
32. Lu Y et al (2020) Ultrahigh power factor and flexible silver selenide-based composite film for thermoelectric devices. Energy Environ Sci 13(4):1240–1249
33. Jin H et al (2019) Hybrid organic–inorganic thermoelectric materials and devices. Angew Chem Int Ed 58(43):15206–15226
34. Lee D et al (2016) Quantitative analyses of enhanced thermoelectric properties of modulation-doped PEDOT: PSS/undoped Si (001) nanoscale heterostructures. Nanoscale 8(47):19754–19760
35. Prunet G et al (2021) A review on conductive polymers and their hybrids for flexible and wearable thermoelectric applications. Mater Today Phys 100402
36. Wang Y et al (2021) Poly (3, 4-ethylenedioxythiophene)/polypyrrole/carbon nanoparticle ternary nanocomposite films with enhanced thermoelectric properties. Polymer 212:123131
37. Nouri-Borujerdi A, Kazemi-Ranjbar S (2021) Thermal and electrical conductivity of a graphene-based hybrid filler epoxy composite. J Mater Sci 56(27):15151–15161
38. Zhang B et al (2010) Promising thermoelectric properties of commercial PEDOT: PSS materials and their Bi2Te3 powder composites. ACS Appl Mater Interfaces 2(11):3170–3178
39. Jood P et al (2013) Thermoelectric properties of Ca3Co4O9 and Ca2. 8Bi0. 2Co4O9 thin films in their island formation mode. J Mater Res. 28(14):1932–1939
40. Culebras M, Gómez CM, Cantarero A (2013) Thermoelectric measurements of PEDOT: PSS/expanded graphite composites. J Mater Sci 48(7):2855–2860
41. Romarís LH et al (2018) Multifunctional electromechanical and thermoelectric polyaniline–poly (vinyl acetate) latex composites for wearable devices. J Mater Chem C 6(31):8502–8512
42. Wang J et al (2018) Thermoelectric and mechanical properties of PLA/Bi0·5Sb1·5Te3 composite wires used for 3D printing. Compos Sci Technol 157:1–9
43. Wang Y, Cai K, Yao X (2011) Facile fabrication and thermoelectric properties of PbTe-modified poly (3, 4-ethylenedioxythiophene) nanotubes. ACS Appl Mater Interfaces 3(4):1163–1166
44. Toshima N, Jiravanichanun N, Marutani H (2012) Organic thermoelectric materials composed of conducting polymers and metal nanoparticles. J Electron Mater 41(6):1735–1742
45. More PV et al (2017) Band engineered p-type RGO–CdS–PANI ternary nanocomposites for thermoelectric applications. Sustain Energ Fuels 1(8):1766–1773
46. An CJ et al (2017) High-performance flexible thermoelectric generator by control of electronic structure of directly spun carbon nanotube webs with various molecular dopants. J Mater Chem A 5(30):15631–15639
47. Khan ZU et al (2015) Acido-basic control of the thermoelectric properties of poly (3, 4-ethylenedioxythiophene) tosylate (PEDOT-Tos) thin films. J Mater Chem C 3(40):10616–10623
48. Anno H et al (2009) Preparation of conducting polyaniline–bismuth nanoparticle composites by planetary ball milling. J Electron Mater 38(7):1443–1449
49. Hammo SM (2012) Effect of acidic dopants properties on the electrical conductivity of poly aniline. Tikrit J Pure Sc 17(2):6–10
50. Meng C, Liu C, Fan S (2010) A promising approach to enhanced thermoelectric properties using carbon nanotube networks. Adv Mater 22(4):535–539
51. Jia Y et al (2021) Wearable thermoelectric materials and devices for self-powered electronic systems. Adv Mater 33(42):2102990
52. Panigrahy S, Kandasubramanian B (2020) Polymeric thermoelectric PEDOT: PSS & composites: synthesis, progress, and applications. Eur Polymer J 132:109726
53. Yun JS, Choi S, Im SH (2021) Advances in carbon-based thermoelectric materials for high-performance, flexible thermoelectric devices. Carbon Energy 3(5):667–708
54. Adekoya GJ et al (2021) Structure-property relationship and nascent applications of thermoelectric PEDOT: PSS/carbon composites: a review. Compos Commun 27:100890

55. Shi W, Yao Q, Chen L (2019) Fabrication and thermoelectric properties of PEDOT films and their composites. Thermoelectric Thin Films 69–96
56. Toshima N, Imai M, Ichikawa S (2011) Organic–inorganic nanohybrids as novel thermoelectric materials: hybrids of polyaniline and bismuth (III) telluride nanoparticles. J Electron Mater 40(5):898–902
57. Toshima N (2013) Metal nanoparticles for energy conversion. Pure Appl Chem 85(2):437–451
58. Hasani A et al (2020) Graphene-based catalysts for electrochemical carbon dioxide reduction. Carbon Energy 2(2):158–175
59. Liu F et al (2019) Synthesis of graphene materials by electrochemical exfoliation: recent progress and future potential. Carbon Energ 1(2):173–199
60. Ding B et al (2010) Electrospun nanomaterials for ultrasensitive sensors. Mater Today 13(11):16–27
61. Cavaliere S et al (2011) Electrospinning: designed architectures for energy conversion and storage devices. Energy Environ Sci 4(12):4761–4785
62. Dalton N et al (2019) Thermoelectric properties of electrospun carbon nanofibres derived from lignin. Int J Biol Macromol 121:472–479
63. Zhang M et al (2018) Synthesis and thermoelectric characterization of lead telluride hollow nanofibers. Front Chem 436
64. Wang Q et al (2012) Enhanced thermoelectric properties of CNT/PANI composite nanofibers by highly orienting the arrangement of polymer chains. J Mater Chem 22(34):17612–17618
65. Jiang Q et al (2020) Colossal thermoelectric enhancement in Cu 2+ x Zn 1–x SnS 4 solid solution by local disordering of crystal lattice and multi-scale defect engineering. J Mater Chem A 8(21):10909–10916
66. Tan C et al (2019) Synergistically optimized thermoelectric performance in Bi0. 48Sb1. 52Te3 by hot deformation and Cu doping. ACS Appl Energ Mater 2(9):6714–6719
67. Wang H et al (2019) Texture development and grain alignment of hot-pressed tetradymite Bi0. 48Sb1. 52Te3 via powder molding. Energ Technol 7(11):1900814
68. Kim J et al (2017) A facile preparation route of n-type carbon buckypaper and its enhanced thermoelectric performance. Compos Sci Technol 153:32–39
69. Hou W et al (2108) Fabrication and excellent performances of Bi0. 5Sb1. 5Te3/epoxy flexible thermoelectric cooling devices. Nano Energ 50:766–776
70. Jiang Q et al (2011) Magneto-electric properties of multiferroic Pb (Zr0. 52Ti0. 48) O_3–$NiFe_2O_4$ nanoceramic composites. J Am Ceram Soc 94(8):2311–2314
71. Jiang Q et al (2014) Enhancement of thermoelectric properties by atomic-scale percolation in digenite Cu x S. J Mater Chem A 2(25):9486–9489
72. Jiang Q et al (2017) Carriers concentration tailoring and phonon scattering from n-type zinc oxide (ZnO) nanoinclusion in p-and n-type bismuth telluride (Bi2Te3): Leading to ultra low thermal conductivity and excellent thermoelectric properties. J Alloy Compd 694:864–868
73. Ge Z-H et al (2018) Improved thermoelectric properties of PEDOT: PSS polymer bulk prepared using spark plasma sintering. Chem Commun 54(19):2429–2431
74. He M et al (2012) Thermopower enhancement in conducting polymer nanocomposites via carrier energy scattering at the organic–inorganic semiconductor interface. Energy Environ Sci 5(8):8351–8358
75. Gao J et al (2016) Enhanced power factor in flexible reduced graphene oxide/nanowires hybrid films for thermoelectrics. RSC Adv 6(38):31580–31587
76. Lin Z et al (2017) A solution processable high-performance thermoelectric copper selenide thin film. Adv Mater 29(21):1606662
77. Varghese T et al (2016) High-performance and flexible thermoelectric films by screen printing solution-processed nanoplate crystals. Sci Rep 6(1):1–6
78. Choi H et al (2018) Enhancement of reproducibility and reliability in a high-performance flexible thermoelectric generator using screen-printed materials. Nano Energy 46:39–44
79. Choi H et al (2017) Enhanced thermoelectric properties of screen-printed Bi 0.5 Sb 1.5 Te 3 and Bi 2 Te 2.7 Se 0.3 thick films using a post annealing process with mechanical pressure. J Mater Chem C 5(33):8559–8565

80. Han C et al (2018) High-performance PbTe thermoelectric films by scalable and low-cost printing. ACS Energ Lett 3(4):818–822
81. Yuan Z et al (2018) Screen-printed radial structure micro radioisotope thermoelectric generator. Appl Energ 225:746–754
82. Wang Y, Zhang S, Deng Y (2016) Flexible low-grade energy utilization devices based on high-performance thermoelectric polyaniline/tellurium nanorod hybrid films. J Mater Chem A 4(9):3554–3559
83. Sundberg P, Karppinen M (2014) Organic and inorganic–organic thin film structures by molecular layer deposition: a review. Beilstein J Nanotechnol 5(1):1104–1136
84. Giri A et al (2016) Reduction in thermal conductivity and tunable heat capacity of inorganic/organic hybrid superlattices. Phys Rev B 93(2):024201
85. Zheng G et al (2017) Shape control in ZIF-8 nanocrystals and metal nanoparticles@ ZIF-8 heterostructures. Nanoscale 9(43):16645–16651
86. Trung NH, Van Toan N, Ono T (2017) Fabrication of π-type flexible thermoelectric generators using an electrochemical deposition method for thermal energy harvesting applications at room temperature. J Micromech Microeng 27(12):125006
87. Huu TN, Van TN, Takahito O (2018) Flexible thermoelectric power generator with Y-type structure using electrochemical deposition process. Appl Energ 210:467–476
88. Yamamuro H et al (2018) Combination of electrodeposition and transfer processes for flexible thin-film thermoelectric generators. Coatings 8(1):22
89. Culebras M et al (2017) Manufacturing Te/PEDOT films for thermoelectric applications. ACS Appl Mater Interfaces 9(24):20826–20832
90. George SM, Yoon B, Dameron AA (2009) Surface chemistry for molecular layer deposition of organic and hybrid organic−inorganic polymers. Acc Chem Res 42(4):498–508
91. George SM (2010) Atomic layer deposition: an overview. Chem Rev 110(1):111–131
92. Cho J, Park J, An J (2017) Low thermal conductivity of atomic layer deposition yttria-stabilized zirconia (YSZ) thin films for thermal insulation applications. J Eur Ceram Soc 37(9):3131–3136
93. Lonkar S, Pillai V, Alhassan S (2018) Facile and scalable production of heterostructured ZnS–ZnO/graphene nanophotocatalysts for environmental remediation. Sci Rep 8:13401
94. Tynell T et al (2014) Efficiently suppressed thermal conductivity in ZnO thin films via periodic introduction of organic layers. J Mater Chem A 2(31):12150–12152
95. Mann HS et al (2015) Infrared and thermoelectric power generation in thin atomic layer deposited Nb-doped TiO_2 films. J Vac Sci Technol A Vac, Surf Films 33(1):01A124
96. Zheng L et al (2015) Direct growth of sb 2 te 3 on graphene by atomic layer deposition. RSC Adv 5(50):40007–40011
97. Liang L et al (2021) Recent advances in organic, inorganic and hybrid thermoelectric aerogels. Chinese Phys B
98. Karttunen AJ et al (2017) Flexible thermoelectric ZnO–organic superlattices on cotton textile substrates by ALD/MLD. Adv Electron Mater 3(6):1600459
99. Shen L et al (2019) Advances in efficient polymerization of solid-state trithiophenes for organic thermoelectric thin-film. ACS Appl Polym Mater 2(2):376–384
100. Cummins G, Desmulliez MP (2012) Inkjet printing of conductive materials: a review. Circuit world
101. Yin Z et al (2010) Inkjet printing for flexible electronics: materials, processes and equipments. Chin Sci Bull 55(30):3383–3407
102. Orrill M, LeBlanc S (2017) Printed thermoelectric materials and devices: fabrication techniques, advantages, and challenges. J Appl Polym Sci 134(3)
103. Kim D, Jeong S, Park B (2006) Moon, direct writing of silver conductive patterns: improvement of film morphology and conductance by controlling solvent compositions. J Appl Phys Lett 89:264101
104. Kuang M, Wang L, Song Y (2014) Controllable printing droplets for high-resolution patterns. Adv Mater 26(40):6950–6958

105. Chen B et al (2017) Inkjet printing of single-crystalline Bi2Te3 thermoelectric nanowire networks. Adv Electron Mater 3(4):1600524
106. Ferhat S et al (2018) Organic thermoelectric devices based on a stable n-type nanocomposite printed on paper. Sustain Energ Fuels 2(1):199–208
107. Park KT et al (2021) High-performance thermoelectric fabric based on a stitched carbon nanotube fiber. ACS Appl Mater Interfaces 13(5):6257–6264
108. Kato K, Hagino H, Miyazaki K (2013) Fabrication of bismuth telluride thermoelectric films containing conductive polymers using a printing method. J Electron Mater 42(7):1313–1318
109. Chen B et al (2019) Flexible thermoelectric generators with inkjet-printed bismuth telluride nanowires and liquid metal contacts. Nanoscale 11(12):5222–5230
110. He M et al (2015) 3D printing fabrication of amorphous thermoelectric materials with ultralow thermal conductivity. Small 11(44):5889–5894
111. Kim F et al (2018) 3D printing of shape-conformable thermoelectric materials using all-inorganic Bi2Te3-based inks. Nat Energy 3(4):301–309
112. Kalsoom U, Nesterenko P, Paull B (2016) Recent developments in 3d printable composite materials. RSC Adv 6(65):60355–60371
113. Maciá-Barber E (2015) Thermoelectric Mater
114. Hewawasam L et al (2020) Waste heat recovery from thermo-electric generators (TEGs). Energy Rep 6:474–479
115. Lan Y et al (2018) Organic/inorganic hybrid nanostructured materials for thermoelectric energy conversion. Functional organic and hybrid nanostructured materials: fabrication, properties, and applications, pp 445–484
116. Yang L et al (2018) High performance thermoelectric materials: progress and their applications. Adv Energy Mater 8(6):1701797
117. Dehkordi AM et al (2015) Thermoelectric power factor: Enhancement mechanisms and strategies for higher performance thermoelectric materials. Mater Sci Eng R Rep 97:1–22
118. Singh D, Ahuja R (2021) Dimensionality effects in high-performance thermoelectric materials: computational and experimental progress in energy harvesting applications. Wiley Interdisciplinary Reviews: Computational Molecular Science, p e1547
119. Tzounis L (2019) Organic thermoelectrics and thermoelectric generators (TEGs). Advanced thermoelectric materials for energy harvesting applications, p 7
120. Wang Y et al (2021) Flexible n-Type abundant chalcopyrite/PEDOT: PSS/graphene hybrid film for thermoelectric device utilizing low-grade heat. ACS Appl Mater Interfaces 13(43):51245–51254
121. Hu H et al (2020) Nucleation and crystal growth control for scalable solution-processed organic–inorganic hybrid perovskite solar cells. J Mater Chem A 8(4):1578–1603
122. Xie C et al (2020) Perovskite-based phototransistors and hybrid photodetectors. Adv Func Mater 30(20):1903907
123. Hou L, Bergmann NW (2012) Novel industrial wireless sensor networks for machine condition monitoring and fault diagnosis. IEEE Trans Instrum Meas 61(10):2787–2798
124. Slobodian P et al (2013) Thermoelectric properties of carbon nanotube and nanofiber based ethylene-octene copolymer composites for thermoelectric devices. J Nanomater 2013

Chapter 20
Organic–Inorganic Nanohybrids in Fuel Cell Applications

Abdul Rauf, Mashhood Urfi, Zaeem Bin Babar, Shahid Iqbal, and Komal Rizwan

1 Introduction

The rapid developments in the field of nanotechnology and nanoscience in twenty-first century rendered a great impact on human life. Nowadays, nanohybrids are one of the latest discoveries in the domains of nanoscience and nanotechnology. Hybrids are the material elements that are usually considered at molecular or nanometer levels. Simplistically, nanohybrids can be defined as "when multiple nanomaterials with unique chemical properties or different spatial properties are combined by physiochemical forces or molecular/macromolecular links the resultant product is called nanohybrid" or "when composite materials are designed in such a way that they are adhere to nanomaterials' surface to enhance the subsisting functionality to accomplish versatile usage". A simple illustration of above-mentioned definition is shown in Fig. 1 [1].

Hybrid materials are usually synthesized through polymerization of metallic alkoxides with macro-monomers [2]. There are many types of nanohybrids, e.g.,

A. Rauf · M. Urfi · Z. B. Babar (✉)
Institute of Energy and Environmental Engineering, University of the Punjab, Lahore, Pakistan
e-mail: zbabar@iese.nust.edu.pk

Z. B. Babar
Institute of Environmental Sciences and Engineering (IESE), School of Civil and Environmental Engineering (SCEE), National University of Sciences and Technology (NUST), Islamabad, Pakistan

S. Iqbal
Department of Chemistry, School of Natural Sciences (SNS), National University of Sciences and Technology (NUST), H-12, Islamabad 46000, Pakistan

K. Rizwan (✉)
Department of Chemistry, University of Sahiwal, Sahiwal 57000, Pakistan
e-mail: komal.rizwan45@yahoo.com

K. Rizwan et al. (eds.), *Hybrid Nanomaterials*, Materials Horizons: From Nature to Nanomaterials, https://doi.org/10.1007/978-981-19-4538-0_20

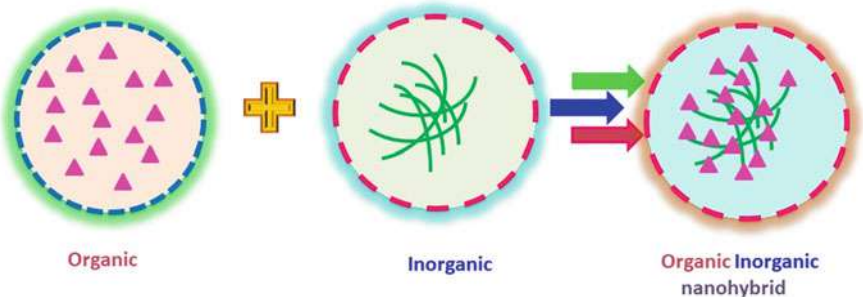

Fig. 1 Organic–inorganic-based nanohybrids

carbon–carbon nanohybrids (CCNHs), carbon–metal nanohybrids (CMNHs), metal–metal nanohybrids (MMNHs), organic molecule-coated nanohybrids (OMCNHs), etc. By combining different multi-scale components, we get a nanohybrid material that has unique properties which can be customized by the defined physical and chemical properties of soul components. These hybrid materials have better corrosion resistance, fire retardancy, thermal conductivity, electrical conductivity, thermo-sensitivity, optical, magnetic, and mechanical properties [3] as shown in Fig. 2.

Nanohybrids have a broader range of applications as presented in Fig. 3. They are extensively used in fuel cells (FCs), which are an important tool to convert chemical energy into electrical energy. FCs extracts chemical energy from specific gaseous fuels other than fossil fuels. Worldwide energy consumption is increasing because of continuous population growth and urbanization. Until now, fossil fuels are being used as a major source to fulfill these energy demands. On the other hand, these sources of energy are damaging environment very because of CO_2, CO, NO_x, SO_2, and particulate emissions. Furthermore, it is predicted that energy demand will increase by more than 50% in next 25 years. Therefore, fossil fuel resources will deplete very rapidly that will eventually lead the world toward energy crisis [4]. Considering these possibilities, it is necessary to explore alternative energy sources that are renewable, long lasting, and greener. FCs are attracting the world's scientists to develop more sustainable and efficient technology for energy production. FCs convert chemical energy into electrical energy without any kind of combustion that saves environment from any kind of hazardous pollutants, and hence, FCs can be considered as zero emission technology [5]. A FC receives its energy from outside of the cell, i.e., oxygen from the atmosphere and hydrogen from the fuel; therefore, it has major applications in automobiles, portable devices, and transportation machines. However, high operating temperature, availability, and pricing of fuel sources are the major constraints that are obstructing further advancement in FCs and their applications in industries.

There are many types of FCs, e.g., alkaline fuel cells (AFC), direct alcohol fuel cells (DAFC), direct glycerol fuel cells (DGFC), solid oxide fuel cell (SOFC), phosphoric acid fuel acid (PAFC), proton exchange membrane fuel cells (PEMFC), and

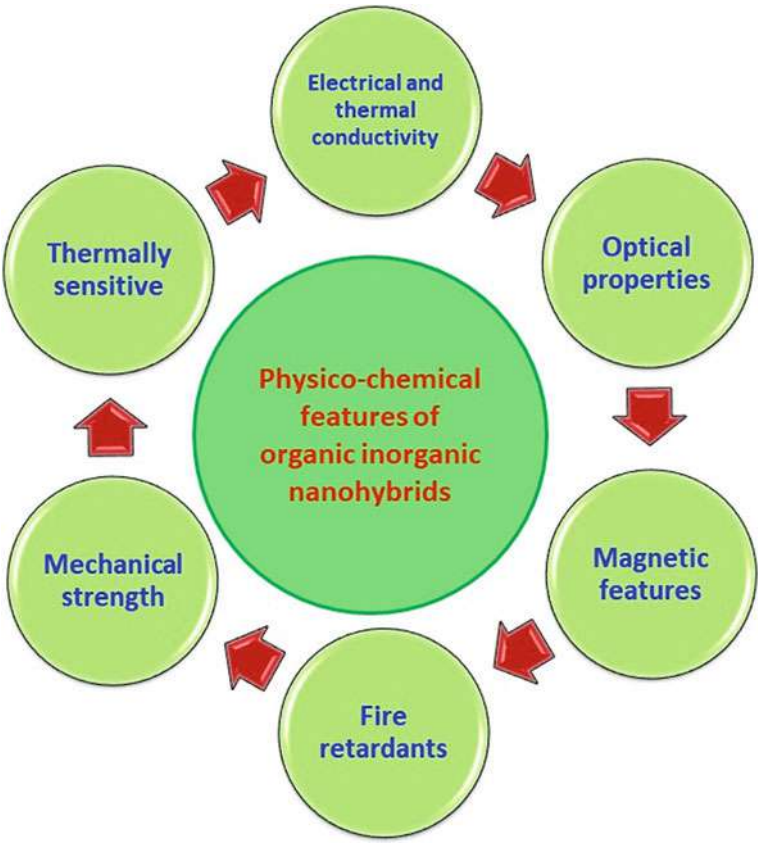

Fig. 2 Physiochemical features of organic–inorganic nanohybrids

molten carbonate fuel cells (MCFC) [6]. Each of these FCs has different working temperature range, carrier of charge, electrolyte, efficiency, and applications [7]. A FC is anticipated to be best replacement for rechargeable batteries and thermal engines in next few coming years as they are free from Carnot restrictions. FCs have many additional advantages, e.g., they can be fabricated in different sizes as per our energy requirements, and have high power density, limitless operating time, and greater capacity of storage to outperform rechargeable and simple batteries [8].

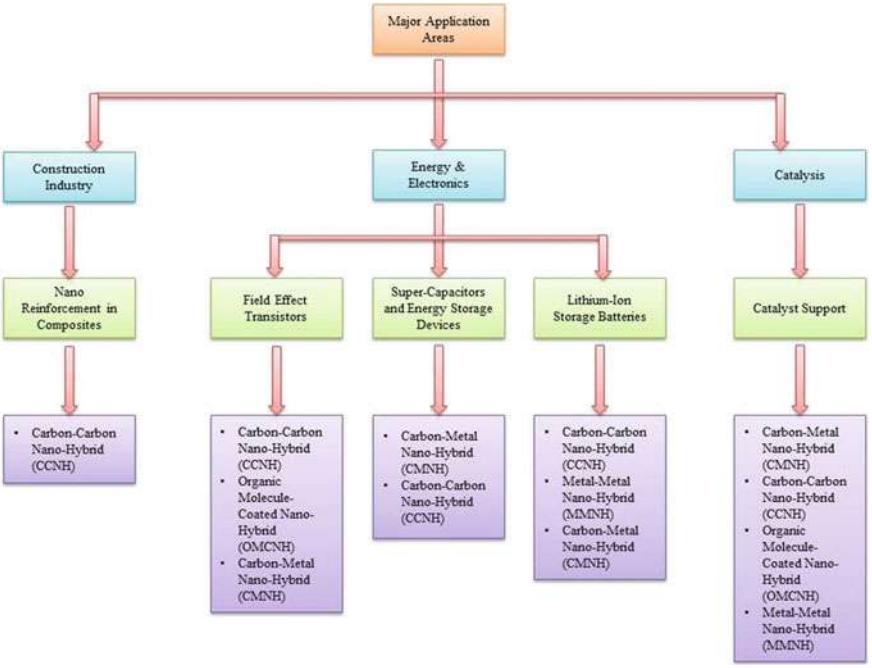

Fig. 3 Applications of nanohybrids

2 Working Principle of Fuel Cells

Fuel cells mainly comprise two electrodes that are separated from each other with the help of a membrane. Remaining parts are just to improve their performance. In more simple words, FCs are basically galvanic cells and have very simple principle of working of reduction and oxidation reactions at cathode and anode, respectively. A basic FC consists of an anode, a cathode, an electrolyte, and a membrane that is sandwiched between the electrodes to form a membrane electrode assembly (MEA) together with gas diffusion layers (GDLs) [9, 10]. During electrochemical reactions, an uninterrupted oxidation of hydrogen fuel and reduction of oxygen takes place at anode and cathode, respectively. Electrons are generated during the process that flows directly to external circuit and generate direct current that can be used instantly to run any appliance. Electrolytic membranes restrict the flow of electrons from inside the cell. Following reactions take place at their respective electrodes,

$$\text{Anodic Reaction:} \quad 2H_2 \rightarrow 4H^+ + 4e^- \tag{1}$$

$$\text{Cathodic Reaction:} \quad O_2 + 4H^+ + 4e^- \rightarrow 2H_2O \tag{2}$$

$$\text{Overall Generalized Reaction:} \quad 2H_2 + O_2 \rightarrow 2H_2O + \text{Heat} \tag{3}$$

Equations (1) and (2) represent the continuous oxidation and reduction of H_2 and O_2, respectively, whereas Eq. (3) is the overall reaction taking place in a FC. Hydrogen ions pass through the membrane at the end of the process to recombine with the electrons discharging at the cathode to regenerate H_2 gas that reacts with O_2 atoms to produce water, which is a by-product of the process [11]. Quality of electrolyte used greatly influence the effectiveness of a FC. Efficiency of a FC can be increased by stopping the movement of electrons generated at anode toward cathode through electrolyte. Therefore, selected electrolyte must have ability to restrict the passage of electrons and should allow only the positive ions to pass through it [12]. A catalyst is employed in order to reduce the energy of reaction occurring at the electrodes [13]. Platinum is a commonly used catalyst in FCs due to its extraordinary electrocatalytic properties during redox reactions. GDLs are used to develop outer layer of catalyst as it helps reactants to pass through catalyst layer to remove water which is a by-product of the reaction. GDLs also provide an electronic connection between electrode and bipolar plate through MEA channels. Furthermore, GDLs helps in reducing corrosion rate of catalyst layer and gives mechanical strength to MEA. Apparently, the anodic material can be hydrogen, kerosene, methane, or even carbon. But hydrogen is always preferred because of its high amount of energy per unit weight, easy availability, and good sensitivity for catalyst [14]. Similarly, oxygen is most commonly used as cathodic material because of its easy availability and high reduction power. The amount of current generated totally depends upon the size and temperature of the cell of FC and also operating conditions of temperature and pressure. A single cell produces a low voltage in the range of around 0.6–0.87 V; therefore, for high voltage value, multiple cells are connected in series or parallel arrangement. These connected cells have bipolar plates between them that helps in distributing oxygen and fuel uniformly in MEA. The resultant current is received by a collector plate which is fixed at MEA terminal.

2.1 Proton Conduction Process

Electrolytic membranes must conduct high number of protons across it in order to get a high value of current which is the prime requirement of the process. Number of protons conducted across the membrane is a key factor that determines the efficiency of a FC. Proton conduction itself depends upon a few factors, e.g., degree of sulfonation, membrane premodifications, operating temperature, and relative humidity [4].

Generally, there are two types of mechanisms for proton conduction,

1. Grotthuss mechanism (proton hopping)
2. Vehicle mechanism (electro-osmotic drag).

In Grotthuss mechanism, it is believed that proton moves across the cross-sectional membrane step by step from one hydrolyzed ionic site to another [5]. In this kind of mechanism, activation energy must be $0.1 < E_{act} < 0.4$ eV for a successful proton conduction [15]. In case of vehicle mechanism, protons tied up with a water molecule that behaves as a dragging agent to transfer a proton from one site to another one. For a successful proton conduction in this kind of mechanism activation energy must be greater than 0.5 eV [16]. In both types of mechanisms, the way of proton transfer mainly depends on the properties and nature of membranes that are being used in FCs. Large number of hydrated protons present in the system increases the relative humidity of the system which in turn increases the proton conductivity. However, excessive water content has unpleasant effects such as methanol pathways, reduced mechanical strength, and swelling in membrane. The maximum upper limit of temperature is 80 °C above which proton conductivity starts decreasing because of water and dry membrane that negatively affects membrane's conducting properties. Therefore, water content must be within optimum level in order to get best conductivity properties of membrane.

3 Organic–Inorganic Nanohybrids in Fuel Cells

3.1 Nafion-Metal Oxide-Based Nanohybrids

Nafion is a sulfonated fluoroethylene-based fluoropolymer that finds its major applications in making FCs especially proton exchange membrane fuel cells. In this nanohybrid, proton on sulfonic acid follows Grotthuss mechanism to move from one site to another one. This helps in promoting proton conduction by suppressing electron transfer through the membrane. However, dehydration problems at elevated temperatures and high operation cost limit Nafion applications in FCs. To overcome these problems, it is necessary to modify Nafion by combining it with other nanomaterials to get desired properties [17]. Recently, proton conduction rate in Nafion nanohybrids was improved by combining it with sulfonate and phosphate silica nanoparticles [18]. The resultant nanohybrid membrane showed very good proton conduction at high temperature and low relative humidity. For instance, sulfonate-based nanohybrids have proton conduction of 50 mS/cm at 30% relative humidity and 130 °C temperature. Additionally, these modified nanohybrids show an improved capacity of water retention and mechanical strength at raised temperature. Nafion can also be combined with metal oxides for synthesis of proton exchange membrane fuel cells. For such purpose, ZrO_2 or TiO_2 nanoparticles were used and the results were tremendously good with increased proton conduction and better ability to retain water that greatly increases the performance of fuel cells [19]. Proton exchange ability greatly enhanced when Nafion membranes that are synthesized in ethanol, water, and ethanol–water solvents are combined with Fe_2TiO_5. On addition of 2% of Fe_2TiO_5, obtained proton conductivity raised to 226 mS/cm. It is observed that

Table 1 Proton conduction and solvent uptake of simple and modified Nafion nanohybrid membranes

Membrane used	Solvent uptake (%)	Proton conduction (mS/cm)			
		Relative humidity (70%)	Operating temperature (110 °C)	Relative humidity 95 (%)	Operating temperature (25 °C)
Membrane synthesized using water solvent	33	240		226	
Membrane synthesized using ethanol solvent	31	–		1	
Membrane synthesized using water–ethanol solvent	29	–		6	

Reprinted with permission from [20]

membrane modified in water solvent has highest efficiency because of the polar nature of water as compared to those membranes that are prepared in ethanol or ethanol–water solvents [20]. Proton conduction and solvent uptake capacities of simple and modified Nafion nanohybrid membranes at different conditions of relative humidity and temperatures are listed in Table 1.

When Nafion was combined with CeO_2, the resultant nanohybrid membrane exhibited enhanced properties for its utilization in fuel cells. Nafion/CeO_2 was assembled between negatively charged SO_3 group of Nafion and positively charged CeO_2 nanoparticles. Below 75% relative humidity, Nafion/CeO_2 nanohybrid membrane showed good dimensional stability and high proton exchange ability as compared to pristine Nafion membrane. The synthesized membrane also showed a very low emission rate of fluoride which is 4.47, 8.67, and 43.05 mg/h against 10, 3, and 1 wt% of CeO_2, respectively. Nafion/CeO_2 membrane was prepared through sol–gel process; therefore, it demonstrated a very low reduction rate (1.13×10^{-4} mV/s) as compared to pristine Nafion membrane or simple Nafion. Modified pristine membrane with propyl sulfonic acid along with TiO_2 nanoparticles to form TiO_2-RSO_3H nanohybrid membrane possessed high proton conduction along with better efficiency. TiO_2-RSO_3H membranes are mostly used in direct methanol fuel cells to increase the performance of fuel cells. Using only 10 wt% of TiO_2-RSO_3H, at 140 °C gives a conductivity of 80 mS/cm in a single cell. Nafion/TiO_2-RSO_3H membrane has almost 40% more power density as compared to simple pristine Nafion membrane.

3.2 Graphene-Based Nanohybrids

Graphene has distinctive properties, for instance, high electrical conductivity, high chemical stability, excellent mechanical strength, more surface-active sites, low metal loading, and high surface area. Therefore, it is extensively used in energy storage devices, sensors, biomedical and electronic devices, and many other applications [21]. Because of the presence of epoxy groups, graphene acts a supporting material, whereas carboxylic groups help in increasing proton conduction ability of the material along with electrocatalyst for redox reaction in FCs. By spreading the metal on graphene, stability of nanocatalyst increases. Many of the graphene-supported and doped graphene nanoelectrocatalysts have been synthesized and analyzed for anodic as well as cathodic materials for FCs. These components are sorted out into following types:

1. Platinum-free alloy nanomaterial and electrocatalyst, supported with graphene, for low-cost material for FCs.
2. Metal-free electrocatalysts, supported with graphene, for oxygen-reduction reactions in alkaline and acidic electrolytic medium.
3. Platinum-based electrocatalysts, supported with graphene, for increasing oxygen-reduction rates in electrolytes.
4. Non-noble metals, supported with graphene, for effective electrocatalysts.

These materials are present at anode of direct methanol fuel cells (DMFCs) and cathode of oxygen-reduction reaction to facilitate electro-oxidation of organic molecules. For various applications in FCs, graphene or co-doped graphene is found to be very cost-effective when combined with nitrogen, sulfur, boron, or phosphorous.

Majorly, platinum-supported graphene and platinum-based alloys in FCs act as electrocatalyst to enhance its performance. To minimize the hazard of catalytic poisoning due to oxidation of methanol, platinum metal is dispersed uniformly on the surface of graphene nanoparticles. Thermal expansion and liquid exfoliation solvo-thermal reaction (TELESTR) is widely used environment friendly and low-cost method for hybridization of graphene with platinum metal or alloys. This method increases the electrocatalytic activity by increasing the oxidation of methanol in FCs. Through electrochemical analysis, methanol oxidation of PtCo/graphene and PtPd/graphene was found to be 1.558 and 1.218, respectively. Graphene-modified nanohybrid has high resistance to poisoning of carbon monoxide and thus shows high conductivity. Recently, Nafion nanohybrid is combined with graphene oxide to get a GO-Nafion nanohybrid. It has very good proton conduction in proton exchange membrane fuel cells [22]. Proton-conducting fields are formed in these nanohybrids when Nafion sulfonic acid units accumulate together. Electrochemical analysis results showed that GO-Nafion nanohybrids have 1.6 times higher proton conduction as compared to commercial Nafion. Graphene sheets doped with nitrogen have their extensive use in microbial fuel cells as an anodic material. Both catalytic activity and electron conduction are affected by nitrogen doping. This kind of doped nanohybrid has very high current density of 6300 mA/m^2 and a power density of around

1008 mW/cm^2. In short, all above-mentioned materials exhibit very good durability and methanol tolerance in both basic and acidic solutions. Such kind of ideal materials are mainly used in energy systems, e.g., metal air batteries and FCs.

3.3 Carbon Nanotube-Based Nanohybrids

An important class of materials that have their extensive applications in the areas of nanotechnology, electronics, energy materials, optics, sensors, and material science are carbon nanotubes (CNT) [4]. CNTs have extraordinary electrical, mechanical, and optical properties. Because of high electrical conductance and light weight, both single-walled CNTs (SWCNT) and multi-walled CNTs (MWCNT) are extensively being used in FC applications [23]. CNTs greatly enhance electron transmission, steadiness, catalytic performance, and corrosion resistance that helps in reducing overall cost of a FC [24]. CNTs are mostly used in microbial fuel cells (MFCs). A hybrid material synthesized from CNT/Pt enriched with effluent from palm oil mill acts as a substitute for catalyst and cathode support in MFCs, as that hybrid material has improved catalytic properties as compared to simple one. This hybrid material increased the output voltage of MFCs from 31.8 to 169.7 mW/m^2 that makes it a novel material for use as a catalyst in FC. By combining imidazole groups with MWCNT nanohybrid membrane using Nafion as a proton-conducting media to yield MWCNT-Im hybrid exhibited low permeability of methanol and high proton conductivity in direct methanol fuel cells [25]. It is because of formation of new electrostatic interactions between Nafion fluoropolymer's negatively charged sulfonic group and mutual interfacial attractions of MWCNT grafted with protonated imidazole units. Recently, MWCNT was compounded with MnO_2/polypyrrole to get a new hybrid MWCNT-MnO_2/PPy that acted as an anode in MFC to utilize sewage water for electricity generation [26]. MWCNT-MnO_2/PPy get deposited on the surface of carbon cloth cathode electrochemically. This fabricated electrode showed power density of 112.5 mW/m^2, electrical conductance of 0.1185 S/m, and with a band gap value 0.8 eV. Another catalyst support for PEMFC is invented by Mirzaei et al. that made up of Pt/MWCNT [27]. This hydrothermally synthesized catalyst support showed good activity even after 4000 runs, whereas a simple Pt/C catalyst lost its activity at around 2000 runs.

3.4 Conducting Polymer-Based Nanohybrids

Polymer electrolyte membrane fuel cells (PEMFCs) exhibited a great potential to deal with issues of generating and consuming renewable energy and to fulfill futuristic energy demands and sustainable environment. In this regard, development and manufacturing PEMs with robust design and high proton affinity is essential to succeed in dealing with the disadvantages of PEMs [28]. Alternative to carbon-based substances

including carbon graphitic structures, carbon nanotubes, and graphene nanosheets, conducting polymers can be applied due to their characteristic superiority. They are highly electrically conductive and chemically stable. Conducting polymer (CP)-based nanohybrids (CPNHs) can be generated by functionalizing polymers using metal oxides. Hence, CPNHs proved to be an eco-friendly polymer with augmented activity as a catalyst and high electrical affinity [29]. The carbon-based substances including carbon black, carbon nanotubes (CNTs), carbon fibers, mesoporous carbon, graphene etc., can be effectively utilized for the manufacturing of highly efficient FCs for the buildup of metallic nanoparticles due to enhanced surface characteristics and a variety of chemical functional species [30].

PEMFCs have a number of distinct and superior properties (i.e., quick boot setup, energy efficient and high power, and can easily handle power fluctuations) [28]. Typically, they work effectively at lower temperatures (100–200 °C) as compared to other FCs. CP-supported nanomaterial is a distinctive group of nanohybrids and specifically electrocatalysts regarding their utilization in FCs that possess the favorable characteristics of its individual components (nanomaterial and CP) [31]. Their higher electronic conductivity than the conventional catalysts is what achieves the level of attention. The manufacturing of Pt-free catalysts layered on CPs also has substantial importance owing to their enhanced catalytic efficiency [29].

CPNH electrocatalysts have been used on vast scale to oxidize low-molecular-weight organic substance utilized in FCs. Typically, in a direct alcohol fuel cell (DAFC), stored chemical energy of alcohol is converted to electricity through anodic oxidation in the presence of catalysts. Till now, platinum-based catalysts have been utilized, and productive attempts were made in lowering the cost of these electrocatalysts by decreasing the Pt content [32]. It can be understood better through example of methanol oxidation.

The oxidation of methanol in acidic or alkaline medium forms CO_2 in a six-stepped process is shown below:

$$\text{Anode Reaction:} \quad CH_3OH + 6\,OH^- \rightarrow CO_2 + 5\,H_2O + 6\,e^- \tag{4}$$

$$CH_3OH + H_2O \rightarrow CO_2 + 6H^+ + 6e^- \tag{5}$$

In MFC, microorganisms (MOs) have significant utilization such as electric power production, wastewater treatment, biological generation of hydrogen, and in other electrochemical devices, when employed as catalysts. MFC generally consists of an anode, a cathode, a polymer electrolyte membrane, substrates, and electrode catalysts [29]. MOs work as the anode, whereas for the cathode, we can use several metals/metal-based catalysts such as platinum, platinum black, manganese dioxide, etc. Nontoxic graphene-based catalysts are also used as an emerging technique to increase the speed of anodic reactions. Anodic oxidation of substrates can produce electrons, protons, and even carbon dioxide:

$$\text{Anode Reaction:} \quad CH_3COO^- + 2H_2O \rightarrow 2CO_2 + 7H^+ + 8e^- \tag{6}$$

$$\text{Cathode Reaction:} \quad O_2 + 4H^+ + 4e^- \rightarrow 2H_2O \tag{7}$$

The formation of metal nanoparticles with the synthesis of CPs leads to the manufacturing of highly efficient catalysts [33]. Generally, CP nanofibers are made at the interface of a micron-sized arrangement with alternating layers of surfactant in the presence of an oxidizing agent and Pd-based compounds [34]. The utilization of nanohybrids based on graphene and CPs in FCs can be promising by acting as electrochemical catalysts with enhanced electrochemical properties. Generally, the consistent dispersion of metallic nanoparticles on the exterior planes of polymer resulted in high transfer rates of charges. Conventional carbon-based supporting materials such as carbon black, carbon nanotubes (CNTs), etc., are highly hydrophobic in nature, which further highlight their utilization in FCs [35].

3.5 Novel Green Nanohybrids

Globally, the major issue faced in selection of a fuel is the environmental impact of its combustion content during and after burning. The efforts of research and development are constantly targeting to find out the most suitable fuel types to eliminate the use of fossil fuels. The reason behind the temptation to use fuel cells is the percentage of efficiency they provide (which is more than 50%) and the low temperature conditions they require to operate. Polymer electrolyte fuel cells such as direct borohydride fuel cells (DBFCs) have the similar advantageous features as mentioned above, over alcohol or hydrogen fuel cells, including efficient operation at relatively lower temperatures and higher cell voltage. Conceptually, DBFCs have the capability to generate eight electrons by oxidizing borohydride ion (BH_4^-), with sodium (Na^+) ions passing through a membrane [36]. The nanohybrid membrane used must be capable of transferring the Na^+ ions efficiently along with providing hindrance to BH_4^- ions. There are basically two groups of membranes categorized as per the charged state of ions being transferred; (i) anion exchange membrane (AEM) for the transportation of positively charged ions and (ii) cation exchange membrane (CEM) for the transportation of negatively charged ions. Doping of Nafion-based nanohybrid membranes with phosphonic acid-modified graphene oxide (PGO) has been manufactured as absolute candidates for their use in CEM-based FCs [37].

The recent developments in the manufacturing of the state-of-the-art polymeric membranes regarding their utilization in FCs have primarily focused on introducing specific functional groups by incorporating doping materials in the polymer matrix. In this aspect, metal oxides are used at a vast scale [38]. The use of TiO_2 in polymer nanohybrids introduces multifaceted properties such as extraordinary superior mechanical toughness, and temperature steadiness [39]. TiO_2 nanoparticles have improved fuel cell and battery performance (as a doping material or as a catalyst). TiO_2 functionalization has become a quite convincing approach to augment ion transfer rates by furnishing interconnection of ionic channels. The increase in

mechanical strength and decrease in fuel permeation could be achieved by utilizing proton-conducting fillers (i.e., titania nanotubes) without substantially decreasing the conductive property of nanocomposite. Additionally, they are hydrophilic nature and have superior surface characteristics (i.e., surface area) and high conductive property (~102−103 mS cm^{-1}) which renders them suitable for their effective use in polymer electrolyte membranes [40]. Using sulfate and phosphate ions in the acid treatment of TiO_2 enables the inculcation of acid into it, which increase hydrophilicity, conductance, and ion interchange capability [41]. Similar properties of polybenzimidazole membrane were observed when doped with TiO_2 in comparison with undoped polybenzimidazole. Addition of TiO_2 nanoparticles to polysulfone membrane increased the performance of FC. Also, enhanced electrochemical efficiency along with decrease in fuel permeation of membrane was obtained by adding TiO_2 nanotubes to a polymer mixture [poly(styrene sulfonic acid) and poly(vinyl alcohol) (PVA)] [42]. This explains the superiority of using titanium oxides in nanocomposites to form highly efficient fuel cells that will neither compromise environmental health and nor the cost of fuel.

PVA, poly (vinyl alcohol), is a low-cost, hydrophilic, and chemically stable polymer that permits convenient formation of film. However, it exhibits low ionic strength. This can be avoided by functionalizing PVA with 4-sulfophthalic acid to yield sulfonated poly (vinyl alcohol) (SPVA). The percentage content of the doped material appreciably affects the H-bonding, and/or interactivity between polymer and the doped material, and the physical and chemical properties of the resultant hybrid membranes which will increase the ion interchanging capability, ion conductance, oxidation potential, and robustness and decrease BH4—crossover, thereby allowing this membrane to be in competition with Nafion-based membranes for utilization in FCs.

4 Conclusion and Future Perspectives

Current developments in research work on nanohybrids and their use in fuel cells have been summarized in this chapter. Fuel cells are zero emission devices that make them environment friendly. They use hydrogen as fuel and exhibit very good efficiency and can be used in many portable electronic devices and automobiles. Because of these attractive features, fuel cells possess potential to replace ordinary energy sources in coming days. Major problems that arise in fuel cells are low proton conduction, high cost, fuel crossover, expensive raw materials, and low membrane stability. All these problems can best be resolved by incorporating fuel cells with nanohybrid materials, e.g., Nafion-metal oxides, graphene oxides, and carbon nanotubes. Cathode, anode, and membranes in fuel cells are basically composed of nanohybrid materials that have better water retention, high proton and low electron conduction through membranes, low chances of fuel crossover, and both high thermal and chemical stability, etc. that are discussed precisely in this chapter. Although very competitive nanohybrid membranes have been produced but to fill existing gaps, it still needs

further study to obtain membranes with good proton conduction and fuel crossover inhibition properties. Nanohybrid membranes can exhibit very good performance even at high temperature. High rate of proton conduction of a nanohybrid membrane is also dependent on water presence that is closely related to additive materials loading inside the nanohybrids. Finding affinity of a nanohybrid for inorganic particles is a big challenge of the day that must be addressed to certify that nanohybrid membrane is best optimized at optimum conditions that also helps in lowering membrane cost. In both Grotthus and Vehicular mechanisms, water is an important medium for proton conduction through membranes. Water intake by membrane greatly affects rate of proton conduction, so a good membrane must not absorb any water ideally as when water reaches on cathode side it acts as very dangerous agent that can cause oxidative or hydrolytic attack on nanohybrid membrane. Water retention ability of a membrane can be increased by introducing a hygroscopic inorganic material with nanohybrid membrane.

Regarding future aspects of nanohybrids, some of the following issues must be addressed:

1. Trade-off challenges
2. Efficient methods for the loading of additive material
3. Additive material's functionalization
4. Fabrication methods of nanohybrid membranes
5. Compatibility between nanohybrid and additive materials
6. Optimization of electrochemical properties.

Computational tools provide very important additional inputs for preparing nanohybrid membranes, since available information interprets many of their properties. Additionally, it will aid scientists to perform real-time experiments.

References

1. Ma W, Yah WO, Otsuka H, Takahara A (2012) Application of imogolite clay nanotubes in organic-inorganic nanohybrid materials. J Mater Chem 22:11887–11892
2. Yin PT, Shah S, Chhowalla M, Lee K-B (2015) Design, synthesis, and characterization of graphene-nanoparticle hybrid materials for bioapplications. Chem Rev 115:2483–2531. https://doi.org/10.1021/cr500537t
3. He H, Li J, Yu C, Luo Z (2019) Surface decoration of microdisk-like g-C3N4/diatomite with Ag/AgCl nanoparticles for application in Cr(VI) reduction. Sustain Mater Technol 22:e00127. https://doi.org/10.1016/J.SUSMAT.2019.E00127
4. Hajilary N, Shahi A, Rezakazemi M (2018) Evaluation of socio-economic factors on CO2 emissions in Iran: factorial design and multivariable methods. J Clean Prod 189:108–115. https://doi.org/10.1016/J.JCLEPRO.2018.04.067
5. Zakaria Z, Shaari N, Kamarudin SK et al (2020) A review of progressive advanced polymer nanohybrid membrane in fuel cell application. Int J Energ Res 44:8255–8295
6. Branco CM, Sharma S, de Camargo Forte MM, Steinberger-Wilckens R (2016) New approaches towards novel composite and multilayer membranes for intermediate temperature-polymer electrolyte fuel cells and direct methanol fuel cells. J Power Sour 316:139–159. https://doi.org/10.1016/J.JPOWSOUR.2016.03.052

7. Hegde RM, Kurkuri MD, Kigga M (2019) Current scenario of nanocomposit materials for fuel cell applications. Springer Nature. https://doi.org/10.1007/978-3-030-05399-4_20
8. Weydahl H, Gilljam M, Lian T et al (2020) Fuel cell systems for long-endurance autonomous underwater vehicles—challenges and benefits. Int J Hydrogen Energ 45:5543–5553. https://doi.org/10.1016/J.IJHYDENE.2019.05.035
9. Inamuddin TS, Kumar MR, Asiri AM (2019) Sustainable polymer composites and nanocomposites. Springer International Publishing, Cham. https://doi.org/10.1007/978-3-030-05399-4
10. Nafil RQ, Majeed MS (2020) Fuel cells as a source of green energy. In: Thermodynamics and energy engineering. IntechOpen
11. Manoharan Y, Hosseini SE, Butler B et al (2019) Hydrogen fuel cell vehicles; Current status and future prospect. Appl Sci (Switzerland) 9.https://doi.org/10.3390/app9112296
12. Lu Y, Zhu B, Cai Y et al (2016) Progress in electrolyte-free fuel cells. Front Energ Res 4:5. https://doi.org/10.3389/fenrg.2016.00017
13. Chong L, Wen J, Kubal J et al (2018) Ultralow-loading platinum-cobalt fuel cell catalysts derived from imidazolate frameworks. Science 362:1276–1281. https://doi.org/10.1126/science.aau0630
14. Flores GH, Poggi-Varaldo HM, Solorza-Feria O, Ponce Noyola MT (2015) Improvement of microbial fuel cell performance by selection of anodic materials and enrichment of inoculum. J New Mater Electrochem Syst
15. Agmon N (1995) The Grotthuss mechanism. Chem Phys Lett 244:456–462. https://doi.org/10.1016/0009-2614(95)00905-J
16. Peighambardoust SJ, Rowshanzamir S, Amjadi M (2010) Review of the proton exchange membranes for fuel cell applications. Int J Hydrogen Energ 35:9349–9384. https://doi.org/10.1016/J.IJHYDENE.2010.05.017
17. Suryani CYN, Lai JY, Liu YL (2012) Polybenzimidazole (PBI)-functionalized silica nanoparticles modified PBI nanocomposite membranes for proton exchange membranes fuel cells. J Membr Sci 403–404:1–7. https://doi.org/10.1016/J.MEMSCI.2012.01.043
18. Boutsika LG, Enotiadis A, Nicotera I et al (2016) Nafion® nanocomposite membranes with enhanced properties at high temperature and low humidity environments. Int J Hydrogen Energ 41:22406–22414. https://doi.org/10.1016/J.IJHYDENE.2016.08.142
19. Mohammadi G, Jahanshahi M, Rahimpour A (2013) Fabrication and evaluation of Nafion nanocomposite membrane based on ZrO_2–TiO_2 binary nanoparticles as fuel cell MEA. Int J Hydrogen Energ 38:9387–9394. https://doi.org/10.1016/J.IJHYDENE.2012.09.096
20. Hooshyari K, Javanbakht M, Naji L, Enhessari M (2013) Nanocomposite proton exchange membranes based on Nafion containing Fe2TiO5 nanoparticles in water and alcohol environments for PEMFC. J Membr Sci 454:74–81. https://doi.org/10.1016/J.MEMSCI.2013.11.033
21. Yang Y, Han C, Jiang B et al (2016) Graphene-based materials with tailored nanostructures for energy conversion and storage. Mater Sci Eng R Rep 102:1–72. https://doi.org/10.1016/J.MSER.2015.12.003
22. Peng KJ, Lai JY, Liu YL (2016) Nanohybrids of graphene oxide chemically-bonded with Nafion: preparation and application for proton exchange membrane fuel cells. J Membr Sci 514:86–94. https://doi.org/10.1016/J.MEMSCI.2016.04.062
23. Georgakilas V, Perman Jason A, Tucek J (2015) Broad family of carbon nanoallotropes: classification, chemistry, and applications of fullerenes, carbon dots, nanotubes, graphene, nanodiamonds, and combined superstructures. In: American Chemical Society. https://doi.org/10.1021/cr500304f
24. Akbari E, Buntat Z (2017) Benefits of using carbon nanotubes in fuel cells: a review. Int J Energy Res 41:92–102. https://doi.org/10.1002/er.3600
25. Tohidian M, Ghaffarian SR (2017) Polyelectrolyte nanocomposite membranes with imidazole-functionalized multi-walled carbon nanotubes for use in fuel cell applications. J Macromol Sci Part B Phys 56:725–738. https://doi.org/10.1080/00222348.2017.1375372
26. Mishra P, Jain R (2016) Electrochemical deposition of MWCNT-MnO_2/PPy nano-composite application for microbial fuel cells. Int J Hydrogen Energy 41:22394–22405. https://doi.org/10.1016/J.IJHYDENE.2016.09.020

27. Mirzaei F, Parnian MJ, Rowshanzamir S (2017) Durability investigation and performance study of hydrothermal synthesized platinum-multi walled carbon nanotube nanocomposite catalyst for proton exchange membrane fuel cell. Energy 138:696–705. https://doi.org/10.1016/J.ENERGY.2017.07.098
28. Zhou Z, Zholobko O, Wu XF et al (2021) Polybenzimidazole-based polymer electrolyte membranes for high-temperature fuel cells: current status and prospects. Energies 14.https://doi.org/10.3390/en14010135
29. Ghosh S, Das S, Mosquera MEG (2020) Conducting polymer-based nanohybrids for fuel cell application. Polymers 12:1–19. https://doi.org/10.1016/j.fuel.2021.121681
30. Gerber IC, Serp P (2019) A theory/experience description of support effects in carbon-supported catalysts. Chem Rev 120:1250–1349. https://doi.org/10.1021/acs.chemrev.9b00209
31. Xu P, Han X, Zhang B et al (2014) Multifunctional polymer-metal nanocomposites via direct chemical reduction by conjugated polymers. Chem Soc Rev 43:1349–1360
32. Ren X, Lv Q, Liu L et al (2019) Current progress of Pt and Pt-based electrocatalysts used for fuel cells. Sustain Energ Fuels 4:15–30. https://doi.org/10.1039/c9se00460b
33. Ghosh S, Maiyalagan T, Basu RN (2016) Nanostructured conducting polymers for energy applications: Towards a sustainable platform. Nanoscale 8:6921–6947. https://doi.org/10.1039/C5NR08803H
34. Ghosh S, Bhandary N, Basu RN (2017) Synergistic effects of polypyrrole nanofibers and Pd nanoparticles for improved electrocatalytic performance of Pd/PPy nanocomposites for ethanol oxidation. Electrocatalysis. https://doi.org/10.1007/s12678-017-0374-x
35. Shifrina ZB, Matveeva VG, Bronstein LM (2019) Role of polymer structures in catalysis by transition metal and metal oxide nanoparticle composites. Am Chem Soc. https://doi.org/10.1021/acs.chemrev.9b00137
36. Stroman RO, Jackson GS (2014) Modeling the performance of an ideal $NaBH_4$–H_2O_2 direct borohydride fuel cell. J Power Sour 247:756–769. https://doi.org/10.1016/J.JPOWSOUR.2013.08.100
37. Zhang B, Cao Y, Jiang S et al (2016) Enhanced proton conductivity of Nafion nanohybrid membrane incorporated with phosphonic acid functionalized graphene oxide at elevated temperature and low humidity. J Membr Sci 518:243–253. https://doi.org/10.1016/J.MEMSCI.2016.07.032
38. Bakangura E, Wu L, Ge L et al (2016) Mixed matrix proton exchange membranes for fuel cells: state of the art and perspectives. Prog Polym Sci 57:103–152. https://doi.org/10.1016/J.PROGPOLYMSCI.2015.11.004
39. Gouda MH, Elessawy NA, Santos DMF (2020) Synthesis and characterization of novel green hybrid nanocomposites for application as proton exchange membranes in direct borohydride fuel cells. Energies 13.https://doi.org/10.3390/en13051180
40. Matos BR, Isidoro RA, Santiago EI et al (2015) Nafion–titanate nanotubes composites prepared by in situ crystallization and casting for direct ethanol fuel cells. Int J Hydrogen Energ 40:1859–1867. https://doi.org/10.1016/J.IJHYDENE.2014.11.102
41. Liu X, Li Y, Peng S et al (2013) Modification of TiO_2 with sulfate and phosphate for enhanced eosin Y-sensitized hydrogen evolution under visible light illumination. Photochem Photobiol Sci 12:1903–1910. https://doi.org/10.1039/c3pp50167a
42. Yang CC, Chien WC, Li YJ (2010) Direct methanol fuel cell based on poly(vinyl alcohol)/titanium oxide nanotubes/poly(styrene sulfonic acid) (PVA/nt-TiO2/PSSA) composite polymer membrane. J Power Sour 195:3407–3415. https://doi.org/10.1016/J.JPOWSOUR.2009.12.024

Chapter 21
Organic–Inorganic Nanohybrids in Advanced Batteries

Aqsa Iqbal, Ataf Ali Altaf, Javeria Shoukat, Anila, Shaheed Ullah, and Samia Kausar

1 Introduction

1.1 Batteries

In batteries, electrical energy is being converted from chemical energy and vice versa, which are made up of stacked cells. Joining the cells in parallel and series electrically yields the necessary battery voltage and current levels. The power as well as energy capabilities of the batteries are measured. The energy and power capability of most types of batteries are not equal and are adjusted during the battery construction method. Energy efficiency is measured throughout battery design stage and is dependent. Efficiency, lifespan (measured in cycles), profundity of liberation (batteries are seldom discharged completely, and profundity of liberation means the degree to which they are discharged), temperature at which they operate, energy density, self-discharge (some batteries are unable to keep their electrical capability when kept on a projection, and self-discharge signifies the degree of discharging) are some of the other important characteristics of the battery [8].

1.2 Types of Batteries

The battery technology is currently undergoing tremendous advancement. Various kinds of batteries are being designed, some of them are accessible at commercial

A. Iqbal · A. A. Altaf (✉) · J. Shoukat · Anila · S. Ullah
Department of Chemistry, University of Okara, Okara 56300, Pakistan
e-mail: atafali_altaf@yahoo.com

S. Kausar
Department of Chemistry, University of Gujrat, Gujrat 50700, Pakistan

K. Rizwan et al. (eds.), *Hybrid Nanomaterials*, Materials Horizons: From Nature to Nanomaterials, https://doi.org/10.1007/978-981-19-4538-0_21

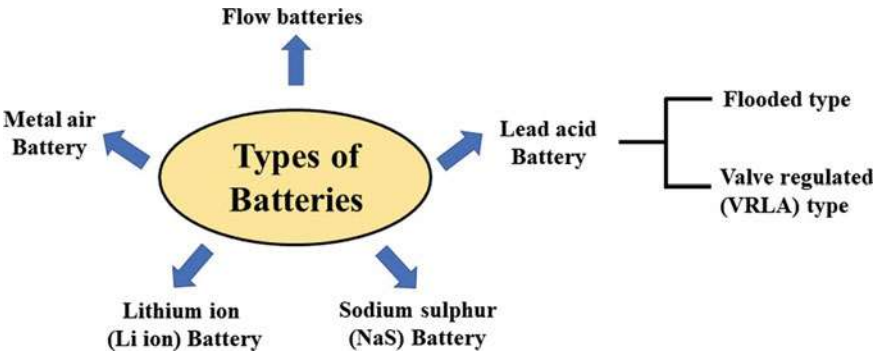

Fig. 1 Types of batteries

scale, and others which are in the trial step till now (Fig. 1). Deep cycle batteries (similar to those used in automobiles that use electricity) with energy capacities extending from 17 to 40 MWh and productivities of 70–80% have been used in power supply applications thus far. Some battery technologies appear to be better suited for power system applications, and these are shortly addressed under [8]:

1.2.1 Lead-Acid Battery

A lead-acid battery cell is composed of a positive electrode of PbO and a cathode of spongy Pb segregated by a microporous substance and dipped in a solution of H_2SO_4 electrolyte. It has two types [8]:

- Flooded type
- Valve regulated (VRLA) type

(a) Flooded Type

Flooded-type series of battery used the solution of H_2SO_4 electrolyte. During discharge, the anode's PbO_2 undergoes reduction to PbO, which interacts with H_2SO_4 to generate $PbSO_4$, while the cathode's sponge Pb undergoes oxidation to Pb^{+2}, which reacts with H_2SO_4 to form $PbSO_4$. Electricity is formed in this manner, and the reaction goes backward while charging [8].

(b) Valve Regulated (VRLA) Type

The VRLA employs the similar fundamental electrical and chemical principles as flooded lead-acid batteries, with the exception that these batteries are wrapped by a valve having function of pressure regulation. Furthermore, the acidic electrolyte is immobilized [8].

1.2.2 Sodium Sulfur (NaS) Battery

A sodium sulfur battery is made up of fused sulfur on the anode and molten sodium on the cathode, which are segregated by a ceramic electrolyte of firm beta Al_2O_3. Only Na^+ undergoes passage through the solution and reacts with sulfur to generate sodium polysulfides. In the course of discharging, Na^+ ions move through the electrolytic solution and negatives ions (e^-s) move through the battery's exterior circuit, creating around 2 V. To permit for this procedure, the battery is kept at about 300 °C [8].

1.2.3 Lithium-Ion (Li-Ion) Battery

The negative electrode in this battery is oxide of metal made of lithium, while the positive electrode is layer-structured carbon having graphite. Salts of Li dissolved in carbonate of organic nature form the electrolytic solution. After the charging of battery, the atoms of lithium in the negative electrode form charged species and pass through the electrolytic solution to positive electrode of carbon, where they unite with external negative charges and are deposited as Li atoms in-between layers of carbon. During liberation, same procedure goes in backward direction [8].

1.2.4 Metal Air Battery

These batteries' anodes are frequently accessible metals with higher energy compactness, such as zinc or aluminum, which liberate electrons after oxidation. Air electrodes or negative electrode is frequently built of spongy carbon structures or metal network coated with appropriate catalysts. Electrolytes, such as potassium hydroxide, are frequently excellent hydroxide (OH–) ion conductors (KOH). The electrolyte might take the shape of a liquid or a compact polymer membrane saturated with KOH [8].

1.2.5 Flow Batteries

Flow battery is made up of two electrolytic reserves through which the electrolyte is cycled (through drives) through an electrolytic cell that includes a negative electrode, a positive electrode, and that separates a membrane. When the two electrolytes flow from the electrochemical cell, the chemical energy is transformed to electricity. Both electrolytes are kept separately outside the electrochemical cell in enormous storage tanks. The density of energy of these batteries is determined by the dimensions of the reservoirs and the number of electrolytes used. The power compactness of flow batteries, on the contrary, is estimated by the speed of reaction of electrode happening at the positive and negative electrodes. Flow batteries are frequently denoted as redox flow batteries due to the redox (oxidation–reduction) interaction that occurs in-between the two electrolytes in the device [8].

2 Nanohybrids

At the nanoscale, materials development has moved beyond one-component production to heterogeneous substances assemblage or hierarchic form, which combines many nanomaterials (NMs) to get versatility. Nanohybrids are the name given to these types of assemblages (NHs). The necessity for versatility has resulted in NMs being chemically and physically modified generally. Hierarchy and hybrid materials are developed by integrating shape and structure modification with physical or chemical fabrication. Surface properties have been altered, and intrinsic hydrophobicity, unique electronic configurations, dissolving properties, and other features have been obtained from nanoscale materials as a result of this functionalization. The success of these modifications has motivated researchers to combine various NMs, each with new and versatile advantages, to achieve a higher level of functionality. Nanoscale nanogold, graphene nanosheets, and iron oxide, for example, each has greater magnetic, plasmon resonance, and charge carrying capabilities. In the material science research, there has been a strong ideal approach to claim simple external variation—with inorganic, organic, and soft molecules—as hybridization. Linking a polymer or monomer molecule to a metallic nanoscale substance, for example, has been claimed to produce an NHs [14]; large polymeric structures coupled with inorganic–organic atoms–molecules are also believed to be NHs [3]. Though small surface alterations can improve material performance, the original physicochemical qualities are likely to be retained; hence, they should not be regarded novel NHs for environmental assessment purposes. When more than one NMs of distinct chemical nature or varying dimensions of space are crosslinked by single molecule or large-sized molecular connections or physical and chemical forces, or when one nanoparticle coats the other holding a distinct chemical uniqueness, or when intricate delicate compounds are designed to attach to nanomaterial surfaces by chemical reactions, all to strengthen the current features or accomplish multi-functional uses, we call it an environmentally unique NH [15]. This definition is similar to the literature description of NHs, but it restricts the materials group to those NHs that are likely to have unexpected and distinctive environmental outcome, transportation, and toxic effects [2].

2.1 Classes of Nanohybrids

Four main classes of nanohybrids are known, i.e., carbon–carbon, metal–metal, carbon–metal, and coated NHs having coating of organic molecules (Fig. 2). The fundamental components of carbon–carbon NHs are single-walled and multi-walled carbon nanotubes (SWNTs and MWNTs), graphene sheets, fullerenes, and which are then connected with other carbonaceous substances to form hierarchies [2]. In the same way, carbon–metal NHs are designed by a combination of materials containing

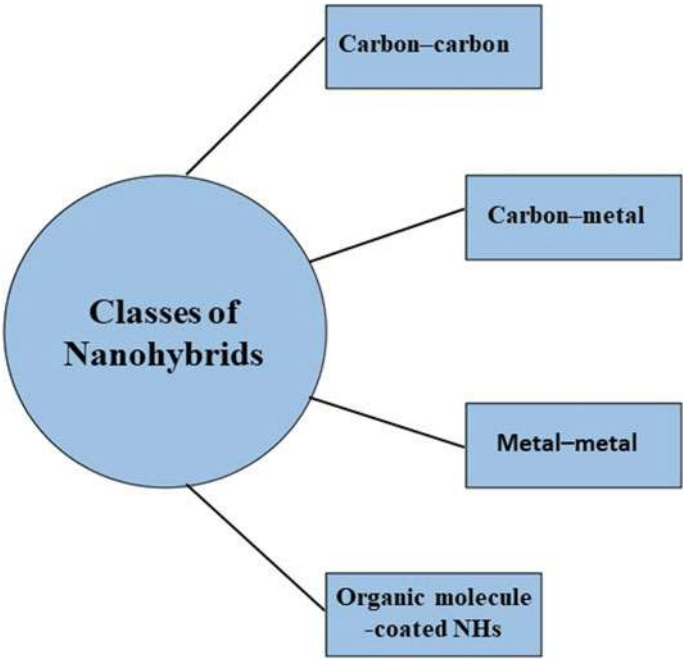

Fig. 2 Classes of nanohybrids

carbon with metallic NMs [11]. Metal–metal NHs, on the other hand, are arrangement of discrete metallic NMs [10] or are synthesized as core–shell structures of different metals [12] and metal oxides [19]. When metallic NMs conjugate with lengthy chain of polymers, cell-synthesized proteins, drug molecules, long-chain organic molecules, nDNA, etc., they form organic molecule-layered NHs [2].

The category of applications of nanohybrid materials is as follows: (1) **electronic**: Li-ion batteries, fuel and solar cells, imaging, superconductors–semiconductors–conductive materials, detection implementations; (2) **environmental**: catalytic–photocatalytic–electrocatalytic applications, membrane technology, devices contaminant sorption, and antimicrobial–antibacterial processes; (3) **medical**: biomaterial–biohybrids, cancer treatment and detection, delivery carriers, UV protection, and drug compound controlled release, etc. [2].

3 Organic–Inorganic Hybrids (OIH)

Organic–inorganic hybrids (OIH) are made up of binary or even additional parts, usually inorganic material (dielectric/semiconductor/particle metal or bulk component) and organic functional groups or molecules, biomolecules, polymers, and so on [23]. These components are linked with one another by unique connection as

a result in the production of the synergetic improvement of their unique features. OIHs have gained great attention in the domains of polymer chemistry, ceramics, physics and material engineering, and organic and inorganic chemistry. Fascinatingly, paint dyestuffs, i.e., Prussian Blue (iron (III) hexa-cyanoferrate) dissolved in organic solutions may be called as the initial illustration of OIHs. Though, the OIHs notion observed only in the 1980s with the progress of soft inorganic chemistry. Then at that time, the synthesis, applications, description of OIHs have developed a rapidly growing part of study in nanotechnology, life science and materials, bio- and environmental monitoring. In the previous years, organic–inorganic hybrids were produced on a commercial level with many utilizations in bio- and environmental monitoring and in analytical chemistry. Such hybrids may be molded into nanofibers, thin films, porous materials, nanoparticles, and nanostructures which show hierarchy, that is, very significant, for example, for designing operative bio-sensing stages with fast information proficiencies for biomedicine and environmental applications [24]. Properties modification, which leads to a change in intrinsic physical and chemical properties such as size, composition, surface and shape chemistry, remains at the center of NH synthesis. As a result of these changes, new qualities develop. The requirement for multi-functionality has led to NMs being chemically and physically modified in general. Hierarchy and hybrid materials are created by combining size and form modification with physical or chemical functionalization. Surface properties have been changed, and novel electronic configurations, dissolving properties, intrinsic hydrophobicity, and other features have been obtained from nanoscale materials as a result of this functionalization. The success of such modifications has motivated researchers to combine various NMs, each with new and versatile advantages, to achieve higher levels of functionality. Nanoscale iron oxide, nanogold, and graphene nanosheets, for example, each has greater magnetic, plasmon resonance, and charge carrying capabilities [2].

4 Organic/Inorganic Nanohybrids (OINHs)

At the nanoscale, materials development has moved beyond one-component production to multi-component, in which two or more already produced nanomaterials (NMs) are coupled to generate versatility. Nanohybrids are the name given to these types of ensembles (NHs) [2]. Nanohybrids are the name given to these types of ensembles (NHs) [28]. In general, nanocomposites having intricately mixed organic (biological) and inorganic networks are known as O–I nanohybrids [20]. OINHs are more probable to be well-arranged structures at the molecule level that have at minutest one constituent, either inorganic or organic at nanoproportions (less than 100 nm). Surprisingly, the ultimate features of OINHs can come from either the total of the distinct integral molecules or the significant interaction formed by the NH interface [21]. To put it another way, organic–inorganic hybrid materials are multi-component structures with minimum one organic and inorganic component in the micro-metric and, more commonly, nanometric size domains [9].

The construction, layout, durability, physical, and physiological features of O–I hybrid nanomaterials are influenced not by the experimental parameters, such as pH, preparation method, temperature, interaction duration, and many more, but by the quantity as well as proportion of inorganic and organic networks used also. Colloid templates, functional nanogels, hollow capsules, optics, biohybrids, nanomembranes, microelectronics, produce smart nanomaterials, stimuli-sensitive nanomaterials, nanobiosensors, and other sectors can all benefit from O–I hybrid nanomaterials [22]. The features of hybrid materials are a result of a significant synergy formed by the existence of a vast hybrid interface, not just the total of the distinct inputs of their constituents. The organic–inorganic interface (energy, kind of interactions, and link ability) does, in fact, play an important part in modifying a diversity of features (separation, optical, catalysis, mechanical, constancy to thermal and chemical pressures). This is why, depending on the kind of the interface among the organic (or biological) and mineral components, distinct hybrid materials have been classified into two primary groups [9].

An inorganic component in hybrid nanomaterials serves numerous functions, including boosting improving charge transfer, mechanical and thermal stability, and redox activity, and giving specialized electromagnetic, electronic, electrochemistry, or chemical capabilities. Organic components, on the other hand, can influence the physical and chemical aspects of the ending surfaces (i.e., specific oxidation–reduction potentials, electrical, electrochemical, photosensitive features, etc.). It is possible to modify the hydrophobic/hydrophilic harmony of the upper layer and manage the attachment behavior, porosity/density of O–I networks by using organic compounds to improve/amend the mechanical features of surfaces, control the sponginess/compactness, and add-on performance of systems. Figure 3 summarizes some of the most frequent organic and inorganic moieties used in the nanohybrid production [22].

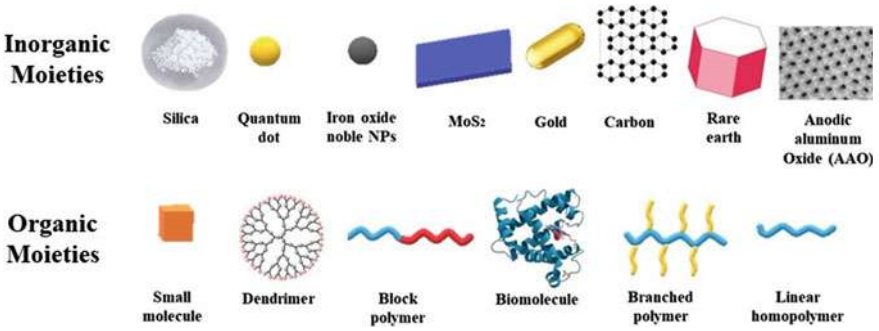

Fig. 3 Organic and inorganic moieties use in nanohybrids

4.1 Classification of OINHs

The OINHs can be divided in two classes:

Class I

Exchange weak links, such as Van der Waals interactions, ionic bond, hydrogen bonding, production, are used to connect inorganic and organic constituents into networks in Class I. Because of their hybrid chemistry, this class of nanohybrids has various application in the production of sensors, biosensors, and catalysts [22].

Class II

Organomineral co-polymers have both O–I constituents connected by covalent or ionocovalent bonding [18]. The existence of covalent chemical bonds between inorganic and organic components has various benefits, which can be grouped into three categories: production of new nanomaterials with enhanced functional characteristics, substantially improved O–I surface formation, and customized hydrophilic-hydrophobic balance. It is also worth noting that numerous hybrid nanomaterials may exhibit both kinds of contacts, such as strong covalent interactions and weak Van der Waals, at the same time, as observed in Class I or Class II as reported by [22].

5 Synthesis of OINHs

The treatment of OIH materials has sparked interest in both industry and academia circles for more than 30 years. The employed synthesized techniques involve "polymerization" or "implantation" procedures of molecular polymeric precursors, or nano-objects in the broadest range (polymers, alkoxides as well as salt of metals, nanoslabs, practical nanoparticles, etc.). These processes can take place at minimum temperatures (20–300 °C) in organic solvents under standard or autogenic compression. Many organic and organometallic chemistry, intercalation chemistry, supramolecular chemistry, and polymer chemistry reactions occurred under these very minor conditions. As a consequence of this methodology, it is able to implement novel OIH materials, which are often mixtures at the molecular or nanometric level, while concurrently generating biological or organic components and inorganic composites. Indeed, merging the features of some biological or organic molecules with those of mineral chemicals at the molecular level in one substance has become a feasible goal. The concern in these multi-functional hybrid materials stems not only from their chemical and physical features, but also from the various alternatives that the combination of the colloidal state with the physical and chemical features of biological systems and complicated fluids provides. The facile processing of many hybrid materials is enabled by the combination of soft chemistry and the multiple engineering approaches used to form soft matter (spin coating,

dip coating, inkjet printing, extrusion, micro-emulsion templating, electrospinning, aerosols processing, 3D/4D printing) [9].

Irrespective of the class of nanohybrid, they can be made in a variety of ways: via conventional hydro- and solvothermal synthesis or sol–gel chemistry (Route A); via/assemblages of already generated monodispersed nano-objects/hybridizing distinct nanobuilding blocks (NBBs) (Route B); via auto-organization of amphiphilic polymers and molecules to produce supramolecular patterns and regulate the quality and (Route D). The traditional sol–gel method enables the generation of simple and inexpensive hybrid networks by hydrolyzing organically altered metallic alkoxides (Route A). Route B is typically utilized to create NHs with a greater inorganic component characterization. The functionalization of NBBs could be done via polymer formation reaction or linked by organic ligands to produce interconnected hybrid networks. Route C leads to the production of self-assembled hybrids with a regulated shape and texture [22].

The following are some examples of OINH grafting strategies [22]:

- Implanting polymers with thiol groups on the surface of metallic carriers frequently involves the creation of metal-sulfur bonds. The most renowned example is bonding of Au-thiol, which is the most common way for Au-NPs to interact with thiolated polymers [6].
- Another example is the use of composites having enzymatic antibody much similar to that of hydrangea to create nanoflowers of inorganic-protein for Enzyme-Linked Immunosorbent Assay (ELISA) [25].

Though, it has be noted that most synthesized nanohybrids are non-crystalline with polyscattered structures, making essential structure connections difficult to examine. Furthermore, a broad range of potential designs may be identified within O–I nanohybrids, ranging from assembly of lattice structure, sandwich-like structures, cellular, spongy constituents, segmented structures, additionally. The multitude of alternative amalgamations of inorganic as well as organic networks, fillers, additives, matrices, and topologies expands the design potentials for OINHs, allowing for additional property enhancement and modifying [22].

5.1 Poly(3,4-Ethylenedioxythiophene)/V_2O_5 Nanohybrid for Li-Ion Batteries

5.1.1 Reaction

The electrical and chemical characterization of novel OIHs generated by insertion of conducting PEDOT into V_2O_5 has been employed as an electrode for Li-ion batteries that can be recharged. PEDOT/V_2O_5 nanocomposite was created by oxidation–reduction process of insertion of ethylenedioxythiophene (EDOT) with crystal of V_2O_5 powder and the chemistry of polymerization linked with this scheme to

show the presence of two stages in the PEDOT–V_2O_5 system consistent to PEDOT insertion into V_2O_5. Several physical and chemical statistics and the micro-structure of PEDOT–V_2O_5 nanocomposites confirm these results, and the resultant nanocomposite exhibits increased ambient thermal conduction and remarkable electrical and chemical performance for high-capacity cathode material for lithium-ion batteries [17].

5.1.2 Preparation of PEDOT–V_2O_5 Nanohybrid

Here, 1.1 mM of vanadium pentoxide and monomer of 0.42 mM ethylenedioxythiophene mixes in double-distilled water were processed in a double-walled Teflon-coated digestion tank, which was positioned on a turn-table for even boiling utilizing a microwave digestor. The reaction vessel's outside shell was made of a strengthening polymer named as Ultem polyetherimide, while the internal lining was made of Teflon. Because these jars were microwave-transparent, the contents could be provided with temperature hydro-thermally. After the reaction contents were subjected to microwave radiations, these caused dipoles inside the fluid to rotate, pushing the dipolar substances to arrange themselves and caused relaxation in the field of vibrating electromagnetic rays, triggering the liquid to heat up. As a result, unlike in other typical systems, the heat generated inside the liquid is not transported from the vessel. For 10 min, computer-controller microwaves-hydrothermal handlings were performed utilizing a 2.45 GHz microwaves at maximum power of 950 W. Following microwaves treatment, the solid was sieved out and repeatedly cleaned with ethanol and water, and the dark blue black powder was air dried [17].

5.2 Gel Polymer-$NaAlO_2$ Nanohybrid

5.2.1 Preparation

The PGPEs were made using the phase-inversion approach described by Yadav et al. To begin, stoichiometric $NaAlO_2$/PVdF-HFP (poly(vinylidinefluoride-co-hexafluoropropylene)) suspensions were liquified in dimethylformamide solution for 12 h. The $NaAlO_2$/PVdF-HFP solutions were then subjected to steam at 100 °C. Subsequently, after 2 h, stretchy white films were formed, which were then rinsed in deionized water to eliminate any remaining solvent before drying at 85 °C for 10 h. Following Fig. 4a depicts a representative picture of a flexible porous film [5]:

The width of the porous films was determined to be between 400 and 780 m. The porous structure of the film is reflected in its white hue. Scanning electron microscopy (SEM) examinations demonstrate the porous character of the film, confirming the existence of small holes in the films as shown in Fig. 4b [5]:

In contrast to GPEs prepared using the solution molding method, the filling of $NaAlO_2$ fillers was held low, up to 0.75 wt%, because the films were unable to hold

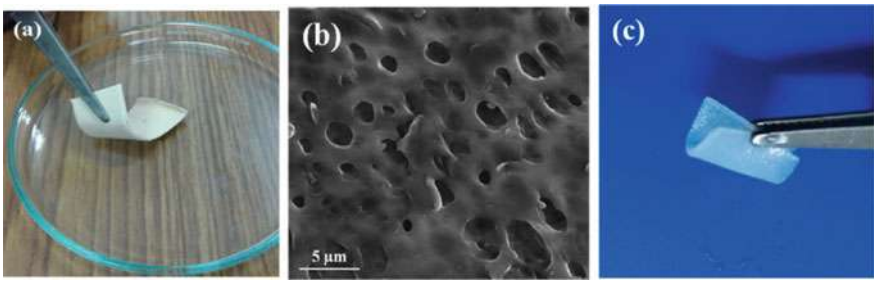

Fig. 4 Porous film (**a**), its SEM image (**b**), image of LE-soaked PGPE (**c**). Reproduced with permission from [5]. (Copyright 2021, Elsevier)

higher filler concentrations, and filler constituents' precipitate formation was detected in the container throughout washing with deionized water. Pictures of a spongy film with 1 wt% $NaAlO_2$ immersed in water are presented in Fig. 4c which clearly shows particle segregate occurrence and precipitate formation. Yet, no such findings are observed in the case of film containing 0.75 wt% $NaAlO_2$. The PGPE films were created by immersing the spongy films in a liquid electrolyte (LE) of 1 molar sodium perchlorate in EC: PC (volume/volume) until weight saturation was reached. After sopping in liquid electrolyte, the PGPE films looked somewhat translucent [5]. The electrolyte films with 0, 0.25, 0.50, and 0.75 wt% $NaAlO_2$ fillers are obtainable as PGPE, PGPE0.25, PGPE0.50, and PGPE0.75, respectively [5].

5.3 *(PEO)$_9$ LiCF$_3$SO$_3$ + Al$_2$O$_3$ Nanohybrids in Lithium Polymer Batteries*

Polymer electrolytes of nanocomposite are being investigated as prospective options for use as membrane of electrolyte in Li-ion batteries of polymer and other gadgets. A review of the literature, however, indicates that methodical research of the influence of ceramic filler amount and superficial zone on the conduction improvement of small-sized and nanocomposite polymer electrolytes is absent. We investigated the heating and electric features of a complex polymer electrolyte $(PEO)_9LiCF_3SO_3$ + Al_2O_3 including Al_2O_3 holding grains of four distinct dimensions with various definite external areas in this study. The outcome demonstrates that the melting temperature of polyethylene oxide crystallites fell by a few degrees in illustrations containing fillers, with a least for samples with greater conduction. The inclusion of the filling significantly increased the ionic conduction greater and lower than 60 °C, with the nanoporous Al_2O_3 grains with 5.8 nm size of pore, 150 m^2/g surface area, and 15 wt% filler concentrations exhibiting the greatest augmentation. The experimental conduction increase has been ascribed to Lewis' acid–base nature of superficial contacts of ionic types with O/OH assemblages on the filler surface, with an extra input below 60 °C coming from the maintenance of an improved part

of the amorphous phase due to the filler's existence. The conductivity versus filler concentration charts show two conductivity maxima that are described in terms of blocking effect, surface interactions, and grain consolidation. Beyond 100 m^2/g grain surface area, the conductivity improvement seems to saturate [7].

5.3.1 Reaction

Aldrich supplied PEO (molecular weight, 5 × 106) and $LiCF_3SO_3$ (lithium triflate, LiTf). The pore size of the nanoporous Al_2O_3 powder (Aldrich) was 5.8 nm, the particle size was 104 mm, the surface area was 155 m^2/g, and the surface groups were acidic. Alfa Aesar supplied the Al_2O_3 powder with grain sizes of 10 mm, 37, and 10–20 nm. The purity of all four varieties of alumina powder was 99.5% or above. Polyethylene oxide (PEO) and lithium triflate were vacuum dried for 24 h before to usage at 50 and 120 °C, correspondingly. Properly measured amounts of PEO and lithium triflate were dissolved in anhydrous acetonitrile to achieve an ethereal oxygen to lithium-ion ratio of 9:1. Al_2O_3 particles were dried in vacuum at 200 °C for 24 h before adding to the aforementioned solution, which was magnetically agitated at ambient temperature for at least 24 h to achieve a homogeneous mixture. The quantity of filler supplied to each Al_2O_3 type ranged from 5 to 25% of the overall poly(ethylene oxide) + lithium triflate weight. After stirring, the resultant slurry was poured onto a Teflon plate and left to gently evaporate the solvent. This technique produced visually homogeneous composite polymer electrolyte sheets with typical thicknesses of 100–200 mm, which were then vacuum dried for 24 h [7].

The melting temperatures of PEO crystallites in various substances were measured using a Mettler Toledo DSC 30 differential scanning calorimeter. The quantities were taken from 140 to 140 °C in the heating cycle at a heating rate of 10 C min1. To avoid contact with ambient moisture, a flow of N_2 gas was kept over the pierced pot. Using a computer-controlled Schlumberger SI 1260 impedance analyzer in the 1 Hz to 10 MHz range of frequency, complex impedance measurements were done on disk-shaped samples sandwiched between two stainless steel electrodes of 13 mm diameter. The sample's temperature was changed from 25 to 110 °C, and measurements were obtained at about 108 °C intervals during heating. The ionic conductivity was calculated using complex impedance data [7].

6 Applications of OINHs in Advanced Batteries

Due to the reduction of fossil fuels and the need to achieve alternative energy sources and a cleaner environment, energy has become one of the most difficult concerns in the twenty-first century. Presently, energy research is divided into two categories: production and preservation. Solar cells, tides, water splitting, and wind are examples of alternative energy sources that have been widely developed. However, progress in power storage appears to be lagging, despite the fact that this sector is currently a

prominent study area. Thermal energy storage, batteries, supercapacitors, fuel energy storage, and other types of energy storage exist. Batteries, as key energy carriers for energy storage, have the benefits of application flexibility, high efficiency, and fast response speed among all storage systems. Batteries are now essential in the energy storage sector as well as other practical uses. Rechargeable metal-ion (Li, Mg, Na, K, Al, Zn, etc.) batteries with long lifetimes, safety, and high energy/power density are preferred and draw a lot of attention as society progresses, and there is an urgent need for clean energy and a friendly environment [29].

Because of their strong ability to efficiently store electric energy in chemical form, rechargeable batteries are becoming increasingly significant in our daily lives [4]. Furthermore, new portable batteries, such as transparent batteries, flexible batteries, and tiny batteries, are gaining favor in today's culture [27].

6.1 *Poly(3,4-Ethylenedioxythiophene)/V_2O_5 Nanohybrid for Li-Ion Batteries*

PEDOT–V_2O_5 nanocomposite was made via oxidation–reduction insertion of ethylenedioxythiophene with crystalline V_2O_5 powder and subsequent polymerization chemistry to establish the existence of two phases in the PEDOT–V_2O_5 system consistent to PEDOT insertion into V_2O_5. Poly(3,4-ethylenedioxythiophene)–V_2O_5 nanocomposite was formed by redox complexing ethylenedioxythiophene (EDOT) with crystalline V_2O_5 powder and then using polymerization chemistry to determine the presence of different stages in the poly(3,4-ethylenedioxythiophene)–V_2O_5 system that corresponded top poly(3,4-ethylenedioxythiophene) complexation into vanadium pentoxide. The produced nanocomposite exhibits better room temperature conduction and outstanding electrical and chemical capabilities as a high-capacity negative electrode material for lithium batteries, according to numerous physical and chemical statistics and micro-structure of poly(3,4-ethylenedioxythiophene)–V_2O_5 nanocomposites [17].

6.2 *Polymer Electrolyte (PE)/Metal-Ion Nanohybrid for Rechargeable Batteries*

The use of inert inorganic fillers in PEs has been extensively researched. TiO_2, Al_2O_3, ZnOx, ZrO_2, and SiO_2 are some of the most often used inorganic fillers. The consequence of these inorganic fillers on electrical and chemical properties, on the other hand, is still a topic of debate. Adding fillers was once expected to upgrade the mechanical properties of PE while diminishing the crystalline structure of PEO, hence increasing ionic conductivity at temperatures less than the melting change. The accumulation of inactive fillers to a polymer electrolyte may improve polymer

chain movement and mechanical strength; but, these inactive nanoparticles will not contribute to the electrolyte's ionic conductivity. In this context, the usage of SPEs in combination with lithium-ion conductive inorganic electrolytes has piqued interest as a means of overcoming the limitations of each component individually. Of all the present inorganic electrolytes, NASICON and garnet have sparked the most scientific interest in the fabrication of nanocomposites [4].

6.3 $(PEO)_9\ LiCF_3SO_3 + Al_2O_3$ Nanohybrids in Lithium Polymer Batteries

Membranes composed of nanocomposite PEs are being investigated as probable use in Li polymer batteries and other technologies. But, a review of the literature shows that no comprehensive study of the outcome of ceramic filler surface area and concentration on the conduction improvement of small-sized and nanocomposite PEs has been conducted. This study looked at the heating and electrical properties of a composite polymer electrolyte $(PEO)_9LiCF_3SO_3 + Al_2O_3$ that included four different sizes of alumina filler grains with different specific surface areas. In samples with fillers, the melting temperature of PEO crystallites is lessened by some degrees, with a minimum for materials with high conduction improvement. The inclusion of the filling significantly increased the ionic conduction greater and lower than 60 °C, with the nanoporous Al_2O_3 grains with 5.8 nm size of pore, 150 m^2/g surface area, and 15 g wt% filler concentrations exhibiting the greatest augmentation. The experimental conduction increase has been ascribed to Lewis' acid–base nature of superficial contacts of ionic types with O/OH groups on the filler surface, with an extra input below 60 °C coming from the maintenance of an improved part of the amorphous phase due to the filler's existence. The conductivity versus filler concentration charts show two conductivity maxima that are described in terms of blocking effect, grain consolidation, and surface interactions. Beyond 100 m^2/g grain surface area, the conductivity improvement seems to saturate [4].

6.4 Polyvinyl Alcohol/Ammonium Nitrate (PVA/NH_4NO_3) Nanohybrid for Batteries

Over the last few decades, researchers have been working on proton-conducting solid polymer electrolytes (SPEs) in order to develop high performance and firm electrical and chemical devices like light-emitting electrochemical cells, electrical and chemical double-layer capacitors, fuel cells, and solid-state batteries. However, the most significant disadvantage of proton-conducting solid polymer electrolytes is their little ionic conduction at ambient temperature, which limits their use in power storing gadgets. Several approaches have been used in recent years to improve ionic

conductivity in proton-conducting solid polymer electrolytes, including blending of polymer, co-polymerization, the adding plasticizers, and the addition of nanosized inorganic fillers to the structure, such as carbon nanotubes, reduced metal oxide, and graphene oxide. The dispersal of a modest quantity of inorganic nanosized fillers into the polymer electrolyte matrix has piqued the attention of many investigators due to their remarkable efficacy in increasing the electrolyte system's room temperature ionic conduction [1].

6.5 PEO/LiFSI Polymer Electrolyte for Li-Ion Batteries

Because of its superior mechanical qualities and compatibility with electrodes, poly(ethylene oxide) (PEO) with a high molecular weight has been widely investigated as a polymer matrix for lithium polymer batteries [16]. The polymer chain's repeat unit, $–CH_2–CH_2–O–$, enables for Li-ion complexion, while the backbone's segmented mobility provides sufficient ion dynamics, as seen in the diagram below [26].

Bis(trifluoromethane) sulfonamide lithium (LiTFSI) possesses a flexible anion, $CF_3–SO_2–N–SO_2–CF_3$ (TFSI), which is advantageous in reducing the crystal nature of poly(ethylene oxide) chains and has superior chemical, electrochemical, and thermal firmness when compared to typical inorganic alkali salts. Furthermore, trifluoromethane) sulfonamide lithium's highly delocalized charge distribution can impair the contacts between Li-ions and trifluoromethane) sulfonamide lithium, facilitating lithium salt dissociation. In contrast, a counterpart of LiTFSI, Li bis(fluorosulfonyl)imide ($Li[N(SO_2F)_2]$ or LiFSI), had a reduced thickness in the melt, which aids Li-ion diffusion. Above 80 °C, the ionic conduction of the polyethylene oxide/LiFSI electrolyte exceeded 103 S/cm^1, which is somewhat more than that of the PEO/LiTFSI electrolyte. Furthermore, when compared to LiTFSI, the LiFSI-based SEI layer produced on an electrode showed improved compatibility with Li metal. Novel Li salts with various negative charged species, such as LiTNFSI ($Li[N(SO_2F)(n–C_4F_9SO_2)]$, LiFTFSI ($Li[N(SO_2F)(SO_2CF_3)]$, and LiDFTFSI ($Li[N(SO_2CF_2H)(SO_2CF_3)]$, have been created and proved to exhibit good ionic conductivity at increased temperatures in recent studies. They can also produce a steady and resilient SEI coating on the surface of the Li metal positive electrode to extend the battery's life, which was linked to the creation of LiF, which formed a shielding film on the anode. Li-ion batteries with such PSEs, on the other hand, still require a temperature above 60 °C to operate. These PSEs would be fused and drop dimensional firmness at such high temperatures, resulting in nonhomogeneity and a reduced capacity to control Li dendrite growth during cycling [26].

6.6 PAN/LiTFSI Polymer Electrolyte

PAN, which comprises the dipolar and EWD CN^-, has great electrochemical stability, a wide electrical and chemical window, strong thermal firmness, and high mechanical strength. PAN-based electrolytes, in particular, have a high oxidation-resistance potential, making them adaptable to high-voltage cathode materials for high energy density. Li ions can be comb-like coupled with as many as four CN groups in the peroxyacetyl nitrate chain in a PAN/$LiClO_4$ system. Even still, at ambient temperature, the ionic conduction of a dry PAN/$LiClO_4$ solid polymer electrolyte is as low as 107 S/cm^1, which is comparable to that of a polyethylene oxide-based electrolyte. Despite the fact that LiTFSI has been shown to reduce PAN crystallinity, unlike polyethylene oxide-based solid electrolytes, the ionic conductivity of PAN-based electrolytes is mostly dependent on the mobility of peroxyacetyl nitrate polymer chains. Two strong EWD groups on the N atom in LiTFSI, on the other hand, make the imide anion stable, and the imide anion's substantial charge delocalization aids ion dissociation. Dry PAN-LiTFSI solid polymer electrolytes have been reported to have ionic conductivity of up to 106 S/cm^1. Wang showed that incorporating plasticizers into PAN-based solid electrolytes was an effective way to break the connection between lithium ions and peroxyacetyl nitrate and boost ionic conduction. Inorganic fillers, in addition to plasticizers, are another technique for improving ionic conductivity in PAN. Based on the Lewis acid–base theory, Wang and colleagues showed that ceramic fillers with changed surfaces could operate as sources of charge carriers, resulting in an increase in ionic conductivity [26].

6.7 Polyoxometalate/Graphene Nanohybrid for Battery

The electrochemical parameters of NHs made of polyoxometalate (POM) and reduced graphene oxide (RGO), in which discrete polyoxometalate subunits are absorbed on surface of reduced graphene oxide, were investigated. The polyoxometalate/reduced graphene oxide-monochlorobenzene (MCB) had an advanced battery capacity and a quicker charging/discharging rate than the microcrystal polyoxometalate/reduced graphene oxide and the POM/SWNT-MCB, according to the charge/discharge measurements. Based on the valence change in polyoxometalate and the capacity of reduced graphene oxide, the fine analysis of the POM/RGO-MCB strongly showed the cooperative amplification of the capacity effects in the polyoxometalate/reduced graphene oxide hybrid materials. This points to POM's good performance as a supercapacitor additive for increasing capacity, as well as a synergetic method to combining a chemical battery and a supercapacitor to provide high energy and high power density energy storages [13].

7 Structure and Characterization of OINHs

Different nanohybrids are being prepared and are characterized by different techniques as follows:

7.1 Powdered X-ray Diffraction

PEDOT–V_2O_5 nanohybrid was prepared, and it was characterized using powered XRD using a Rigaku miniflex X-ray diffractometer with Ni-filtered Cu Kalpha (1.542 A) radiation and a graphite crystal monochromator [17].

The powder XRD diffraction patterns of (a) crystalline V_2O_5 and (b) PEDOT–V_2O_5 composite are shown in Fig. 5 to indicate the subtle structural changes that occur during chemical interaction. The interlayer spacing is directly related to the strongest peak found at the small angle of equivalent to the (0 0 1) plane of the covered V_2O_5 assembly. The presence of a high-frequency diffused scattering feature modifies the key structures of the V_2O_5 diffraction form in the composites, and the d-spacing

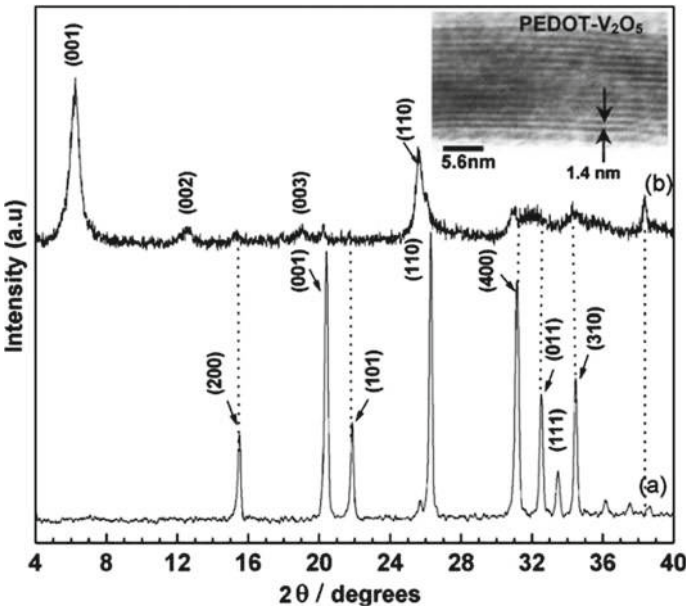

Fig. 5 Powder X-ray diffraction patterns of **a** pure V_2O_5 and **b** microwave-prepared PEDOT–V_2O_5 nanocomposite. The HRTEM image of PEDOT nanoribbons inserted into V_2O_5 layers to form a nanocomposite is shown in the inset figure. Reproduced with permission from [17]. (Copyright 2006, Elsevier)

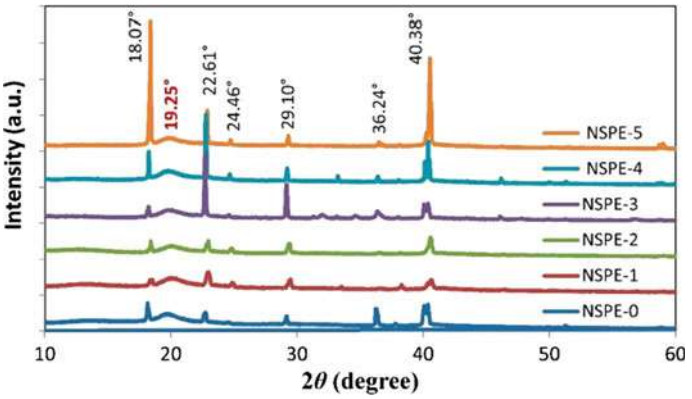

Fig. 6 XRD pattern plots for PVA/NH_4NO_3/ZnO NSPEs with changed ZnO-nanoparticle (NP) contents. Reproduced from an open access article by [1], published under creative commons attributions license

upsurges from 4.3 to 14.1 A. This would imply that the extension continues, forming a polymer monolayer between the V_2O_5 layers [17].

Polyvinyl alcohol/ammonium nitrate (PVA/NH_4NO_3) nanohybrid was synthesized, and XRD technique was used for its characterization. The XRD patterns for PVA/NH_4NO_3/ZnO NSPEs with changing ZnO-NP insides are shown in Fig. 6 given below:

The low relative crystal nature of the NSPE-2 sample is revealed by the lowest strength of the characteristic peaks after loading 2 wt% ZnO-NP. Above this concentration, the strength of the ammonium nitrate peaks increases as the zinc oxide-NP quantity rises, resulting in a decrease in conduction due to dissociated ions re-combination to form ammonium nitrate salt. It has long been known that even little changes in the crystal structure of polymer samples have a significant impact on conductivity [1].

7.2 High-resolution Transmission Electron Microscopy (HRTEM)

For transmission electron microscope modeling, PEO–V_2O_5 nanohybrid was studied and is shown in the inserted image in above Fig. 7. The nanoribbon shape of the PEDOT–V_2O_5 nanocomposite is shown in a high-resolution transmission electron microscopy (HRTEM) image, as shown in Fig. 7. As a result, the in situ oxidation–reduction intercalation polymerization appears to be topotactic, and the host construction remains unchanged. The V_2O_5 host comprises of numerous conducting polymer nanoribbons, as can be seen in the HRTEM image, and the low scattering power results great difference for white lines, each approximately 1.4 nm between

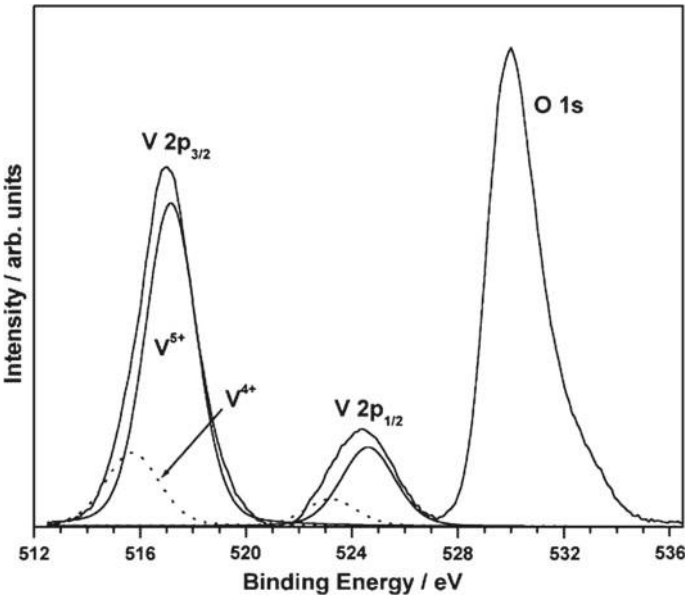

Fig. 7 PEDOT–V_2O_5 nanocomposite X-ray photoelectron spectra generated by redox intercalative polymerization. Reproduced with permission from [17]. (Copyright 2006, Elsevier)

two dark fringes of vanadate films. The most distinct intensity maximum found in the broad X-ray diffraction pattern can be used to estimate the same ribbon thickness of roughly 1.41 nm (0 0 1). As a result of the HRTEM image of the nanocomposite material, we can deduce that the highly crystallinity of V_2O_5 is detached in this hybrid material by alternating organic conducting polymer nanoribbons [17].

7.3 X-ray Photoelectron Spectroscopy (XPS)

After redox polymer intercalation, X-ray photoelectron spectroscopy (XPS) is a surface-specific approach for studying the polymer–vanadium oxide interface and vanadium (V^{5+}/V^{4+}) oxidation state. In the figure below, XPS data from the V 2p and O 1 s core levels of a polymer intercalated nanocomposite are shown:

X-ray photoelectron spectra revealed the presence of both V^{4+}/V^{5+} species in the nanocomposite, implying that oxidative polymerization reduced the V^{4+} species in the V_2O_5 slabs. The oxidation–reduction insertion process and charge transfer from the polymer to the V_2O_5 framework are also confirmed by these findings [17].

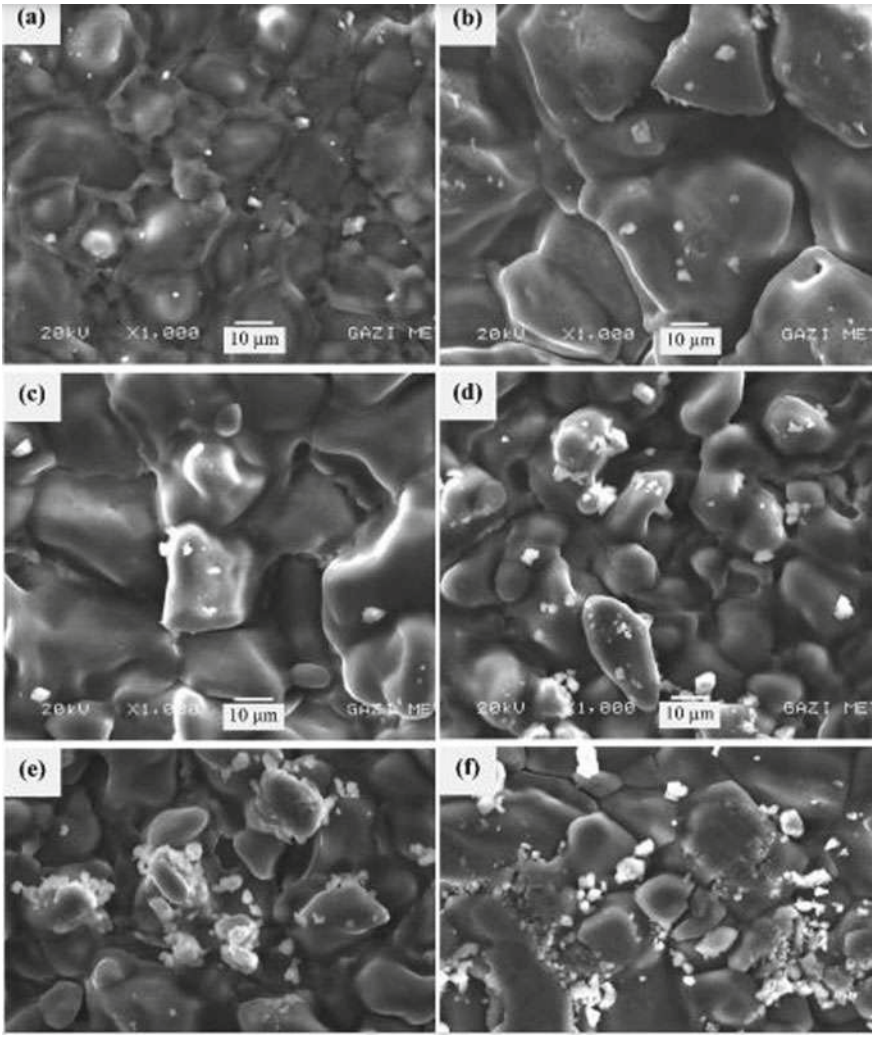

Fig. 8 Scanning electron microscope (SEM) micrographs of PVA/NH_4NO_3/ZnO NSPEs with different ZnO-NP concentrations: **a** NSPE-0, **b** NSPE-1, **c** NSPE-2, **d** NSPE-3, **e** NSPE-4, and **f** NSPE-5. Reproduced from an open access article by [1], published under creative commons attributions license

7.4 Scanning Electron Microscopy (SEM)

The morphology of polyvinyl alcohol/ammonium nitrate (PVA/NH_4NO_3) nanohybrid was studied by scanning electron microscopy (SEM). Scanning electron microscope (SEM) micrographs of PVA/NH_4NO_3/ZnO NSPEs with various ZnO-NP

contents are shown in Fig. 8. The sound structure of undoped and doped proton-conducting PEs shows solid structures protruding from the membrane surface, indicating that the NH_4NO_3 salt has recrystallized out of the NSPE surface [1].

The density of the solid formations was likewise lowered after the adding 2 wt% ZnO-NPs. The density of these solid formations in the polymer electrolytes increased as the ZnO-NP content was increased further [1].

8 Conclusion

At the nanoscale, materials development has developed above single-particle formation to multi-component assemblies or hierarchic structures that combine two or more pre-synthesized nanomaterials (NMs) to extract multi-functionality. The need for multi-functionality has resulted in NMs being physically and chemically transformed at the nanoscale in general, and these alterations in nanomaterials lead to nanohybrids. These nanohybrids are employed in modern batteries to increase their efficiency and longevity. To study the properties of nanohybrids, various methods such as chemical vaporization deposition, hydrothermal/solvothermal, ultrasonification, layer-by-layer deposition, and different characterization techniques such as powered scanning electron microscopy (SEM), X-ray photoelectron spectroscopy (XPS), high-resolution transmission electron microscopy (HRTEM), X-ray diffraction (XRD) can be utilized to study their properties.

References

1. Abdullah OG, Salman YA, Tahir DA, Jamal GM, Ahmed HT, Mohamad, AH, Azawy AK (2021) Effect of ZnO nanoparticle content on the structural and ionic transport parameters of polyvinyl alcohol based proton-conducting polymer electrolyte membranes. Membranes 11(3):163
2. Aich N, Plazas-Tuttle J, Lead JR, Saleh NB (2014) A critical review of nanohybrids: synthesis, applications and environmental implications. Environ Chem 11(6):609–623
3. Arribas A, Bermudez M, Brostow W, Carrion-Vilches F, Olea-Mejia O (2009) Scratch resistance of a polycarbonate + organoclay nanohybrid. Express Polym Lett 3:621–629
4. Boaretto N, Meabe L, Martinez-Ibañez M, Armand M, Zhang H (2020) Polymer electrolytes for rechargeable batteries: from nanocomposite to nanohybrid. J Electrochem Soc 167(7):070524
5. Chauhan AK, Kumar D, Mishra K, Singh A (2021) Performance enhancement of Na^+ ion conducting porous gel polymer electrolyte using $NaAlO_2$ active filler. Mater Today Commun 26:101713
6. del Mar Encabo-Berzosa M, Sancho-Albero M, Crespo A, Andreu V, Sebastian V, Irusta S, Arruebo M, Martín-Duque P, Santamaria J (2017) The effect of PEGylated hollow gold nanoparticles on stem cell migration: potential application in tissue regeneration. Nanoscale 9(28):9848–9858
7. Dissanayake M, Jayathilaka P, Bokalawala R, Albinsson I, Mellander B-E (2003) Effect of concentration and grain size of alumina filler on the ionic conductivity enhancement of the $(PEO)_9LiCF_3SO_3$: Al_2O_3 composite polymer electrolyte. J Power Sources 119:409–414

8. Divya K, Østergaard J (2009) Battery energy storage technology for power systems—an overview. Electr Power Syst Res 79(4):511–520
9. Faustini M, Nicole L, Ruiz-Hitzky E, Sanchez C (2018) History of organic–inorganic hybrid materials: prehistory, art, science, and advanced applications. Adv Funct Mater 28(27):1704158
10. Feng J-J, Gernert U, Sezer M, Kuhlmann U, Murgida DH, David C, Richter M, Knorr A, Hildebrandt P, Weidinger IM (2009) Novel Au−Ag hybrid device for electrochemical SE(R)R spectroscopy in a wide potential and spectral range. Nano Letters 9(1):298–303
11. Fu D, Han G, Chang Y, Dong J (2012) The synthesis and properties of ZnO–graphene nano hybrid for photodegradation of organic pollutant in water. Mater Chem Phys 132(2–3):673–681
12. Ilaria F, Venditti I, Battocchio C, Polzonetti G, Cesare C, Russo MV (2011) Core shell hybrids based on noble metal nanoparticles and conjugated polymers: synthesis and characterization. Nanoscale Res Lett
13. Kume K, Kawasaki N, Wang H, Yamada T, Yoshikawa H, Awaga K (2014) Enhanced capacitor effects in polyoxometalate/graphene nanohybrid materials: a synergetic approach to high performance energy storage. J Mater Chem A 2(11):3801–3807
14. Leonard K, Kawashima M, Okamura H, Kurawaki J (2010) One-pot sonochemical synthesis of dendron-stabilized gold nanoparticles as promising nano-hybrid with potential impact in biological application. Mater Lett 64(20):2240–2243
15. Liu C-H, Chiu L-K, Yeh J-Y, Tsiang RC (2012) Making organic–inorganic nanocomposites via selective dispersion of PS-tethered SiO_2 particles in polystyrene-block-polymethylmethacrylate copolymer. J Nanomaterials
16. Meyer WH (1998) Polymer electrolytes for lithium-ion batteries. Adv Mater 10:439
17. Murugan AV (2006) Novel organic–inorganic poly (3,4-ethylenedioxythiophene) based nanohybrid materials for rechargeable lithium batteries and supercapacitors. J Power Sources 159(1):312–318
18. Nicole L, Rozes L, Sanchez C (2010) Integrative approaches to hybrid multifunctional materials: from multidisciplinary research to applied technologies. Wiley Online Library
19. Ohno T, Tagawa S, Itoh H, Suzuki H, Matsuda T (2009) Size effect of TiO_2–SiO_2 nano-hybrid particle. Mater Chem Phys 113(1):119–123
20. Pomastowski P, Sprynskyy M, Zuvela P, Rafinska K, Milanowski M, Liu JJ, Yi M, Buszewski B (2016) Silver-lactoferrin nanocomplexes as a potent antimicrobial agent. J Am Chem Soc 138(25):7899–7909
21. Sanchez C, Rozes L, Ribot F, Laberty-Robert C, Grosso D, Sassoye C, Boissiere C, Nicole L (2010) Chimie douce: a land of opportunities for the designed construction of functional inorganic and hybrid organic–inorganic nanomaterials. C R Chim 13(1–2):3–39
22. Semenova D, Silina YE (2019) The role of nanoanalytics in the development of organic–inorganic nanohybrids—seeing nanomaterials as they are. Nanomaterials 9(12):1673
23. Shakeel A, Rizwan K, Farooq U, Iqbal S, Altaf AA (2022) Advanced polymeric/inorganic nanohybrids: an integrated platform for gas sensing applications. Chemosphere 294:133772. https://doi.org/10.1016/j.chemosphere.2022.133772
24. Silina YE, Gernaey KV, Semenova D, Iatsunskyi I (2020) Application of organic–inorganic hybrids in chemical analysis, bio-and environmental monitoring. Appl Sci 10(4):1458
25. Wei T, Du D, Zhu M-J, Lin Y, Dai Z (2016) An improved ultrasensitive enzyme-linked immunosorbent assay using hydrangea-like antibody–enzyme–inorganic three-in-one nanocomposites. ACS Appl Mater Interfaces 8(10):6329–6335
26. Xi G, Xiao M, Wang S, Han D, Li Y, Meng Y (2021) Polymer-based solid electrolytes: material selection, design, and application. Adv Funct Mater 31(9):2007598
27. Yu F, Du L, Zhang G, Su F, Wang W, Sun S (2020) Electrode engineering by atomic layer deposition for sodium-ion batteries: from traditional to advanced batteries. Adv Funct Mater 30(9):1906890

28. Zhao N, Yan L, Zhao X, Chen X, Li A, Zheng D, Zhou X, Dai X, Xu F-J (2018) Versatile types of organic/inorganic nanohybrids: from strategic design to biomedical applications. Chem Rev 119(3):1666–1762
29. Zhou W, Zhang M, Kong X, Huang W, Zhang Q (2021) Recent advance in ionic-liquid-based electrolytes for rechargeable metal-ion batteries. Adv Sci 2004490

Chapter 22
Toxicology, Stability, and Recycling of Organic–Inorganic Nanohybrids

Shahzad Maqsood Khan, Sidra Saleemi, and Hafiz Abdul Mannan

1 Introduction

Nanoparticles (NPs) are promising materials in science now, and further progress with different properties is continued. NPs have unique properties owing to their high surface area and exceptional chemical and physical properties. These NPs with low toxicity can be used for catalyst synthesis and their environmental and medical applications. Change in surface composition and their direct interaction with the environment can influence and change their properties. NPs especially for biomedical applications meet biological fluids, and this contact instantly forms protein cornea deteriorating the colloidal stability and disturbing the interaction between NPs and tissues. Also, the external forces can create a region-specific accumulation of materials due to exerted force. Such behavior of nanohybrid materials can be affected by crystal lattice, coating on materials, their shape and size, and their synthetic methods [1]. Recent material development is focused on the conjugation of multiple nanomaterials. This new class of materials is also termed nanohybrids or "horizon nanomaterials". Material performances are enhanced by metal doping or overcoating or by metal or metal oxides conjugation with carbonaceous NPs. This modification could lead hybrid nanomaterials to multi-functionality due to incorporating nanoparticles or materials for composite applications. Nanohybrids have wide applications in energy, electronics, medical products, etc. These fields are in demand of stringent intention to evaluate their safety. These nanohybrids have multiple and unique physicochemical properties compared to their individual components. Such attributes, hence, make and increase uncertainty in the risk evaluation, toxicity, stability, and recycling ability of these materials. Developed toxicological testing strategies are therefore required to be re-evaluated for assessing properties of nanohybrid materials [2]. While considering the applications of hybrid nanomaterials, hybrid super-capacitors are well known

S. M. Khan (✉) · S. Saleemi · H. A. Mannan
Institute of Polymer and Textile Engineering, University of the Punjab, Lahore 54590, Pakistan
e-mail: shahzad.ipte@pu.edu.pk

K. Rizwan et al. (eds.), *Hybrid Nanomaterials*, Materials Horizons: From Nature to Nanomaterials, https://doi.org/10.1007/978-981-19-4538-0_22

materials due to their high energy density. This is achieved without changing the power density. Such an asymmetric approach in nanohybrid materials starts a new era for most required non-toxic, pollution-free, stable, long shelf life, and energy proficient storing performance. Due to their applications in many power devices, research and development for development of stable advanced storage devices have a bright and enormous future [3].

The enhanced demand of novel and compelling antimicrobial agents for tackling with contagions and ailments, different metal-based NPs are deposited on montmorillonite or polymers. Materials based on Ag NPs and Cu NPs on different materials are reported, and other toxicological properties on human cell lines have not been reported in detail. Such nanohybrid materials are with enhanced antimicrobial properties and involvement of more advanced materials having less toxicity and high potent behavior are important candidates for new generation of nanohybrid materials. To control the diseases and infections caused due to microbial attacks and infections acquired by hospital cross-infections, control and prevention of toxic contaminations on the surface of nanohybrid materials are important to study and evaluate. Therefore, novel synthesis of such novel, non-toxic, and highly potent nanohybrid materials with easy technology is the need of the hour. In current scenario, multi-drug-resistant pathogen strains are generating disorder in human bodies which is countered by disinfectants, antibiotics. To combat threatening health problems, nano-engineered hybrid materials with exceptional tailorable properties currently provide promising solutions. Especially, NPs of Ag and Cu even at low concentration and multi-targeted mechanism are in use as bio-active nanomaterials. Ag- and Cu-based nanohybrids have wider use in traditional drugs used for disinfection and sanitization since pre-historic periods. Invention of nanotechnology provides huge breakthrough for synthesizing non-toxic, stable, and recyclable nanohybrids of multiple shapes, sizes, and enhanced functional properties [4].

Rapid increase in the industry and population also enhanced the presence and release of toxic and hazardous contaminants in the environment. These toxic substances pollute the ecosystem. Nanotechnology especially in biochemical engineering constructed nanohybrid materials for target uptake of toxic pollutants. Modified and tailored nanohybrid materials were designed with less toxicity, more stability enabling high specificity and efficiency. These biopolymer-based, biodegradable, eco-friendly, and economical nanohybrids are promisingly taking part for removal of hazardous environmental pollutants as well. Nanostructures, e.g., carrageenan, silica, non-magnetic and magnetic, carbon nanotubes or nanorods, nanoclay, nanomembrane, metal organic frameworks, graphene oxide, and other nanomaterials are some examples of most recently used nanohybrids [5–7]. This supreme improvement of organic–inorganic hybrid nanomaterials is covering chemistry, physics, life sciences, medicine, and technology. This in-depth understanding of nanohybrids at the atomic and molecular levels produces new design of advanced less toxic, more stable, and recyclable nanohybrid materials. Nanostructured materials based on graphene, fullerene, carbon nanotubes, etc., have been developed with enhanced optical, electrical, thermal properties. Carbon-based nanomaterials are also in practice, and research is ongoing for specific carbon-based nanohybrids and

their heteroatom-doped derivatives for progressive materials production with tunable properties for energy storage, electrocatalysis, and for optoelectronic devices. Huge development in organic inorganic nanohybrid systems is also shooting upward in the field of catalysis. The catalysts expedition by using nanohybrid materials is applied in designing hybrid nanomaterials with better selectivity, higher activity, and improved stability. The formation of sustainable, non-toxic, eco-friendly, and stable nanohybrids is a challenging issue [8]. This chapter summarizes recent advances in toxicity, stability, and recycling of hybrid nanomaterials which are used in various biomedical, environmental, and energy applications.

2 Toxicity of Hybrid Nanomaterials

The manufacturing and consumption of hybrid nanomaterials were considered as hot area and keep growing, to be the cause of many issues and concerns among scientific, public, and regulatory authorities regarding their utilization in human-related applications. Hybrid nanoparticles composed of nanoparticles could be categorized in two major groups: anthropogenic (synthetic) and natural nanoparticles. Natural nanoparticles present in the atmosphere long before the nanotechnology period began. For example, bio-nanoparticles include fullerenes, soil colloids, carbon nanotubes, etc. [9, 10]. Soils hold variety of inorganic and organic nanoparticles, namely metal oxides, clay minerals, and hydroxides [11]. Mostly, natural vegetation contains organic nanoparticles [12]. Synthetic nanoparticles could be divided into two classes: accidentally prepared nanoparticles, which are nanoparticles produced inadvertently in artificial processes (e.g., carbon nanotubes and fullerenes, carbon black, platinum nanoparticles obtained as a by-product from combustion process), and designed nanoparticles are those nanoparticles that are formed purposefully because of their unique properties.

The major concern of existing research on the toxicity of hybrid nanomaterials is synthetic nanoparticles, such as carbon nanotubes, metals, metal oxides, and polymeric nanoparticles used as quantum dots and drug carriers. The reduction in particle size results in increased surface area which gives rise to improved and innovative material characteristics; however, it also reduces their biological reactivity [13, 14]. Reduction of particles toward nanosize can also provide them entry into different regions of human body [15].

The emission of nanoparticles into the atmosphere can occur via numerous processes, such as washing/laundering of end-user products having nanoparticles; spilling during designing and manufacture; as an unintentional discharge during carrying them or moving them according to the use; from productions that use nanotechnology, for example, drug delivery; hybrid composite materials and effluent treatment. Ecological pollution and bionetwork troubles signify yet another alarm. These trepidations request the corresponding toxicity evaluation of these particles with their synthesis, manufacturing, and utilization in hybrid nanomaterials.

However, there are fewer publications on hybrid nanomaterials regarding the toxicity of nanoparticles in hybrid nanomaterials. The health and safety features of nanomaterials are not considered in new advancements. Nanoparticles were revealed to produce inflammatory cytotoxicity, damage of lungs, and oxidative pressure replies in various in vitro studies [16–18]. The damage of human health is also investigated through in vivo testing to evaluate their impact on human and animal health [19]. Table 1 presents the existing data and information concerning about the usage of nanoparticles with biological systems. These adverse effects lead to numerous issues and experimental challenges handled while measuring the severity/toxicity of nanoparticles in hybrid composite material. Most of the methods used for toxicity evaluation are standardized and designed by keeping in mind the chemical toxicity of these particles. However, nanoparticles show numerous exceptional physicochemical characteristics which can be challenging and restrict the use of typical toxicity analysis. More detailed examination of toxicity is vital aspect in terms of elemental purity, surface area, size, shape, solubility, agglomeration, etc. Insufficient data will

Table 1 Toxicity of commonly used nanoparticles (NPs)

Type of nanoparticles	Toxicity	References
Quantum dots	• induce inflammatory response • cytotoxic • oxidative stress	[21, 22]
Fullerenes	• oxidative stress • DNA damage	[23, 24]
Gold NPs	• effect autophagy • inflammation • bioaccumulation in important body organs • oxidative stress	[25–27]
Silver NPs	• cytotoxicity • neuronal degeneration • causing brain edema or swelling • oxidative stress	[28, 29]
Multi-walled carbon nanotubes (MWCNTs)	• DNA damage • inflammation • formation of granuloma • fast growth of fibrosis in lungs • oxidative stress	[30–33]
Single-walled carbon nanotubes (SWCNT)	• fibrogenic effects in lung cells • inflammation • promote allergic response • oxidative stress	[34–36]
Metal oxide NPs	• cytotoxicity • oxidative stress • membrane damage • inflammatory response	[37–39]

lead to many issues related to toxicity and stability of nanomaterials. Their different optical properties, high adsorption capacities, and improved catalytic schemes can stimulate the outcomes of various in vitro toxicity, dive into the misapprehension of related findings. Also lack of information related to standardized procedures and strategies makes it complicated to relate the safety/toxicity analysis from recent studies. These major concerns affect nanotoxicology and their proper evaluation of the probable adverse health and environmental implications of nanomaterials [20]. In this chapter, we address some significant approaches associated with analysis of toxicity of nanoparticles in hybrid nanomaterials.

Occasionally, extremely lesser quantity of nanoparticles in the ecosystem or biological schemes makes qualitative analysis by microscopic techniques very hard to diagnose. Furthermore, electron microscopy procedures become useless while considering analytical quantification of nanoparticles. Within this frame of reference, Inductively Coupled Plasma Mass Spectrometry (ICPMS) could be effectively used as a quantitative and sensitive method for the analysis of quantities of nanoparticles. ICPMS becomes particularly essential in the perspective of an in vivo situation, where it recognizes the marked organs for nanoparticles [40]. Using this characterization, even small amounts of particles that go into various body organs through a different route can be detected. Moreover, this testing needs intense care as during the digestion step, it leads to contamination and dilution [41].

2.1 Agglomeration and Dispersion of Nanoparticles in Hybrid Nanomaterials

The chemistry of agglomeration contains formation of cluster of nanoparticles, which is mostly due to weak forces, that addresses at the nanoscale because of greater surface area-to-volume ratio [42]. Many researches show that nanoparticles begin to agglomerate during manufacturing, both in suspension and dry condition. It always remains challenging for researchers to prevent these nanoparticles from agglomeration during synthesis process, especially biomedical application. Together with other forces, Brownian motion also took part in the agglomeration of nanoparticles, which eventually settle down because of gravitational forces. The agglomeration is an alarming symbol while considering the physicochemical characteristics of the nanoparticles. The vital characteristics affected are their size, volume-to-surface ratio, their surface reactivity, and size distribution. Since, these factors took an important part in the severity of nanoparticles [43]. Agglomeration is affected by several intrinsic and extrinsic parameters, such as dispersant, concentration of the nanoparticle, surface coating, size, zeta potential, temperature, sonication time [44]. Many researches show that nanoparticles begin to agglomerate during manufacturing, both in suspension and

dry condition. It always remains challenging for researchers to prevent these nanoparticles from agglomeration during synthesis process, especially biomedical application. Together with other forces, Brownian motion also took part in the agglomeration of nanoparticles, which eventually settle down because of gravitational forces. The agglomeration is an alarming symbol while considering the physicochemical characteristics of the nanoparticles. The vital characteristics affected are their size, volume-to-surface ratio, their surface reactivity, and size distribution. Since, these factors took an important part in the severity of nanoparticles [45]. For instance, when these particles were presented into deionized water, they may agglomerate with increased concentration [45]. Therefore, agglomeration is a crucial property for the precise analysis of the biotic behavior to any modified hybrid nanomaterial. Agglomeration may also lead to change in the constructural behavior of the material; it becomes rigid and performs like asbestos particles [46]. Nanoparticles are known to pass through biotic barriers because of their size. Therefore, agglomeration may alter biotic behavior due to the reduction in total available surface area, leading to toxicity, especially in toxicity assessments and drug delivery [47]. The rate and extent of aggregation of nanoparticles after entry into cells may vary due to their interactions with macromolecules [48]. Although there are different methods for depolymerizing nanoparticles (polyethylene glycol, serum, sonication, detergents, lung surfactants, etc.), sonication is the most widely used method. It disperses the nanoparticles in the liquid by cavitation. However, the dispersion of nanoparticle does not reach the ideal dispersion; i.e., the particles have not achieved their pristine particle size and presented a propensity to re-agglomerate by the passage of time. Murdock et al. also measured the consequence of agglomeration due to surface change and sonication [45]. The zeta potential and size distribution were used to confirm that the probe sonication is unable to disperse these particles to their primary particle size at different time span; it also gives unstable suspension of nanoparticles [45]. Surface modification is another effective way to avoid agglomeration of nanoparticles as it involves even dispersion of these particles in liquids. These modifications can be acquired by using numerous methods depending on their utilization. These particles can also be modified with number of ionic or nonionic surfactants and polymers [46].

3 Stability of Hybrid Nanomaterials

Stability of hybrid nanomaterials is of great importance due to their application in various environments and harsh operating conditions. Often, these materials are used at elevated temperatures, and their thermal stability should be considered at the designing stage. In addition, these hybrid materials are subjected to various mechanical stresses, loads, and movements especially in biomedical applications, and their mechanical stability determines their stable operational range. Finally, environmental stability determines the service life of any hybrid nanocomposite under various environments. All these aspects are briefly discussed below.

3.1 Thermal Stability of Hybrid Nanomaterials

The ability of nanomaterials to resist heat action and to sustain their properties like toughness, elasticity, and strength at the given temperature is a unique feature of these materials [49]. Thermal stability of nanomaterials is usually measured by thermal gravity analyzer (TGA). Nanostructure materials show high thermal stability. Hybrid nanomaterials are used for effective applications such as industrial materials, heat-resistant materials, and corrosion-resistant materials. In the nuclear units, nanostructure materials are used because of radiation tolerance since these materials can withstand long-term strong radiation exposure under high stress, high temperature, and corrosive environment [50]. Goikuria et al. showed novel strategies for enhanced thermal stability of hybrid nanomaterials. In this study, they fabricated hybrid nanomaterial using different nanoparticles in the cellulose nanocrystals (CNC-based) nanocomposites. The nanoparticles included ZnO_2, TiO_2, SiO_2, Al_2O_3, Fe_2O_3. CNC-based nanocomposites were fabricated with these nanoparticles by co-assembly method. By addition of the nanoparticles, remarkable improvements in thermal stability were seen [51].

3.2 Mechanical Stability of Hybrid Nanomaterials

Mechanical stress tends to endorse modification in molecular properties. The existing state of the art by means of growth of composite from one phase to another can extremely transform their characteristics. Nevertheless, besides some early clues on the chemical connections and physical properties of the existing hybrids, the existing research has still room to deprive a massive effort to formulate a better systems that can forecast the result when the polymer is induced in mixture [52]. Numerous studies formulate a bio-based system to assess the properties under different combinations to achieve the targeted approaches of mechanical properties with respect to polymeric modification in hybrid nanomaterials. Furthermore, this systems will not be directly comparable, since the synthetic routes in nature, resulting materials and properties, and the target applications will be different [53].

3.3 Environmental Stability of Hybrid Nanomaterials

Nanomaterials are used for different applications due to their reduced size and effective surface area. Nanoparticles sustain in the surroundings which may be hazardous. So, their use is limited in some ways. Usually, the presence of an extreme number of particle boundaries inclines to damagingly affect the deterioration characteristics of nanomaterials, since places where the material is disordered are most exposed to attack from their atmospheres. Though, on the other hand, the dispersion needs to

form defensive layers, i.e., surface passivation may be increased, lowering the corrosion rate. So, only two factors are identified to prevent the nanomaterials from harsh atmospheres (such as acidic or oxidizing environments). Other factors may comprise the features of the protective layers and the presence of residual stresses. Hence, it is very difficult to forecast the interaction of corrosive environment with the result of an interaction between nanomaterials. Different nanomaterials such as TiO2, carbon nanotubes, and organic conducting polymers (OCP) have good characteristics such as excellent electrical and mechanical properties, structural and chemical properties, and especially eco-stable. Nanomaterials show limited individual properties. So, the composites of the nanomaterials are formed to improve their properties such as environmental stability. For example, carbon nanotubes discovered by Kroto [52] are highly water repellent in the nature and do not have specific attraction to metal ions and cannot be used for the sensing applications of metal ion [54], while OCPs show good environment stability as well as greater affinity toward metal ion sensing applications [55–57]. The OCPs and CNTs composites show high environmental stability which individual ones cannot see [56].

4 Recycling of Hybrid Nanomaterials

While designing an organic–inorganic hybrid nanomaterial, it is very important to take into account the entire life cycle of the material starting from manufacturing step to end-of-life stage and possibilities of reuse and recycle. Disposal of scrap and end-of-life materials is a serious environmental challenge and demands serious considerations. The primary objective of the recycling process is the reclamation of material or otherwise energy which is obtained by combustion, incineration, or pyrolysis process.

The material loses its value because of its use, and the value decreases over the time. However, the recycled material may be used in less demanding and less strategic applications because of reduced quality and lifetime wear [58]. Recycling of organic materials made from polymers is generally known, whereas nanocomposites and nanohybrid materials pose some exceptional challenges. Little information is available in literature about the effect of nanoscale fillers and fibers on the recycling process because recycling of hybrid nanomaterials is different from the recycling of conventional filled polymers [59].

During the recycling of hybrid nanomaterials, an important issue is human exposure to nanofillers and their fragmented parts, which may pose some serious concern toward human health and safety. Recycling of hybrid nanocomposites is limited by the heterogeneous nature of these composites, making it inherently difficult to process different materials by the same recycling process. Sometimes, the associated cost and energy requirement of recycling are so high that the price of the virgin material offsets the recycling possibility. For example, no commercial process can recycle glass fibers at competitive price with the same characteristics as virgin fibers because of extremely low price of virgin glass fibers [60].

Recycling process is also dependent on nature of the material. For example, self-reinforced thermoplastic-based hybrid nanocomposites can be recycled very easily since the matrix and the reinforcement are the same material in different forms. A hybrid composite made of polypropylene fibers in polypropylene matrix can be quoted as an example which can be simply recycled by re-melting and re-granulation. However, in case of crosslinked thermosetting polymer-based hybrid nanomaterials, the process is not straightforward because of crosslinking. Similarly, paint removal of a hybrid nanocomposite also reduced the efficiency of recycling process. Recovery of continuous fibers in fiber reinforced composites is also a difficult task [61].

Many recycling methods are available for polymer-based hybrid composites, such as mechanical, thermal, and chemical recycling techniques. In mechanical technology, composites are grinded and recycled into different sizes which can be used as fillers for new composite development. Chemical recycling recovers polymers or monomers at relatively lower processing temperatures depending upon the selected process of recovery. In thermal recycling, polymer is volatized in lower molecular weight components. Material is often used for energy recovery by pyrolysis, combustion, or incineration [58]. Zhang et al. [59] investigated the recycling of carbon nanotubes filled polypropylene composite by injection molding and granulation process and found that up to 20 recycling runs, no substantial change was observed in the properties of the composite. The process has limited exposures and can be performed with proper exposure controls. Recyclable glass bottles covered with hybrid organic–inorganic material have also been reported [62].

Most of the studies reported in the literature on recycling of organic–inorganic hybrid nanomaterials deal with regeneration by filtration, centrifugation or magnetic decantation process, and reusability of catalysts and adsorbents over a few numbers of cycles [63, 64]. Although this can be regarded as recycling in principle, however, these are the essential performance criteria of adsorbents and catalysts in industrial applications. These studies lack in end-of-use recycling details of organic–inorganic hybrid nanomaterials. For example, Hoseini et al. [65] studied recycling of nanohybrid material, P_2Mo_{18}/MIL-101(Cr), for the removal of methylene blue (MB) by adsorption process. The nanohybrid material was recycled by simple centrifugation and washed with water and ethanol solution. The characterization results of the regenerated adsorbent showed that it did not exhibit significant changes in comparison with the fresh adsorbent. The nanohybrid material maintained its adsorption performance after six cycles, and an adsorption efficiency of 94% was achieved. Conversely, Ji et al. [66] developed organic/inorganic nanohybrid films that can be recycled without centrifugation and filtration. These nanohybrid composites were synthesized by electrospinning process and composed of silk fibroin and $Bi_2O_2CO_3$–Cu_2O for the photocatalytic degradation of chloramphenicol. Both the studies did not discuss the strategies to recycle end-of-use hybrids.

For sustainable development and to address the drawbacks in current recycling procedures such as high recycling cost, lower quality, energy requirements, there is a need to develop more suitable strategies for recycling and reuse of hybrid nanomaterials. More stringent environmental legislations are needed to promote recycling. New materials should be designed for easy recycling approaches. More efficient

and novel separation, purification, and processing methods should be developed for recycling of hybrid nanomaterials.

5 Conclusion

This chapter analyzes and critically assembled the toxicity, stability, and recycling of hybrid nanomaterials to address their challenges and opportunities for upcoming studies. These findings conclude that the characterization, toxicity, stability, and recycling are important aspects of manufacturing innovative hybrid nanomaterials. Toxicity of synthetic nanoparticles and hybrid nanomaterials is a serious concern. Stability of hybrid nanomaterials is of great importance due to their application in various environments and harsh operating conditions. Often, these materials are used at elevated temperatures, and their thermal stability should be considered at the designing stage. Similarly, while designing a hybrid nanomaterial, its recycling aspect should be considered at design stage. Most of the studies reported in literature deal with reuse of hybrid nanomaterial. End-of-life recycling should also be considered and investigated in the future studies. For better sustainability, innovative materials and recycling techniques are required.

References

1. Friedrich RP, Janko C, Unterweger H, Lyer S, Alexiou C (2021) SPIONs and magnetic hybrid materials: synthesis, toxicology and biomedical applications. Phys Sci Rev
2. Saleh NB et al (2014) Emergent properties and toxicological considerations for nanohybrid materials in aquatic systems. Nanomaterials (Basel) 4(2):372–407
3. Muzaffar A, Ahamed MB, Deshmukh K, Thirumalai J (2019) A review on recent advances in hybrid supercapacitors: design, fabrication and applications. Renew Sustain Energy Rev 101
4. Roy A, Joshi M, Butola BS, Malhotra S (2018) Antimicrobial and toxicological behavior of montmorillonite immobilized metal nanoparticles. Mater Sci Eng 93
5. Li W, Qamar SA, Qamar M, Basharat A, Bilal M, Iqbal HM (2021) Carrageenan-based nanohybrid materials for the mitigation of hazardous environmental pollutants. Int J Biol Macromol 190
6. Shakeel A et al (2022) Advanced polymeric/inorganic nanohybrids: an integrated platform for gas sensing applications. Chemosphere 294:133772
7. Rasheed T, Rizwan K (2022) Metal-organic frameworks based hybrid nanocomposites as state-of–the-art analytical tools for electrochemical sensing applications. Biosens Bioelectron 199:113867
8. Ananikov VP (2019) Organic–Inorganic hybrid nanomaterials. Nanomaterials 9
9. Buffle J (2006) The key role of environmental colloids/nanoparticles for the sustainability of life. Environ Chem 3(3):155–158
10. Nowack B, Bucheli TD (2007) Occurrence, behavior and effects of nanoparticles in the environment. Environ Pollut 150(1):5–22
11. Theng BK, Yuan G (2008) Nanoparticles in the soil environment. Elements 4(6):395–399
12. Xia L et al (2010) Naturally occurring nanoparticles from English ivy: an alternative to metal-based nanoparticles for UV protection. J Nanobiotechnol 8(1):1–9

13. Nel A et al (2006) Toxic potential of materials at the nanolevel. Science 311(5761):622–627
14. Kahru A, Savolainen K (2010) Potential hazard of nanoparticles: from properties to biological and environmental effects. Toxicology 2(269):89–91
15. Oberdörster G, Oberdörster E, Oberdörster J (2005) Nanotoxicology: an emerging discipline evolving from studies of ultrafine particles. Environ Health Perspect 113(7):823–839
16. Donaldson K et al (2006) Carbon nanotubes: a review of their properties in relation to pulmonary toxicology and workplace safety. Toxicol Sci 92(1):5–22
17. Lewinski N, Colvin V, Drezek R (2008) Cytotoxicity of nanoparticles. Small 4(1):26–49
18. Yang X et al (2010) SiO_2 nanoparticles induce cytotoxicity and protein expression alteration in HaCaT cells. Part Fibre Toxicol 7(1):1–12
19. Samberg ME, Oldenburg SJ, Monteiro-Riviere NA (2010) Evaluation of silver nanoparticle toxicity in skin in vivo and keratinocytes in vitro. Environ Health Perspect 118(3):407–413
20. Baer DR et al (2010) Application of surface chemical analysis tools for characterization of nanoparticles. Anal Bioanal Chem 396(3):983–1002
21. Li K et al (2009) Intracellular oxidative stress and cadmium ions release induce cytotoxicity of unmodified cadmium sulfide quantum dots. Toxicol In Vitro 23(6):1007–1013
22. Cho SJ et al (2007) Long-term exposure to CdTe quantum dots causes functional impairments in live cells. Langmuir 23(4):1974–1980
23. Zhang LW et al (2009) Endocytic mechanisms and toxicity of a functionalized fullerene in human cells. Toxicol Lett 191(2–3):149–157
24. Jacobsen NR et al (2008) Genotoxicity, cytotoxicity, and reactive oxygen species induced by single-walled carbon nanotubes and C_{60} fullerenes in the FE1-Muta™ Mouse lung epithelial cells. Environ Mol Mutagen 49(6):476–487
25. Li JJ et al (2010) Autophagy and oxidative stress associated with gold nanoparticles. Biomaterials 31(23):5996–6003
26. Pan Y et al (2009) Gold nanoparticles of diameter 1.4 nm trigger necrosis by oxidative stress and mitochondrial damage. Small 5(18):2067–2076
27. Tarantola M et al (2009) Cytotoxicity of metal and semiconductor nanoparticles indicated by cellular micromotility. ACS Nano 3(1):213–222
28. Asharani P, Hande MP, Valiyaveettil S (2009) Anti-proliferative activity of silver nanoparticles. BMC Cell Biol 10(1):1–14
29. Foldbjerg R, Dang DA, Autrup H (2011) Cytotoxicity and genotoxicity of silver nanoparticles in the human lung cancer cell line, A549. Arch Toxicol 85(7):743–750
30. Cheng C et al (2009) Toxicity and imaging of multi-walled carbon nanotubes in human macrophage cells. Biomaterials 30(25):4152–4160
31. Cveticanin J et al (2009) Using carbon nanotubes to induce micronuclei and double strand breaks of the DNA in human cells. Nanotechnology 21(1):015102
32. Patlolla A, Patlolla B, Tchounwou P (2010) Evaluation of cell viability, DNA damage, and cell death in normal human dermal fibroblast cells induced by functionalized multiwalled carbon nanotube. Mol Cell Biochem 338(1):225–232
33. Ravichandran P et al (2009) Induction of apoptosis in rat lung epithelial cells by multiwalled carbon nanotubes. J Biochem Mol Toxicol 23(5):333–344
34. Lindberg HK et al (2009) Genotoxicity of nanomaterials: DNA damage and micronuclei induced by carbon nanotubes and graphite nanofibres in human bronchial epithelial cells in vitro. Toxicol Lett 186(3):166–173
35. Herzog E et al (2009) SWCNT suppress inflammatory mediator responses in human lung epithelium in vitro. Toxicol Appl Pharmacol 234(3):378–390
36. Migliore L et al (2010) Carbon nanotubes induce oxidative DNA damage in RAW 264.7 cells. Environ Mol Mutagen 51(4):294–303
37. Chen Y-C et al (2010) The inhibitory effect of superparamagnetic iron oxide nanoparticle (Ferucarbotran) on osteogenic differentiation and its signaling mechanism in human mesenchymal stem cells. Toxicol Appl Pharmacol 245(2):272–279
38. Choi S-J, Oh J-M, Choy J-H (2009) Toxicological effects of inorganic nanoparticles on human lung cancer A549 cells. J Inorg Biochem 103(3):463–471

39. Eom H-J, Choi J (2009) Oxidative stress of CeO_2 nanoparticles via p38-Nrf-2 signaling pathway in human bronchial epithelial cell, Beas-2B. Toxicol Lett 187(2):77–83
40. Tang J et al (2009) Distribution, translocation and accumulation of silver nanoparticles in rats. J Nanosci Nanotechnol 9(8):4924–4932
41. Allabashi R et al (2009) ICP-MS: a powerful technique for quantitative determination of gold nanoparticles without previous dissolving. J Nanopart Res 11(8):2003–2011
42. Powers KW et al (2007) Characterization of the size, shape, and state of dispersion of nanoparticles for toxicological studies. Nanotoxicology 1(1):42–51
43. Borm P et al (2006) Research strategies for safety evaluation of nanomaterials, part V: role of dissolution in biological fate and effects of nanoscale particles. Toxicol Sci 90(1):23–32
44. Teeguarden JG et al (2007) Particokinetics in vitro: dosimetry considerations for in vitro nanoparticle toxicity assessments. Toxicol Sci 95(2):300–312
45. Murdock RC et al (2008) Characterization of nanomaterial dispersion in solution prior to in vitro exposure using dynamic light scattering technique. Toxicol Sci 101(2):239–253
46. Wick P et al (2007) The degree and kind of agglomeration affect carbon nanotube cytotoxicity. Toxicol Lett 168(2):121–131
47. Sager TM et al (2007) Improved method to disperse nanoparticles for in vitro and in vivo investigation of toxicity. Nanotoxicology 1(2):118–129
48. Balbus JM et al (2007) Meeting report: hazard assessment for nanoparticles—report from an interdisciplinary workshop. Environ Health Perspect 115(11):1654–1659
49. Król-Morkisz K, Pielichowska K (2019) Thermal decomposition of polymer nanocomposites with functionalized nanoparticles. Polymer composites with functionalized nanoparticles. Elsevier, pp 405–435
50. Andrievski R (2014) Review of thermal stability of nanomaterials. J Mater Sci 49(4):1449–1460
51. Goikuria U et al (2017) Thermal stability increase in metallic nanoparticles-loaded cellulose nanocrystal nanocomposites. Carbohydr Polym 171:193–201
52. Kroto HW et al (1985) C_{60}: buckminsterfullerene. Nature 318(6042):162–163
53. Lau KK et al (2003) Superhydrophobic carbon nanotube forests. Nano Lett 3(12):1701–1705
54. Lange U, Roznyatovskaya NV, Mirsky VM (2008) Conducting polymers in chemical sensors and arrays. Anal Chim Acta 614(1):1–26
55. Sotiropoulou S, Chaniotakis NA (2003) Carbon nanotube array-based biosensor. Anal Bioanal Chem 375(1):103–105
56. Besteman K et al (2003) Enzyme-coated carbon nanotubes as single-molecule biosensors. Nano Lett 3(6):727–730
57. Deshmukh MA et al (2018) Composites based on conducting polymers and carbon nanomaterials for heavy metal ion sensing. Crit Rev Anal Chem 48(4):293–304
58. Yang Y et al (2012) Recycling of composite materials. Chem Eng Process 51:53–68
59. Zhang J et al (2016) The effects of recycling on the properties of carbon nanotube-filled polypropylene composites and worker exposures. Environ Sci Nano 3(2):409–417
60. Oliveux G, Dandy LO, Leeke GA (2015) Current status of recycling of fibre reinforced polymers: review of technologies, reuse and resulting properties. Prog Mater Sci 72:61–99
61. Chawla KK (2019) Repair and recycling of composites. Composite materials: science and engineering. Springer International Publishing, Cham, pp 517–528
62. Sanchez C et al (2005) Applications of hybrid organic–inorganic nanocomposites. J Mater Chem 15(35–36):3559–3592
63. Bhanja P, Bhaumik A (2016) Organic–Inorganic hybrid metal phosphonates as recyclable heterogeneous catalysts. ChemCatChem 8(9):1607–1616
64. Asadian M et al (2019) The first pyrazolium-based ionic liquid containing phosphotungstic acid immobilized on $CuFe_2O_4@SiO_2$: a recyclable organic–inorganic nanohybrid catalyst for the synthesis of polyhydroquinolines. Iran J Chem Chem Eng (IJCCE) 38(5):65–77
65. Hoseini A-A et al (2020) An organic–inorganic hybrid nanomaterial composed of a Dowson-type $(NH_4)_6P_2Mo_{18}O_{62}$ heteropolyanion and a metal–organic framework: synthesis, characterization, and application as an effective adsorbent for the removal of organic dyes. RSC Adv 10(66):40005–40018

66. Ji S et al (2020) Electrospun organic/inorganic hybrid nanofibers as low-cytotoxicity and recyclable photocatalysts. Appl Surf Sci 532:147430

Chapter 23
Application Scope, Challenges and Future Perspectives of Organic–Inorganic Nanohybrids

Hina Liaquat, Shoomaila Latif, Muhammad Imran, Nazim Hussain, and Muhammad Bilal

1 Introduction

Single particle synthesis on nanoscale has been advanced to hierarchical multi-component assemblies. This progress in materials science has brought up multi-functional nanomaterials to aid the ongoing development [1]. The term used to denote these ensembles is nanohybrids (NHs) [2, 3]. The alteration in inherited well-established physicochemical properties such as shape, surface chemistry, size and composition of nanohybrids put main focus on their property-modulated synthesis. These alterations have driven the attention of the world toward emergent novel properties [4]. Nanohybrids formed by combining graphene nanosheets with quantum dots, titanium dioxide, porphyrin, carbon nanotubes, etc., have been considered a successful manipulation to attain functionality of higher degree with each combination being novel advantages like lithium-ion batteries [5, 6], supercapacitors [7], transparent conductors [8], optical limiting and emitting [9, 10] devices.

Assembly and conjugation of different materials have given rise to a large domain of nanohybrids having a wide range of applications with greater magnitude. Among

H. Liaquat · M. Imran (✉)
Centre for Inorganic Chemistry, School of Chemistry, University of the Punjab, Lahore 54000, Pakistan
e-mail: imran.hons@pu.edu.pk

S. Latif
School of Physical Sciences, University of the Punjab, Lahore 54000, Pakistan

N. Hussain
Center for Applied Molecular Biology (CAMB), University of the Punjab, Lahore, Pakistan

M. Bilal (✉)
School of Life Science and Food Engineering, Huaiyin Institute of Technology, Huaian, China
e-mail: bilaluaf@hotmail.com

K. Rizwan et al. (eds.), *Hybrid Nanomaterials*, Materials Horizons: From Nature to Nanomaterials, https://doi.org/10.1007/978-981-19-4538-0_23

different nanohybrids, grouping of organic nanoparticles to the inorganic nanoparticles by covalent and non-covalent forces forms a class of functional organic–inorganic nanohybrids. This unique assembly provides us with many exceptional properties of higher stability, biocompatibility, multifunctionality, improved mechanical and physical characteristics and eco-friendliness [11]. Another interesting feature of organic–inorganic hybrid is their intracomponent interactions which have led to innovative synergistic properties. Modulated chemical and physical characteristics can be obtained by hybrid nanoparticles formed by coupling of 2 or more constituents. A diversity in applications such as light harvesting, biomedicine, catalysis and energy storage is achieved by unique optoelectronic and chemical characteristics of organic–inorganic nanohybrids [12–14].

The fascinating combination of organic and inorganic nanoparticles to form nanohybrids is not new, but it can be largely found in nature in the form of mollusk teeth and shells, which are made up of inorganic and bio-macromolecular nanoparticles via nanoscale hybridization [15]. Therefore, organic–inorganic nanohybrids can be defined as hetero-nanoparticles formed by the coupling of inorganic and organic parts, each having discrete domains. The organic–inorganic nanohybrids have some new properties raised from synergic effects of organic and inorganic components like desirable magnetic, electrical and optical properties in addition to general characteristics of individual components [16]. The distinct feature of nanoscale hybridization exhibits considerably distinctive properties than consistent bulk materials [17].

Organic–inorganic hybrid materials, on the other hand, are more than just physical mixtures. They are widely described as nanocomposites with intimately mixed organic and inorganic species [18]. A lot of organic–inorganic nanohybrids have been prepared for their diverse applications, and some are described here. Aripiprazole (APZ) is a novel cationic drug to treat schizophrenia both positive and negative types with less risk of extrapyramidal side effects in comparison with other drugs. The drug delivery into human is done with the help of a nanohybrid of the cationic APZ with montmorillonite (MMT). MMT is an inorganic material containing alternate layers of silicon and aluminum and is negatively charged. APZ couples MMT by ionic interactions. APZ-MMT hybrid was further treated with a polymer that is cationic like polyvinylacetal diethylaminoacetate to avoid the release of drug buccal cavity. This has also improved the APZ dissolution in stomach [19]. The cationic inorganic lamella of Mg–Al-LDH (layered double hydroxide) was combined with naphthol blue-black anionic dye to form a composite which is useful as biological and protein stain in electrophoresis and chromatography, a dye in nylon, silk, textile, wool, wood stain, writing ink and soap industry [20].

An organic–inorganic hybrid of polyaniline with CdS has been modified by doping camphor sulfonic acid to enhance gas (H_2S) sensing at room temperature [21]. Cerasome, self-assembled, lipidicorganotrialkoxysilanes has bilayer of lipids like in liposome which are covered by silicate frameworks. Cerasome forms stable biomembrane model and functional nanocapsules with the help of silicates present in it [22]. The unique properties of organic–inorganic nanohybrids are attributed to both their organic and inorganic parts which can be briefly described as follow.

2 Organic Species

Organic species constitute a crucial part of the nanohybrid, and there is huge diversity of organic species to choose from. Surface modification of inorganic nanoparticles is essential for interaction with organisms [23–25]. Inorganic nanoparticles with toxic or hydrophobic capping ligands are inappropriate for biomedical applications, so capping ligands of organic nature are used to improve the properties and reduce cytotoxicity [26]. Nature of the inorganic nanoparticles decides the type of organic specie that will be attached on the surface [27]. The organic species containing terminal thiol group usually attaches with Au NPs; the functionalization of silica nanoparticles could be done with silane containing organic species, and LDH can be used with organic anions and biomolecules [28].

3 Inorganic Nanoparticles

Inorganic NPs could be prepared using either chemical or physical methods by bottom-up or top-down approaches within the range of 1–100 nm in no less than one dimension [26]. Effective therapeutic and diagnostic applications are achieved by controlling the shape, surface engineering, size and composition of inorganic NPs. The capability of inorganic NPs to effectively monitor therapeutic process and facilitate imaging is way ahead the organic biomaterials [29]. Inorganic NPs like iron oxide, carbon, gold, quantum dots, rare earth and silica NPs have been applied in biomedicine fields through in vivo or in vitro systems [30].

4 Applications Prospects of Organic–Inorganic Nanohybrids

Numerous organic–inorganic hybrids have been synthesized till this day and are utilized in many fields for their unique properties.

4.1 Biomedical Applications

Novel functional therapeutic mediators have been developed with exclusive physical or optical properties of inorganic nanoparticles which can carry drug with the help of organic surface polymer could be utilized in biomedical imaging. Ceramic containing inorganic nanoparticles are applied as bone graft materials due to their strong mechanical properties [31, 32]. Nanomedicine is the branch of nanotechnology which recognizes medical application of nanoparticles to treat and prevent

diseases [33]. Nanoscale agents carry exceptional properties as diagnosis systems, drug delivery systems and biosensors. Biodistribution and pharmacokinetics of many drugs are controlled by attaching suitable drug delivery systems. Nanomedicines tend to accumulate in the cancer tissues via vascular tumor structure. This process is the base to drug delivery in tumor cells [34]. Same nanoformulation is used to diagnose and treat cancer by theranostic agents at the same time. Min et al. acquired doxorubicin-based $CaCO_3$ hybrid nanoparticles for chemotherapy and ultrasound imaging specifically for cancer [35]. Nanotechnology is now advanced to the level of developing nanovaccines, utilization of patient's immune system to combat cancer. This phenomenon is termed as cancer immunotherapy. Nanoparticles carry immunostimulants to elicit an adaptive response by immune system [36–38]. The technology which breaks a specific part in double stranded helix, then replaces, inserts or modifies a gene is called gene editing. Lately, short palindromic repetitions that are clustered and interspaced from bacterial adaptive immune system are considered a great tool to edit genome [39]. Mout et al. came up with a direct cytosolic carrier for genome editing. The delivery system is cationic arginine-Au nanohybrid which enhances the efficiency of cytoplasmic nuclear delivery up to ~90% [40]. Silicate-based nanohybrids with large surface areas and hydrophilic nature are bioactive molecules. These bioactive moieties have high biocompatibility and tissue regeneration capacity as compared to other nanomaterials with absorbable and non-toxic degradation products [41, 42].

4.2 Photocatalytic Applications

Combination of inorganic nanoparticles with semiconductive organic polymers gives potential photocatalytic hybrids to carry CO_2 reduction and water splitting. Five mechanisms involved in charge transfer and light absorption in the organic–inorganic heterojunctions are: type I heterojunction, sensitization, z-scheme heterojunction, z-scheme through conductive intermediate and double transfer mechanism [43–45]. The environmental application of nanohybrids involves the removal of pollutant based on the nature of semiconductor polymer and inorganic nanoparticles. Most known inorganic semiconductors include ZnO and TiO_2, while most popular polymeric organic photocatalyst is g–C_3N_4 [46]. The interfaces in organic–inorganic nanohybrids are the base of photocatalytic activity and charge transfer process. If the organic ligand contains an electronegative element, it will help enhance the coating of inorganic particles. Some examples of N-atom containing ligands are polypyrrole, g–C_3N_4 and polyaniline, while polythiophenes are S-atom containing polymers [47]. Lei et al. developed a PVA-coated TiO_2 hybrid, effective against photodegradation of phenol and MO. Here, PVA is not the actual coupling polymer rather than post-treatments convert it to unsaturated conductive polymer [48]. Karthik et al. reported a special charge transfer mechanism by poly(catechol)-TiO_2 hybrid used to remove Cr (VI) from environment and for production of H_2 from water [49]. Yang et al. presented a combination of TiO_2 with pyrene and 3% Pt. This combination increased

production of hydrogen to a value of 15.020 $mmolg^{-1}$ h^{-1}. Close interfacial contact between TiO_2 and pyrene enhances the photocatalytic activity [50].

4.3 Electrochemical Sensors

The conventional undoped or doped inorganic sensors are used to detect reducing gases with low cost, simple methods and good response [51].However, these sensors have some flaws like their working temperature is way too high which results in high power consumption and also compromise the safety [52, 53]. On the other hand, organic polymer-based sensors work effectively at room temperature [54]. These polymers are also not free of shortcomings like long response time, low response and less thermally stable [55]. The problems of both organic and inorganic sensors could be overcome by combining both materials [56]. SnO_2-polyaniline hybrid materials have been developed to work as gas sensors. Deshpande et al. showcased that the presence of SnO_2 has drastically changed the sensor properties of polyaniline fore ammonia gas by faster response time, grater reproducibility and good response at room temperature [57]. Li et al. carried in situ synthesis of ZnO-sodium polystyrenesulfonate nanocomposite which could be used as humidity sensors. This sensor showed better linearity, higher response, quicker response and small hysteresis than simply sodium polystyrenesulfonate sensors. The improvement in the results is attributed to presence of ZnO and synthesis at nanoscale [58].

5 Challenges and Future Perspectives of Organic–Inorganic Nanohybrids

We have emphasized on some of the recent advances of organic–inorganic nanohybrids in this chapter. The given work present functionality of organic–inorganic hybrids in different fields. Recent achievements made in this field are pretty encouraging, but there is still space for further progress. Many improvements are needed to enhance the applications of these hybrids. First, biocompatibility and toxicity are two major concerns regarding in vivo utilization of organic–inorganic nanohybrids. Advanced screening and deigning of nanohybrids should be done to make them nontoxic with excretion from organism by completing the task. Second, site specificity is another challenge which can be improved by using certain targeting ligands like antibodies, oligosaccharides, fusogenic residues, viral proteins, polypeptides and folic acid to take the drug to the disease site. Another big problem is to commercialize those nanohybrids in practical field which is impossible without interdisciplinary collaborations.

One of the many challenges is that the synthesis design for distinct organic–inorganic nanohybrids must attain, controllability, safety and high efficiency for biomedical application and it should be simple at the same time. Nowadays, nanohybrids synthesis approaches are way too complicate for this idea. Synthetic designs are delicate and tedious most of the time rather than easily scaled-up and reproduceable. Considering intricacy of biological systems, tremendous trial with efficient nanohybrids has failed. To avoid this problem, we must explore the behavior of nanohybrids in biological system like their degradation potential, biocompatibility and biodistribution in vivo. This will decrease the spread of nanohybrids in normal cells and tissues.

Nitrogen fixation and its photoreduction to ammonia are an emerging topic nowadays. The literature proves that the usage of organic–inorganic hybrid photocatalyst gives us better performance than mere semiconductors. The production of ammonia has gained importance commercially and environmentally and is increasing the interest of contributors. The current progress in this field forces us to believe that conjugation of inorganic and polymer semiconductor has a strong potential for enhanced photocatalytic and optoelectronic properties. These hybrid structures could cause dramatic changes not only in environmental mechanisms but also in the production of solar fuel through artificial photosynthesis to overcome climate changes.

The cost of using noble metal nanoparticles as commercial photocatalysts is too high to use them. That is why, abundant and cheaper organic–inorganic nanohybrids need to be synthesized to replace metal nanoparticles. The metal and polymer nanoparticles rarely remove multiple pollutants at the same time, but nanocomposites based on organic and inorganic particles have been developed to degrade multi-pollutants. This has been a futuristic approach to synthesize more effective nanohybrids. Beside the availability of a lot of organic−inorganic hybrids synthesized so far, many are still not tested for their application as catalysts and only few are reused as catalysts. Hence, there lies a great opportunity to investigate those available hybrids as catalyst. A lot of hybrids with single functional group are known but only a few materials with more than one functional group. This area needs to be explored to incorporate hybrid materials with multiple functional groups either in specific or in random spatial arrangements. Efforts must be made to discover and test new hybrid materials. The illuminating points are the interactive functions and properties of individual parts of organic–inorganic nanohybrids. A keen study of demanding systems for nanohybrids will lead to a clear practical design. The overall review on diversity of organic–inorganic nanohybrids could suggest an unconventional proposal to futuristic biomedical, catalytic and electrochemical properties.

6 Conclusion

The captivating organic–inorganic nanohybrids are the most promising nanomaterials which can be easily synthesized with excellent crystallinity, uniform composition throughout the matrix and intercalation of polymer films coated on inorganic NPs. The main focus of this chapter is the recent advancement in organic–inorganic nanocomposites, their applications in biomedical, photocatalytic and electrochemical field and the challenges and future perspectives faced in this field of research. High and quicker response, large surface area, improved adsorption efficiency, affinity for biomolecules, thermal stability and excellent conductivity makes organic–inorganic hybrids a pledging choice for biomedical applications such as biomedicine, as therapeutic agents and in cancer therapy as well as for environmental applications like removal of pollutants from water and environment, biosensors and electrolysis. The present chapter also highlighted some challenges that are faced in this field and what progress we can make to minimize those problems so that organic–inorganic hybrids can be used commercially. In the future, a large number of efficient organic–inorganic nanocomposites are believed to be prepared with a variety of polymers and inorganic cations and anions for further enhanced applications.

References

1. Paek SM, Oh JM, Choy JH (2011) A lattice-engineering route to heterostructured functional nanohybrids. Chem Asian J 6(2):324–338
2. Banin U, Ben-Shahar Y, Vinokurov K (2014) Hybrid semiconductor–metal nanoparticles: from architecture to function. Chem Mater 26(1):97–110
3. Liu, C. H., Chiu, L. K., Yeh, J. Y., & Tsiang, R. C. C. (2012). Making organic-inorganic nanocomposites via selective dispersion of PS-tethered SiO2 particles in polystyrene-block-polymethylmethacrylate copolymer. *Journal of Nanomaterials*, *2012*.
4. Saleh NB, Afrooz ARM, Bisesi JH, Aich N, Plazas-Tuttle J, Sabo-Attwood T (2014) Emergent properties and toxicological considerations for nanohybrid materials in aquatic systems. Nanomaterials 4(2):372–407
5. Chen S, Chen P, Wang Y (2011) Carbon nanotubes grown in situ on graphene nanosheets as superior anodes for Li-ion batteries. Nanoscale 3(10):4323–4329
6. Wang D, Choi D, Li J, Yang Z, Nie Z, Kou R, Hu D, Wang C, Saraf LV, Zhang J, Aksay IA, Liu J (2009) Self-assembled TiO_2-graphene hybrid nanostructures for enhanced Li-ion insertion. ACS Nano 3(4):907–914
7. Wang Y, Tang S, Vongehr S, Ali Syed J, Wang X, Meng X (2016) High-performance flexible solid-state carbon cloth supercapacitors based on highly processible N-graphene doped polyacrylic acid/polyaniline composites. Sci Rep 6(1):1–10
8. Watcharotone S, Dikin DA, Stankovich S, Piner R, Jung I, Dommett GH et al (2007) Graphene−silica composite thin films as transparent conductors. Nano Lett 7(7):1888–1892
9. Son DI, Kwon BW, Park, DH, Seo WS, Yi Y, Angadi B, Lee C-L, Choi WK (2012) Emissive ZnO–graphene quantum dots for white-light-emitting diodes. Nat Nanotechnol 7(7):465–471
10. Xu Y, Liu Z, Zhang X, Wang Y, Tian J, Huang Y, Ma Y, Zhang X, Chen Y (2009) A graphene hybrid material covalently functionalized with porphyrin: synthesis and optical limiting property. Adv Mater 21(12):1275–1279

11. Mu Q, Jiang G, Chen L, Zhou H, Fourches D, Tropsha A, Yan B (2014) Chemical basis of interactions between engineered nanoparticles and biological systems. Chem Rev 114(15):7740–7781
12. Nguyen KT, Zhao Y (2014) Integrated graphene/nanoparticle hybrids for biological and electronic applications. Nanoscale 6(12):6245–6266
13. Liang R, Wei M, Evans DG, Duan X (2014) Inorganic nanomaterials for bioimaging, targeted drug delivery and therapeutics. Chem Commun 50(91):14071–14081
14. Naoi K, Naoi W, Aoyagi S, Miyamoto JI, Kamino T (2013) New generation "nanohybrid supercapacitor." Acc Chem Res 46(5):1075–1083
15. Ruiz-Hitzky E, Darder M, Aranda P, Ariga K (2010) Advances in biomimetic and nanostructured biohybrid materials. Adv Mater 22(3):323–336
16. Nguyen KT, Zhao Y (2015) Engineered hybrid nanoparticles for on-demand diagnostics and therapeutics. Acc Chem Res 48(12):3016–3025
17. Sanchez C, Julián B, Belleville P, Popall M (2005) Applications of hybrid organic–inorganic nanocomposites. J Mater Chem 15(35–36):3559–3592
18. Sanchez C, Ribot F, Lebeau B (1999) Molecular design of hybrid organic-inorganic nanocomposites synthesized via sol-gel chemistry. J Mater Chem 9(1):35–44
19. Oh YJ, Choi G, Choy YB, Park JW, Park JH, Lee HJ et al (2013) Aripiprazole—montmorillonite: a new organic–inorganic nanohybrid material for biomedical applications. Chem Eur J 19(15):4869–4875
20. bin Hussein MZ, Zainal Z, Yahaya AH, binti Abd Aziz A (2002) Synthesis of layered organic–inorganic nanohybrid material: an organic dye, naphthol blue black in magnesium–aluminum layered double hydroxide inorganic lamella. Mater Sci Eng B 88(1):98–102
21. Raut BT, Chougule MA, Nalage SR, Dalavi DS, Mali S, Patil PS, Patil VB (2012) CSA doped polyaniline/CdS organic–inorganic nanohybrid: physical and gas sensing properties. Ceram Int 38(7):5501–5506
22. Katagiri K, Hashizume M, Ariga K, Terashima T, Kikuchi JI (2007) Preparation and characterization of a novel organic–inorganic nanohybrid "cerasome" formed with a liposomal membrane and silicate surface. Chem A Eur J 13(18):5272–5281
23. Albanese A, Tang PS, Chan WC (2012) The effect of nanoparticle size, shape, and surface chemistry on biological systems. Annu Rev Biomed Eng 14:1–16
24. Verma A, Uzun O, Hu Y, Hu Y, Han HS, Watson N, Chen S, Irvine DJ, Stellacci F (2008) Surface-structure-regulated cell-membrane penetration by monolayer-protected nanoparticles. Nat Mater 7(7):588–595
25. Kim B, Han G, Toley BJ, Kim CK, Rotello VM, Forbes NS (2010) Tuning payload delivery in tumour cylindroids using gold nanoparticles. Nat Nanotechnol 5(6):465–472
26. Burda C, Chen X, Narayanan R, El-Sayed MA (2005) Chemistry and properties of nanocrystals of different shapes. Chem Rev 105(4):1025–1102
27. Xu ZP, Zeng QH, Lu GQ, Yu AB (2006) Inorganic nanoparticles as carriers for efficient cellular delivery. Chem Eng Sci 61(3):1027–1040
28. Huang X, Li L, Liu T, Hao N, Liu H, Chen D, Tang F (2011) The shape effect of mesoporous silica nanoparticles on biodistribution, clearance, and biocompatibility in vivo. ACS Nano 5(7):5390–5399
29. Ulbrich K, Holá K, Šubr V, Bakandritsos A, Tucek J, Zboril R (2016) Chem Rev 116:5338–5431
30. Liu K, Zhao N, Kumacheva E (2011) Self-assembly of inorganic nanorods. Chem Soc Rev 40(2):656–671
31. Liu H, Webster TJ (2010) Mechanical properties of dispersed ceramic nanoparticles in polymer composites for orthopedic applications. Int J Nanomed 5:299
32. Hong Z, Reis RL, Mano JF (2008) Preparation and in vitro characterization of scaffolds of poly (L-lactic acid) containing bioactive glass ceramic nanoparticles. Acta Biomater 4(5):1297–1306
33. He Q, Shi J (2014) MSN anti-cancer nanomedicines: chemotherapy enhancement, overcoming of drug resistance, and metastasis inhibition. Adv Mater 26(3):391–411
34. Prabhakar U, Maeda H, Jain RK, Sevick-Muraca EM, Zamboni W, Farokhzad OC, et al (2013) Challenges and key considerations of the enhanced permeability and retention effect for nanomedicine drug delivery in oncology

35. Min KH, Min HS, Lee HJ, Park DJ, Yhee JY, Kim K et al (2015) pH-controlled gas-generating mineralized nanoparticles: a theranostic agent for ultrasound imaging and therapy of cancers. ACS Nano 9(1):134–145
36. Shin H, Na K (2019) In situ vaccination with biocompatibility controllable immuno-sensitizer inducing antitumor immunity. Biomaterials 197:32–40
37. Shao, K., Singha, S., Clemente-Casares, X., Tsai, S., Yang, Y., & Santamaria, P. (2015). Nanoparticle-based immunotherapy for cancer. ACS Nano 9(1):16–30
38. Li S, Feng X, Wang J, He L, Wang C, Ding J, Chen X (2018) Polymer nanoparticles as adjuvants in cancer immunotherapy. Nano Res 11(11):5769–5786
39. Doudna JA, Charpentier E (2014) The new frontier of genome engineering with CRISPR-Cas9. Science 346(6213):1258096
40. Mout R, Ray M, Yesilbag Tonga G, Lee YW, Tay T, Sasaki K, Rotello VM (2017) Direct cytosolic delivery of CRISPR/Cas9-ribonucleoprotein for efficient gene editing. ACS Nano 11(3):2452–2458
41. Xavier JR, Thakur T, Desai P, Jaiswal MK, Sears N, Cosgriff-Hernandez E, Kaunas R, Gaharwar AK (2015) Bioactive nanoengineered hydrogels for bone tissue engineering: a growth-factor-free approach. ACS Nano 9(3):3109–3118
42. Mihaila SM, Gaharwar AK, Reis RL, Khademhosseini A, Marques AP, Gomes ME (2014) The osteogenic differentiation of SSEA-4 sub-population of human adipose derived stem cells using silicate nanoplatelets. Biomaterials 35(33):9087–9099
43. Xie S, Zhang Q, Liu G, Wang Y (2016) Photocatalytic and photoelectrocatalytic reduction of CO_2 using heterogeneous catalysts with controlled nanostructures. Chem Commun 52(1):35–59
44. Li K, Peng B, Peng T (2016) Recent advances in heterogeneous photocatalytic CO2 conversion to solar fuels. ACS Catal 6(11):7485–7527
45. Safaei J, Mohamed NA, Noh MFM, Soh MF, Ludin NA, Ibrahim MA, Wan Isahak WNR, Asri M, Teridi, M. A. M. (2018) Graphitic carbon nitride (gC_3 N_4) electrodes for energy conversion and storage: a review on photoelectrochemical water splitting, solar cells and supercapacitors. J Mater Chem A 6(45):22346–22380
46. Ong WJ, Tan LL, Ng YH, Yong ST, Chai SP (2016) Graphitic carbon nitride (g-C3N4)-based photocatalysts for artificial photosynthesis and environmental remediation: are we a step closer to achieving sustainability? Chem Rev 116(12):7159–7329
47. Yang L, Yu Y, Zhang J, Chen F, Meng X, Qiu Y, Dan Y, Jiang L (2018) In-situ fabrication of diketopyrrolopyrrole-carbazole-based conjugated polymer/TiO_2 heterojunction for enhanced visible light photocatalysis. Appl Surf Sci 434:796–805
48. Lei P, Wang F, Zhang S, Ding Y, Zhao J, Yang M (2014) Conjugation-grafted-TiO_2 nanohybrid for high photocatalytic efficiency under visible light. ACS Appl Mater Interfaces 6(4):2370–2376
49. Karthik P, Vinoth R, Selvam P, Balaraman E, Navaneethan M, Hayakawa Y, Neppolian B (2017) A visible-light active catechol–metal oxide carbonaceous polymeric material for enhanced photocatalytic activity. J Mater Chem A 5(1):384–396
50. Yang Q, Peng P, Xiang Z (2017) Covalent organic polymer modified TiO_2 nanosheets as highly efficient photocatalysts for hydrogen generation. Chem Eng Sci 162:33–40
51. Mousty C (2004) Sensors and biosensors based on clay-modified electrodes—new trends. Appl Clay Sci 27(3–4):159–177
52. Leroux F, Taviot-Guého C (2005) Fine tuning between organic and inorganic host structure: new trends in layered double hydroxide hybrid assemblies. J Mater Chem 15(35–36):3628–3642
53. Shakeel A, Rizwan K, Farooq U, Iqbal S, Altaf AA (2022) Advanced polymeric/inorganic nanohybrids: an integrated platform for gas sensing applications. Chemosphere 294:133772
54. Geng W, Li N, Li X, Wang R, Tu J, Zhang T (2007) Effect of polymerization time on the humidity sensing properties of polypyrrole. Sens Actuators B Chem 125(1):114–119
55. Wallace GG, Teasdale PR, Spinks GM, Kane-Maguire LA (2008) Conductive electroactive polymers: intelligent polymer systems. CRC Press

56. Wu Y, Xing S, Fu J (2010) Examining the use of TiO_2 to enhance the NH_3 sensitivity of polypyrrole films. J Appl Polym Sci 118(6):3351–3356
57. Deshpande NG, Gudage YG, Sharma R, Vyas JC, Kim JB, Lee YP (2009) Studies on tin oxide-intercalated polyaniline nanocomposite for ammonia gas sensing applications. Sens Actuators B Chem 138(1):76–84
58. Li Y, Yang MJ, She Y (2004) Humidity sensors using in situ synthesized sodium polystyrene-sulfonate/ZnO nanocomposites. Talanta 62(4):707–712